Conceptual Design of Deployable Space Structures

Von der Fakultät für Maschinenbau
der Technischen Universität Carolo-Wilhelmina zu Braunschweig

zur Erlangung der Würde

eines **Doktor-Ingenieurs (Dr.-Ing.)**

genehmigte Dissertation

von:	**Dipl.-Ing. Martin Hillebrandt**
geboren in (Geburtsort):	Braunschweig

eingereicht am:	31.01.2019
mündliche Prüfung am:	17.04.2019
Vorsitz:	Prof. Dr.-Ing. Christian Hühne
Gutachter:	Prof. Dr.-Ing. Michael Sinapius
	Prof. Dr. rer. nat. Hansjörg Dittus

2020

Preface

This doctoral thesis was inspired by my work as a project engineer in the field of deployable space structures at the Institute of Composite Structures and Adaptive Systems of the German Aerospace Center (DLR) and was supervised at the Institute of Adaptronics and Function Integration of the Technical University Carolo Wilhelmina in Braunschweig, Germany.

Many people have contributed to the development of this thesis through scientific discussions, advice, the introduction of different viewpoints and many other types of support. I would like to take this opportunity to thank some of them who have contributed in a special way.
First of all, I would like to thank my supervisor Prof. Dr.-Ing. Michael Sinapius for his support and guidance and especially for the many discussions about the scientific focus of this thesis. Furthermore, I would like to thank the head of my department Prof. Dr.-Ing. Christian Hühne for his support over many years and for providing the resources and professional free time necessary to carry out this work. I would also like to thank Prof. Dr. rer. nat. Hansjörg Dittus for his agreement to provide the second opinion to this thesis.
My special thanks go to Dr.-Ing. Marco Straubel, who has supported me in my professional career not only during the preparation of this work, but already since my academic studies as a graduate student. I would also like to thank Martin Zander and Olaf Mierheim for the many discussions, valuable suggestions and their advice not only on the scientific issues involved with the preparation of this work. I should also mention the manifold support I received from the members of the Spacecraft Structures Team at the Institute of Composite Structures and Adaptive Systems in Braunschweig.

I am especially grateful to my fiancée Nina, my sister Claudia and my parents Marion and Fritz, who have always supported me unconditionally, even long before this work began, and have thus created the basis without which the presented thesis would not have been possible.

This work is dedicated to my brother Jan.

Abstract

Deployable Structures are utilized in space applications in a multiplicity of different fields. They provide the backbone structure of solar arrays for power generation, reflectors for earth observation, drag sails for de-orbiting, solar sails for propulsion and also serve as deployable instrument booms. Deployable structures are applied where the dimensions of a spacecraft or its subsystem exceeds the dimensions of the launchers payload bay. Hence means for folding to enable space transport and for deployment to enable the transition on-orbit into the required operational form have to be implemented in their design. The primary goals of the design task are thereby a low mass and a small stowed volume to enable compatibility with a variety of host spacecraft and launchers and to minimize launch costs. Within this thesis a conceptual design methodology is developed that aims on generating such lightweight and compactly packaging deployable structures. The approach for its development is a system analysis of a deployable structure consisting of a deformable structure and a deployment mechanism. Goal of this analysis is the identification of design drivers and specific characteristic of this category of structures as a basis for the development of the design methodology. Therefore analytic sizing expressions for several deployable masts and their deployment mechanism components are established and their scaling behaviors regarding a solar array and solar sail application are examined. A particular focus is thereby on the design dependencies and interactions between the deformable structure and the deployment mechanism and how these need to be considered in the design process. Furthermore the form transition between the stowed and deployed state under external loads is analyzed and the impact of this unique load case of deployable structures on their design is studied. Another analysis focus addresses performance evaluation methods of deployable space structures applicable in early design stages. Such methods are required to identify the most promising design concepts despite the uncertainties regarding the actual mass and volume specific performance of the fully developed system. The combined results of these analyses are subsequently implemented in the processes of the new conceptual design methodology for deployable space structures. Furthermore a variety of design principles are deduced from these analyses results that enable high solution qualities regarding lightweight and compactly packaging deployable space structures. Finally the methodology is demonstrated for the conceptual design of the deployable structure of a solar array.

Zusammenfassung

Entfaltbare Strukturen werden für Weltraumanwendungen in einer Vielzahl von unterschiedlichen Bereichen eingesetzt. Sie dienen als Stützstrukturen für Solarmodule zur Stromerzeugung, als Reflektoren zur Erdbeobachtung, Bremssegel für das De-Orbiting von Satelliten und als Sonnensegel zum Antrieb von Raumsonden sowie als entfaltbare Instrumententräger. Sie werden überall dort eingesetzt, wo die Abmessungen des Raumfahrzeugs oder eines seiner Teilsysteme das verfügbare Nutzlastvolumen der Trägerrakete überschreiten. Daher ist es nötig die jeweiligen Systeme und deren Stützstrukturen faltbar zu gestalten, um den Transport in den Orbit zu ermöglichen. Weiterhin müssen sie dort in ihre Zielform automatisch entfaltet werden können. Die wesentlichen Entwurfsziele sind dabei eine geringe Masse und ein kleines Stauvolumen, da diese die Kompatibilität mit möglichen Trägersatelliten und -raketen bestimmen sowie entscheidend für die Startkosten sind. Im Rahmen dieser Arbeit wird eine Methodik für den Entwurf solcher entfaltbarer Raumfahrtstrukturen entwickelt, deren Ziel es ist die Entwicklung von leichten und kompakt staubaren entfaltbaren Strukturen zu ermöglichen. Der Ansatz für die Entwicklung der Methodik ist die Systemanalyse einer entfaltbaren Raumfahrtstruktur, deren Hauptbestandteile eine verformbare Struktur und ein entsprechender Entfaltungsmechanismus sind. Ziel der Systemanalyse ist die Identifizierung von spezifischen Merkmalen und entwurfsbestimmenden Anforderungen entfaltbarer Strukturen, welche als Grundlage für die Entwicklung der Entwurfsmethodik dienen. In der Systemanalyse werden mehrere Typen entfaltbarer Masten untersucht und für diese und deren Entfaltungsmechanismen analytische Skalierungsfunktionen aufgestellt. Anhand dieser Funktionen wird das Skalierungsverhalten der Masten bezüglich einer Anwendung als Stützstruktur eines entfaltbaren Solarmoduls und eines Sonnensegels untersucht. Betrachtet werden dabei insbesondere Abhängigkeiten und Interaktionen in der Auslegung zwischen der verformbaren Struktur und dem Entfaltungsmechanismus und es werden Maßnahmen abgeleitet wie diese im Entwurfsprozess zu berücksichtigen sind. Ein weiterer Schwerpunkt der Analyse ist der Formübergang der entfaltbaren Struktur zwischen dem gestauten und dem entfalteten Zustand, wenn dabei äußere Lasten einwirken. Darüber hinaus werden Methoden zur Leistungsbewertung von entfaltbaren Raumfahrtstrukturen untersucht, die auch in frühen Entwurfsphasen eingesetzt werden können. Solche Methoden sind von besonderer Bedeutung für den Entwurfsprozess, da an dessen Ende die Auswahl eines möglichst leistungsfähigen Konzeptes steht, obwohl aufgrund des geringen Entwicklungsstandes erhebliche Unsicherheit über deren tatsächliche Leistungsfähigkeit bzgl. Massen- und Volumeneffizienz besteht. Die Ergebnisse der genannten Teilschritte der Systemanalyse fließen anschließend in die Gestaltung der Prozesse der neuen Entwurfsmethodik für entfaltbare Raumfahrtstrukturen ein. Darüber hinaus werden aus ihnen Konstruktionsprinzipien abgeleitet, die zur Entwicklung von leichten und kompakt staubaren entfaltbaren Raumfahrtstrukturen besonders geeignet sind. Abschließend wird die Methodik anhand des Entwurfs der entfaltbaren Struktur eines Solarmoduls demonstriert.

Table of Contents

List of Figures

List of Tables

List of Parameters

Parameter	Expression	Unit	Remarks
A	Mast Cross-Sectional Area	m²	Mast Design Variable
A_0	Base Segment Area of the Telescopic Tubular Mast	m²	
A_n	Tip Segment Area of the Telescopic Tubular Mast	m²	
A^*	Minimum Mass Area Solution	m²	
a_{acc}	Acceleration Load	m/s²	
A_l	Truss Longeron Cross-Sectional Area	m²	
b_M	Mast Flattened Width	m	
c_c	Wall Buckling Stress Approximation Factor for Compression	-	
c_b	Wall Buckling Stress Approximation Factor for Bending	-	
c_t	Truss Axial Mass Fraction Approximation Factor	-	
D	Flexural Rigidity	Nm	
D_M	Mast Diameter	m	
d	Diameter	m	
d_{AE}	Solar Sail Distance relative to the Sun	AE	
d_c	Wall Buckling Stress Approximation Factor for Compression	-	
d_b	Wall Buckling Stress Approximation Factor for Bending	-	
d_t	Truss Axial Mass Fraction Approximation Factor	-	
E	Young's Modulus	N/m²	
E_{tan}	Tangent Modulus	N/m²	
EI	Bending Stiffness	Nm²	
F	Force	N	
f	Eigenfrequency	Hz	
F_S	Safety Factor	-	
g	Mast-Mechanism Interaction Factor	-	
h	Element height	m	
I	Second Moment of Area	m⁴	
i	Mast Constraint Function Exponent Term	-	
j	Mast Constraint Function Exponent	-	

	Term	
k	Factor	-
k_A, $k_{A,l}$	Cross-Section Area Factor	-
k_a	Acceleration Load Amplification Factor	-
k_C, $k_{C,l}$	Mounting Factor	-
k_D	Plate Rigidity Factor	-
$k_{E,0}$	Initial Modulus Knockdown Factor	-
k_f	Eigenfrequency Amplification Factor	-
k_G	Gear Ratio	-
k_I, $k_{I,l}$	Cross-Section Second Moment of Area Factor	-
k_{IF}	Interface Size Factor	-
k_{MI}	Mechanical Interface Mass Factor	-
k_m	Plate Mass Factor	-
k_{PV}	Effective Photovoltaic Cell Area Factor	-
k_z	Solar Sail Tip Displacement Factor	-
k_y	Cross-Section Neutral Layer Offset Factor	-
k_γ	Solar Sail Mass Distribution Factor	-
k_ζ	Truss Compression Strength Knockdown Factor	-
k_ρ	Density Factor	-
L	Mast Length	m
l	Element or Longeron Length	m
l_{tz}	Support Length of the Transition Zone	m
M	Bending Moment	Nm
m	Mass	kg
M_{CS}	Spring Moment	Nm
M_{Mr}	Mast Reeled Spring Moment	Nm
m_M	Mast Mass	kg
m_0	Supported Mass	kg
n	Number of Longerons or Cylinder Segments	-
P	Compression Load	N
P_E	Euler Load	N
P_{elec}	Solar Array Power	W
$P_{elec,m}$	Mass Specific Solar Array Power	W/kg
$P_{elec,V}$	Volume Specific Solar Array Power	W/m³
p	Pressure	N/m²
p_{sol}	Solar Pressure at 1AE	

$p_{t,max}$	Maximum Line Pressure	N/m	
R	Mast Radius	m	Mast Design Variable
R_0	Base Segment Radius of the Telescopic Tubular Mast	m	
R_n	Tip Segment Radius of the Telescopic Tubular Mast	m	
R^*	Minimum Mass Radius Solution	m	
r	Radius	m	
$r_{i,l}$	Longeron Radius of Gyration	m	
r_l	Truss Longeron Radius	m	
r_M	Mast Reeling Radius	m	
$r_{M,i}$	Mast Radius of Gyration	m	
S_a	Deployment Mechanism Envelope Length	m	
S_b	Deployment Mechanism Envelope Height	m	
S_c	Deployment Mechanism Envelope Width	m	
T	Torque	Nm	
t	Element thickness	m	
t_M	Tubular Shell Mast Thickness	m	
t_{PV}	Photovoltaic Blanket Thickness	m	
V	Volume	m³	
v	Length Specific Volume	m³/m	
W	Section Modulus	m³	
w	Length Specific Mass	kg/m	
Y, Z	Transition Zone Form Functions	m	
$\hat{Y}, \hat{Z}$	Related Transition Zone Form Functions	-	
x, y, z	Coordinates and Directional Offsets	m	
$\hat{x}, \hat{y}, \hat{z}$	Related Coordinates	-	
α	Arc Angle	rad	
β	Truss Axial Mass Ratio	-	
γ	Areal Mass	kg/m²	
γ_{BL}	Areal Solar Array Blanket Mass	kg/m²	
Γ	Ratio	-	
Γ_{bL}	Solar Array Side Length Ratio	-	
Γ_{PVL}	Photovoltaic Blanket Fold Height Ratio	-	
Γ_R	Telescopic Tubular Mast Taper Ratio	-	

Γ_{Rt}	Inverse Wall Thickness Ratio	-	
Γ_{SB}	Spreader Bar Thickness Ratio	-	
Γ_t	Thickness Ratio	-	
Γ_ρ	Density Ratio	-	
ΔR	Segment Clearance of the Telescopic Tubular Mast	-	
δ	Solar Array Eigenfrequency Knockdown Factor	-	See Banik [120]
ε	Strain	-	
ε_f	Flattening Strain	-	
ε_r	Reeling Strain	-	
ζ	Truss Longeron Imperfection Ratio	-	
η	Efficiency	-	
η_G	Gear Efficiency	-	
η_{PV}	Photovoltaic Efficiency	-	
Θ	Truss Diagonal Angle	rad	
K	Transition Zone Curvature Function	1/m	
κ	Curvature	1/m	
ν	Poisson Ratio	-	
ρ	Density	kg/m³	
ρ^*	Reference Density	kg/m³	
σ	Stress	N/m²	
τ	Shear stress	N/m²	
ω	Angular Frequency	rad/s	

List of Indices

Index	Expression	Remarks
0	Initial or Starting Value	
$crit$	Critical	
l	Longeron	
min	Minimum	
max	Maximum	
opt	Optimum	
req	Requirement	
sys	System	
TZ	Transition Zone	

Deployable Structure Element Hierarchy and List of According Indices

Main Component	Module	Component	Index
Deployment Mechanism			-
	Energy Source		ES
	Mast Spool		MS
		Spool Cylinder	MSC
		Spool End Cap	MSE
		Spool Axle	MSA
	Spool Brake Mechanism		SP
		Spool Brake Tooth Ring	SBT
		Spool Brake Arm Mount	SBM
		Spool Brake Arms	SBA
		Spool Brake Spring	SBS
	Mast Guidance and Root Support		MG
		Mast Guide and Support Shells	MGS
		Mast Guide Rolls	MGR
	Drive Mechanism		DM
		Belt	DMB
		Belt Spool	DMS
		Gear	DMG
		Electric Motor	DMM
	Support Structure		SS
	Mechanical Interface		MI
Mast			M
	Tubular Shell Mast		TSM
	Tubular Shell Mast with Transition Zone		TSZ
	Solid Rod Truss		SRT
	Telescopic Tubular Mast		TTM

1. Observations on Deployable Space Structures

Spacecraft often rely in their functionality and operational capabilities on deployable sub-systems. They serve as solar arrays for power generation, antennas for communication, reflectors for earth observation, radiators and sun shields for thermal control, solar sails for propulsion and masts for instrument positioning. They all have in common that their required dimensions often exceed the dimensions of the payload bays of considered launchers. Prominent examples are the eight solar array wings of the International Space Station (ISS) as shown in Figure 1-1. Each wing has a size of 30 m x 12 m whereby they surpass the transport capabilities of even the largest launchers available today.

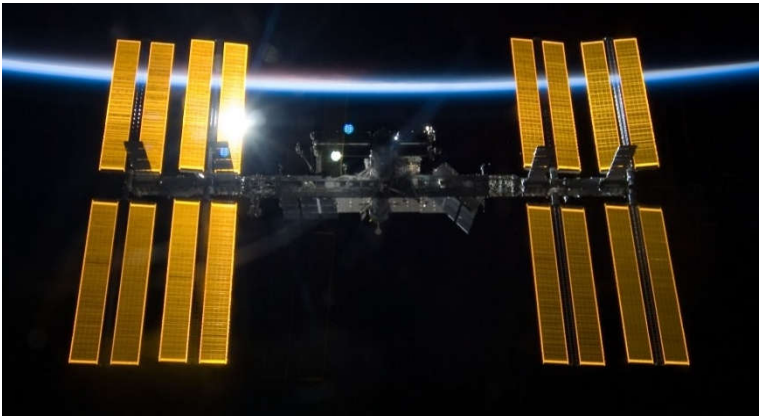

Figure 1-1: Image of the International Space Station (ISS) with its eight deployed Solar Arrays [1].

Hence, for transport into space a more compact form is required, wherefore means for foldability need to be introduced in the design. Once on orbit they autonomously unfold from this stowed configuration to the desired form that is necessary for their function. This change in shape is enabled by deployable structures. Deployable structures generate and induce the forces necessary for the transition from the stowed to the deployed form and provide the required stiffness and stability during and after deployment. Thus, the special characteristic and challenge in the design of Deployable Space Structures is to efficiently combine the mechanical requirements of the structure with the functional demands of shape changing with respect to certain design objectives and constraints such as compact stowage. The thesis at hand aims on contributing to the design of efficient Deployable Space Structures.

1.1. Principle Design and Main Design Objectives

The principle design of a deployable structure is described using a single ISS solar array wing as an example (see also Figure 1-1). A schematic of the design is displayed in Figure 1-2. Its main components are two blankets which carry the photovoltaics, two spreader bars which laterally support the blankets and a centrally aligned deployable truss.

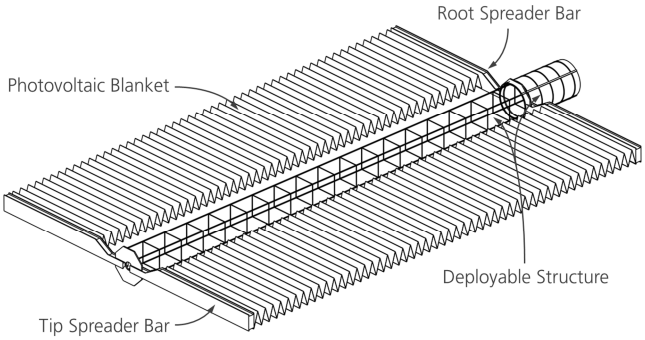

Figure 1-2: Schematic of the main components of an ISS solar array wing in a semi-deployed state.

The truss is the deployable structure of the array which deploys, stretches and supports the photovoltaic blankets. It becomes foldable by hinges at the joints of longerons and battens. At its root a mechanism is located which deploys the truss from its stowed state. It has a cylindrical form and is equipped with an internal sliding mechanism that unfolds the truss bay by bay and pushes it out of its stowage compartment. Thereby it also introduces the forces necessary to unfold and stretch the two photovoltaic blankets.
In conclusion the deployable truss in the example and deployable structures in general can roughly be subdivided into two components[1]:

(1) A *Deformable Structure* that transmits the forces necessary to perform the change of shape and provides the required stiffness and stability and
(2) A *Deployment Mechanism* that acts on the Deformable Structure and provides the capabilities necessary to perform the deployment such as unfolding of the Deformable Structure and generation of the required deployment force.

The design of Deployable Space Structures has two main objectives: a low mass and a small stowed volume. Both are primarily results of the afore mentioned mass and

[1] Throughout this thesis the term *deployable structure* or *Deployable Space Structure* stands for the combination of a *Deformable Structure* with a *Deployment Mechanism*. The *deployable structure* is part of a *deployable sub-system* of a *spacecraft*.

volume constraints during space transport and directly translate into launch costs. On-orbit a low mass leads to small mass moments of inertia whereby stiffness and stability requirements as well as requirements on the performance of the attitude control system of the host spacecraft are reduced.

1.2. Disproportion in the Mass and Stowage Volume Distribution

In the following the distributions of the mass and the stowage volume among the two components of a Deployable Space Structure are examined. Subject of the examination are various types of deployable masts which are often used as primary elements of deployable structures like for the example of the ISS solar array wings.
Table 1-1 gives the masses of the Deformable Structure m_S and the Deployment Mechanism m_M of the deployable masts. As can be seen, the Deployment Mechanism is always a significant and in many cases by far the dominating contributor. The ratio of the mechanism mass towards the overall mass reaches values between 23 % and 91 % and is in most cases well above 50 %.

Mast Type or Mission	Type of architecture	Deformable Structure mass m_S [kg]	Deployment Mechanism mass m_M [kg]	Deployment Mechanism mass ratio $\frac{m_M}{m_S + m_M}$	Remarks
De-Orbit Sail (4 x 2.86m)	Tubular	0.217 (measured)	0.64 (measured)	**75 %**	
GOSSAMER (4 x 4.3m)[2]	Tubular	0.619 (measured)	~6 (measured)	**91 %**	Mechanism mass contains only boom deployment components of Boom and Sail Deployment Unit
Northrop-Grumman 0.86" High Force STEM (20ft) [2] [3]	Tapespring	0.617 (measured)	1.59 (measured)	**72 %**	Maximum allowable mast length unknown
Northrop-Grumman Nano STEM (20ft) [2]	Tapespring	0.227 (measured)	0.163 (measured)	**42 %**	
ATK-ABLE ISS FAST (104ft) [4] [5]	Articulated	204 (estimated)	204 (estimated)	**50 %**	

[2] GOSSAMER is a solar sail that is designed to abandon the Deployment Mechanisms after deployment.

ATK-ABLE SRTM ADAM (60m) [6] [7]	Articulated	290 (measured)	695 (measured)	**71 %**	
Northrop-Grumman AstroMast Model 12027 (14m) [8]	Coilable	4.48 (measured)	12.32 (measured)	**73 %**	
ATK ORU Transfer Device (OTD) Boom [9]	*Telescopic*	*15.69 (estimated)*	*4.720 (estimated)*	***23 %***	*Estimated shell thickness averaged to 0.1 in*

Table 1-1: Structural mass compared to mechanism mass for various deployable mast systems.

Table 1-2 displays the contribution of the volume of the Deformable Structure V_S to the total volume V_T of the stowed configuration. The volume of the Deformable Structure is given in terms of the volume occupied by the pure structural material [3]. It is derived from the mass of the Deformable Structure m_S and its mean density ρ_S:

$$V_S = \frac{m_S}{\rho_S}$$

It can be seen that for the stowed volume an even stronger trend for dominance of the Deployment Mechanism is present. The values of the structure volume ratio vary between 1.9 % and 29 % and are in most cases well below 10 %.

Mast Type or Mission	Type of architecture	Deformable Structure Volume V_S [m³]	Total Volume V_T [m³]	Deformable Structure volume ratio $\frac{V_S}{V_T}$	Remarks
De-Orbit Sail (4 x 2.86m)	Tubular	0.215 x 10^{-3} (measured)	1.046 x 10^{-3} (measured)	**12 %**	Shell Material: CFRP
GOSSAMER (4 x 4.3m)	Tubular	0.520 x 10^{-3} (measured)	7.301 x 10^{-3} (measured)	**5.3 %**	Shell Material: CFRP
Northrop-Grumman 0.86" High Force STEM (20ft) [2] [3]	Tapespring	0.078 x 10^{-3} (calculated)	2.572 x 10^{-3} (measured)	**3.1 %**	Longeron Material: Stainless Steel
Northrop-Grumman Nano STEM (20ft) [2]	Tapespring	0.029 x 10^{-3} (calculated)	0.110 x 10^{-3} (estimated)	**26 %**	Longeron Material: Stainless Steel
ATK-ABLE ISS FAST [5] [10]	Articulated	75.60 x 10^{-3} (calculated)	2960 x 10^{-3} (measured)	**2.6 %**	Longeron Material:

[3] The material volume is chosen to prevent that the stowage efficiency of the corresponding mast compromises the comparability. Thus, the structure volume ratio describes the percentage of the overall stowed volume that is allocated by the Deformable Structure.

ATK-ABLE SRTM ADAM [6] [7]	Articulated	192.2 x 10^{-3} (calculated)	4242 x 10^{-3} (measured)	**4.5 %**	Aluminum Longeron Material: CFRP
Northrop-Grumman AstroMast Model 12027 (14m) [8]	Coilable	2.218 x 10^{-3} (calculated)	114.3 x 10^{-3} (measured)	**1.9 %**	Longeron Material: GFRP
ATK ORU Transfer Device (OTD) Boom [9]	Telescopic	*5.812 x 10^{-3} (estimated)*	*20.39 x 10^{-3} (estimated)*	***29 %***	*Shell Material: Aluminum*

Table 1-2: Structural material volume compared to overall mast stowage volume for various mast systems.

Hence, a disproportion in the distribution of mass and stowage volume towards the Deployment Mechanism is identified.

1.3. Research Question and Leading Hypothesis

The preliminary investigations summarized in Table 1-1 and Table 1-2 show that the Deformable Structure contributes little to the overall mass and stowage volume of the deployable structure. In consequence, only a small percentage of mass and stowed volume actually participates in the main tasks of carrying the deployment loads and providing the required stiffness and stability during and after transition. Furthermore, the Deployment Mechanism and thereby the predominant part of the deployable structure loses its function once the deployment process is completed. These observations lead to the research question that is at the basis of this thesis:

> *In how far are current deployable structures 'optimal' designs in terms of mass and stowed volume and in how far do current design methods lead to 'optimal' designs?*

It is assumed that the observed disproportion in the mass and stowed volume between Deformable Structure and Deployment Mechanism is symptomatic for design flaws that lead to augmented mass and stowage volume. The above formulated research question implicitly contains the leading hypothesis of this thesis on the cause for these design flaws:

> *There is a methodological gap in the state of the art that causes deployable structures to be overly heavy and voluminous.*

The aim of this thesis is to answer the above formulated research question, examine the validity of the leading hypothesis and develop methods for the design of lightweight and compactly packaging Deployable Space Structures.

1.4. Thesis Outline

The thesis is structured into 11 chapters. Following on the introduction, the state of the art is reviewed in the chapter 2 '*Current Deployable Space Structures and Methods for their Design*'. It provides the basis for chapter 3 '*Hypotheses on the Design of Lightweight and Compactly Packaging Deployable Space Structures*' in which gaps in the state of the art are identified and detailed hypotheses on addressing these gaps are formulated. Thereby each of the following chapters 4 to 8 are dedicated to one hypothesis.

The tool for verification of these hypotheses is the system analysis of a deployable structure. The analysis focuses on gaining insight into the highly linked interaction between Deformable Structure and Deployment Mechanism. Therefore, first a mathematical expression of the Deployment Mechanism is established in the chapter 4 '*Deployment Mechanism Parameterization and Derivation of Scaling Functions*'. In chapter 5 '*Design Interactions of Deformable Structure and Deployment Mechanism*' the design relevant influence among the Deformable Structure and the Deployment Mechanism is examined. In chapter 6 '*Consideration of the Transition under Load*' the case of significant loading during deployment when the structure is in the state of transition is analyzed. Chapter 7 '*Function Integration in the Design of Deployable Space Structures*' addresses the potential advantages of the design principle of concentrating functions in few components for the case of deployable structures. In chapter 8 '*Performance Evaluation of Deployable Space Structures*' the selection process at the end of the phase of conceptual design is demonstrated based on a performance description through quantification.

The results of the system analysis performed in chapters 4 to 8 are evaluated and concluded in the chapter 9 '*Development of the Conceptual Design Methodology for Deployable Space Structures*'. This method is exemplary demonstrated for the conceptual design of the deployable structure of a flexible blanket solar array in chapter 10 '*Conceptual Design of a Solar Array*'. Finally in chapter 11 *'Application and Discussion'* the application and corresponding limitations of the new conceptual design methodology are outlined and the results with the underlying approach and corresponding assumptions and simplifications are discussed.

2. Current Deployable Space Structures and Methods for their Design

The basis for validation of the initial assumption of a methodological gap in the design of Deployable Space Structures is provided by a review of the literature on current Deployable Space Structures, their characteristics and procedures and methods for their design. In addition general design methods and methods for morphing aircraft structures may contain procedures applicable to Deployable Space Structures and described as well.

2.1. Deployable Masts and Related Structures

Deployable structures are utilized in space applications from the beginning of spaceflight. Since then they have evolved to structures that reach dimensions of several tens of meters [11] or even hundreds of meters [12] and achieve packaging ratios between stowed and deployed state of several magnitudes. Deployable Space Structures exist in a variety of designs which differ in their structural architectures, methods for folding and deployment as well as materials. Among Deployable Space Structures deployable masts can be seen as universal construction elements which serve as primary structural elements of other deployable structures. Thereby they show a particular diversity in their designs. Their characteristics and fields of application are described in the following and are representative for Deployable Space Structures in general.

2.1.1. Structural Architectures

Deployable masts are realized with several different types of structural architectures. One architecture category particularly applied for smaller deployable masts are shell structures (see left Figure 2-1) which consist of thin-walled, curved shells of open or closed cross-section [13]. A prominent example for open profile shell masts is the Storable Tubular Extendible Member (STEM) [14] [15] which consists of a single shell that forms in deployed state a circular cross-section with a slight overlap of its edges. STEM booms have a broad flight heritage and are available in a variety of different variants and sizes [16] [3] [2] [17].

A shell mast with open cross-section but formed from two shells is the Triangular Rollable and Collapsible (TRAC) mast [18] [19]. Its two outward curved tapespings are joined along one flange and thereby create a cross-section whose corner points form a triangle. The TRAC boom is particularly developed for small satellite applications where generation of a high bending stiffness out of a small stowage volume is desired.

Examples for shell masts with closed profiles are lenticular booms such as the Collapsible Tube Mast [20] [21]. They consist of two symmetric half-shells with omega-shaped profile which are connected towards each other at their outward flanges. Due to their closed cross-section they feature a significantly higher torsional stiffness than

the open cross-section masts which makes them less vulnerable to flexural torsional buckling.
Another category of architectures are trusses (see middle Figure 2-1). These consist of a series of similar bays each constructed in general from three to six longerons that are interconnected by joints with the battens and diagonals. Longerons and battens and often also the diagonals are realized as slender rods. Therefore trusses achieve high deployed volumes and subsequently high bending stiffness. As a truss is an assembly of several structural members it can be realized as a combination of different structural architectures such as trusses of solid rods like the Superstring [22] [23], trusses of tapes like the Collapsible Tape Truss (CTT) [24] [25] or even potentially a truss of trusses. Prominent examples for this category of architectures with significant flight heritage are the ABLE Deployable Articulated Mast (ADAM) [26] as utilized for the Shuttle Radar Topography Mission (SRTM) [11] [27] [28], the Folding Articulated Square Truss (FAST) [29] [30] which provides the backbone structure of the ISS solar arrays and the CoilABLE booms [31] [32] [33] or AstroMasts [8]. An example for the combination of a truss and shell mast architecture is the Collapsible Rollable Tube [34].
Trusses are voluminous designs which combine elements made of different materials. Hence, thermal stability to avoid slackness and subsequently loss in stiffness needs to be ensured which is often done by pretension. The FAST mast and the CoilABLE booms use their battens for this purpose as spring elements through integrating these in buckled state.
The third category of structural architectures are grid-structures (see right Figure 2-1). These feature in general circular cross-sections that are formed through several frequently crossing longitudinal, lateral and diagonal rows of rods or tapes [35]. Thereby grid masts can be seen as hybrids of shell and truss structures. Examples from this category are the UltraBoom [36] and the Isogrid Truss [37] [28].

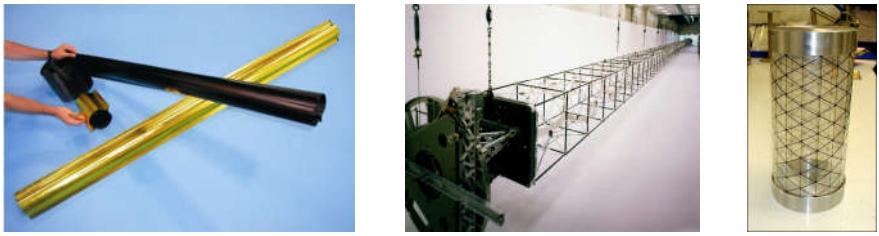

Figure 2-1: DLR's deployable, lenticular shell masts [Source: DLR] (left), deployed ADAM [38] mast consisting of four-longeron truss-bays (middle) and a sample of the ROC isogrid (from [37] Figure 6: "ROC isogrid boom testing sample") inflatable mast (right).

2.1.2.Folding Methods

Folding of the structures is mainly achieved through methods based on distributed or concentrated deformation or combinations of both. Distributed deformation (see left Figure 2-2) refers to the folding of the entire structure. This principle is utilized

particularly for shell and grid masts which are stowed by flattening of their cross-sections to a narrow band with subsequent reeling on a drum.
Concentrated deformation (see right Figure 2-2) is based on the use of rigid elements interconnected by hinges or other flexible elements that allow localized high concentrations of deformation. This folding method is often utilized for truss structures which are designed from rigid members and become foldable through hinged joints.
A third method is the on-orbit assembly of sub-structures that do not possess a permanent rigid connection. Examples are various locking versions of the STEM boom [2] [39] [40] or the TriLok mast [28] [41]. Both are utilizing a series of unlockable edge connectors consisting of pins attached to one structural member which latch into accordingly formed cut-outs in the adjacent member. The Interlocking-STEM [40] uses two nesting STEM booms whereby the inner shell is equipped with the pins along its edges and the outer shell with the corresponding cut-outs. The TriLok mast is assemble from three separately reeled, flexible truss faces that interconnect along their edges to form a triangular truss.
Another method is the use of telescopic elements which also do not possess a rigid connection among each other and are stowed through nesting. The in general cylindrical elements are able to slide inside the enclosing ones along the masts longitudinal axis. The ends of the cylinders are equipped with locking mechanisms that enable latching among each other in the deployed state. Examples for such masts are the Astro Telescopic Mast [42], AstroTube Max [43] and ORU Transfer Device (OTD) [9].
There are several hybrids of the above introduced folding methods. An example for combined use of distributed and concentrated deformation is the Deployable Elastic Composite Shape Memory Alloy Reinforced (DECSMAR) truss [28] [44] [45]. The three longeron truss is constructed from longerons and battens made of thin-walled shells which utilize a distributed deformation approach similar to a tapespring. However, the longerons possess additional zones of concentrated strain which enable a more compact folding. Therefore the composite shell material is thinned out at desired folding lines but possesses edge reinforcements made of shape memory alloy wires to compensate for the local loss in material. These wires enable much higher strains during folding due to super-elasticity and thereby high degrees of deformation.
A combination of distributed deformation, concentrated deformation and telescopic elements is the Superstring [23]. Its longerons are slender rods or tapes that are reeleable through distributed deformation. Attachment of battens and diagonals is done through hinged joints. The necessary degrees of freedom to enable folding are achieved through use of telescopic diagonals. Each diagonal is composed of two rods that are interconnected by a sliding joint which latches in the unfolded position. Thereby the upper and lower truss faces can be folded on top of each other whereby the entire truss becomes reelable.

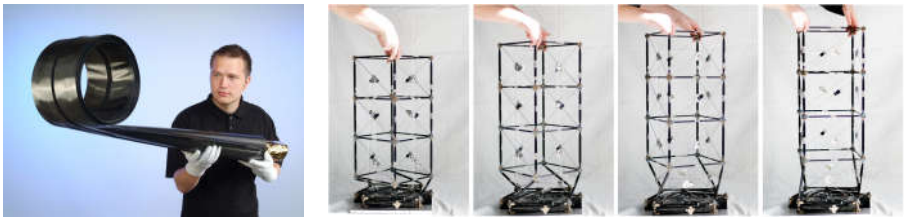

Figure 2-2: Folding method based on distributed deformation (left) for the example of DLR's CFRP boom [Source: DLR] and based on concentrated deformation (right) for the example of the ADAM mast (from [46] Figure 2.8: "The WSOA sample mast, shown with three fully deployed bays and a single partially deployed bay.").

2.1.3.Deployment Methods

The deployment methods of Deployable Space Structures differ in their sources to provide the required energy for the form transition whereby often combinations of these are utilized. A widely applied approach is the use of strain energy although it is seldom used as single deployment method. Deployment by strain energy makes use of the elastically stored energy that is introduced into the structure during the folding process. When the external constraining forces are removed the structures return to their original shape. However, the release of strain energy is instant and the resulting deployment behavior of the structure is often chaotic wherefore further means to achieve a controlled deployment have to be applied [47]. Structures that are using strain energy as main energy source for deployment are the CoilABLE boom and the AstroMast. These trusses possess a well-defined Transition Zone with localized release of strain energy.

A second method for unfolding of the deployable structures is the motorized deployment (see left Figure 2-3). Therefore in general electric motors are combined with mechanical mechanism components which transform the generated motion and enable its transmission to the structure. An example for such a deployment is the ADAM mast. Its stowage cylinder is equipped with as set of motor driven sliders that gear into the joints of the helically stowed truss [46]. The sliders unfold the truss sequentially bay by bay and push it out of the stowage cylinder whereby also high deployment forces can be generated. The motorized deployment is often used in combination with strain energy such as for the CFRP Boom [48] [49]. This is a lenticular shell boom which uses strain energy to regain its tubular cross-sectional shape. However, the tendency of this mast for self-deployment is suppressed through external constraint forces and it is primarily deployed by a motor driven mechanism that applies the deployment force through a co-coiled steel belt [50] [51].

A third method is deployment by inflation (see right Figure 2-3) of a gastight structure [52]. The required gas is provided by a pressure tank or chemical gas generator. The structures are in general of tubular shape and consist of thin-walled shells or plastic foil laminates. An example are the Space Solar Power truss which is composed of three inflatable, tubular longerons [28] [53] and the inflatable offset boom of InflateSail [54].

The use of inflation is often connected with the chaotic release of energy due to the force-controlled deployment. A controlled and localized generation of deployment forces that leads to a well-defined deployment path is difficult to achieve.

Figure 2-3: Motorized stowage and deployment canister of the SRTM truss [55] (left) and Inflatable Antenna Experiment (from [56] Figure 6: "Partial Orbital Deployment") during the deployment process through inflation (right)

2.1.4.Materials

The material selection for a deployable structure largely depends on the intended folding and deployment methods. Structures utilizing strain energy make use of materials with high elastic strains [57] such as copper-beryllium, spring steel-alloys, carbon fiber-reinforced silicon (CRFS) [58] and glass and high strength carbon fiber composites. In this regard also composite materials that enable high strains due to elastic fiber micro-buckling embedded in a soft matrix [59] [60] (see right Figure 2-4) and materials featuring super-elasticity [44] are examined.

For articulated structures particularly high modulus materials such as according carbon fiber composites and steel alloys are used. An impact on the material selection also has the consideration of thermal distortions which result from internal thermal gradients. Here, again carbon fiber composite materials have an advantage due to their low coefficients of thermal expansion [47] [61].

Fiber composite materials enable the realization of bi-stabile structures [62] [63]. The Bi-Stable Over the Whole Length (BOWL) boom [64] (see left Figure 2-4) is a shell boom with a semi-circular cross-section that is stowed through distributed deformation by flattening and reeling. The lateral contraction of the utilized carbon fiber laminate is tailored through according variation of the local fiber angle in a way that an energy minimum in the reeled, stowed state is achieved. Thereby the boom does not require additional constraint forces to maintain its stowed state as is necessary for similar masts such as the STEM boom. This principle is further applied to TRAC and lenticular booms [65] [13].

There are several materials which are specifically developed for use in combination with inflation as deployment method [66] and enable very high packaging efficiencies. One group consists of materials which become deformable through heating above

their glass transition temperature. These materials are in general composites with a thermoplastic matrix that possesses a tailored glass transition temperature (T_G). Through heating above T_G the structure becomes deformable and is frozen in this state by cooling below T_G [53]. Deployment is achieved through the reversed procedure.
A similar method that allows high degrees of deformation is the use of uncured fiber composite materials. Thereby the matrix is in an uncured state before and during deployment and is hardened afterwards through application of heat or orbital radiation [67] [68].
Other materials utilized in combination with inflation are aluminum laminates [69] [70]. These consist of several layers of thin aluminum sheets combined with plastic membranes like Kapton. Such laminates are also compactly foldable and can be hardened by overstretching of the aluminum in the deployed state through applying according overpressure.

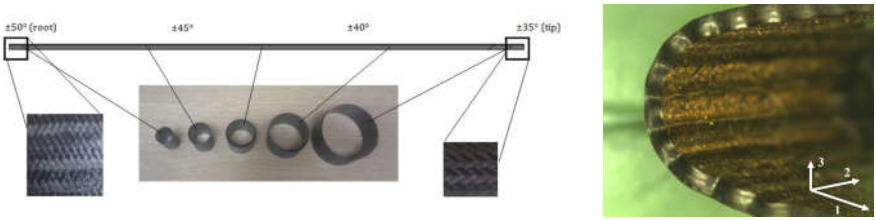

Figure 2-4: Fiber angle variation in a carbon fiber composite on the BOWL boom (from [64] Figure 6: "Variable braid angle BOWL boom for CubeSail.") to achieve bi-stability over its entire length (left) and micro-buckling pattern (from [60] Figure 1: "Packaged EMC laminate showing inplane microbuckling.") in a fiber composite with a soft matrix (right)

2.1.5.Deployable Systems Based on Deployable Masts

Deployable masts provide the backbone structure of a variety of deployable systems. Medium and large size solar arrays utilize a design where a flexible photovoltaic blanket is supported and tensioned by one or several masts which are deployed along their main axis. The blanket is spanned between lateral spreader bars attached to root and tip of the mast(s). In general mast and blanket are thereby deployed in parallel. Examples for flexible blanket solar arrays are the solar array experiment OAST aboard STS-41D [71] and the Earth Observing System (EOS) AM-1 satellite [72] which both utilize CoilABLE booms and the eight ISS solar array wings which are based on the FAST mast. Examples for solar arrays utilizing two simultaneously deploying masts are the early solar arrays of the Hubble Space Telescope [73] [74] and the Roll Out Solar Array (ROSA) recently demonstrated in an on-orbit deployment experiment [75] [76] [77]. Both are using Bi-STEM [78] or STEM booms.
Drag and solar sails (see left Figure 2-5) make use of deployable masts to support their sail membranes. Thereby four masts aligned in a cross configuration are supporting a rectangular sail. Deployment of masts and sails is done from the center and performed either simultaneously or sequentially with the sail unfolding last. Examples for such

deployable systems are NanoSail-D [79] which utilizes TRAC booms, Inflatesail [54] that is based on Bi-Stable tapespring booms or Sunjammer [80] [81] [82] that applies telescopically folded, inflatable Tubular Shell Masts.
Furthermore there are some examples for deployable reflector antennas which also make use of deployable masts as primary structures such as the Tension Truss Antenna developed for the HALCA satellite [83] [84] (see right Figure 2-5).

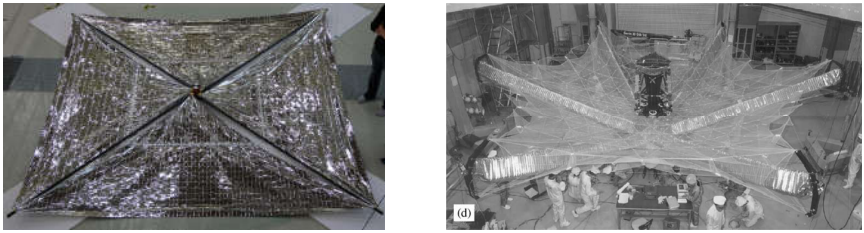

Figure 2-5: Deployed drag and solar sail De-Orbit Sail [Source: DLR] utilizing four lenticular shell booms (left) and deployed Tension truss Antenna (from [84] Figure 3 (d): "Deployment test of the main reflector of the large antenna: (a) the start, (b) and (c) during deployment, (d) completely deployed.") based on six pantographic masts (right).

2.2. Circular and Modular Deployable Structures

More application specific Deployable Space Structures are developed particularly in the fields of large deployable reflectors and solar arrays. It is noticeable that many of these are of circular shape which is either beneficial for their function such as for reflectors or beneficial regarding mechanical properties, folding and deployment methods. Particularly for large structures modular designs are developed which consist of assemblies of similar unit cells. Both groups of deployable structures are described in the following and in addition some specific deployable structure designs are presented.

2.2.1.Torus and Radial Rib Structures

A variety of Deployable Space Structures possess or require a circular form that is achieved through toroidal structures, use of radial ribs or solid petals [62] [85] [86]. Toroidal structures are mainly utilized for mesh reflectors which support on the inside of the ring the tension net that enforces the required form upon the underlying reflecting mesh. These rings consist of articulated trusses which perform a simultaneous deployment in two spatial axes. During deployment the circumferential length of the torus is increased whereby also the ring diameter increases until the net is fully tensioned. The deployment forces are thereby provided by spring mechanisms or electric motors which act on linkages, tension cables or directly on the articulated truss. An example for such a reflector is the AstroMesh [87] [88] [89] (see left Figure 2-6).

On the basis of toroidal architectures also inflatable reflectors are realized [90]. One example whose deployment is demonstrated on-orbit is the Inflatable Antenna Experiment [56] (see right Figure 2-3). Three inflatable booms support an inflatable torus which spans a reflector on its inside. The reflector gains its required shape from an inflatable lens whereby only one side of the lens has a reflective coating while the other is translucent. Also based on inflatable toroidal structures is the Hypersonic Inflatable Aerodynamic Decelerator (HIAD) developed for re-entry purposes [91].
Another common design approach for circular deployable structures is based on radial ribs. The ribs are hinged in the center and may be further divided into segments interconnected by additional hinges and unfold to the outside. In between the ribs the functional surface is spanned which is in case of mesh reflectors again a combination of a tension net with the underlying mesh. An example for such a design is the Hinged-Rib-Antenna [85] reflector.
The Wrap-Rib-Antenna [92] also uses radial ribs but is based on a distributed deformation approach for stowage. It uses a high number of flexible ribs whose cross-section can be flattened for subsequent coiling on a cylindrical hub located in the center of the reflector.
For the deployable solar arrays UltraFlex and MegaFlex [76] [93] [94] (see right Figure 2-6) a structural concept is selected that is similar to a hand fan with radial ribs pivoted in the circle center. Thereby the ribs support triangular segments of a photovoltaic blanket in between. For deployment the ribs are rotated by a motor driven belt until a full circle is reached and the first and the last rib are joined.
Deployable structures that provide high surface accuracies are required for antenna reflectors operating in a high frequency range and optics. For such applications deployable apertures based on foldable rigid or semi-rigid surfaces are utilized [62] [85] [95].

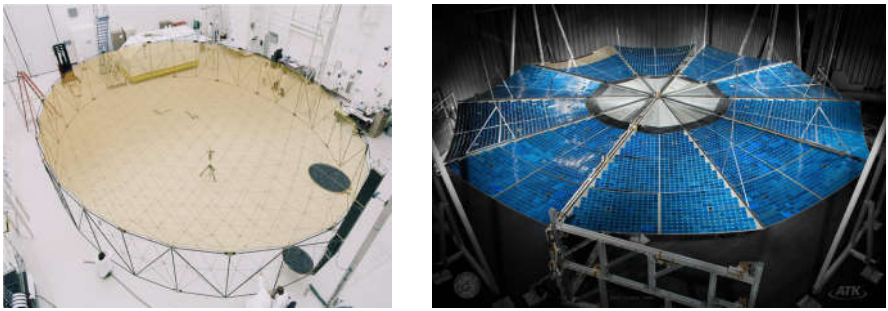

Figure 2-6: AstroMesh (from [89] Figure 2) reflector antenna with toroidal truss structure (left) and MegaFlex (from [76] Figure 7: "ATK Engineering development unit MegaFlex solar") solar array with radial rib structure (right).

2.2.2. Modular Structures

Particularly for the realization of large Deployable Space Structures modular designs are considered. Therefore a number of similar or identical modules are joined to form a larger structure. Advantages are strived in development costs, manufacturing, testing and specifically flexibility towards varying size requirements.

One example in the field of deployable reflectors is the large deployable reflector of the Engineering Test Satellite VIII (ETS-VIII) [96] [97] (see left Figure 2-7). It consists of fourteen hexagonal modules interconnected to a nearly circular structure. Each module possesses six radial ribs realized as four bar linkages with an additional diagonal member. The ribs span the tension net that provides the required form to the underlying reflecting mesh. Their deployment is driven by a spring driven lever mechanism in the modules center. The modules are interconnected at the tips of the ribs and unfold simultaneously.

An example for a modular design in the field of large solar array is the SquareRigger [98] [99] [100]. Square Rigger consists of several rectangular modules with a side length ratio of 1:2. The supporting structure of each module consists of a frame realized as a six bar linkage. One bar at the shorter side contains a zigzag folded membrane or blanket which is linearly deployed within the frame after unfolding of the frame itself. The SquareRigger modules are joined along their frame sides and deploy simultaneously.

A widely used design of a modular Deployable Space Structure is a hinged panel solar array such as the Planar Unfolding Modular Array (PUMA) [101] [102]. This type of Deployable Space Structure consists of lightweight sandwich panels which carry the photovoltaics. They are interconnected by spring loaded hinges which also provide the necessary deployment energy. For stowage the panels fold on top of each other. The panels are in general arranged in a line but may also combine longitudinally and laterally deploying elements.

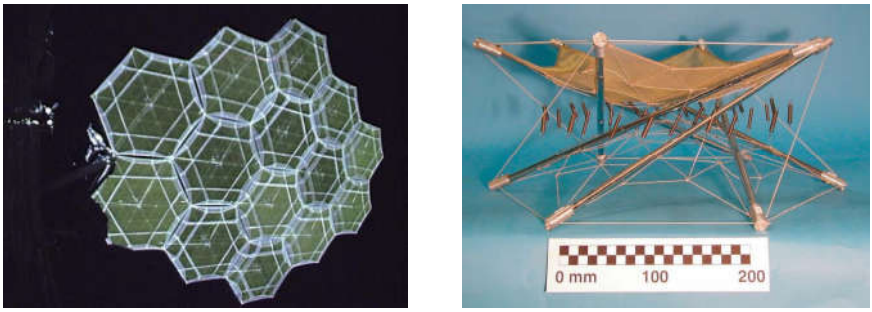

Figure 2-7: Modular mesh reflector deployed aboard ETS-VIII (from [97] Figure 17: "RX-LDR successful deployment in orbit (full deployment in distant view).") (left) and model of a deployable mesh reflector (from [103] Figure 7.12: "Side view of demonstration model") based on a deployable tensegrity structure (right).

2.2.3. Other Deployable Structure Designs

Examples for other designs of Deployable Space Structures are the spherical Echo-1 and 2 balloons [104] with a diameter of up to 41m used for signal reflection in an early communication experiment. Both balloons are deployed by inflation but Echo-2 further utilized a rigidization mechanism based on overstretching of thin aluminum foils applied on both sides of a Mylar base layer which makes it independent from the internal gas pressure. Other examples for large inflatable structures are inflatable space habitats [105].

A specific construction type that can be applied to Deployable Space Structures are tensegrity structures [103] [106] (see right Figure 2-7). These structures are trusses that are strictly subdivided into compression and tension loaded elements whereby the tension elements are realized as cables. Thereby the solid rods which carry the compression loads are not in direct contact but are connected through the cables. The cables are held under pretension to maintain the structural integrity and avoid loss in stiffness due to slackness from deformation under load.

2.3. Design Procedures and Methodologies for Deployable Space Structures

In the following the literature addressing the design of Deployable Space Structures is described. First some sources for design requirements that are specific to this category of structures are presented. Subsequently publications on the imperfection sensitivity of Deployable Space Structures and their consideration in the design process are addressed. Thereafter methods for the performance evaluation in early design stages are described and finally current design methods for various types of Deployable Space Structures in different design stages are presented.

2.3.1. Specific Sources of Design Requirements

The first step in every design task is the definition of requirements. Specific requirements for large and lightly loaded Deployable Space Structures are investigated by Hedgpeth [107]. The investigation focusses on requirements that are mostly neglected in smaller and/or higher loaded systems:

→ *External operational loads*: Discussed are external operational loads whose significance increases with the size of the structure. These are inertial loads from tracking and station keeping, gravity gradient, solar pressure and atmospheric drag in the low earth orbit.

→ *Stiffness requirements of the deployed system*: Stiffness requirements result from closed-loop control systems of the spacecraft to avoid critical interaction as well as limits in the allowable deformation of the structure under loading.

→ *Deployment precision requirements*: Precision requirements apply primarily to instrument booms, reflectors and other antenna structures where a high pointing accuracy and minimal shape errors of functional surfaces are crucial for their function.

→ *Impact of member slenderness*: The impact of the member slenderness on strength and stiffness refers to the increasing sensitivity towards geometrical imperfections with higher member slenderness.

The latter point is addressed by several other authors and is reviewed in the following subsection.

2.3.2. Consideration of Imperfections

Deployable Space Structures feature structural elements of high slenderness and low wall thickness and are therefore sensitive in their mechanical properties to geometric imperfections. The importance of considering imperfections already on the level of conceptual design is emphasized by several authors (Hedgepeth [107], Mikulas [108], Hinkle et al. [109], Murphey and Hinkle [110], Murphey [111], Jenkins and Murphey [112]). A detailed analysis is done by Crawford and Benton [113]. Based on investigations by Crawford and Hedgepeth [114] the effects of local and global straightness imperfections in slender solid rod trusses loaded in compression are investigated. It is shown that due to the imperfections the effective axial stiffness becomes a function of the axial load due to bending deflection in the longerons and the overall mast. As a result it is found that even small imperfections lead to a significant reduction in the axial strength of the mast whereby the combined occurrence of local and global imperfections amplifies the effect. For the analyzed truss of solid rods already the presence of moderate out-of-straightness imperfections leads to losses in the order of 50% compared to the solutions of the ideally straight mast.

Sickinger [47] addresses local variations in the shell thickness and fiber angle of a lenticular composite boom as a result of the manufacturing process. Through Monte-Carlo-Simulations with variation of the imperfection patterns a significant effect on the thermomechanical behavior is demonstrated that has to be considered particularly when high shape accuracies are desired.

2.3.3. Performance Evaluation Methods

Performance description of Deployable Space Structures is often done through scaling functions (also scaling laws; cf. similarity principles [115]). A scaling function describes the sizing result of a structure regarding a specific property dependent on certain design requirements. Hence such functions describe how the respective structural property scales with the requirements.

On the basis of structural scaling functions Crawford [116] compares the geometrical dimensions and masses of cylindrical shell masts, coilable booms and articulated trusses applied in three different load cases. Thereby he also considers scaling limits in terms of maximum material stresses for the first two mast categories whose deployment methods are based on strain energy. Crawford further utilizes empirical data to adjust the mass scaling function results to measurements made on existing hardware. In case of the Coilable booms also the Deployment Mechanism mass is partially included in the functions through adding an empirical mass equation for the deployment canisters. However, the results are valid only in the vicinity of the specific

canister point design. Crawford concludes with a comparative evaluation of the masses and geometric dimensions of the three different mast types in which he points out that the articulated lattice boom is superior in most of the considered applications.
Garba et al. [117] comparatively investigate through use of scaling functions structural concepts for two flexible blanket solar arrays in a power range of 10 kW to 80 kW per wing. The concepts differ primarily in their blanket folding method which is done through zigzag-folding and reeling. The scaling functions are developed from existing point designs utilized as baseline configurations and are extrapolated through development of according component scaling laws which are adjusted by comparison with empirical data. Thereby the parameterization of the two solar arrays is very detailed and also considers the main Deployment Mechanisms components. The evaluation is done primarily through comparison of their mass scaling behavior.
Also on the basis of scaling functions Mikulas [108] compares for the load case of axial compression the mass efficiency of tubular columns, trusses of solid rods, trusses of tubes and isogrid trusses. Thereby he differs three design cases and assigns Deployable Space Structure to the latter two: short column length and/or high load, intermediate column length and/or intermediate load and high column length and/or small load. Mikulas considers in the formulation of the scaling functions the impact of scaling limits through minimum dimensions of structural members as well as the impact of geometrical imperfections. The comparison of the mass specific performances of the different mast concepts is described in relation to the results of the tubular column. Mikulas shows that for the design cases of low and intermediate loads the mass of the tubular column can be expressed independent of size (column length) and becomes a function of the compression load only. The related ratio between mass m and column length L which is the function value of the derived scaling functions is described by Equation 2-1:

$$\frac{m}{L^{5/3}} \qquad 2\text{-}1$$

However, the results of the non-tubular column architectures remain a function of the size due to different forms of the scaling functions. Based on this performance comparison Mikulas concludes that in the low loading region trusses of solid rods are efficient while tubular columns provide good performance in the intermediate load range. Isogrid trusses show a good efficiency in the low loading region as well but it is stated that further analysis on the strength prediction which is the basis for the scaling function is necessary.
Mikulas and Cassapakis [118] further utilize mass scaling functions for performance comparison of Bi-STEM booms and CoilABLE booms with tubular inflatable booms based on a rigidizable matrix and an aluminum laminate. The design load case is a mast with fixed root and a tip mass. Design constraints are a bending moment resulting from root acceleration and a eigenfrequency requirement. For this design case mass scaling functions are developed. These include scaling limits in terms of a minimum wall thickness for the Tubular Shell Masts and a maximum strain constraint for the CoilABLE boom. The comparison is performed within a length interval of 3.5 m to 28 m and an eigenfrequency interval from 0.02 Hz to 1 Hz. A comparison over the mast length is performed for an eigenfrequency constraint of 0.2 Hz. Thereby it is

concluded that for most applications the tubular rigidizable and aluminum laminate masts perform best in terms of mass and stowage volume which is deduced from evaluation of the resulting beam diameters.

On the basis of structural scaling functions a variety of performance metrics and indices are developed inspired by similar approaches utilized for aircraft structures. These metrics and indices express the efficiency of a structure through relating its performance regarding a specific design objective to the associated expenditure of mass or stowage volume.
Mikulas et al. [119] present three performance metrics for performance evaluation of deployable trusses. The first metric relates bending stiffness EI to specific truss mass w (mass per length). It is used to discuss the bending stiffness performance as a function of the truss diameter D_M which is seen as a characteristic value that represents the stowed dimensions and may be limited by certain design constraints. The metric given by Equation 2-2 is derived from the expression for the theoretical truss bending stiffness:

$$\frac{EI}{w} = \frac{1}{8}\frac{E}{\rho\Sigma}D_M^2 \qquad 2\text{-}2$$

The parameters E and ρ are the modulus and density of the longeron material while the parameter Σ is a factor to account for the mass of battens, diagonals and joints. Mikulas et al. demonstrate the use of this metric for comparative performance evaluation of a variety of mast point designs which differ strongly in design and size. Furthermore the metric enables the evaluation in relation to theoretical performance limits such as for $\Sigma = 1$ when all mass is concentrated in the longerons.
The second metric presented by Mikulas et al. relates specific stowage volume v (volume per length) to bending stiffness EI and is expressed by Equation 2-3:

$$\frac{v}{EI} = \beta\frac{8\Sigma}{ED_M^2} \qquad 2\text{-}3$$

The parameter β gives the ratio of the actually stowed volume towards the pure material volume and thereby describes the packaging efficiency. Through application of this metric it is found that the majority of current deployable trusses possess rather small volume efficiencies with packaging parameter values in the order of $\beta = 100$.
The third metric presented by Mikulas et al. relates critical bending moment M to specific truss mass w and describes the bending moment performance depending on the truss diameter D_M according to Equation 2-4:

$$\frac{M}{w} = \frac{\pi^2\sqrt{2}}{4\Sigma}\frac{E}{\rho}\frac{1}{\left(\frac{l}{r_{i,l}}\right)^2}D_M \qquad 2\text{-}4$$

The parameter l is the longeron length and $r_{i,l}$ describes the longeron radius of gyration.
The three metrics are used to derive reference curves to enable a comparative performance evaluation of specific trusses with other designs or regarding theoretical design limits. Furthermore they can be used in the design process to identify specific performance sensitivities.

Murphey [28] [111] presents two performance indices for deployable trusses for the load cases of axial compression and bending. The formulation of the indices is fully independent of size wherefore the index value is a direct measure for the efficiency of a structure with respect to the underlying load case. The performance index μ_c for the load case of axial compression relates the associated design requirements of compression load P and column length L to the specific truss mass w (mass per length) as shown by Equation 2-5:

$$\mu_c = \frac{(L \cdot P)^{\frac{2}{3}}}{w} \tag{2-5}$$

The performance index μ_b for the load case of bending relates the design requirements of bending stiffness EI and critical bending moment M to the specific mass w and is expressed by Equation 2-6:

$$\mu_b = \frac{(EI \cdot M^2)^{\frac{1}{5}}}{w} \tag{2-6}$$

Both indices can be written as products of constant sub-indices μ_i as given by Equations 2-7 and 2-8:

$$\mu_c = \left(\frac{\pi^4}{2}\right)^{\frac{1}{3}} \mu_{m,c}\mu_{t,c}\mu_{l,c}\mu_{n,c} \tag{2-7}$$

$$\mu_b = \left(\frac{\pi^4}{2^3}\right)^{\frac{1}{5}} \mu_{m,b}\mu_{t,b}\mu_{l,b}\mu_{n,b} \tag{2-8}$$

Thereby μ_m is the material index, μ_t the truss architecture index, μ_l the longeron architecture index and μ_n the longeron number index. The specific indices are functions of material and architectural properties and thereby constant for a given architecture and material (for a detailed description see [28]). They can be used to optimize the design and select proper materials. The advantage of the approach presented by Murphey is that the performance potential of a truss design is characterized by a single value independent of its specific size. The higher the performance index, the higher is the structural efficiency regarding the related load case. However, the underlying scaling functions are based on Euler column buckling for both indices. For trusses whose scaling laws deviate from this approach, the performance values become dependent on size.

The performance indices developed by Murphey are utilized by Banik [120] in performance metrics for tensioned blanket solar arrays whose main structural elements are deployable trusses. The metrics are developed from analytical and numerical analyses of a solar array with an arbitrary number of longitudinal masts which tension the photovoltaic blanket. The formulations of the metrics aim on finding a solar array design that is balanced with respect to mass and complexity. Thereby a high structural efficiency of the masts is associated with a high system complexity and the performance index by Murphey is used as an according indicator. Hence, aside from their use in structural design and optimization, the metrics by Banik enable to assess the balance of the solar array design in terms of mass and complexity.

2.3.4.Specific Design Methodologies

A variety of publications describe design, sizing and analysis methods for specific types of deployable structures and related design issues. Gantes [121] and Gantes et al. [122] [123] describe a design methodology for deployable space frames that are based on pantographic elements. Thereby the design focus is on the associated kinematics which are further addressed by several other authors such as Farrugia [124] or Chen and You [125]. Guest [126] presents the design and analysis of foldable cylinders, wrapping of flat membranes and a solid surface reflector. The design and analysis of a modular mesh antenna based on space frames is presented by Meguro et al. [127]. Sickinger [47] describes a procedure for the verification of Deployable Space Structures and Straubel [128] presents a design and sizing method applicable for the preliminary and detailed design of deployable antennas. Overviews on the fields of Deployable Space Structures and their design are given by Pellegrino [62], Jenkins [129] [112], Kiper [130] or Puig et al. [131]. However, a design method of general applicability is missing.

Among the specific design methods presented above, the design and sizing method for the deployable structure of a large, space antenna presented by Straubel [128] possesses a more general applicability in the phases of preliminary and detailed design. As a basic consideration for the development of the method it is pointed out by the author that the design of a deployable antenna or a similar deployable system is a highly multidisciplinary task with several parallel design processes that possess a high degree of interdependency. Hence, frequent sizing iterations are required throughout the development process wherefore a design and sizing method needs to provide a high flexibility towards changing requirements. To achieve this flexibility the method utilizes parameterized FE-models that are robust regarding changes and allow rapid re-sizing. In this regard it is shown by Straubel that the sizing of the components can be done in a successive manner thus containing only a minimum of iteration loops for sizing and optimization. The design procedure is demonstrated for the example of a membrane SAR-antenna. Straubel concludes with the presentation of several different versions of the SAR-antennas resulting from different sets of requirements. The quality of the predominantly sequential design approach is demonstrated by the derivation of SAR-antenna concepts that are significantly more lightweight than solutions of the state-of-the-art.

2.4. General Applicable Design Methodologies

For the design of Deployable Space Structures other design methodologies are potentially applicable. These are general design methods such as described in VDI 2221 [132] and Pahl et al. [133] and methods for the design of morphing structures which also address structures that perform a change in shape.

2.4.1. VDI 2221: Systematic Approach to the Development and Design of Technical Systems and Products

A general design methodology for technical systems and products is described in the guideline 2221 [132] edited by the Verein Deutscher Ingenieure (VDI). This guideline summarizes a variety of publications on design methods from different technical disciplines in a single methodology of general applicability. An overview on the development history of this design guideline is given by Jaensch and Birkhofer [134]. The presented methodology is structured into seven processes and is displayed in Figure 2-8 as a flow-diagram including the intermediate process outputs. Addressed is the design process starting with the detailed definition of the design task up to the necessary documentation before product introduction.

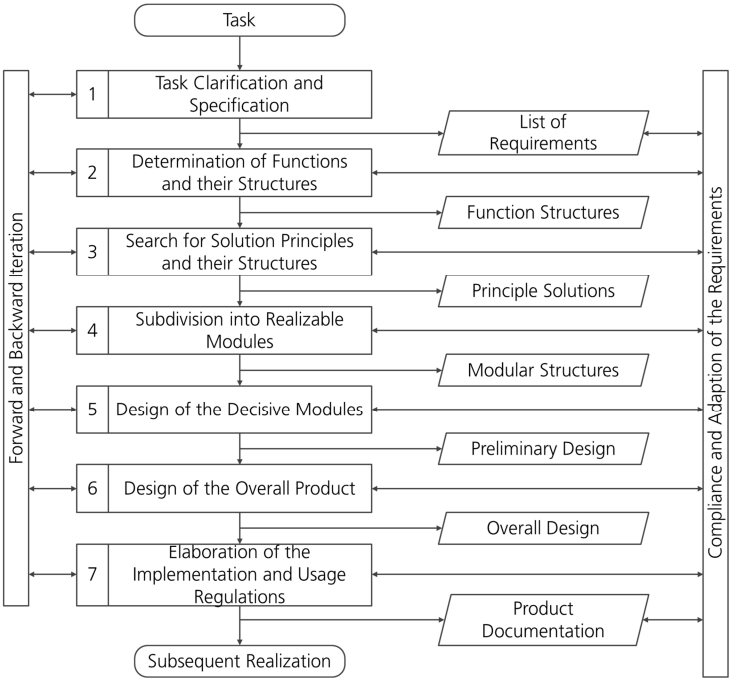

Figure 2-8: Flow diagram of the design methodology according to VDI 2221.

The design processes of VDI 2221 are defined as follows whereby iteration loops may be performed where applicable:

→ *Process 1 'Task Clarification and Specification'*: The design task is defined in detail. Output is the 'List of Requirements' which is constantly updated throughout the development process.

→ *Process 2 'Determination of Functions and their Structures'*: The design object is described regarding its behavior through overall, main and sub-functions. Output is the design objects 'Functional Structure'.
→ *Process 3 'Search for Solution Principles and their Structures'*: Solution principles for the decisive functions and functional structures are established and combinations of specific solutions are selected. Outputs are one or several 'Principle Solutions' of the design object.
→ *Process 4 'Subdivision into Realizable Modules'*: The principle solution is subdivided into modules which represent to some extend already its realization in specific elements. Furthermore modularization enables subdivision of the development process into several parallel design tasks. Output of this design step is the 'Modular Structure'.
→ *Process 5 'Design of Decisive Modules'*: The design of the decisive modules is performed and initial optimization is done. Outputs are the 'Preliminary Designs' of the related modules.
→ *Process 6 'Design of the Overall Product'*: The design of the decisive modules is detailed and the design of the remaining modules is conducted. Output is the 'Overall Design' of the design object.
→ *Process 7 'Elaboration of the Implementation and Usage Regulations'*: The documentation of the design object and the regulations for its application are established. Output is the 'Product Documentation'.

The general design guideline VDI 2221 is supplemented by VDI 2222 [135] which addresses the processes 1 to 3 and is described in the following and VDI 2223 [136] which addresses the processes 4 to 6.

2.4.2. VDI 2222: Methodic Development of Solution Principles

The guideline VDI 2222 (Blatt 1) [135] describes a general conceptual design methodology of technical products. It concentrates on the processes 1 to 3 of VDI 2221 and addresses the generation of principle solutions. Figure 2-9 displays the methodology with the intermediate outputs and knowledge repositories (see VDI 2222 Blatt 2 [137]) which provide inputs for the solution processes.

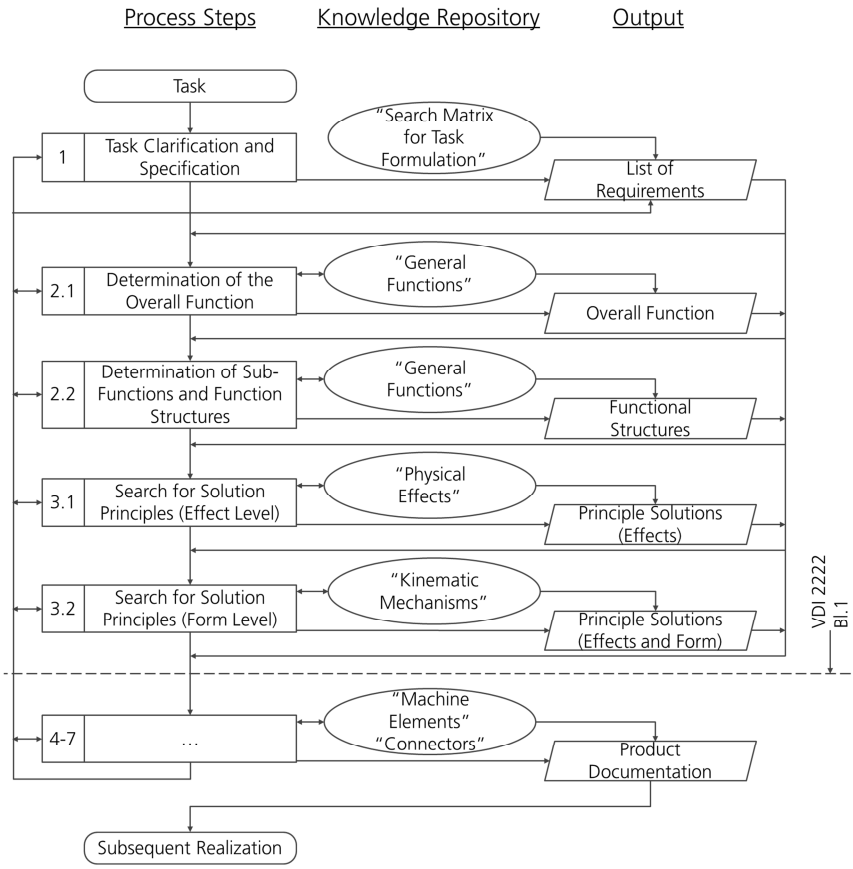

Figure 2-9: Flow diagram of the conceptual design methodology according to VDI 2222.

Within the VDI 2222 the processes 2 to 3 of VDI 2221 are further subdivided as follows:

→ *Process Step 2.1 'Determination of the Overall Function'*: The overall function is defined based on the beforehand clarification and specification of the design task.

→ *Process Step 2.2 'Determination of Sub-Functions and Function Structures'*: The overall function is subdivided into main and sub-functions and connected to the functional structure.

→ *Process Step 3.1 'Search for Solution Principles – Effect Level'*: A search for applicable physical effects for realization of the defined functions is conducted.

→ *Process Step 3.2 'Search for Solution Principles – Form Level'*: The basic realization of the selected physical effects through initial definitions on geometrical forms and materials is conducted.

The VDI 2222 further illustrated the generation of principle solutions through case studies and description of applicable methods and procedures. The authors emphasize the importance of the initially high level of abstraction and the step-by-step implementation of the described processes in order to gain a large solution space that enables finding new and innovative solutions.

2.4.3.Design Methodologies for Morphing Aircraft Structures

Other potentially applicable design methodologies are described in the literature on the design of morphing structures. Morphing structures use deploying structures as part of their "inner mechanisms" to enable a change in shape of a functional surface. A main field of application of these structures is the adaptation of aircraft wing properties to the current state of flight. Here especially leading und trailing edges that are used to enlarge the wing area and change the wing profile are focal points. In the following some design methods for morphing structures are described as they contain to some extend also the design of the associated deploying structures.

Lajux [138] develops a design methodology for leading edges in the phases of conceptual to detailed design. The main focus of the methodology is compliance of the generated morphing structure with the shape requirements. Mass, cost and reliability are additional objectives. To address the latter, Lajux introduces tools for assessment of mass, reliability and cost of initial designs as a basis for pre-selection of the most promising concepts. The tools are based on empirical data (cf. knowledge repositories), the targeted wing dimensions and performance as well as user estimates on established concepts. It is pointed out that this pre-evaluation and pre-selection is essential to reduce overall development efforts.

Based on the assessment tools, the design of the deploying structure starts with the pre-selection of promising concepts among established solutions for aircraft leading edges. In the next step the kinematics necessary to comply with the form requirements are established. Special attention is thereby paid to constraints set by the limited space inside the wing structure. This is done on the basis of a CAD model, initial and target shape and a special CAE software tool. Subsequently the kinematic model is transferred into a finite element model for structural analysis and design. Following the structural design, the integration with the overall wing design is performed and final assessments of mass, reliability and cost of the overall system are done.

Li et al. [139] present a conceptual design method for the inner mechanisms of morphing structures. The method is demonstrated on the basis of a morphing nose cone for rockets that have to deal with different aerodynamic and thermal requirements during high velocity flight inside the atmosphere and re-entry. The nose cone consists of a flexible skin with a solid spherical tip. By adjusting the length of the cone its aerodynamic properties are altered according to the requirements of the current state of flight. The focus of the method is again on achieving compliance with the form requirements.

The design methodology for the inner mechanism consists of two blocks. In the first block a mechanism is selected that includes a certain type of kinematic principle. In the presented example this mechanism is based on sliders with a single degree of freedom.

In the second block the kinematic is analyzed, optimized and the achievable shape is computed. By comparison with the target shape the shape error is derived and the procedure is repeated in case of an unacceptable difference. The mechanical design of the deploying and morphing structure is subsequently done in the phases of integrated and detailed design but is not further addressed.
Kintscher [140] develops a design methodology for a morphing aircraft leading edge that comprises the phases of conceptual to detailed design. The methodology is presented for the example of a leading edge which consists of a flexible skin that is deformed by an inner mechanism. The skin is designed to participate in the task of carrying aerodynamic forces by use of discrete stiffeners, skin materials of high strength and stiffness and reduction of the skin flexibility to a necessary minimum. However, the inner mechanism still needs to stiffen the structure and transmit a considerable part of the applied loads to the inner wing structure. Thereby again the primary focus of the presented methodology is on compliance with the form requirements.
The design of the inner mechanism starts with the definition of the kinematic requirements from the shape changing leading edge. For each attachment point of the inner mechanism to the stiffened skin a deployment path is defined that needs to be followed by the deploying structure of the inner mechanism. Thereby the kinematic is fixed and an adequate deploying structure is designed. In the presented example an articulated deploying structure actuated by servomotors is chosen. Kintscher points out that the selection of the articulated deploying structure is not the outcome of a comprehensive study and structural optimization is not done. However, he states that the consideration of alternative concepts and the optimization towards reduction of required actuator forces may lead to significantly decreased system mass.

2.5. Summary of the State-of-the-Art

Deployable Space Structures described in the literature span a large solution space regarding their sizes and forms of realization. They make use of a multiplicity of different structural architectures, folding and deployment methods and materials. Designs range from tubular inflatable, rigidizable structures over bi-stable shell masts to modular, articulated truss structures deployed through complex motorized mechanisms. They consist in general of slender and thin walled structural elements as they are only lightly loaded in their operational environment on-orbit. Thereby Deployable Space Structures feature a large change in size up to several magnitudes between stowed and deployed state.
Concerning the design of Deployable Space Structures there is a particular focus in the literature on performance evaluation of deployable masts and associated systems through scaling functions, performance metrics and indices. These are used to comparatively discuss the performance potentials of different categories of structures. Thereby particularly the performance indices can also be applied for design purposes to identify design drivers and sensitivities and to provide initial sizing results. Also considered in these discussions are the impact of scaling limits and geometrical

imperfections. Few publications address the influence of the Deployment Mechanisms but only at a very basic level.
Publications on design methodologies for Deployable Space Structures are scarce and address specific types of deployable structures and related design issues such as deployable space frames and their kinematics. A more general methodology for the phases of preliminary and detailed design is presented by Straubel [128]. The focus is thereby on a fast sizing procedure for multidisciplinary development processes that is flexible regarding frequent changes in design requirements.
General design methodologies such as VDI 2221 and VDI 2222 are well-developed and cover the entire design process from conceptual to detailed design and product introduction. Furthermore several design methodologies are published for morphing aircraft structures. These focus primarily on the design of a kinematic that enables compliance with the several required states of form.

3. Hypotheses on the Design of Lightweight and Compactly Packaging Deployable Space Structures

The motivation for this thesis is the presumption that current deployable structures are not 'optimal' designs in terms of a low mass and small stowage volume caused by a methodological gap in the state-of-the-art. For verification of this hypothesis, firstly the beforehand presented literature on Deployable Space Structures and their design is analyzed regarding indications for this conjecture. Subsequently hypotheses on means to address this methodological gap are formulated and the approach for their verification is outlined.

3.1. Definition of the Design Task

For the identification of methodological gaps firstly the design task needs to be defined. Deployable structures have a long history of application aboard spacecraft wherefore new applications that require entirely new solutions are scarce. Instead new developments of deployable structures target fields of applications such as solar arrays or antenna reflectors where several solutions already exist. Hence, a particular focus in the design task is to generate solutions that outperform the state-of-the-art in terms of certain design objectives such as a low mass and small stowage volume. Therefore, in addition to functional compliance, the design objectives need to be reflected accordingly in a design methodology to generate lightweight and compactly packaging Deployable Space Structures.

3.2. Significance of the Phase of Conceptual Design

The goal of the design task is defined by finding a valid solution for a deployable structure that excels regarding certain design objectives. These design objectives that refer to specific properties such as mass or stowage volume are determined by the decisions made within the design process. Hence, to search for indications that support the hypothesis of a methodological gap, firstly it needs to be analyzed which design decisions determine those properties that reflect the design objectives.
The design decisions that determine the properties of mass and stowage volume of a deployable structure are those that define its physical form. Each decision contributes to the concretization of this physical form and thereby constrains the solution space for the subsequent. Hence, the significance of a decision depends not only on its direct impact on the specific design objective but also on its impact on the solution space. For example the selection of a folding principle does not necessarily have a high impact on the mass of the Deformable Structure but it largely constrains the solution space for the design of the Deployment Mechanism which is a main mass contributor.
The importance of a design decision further depends on its accessibility to alterations at later design stages. During optimization or when its impact on the design objectives becomes more apparent, revision of a specific design decision may become of interest.

However, the accessibility towards such alterations is different for each decision and depends on its position in the chain of the design process and its impact on the solution space. The earlier the decision in the design process and the higher its impact on the solution space, the lower is its accessibility at later design stages. For example, changing the folding principle in late design stages will in most cases be linked with unreasonable efforts as it is made early in the design process and largely determines the functional interaction between the foldable structure and the Deployment Mechanism with its sub-components. In contrast the selection of a material for the support structure of the Deployment Mechanism may have a high impact on the overall mass but its impact on the solution space is small. Thereby, substitution by a more mass efficient material is easily done at all phases of design.
In consequence to these considerations, the primary design decisions that are of particular importance for the efficiency of a solution regarding specific design objectives are those decisions that possess a high impact on the solution space and a low accessibility in later design stages. For the case of a deployable structure, such primary design decisions are in particular the selection of the folding and deployment principles as they define the stowed form, the required mechanism functionalities and the interface between the Deformable Structure and the Deployment Mechanism. Other examples are the selection of the structural architecture of the Deformable Structure and the type of energy source to enable the form transition.
These primary design decisions are made early in the design process in the phases of conceptual design and early preliminary design. Hence, a design methodology has to focus in particular on these design stages.

3.3. Conclusions on Current Conceptual Design Methods

In the current literature there are no conceptual design methods specific for Deployable Space Structures published that are of general applicability. Some methods describe the kinematic design of deployable space frames but do not contain design procedures that can be generalized. However, general design methods are available and a design procedure that is applied in practice for conceptual design can be deduced particularly from the literature on performance evaluation methods (see subsection 2.3.3).

3.3.1. General Design Methods

Well-developed general design methods that can be applied in the phase of conceptual design are available such as described in VDI-2221 and VDI-2222 (see subsections 2.4.1 and 2.4.2). These methods are not problem-specific and thereby universally applicable to engineering design tasks like for the conceptual design of Deployable Space Structures. Their approach features in the initial design steps a high level of abstraction that focusses purely on functional compliance without consideration of design objectives. Starting point after definition of the design task and the design requirements is the functional description of the design object. In Figure 3-1 the general functional description of a Deployable Space Structure is shown

with a rough sub-division into material, energy and information flows. Based on this functional description principle solutions are generated as the primary output of the phase of conceptual design.

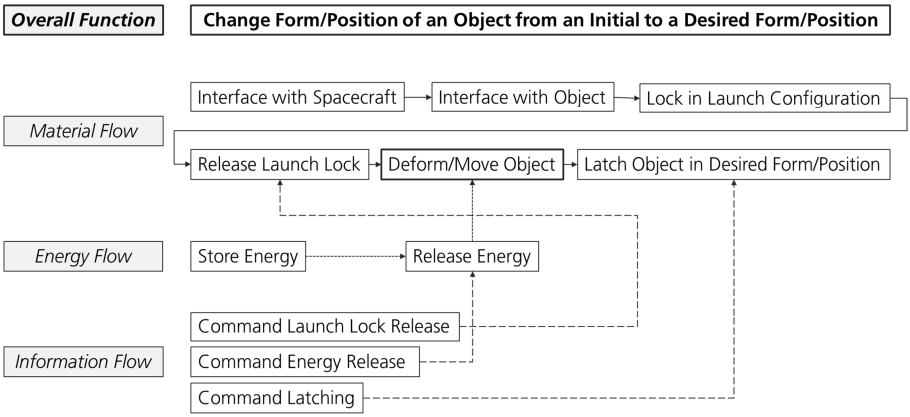

Figure 3-1: Overall function and basic functional structure of a Deployable Space Structure.

This design point of view promotes an unbiased concept generation process and an open solution space that remains largely unconstrained from certain preferences of the designer towards specific solutions. The approach thereby allows for finding of new, innovative and non-obvious solutions which is a key aspect to enable high solution qualities regarding certain design objectives. However, due to their general applicability general design methods do not reflect specific design characteristics and tasks of Deployable Space Structures. These have to be identified and implemented throughout the development process by the designer.

3.3.2. Current Design Practice

Although there are no conceptual design methods specific for Deployable Space Structures published, there is a variety of literature on performance evaluation methods and design descriptions targeting this development phase that allow deduction of a design procedure that is currently applied in practice. This procedure is displayed in Figure 3-2 and addresses the Deformable Structure. Firstly mechanical requirements, size and load cases are defined. In a second step a number of concepts are established by selection of the structural architecture and basic considerations on the folding principle introduced through according design constraints. The designs are detailed up to a level where quantification of the structural performance by use of performance indices, metrics, scaling functions or specific property values is possible for evaluation. Subsequently the best performing concept is selected for further design steps through performance comparison for the targeted design point or design range.

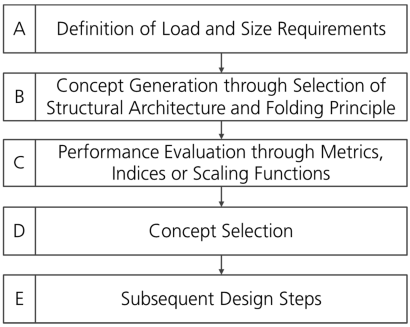

Figure 3-2: Deduced design procedure of Deployable Space Structures applied in practice.

3.4. Identified Gaps in the State-of-the-Art

The absence of a conceptual design method specific for Deployable Space Structures raises the question in how far the literature provides already the basis for its development e.g. through according adjustment of general design methods. This requires knowledge on the design driving requirements and specific characteristics of Deployable Space Structures and in how far these need to be addressed in early design stages.

3.4.1. Negligence of the Deployment Mechanism

The current literature that addresses the phase of conceptual design and is the basis for the design procedure displayed in Figure 3-2 focusses on the Deformable Structure and neglects the Deployment Mechanism. In current concept and design descriptions the design of the Deformable Structure includes dimensioning and initial optimization while the design of the Deployment Mechanism remains on a pure functional level. The same is true for literature on performance evaluation methods. For the Deformable Structure several performance indices and metrics are published which also enable identification of design drivers and provide knowledge on the performance potential of certain structural architectures. However, similar publications are missing for the Deployment Mechanism and the overall deployable structure.

3.4.2. Negligence of Design Requirements and Characteristics

Aside from the lack in overall consideration in the design of Deployable Space Structures, a variety of other characteristics and design requirements are not addressed in the current literature. Such characteristics and requirements are as follows:

→ The *load case of space transport* can impose high dynamic and acoustic loads on the deployable structure in stowed configuration and particularly drive the design of spatially extended components,

→ The *load case of deployment* can be design driving especially when robustness against deployment errors is required such as a sticking photovoltaic blanket of a solar array,
→ The *transition from the stowed to the deployed state* can be connected with significant changes in stiffness and stability when the deployable structure has a pronounced *Transition Zone* or undergoes a change of shape as a whole such as a pantograph,
→ *Design interactions* between the Deformable Structure and the Deployment Mechanism can require significant optimization to avoid misjudgment of the actual performance.

Hence, it can be concluded that the current literature does not provide the required basis for the development of a conceptual design method for Deployable Space Structure. The Deployment Mechanism is largely neglected and comprehensive information on design drivers and design relevant characteristics are missing.

3.4.3. Drawbacks of the Design Principle of Function Separation

In addition to the gap in knowledge identified in the current literature, there is a methodological gap in the concept generation process of general design methods.

The literature on deployable masts provides some examples that feature a particular design focus on function integration. Motivations are reduced complexity, enhanced compatibility between the Deformable Structure and the Deployment Mechanism and better compliance with other design objectives. Prominent examples are bi-stable booms that possess a stable configuration in the deployed and stowed configuration. Due to the stability in the stowed form the required functional capabilities of the Deployment Mechanism regarding containment and deployment control are largely reduced. This is achieved through the expense of stiffness and stability of the Deformable Structure as a specifically tailored fiber orientation in the booms composite shell is required to achieve bi-stability. This trade of integrating Deployment Mechanism functions into the Deformable Structure by the expense of structural efficiency makes this type of deployable mast particularly competitive in the small scale region such as CubeSat applications where a small stowage volume is a major design objective.

However, finding solutions such as the bi-stable boom that feature function integration is complicated by the approach of a detailed functional description of the design object as used in general design methods. After establishing the overall function it is further subdivided into main and sub-functions to enhance understanding of the design task and simplify the solution process through sub-division into independently solvable partial problems. In consequence, this design principle of function separation creates a design point of view that hinders to some extent finding solutions with function integration and favors solutions with function separation that reflect the functional structure.

3.5. Hypotheses on a New Conceptual Design Method

The review and analysis of the literature addressing the design of Deployable Space Structures supports the leading hypothesis of this thesis that there is a methodological gap in the state of the art. There is no specific design methodology published and the literature does not provide the basis for its development. Furthermore, current design methods hinder to some extent finding solutions that enable high solution quality through function integration. To fill these gaps detailed system analyses of Deployable Space Structures are necessary to identify design drivers and specific system characteristics as a basis for the development of efficient and focused design processes and procedures. In the following hypotheses on design aspects are formulated that need to be addressed in such processes and procedures of a conceptual design method for Deployable Space Structure.

3.5.1. Deployment Mechanism Parameterization

For performing the system analyses a mathematical description of a deployable structure regarding the design objectives is required. Thereby the impact of certain requirements and design interdependencies can directly be observed and assessed in a quantifiable form. For the Deformable Structure such mathematical descriptions are available through performance indices, metrics and scaling functions but need to be developed for the Deployment Mechanism.
For the mathematical description of the Deployment Mechanism parameterization is necessary. It is hypothesized that this can be done on the basis of the geometry parameters of the Deformable Structure and the overall requirements without introducing additional design variables. Thereby the consideration of the Deployment Mechanism does not increase the complexity of the solution process. This hypothesis is based on the observation that the design of the Deployment Mechanism largely depends on the Deformable Structure. Its form and dimensions are linked to the form and dimensions of the stowed Deformable Structures and its required functional capabilities and interface design depend on the structures folding and deployment principle.

The hypothesis is summarized as follows:
The parameterization of the Deployment Mechanism can be done on the basis of the geometry parameters of the Deformable Structure and the overall requirements without introducing additional design variables.

3.5.2. Design Interactions of Deformable Structure and Deployment Mechanism

Main subjects to be addressed in a conceptual design method are design interactions between the Deformable Structure and the Deployment Mechanism. In this regard it is hypothesized that there are significant design interactions that do not allow for a sequential sizing procedure where the Deformable Structure is sized first according to the mechanical requirements and subsequently the Deployment Mechanism. In

consequence to this hypothesis it is predicted that an optimization process regarding the design objectives is required already in the phase of conceptual design to avoid misjudgment of the performance potential. This hypothesis is based on the observation that the designs of the Deformable Structure and the Deployment Mechanism are highly linked due to the high degree of functional interaction.

The hypothesis is summarized as follows:
There are design interactions between the Deformable Structure and the Deployment Mechanism that do not allow for a sequential sizing procedure and require an optimization process already in the phase of conceptual design.

3.5.3. Impact of Transition Zones

For many deployable structures the transition from the stowed to the deployed configuration is connected with a change in stiffness and stability. Here it is hypothesized that this variation in mechanical properties is a design driving factor whose consideration leads to significant differences in the sizing results of Deformable Structure and Deployment Mechanism in comparison to the deployed, operational configuration. The hypothesis is derived from observations that the form transition of various deployable structures is connected with a significant local or global change in shape. Thereby the load case of deployment can become a design driving factor even when the applied loads are considerably below the operational load case.

The hypothesis is summarized as follows:
The consideration of load carrying Transition Zones cause significant differences in the sizing results of the Deformable Structure and Deployment Mechanism in comparison to sizing based on the fully deployed structure.

3.5.4. Design Principle of Function Integration

For the field of Deployable Space Structures it is hypothesized that solutions with function integration enable superior results in comparison to solutions based on function separation. This hypothesis results from the observation that deployable structures feature a high degree of functional interaction among its components. In parallel their competitiveness regarding the design objectives is a major design goal. Thus, reducing the number of components, enhancing their compatibility among each other or reducing their required functional capabilities through function integration is of high interest to achieve benefits on the side of the overall properties that reflect the design objectives.

The hypothesis is summarized as follows:
The application of the design principle of function integration in Deployable Space Structures allows reduction in mass and stowage volume.

3.5.5. Evaluation on the Basis of an Overall View

The process of concept selection is based on a performance evaluation of the competing concepts. In the literature an evaluation process of deployable structures on the basis of the Deformable Structure only is indicated. Here it is hypothesized that such an evaluation procedure is not representative for the overall system and causes misjudgments regarding the actual performance potentials wherefore not necessarily the best performing is selected. Instead the performance evaluation process needs to be done on the basis of an overall consideration including the Deployment Mechanism already in the phase of conceptual design. This hypothesis is largely based on the observations regarding the mass and volume distribution among Deformable Structure and Deployment Mechanism presented in chapter 1 '*Observations on Deployable Space Structures*' which shows a dominance of the Deployment Mechanism in several design examples.

The hypothesis is summarized as follows:
Performance evaluation on the basis of the Deformable Structure only is not representative for the overall deployable structure and leads to misjudgments in the concept selection process.

3.6. Outline of the Verification Approach

The approach for verification of the hypotheses introduced in section 3.5 consists of the system analysis of a Deployable Space Structure exemplary performed for the category of deployable masts. The analysis is described throughout the chapters 4 to 8 whereby each chapter addresses one hypothesis. Goal is the identification of design drivers and specific characteristics that need to be implemented in the processes and procedures of a conceptual design methodology for Deployable Space Structures. However, the chapters 4 to 8 do not necessarily reflect in their composition such processes or procedures. Instead these are subsequently developed in chapter 9 '*Development of the Conceptual Design Methodology for Deployable Space Structures*' based on the analysis results.

In chapter 4 '*Deployment Mechanism Parameterization and Derivation of Scaling Functions*' firstly a model of the Deployment Mechanism is established. This model features a high level of detail to allow identification of those components that are decisive for the performance regarding the design objectives of low mass and small stowed volume. Subsequently a mathematical description of the Deployment Mechanism through component scaling functions according to the hypothesis described in subsection 3.5.1 is performed. The scaling functions are derived in the same way as those described in the literature for the Deformable Structure from basic equations on stiffness and stability. The results are simple mathematical expressions of the main design objectives of mass and stowage volume that allow direct deduction of design drivers and design interactions between components on a quantifiable basis.

Based on the mathematical model, verification of the remaining hypotheses is conducted. In chapter 5 '*Design Interactions of Deformable Structure and Deployment Mechanism*' the hypothesis on component design interactions detailed in subsection 3.5.2 is addressed. It is examined if there are design interactions between the Deformable Structure and the Deployment Mechanism. Based on this examination the questions are answered in how far an optimization process is necessary already in the phase of conceptual design or if a sequential sizing procedure is possible.

The impact of Transition Zones and means for their analysis are described in chapter 6 '*Consideration of the Transition under Load*'. This chapter covers the related hypothesis formulated in subsection 3.5.3 by establishing a mathematical model of the Transition Zone of a Tubular Shell Mast and implementing this model into the scaling function of the Deformable Structure. Furthermore it is addressed in how far Transition Zones cause particular design interaction of Deformable Structure and Deployment Mechanism.

The hypothesis on the design principle of function integration presented in subsection 3.5.4 is addressed in chapter 7 '*Function Integration in the Design of Deployable Space Structures*'. A Telescopic Tubular Mast that features a high degree of function integration in its design is compared regarding its competitiveness in mass and stowage volume with other widely used types of deployable masts. It is analyzed if there are advantages in design objective related performance due to the function integration.

In chapter 8 '*Performance Evaluation of Deployable Space Structures*' the approach of evaluating deployable structures on the basis of the Deformable Structure only as indicated in the literature is evaluated. Therefore performance comparisons of several deployable masts are conducted on the basis of the Deformable Structure only and on the basis of the overall deployable structure. This comparison addresses the hypothesis detailed in subsection 3.5.5 that predicts different outcomes of the concept selection process between the two evaluation approaches.

4. Deployment Mechanism Parameterization and Derivation of Scaling Functions

The basis for the following system analysis of Deployable Space Structures is the mathematical description of their components through scaling functions of their mass and stowage volume. While for the Deformable Structures of deployable masts the literature provides such scaling functions, the equivalents for the Deployment Mechanism are derived within this chapter. Therefore, a baseline Deployment Mechanism is selected whose design is known in detail and that is based on actual Deployment Mechanism designs which are applied in practice. The derivation of the mechanism scaling functions is done on the basis of the design variables of the Deformable Structure without introduction of additional variables as is hypothesized in subsection 3.5.1. Design interdependencies towards the Deformable Structure are identified through inspection of the Deployment Mechanism scaling functions.

4.1. Baseline Deployment Mechanism Design for the System Analysis

The baseline design for derivation of the scaling functions is DLR's Deployment Mechanism developed for the tubular, double omega booms. It is the basis for various missions and projects such as the solar and drag sails GOSSAMER [50] and De-Orbit Sail [51]. Thereby it is ensured that the analysis is performed for a design that is on a high level of development and actually meets mission requirements applied in practice. Furthermore, this mechanism design is versatile in its application as it is compatible with all types of masts that are stowed by reeling along the longitudinal mast direction such as tapesprings, TRAC-booms [18], double-omega booms [49] or trusses like SuperString [23] and CTT [24]. The mechanism components are designed to allow scalability over a wide size range to enable analysis of masts in different size categories.

4.1.1. Overall Mechanism

Figure 4-1 shows the baseline Deployment Mechanism design in assembled state and with parts of the outer walls removed. The inner mechanism components reflect in their form and alignment the stowed form of the mast. A spool contains and supports the reeled mast while other components enclose the opening part to guide and direct its deployment. The stowed mast with the inner mechanism components is contained and supported by a box-shaped structure assembled in the presented version from sandwich plates. At the rear side of this box a frame with flanges is attached that provides the mechanical interface to the spacecraft.

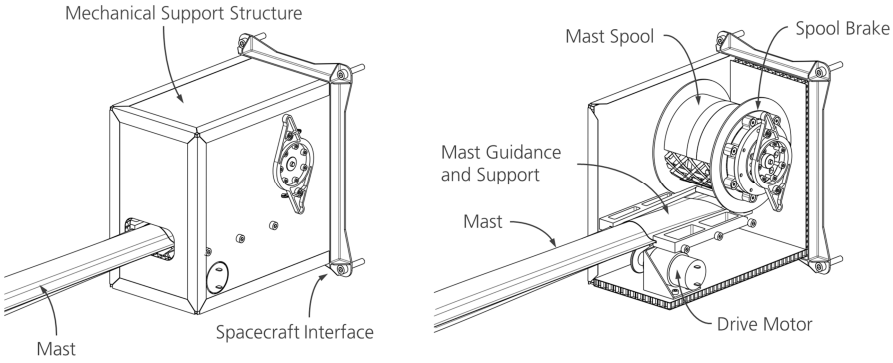

Figure 4-1: Baseline Deployment Mechanism model (left) and mechanism details with removed support structure walls (right).

Figure 4-2 shows the mechanism design in exploded state and reveals some of the subcomponents and way of assembly.

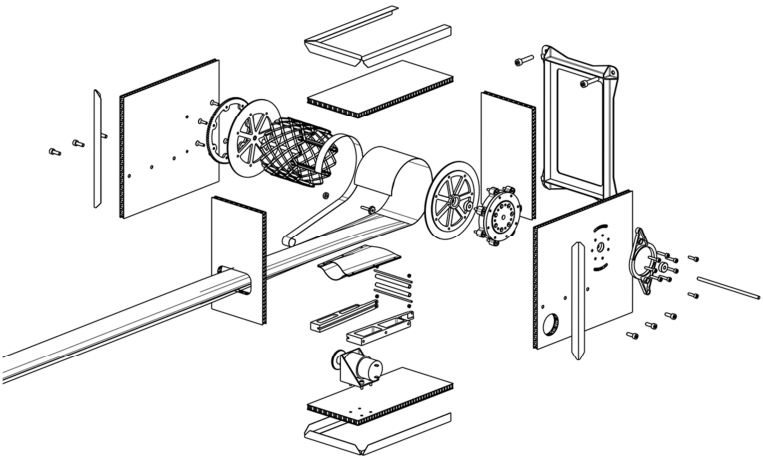

Figure 4-2: Exploded view of the baseline design of the Deployment Mechanism displayed for a tubular, double-omega shell mast.

4.1.2.Mechanism Modules

The baseline Deployment Mechanism can be separated into five main modules that reflect specific functional tasks. These main modules and their functions are described in the following.

4.1.2.1. Mast Spool

The mast is reeled for stowage on a cylindrical spool that contains the mast in stowed state and provides the mechanical support to the stowed package necessary during launch. It consists of a central cylinder, two end-caps, two roller bearings and an axle. In addition there is a gear attached to the hub that enables re-winding after deployment. Figure 4-3 shows the boom spool with coiled boom as well as the separated components.

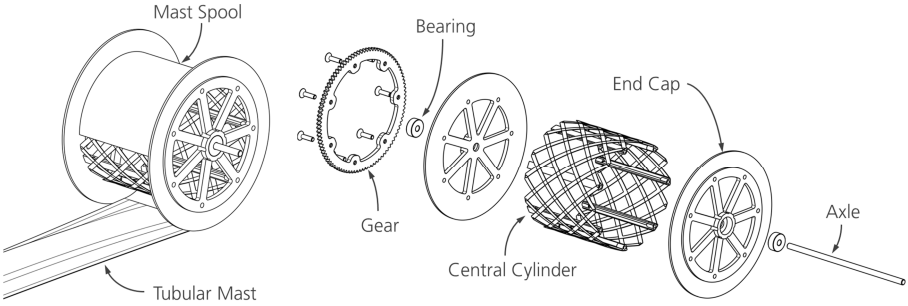

Figure 4-3: Mast Spool in assembled state with coiled tubular boom (left) and in exploded state detailing its subcomponents (right).

The central cylinder is designed as a grid with longitudinal stringers and helical diagonals. Such a design is chosen to enable scalability to high dimensions as a cylinder of solid walls would lead to unreasonable high mass. For the same reason the end-caps primarily consist of radial bars whose cross-sectional profile may be adjusted accordingly.

4.1.2.2. Spool Brake Mechanism

The masts that are compatible with this mechanism design are reelable through elastic deformation. Without bi-stability such a mast acts in stowed state as a spiral spring and is not stable in this configuration. Hence, self-deployment needs to be prevented which is done by applying a Brake Mechanism to the Mast Spool whose braking torque is above the spring moment. The brake is designed similar to a free-wheel-clutch and is displayed in Figure 4-4. A number of spring loaded arms gear into a toothed ring each with a different angle. Thereby each arm applies a small force to the Tooth Ring opposite to the direction of motion whereby a braking torque is generated. By using several spring loaded arms the variance in the generated torque can be reduced. The Brake Mechanism is directly attached to the Mast Spool and the counterpart to the surrounding support structure.

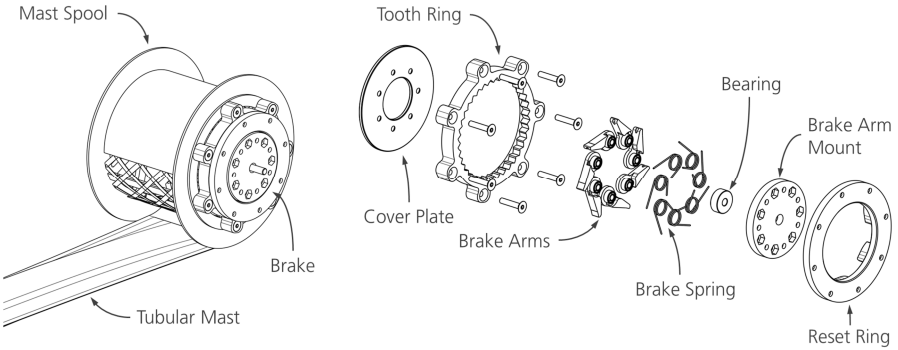

Figure 4-4: Brake Mechanism attached to the Mast Spool (left) and in exploded state detailing its subcomponents (right).

4.1.2.3. Mast Root Support and Guidance

The masts that are compatible with the selected Deployment Mechanism are stowed by elastic deformation through reeling. Such masts are tapsprings, TRAC-booms [18], lenticular booms [48] or trusses like the Superstring [23] or CTT [24]. All these masts possess a Transition Zone between the fully flattened and fully deployed state with reduced cross-sectional dimensions and thereby also reduced mechanical performance. To enhance the stiffness and stability in this region an external support structure is used. For the example of a tubular, double-omega mast this external support consists of two Guide and Support Plates which fully enclose the mast from the outside as shown in Figure 4-5.

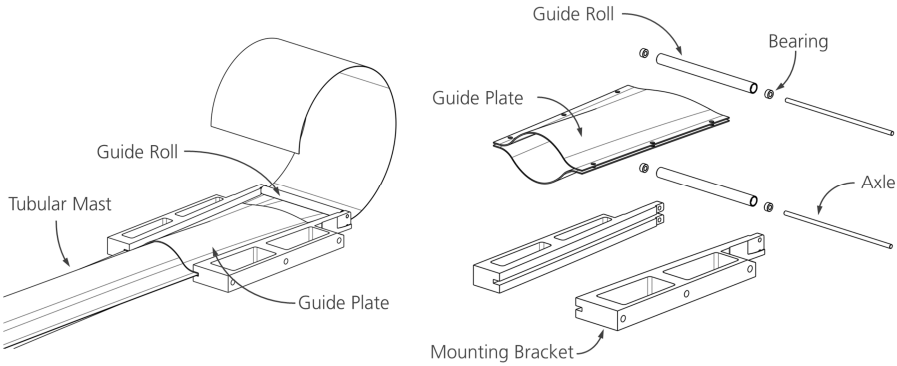

Figure 4-5: Boom support and guiding components with semi-coiled tubular boom (left) and in exploded state detailing its subcomponents (right).

In addition to supporting the Transition Zone, it is of high importance to guide and direct the motion of the deploying mast. This is also achieved by the Guide and Support Plates but to gain a controlled detachment of the mast off the spool and ensure proper alignment with the Guide and Support Plates, two Guide Rolls constrain any vertical motion at the beginning of the Transition Zone where the mast is still fully flattened. Guide and Support Plates and Rolls are attached to the surround support structure by two mounting brackets.

4.1.2.4. Drive Mechanism

The Drive Mechanism generates and introduces the forces necessary to deploy the mast. An electric motor transforms the electric energy that is provided by the host spacecraft wherefore a dedicated energy source is not considered. The motor is attached to a gear which drives a spool that coils a steel belt that is co-coiled with the stowed mast. For deployment the motor turns the Belt Spool and thereby pulls the mast off the Mast Spool. The belt also constrains the motion of the stowed mast in combination with the Spool Brake Mechanism. As it encloses the reeled boom, any movement of the mast in radial direction is prevented by the tensioned belt while the Brake Mechanism prevents any motion of the Mast Spool. Figure 4-6 shows the Drive Mechanism with the belt attached to the Mast Spool and gear as well as the related disassembled subcomponents.

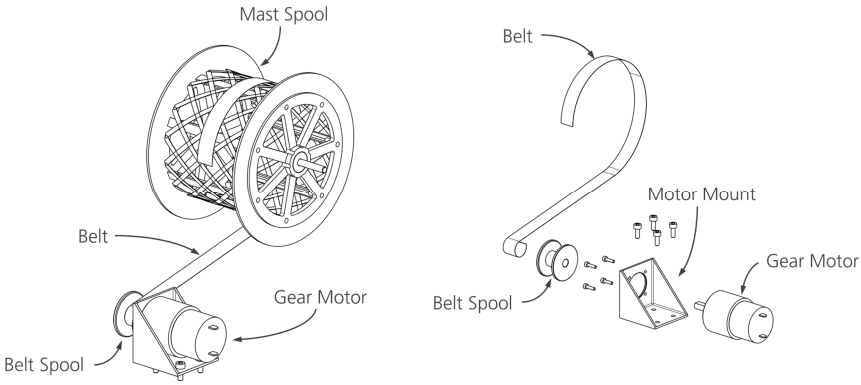

Figure 4-6: Drive Mechanism with attached belt and boom spool (left) and exploded state detailing its subcomponents (right).

4.1.2.5. Mechanical Support Structure and Spacecraft Interface

The mechanism components are mounted to the Mechanical Support Structure which transfers mechanical loads to the host spacecraft and provides the strength and stiffness that is required for space transport. In the selected baseline design the

support structure consists of a rectangular box whose panels may be designed as solid, sandwich or stiffened plates. Figure 4-7 shows the Mechanical Support Structure realized with sandwich panels that are connected by L-shaped profiles along the edges. Inserts are placed at locations of screw connections. The mechanical interface towards the host spacecraft is realized as a rectangular frame with mounting holes that is attached to the backside of the box.

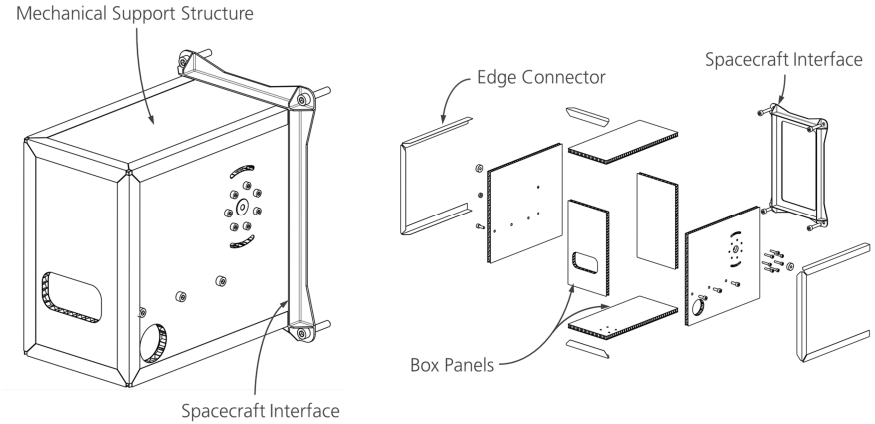

Figure 4-7: Support Structure with mechanical interface towards the host spacecraft in assembled state (left) and in exploded state detailing its subcomponents (right).

4.2. Parameterization of the Deployment Mechanism

The derivation of scaling functions for the baseline Deployment Mechanism requires parameterization of its modules and components. The basis for this parameterization and subsequent development of scaling functions is the identification of design parameters. Therefore, firstly the dependency of the mechanism design on the Deformable Structure particularly its stowed form is examined. Based on the identified dependencies the according parameters of the stowed mast are extracted. Subsequently general design parameters are identified and the procedure for component parameterization is presented.

4.2.1. Design Dependency on the Deformable Structure

The accommodation and design of the mechanism components – particularly their dimensions – depends in a high degree on the Deformable Structures stowed form. For initial identification of such geometrical dependencies a design sketch that represents the stowed Deformable Structure and the mechanism component accommodation is used. Figure 4-8 shows such a sketch for the baseline Deployment

Mechanism design with the main geometrical parameters for a reelable, tubular double omega boom and some initial size definitions.

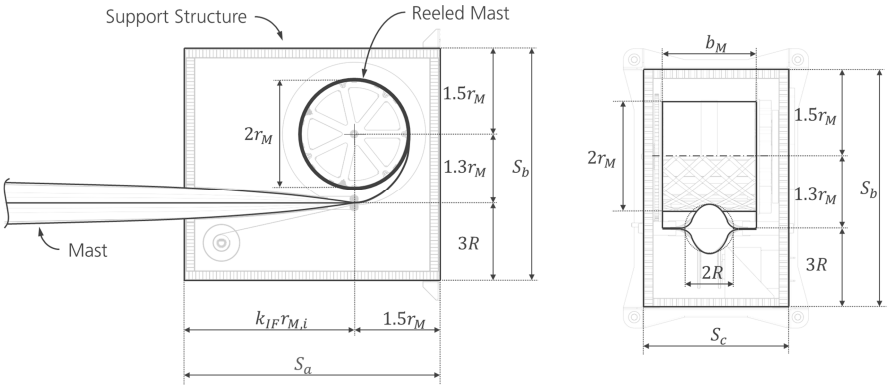

Figure 4-8: Design sketch of the stowed mast with its geometrical relation to the Deployment Mechanism design.

The mechanism dimensions are expressed through multiples of the mast radius R, flattened mast width b_M and mast reeling radius r_M. Thereby the dimensions of the surrounding Mechanical Support Structure, the Mast Spool, the Spool Brake radius and the size of the components for mast root support and guidance are defined. The length of the mast root support is given by a multiple of the mast radius through the mast-mechanism interface parameter k_{IF} (see left side of Figure 4-8).
However, aside from geometrical dependencies other functional mechanism requirements depend on the Deformable Structures properties particularly the Spool Brake Mechanism and the Drive Mechanism. The Spool Brake Mechanism has to counter the self-deployment of the reeled mast and the Drive Mechanism has to provide a certain deployment force. The required braking torque is deduced from the moment M_{Mr} generated by the flattened and reeled mast which acts similar to a spiral spring and depends solely on the mast properties and reeling radius. The deployment force can either be defined by a design requirement but may also be coupled to the masts compression strength P_{crit}.
Another dependency in the design is related to those components that give structural support to the mast and mechanism components such as the Mast Spool and the Mechanical Support Structure. These components are primarily sized according to the load case of space transport through stiffness requirements in the form of minimum eigenfrequencies and inertial acceleration loads. Hence, the mast mass m_M that needs to be supported by the corresponding support structure is required for its sizing.
Table 4-1 summarizes the design dependencies between mechanism components and modules towards the Deformable Structure properties and stowed form. The presented dependencies are based on the above presented initial observations and

considerations and are thereby not complete. Further dependencies may be identified during development of the scaling functions.

Mast Parameter	Symbol	Unit	Related Components	Remark
Radius	R	m	Mechanical Support Structure (Length, Height), Root Support and Guidance (Length)	
Reeling Radius	r_M	m	Mast Spool (Radius), Mechanical Support Structure (Length, Height), Spool Brake (Radius)	
Flattened Width	b_M	m	Mast Spool (Width), Mechanical Support Structure (Width), Root Support and Guidance (Width)	
Mass	m_M	kg	Mast Spool (Stiffness, Stability), Mechanical Support Structure (Stiffness, Stability)	
Reeled Spring Moment	M_{Mr}	Nm	Spool Brake (Braking Torque)	
Compression Strength	P_{crit}	N	Drive Mechanism (Deployment Force)	Depending on definition

Table 4-1: Design dependencies of the Deployment Mechanism Modules towards the Deformable Structures properties.

4.2.2.Parameters dependent on the Stowed Deformable Structure

In the previous subsection basic design dependencies between mechanism components and the stowed form and properties of the Deformable Structure are identified. In the following the parameters that represent these design dependencies (summarized in Table 4-1) are exemplary developed for a reelable Tubular Shell Mast as displayed in Figure 4-8 and Figure 4-9. As design variables the masts cross-sectional area A (Equation 4-1) and radius R are selected in accordance with the literature on mast scaling functions and performance metrics specifically the indices developed by Murphey [28].

Note: In the following equations the design variables A and R are always written last in the equation as a set and with negative exponents where necessary to highlight their contribution to the function value. Furthermore equation parameters are separated in the equations regarding context, e.g. all material related parameters are grouped.

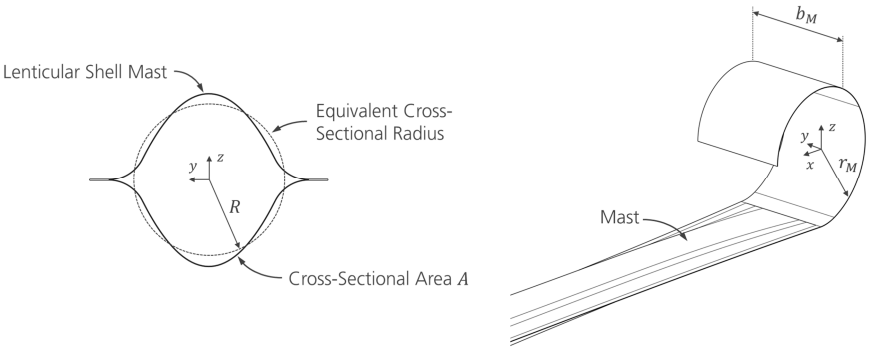

Figure 4-9: Example of a reelable lenticular shell mast that is compatible with the baseline Deployment Mechanism design in cross-sectional view (left) and partly reeled (right).

4.2.2.1. Mast Reeling Radius

The reeling radius r_M of a tubular mast of uniform shell thickness t_M (Equation 4-2) depends on the cross-sectional shape of the mast defined by the cross-section parameter k_A and the reeling strain ε_r and is given by Equation 4-3:

$$A = k_A R t_M \tag{4-1}$$

$$t_M = \frac{1}{k_A} A R^{-1} \tag{4-2}$$

$$r_M = \frac{t_M}{\varepsilon_r} = \frac{1}{\varepsilon_r k_A} A R^{-1} \tag{4-3}$$

4.2.2.2. Flattened Mast Width

The flattened width b_M of the mast also depends on the masts cross-sectional shape parameter k_A and is given by Equation 4-4:

$$b_M = k_A R \tag{4-4}$$

4.2.2.3. Mast Mass

The mass of the mast m_M is simply derived through multiplication of the cross-sectional area A by the mast length L and material density ρ as described by Equation 4-5:

$$m_M = \rho L A \tag{4-5}$$

4.2.2.4. Compression Strength

The required deployment force that needs to be generated by the Drive Mechanism may be expressed by the masts compression strength P_{crit} to ensure that the Drive Mechanism is not a limiting factor. The compression strength may be expressed for a

slender mast by the Euler buckling load P_E that depends on the second moment of area I (Equation 4-6) expressed by the architecture coefficient k_I and the materials Young's modulus E. The deployment force derived from the Euler buckling load is described by Equation 4-7 which includes a factor k_C that accounts for the boundary conditions:

$$I = k_I A R^2 \quad 4\text{-}6$$

$$P_{crit} = P_E = \frac{\pi^2 EI}{(k_C L)^2} = \frac{\pi^2 E k_I}{(k_C L)^2} AR^2 \quad 4\text{-}7$$

4.2.2.5. Reeled Spring Moment

The Spool Brake Mechanism needs to provide a braking torque M_{Mr} that results from the stress in the stowed mast similar to a spiral string. The approximate torque generated by the mast in reeled state is given by Equations 4-8 and 4-9 depending on the mast flattened bending stiffness $(EI)_{flat}$:

$$(EI)_{flat} \approx \frac{2}{3} E b_M t_M^3 = \frac{2}{3} E \frac{1}{k_A^2} A^3 R^{-2} \quad 4\text{-}8$$

$$M_{Mr} \approx \frac{(EI)_{flat}}{r_M} = \frac{2}{3} \varepsilon_r \frac{1}{k_A} E A^2 R^{-1} \quad 4\text{-}9$$

However, this simplified approach neglects the stresses that arise from previous flattening of the mast and considers only those from reeling.

4.2.3. General Parameters

General parameters for the Deployment Mechanism result from the design task and the design objectives whereby the latter define the scaling function values. These scaling functions are developed on the basis of the design variables of the Deformable Structure.

4.2.3.1. Design Requirements

Design requirements for Deployable Space Structures result among others from mission constraints, functional requirements, environmental conditions, mechanical load cases, verification processes and integration and handling procedures. In the following only design requirements are considered that can be attributed as universally applicable to space missions. Such requirements result from the necessary size of the deployable structure and the load cases of space transport, deployment and operation. Table 4-2 gives the requirements that are considered for the derivation of the mechanism scaling functions.

Requirement	Symbol	Unit	Load Case
Mast length	L	m	Operation
First eigenfrequency	f	Hz	Space transport
Maximum acceleration	a_{acc}	g	Space transport
Bending stiffness	EI	Nm²	Deployment/operation
Critical bending moment	M	Nm	Deployment/operation
Compression strength	P	N	Deployment/operation

Table 4-2: List of design requirements for Deployment Mechanism parameterization.

The length of the mast L is derived from the type of application of the deployable mast and the mission requirements that define the required size of the deployable system.
First eigenfrequency f and maximum acceleration a_{acc} result from requirements for the stability and dynamic behavior of the stowed system during launch. The static acceleration load requirement is a simplification as the actual load environment is complex. In general the launch loads are described by several load events that can be addressed in separate tests such as acoustic pressure, random vibration, sine vibration, shock or sine-burst. However, the definition of static acceleration loads for basic design steps is a common method.
The mechanical load cases applied to the deployed and deploying structure are reflected by the required compression strength P, critical bending moment M and bending stiffness EI. These mechanical load cases are axial compression and bending and well represented in the literature [113] [108] [28].

4.2.3.2. Design Objectives

As introduced beforehand, the design objectives are to minimize mass m and stowed volume V of the deployable structure as these are often the main factors for the competitiveness of a Deployable Space Structure. The design objectives considered for this analysis are listed in Table 4-3. They are applied in the design either separately or combined with according weighting.

Objective	Symbol	Unit	Remark
Minimize mass	m	kg	
Minimize stowage volume	V	m³	Volume measured on the outer envelope including voids

Table 4-3: List of design objectives for mechanism parameterization.

4.2.3.3. Design Variables

In subsection 4.2.1 it is demonstrated that the design of the Deployment Mechanism largely depends on the Deformable Structures stowed form. This led to the hypothesis that the design variables for the Deployment Mechanism are the same as for the

Deformable Structure as detailed in subsection 3.5.1. It is assumed that aside from requirements, architectural parameters and material selections the geometry and thereby mass and stowed volume of each mechanism component is dependent on the design variables of the Deformable Structure. Table 4-4 gives these design variables which are the cross-sectional area A and radius R of the mast.

Design Variable	Symbol	Unit	Remark
Cross-sectional mast area	A	m²	Describes the mean cross-sectional mast area (includes in case of trusses battens and diagonals)
Mast radius	R	m	Specific definition depends on the type of mast architecture

Table 4-4: List of Deployment Mechanism design variables.

4.2.4.Procedure for Component Parameterization and Scaling Function Derivation

The parameterization of the mechanism components is done based on the above derived design requirements, objectives and variables. For each component of the baseline mechanism model the following parameterization procedure is conducted:

(1) *Identification of design relations*: It is analyzed in how far the design of the corresponding component is related to other mechanism components, the Deformable Structure or directly to the design requirements,
(2) *Identification of design driving component elements*: It is examined which elements of the component are decisive for those properties that reflect the design objectives,
(3) *Derivation of a simplified component approximation model*: A model of the component is established that is reduced to its main elements and mathematically describable,
(4) *Identification of scaling limits*: The component and its elements are analyzed regarding limitations in the scaling process,
(5) *Derivation of the component scaling function*: Mathematical expressions describing the component element properties are combined to an overall scaling function that reflects the design objectives; the function is formulated on the basis of the overall design requirements and the design variables of the Deformable Structure; the application of the scaling function is done considering the scaling limits.

Critical for the derivation of the component scaling functions is the simplified approximation model in step (3). For the identification of design drivers and an easy implementation into an overall scaling function, a low complexity is favored. However, this simplified model still needs to represent the actual component scaling behavior.

4.3. Scaling Functions of the Deployment Mechanism Components

The overall mechanism scaling function is derived from the component scaling functions. The scaling functions are established for the design objectives of mass m and stowed volume V on the basis of the Deformable Structures design variables of cross-sectional mast area A and radius R. The stowed volume is derived from the outer envelope of the mechanism that coincides with the volume of the surrounding support structure. Hence, a volume scaling function is developed only for the support structure. However, as the volume is a result of a sizing process, the volume scaling function is dependent on the mass scaling functions particularly on the mast scaling results.
In the following the simplified component models, the thereby established scaling functions and the component specific scaling limits are presented. The detailed descriptions of the mechanism component scaling function derivations are given in the Appendix B based on basic construction element scaling functions presented in Appendix A.

4.3.1. Energy Source

For the baseline mechanism design the required electric energy is provided by the host spacecraft wherefore an energy source is not included in the scaling function. However, to demonstrate the component parameterization procedure given in 4.2.4 the derivation of a simple energy source mass scaling function is described in the following. For the subsequent components this procedure is not described in detail to limit the extent of this section.

(1) *Identification of design relations:*
The mass of the energy source components are related to the energy that needs to be provided for the deployment process. The required energy depends on the work that is done during deployment J_{deploy} and the efficiency of the energy translation η_J. Furthermore, in the project may be some robustness required against off-nominal energy consumption that is covered by a safety factor F_J.

(2) *Identification of design driving component elements:*
As there is no energy source design, specific design driving components cannot be identified. However, for the examples of pressure tanks or batteries design driving in terms of mass is the energy storing medium and the component for its containment.

(3) *Derivation of a simplified component approximation model:*
A battery or pressure tank can be approximated as a mass block with a certain energy density ψ_{Jm} that linearly relates stored energy to component mass.

(4) *Identification of scaling limits:*
Scaling limits may be reached in the small scale region as down-scaling of batteries or pressure tanks are constrained by manufacturing limits. The simplest form of an according scaling limit is the definition of a minimum mass m_{min} that may be derived from an analysis of commercially available products.

(5) *Derivation of the component scaling function:*

The component scaling function is derived based on the beforehand considerations. The work J_{deploy} that is done during deployment by the mast is given by the deployment force P_{deploy} and the required mast length L_{req}:

$$J_{deploy} = P_{deploy} L_{req} \tag{4-10}$$

The maximum deployment force may be defined equivalent to the masts Euler buckling load P_E given by Equation 4-7:

$$P_{deploy} = P_E = \frac{\pi^2 E k_I}{(k_C L)^2} AR^2 \tag{4-11}$$

The total energy J is derived by the efficiency factor η_J and the factor of safety $F_J \geq 1$:

$$J = \frac{F_J}{\eta_J} J_{deploy} \tag{4-12}$$

The mass m_{ES} of the energy source can now be calculated through the energy density factor ψ_{Jm}:

$$m_{ES} = \frac{J}{\psi_{Jm}} \tag{4-13}$$

Substitution of the total energy gives the mass scaling function of the energy storage system expressed by Equation 4-14 whereby it needs to be checked that the minimum mass scaling limit $m_{ES,min}$ is not violated:

$$m_{ES} = \pi^2 \frac{F_J}{\eta_J} \frac{1}{\psi_{Jm}} \frac{k_I}{k_C^2} \frac{1}{L_{req}} EAR^2 \geq m_{ES,min} \tag{4-14}$$

The design variables of the mass scaling function of the energy source are the mast cross-sectional area A and radius R through selecting the masts Euler buckling load as the deployment load criterion. The remaining parameters reflect the design requirements and specific design characteristics of the Deformable Structure and the component itself. The influence of specific design decisions can directly be identified through inspection of Equation 4-14. The parameters of the energy source scaling function are summarized in Table 4-5.

Parameter	Symbol	Unit	Parameter Category	Remarks
Safety factor	F_J	-	Project factor	-
Energy conversion efficiency	η_J	-	Component characteristic	-
Energy density	ψ_{Jm}	kg/J	Component characteristic	-
Mast mounting factor	k_C	-	System architecture	-
Mast moment of inertia factor	k_I	-	Mast architecture	-
Mast material modulus	E	N/m²	Mast material	-
Mast length	L_{req}	m	Design requirement	-
Mast cross-sectional area	A	m²	Design variable	-
Mast radius	R	m	Design variable	-

Table 4-5: Scaling function parameters of the energy source.

4.3.2.Mast Spool

The Mast Spool is an assembly of several subcomponents consisting of a central cylinder, two end-caps, two bearings, several screw connectors and an axle (the components for re-winding of the mast indicated in Figure 4-3 are neglected). The spool supports the stowed mast during launch and is thereby sized for the load case of space transport. This load case is represented by the minimum eigenfrequency requirement f_{req} and an acceleration load a_{acc}. The sizing of the subcomponents is dependent on each other wherefore it needs to be done in a specific order. In this order each subcomponent structurally supports the preceding wherefore their masses influence the sizing result of the subsequent. For the Mast Spool the sizing starts with the central cylinder which directly supports the stowed mast (the sizing of connector elements and bearings is described separately in subsection 4.3.8). The scaling functions for the Mast Spool components are addressed in Appendix B1.

4.3.2.1. Spool Cylinder

The Spool Cylinder is a grid structure built from a set of longitudinal stringers that are interconnected by helical diagonals. This design ensures a good scalability even in the large size region where planar structures may become unreasonable heavy. The cylinder length depends on the flattened width and its radius on the initial reeling radius of the mast. Figure 4-10 shows the central cylinder and the simplified model that is the basis for the derivation of the scaling function.

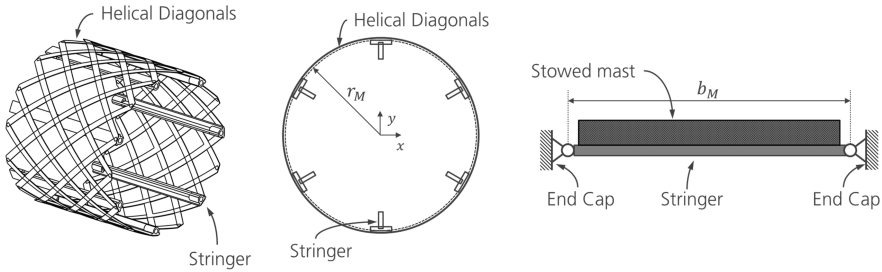

Figure 4-10: Central cylinder of the Mast Spool consisting of stringers and helical diagonals (left), cross-sectional view (middle) and simplified mechanical model of a single stringer as a simply supported beam with supported stowed mast (right).

For derivation of the scaling function it is assumed that the stringers solely carry the inertial loads applied during launch and define the central cylinders dynamic behavior. The stringers are idealized as beams that are simply supported at their ends by the spools end caps. Any structural support given by the helical diagonals is neglected wherefore the approach can be considered conservative.

The central cylinder structurally supports the stowed mast. As the stringers are designed to comply with certain eigenfrequency and inertial load requirements, the mass added by the mast needs to be considered. The additional mass that is carried by each stringer is a fraction of the mast mass m_M given by the number of stringers n_{st} and the parameter k_{Mm}. Thereby the mast mass is uniformly distributed throughout the stringer length.
In the scaling function a scaling limit is considered for the small scale region in the form of a minimum cross-sectional stringer size.

Based on the above described model two separate scaling functions are derived for the eigenfrequency requirement f_{req} and the inertial load requirement a_{acc}. For each calculation point the function values are compared and the higher mass is selected.
Equation 4-15 gives the mass scaling function $m_{MSC,f}$ of the central cylinder derived for the eigenfrequency requirement (see Appendix B1.1):

$$m_{MSC,f} = k_{MSC,m} n_{st} \left(\Phi + \sqrt{\Phi^2 + 2\Phi k_{Mm} \frac{m_M}{n_{st}}} \right) \qquad 4\text{-}15$$

$$\Phi = \frac{2}{\pi^2} \frac{k_A}{k_I} \frac{k_\rho^2 \rho^{*2}}{E} k_f^2 f_{req}^2 b_M^5$$

Equation 4-16 gives the mass scaling function $m_{MSC,a}$ of the central cylinder derived for the inertial load requirement (see Appendix B1.1):

$$m_{MSC,a} = k_{MSC,m} n_{st} k_\rho k_A \rho^* \left(u + v - \frac{a}{3} \right)^2 b_M \qquad 4\text{-}16$$

$$u = \sqrt[3]{-\left(\frac{a}{3}\right)^3 - \frac{c}{2} + \sqrt{\frac{1}{27} a^3 c + \frac{1}{4} c^2}}$$

$$v = \sqrt[3]{-\left(\frac{a}{3}\right)^3 - \frac{c}{2} - \sqrt{\frac{1}{27} a^3 c + \frac{1}{4} c^2}}$$

$$a = -\frac{1}{8} \frac{k_y}{k_I} \frac{k_\rho \rho^*}{\sigma_{crit}} k_a a_{acc} b_M^2$$

$$c = -\frac{1}{8} \frac{1}{\sigma_{crit}} \frac{k_y}{k_A k_I} k_a a_{acc} k_{Mm} \frac{m_M}{n_{st}} b_M$$

Both scaling functions are dependent on the properties of the Deformable Structure through the length of the cylinder that is equal to the flattened mast width b_M and the mass term m_M. Both parameters and thereby also the central cylinder scaling function are functions of the mast design variables of cross-sectional area A and radius R.
The mass efficiency of the component can be adjusted through selection of the stringer architecture that is expressed by the beam architecture parameters k_A, k_I, k_y and k_ρ (see Appendix A1.1) as well as the stringer material represented by the Young's modulus E, the mean density ρ^* and the critical stress σ_{crit}. For selection of the stringer architecture the difference in the scaling limits in the small scale region have to

be taken into account. Thereby a less efficient design may still lead to lower masses due to a less strict scaling limit.
Table 4-6 lists the parameters of both scaling functions. Detailed description of the derivation of the scaling functions is given in the Appendix B1.1.

Parameter	Symbol	Unit	Value	Remarks
Flattened mast width	b_M	m	Input value	Depending on mast design variables A and R
Mast mass	m_M	kg	Input value	Depending on mast design variables A and R
Number of stringers	n_{st}	-	6	
Material density	ρ^*	kg/m³	2700	
Material modulus	E	N/m²	70 GPa	
Material critical stress	σ_{crit}	N/m²	200 MPa	
Beam density factor	k_ρ	-	1	Stiffened beam
Beam cross-section factor	k_A	-	0.4	Stiffened beam
Beam moment of area factor	k_I	-	0.417	Stiffened beam
Beam neutral layer factor	k_y	-	1.5	Stiffened beam
Mass amplification factor to account for diagonal mass	$k_{MSC,m}$	-	2	
Distributed mass factor	k_{Mm}	-	1/3	
Eigenfrequency requirement adjustment factor	k_f	-	1.5	
Acceleration load adjustment factor	k_a	-	1.5	
Lateral acceleration	a_{acc}	m/s²	30 g	
Eigenfrequency requirement	f_{req}	Hz	100	

Table 4-6: Summary of the parameters of the mass scaling functions of the Mast Spool Cylinder.

4.3.2.2. Spool End Cap

The Spool End Caps consist of a set of radial ribs that are joined in the center by a ring and possess a flange on the outside that avoids slippage of the stowed mast off the spool. The dimensions of the end cap are determined by the inner reeling radius of the mast r_M that defines the length of the ribs. Figure 4-11 shows the end cap and the simplified model for derivation of the scaling function.

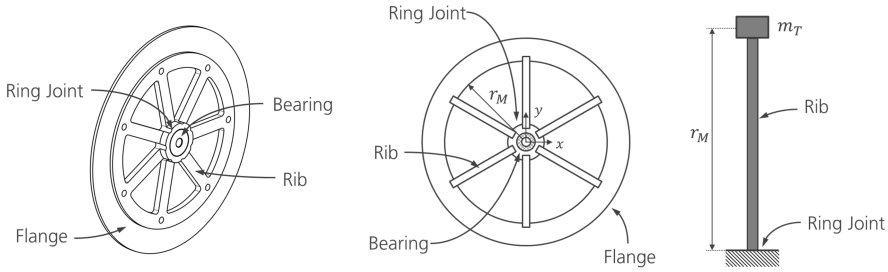

Figure 4-11: End cap of the Mast Spool consisting of a set of radial ribs connected by an inner ring and a circular flange (left), reduced model (middle) and simplified mechanical model of a single rib as a fixed beam with end mass (right).

For derivation of the scaling functions it is assumed that the scaling behavior of the end caps is dominated by the radial ribs as these determine the dynamic behavior and transfer the loads from the central cylinder to the axle. The ribs are idealized as beams with a root that is fixed at the ring joint and an end mass m_T. The end mass corresponds the sum of the central cylinder mass m_{MSC} and mast mass m_M reduced by the number of ribs n_{rib}.
In the scaling function a scaling limit is considered for the small scale region in the form of a minimum cross-sectional rib dimension.

Based on the above described model again two separate scaling functions are derived for the eigenfrequency requirement f_{req} and the inertial load requirement a_{acc}. For each calculation point the function values are compared and the higher mass is selected.
Equation 4-17 gives the mass scaling function $m_{MSE,f}$ of a single end cap derived for the eigenfrequency requirement (see Appendix B1.2):

$$m_{MSE,f} = k_{MSE,m} n_{rib} \left(\Phi + \sqrt{\Phi^2 + \frac{1}{0.23} \Phi \frac{m_{MSC} + m_M}{n_{rib}}} \right) \qquad 4\text{-}17$$

$$\Phi = \frac{0.23}{2} \frac{4\pi^2}{3} \frac{k_\rho^2 \rho^{*2}}{E} \frac{k_A}{k_I} k_f f_{req}^2 r_M^5$$

Equation 4-18 gives the mass scaling function $m_{MSE,a}$ of a single end cap derived for the inertial load requirement (see Appendix B1.2):

$$m_{MSE,a} = k_{MSE,m} n_{rib} k_\rho k_A \rho^* \left(u + v - \frac{a}{3} \right)^2 r_M \qquad 4\text{-}18$$

$$u = \sqrt[3]{-\left(\frac{a}{3}\right)^3 - \frac{c}{2} + \sqrt{\frac{1}{27} a^3 c + \frac{1}{4} c^2}}$$

$$v = \sqrt[3]{-\left(\frac{a}{3}\right)^3 - \frac{c}{2} - \sqrt{\frac{1}{27}a^3c + \frac{1}{4}c^2}}$$

$$a = -\frac{1}{2}\frac{k_y}{k_I}\frac{k_\rho \rho^*}{\sigma_{crit}} k_a a_{acc} r_M^2$$

$$c = -\frac{k_y}{k_I k_A}\frac{1}{\sigma_{crit}}\frac{m_{MSC} + m_M}{2n_{rib}} k_a a_{acc} r_M$$

The scaling functions are dependent on the design variables of the Deformable Structure through the length of the ribs that equals the masts reeling radius r_M and the tip mass term that includes the mast mass m_M.

The mass efficiency of the end cap can be influenced through the beam architecture and material parameters of the ribs as described above for the stringers of the central Mast Spool Cylinder.

Table 4-7 gives the parameters that are included in the end cap scaling functions. Detailed description of the derivation of the scaling functions is given in the Appendix B1.2.

Parameter	Symbol	Unit	Value	Remarks
Mast reeling radius	r_M	m	Input value	Depending on mast design variables A and R
Mast mass	m_M	kg	Input value	Depending on mast design variables A and R
Central cylinder mass	m_{MSC}	kg	Input value	Depending on mast design variables A and R
Number of ribs	n_{rib}	-	6	
Material density	ρ^*	kg/m³	2700	
Material modulus	E	N/m²	70 GPa	
Material critical stress	σ_{crit}	N/m²	200 MPa	
Beam density factor	k_ρ	-	1	Stiffened beam
Beam cross-section factor	k_A	-	0.8	Stiffened beam
Beam moment of area factor	k_I	-	0.417	Stiffened beam
Beam neutral layer factor	k_y	-	1.5	Stiffened beam
Flange and joint mass factor	$k_{MSE,m}$	-	1.3	
Eigenfrequency requirement adjustment factor	k_f	-	1.5	
Acceleration load adjustment factor	k_a	-	1.5	
Lateral acceleration	a_{acc}	m/s²	30 g	
First eigenfrequency	f_{req}	Hz	100	

Table 4-7: Summary of the parameters of the mass scaling functions of the Mast Spools End Caps.

4.3.2.3. Spool Axle

The Spool Axle is a circular rod whose length is dependent on the flattened width of the mast b_M and the width of the end caps and the mounting points in the support structure considered by a factor $k_{MSA,m} > 1$. The diameter of the axle is derived from a maximum shear stress τ_{max} that shall not be exceeded when subjected to an acceleration a_{acc}. The eigenfrequency requirement is not considered for sizing of the axle as the supporting points of the end caps are close to the mounting points.
A scaling limit is introduced for the small scale region through definition of a minimum axle diameter that reflects the availability, manufacturing, handling and integration restrictions.

Equation 4-19 gives the mass scaling function m_{MSA} of the Spool Axle (see Appendix B1.3):

$$m_{MSA} = \frac{\rho}{\tau_{max}}(m_M + m_{MSC} + 2m_{MSE})k_a a_{acc} k_{MSA,m} b_M \qquad 4\text{-}19$$

The scaling function for the Mast Spool Axle is dependent on the design variables of the Deformable Structure through the mass terms of the mast m_M, Spool Cylinder m_{MSC} and end caps m_{MSE} as well as the width of the flattened mast b_M.
The mass efficiency of the axle can be adjusted through selection of the material that is expressed by the density ρ and maximum shear stress τ_{max}.
Table 4-8 lists the scaling function parameters of the Mast Spool Axle. Detailed description of the derivation of the scaling functions is given in the Appendix B1.3.

Parameter	Symbol	Unit	Value	Remarks
Mast flattened width	b_M	m	Input value	Depending on mast design variables A and R
Mast mass	m_M	kg	Input value	Depending on mast design variables A and R
Central cylinder mass	m_{MSC}	kg	Input value	Depending on mast design variables A and R
End cap mass	m_{MSE}	kg	Input value	Depending on mast design variables A and R
Material density	ρ	kg/m³	7800	
Maximum shear stress	τ_{max}	N/m²	150 MPa	
Mass amplification factor to account for higher length	$k_{MSA,m}$	-	1.2	
Acceleration load adjustment factor	k_a	-	1.5	
Lateral acceleration	a_{acc}	m/s²	30 g	

Table 4-8: Summary of the parameters of the mass scaling functions of the Mast Spools Axle.

4.3.3.Spool Brake Mechanism

The Spool Brake Mechanism counters the spring effect of the stowed mast to avoid self-deployment. The brake is similar designed to a free-wheel clutch with an outer Tooth Ring, spring loaded Brake Arms, a mounting plate for the arms and several screw connector elements (see subsection 4.3.8). Its design is driven by the mast spring moment M_{Mr} that needs to be countered and the dimensions of the Mast Spool to which the brake is attached. The outer radius of the circular Brake Mechanism equals the reeling radius r_M of the mast which coincides with the cylinder radius of the Mast Spool. The main dimensions of all other Brake Mechanism subcomponents are linearly scaled in relation to the reeling radius on the basis of geometrical ratios extracted from the baseline Brake Mechanism design. Figure 4-12 shows the subcomponents of the Brake Mechanism and the simplified model that is the basis for derivation of the scaling functions. The scaling functions for the Brake Mechanism components are addressed in Appendix B2.

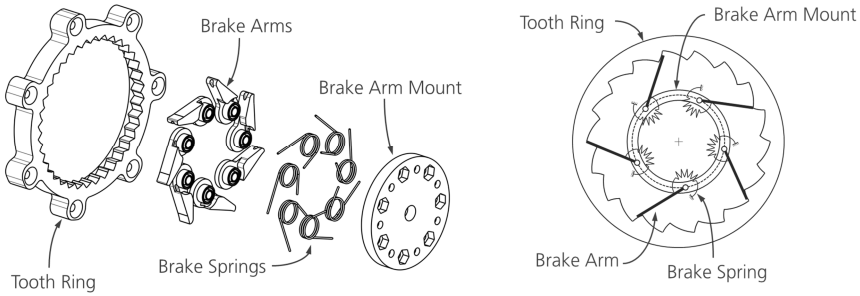

Figure 4-12: Main component elements of the Mast Spool brake (left) and sketch of the simplified model for scaling function derivation (right).

4.3.3.1. Tooth Ring

The outer Tooth Ring possesses several teeth on the inside for generation of the brake moment. Figure 4-13 shows the ring and its simplified model.

Figure 4-13: Tooth Ring of the spool brake (left) and simplified model (right).

As introduced beforehand the outer radius coincides with the mast reeling radius r_M. For derivation of the scaling function all dimensions are linearly scaled in relation to the reeling radius by according size ratios except for the height of the ring. These ratios are derived from the baseline Brake Mechanism design that is taken as a role model. The height of the ring is derived in a different way from an allowable line pressure $p_{t,max}$ at the contact area between Tooth Ring and spring loaded Brake Arms (see also subsection 4.3.3.4).
A scaling limit is applied for the minimum height of the Tooth Ring that shall not be exceeded.

Equation 4-20 gives the mass scaling function m_{SBT} of the Tooth Ring of the Spool Brake Mechanism (see Appendix B2.4):

$$m_{SBT} = \pi \frac{1}{\Gamma_{lla}} \left(1 - \left(\frac{\Gamma_{rta} + \Gamma_{rti}}{2}\right)^2\right) \frac{M_{cs}}{p_{t,max}} \rho r_M \qquad 4\text{-}20$$

It is noticeable that the mass scaling function is not dependent on any load case requirements. The design variables of the Deformable Structure are represented through the reeling radius r_M and the spring moment M_{cs} that depends on the masts spring moment M_{Mr} (see Appendix B2.2, B2.3 and Tab. B - 8).
The mass efficiency of the Tooth Ring can be influenced through the material selection expressed by the density ρ and the allowable line pressure $p_{t,max}$. Furthermore adjustment of the geometry ratios Γ_{rta}, Γ_{rti} and Γ_{lla} allows influencing the component mass but the influence on the Brake Mechanism components needs to be considered.
Table 4-9 summarizes the parameters of the spool brake Tooth Ring of the Spool Brake Mechanism. Detailed description of the derivation of the scaling functions is given in the Appendix B2.4.

Parameter	Symbol	Unit	Value	Remarks
Mast reeling radius	r_M	m	Input value	Depending on mast design variables A and R
Spring moment	M_{cs}	Nm	Input value	Depending on mast design variables A and R thorugh mast spring moment M_{Mr} (see Tab. B - 8)
Material density	ρ	kg/m³	2700	
Allowable line pressure	$p_{t,max}$	N/m	1000	
Ratio of outer tooth radius to mast reeling radius	Γ_{rta}	-	0.88	
Ratio of inner tooth radius to mast reeling radius	Γ_{rti}	-	0.82	
Ratio of Brake Arm length to mast reeling radius	Γ_{lla}	-	0.52	

Table 4-9: Summary of the parameters of the mass scaling functions of the Tooth Ring of the Spool Brake Mechanism.

4.3.3.2. Brake Arm Mount

The Brake Arm Mount is utilized for mounting of the Brake Arms and is a ring with several threaded holes. It is attached to the surrounding support structure while the Tooth Ring is mounted to the Mast Spool. Figure 4-14 shows the Brake Arm Mount and its simplified model.

Figure 4-14: Mounting ring for the Mast Spool Brake Arms (left) and simplified model with main parameters (right).

The scaling function of the Brake Arm is derived in the same way as the Tooth Ring through definition of size ratios derived from the baseline Spool Brake Mechanism design that relate all dimensions to the masts reeling radius r_M. The height of the ring is set equal to the height of the Tooth Ring.

Equation 4-21 gives the mass scaling function m_{SBM} of the Brake Arm Mount of the Spool Brake Mechanism (see Appendix B2.5):

$$m_{SBM} = 4\pi \frac{\Gamma_{rla}\Gamma_{rcs}}{\Gamma_{lla}} \frac{M_{cs}}{p_{t,max}} \rho r_M \qquad 4\text{-}21$$

The mass scaling function is similar to that of the Tooth Ring and is also dependent on the design variables of the Deformable Structure through the reeling radius r_M and the spring moment M_{cs}. Influencing the mass efficiency can again be done through selection of the size ratios and material.

Table 4-9 lists all parameters of the Brake Arm Mount scaling function. Detailed description of the derivation of the scaling functions is given in the Appendix B2.5.

Parameter	Symbol	Unit	Value	Remarks
Mast reeling radius	r_M	m	Input value	Depending on mast design variables A and R
Spring moment	M_{cs}	Nm	Input value	Depending on mast design variables A and R thorugh mast spring moment M_{Mr} (see Tab. B - 8)
Material density	ρ	kg/m³	2700	
Allowable line pressure	$p_{t,max}$	N/m	1000	

Ratio of mount radius to mast reeling radius	Γ_{rla}	-	0.5
Ratio of mount width to mast reeling radius	Γ_{rcs}	-	0.12
Ratio of Brake Arm length to mast reeling radius	Γ_{lla}	-	0.52

Table 4-10: Summary of the parameters of the mass scaling functions of the Brake Arm Mount of the Spool Brake Mechanism.

4.3.3.3. Spring Loaded Brake Arms

A set of spring loaded Brake Arms generates the brake moment by gearing into the outer Tooth Ring. The Brake Arms are equipped with springs that apply the required moment to generate the braking torque. Figure 4-15 displays the set of Brake Arms with mounted springs and the simplified model for derivation of the scaling function.

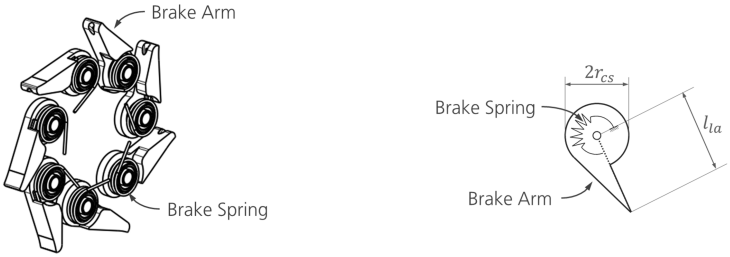

Figure 4-15: Set of spring loaded Brake Arms that generate the braking torque (left) and simplified model of a single Brake Arm and spring with main parameters (right).

The shape of the Brake Arms is determined in the same way as for the Tooth Ring and the Brake Arm Mount through size ratios that cause linear scaling of the arm with the mast reeling radius r_M. The height is the same as for the Tooth Ring.

Equation 4-22 gives the mass scaling function m_{SBA} of the Brake Arm of the Spool Brake Mechanism (see Appendix B2.6):

$$m_{SBA} = n_{la}\frac{1}{\Gamma_{lla}}\left(\frac{1}{2}\Gamma_{lla}\Gamma_{rcs} + \pi\Gamma_{rcs}^2\right)\frac{1}{p_{t,max}}M_{cs}\rho r_M \qquad 4\text{-}22$$

In accordance with the previous scaling functions, the Brake Arm scaling function consists largely of size ratios and is dependent on the Deformable Structures design variables through the reeling radius r_M and the spring moment term M_{cs}. Means to influence the component mass efficiency are again adjustment of the size ratios and selection of the material but also the number of Brake Arms n_{la}.

Table 4-11 lists the parameters of the Brake Arm scaling function. Detailed description of the derivation of the scaling functions is given in the Appendix B2.6.

Parameter	Symbol	Unit	Value	Remarks
Mast reeling radius	r_M	m	Input value	Depending on mast design variables A and R
Spring moment	M_{cs}	Nm	Input value	Depending on mast design variables A and R through mast spring moment M_{Mr} (see Tab. B - 8)
Number of Brake Arms	n_{la}	-	7	
Material density	ρ	kg/m³	2700	
Allowable line pressure	$p_{t,max}$	N/m	1000	
Ratio of mount width to mast reeling radius	Γ_{rcs}	-	0.12	
Ratio of Brake Arm length to mast reeling radius	Γ_{lla}	-	0.52	

Table 4-11: Summary of the parameters of the mass scaling functions of the Brake Arms of the Spool Brake Mechanism.

4.3.3.4. Brake Springs

The Brake Springs are attached to the Brake Arms and press these into the Tooth Ring whereby the required braking torque to avoid self-deployment of the stowed mast is generated. Therefore, the spring dimensions are depending on the required braking torque that equals the masts spring moment M_{Mr} and are not solely dependent on certain size ratios.

Equation 4-23 gives the mass scaling function m_{SBS} of the Brake Springs of the Spool Brake Mechanism formulated with sub functions for the spring wire diameter d_{cs} and number of coils of each spring n_{cs} (see Appendix B2.7):

$$m_{SBS} = \frac{\pi}{4} n_{la} d_{cs}^2 (2\Gamma_{lla} + 2\pi n_{cs} \Gamma_{rcs}) \rho r_M \qquad 4\text{-}23$$

$$d_{cs} = \left(\frac{32}{\pi} \frac{\Phi_{B,1}}{\Phi_{B,2}\Phi_{B,3}} \frac{1}{(n_{la}-1)} \frac{1}{\sigma_{cs,crit}} k_B M_{Mr} \right)^{\frac{1}{3}}$$

$$n_{cs} = \left(\frac{1}{2\pi^4} \frac{\Phi_{B,1}^4}{\Phi_{B,2}\Phi_{B,3}} \frac{1}{(n_{la}-1)} \frac{E^3}{\sigma_{cs,crit}^4} k_B M_{Mr} \frac{1}{r_M^3} \right)^{\frac{1}{3}}$$

$$\Phi_{B,1} = \frac{1}{\Gamma_{rcs}} \left(\pi - \arccos\left(\frac{\Gamma_{rla}^2 + \Gamma_{lla}^2 - \Gamma_{rti}^2}{2\Gamma_{rla}\Gamma_{lla}} \right) + \gamma_{la,0} \right)$$

$$\Phi_{B,2} = \left(\pi - \arccos\left(\frac{\Gamma_{rla}^2 + \Gamma_{lla}^2 - \frac{1}{4}(\Gamma_{rti} + \Gamma_{rta})^2}{2\Gamma_{rla}\Gamma_{lla}} \right) + \gamma_{la,0} \right)$$

$$\Phi_{B,3} = \frac{\Gamma_{lla}^2 + \frac{1}{4}(\Gamma_{rti} + \Gamma_{rta})^2 - \Gamma_{rla}^2}{2\Gamma_{lla}^2\Gamma_{rcs}}$$

The scaling function for the Brake Springs also largely depends on the size ratios of the Brake Mechanisms components. The Brake Springs are dependent on the Deformable Structure through the spring moment M_{Mr} and reeling radius r_M of the stowed mast.
The mass efficiency of the springs can be adjusted through selection of the spring wire material that is expressed by the material modulus E, density ρ and critical stress $\sigma_{cs,crit}$. Furthermore the mass can be influenced by according selection of the brake size ratios and the mounting angle of the springs $\gamma_{la,0}$.
Table 4-12 lists the parameters of the Brake Spring scaling function. Detailed description of the derivation of the scaling functions is given in the Appendix B2.7.

Parameter	Symbol	Unit	Value	Remarks
Mast reeling radius	r_M	m	Input value	Depending on mast design variables A and R
Mast spring moment	M_{Mr}	Nm	Input value	Depending on mast design variables A and R
Number of Brake Arms	n_{la}	-	7	
Material modulus	E	N/m²	210 GPa	
Material density	ρ	kg/m³	7800	
Maximum allowable stress	$\sigma_{cs,crit}$	N/m²	600 MPa	
Allowable line pressure	$p_{t,max}$	N/m	1000	
Brake moment amplification factor	k_B	-	1.5	
Ratio of mount width to outer brake radius	Γ_{rcs}	-	0.12	
Ratio of Brake Arm length to outer brake radius	Γ_{lla}	-	0.52	
Ratio of mount radius to outer brake radius	Γ_{rla}	-	0.5	
Ratio of inner tooth radius to outer brake radius	Γ_{rti}	-	0.82	
Ratio of outer tooth radius to outer brake radius	Γ_{rta}	-	0.88	
Spring initial mounting angle	$\gamma_{la,0}$	rad	π/4	

Table 4-12: Summary of the parameters of the mass scaling functions of the Brake Springs of the Spool Brake Mechanism.

4.3.4.Mast Root Support and Guidance

The deploying part of the mast is supported in the opening part by enclosing Support Plates. To enable unobstructed entering of these plates Guide Rolls are installed where the mast comes off the spool to ensure proper alignment. The dimensions of the Support Plates and Guide Rolls are determined by the form of the stowed and deploying mast and they are sized according to requirements of the load case of space transport. As both subcomponents do have to support only their own weight, it is assumed that their mass will be relatively low and their design dominated by stiffness requirements. Hence, the scaling functions are developed for the eigenfrequency requirement f_{req}. Scaling functions for the mast root support and guidance components are addressed in Appendix B3.

4.3.4.1. Support Plates

The Support Plates possess the form of the deploying mast to constrain its lateral motion during deployment and under load. They are attached to the surrounding mechanism support structure by planar mounting brackets. The Support Plates and the simplified model are displayed in Figure 4-16.

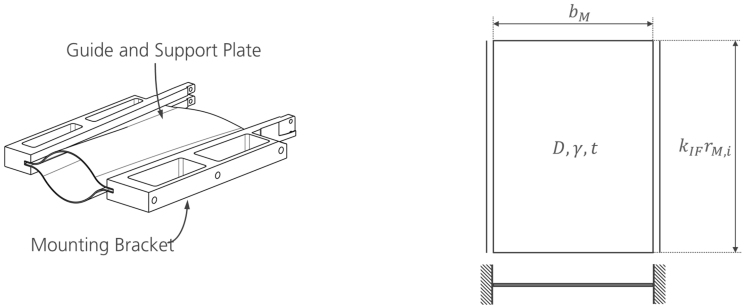

Figure 4-16: Guide and Support Plates of the mast with mounting brackets (left) and simplified model of a single plate with fixed longitudinal edges (right).

The Support Plates and the mounting brackets are idealized as two stacked plates that are fixed along their longitudinal edges by the Deployment Mechanism support structure to which they are attached. The width of the plates is determined by the width of the flattened mast b_M. Their length is the required supported length of the mast root that is predefined for each mast type in terms of multiples k_{IF} of the masts radius of gyration $r_{M,i}$ (see also subsection 4.3.6). The plate thickness results from sizing according to the eigenfrequency requirement f_{req} of the load case of space transport.
A scaling limit is applied in the form of a minimum plate thickness that results from manufacturing limits and depends on the plate architecture.

Equation 4-24 gives the mass scaling function m_{MGS} of the Support Plates (see Appendix B3.1):

$$m_{MGS} = \left(4\pi^2 \frac{1}{k_C^4} \frac{k_m^3}{k_D} \frac{k_\rho^3 \rho^{*3}}{E} \left(k_{IF} r_{M,i}\right)^2 b_M^6 k_f^2 f_{req}^2\right)^{\frac{1}{2}} \quad 4\text{-}24$$

The scaling function depends on the design variables of the Deformable Structure through the length depending on the mast radius of gyration $r_{M,i}$ and width b_M which result from the stowed form of the mast.

Means to influence the mass efficiency of the plates are the selection of plate architecture described through the parameters k_m and k_D (see Appendix A3.1), plate mounting conditions through parameter k_C and plate material expressed through the Young's modulus E and density ρ^*. For the selection of the plate architecture, in the small scale region also the different scaling limits need to be considered as e.g. a solid plate can be realized thinner than a sandwich or stiffened plate.

Table 4-13 summarizes the parameters included in the Support Plate scaling function. Detailed description of the derivation of the scaling functions is given in the Appendix B3.1.

Parameter	Symbol	Unit	Value	Remarks
Mast radius of gyration	$r_{M,i}$	m	Input value	Depending on mast design variables A and R
Mast flattened width	b_M	m	Input value	Depending on mast design variables A and R
Material modulus	E	N/m²	60 GPa	
Material density	ρ	kg/m²	1600	
Eigenfrequency requirement	f_{req}	Hz	100	
Mast-mechanism interface factor	k_{IF}	-	5	
Eigenfrequency amplification factor	k_f	-	1.5	
Plate boundary factor	k_C	-	4.73	Fixed edges
Density factor	k_ρ	-	50/1600	Sandwich architecture
Plate architecture mass factor	k_m	-	0.111	Sandwich architecture
Plate rigidity architecture factor	k_D	-	0.0125	Sandwich architecture

Table 4-13: Summary of the parameters of the mass scaling functions of the Support Plates.

4.3.4.2. Guide Rolls

A set of two Guide Rolls ensures that the mast enters the Support Plates in the correct alignment when it comes off the spool. Each spool consists of a roller, two bearings

and an axle. Figure 4-17 shows the Guide Roll and the simplified model for derivation of the scaling function.

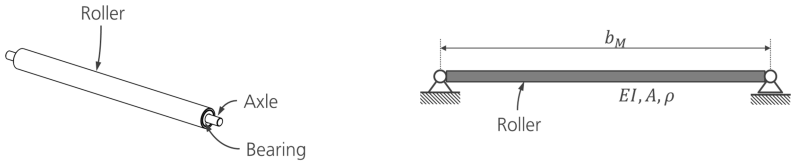

Figure 4-17: Guide Roll of the flattened mast with axle and roller (left) and simplified model as a simply supported beam (right).

The Guide Roll is idealized as a tubular beam with simply supported ends and no external loading. The length of the Guide Roll depends on the flattened width of the mast b_M and its radius is sized according to the eigenfrequency requirement of the load case of space transport.
A scaling limit is defined in the small scale region for the minimum radius of the roller to account for manufacturing limits.

Equation 4-25 gives the mass scaling function of the Guide Roll m_{MGR} (see Appendix B3.2):

$$m_{MGR} = \frac{4}{\pi^2} k_{MGR,m} \frac{k_A}{k_I} \frac{k_\rho^2 \rho^{*2}}{E} b_M^5 k_f^2 f_{req}^2 \qquad 4\text{-}25$$

The scaling function is dependent on the Deformable Structure and its design variables through its length that results from the flattened width of the mast b_M. The mass of the axle is considered by a linear mass amplification factor $k_{MGR,m}$ as the axle loading scales with the roller mass.
The mass efficiency of the Guide Roll can be influenced through the material selection expressed by the Young's modulus E and the density ρ^* and the roller architecture represented by the beam parameters k_A, k_I and k_ρ (see Appendix A1.1).
Table 4-14 lists the parameters of the Guide Roll scaling function. Detailed description of the derivation of the scaling functions is given in the Appendix B3.2.

Parameter	Symbol	Unit	Value	Remarks
Mast flattened width	b_M	m	Input value	Depending on mast design variables A and R
Material modulus	E	N/m²	70 GPa	
Material density	ρ^*	kg/m³	2700	
Eigenfrequency requirement	f_{req}	Hz	100	
Mass amplification factor to account for axle mass	$k_{MGR,m}$	-	1.2	
Beam cross-section factor	k_A	-	0.2π	Circular tube
Beam moment of area	k_I	-	0.5	Circular tube

factor				
Beam density factor	k_ρ	-	1	Circular tube
Eigenfrequency adjustment factor	k_f	-	1.5	≥ 1

Table 4-14: Summary of the parameters of the mass scaling function of the Guide Roll.

4.3.5.Drive Mechanism

The Drive Mechanism generates and introduces the required forces necessary for deployment of the mast. It consists of an electric motor, a gear, a Belt Spool and a belt. The belt is co-coiled with the mast on the Mast Spool and introduces the deployment forces generated by the motor. Sizing of the subcomponents is depending on the required deployment forces that need to be generated and transmitted. For calculation of the torque the gear-motor also the gear ratio of the secondary transmission caused by coiling of the belt on the Belt Spool needs to be considered. Hence, sizing of the belt and Belt Spool needs to be done beforehand. Scaling functions for the Drive Mechanism are addressed in Appendix B4.

4.3.5.1. Belt

The belt is a thin cord that is co-coiled with mast on the Mast Spool. By applying a pulling force to the belt the same force is applied to the mast and causes its deployment. Due to reeling of the belt on the boom spool and the much smaller Belt Spool that is attached to the gear motor, the belt has to comply with significant elastic deformation. The belt in its integrated form in the Deployment Mechanism and the simplified model for derivation of the scaling function are displayed in Figure 4-18.

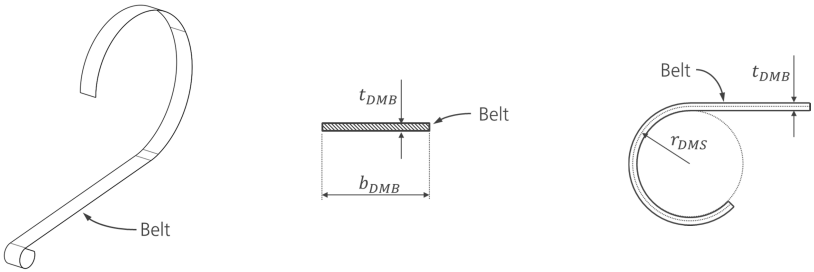

Figure 4-18: Belt in its assembled shape (left), and model for dimensioning (middle and right).

The belt is sized by the stress in the material that is caused by the pulling force that needs to be transmitted and the elastic deformation when the belt is coiled on the Belt Spool.

Equation 4-26 gives the mass scaling function of the belt m_{DMB} (see Appendix B4.1):

$$m_{DMB} = \frac{F_{S,\varepsilon,B}}{\Gamma_{\varepsilon,P,B}} \frac{\rho}{E\varepsilon_{max}} L_{req} P \qquad 4\text{-}26$$

The dependency of the belt scaling function on the properties and design variables of the Deformable Structure is related to the selection of the deployment force requirement P. Here the deployment force is set equal to the required column compression strength P_{req} wherefore there is no direct design relation to the Deformable Structure.

The mass efficiency of the belt is adjustable through the material selection expressed by the Young's modulus E, the material density ρ and the allowable elastic strain ε_{max} as well as the belt cross-sectional size ratio $\Gamma_{\varepsilon,P,B}$ which relates the belt thickness to its width.

The parameters of the belt scaling function are given in Table 4-15. Detailed description of the derivation of the scaling functions is given in the Appendix B4.1.

Parameter	Symbol	Unit	Value	Remarks
Deployment force	P	N	Input value	Potentially depending on mast design variables A and R
Mast length	L_{req}	m	Input value	
Material modulus	E	N/m²	210 GPa	
Material density	ρ	kg/m³	7800	
Maximum allowable strain	ε_{max}	-	0.008	
Factor of safety	$F_{S,\varepsilon,B}$	-	2	
Belt strain ratio	$\Gamma_{\varepsilon,P,B}$	-	0.25	

Table 4-15: Summary of the parameters of the mass scaling function of the belt.

4.3.5.2. Belt Spool

The Belt Spool is attached to the gear-motor and transmits the deployment force to the belt through coiling. The spool consists of a central cylinder with two end-caps that prevent the belt to slip off the spool. Its design and simplified model for derivation of the scaling function is displayed in Figure 4-19.

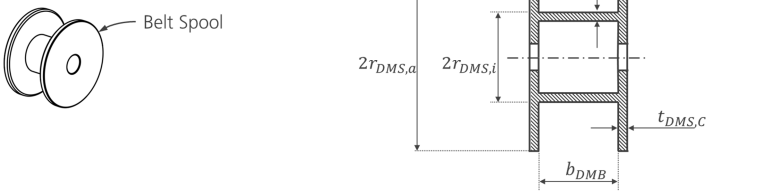

Figure 4-19: Spool for winding of the belt (left) and cross-sectional view with main geometric parameters (right).

The Belt Spool is idealized as a hollow spool with thin-walled central cylinder and end caps. The wall thicknesses are scaled linearly through according size ratios that are extracted from the baseline Belt Spool design. The spool is sized depending on the belt dimensions and the belts minimum reeling radius which is related to the allowable reeling strain.

Equation 4-27 gives the scaling function of the Belt Spool (see Appendix B4.2):

$$m_{DMS} \approx 2\pi \left(k_{DMS,ra}^2 \left(\frac{1}{4} \frac{F_{S,\varepsilon,B}^2}{\left(1 - \Gamma_{\varepsilon,P,B}\right)^2} \Upsilon + \frac{1}{\pi} L_{req} \sqrt{\Upsilon} \right)^2 \frac{\Gamma_{t,E}}{\Gamma_b} \sqrt{\Upsilon} + \frac{\Gamma_{t,C}}{\Gamma_b^2} \sqrt{\frac{F_{S,\varepsilon,B}^2}{4\left(1 - \Gamma_{\varepsilon,P,B}\right)^2} \Upsilon^3} \right) \rho \qquad 4\text{-}27$$

$$\Upsilon = \Gamma_b \frac{F_{S,\varepsilon,B}}{\Gamma_{\varepsilon,P,B}} \frac{P}{E \varepsilon_{max}}$$

Just like the belt, the Belt Spool scaling function is not necessarily related to the design of the Deformable Structure which depends on the definition of the pulling force P.
The mass efficiency of the spool can be influenced through selection of the spool material expressed by the material density ρ as well as the spool architecture defined by the wall thickness coefficients for the end caps and central cylinder $\Gamma_{t,E}$ and $\Gamma_{t,C}$.
Table 4-16 lists the parameters of the Belt Spool scaling function. Detailed description of the derivation of the scaling functions is given in the Appendix B4.2.

Parameter	Symbol	Unit	Value	Remarks
Deployment force	P	N	Input value	Potentially depending on mast design variables A and R
Mast length	L_{req}	m	Input value	
Belt Spool density	ρ	kg/m³	2700	
Belt material modulus	E	N/m²	210 GPa	
Belt allowable elastic strain	ε_{max}	-	0.008	
Belt volume factor	$k_{DMS,ra}$	-	1.5	≥ 1
Belt factor of safety	$F_{S,\varepsilon,B}$	-	2	
Belt thickness ratio	Γ_b	-	0.0025	
Belt strain ratio	$\Gamma_{\varepsilon,P,B}$	-	0.25	
Belt Spool End Cap wall thickness ratio	$\Gamma_{t,E}$	-	0.05	
Belt Spool central cylinder wall thickness ratio	$\Gamma_{t,C}$	-	0.05	

Table 4-16: Summary of the parameters of the mass scaling function of the Belt Spool.

4.3.5.3. Gear

The gear generates the high torque at low rpms that are required for the deployment process. The required torque results from the desired deployment force and the dimensions of the Belt Spool. As the gear is a complex assembly the scaling function is not derived directly through parameterization of its subcomponents. Instead commercially available products that are suited for high vacuum or space applications are reviewed regarding their mass and operation torque. Figure 4-20 shows the gear data derived from catalogue data of the companies Maxon Motor GmbH [141] and Dr. Fritz Faulhaber GmbH & Co. KG [142].

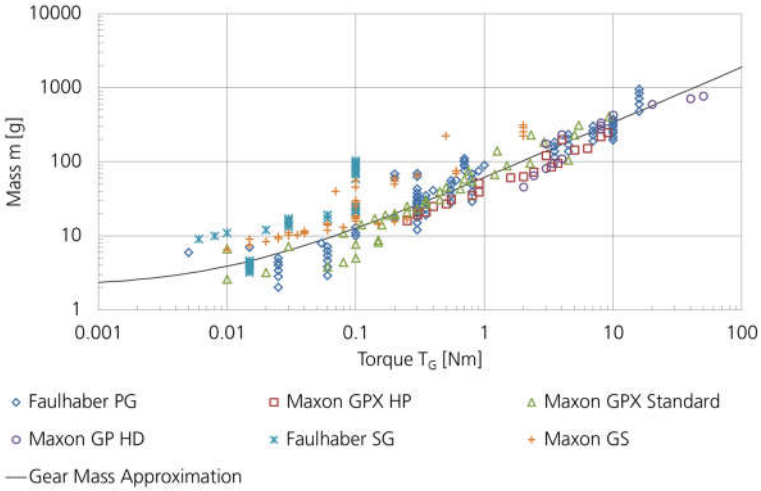

Figure 4-20: Gear mass plotted over output torque of commercially available gears suited for high vacuum and space applications [141] [142].

Equation 4-28 gives the scaling function of the gear that relates gear mass m_{DMG} to the output torque T_G through approximation of the gear data by a power function (see Appendix B4.3):

$$m_{DMG} = \xi_{G,1} T_G^{\xi_{G,2}} + \xi_{G,3} \qquad 4\text{-}28$$

The scaling function includes a scaling limit in terms of a minimum gear mass represented by the coefficient $\xi_{G,3}$ that is set equal to the gear with the lowest mass found in the review. The coefficients $\xi_{G,1}$ and $\xi_{G,2}$ can be adjusted to represent more mass efficient gears but by the expense of potential candidate products especially for high transmission ratios.

The require output torque T_G results from the dimensions of the Belt Spool, the belt and the required deployment force. The gear torque scaling function is given by Equation 4-29 (see Appendix B4.3 :

$$T_G = \left(\frac{1}{4} \Gamma_b \frac{F_{S,\varepsilon,B}^3}{\Gamma_{\varepsilon,P,B}\left(1-\Gamma_{\varepsilon,P,B}\right)^2} \frac{1}{E\varepsilon_{max}^3} P^3 + \left(\frac{1}{\pi^2} \Gamma_b \frac{F_{S,\varepsilon,B}}{\Gamma_{\varepsilon,P,B}} \frac{1}{E\varepsilon_{max}} P^5 L_{req}^2 \right)^{\frac{1}{2}} \right)^{\frac{1}{2}} \quad 4\text{-}29$$

Table 4-17 lists the parameters of the gear mass and torque scaling functions. Detailed description of the derivation of the scaling functions is given in the Appendix B4.3.

Parameter	Symbol	Unit	Value	Remarks
Deployment force	P	N	Input value	Potentially depending on mast design variables A and R
Mast length	L_{req}	m	Input value	
Liner mass approximation coefficient	$\xi_{G,1}$	$\frac{\text{g}}{(\text{Nm})^{\xi_{G,2}}}$	60	
Power mass approximation coefficient	$\xi_{G,2}$	-	0.75	
Constant mass approximation coefficient	$\xi_{G,3}$	g	2	
Belt material modulus	E	N/m²	210 GPa	
Belt allowable elastic strain	ε_{max}	-	0.008	
Belt thickness ratio	Γ_b	-	0.0025	
Belt strain ratio	$\Gamma_{\varepsilon,P,B}$	-	0.25	
Belt factor of safety	$F_{S,\varepsilon,B}$	-	2	

Table 4-17: Summary of the parameters of the gear torque and mass scaling functions.

4.3.5.4. Electric Motor

The mass scaling function for the electric motor is derived in the same way as the gear scaling function through review of catalogue data of electric motors that are suited for high vacuum or space applications. Figure 4-21 shows the catalogue data of electric motors of the companies Maxon Motor GmbH [141], Dr. Fritz Faulhaber GmbH & Co. KG [142] and Phytron GmbH [143].

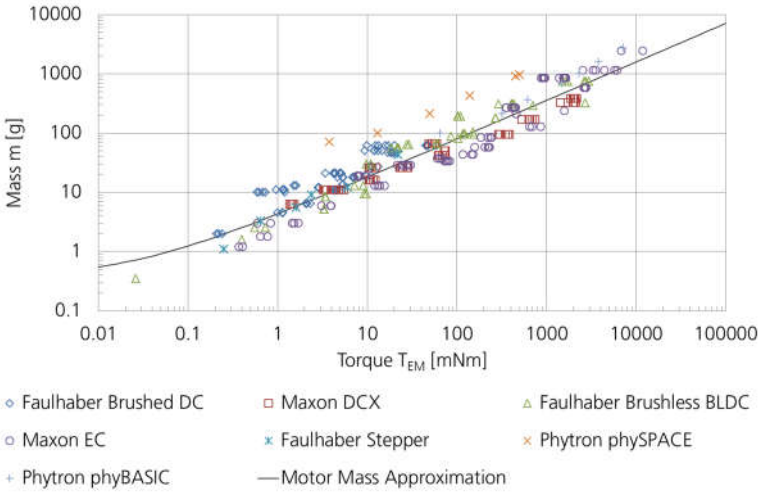

Figure 4-21: Motor mass plotted over output torque for commercially available electric motors suited for high vacuum and space applications.

Equation 4-30 gives the scaling function of the electric motor that relates motor mass m_{DMM} to the output torque T_{EM} through approximation of the motor data by a power function (see Appendix B4.4):

$$m_{DMM} = \chi_{EM,1} T_{EM}^{\chi_{EM,2}} + \chi_{EM,3} \qquad 4\text{-}30$$

$$T_{EM} = \frac{1}{\eta_G} \frac{T_G}{k_G}$$

The required motor output torque T_{EM} is dependent on the required gear output torque T_G through the gear ratio k_G and the gear efficiency factor η_G.

lists the parameters of the gear mass and torque scaling functions. Detailed description of the derivation of the scaling functions is given in the Appendix B4.4.

Parameter	Symbol	Unit	Value	Remarks
Deployment force	P	N	Input value	Potentially depending on mast design variables A and R
Mast length	L_{req}	m	Input value	
Liner mass approximation coefficient	$\chi_{EM,1}$	$\frac{\text{g}}{(\text{mNm})^{\chi_{EM,2}}}$	4	
Power mass approximation coefficient	$\chi_{EM,2}$	-	0.65	
Constant mass	$\chi_{EM,3}$	g	0.35	

approximation coefficient				
Gear efficiency	η_G	-	55%	Potentially depending on mast design variables A and R
Gear ratio	k_G	-	1:300	

Table 4-18: Summary of the parameters of the electric motor torque and mass scaling functions.

4.3.6. Mechanical Support Structure

The Support Structure encloses the stowed mast and the other Deployment Mechanism components and provides the required structural support particularly during space transport. The box-shaped structure is composed of rectangular plates that are interconnected by bonded edge connectors. Figure 4-22 shows the design and the simplified model for derivation of the scaling function.

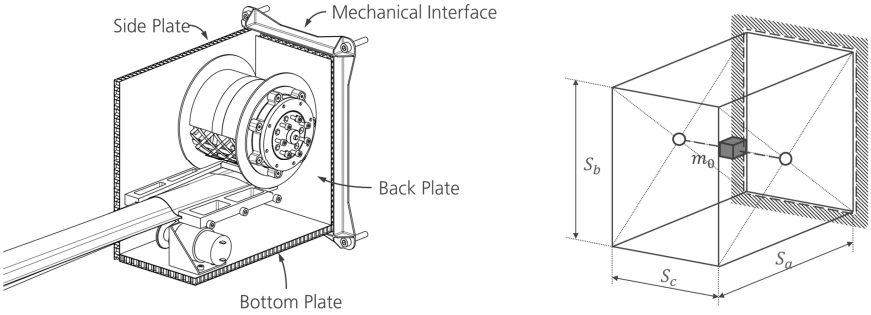

Figure 4-22: Mechanical Support Structure with removed side, top and front plate (left) and simplified model with remaining mechanism components concentrated in one central mass point that is attached to both side walls (right).

The structure scaling function is derived for the load case of space transport. The loads resulting from the inertial forces of the masses of the other mechanism components is accounted for by assuming that this mass is concentrated within a single mass point in the center of the box. Furthermore it is assumed that this mass is attached to the two side walls (see right side in Figure 4-22).

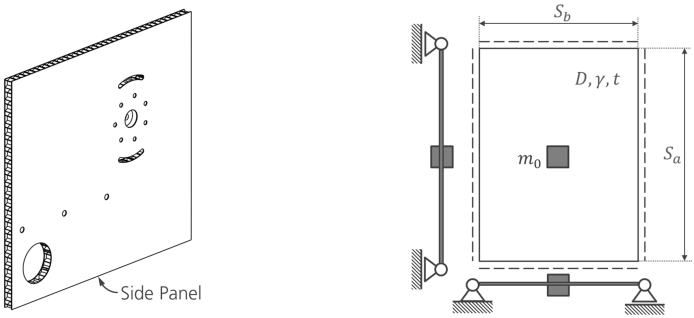

Figure 4-23: Side panel of the Support Structure realized as a sandwich panel with cut-outs and inserts (left) and simplified model of a plate with simply supported edges and point mass in its center (right).

For derivation of the scaling function it is assumed that the design is dominated by the stiffness requirements in the form of the minimum first eigenfrequency f_{req}. Furthermore it is assumed that the first eigenmode is a local mode of the highest loaded side walls which also are the largest panels of the box shaped structure. Hence, the support structure scaling function is developed based on the sizing of a side wall panel with an attached center mass according to the requirements of the load case of space transport. For calculation of the box mass it is assumed that all remaining panels possess the same composition, thickness and area mass. The dimensions of the panel are derived according to Figure 4-8.
A scaling limit is applied for the minimum thickness of the panel in the small scale region. Different scaling limits are defined depending on the specific panel architecture.

Equation 4-31 gives the scaling function of the support structure mass m_{SS} (see Appendix B5):

$$m_{SS} = \left(\frac{128}{\pi^2} k_m^3 \frac{(S_a S_b + S_a S_c + S_b S_c)^3}{S_a S_b \left(\frac{1}{S_a^2} + \frac{1}{S_b^2} \right)^2} \frac{(1-\nu^2) k_\rho^3 \rho^{*3}}{k_D E} f_{req}^2 m_0 \right)^{\frac{1}{3}} \qquad 4\text{-}31$$

The scaling function is dependent on the Deformable Structures properties and design variables through its dimensions S_a, S_b and S_c as well as the center mass m_0 which reflects the sum of the mast and mechanism component masses presented beforehand.
The mass efficiency of the support structure can be influenced through selection of the plate architecture parameters represented by the coefficients k_m and k_D and the panel material expressed by the Young's modulus E, Poisson ratio ν and the density ρ.

The parameters of the support structure scaling function are listed in Table 4-19. Detailed description of the derivation of the scaling functions is given in the Appendix B5.

Parameter	Symbol	Unit	Value	Remarks
Box length	S_a	m	Input value	Depending on mast design variables A and R
Box height	S_b	m	Input value	Depending on mast design variables A and R
Box width	S_c	m	Input value	Depending on mast design variables A and R
Supported center mass	m_0	kg	Input value	Depending on mast design variables A and R
Eigenfrequency requirement	f_{req}	Hz	100	
Material modulus	E	N/m²	60 GPa	
Reference density	ρ^*	kg/m³	1600	
Material Poisson's ratio	ν	-	0.3	
Density factor	k_ρ	-	100/1600	Sandwich Architecture
Plate stiffness factor	k_D	-	0.0125	Sandwich Architecture
Plate mass factor	k_m	-	0.111	Sandwich Architecture

Table 4-19: Summary of the parameters of the Support Structure scaling function.

4.3.7. Mechanical Interface

The interface of the Deployment Mechanism to the host spacecraft is a rectangular frame which is directly attached to the backside of the support structure box. It provides a flange with bolt holes for mounting of the structure. The design is displayed in Figure 4-24.

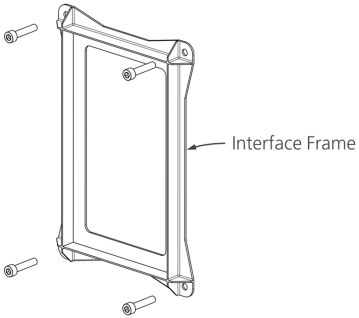

Figure 4-24: Mechanical interface frame for attachment to the host spacecraft.

The loading on the interface scales with the attached mechanism mass. In the following the interface mass is considered by a linear mass factor $k_{MI} > 1$ that is applied to the overall mechanism mass m_{all}. Equation 4-32 gives the interface mass m_{MI}:

$$m_{MI} = (1 - k_{MI}) m_{all} \qquad 4\text{-}32$$

4.3.8. Connector and Construction Elements

The Deployment Mechanism assembly utilizes some standard components such as bolted joints and bearings that may add a significant amount of mass as they often consist of steel or other high density materials. The baseline Deployment Mechanism design includes primarily screw connectors for component assemblies and ball bearings for rotating parts such as the Mast Spool or Guide Rollers. In the following the related scaling functions are presented.

4.3.8.1. Screw Connectors

The screw connector consists of a screw that is based on ISO 4762 and a threaded counterpart. The shape of the counterpart depends on the joining component and is different e.g. for a solid or sandwich panel. The simplified model for derivation of the scaling function is shown in Figure 4-25.

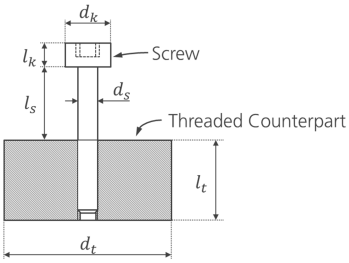

Figure 4-25: Model of a screw connection for scaling function derivation.

The size of the connector element depends on the loads that need to be transmitted. As the loading conditions can become complex here it is assumed that the connectors are sized by axial loads only. This axial load results from a lateral acceleration a_{acc} of the attached mass m_0 while it is assumed that corresponding shear loads are decoupled from the connectors e.g. by use of undercuts or bolts and bending loads are negligible. Furthermore, stresses from preloads on the screw are considered by adjustment of the critical stress σ_{crit}. The screw and thread dimensions are derived by size ratios as is done for the Brake Mechanism components.
A scaling limit is applied for the minimum screw size which results primarily from associated handling and integration issues.

Equation 4-33 gives the scaling function of a screw connection with a high strength counterpart such as a solid or stiffened metal plate that allows a direct attachment (see Appendix A5.2):

$$m_{CE} = \left(\frac{4}{\pi}\frac{a_{acc}^3 m_0^3}{\sigma_{crit}^3}\right)^{\frac{1}{2}} \rho_s \left(\Gamma_{dk}^2 \Gamma_{lk} + \Gamma_{ls} + \Gamma_{lt} + \Gamma_\rho \Gamma_{lt}\left(\Gamma_{dt}^2 - 1\right)\right) \quad 4\text{-}33$$

Equation 4-34 gives the scaling function of a screw connection with a low strength counterpart such as a sandwich that requires an insert for attachment (see Appendix A5.3):

$$m_{CE} = \left(\frac{4}{\pi}\frac{a_{acc}^3 m_0^3}{\sigma_{crit}^3}\right)^{\frac{1}{2}} \rho_s \left(\Gamma_{dk}^2 \Gamma_{lk} + \Gamma_{ls} + \Gamma_{lt} + \Gamma_\rho \Gamma_{lt}\left(\left(\frac{1}{4\Gamma_{lt}}\frac{\sigma_{crit}}{\tau_{crit}}\right)^2 - 1\right)\right) \quad 4\text{-}34$$

The mass of the screw connector can be influenced through selection of the screw material represented by its density ρ_s and critical stress σ_{crit} as well as the core material properties expressed by the critical shear stress τ_{crit} in case of a sandwich as counterpart.
Table 4-20 lists the scaling function parameters of the screw connector. Detailed description of the derivation of the scaling functions is given in the Appendix A5.

Parameter	Symbol	Unit	Value	Remarks
Attached mass	m_0	kg	Input value	
Lateral acceleration	a_{acc}	m/s²	30g	
Maximum allowable normal stress	σ_{crit}	N/m²	32 MPa	
Maximum allowable shear stress	τ_{crit}	N/m²	0.344 MPa	
Material density	ρ_s	kg/m³	7800	
Screw head diameter ratio	Γ_{dk}	-	7/4	
Screw head length ratio	Γ_{lk}	-	1	
Screw shaft ratio	Γ_{ls}	-	3	
Counterpart thread length	Γ_{lt}	-	3	
Counterpart thread diameter	Γ_{dt}	-	High strength: 21/5 Low strength: 11.6	
Material density ratio	Γ_ρ	-	27/78	

Table 4-20: Summary of the parameters of the screw connector scaling functions.

4.3.8.2. Ball Bearings

Ball bearings are required for many mechanism components with moving parts. The main elements of such a bearing regarding mass are the inner and outer bearing races and the balls in between. Figure 4-26 shows the ball bearing model that is used for derivation of the mass scaling function.

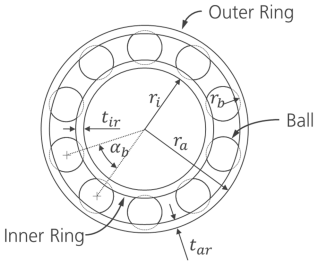

Figure 4-26: Model of a ball bearing for scaling function derivation.

Like the screw connectors and the Mast Spool brake, the sizes of the bearing elements are expressed through size ratios that are extracted from a role model. The primary dimension the ratios relate to is the radius of the corresponding axle which coincides with the bearings inner radius.
A scaling limit for the small size region is not applied as this is already done for the axles the bearings are attached to.

Equation 4-35 gives the mass scaling function of the ball bearing (see Appendix A6):

4-35

$$m = 2\pi\left(\left[\pi\left(\arcsin\left(\frac{\Gamma_b}{1+\frac{1}{2}\Gamma_t+\Gamma_b}\right)\right)^{-1}\right]\frac{2}{3}\Gamma_b^2 + (2+\Gamma_t+2\Gamma_b)\Gamma_t\Gamma_w\right)\Gamma_b\rho r_i^3$$

Table 4-21 lists the scaling function parameters. Detailed description of the derivation of the scaling function is given in the Appendix A6.

Parameter	Symbol	Unit	Value	Remarks
Axle radius	r_i	m	Input value	
Material density	ρ	kg/m³	7800	
Ball size ratio	Γ_b	-		
Bearing race thickness ratio	Γ_t	-		
Bearing width ratio	Γ_w	-		

Table 4-21: Summary of the parameters of the ball bearing scaling function.

4.3.9. Electronics

Electronic components are not included in the baseline Deployment Mechanism design as it is assumed that a motor control unit is provided by the host spacecraft and other electrical components are not considered. However, particularly a harness for power distribution, sensor connection and actuator and motor control may add significant mass in other designs.

4.4. Conclusions on Design Interdependencies between Deformable Structure and Deployment Mechanism

The inspection of the scaling functions of the Deployment Mechanism components show that they are strongly related in their design to the properties of the Deformable Structure. In particular its stowed form defines the accommodation, shape and size of most mechanism components. Thereby it is possible to parameterize the mechanism components and formulate its scaling functions on the basis of the design variables of the Deformable Structure as is hypothesized in subsection 3.5.1. This emphasizes the importance of the stowed form of the Deformable Structure for the mechanism design and thereby the mass and volume related performance of the overall deployable structure. Hence within the design process of Deployable Space Structures the design of the Deformable Structure has to be concretized regarding its stowed, deploying and deployed form before the design of the Deployment Mechanism can be detailed. Furthermore, it is demonstrated within this chapter that component scaling functions that reflect these design dependencies can be established through basic considerations such as expressed by the design sketch displayed in Figure 4-8. This is possible also in the phase of conceptual design with a significantly lower state of knowledge.
However, the parameterizations of the mechanism components are done based on simplified models and some assumptions on scaling relations between subcomponents

wherefore the deduced scaling functions are not fully representative for the actual scaling behavior. Especially components that are sized regarding mechanical loading during space transport are subjected to scaling uncertainty as the complex load cases cannot be fully represented by the chosen parameterization approach. Furthermore, interdependencies in the dynamic behavior of a complex assembly cannot be considered as well.

5. Design Interactions of Deformable Structure and Deployment Mechanism

The parameterization and derivation of the mechanism scaling functions presented in the previous chapter shows that there is a high dependency of most mechanism components in design and scaling behavior on the Deformable Structure. This observation causes the question in how far an optimization process regarding the design objectives is required to accurately predict the actual system performance. In subsection 3.5.2 it is hypothesized that such design interactions between Deformable Structure and Deployment Mechanism exist and an optimization process needs to be considered already in early design stages as a sequential design would lead to significant misjudgments in the performance evaluation.
In the following the need for optimization regarding the design objectives to minimize mass and stowed volume is examined. Therefore the system scaling function that combines the scaling functions of the Deformable Structure and the Deployment Mechanism is developed in a form that allows for identification and quantification of design interactions between these parts. The thereby considered Deformable Structures are a Tubular Shell Mast and a truss with longerons of solid rods which are both compatible with the above presented Deployment Mechanism design. Their scaling functions are introduced in the following before the systems scaling function can be established and the search for design interactions can be conducted.

5.1. Procedure for Derivation of the Deformable Structures Scaling Functions

Within this section the basic procedure for the derivation of the scaling functions for the Deformable Structure is described. The description includes the presentation of the load cases considered for the following analysis steps. On this basis the specific scaling functions for a Tubular Shell Mast and a Solid Rod Truss are derived in sections 5.2 and 5.3.

5.1.1. Procedure for Derivation of the Deformable Structure Scaling Functions

The scaling functions for the Deformable Structure are developed for specific load cases and describe their according mechanical sizing. First a set of constraint functions on the required mechanical performance are deduced from the selected load case. In a second step basic equations describing the sizing of the Deformable Structure according to this load case are established based on the Deformable Structures architecture. The load case specific scaling functions are now derived through equating these two sets of constraint functions and solving for the design variables which are for deployable masts the cross-sectional area A and mast radius R as introduced in subsection 4.2.3.3. For the derivation of scaling functions for the Deformable Structure

the impact of scaling limits and geometrical imperfections need to be considered which are described in the following.

5.1.2. Consideration of Scaling Limits

As is shown in the literature (cf. Mikulas [108]) scaling limits can greatly affect the scaling behavior of a large and lightly loaded space structure and in particularly geometrical scaling limits. Due to the small loading the designs are mostly dominated by stiffness requirements and lead to structures composed of slender or thin walled elements. Hence, in the small scale region scaling limits that result from manufacturing constraints, material availability or even handling and robustness criteria need to be considered. Examples for sources of scaling limits are the availability of thin fiber material that limits the realizable thickness of composite shells or the maximum strain that shall not be exceeded by Deformable Structures that are stowed through elastic deformation.
Scaling limits require the derivation of separate scaling functions and the validity of each scaling result needs to be checked for violation of these limits.

5.1.3. Consideration of Imperfections

To accurately represent the scaling behavior of slender structures that consist of thin walled or slender elements the sensitivity of local and global buckling strength towards imperfections needs to be considered. In [144], [113] and [28] the impact of such imperfections on the actual mechanical performance are demonstrated for geometrical imperfections of shells and compression members depending on certain size ratios. These relations need to be considered in the description of the mechanical performance of the Deformable Structure.

5.1.4. Design Load Cases for the System Analysis

For the following system analysis load cases are derived for a solar sail and a solar array application that feature different sizes and load intensities. The derivation of the design loads for the two load cases is described in Appendix D.

5.1.4.1. Solar Sail Application

For the solar sail described in Appendix D1 a mast length interval of 1 m to 1000 m is considered. The sail design is selected to be similar to that of Sunjammer developed by L'Garde [82] which does not require any tension forces on the sail in operational state due to the underlying net of suspension cables. Hence the operational load case is bending from the solar pressure p_{sol} (neglecting shear loads). The corresponding constraint functions are given by Equation 5-1 for the bending stiffness EI and 5-2 for the critical bending moment M:

$$EI \geq EI_{req} \quad 5\text{-}1$$

$$M \geq M_{req} \quad 5\text{-}2$$

For calculation of the required critical bending moment M_{req} it is assumed that the sails minimum distance to the sun is d_{AE} normalized to 1 AE. The mass distribution throughout the sail is expressed by a factor k_γ that gives the ratio between the bus mass in the sails center and the mass distributed throughout the sail. The resulting required critical bending moment M_{req} of the solar sail mast is given by Equation 5-3 (see Appendix D1.2):

$$M_{req} = \frac{1}{2}\left(1 - k_\gamma\right)\frac{p_{sol}}{d_{AE}^2} L_{req}^3 \tag{5-3}$$

An additional requirement is formulated for the bending stiffness EI_{req} to ensure a certain flatness of the sail under load. Equation 5-4 gives the required bending stiffness to limit the tip displacement to a fraction k_z of the mast length L (see Appendix D1.3):

$$EI_{req} = \frac{15}{96}\frac{1}{k_z}\left(1 - k_\gamma\right)\frac{p_{sol}}{d_{AE}^2} L_{req}^4 \tag{5-4}$$

5.1.4.2. Solar Array Application

For the solar array application (see Appendix D2) a mast length interval of 1 m to 100 m is considered. The design is selected to be similar to that of the ISS solar arrays (see Figure 1-2) with the mast and the photovoltaic blanket in the same plane. Hence, the load case for deployment and operation is axial compression. Equations 5-5 and 5-6 give the resulting constraint functions for the global and local buckling strength P_{global} and P_{local}:

$$P_{global} \geq P_{req} \tag{5-5}$$

$$P_{local} \geq P_{req} \tag{5-6}$$

The required compression strength P_{req} of the mast is derived for a minimum eigenfrequency requirement f_0 for the deployed array according to Banik [120]. The eigenfrequency requirement defines the tension load in the blanket that needs to be provided through compression of the mast. Thereby the compression load requirement is given by Equation 5-7 and depends on the areal mass of the array γ, its aspect ratio Γ_{bL} and a knockdown factor δ (see Appendix D2.3):

$$P_{req} = \left(\frac{2\pi^2}{3.516}\right)^2 \left(\frac{f_0}{\delta}\right)^2 \gamma_{BL}\Gamma_{bL} L_{req}^3 \tag{5-7}$$

5.2. Scaling Functions of the Tubular Shell Mast

In the following the scaling function of a Tubular Shell Mast is developed according to subsection 5.1. The detailed description is given in Appendix E.

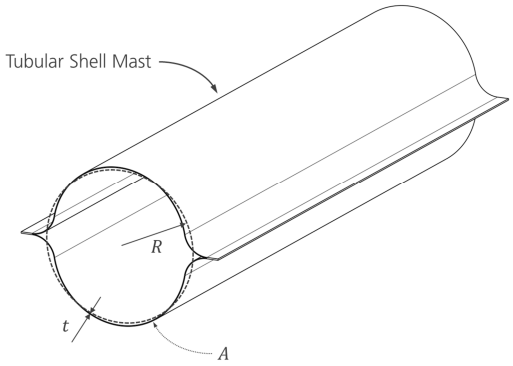

Figure 5-1: A lenticular boom as an example for a Tubular Shell Mast with main cross-sectional properties.

A Tubular Shell Mast as displayed in Figure 5-1 possesses a closed cross-section and is designed from thin-walled shells that can be elastically deformed for stowage. Prominent examples are lenticular masts such as DLR's double-omega boom [47]. The approximated cross-sectional shape of the mast is assumed to have a constant wall thickness t that is significantly smaller than the cross-sectional radius R. Thereby the cross-sectional area A and the second moment of area I can be expressed through the constant mast architecture coefficients k_A and k_I as given by Equation 5-8 and 5-9 (see Appendix E1):

$$A \approx k_A R t \tag{5-8}$$

$$I \approx k_I R^2 A \tag{5-9}$$

The values of these parameters are defined according to the corresponding cross-sectional form of the mast. To limit the complexity of the scaling functions an isotropic material is selected for the Tubular Shell Mast that is represented by the Young's modulus E, density ρ and Poisson's ratio ν. Thereby the mass m and specific mass w are derived according to Equations 5-10 and 5-11 whereby L gives the mast length (see Appendix E1):

$$m = \rho A L \tag{5-10}$$

$$w = \frac{m}{L} = \rho A \tag{5-11}$$

5.2.1.Shell Mast Scaling Limits

For the Tubular Shell Mast two scaling limits are derived which are the minimum wall thickness t_{min} and the maximum allowable material strain ε_{max} as given by Equations 5-12 and 5-13:

$$\varepsilon \leq \varepsilon_{max} \tag{5-12}$$

$$t \geq t_{min} \tag{5-13}$$

The scaling limits result from considerations such as discussed in subsection 5.1.2 and introduce additional constraint functions.

5.2.2.Shell Imperfections

The shell imperfections of the Tubular Shell Mast are approximated through application of the critical wall buckling stresses σ_{crit} of cylinders under compression and bending loads as given by NASA SP-8007 [144]. The stress is expressed as a function of the wall thickness ratio $\frac{t}{R}$ as given by Equation 5-14 for compression and Equation 5-15 for bending loading (see Appendix E2):

$$\sigma_{crit} = \frac{E}{\sqrt{3(1-\nu^2)}}\frac{t}{R}\gamma_c \qquad 5\text{-}14$$

$$\gamma_c = 1 - 0.901\left(1 - e^{-\phi}\right)$$

$$\phi = \frac{1}{16}\sqrt{\frac{R}{t}}$$

$$\sigma_{crit} = \frac{E}{\sqrt{3(1-\nu^2)}}\frac{t}{R}\gamma_b \qquad 5\text{-}15$$

$$\gamma_b = 1 - 0.731\left(1 - e^{-\phi}\right)$$

The actual wall thickness ratios of a Tubular Shell Mast varies in a narrow interval limited by the maximum allowable strains induced during flattening of the cross-section and subsequent reeling. To simplify the expression and allow an analytical solution for the design variables Equations 5-14 and 5-15 are approximated within this interval by a power function. Therefore the terms expressing the wall thickness ratio are approximated as given in Equation 5-16 (see Appendix E2):

$$\frac{1}{\Gamma_{Rt}}\gamma(\Gamma_{Rt}) \approx \frac{1}{c\Gamma_{Rt}^{d}} \qquad 5\text{-}16$$

$$\Gamma_{Rt} = \frac{R}{t}$$

The resulting buckling stress is given by Equation 5-17:

$$\sigma_{crit} = \frac{E}{\sqrt{3(1-\nu^2)}}\frac{1}{c\Gamma_{Rt}^{d}} \qquad 5\text{-}17$$

The approximation interval is constrained by the strain ε_f in the shell during flattening that corresponds to the wall thickness ratios as described by Equation 5-18:

$$\varepsilon_f = \frac{1}{2}\frac{t}{R} = \frac{1}{2}\frac{1}{\Gamma_{Rt}} \qquad 5\text{-}18$$

The considered approximation interval for the flattening strain ε_f is $[0.01, 0.00025]$. This interval corresponds to an inverse wall thickness ratio interval Γ_{Rt} of $[50, 2000]$. The resulting coefficients for the two load cases are summarized in Table 5-1. An analysis of the associated approximation error is given in Appendix E2.

Load Case	Flattening Strain Approximation Interval $\boldsymbol{\varepsilon_f}$	Wall Thickness Ratio Approximation Interval Γ_{Rt}	Linear Coefficient $\boldsymbol{c}$	Power Coefficient $\boldsymbol{d}$
Axial Compression	$[0.01, 0.00025]$	$[50, 2000]$	0.2431	1.4258
Bending	$[0.01, 0.00025]$	$[50, 2000]$	0.4937	1.2455

Table 5-1: Coefficients for the approximation function of the buckling stress for a cylinder loaded in compression and bending.

Through substitution of the inverse wall thickness ratio Γ_{Rt} by application of Equations 5-8 and 5-16 the buckling stress σ_{crit} with consideration of shell imperfections can be written as a function of the mast design variables A and R given by Equation 5-19:

$$\sigma_{crit} = \frac{E}{\sqrt{3(1-\nu^2)}} \frac{1}{c k_A^d} A^d R^{-2d} \tag{5-19}$$

5.2.3. Tubular Shell Mast Scaling Constraint Functions for Axial Compression

For derivation of the mast scaling function for the load case of axial compression firstly the constraint equations are formulated depending on the masts design variables of cross-sectional area A and radius R. A detailed description of the scaling function derivation for the Tubular Shell Mast loaded in compression is given in Appendix E3 and is summarized in E3.5.

5.2.3.1. Column Buckling

The global column buckling is derived through the Euler buckling load P_E as given by Equation 5-20 (see Appendix E3.1):

$$P_{req} \leq P_{global} = P_E \tag{5-20}$$

$$P_E = \frac{\pi^2 EI}{(k_C L)^2}$$

Substitution of the bending stiffness EI gives the constraint function for column buckling expressed by Equation 5-21 (see Appendix E3.1):

$$P_{req} \leq \frac{\pi^2 E k_I}{\left(k_C L_{req}\right)^2} A R^2 \tag{5-21}$$

The factor k_C gives the Euler buckling boundary condition of the column.

5.2.3.2. Local Wall Buckling

The strength due to local wall buckling is derived through the wall buckling stress for a cylinder loaded in compression and is given by Equation 5-22 (see Appendix E3.2):

$$P_{req} \leq P_{local} = \sigma_{crit} A \tag{5-22}$$

Substitution of the critical stress by Equation 5-19 gives the constraint equation for

the compression strength from local wall buckling described by Equation 5-23 (see Appendix E3.2):

$$P_{req} \leq \frac{E}{\sqrt{3(1-\nu^2)}} \frac{1}{c_c k_A^{d_c} R^{2d_c}} A^{1+d_c} \quad 5\text{-}23$$

5.2.3.3. Minimum Wall Thickness

The constraint equation for the minimum wall thickness scaling limit t_{min} is derived from Equation 5-13 through substitution of the wall thickness t by Equation 5-8 and is given by Equation 5-24 (see Appendix E3.3):

$$A \geq k_A R t_{min} \quad 5\text{-}24$$

5.2.3.4. Maximum Material Strain

Equation 5-25 gives the constraint equation for the maximum material strain scaling limit ε_{max}. It is derived from Equation 5-12 through substitution of the strain ε and wall thickness t according to Equations 5-18 and 5-8 (see Appendix E3.4):

$$\frac{1}{2k_A} \frac{A}{R^2} \leq \varepsilon_{max} \quad 5\text{-}25$$

5.2.4.Tubular Shell Mast Scaling Constraint Functions for Bending

The scaling function for the load case of bending is derived in the same way as for the load case of axial compression. Firstly the constraint equations are formulated based on the load case and the masts structural architecture and are subsequently re-written in the required form for the design interaction analysis described in section 5.4. The detailed description of the scaling function derivation of a Tubular Shell Mast loaded in bending is given in Appendix E4 and is summarized in E4.3.

5.2.4.1. Bending Stiffness

The constraint function for the bending stiffness EI of the Tubular Shell Mast is given by Equation 5-26 (see Appendix E4.1):

$$EI_{req} \leq EI \quad 5\text{-}26$$

Substitution of the second moment of area I by equation 5-9 gives the bending stiffness constraint function expressed by Equation 5-27 (see Appendix E4.1):

$$EI_{req} \leq E k_I A R^2 \quad 5\text{-}27$$

5.2.4.2. Critical Bending Moment

The constraint equation for the masts critical bending moment M is given by Equation 5-28 (see Appendix E4.2):

$$M_{req} \leq M = \sigma_{crit} \frac{I}{R} \quad 5\text{-}28$$

Substitution of the local wall buckling stress σ_{crit} due to bending and the second moment of area I by Equations 5-19 and 5-9 gives the critical bending moment buckling equation described by Equation 5-29 (see Appendix E4.2):

$$M_{req} \leq \frac{E}{\sqrt{3(1-\nu^2)}} \frac{1}{c_b} \frac{k_I}{k_A^{d_b}} A^{1+d_b} R^{1-2d_b} \qquad 5\text{-}29$$

5.2.4.3. Minimum Wall Thickness and Maximum Material Strain

The constraint equations for the minimum wall thickness and maximum material strain are the same as for the load case of axial compression and given by Equations 5-24 and 5-25.

5.3. Scaling Functions of the Truss of Solid Rods

In this section the scaling functions of the Solid Rod Truss are developed according to the procedure described in section 5.1. A detailed description is given in Appendix F.
A truss of solid rods as displayed in Figure 5-2 consists of a number of n longerons that are interconnected through diagonals and battens. Thereby the parameterization of the cross-section is more complex as it is not continuous and is done in the following according to Murphey [28] (see Appendix F1).

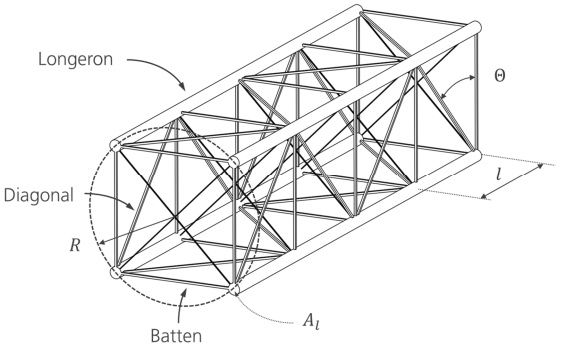

Figure 5-2: Example of a four longeron truss with main elements and geometrical parameters.

As a conservative approximation it is assumed that the diagonals and battens possess the same linear mass as the longerons. Thereby the mean cross-sectional truss area A can be expressed through the cross-sectional longeron area A_l and an axial mass ratio β as given by Equation 5-30 (see Appendix F1):

$$A = n\beta A_l \qquad 5\text{-}30$$

The axial mass fraction β depends on the diagonal angle Θ and is given by Equation 5-31 (see Appendix F1):

5-31

$$\beta = 1 + \frac{1}{\tan(\Theta)} + \frac{1}{\sin(\Theta)}$$

The diagonal angle and thereby the axial mass fraction is for different scaling functions either constant or becomes a third design variable. These two design cases are addressed in Appendix F2.1 and F2.2. The resulting truss mass m and specific mass w can be derived by Equations 5-32 and 5-33:

$$m = A\rho L = n\beta A_l \rho L \quad \text{5-32}$$

$$w = A\rho = n\beta A_l \rho \quad \text{5-33}$$

5.3.1.Longeron Imperfections

The longerons differ from their ideal, fully straight shape through initial lateral deformations. These geometrical longeron imperfections and their impact on the truss performance are addressed in Appendix F3. Thereby axial loads cause additional bending loads in the longeron that result in a lateral displacement. Due to this lateral displacement also some axial shortening is caused which lowers the longerons effective axial stiffness. The shape of the imperfection is approximated as a sine half-wave with a maximum middle displacement a_0 in unloaded state. As a measure for the imperfection a ratio ζ is defined that relates the initial displacement a_0 to the longerons radius of gyration $r_{i,l}$ according to Equation 5-34 (see Appendix F3.3):

$$\zeta = \frac{a_0}{r_{i,l}} \quad \text{5-34}$$

The loss in axial stiffness is described in Appendix F3.3 and can be expressed through a tangent modulus $E_{tan,0,l}$ that gives the initial axial stiffness of the unloaded longeron. The tangent modulus is given in Equation 5-35 (see Appendix F3.3):

$$E_{tan,0,l} = \frac{E}{\frac{1}{2}\zeta^2 + 1} \quad \text{5-35}$$

For the following derivation of the scaling functions a certain design value for the imperfection ratio ζ is defined. Therefore the corresponding expression in Equation 5-35 becomes a constant that is expressed through the knockdown factor $k_{E,0}$ in relation to the material modulus E (see Appendix F3.3):

$$k_{E,0} = \frac{E_{tan,0}}{E} \quad \text{5-36}$$

The loss in axial stiffness of the longerons also has an impact on the column buckling strength P_{crit} (cf. Crawford [113]) which is described in Appendix F3.4. The strength of a truss column with imperfect longerons depending on the imperfection ratio is described by Equation 5-37 in relation to the trusses Euler buckling load P_E (see Appendix F3.4):

$$P_{crit} = P_E \left(1 + \frac{1}{2} \left(\sqrt{-(u+v)} - 2\sqrt{\frac{2\sqrt{u^2 - uv + v^2} + u + v}{4}} \right) \right) \quad \text{5-37}$$

$$u = \frac{\zeta}{2}\sqrt[3]{\sqrt{\zeta^2 + \frac{512}{27}} - \zeta}$$

$$v = -\frac{\zeta}{2}\sqrt[3]{\sqrt{\zeta^2 + \frac{512}{27}} + \zeta}$$

For the design value of the imperfection ratio the corresponding expression in Equation 5-37 becomes a constant and is replaced by the knockdown factor k_ζ in relation to the Euler buckling load as given in Equation 5-38 (see Appendix F3.4):

$$k_\zeta = \frac{P_{crit}}{P_E} \qquad 5\text{-}38$$

Figure 5-3 shows the curves of the knockdown factor $k_{E,0}$ for the initial axial modulus of a longeron and the knockdown factor k_ζ for the column axial compression strength in relation to the imperfection ratio ζ.

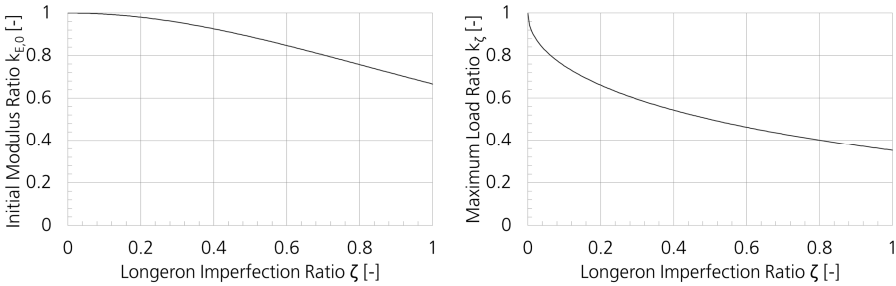

Figure 5-3: Initial modulus of a longeron with imperfection (left) and maximum load ratio of a truss column with imperfect longeron (right) both plotted over the imperfection ratio ζ.

5.3.2. Truss Scaling Limits

For the truss of solid rods scaling limits are defined for the minimum longeron radius $r_{min,l}$ and a minimum and maximum diagonal angle θ_{min} and θ_{max}. The resulting constraint equations are given by Equations 5-39 to 5-41:

$$r_l \geq r_{min,l} \qquad 5\text{-}39$$

$$\theta \geq \theta_{min} \qquad 5\text{-}40$$

$$\theta \leq \theta_{max} \qquad 5\text{-}41$$

The scaling limits result in the case of the minimum longeron radius from manufacturing issues. The definition of a minimum diagonal angle ensures a certain minimum length of the longeron in relation to the battens and diagonals and sets a limit to the number of nodes that add additional mass. The same is done for the battens in relation to diagonals and longerons through definition of the maximum diagonal angle.

5.3.3. Truss Scaling Constraint Functions for Axial Compression

The mast scaling functions for axial compression of a truss of solid rods are the column buckling strength and the local longeron buckling strength both given by Euler. As introduced beforehand the truss mass ratio β depends on the diagonal angle Θ and becomes a third variable when certain scaling limits are reached. Thereby the related scaling limit provides the additional constraint equation to solve for the diagonal angle. In the following the general scaling constraint functions are given to shorten the description but are further described in detail in Appendix F4 and particularly F4.3.

5.3.3.1. Global Column Buckling

The global buckling strength of a truss of solid rods is derived from the Euler buckling strength of a column loaded in compression as given by Equation 5-20 (see also Appendix F4.1). Equation 5-42 gives the resulting constraint function (see Appendix F4.2 and F4.3):

$$P_{req} \leq \frac{\pi^2}{2} k_\zeta \frac{1}{k_C^2} \frac{1}{L_{req}^2} \frac{1}{\beta} EAR^2 \qquad 5\text{-}42$$

5.3.3.2. Local Longeron Buckling

The local buckling strength is determined through the buckling load of a single longeron given by Equation 5-43 (see Appendix F4.1):

$$P_{req} \leq P_{local} = nP_{E,l} \qquad 5\text{-}43$$

$$P_{E,l} = \frac{\pi^2 (EI)_l}{\left(k_{C,l} l\right)^2}$$

The resulting constraint function for local longeron buckling is given by Equation 5-44 (see Appendix F4.2 and F4.3):

$$P_{req} \leq \frac{\pi^2}{4} \frac{1}{n} \frac{1}{\left(\tan(\Theta) \sin\left(\frac{\pi}{n}\right)\right)^2} \frac{1}{k_{C,l}^2} \frac{k_{I,l}}{k_{A,l}} \frac{1}{\beta^2} EA^2 R^{-2} \qquad 5\text{-}44$$

The coefficients $k_{A,l}$, $k_{I,l}$ and $k_{C,l}$ are the longeron architecture and boundary parameters that correspond to the mast architecture and boundary parameters k_A, k_I and k_C introduced above for the Tubular Shell Mast (see section 5.2 and Appendix F1).

5.3.4. Truss Scaling Constraint Functions for Bending

The constraint functions for the load case of bending are given by the bending stiffness and critical bending moment of the truss. A detailed description of the derivation of the scaling functions for the load case of bending is given in Appendix F5.

5.3.4.1. Bending Stiffness

The bending stiffness constraint equation for the Solid Rod Truss is given by Equation 5-45 (see Appendix F5.1):

$$EI_{req} \leq \frac{1}{2} k_{E,0} E \frac{1}{\beta} A R^2 \tag{5-45}$$

5.3.4.2. Critical Bending Moment

The critical bending moment M results from the buckling strength P_l of the longerons as described by Equation 5-46 [28] (see Appendix F5.1):

$$M_{req} \leq M = \frac{n}{2} P_l R \tag{5-46}$$

The resulting constraint equation is given by Equation 5-47 (see Appendix F5.2 and F5.3):

$$M_{req} \leq \frac{\pi^2}{8} \frac{1}{n} \frac{1}{\beta^2} \frac{k_{I,l}}{k_{A,l}} \frac{1}{\left(\tan(\Theta) \sin\left(\frac{\pi}{n}\right)\right)^2} E A^2 R^{-1} \tag{5-47}$$

5.4. Derivation of the System Scaling Function

The system scaling function can now be derived from the combination of the scaling function of the Deformable Structure with those of the Deployment Mechanism. In the following only the derivation of the mass scaling function is presented as the procedure for the volume scaling function is the same. The derivation of the system scaling function is described in detail in Appendix C.

5.4.1. Sequential Sizing of Deformable Structure and Deployment Mechanism without Optimization

The system mass m_{sys} of the deployable structure is the sum of the component masses m_i (see Equation 5-48) that are functions of the Deformable Structures design variables of cross-sectional area A and radius R:

$$m_{sys} = \sum_{i=1}^{n} m_i(A, R) \tag{5-48}$$

The solution is done sequentially whereby the Deformable Structure is sized first according to the load cases defined in subsection 5.1.4 and subsequently based the Deployment Mechanism Components are sized as these depend on the Deformable Structures size. To solve for the two design variables two constraint equations are required. The scaling constraint functions developed beforehand for the Tubular Shell Mast and the Solid Rod Truss are power functions that can be written in the form as given by Equations 5-49 and 5-50 (see Appendix C1):

$$c_1 \leq A^{i_1} R^{j_1} \tag{5-49}$$

$$c_2 \leq A^{i_2} R^{j_2} \tag{5-50}$$

Thereby a general sizing solution for the Deformable Structures can be given

expressed by the variables A^* and R^* in the Equations 5-51 and 5-52 (see Appendix C1):

$$A^* = \left(\frac{c_1^{j_2}}{c_2^{j_1}}\right)^{\frac{1}{i_1 j_2 - i_2 j_1}} \quad 5\text{-}51$$

$$R^* = \left(\frac{c_2^{i_1}}{c_1^{i_2}}\right)^{\frac{1}{i_1 j_2 - i_2 j_1}} \quad 5\text{-}52$$

With the sizing results A^* and R^* of the Deformable Structure the masses of the mechanism components m_i are then fully determined due to their design dependency on the Deformable Structure. Thereby, in the sequential sizing process the system mass is a consequence of the Deformable Structures sizing result and mutual design interactions that may require optimization are not represented.

5.4.2. Sizing of Deformable Structure and Deployment Mechanism with Optimization

The sizing result of the Deformable Structure expressed by the reference solution A^* and R^* represents the minimum mass solutions for the Deformable Structure. However the minimum mass of the system may deviate from this reference solution caused by design interactions between the Deformable Structure and the Deployment Mechanism as is hypothesized in subsection 3.5.2. In this case an optimization process is required that is not considered in the sequential sizing approach. The hypothesis contains the assumption that it is beneficial to "invest" additional mass into the Deformable Structure to gain degrees of freedom in its design as subsequently other mechanism components can be made more lightweight in response which lowers the overall system mass.

The approach to derive the minimum system mass is to "invest" additional mass through increasing the masts cross-sectional area A above the reference solution A^*. Thereby the cross-sectional geometry can be altered in a certain interval while still complying with the constraint functions. Figure 5-4 shows an example of a tubular column under compression load P_{req}. The corresponding constraint functions are compliance of the mast design with the global Euler buckling load P_E and the local wall buckling load P_σ as described by Equations 5-53 and 5-54:

$$P_E \geq P_{req} \quad 5\text{-}53$$

$$P_\sigma \geq P_{req} \quad 5\text{-}54$$

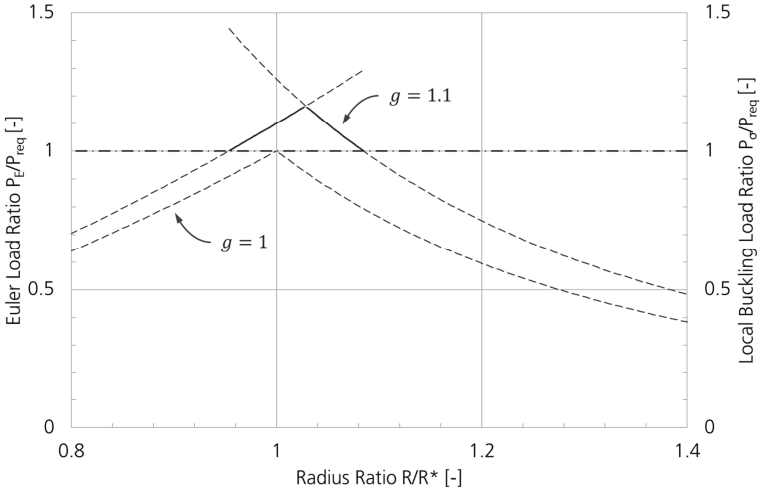

Figure 5-4: Gain in degree of freedom in cross-sectional design of a thin-walled Tubular Shell Mast under compression load through increase of the cross-sectional area A over the minimum mass solution A^* (solid lines give valid solutions that comply with).

In Figure 5-4 the primary ordinate shows the masts Euler buckling load P_E normalized by the required compression strength P_{req} and the secondary ordinate the masts local wall buckling load P_σ normalized in the same way. The abscissa gives the mast radius R normalized by the radius of the minimum mass solution of the sequential approach R^*. Displayed are the curves of the constraint equations for two cases: the first case gives the solution of the minimum mass of the Deformable Structure with the cross-sectional area A^* and the second case the solution for the mast with increased cross-sectional area A. The curves with positive slope represent the constraint equations for global Euler buckling and the decreasing the constraint equations for local wall buckling. One can see that for the minimum mass solution (lower curves) the constraints are satisfied in exactly one point at $[1,1]$. By increasing the cross-sectional area A through "investment" of 10% additional mass the requirements are satisfied for a radius ratio interval between 0.95 and 1.08. Thereby, degrees of freedom to search for a minimum in system mass m_{sys} are gained.

5.4.3. Design Interaction Factor

The increase in cross-sectional area (and thereby mass) of the Deformable Structure relative to the reference solution A^* is used in the following as a measure for the design interaction of Deformable Structure and Deployment Mechanism. Thereby this interaction is quantified through the parameter g as given by Equation 5-55 and described in Appendix C2:

5-55

$$\frac{A}{A^*} = g$$

For $g > 1$ the constraint equations are satisfied not only in a single point but in an interval allowing variation of the cross-sectional shape. Of interest is the value g that gives the minimum system mass. For $g = 1$ there is no design influence of the Deployment Mechanism on the Deformable Structure wherefore a sequential sizing procedure would be applicable.

The minimum system mass is gained at the boundaries of the interval where one constraint is exactly met and the other exceeded. Otherwise an overly large value for g is chosen and thereby an overly heavy mast is used. The solutions for the cross-sectional area A and radius R for the interval boundary are given by Equations 5-56 and 5-57 (see Appendix C2):

$$A = gA^* \quad \text{5-56}$$

$$R = g^{-\frac{i}{j}}R^* \quad \text{5-57}$$

Thereby the higher the value of g the larger is the deviation from the minimum mass solution of the Deformable Structure and the higher is the influence of the Deployment Mechanism on the Deformable Structure design.

5.4.4.Procedure for Derivation of the System Scaling Function

The system mass is now derived according to the flow diagram displayed in Figure 5-5. It includes an optimization process through searching for the values of g_{opt} where the system mass is minimized which also is a measure for the interaction of Deformable Structure and Deployment Mechanism. Outputs of the procedure are the scaling mass functions of the system, the Deformable Structure and the Deployment Mechanism components. Therefore first an outer analysis loop for a design interval $[L_0, L_{max}]$ for the mast length L and a length increment ΔL are defined. Based on the mast length the design loads are calculated for each analysis step as in many cases the loading of a deployable structure utilized in a specific application can be coupled with its size (see subsection 5.1.4). The inner analysis loop incorporates the optimization process by use of the interaction factor g. It starts with the calculation of the solution for an interaction factor of $g = 1$ which is the above described minimum mass solution of the Deformable Structure. Based on this reference solution the calculation loop is conducted over a certain interval of interaction factors $[g_0 = 1, g_{max}]$. The results of this procedure are the mass scaling functions of the Deformable Structure and the Deployment Mechanism components depending on the interaction factor g for each length L_k. The sum of these masses represents the system mass scaling function.

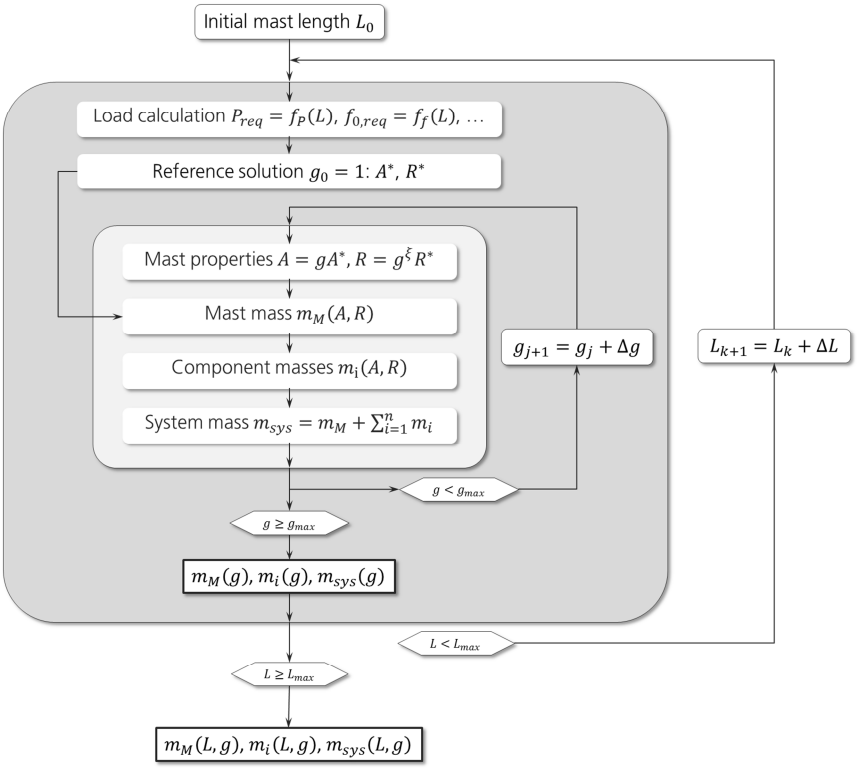

Figure 5-5: System analysis flow to derive the functions of component masses m_i, system mass m_{sys} and related interaction factor g_{opt} for the mast length interval $[L_0, L_{max}]$ of the analysis.

The system mass is analyzed regarding those interaction factor values g_{opt} which provide the minimum system mass. Thereby it is derived in how far design interactions between Deployment Mechanism and Deformable Structure occur and if their intensity justifies an optimization process already in early design stages.

5.5. Investigation of Design Interactions

Within this section the identification of design interactions and thereby verification of the hypothesis formulated in subsection 3.5.2 is done based on the beforehand described procedure for derivation of the system scaling function. The influence of the mechanism on the sizing result of the Deformable Structure and therefore the need for optimization is identified through the design interaction factor g (see subsection 5.4.3). For the case of $g = 1$ there is no interaction and a sequential sizing of the Deformable Structure and the Deployment Mechanism is valid.

The analysis reveals that there is an influence of the Deployment Mechanism on the sizing result of the Deformable Structure. However, these interactions are observed only for the Tubular Shell Mast wherefore in the following the results for the Solid Rod Truss are not presented. Furthermore it is found that design interactions occur only in the large size region for both design objectives of minimum mass and minimum volume.

Figure 5-6 shows the specific volume v (in m³/m) of a Tubular Shell Mast in the solar sail application. The solid line shows the solution without and the dashed line with design interactions and the dot-dash-line the corresponding interaction factor g. One can see that initially the specific volume decreases with the mast length which is a result of the scaling limits of the deformable and Deployment Mechanism components that are particularly dominating in the small scale region. The scaling limits also cause the discontinuities in the curves due to change overs in the scaling laws when different scaling limits become active.

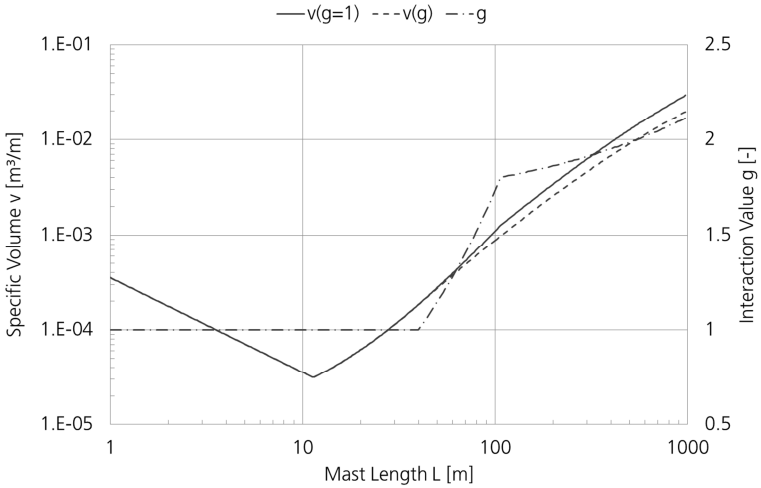

Figure 5-6: Specific volume of a Tubular Shell Mast in a solar sail application plotted over the mast length for the case of sequential design without (solid line) and with consideration of interaction (dashed line) given by the design interaction factor g.

Up to a mast length of 40 m the curves coincide and the interaction factor remains 1. Above this length the curves start to separate with increasing g. The maximum value is reached at a mast length of 1000 m where the mass of the Deformable Structure is 2.1-times above the minimum mass solution of the Deformable Structure derived through a sequential design. Thereby significant volume savings are gained in the large scale region which amount for the overall deployable structure at a mast length of 1000 m to 33 %.

Figure 5-7 shows the development of the specific mass of a Tubular Shell Mast in a solar array application with and without consideration of design interactions. The principle forms of the curves are the same as for the previous example. Again the influence of the scaling limits is visible through a decreasing specific mass with increasing mast length in the small scale region and is expressed by the discontinuities in the plots. Design interactions are observed above 30 m mast length whereby a maximum value of 1.6 for the design interaction factor g is reached for a mast length of 100 m. The mass saving gained through consideration of the interaction results to 17 %.

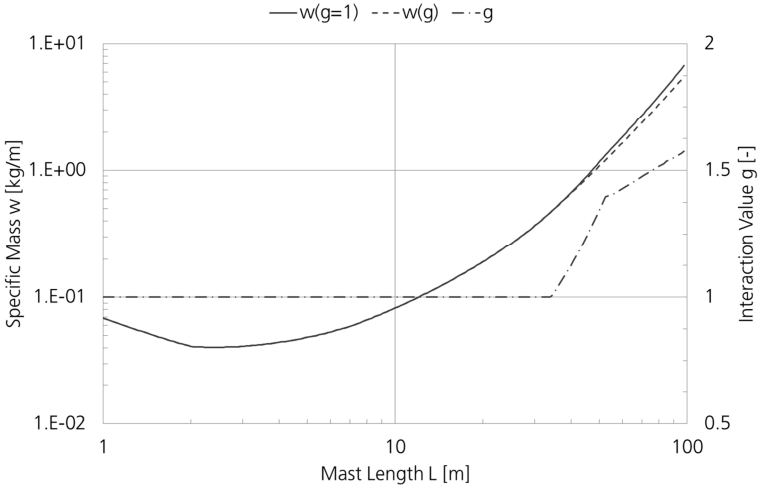

Figure 5-7: Specific mass of a Tubular Shell Mast in a solar array application plotted over the mast length for the case of sequential design without (solid line) and with consideration of interaction (dashed line) given by the design interaction factor g.

Of particular interest is the source of the design interaction. Figure 5-8 shows for the Tubular Shell Mast used in a solar array application the corresponding change in component masses in relation to the overall mass of the deployable structure. The component masses are combined in functional groups corresponding to subsections 4.3.2 to 4.3.6 to enhance the readability of the diagram. The masses of the mast and the Spool Brake Mechanism increase while the Mast Spool and the Drive Mechanism remain constant. In case of the Drive Mechanism this is due to the fact that the scaling functions do not depend on the properties of the Deformable Structure. Hence, the mass savings result primarily from the support structure and the components of the mast root support and guidance. These components depend in their dimensions directly on the compactness of the reelable masts stowed form and particularly its flattened width. The flattened width is lowered through an increase in shell thickness

which allows reduction of the mast radius and results in a more compact stowed form. Furthermore the mass of the support structure is dependent on the mass of the supported components. Therefore, savings in component masses also lead to savings in the support structure mass.

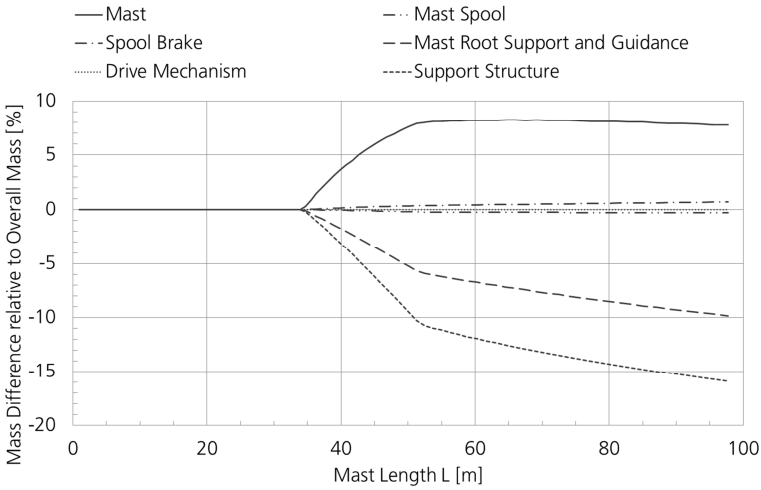

Figure 5-8: Difference in the masses of the mast and the mechanism modules in relation to the solution with sequential design plotted over the mast length for a Tubular Shell Mast in a solar array application.

5.6. Conclusions on Design Interactions and their Significance for the Conceptual Design

The analysis of the interaction in the design between Deployment Mechanism and Deformable Structure reveals that there are such interactions thus supporting the hypothesis formulated in subsection 3.5.2. However, design interactions are not observed for the truss of solid rods and occur in relevant intensity mainly for large structures that are designed with the objective of minimum stowage volume. Figure 5-6 and Figure 5-7 show relatively small gains in overall mass and volume despite of interaction values that are well above 1.

In the small to middle size region it is found that the scaling behavior of both masts is largely dominated by scaling limits. Scaling limits may also cause the absence of design interactions in these regions as they significantly constrain the sizing results of the Deformable Structure. Only in the large size region the mast is sized according to the stiffness and strength criteria and subsequently provides higher degrees of freedom for variation of the cross-sectional shape.

Another aspect that favors design interactions in the large size region is the wide analysis interval combined with a missing adjustment of the architectural parameters of the component scaling laws with the component size. Such adjustments apply particularly to the structural components which require proper selection of their architecture parameters such as thickness ratios in a sandwich to gain high mass efficiencies. Hence, the intensity and potentially the occurrence of design interactions may be lowered through enhancing the component mass efficiency by size adequate selection of their architectural properties.

In conclusion the presented analysis supports a design point of view where design interactions can in most cases be neglected in early design phases. The potential gain in overall mass and stowed volume is small even for deployable structures with a considerably high mass contribution of the Deployment Mechanism (cf. Figure 5-6 and Figure 5-7). For large deployable structures which are dominated by volume constraints an optimization process may be considered but in general a sequential sizing is sufficient especially for small and medium sized structures that are designed for a narrow size interval. This finding disagrees with the hypothesis formulated in subsection 3.5.2 regarding the significance of design interactions for the phase of conceptual design. The analysis further reveals that the implementation of scaling limits in the scaling functions is of particular importance to adequately represent the components scaling behavior. This is especially true for the scaling function of the Deformable Structure combined with low loading as thereby the dimensions of the structural elements become small and particularly sensitive to geometrical scaling limits.

The consideration of scaling limits and the importance of a compact stowed form is further analyzed in the following chapters.

6. Consideration of the Transition under Load

The transition of a Deployable Space Structure from its stowed to the deployed configuration is connected with a significant change in shape. This change in shape can be local such as in a tapespring or global such as in a pantograph. The form transition is often associated with significant variations in the Deformable Structures mechanical properties. Therefore even small deployment loads can become a design driving factor and require consideration already in early design stages as is hypothesized in subsection 3.5.3. In the following the scaling behavior of a Deployable Space Structure with consideration of the form transition is analyzed and exemplary demonstrated for a specific design and application. The results gained through this examination are discussed subsequently regarding their validity for general use in a design methodology. The description of the analysis process is detailed in Appendix G.

6.1. Analysis Approach

The analysis of the transition of a deployable structure under load and its impact on the design objectives is done through according scaling functions that are formulated for the deformed state during transition. Therefore firstly a geometric model of the shape changing Deformable Structure is established and parameters that define this form are identified. Subsequently a parameter and sensitivity study is performed to derive the interdependencies between shape and design parameters. Based on the parametric geometry model with incorporated design dependencies the mechanical properties of the Deformable Structure during transition are derived and the scaling functions are established. The sections 6.2, 6.3 and 6.4 reflect this procedure.
The analysis of the Deformable Structure during transition is demonstrated in the following for a Tubular Shell Mast design that consists of two semi-circular half-shells that are connected along their edges through line-hinges. Figure 6-1 shows the transition of such a mast with the main mechanism components that contain the mast in stowed form and support and guide the partly deployed root. Decisive for the scaling behavior of the mast are the mechanical properties at the end of the root support in a distance l_{tz}. Here the cross-sectional dimensions are still significantly smaller in the z-direction than in the fully deployed state. Therefore its stiffness and strength are reduced accordingly which needs to be considered in the design and sizing process. Enclosing the Transition Zone entirely with the external root support will in most cases collide with volume and shape constraints due to its high length.

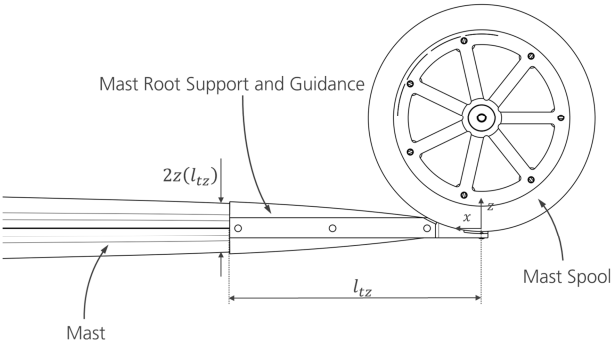

Figure 6-1: Transition Zone and externally supported length of a Tubular Shell Mast with the Mast Spool and the Root Support and Guidance components.

6.2. Geometry Model of the Transition Zone

The geometry model reflects the form of the Deformable Structure during transition. Based on its parameterization, the impact of boundary conditions, geometrical properties, kinematic definitions, material properties and mechanical loading on the shape development of the Deformable Structure during transition is studied. The results of this parameter study are then summarized in a geometry model that incorporates the derived dependencies.
For the example of the Tubular Shell Mast firstly the cross-section is parameterized and an assumption on the deformed shape within the Transition Zone is made. The parameter study is done by use of finite element analysis and considers variation of the material and geometry properties. The derived dependencies of the shape of the Transition Zone on the variation parameters are subsequently used for calculation of the masts mechanical properties.

6.2.1.Parameterization

The parameterization of the Deformable Structure in the state of transition (see Appendix G1) requires identification of the parameters that likely have an impact on its shape, stiffness and load carrying capabilities. The parameterization is done for the states of form that are considered most critical for the given loading conditions. Furthermore, if the deployment is associated with a low stiffness of the Deformable Structure, potential deformation under load has to be considered as well.
Tubular Shell Masts possess a local Transition Zone at their root where the mast comes off the Mast Spool. The parameters with an impact on the shape of the Transition Zone are the cross-sectional dimensions and the properties of the selected material. The stiffness of the mast when it comes off the Mast Spool is small wherefore the mechanism provides additional support through the components of the mast root support and guidance displayed in Figure 6-1.

For the parameterization it is assumed that the shape of the Transition Zone is independent of the mast length and its cross-section is always a segment of a circle. The cross-section of the mast in fully deployed state and the approximation for the deformed state is displayed in Figure 6-2. They are parameterized by a radius R, wall thickness t, arc-angle α and radius of Gyration $r_{M,i}$. The development of the cross-section throughout the Transition Zone is defined by the centerline profile $Z(x)$ and the flange profile $Y(x)$. In addition the curvature of the centerline $K(x)$ is of interest for later calculation of the local buckling stresses.

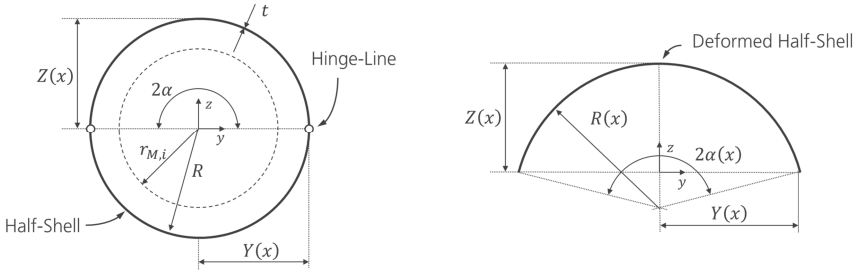

Figure 6-2: Parameterization of the cross-section of the Tubular Shell Mast with two semi-circular half-shells connected by hinge-lines (left) and shape approximation for the deformed cross-section within the Transition Zone (right).

For the derivation of the scaling functions a dimensionless description is advantageous. Therefore, the cross-section, length coordinate and geometry functions are described in normalized form through size ratios. The shell thickness is given by the size ratio Γ_t that relates the thickness to the deployed mast radius as expressed by Equation 6-1:

$$\Gamma_t = \frac{t}{R} \tag{6-1}$$

The length coordinate x is normalized through the masts deployed radius of gyration according to Equation 6-2:

$$\hat{x} = \frac{x}{r_{M,i}} \tag{6-2}$$

Thereby the geometry approximation functions can be written in non-dimensional form as expressed by Equation 6-3 whereby the curvature is normalized through the deployed centerline curvature κ:

$$\hat{Y}(\hat{x}) = \frac{Y(\hat{x})}{R}, \hat{Z}(\hat{x}) = \frac{Z(\hat{x})}{R}, \hat{K}(\hat{x}) = \frac{K(\hat{x})}{\kappa} \tag{6-3}$$

The length of the root support l_{tz} is normalized by the masts deployed radius of gyration $r_{M,i}$ expressed through the coefficient k_{IF} that is given by Equation 6-4:

$$k_{IF} = \frac{l_{tz}}{r_{M,i}} \tag{6-4}$$

For simplification of the description in the following the functions $Y(x)$, $Z(x)$ and $K(x)$ are written as Y, Z and K. The same is done for the normalized forms. Specific function values at a location x are expressed by Y_x, Z_x and K_x.

6.2.2.Parameter Study

The parameter study reveals the dependencies between the design parameters and the geometry of the Deformable Structure during transition. These dependencies are used to establish a geometry model that already contains the basic relations that need to be reflected within the scaling functions.

The shape of the Transition Zone of the Tubular Shell Mast and the impact of the design variables are derived through a parameter study based on finite element analysis. A single, semi-circular half-shell is modelled with boundary conditions along its edges according to the line-hinges. Subsequently the half-shell is flattened at one end and the geometry data for the centerline profile Z, flange profile Y and centerline curvature K are extracted. For the analysis the finite element software PATRAN 2014 with the solver NASTRAN 2014 is used with the solution type Sol106 and shell elements of the type quad4. Figure 6-3 shows the model with the overlaid geometry functions.

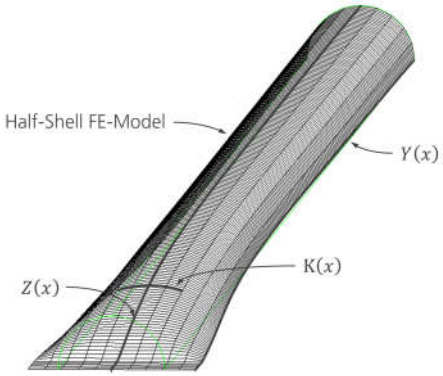

Figure 6-3: Finite element model of a single half-shell of a Tubular Shell Mast with corresponding geometry approximation functions.

Within the analysis the cross-sectional dimensions and the material properties are varied to derive their influence on the shape of the Transition Zone. The cross-section is varied through the wall thickness ratio Γ_t while the arc-angle is held constant. On the material side the shear modulus is altered through the Poisson ratio ν as an isotropic material is used. The analysis parameters, their values and variation intervals are summarized in Table 6-1.

Parameter	Symbol	Unit	Value
Wall thickness	t	mm	0.2 – 0.6
Deployed Radius	R	mm	30
Deployed Radius of Gyration	$r_{m,i}$	mm	21.2
Deployed arc length	α	rad	$\pi/2$
Mast length	L	mm	3600
Wall thickness ratio	Γ_t	-	$6.7 \cdot 10^{-3}$ – $20 \cdot 10^{-3}$
Young's modulus	E	N/mm²	70000
Poisson ratio	ν	-	0.1 – 0.5

Table 6-1: Summary of the Transition Zone analysis parameters and values.

6.2.3.Sensitivity Analysis

The sensitivity analysis is done to identify those design dependencies that are to be incorporated in the geometry model and scaling functions and those that can be neglected.

In the following the sensitivities of the Tubular Shell Mast towards variation of its cross-sectional shape and material properties is described. Thereby the geometry of the Transition Zone is presented in non-dimensional form through the centerline profile $\hat{Z}$, the flange profile $\hat{Y}$ and the centerline curvature $\hat{K}$ as introduced in subsection 6.2.1.

Figure 6-4 shows the centerline profile $\hat{Z}$ for variation of the wall thickness ratio Γ_t (left side) as well as the Poisson's ratio ν (right side). The wall thickness ratio shows a high impact on the profile of the Transition Zone whereby high relative wall thicknesses are beneficial to reduce its length. The shear modulus shows only a small influence which is also true for the Young's modulus E whose variation shows no effect on the form of the Transition Zone.

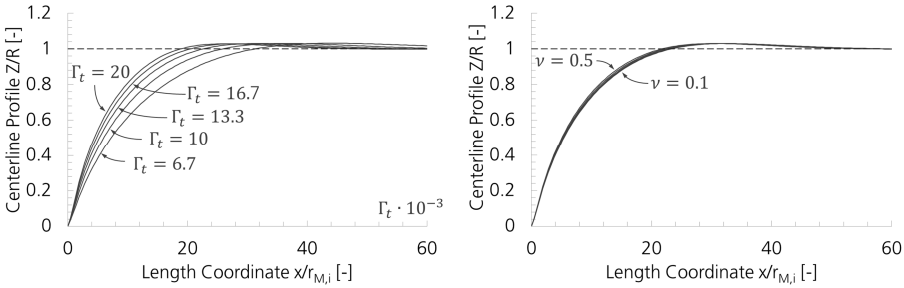

Figure 6-4: Development of the centerline profile height plotted over the length coordinate normalized by the radius of gyration for variation of the wall thickness ratio (left) and the Poisson's ratio (right).

The same high impact of the wall thickness ratio is visible in the flange profile $\hat{Y}$ and the centerline curvature $\hat{K}$ displayed in Figure 6-5. Hence, while the material properties

can be neglected for the case of an isotropic material, the impact of the wall thickness ratio needs to be considered in the derivation of the Transition Zone scaling functions.

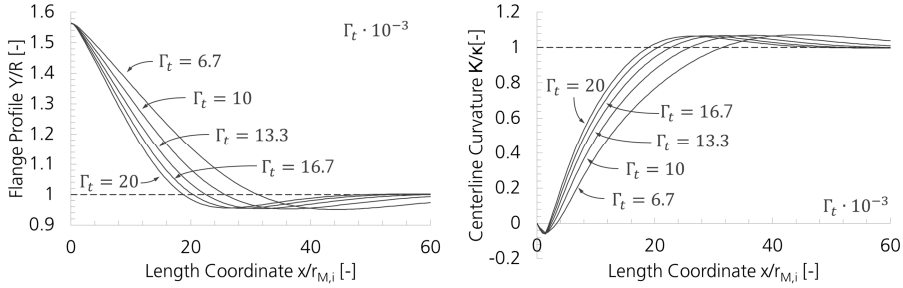

Figure 6-5: Development of the flange profile (left) and the centerline curvature (right) plotted over the length coordinate normalized by the radius of gyration for variation of the wall thickness ratio.

6.3. Mechanical Properties within the Transition Zone

On the basis of the geometry model the stiffness and the strength of the Deformable Structure during transition is calculated. Due to the incorporated dependencies towards the design parameters in the geometry model, the derived expressions for the mechanical properties already largely reflect the actual scaling functions.
The mechanical properties of the Tubular Shell Mast that are of interest for the considered applications and load cases are the bending stiffness EI, the critical bending moment M and the compression strength P due to local wall buckling. Their development throughout the Transition Zone is described in the following.

6.3.1.Bending Stiffness

The bending stiffness around the weak axis EI_y is given by the second moment of area I_y. It is derived from the centerline profile Z and the beforehand introduced assumption that the deformed shape of the cross-section corresponds to a segment of a circle (see Figure 6-2). The second moment of area $I_{y,x,s}$ of a circle segment at a location x is defined by the segment radius R_x, the segment arc-angle α_x and the wall thickness t given by Equations 6-5 to 6-7 (see Appendix G1):

$$I_{y,x,s} = R_x^3 t \left(\alpha_x + \frac{\sin(2\alpha_x)}{2} - \frac{2\sin^2(\alpha_x)}{\alpha_x} \right) \quad 6\text{-}5$$

$$R_x = \frac{Z_x^2 + Y_x^2}{2Z_x} \quad 6\text{-}6$$

$$\alpha_x = \arcsin\left(\frac{Z_x}{R_x}\right) \quad 6\text{-}7$$

The resulting second moment of area $I_{y,x}$ at a location x of the mast is given by Equation 6-8 whereby the offset of the circle segment Δz_x is derived according to Equation 6-9 (see Appendix G1):

$$I_{y,x} = 2I_{y,x,s} + \Delta z_x^2 A \tag{6-8}$$

$$\Delta z_x = Z_x + \left(\frac{\sin(\alpha_x)}{\alpha_x} - 1\right) R_x \tag{6-9}$$

The bending stiffness is written in non-dimensional form through normalization by the bending stiffness of the deployed mast $EI_{y,0}$. Thereby the bending stiffness coincides with the non-dimensional second moment of area as expressed by Equation 6-10:

$$\widehat{EI}_{y,x} = \frac{EI_{y,x}}{EI_{y,0}} = \frac{I_{y,x}}{I_{y,0}} = \hat{I}_{y,x} \tag{6-10}$$

Figure 6-6 shows the bending stiffness $\widehat{EI}_{y,\hat{x}}$ plotted over the normalized length coordinate $\hat{x}$. The discontinuities at the function value 1 are secondary effects of the geometry approximation that does not fully coincide with the actual form of the Transition Zone derived by the finite element analysis. However as the root support does not enclose the entire Transition Zone the interval for the following approximation is limited regarding the length coordinate $\hat{x}$ to $[5, 20]$ and regarding the centerline profile $\hat{Z}$ to $[0.2, 0.9]$.

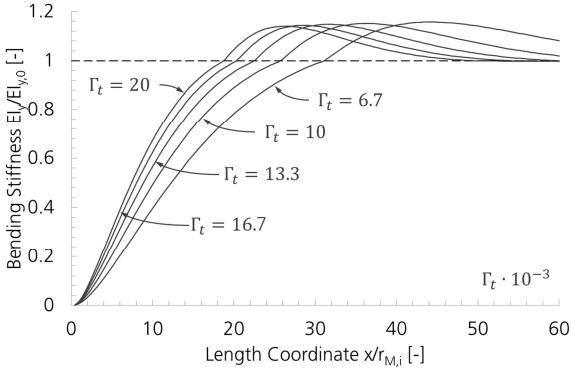

Figure 6-6: Development of the bending stiffness throughout the Transition Zone of the Tubular Shell Mast.

For derivation of the scaling function the bending stiffness of the mast is approximated by a cubic polynomial given by Equation 6-11 (see Appendix G4):

$$\widehat{EI}_{y,\hat{x}} = \hat{I}_{y,\hat{x}} = d_1\hat{x}^3 + d_2\hat{x}^2 + d_3\hat{x} + d_4 \tag{6-11}$$

The coefficients d_k depend on the shell thickness ratio Γ_t and are approximated by quadratic polynomials expressed through Equation 6-12 (see Appendix G4):

$$d_k = \omega_{1,k}\Gamma_t^2 + \omega_{2,k}\Gamma_t + \omega_{3,k} \tag{6-12}$$

Table 6-2 gives the coefficients of the bending stiffness approximation function for the Transition Zone of the Tubular Shell Mast.

Coefficient	$\omega_{1,k}$	$\omega_{2,k}$	$\omega_{3,k}$
d_1	$4.376 \cdot 10^{-2}$	$-2.882 \cdot 10^{-3}$	$1.588 \cdot 10^{-6}$
d_2	-1.513	$-5.787 \cdot 10^{-2}$	$3.306 \cdot 10^{-4}$
d_3	-63.73	5.216	$2.146 \cdot 10^{-2}$
d_4	58.66	-4.738	$-7.836 \cdot 10^{-2}$

Table 6-2: Parameter values for the coefficients of the bending stiffness approximation function.

6.3.2. Compression Strength from Local Wall Buckling

The compression strength P due to local wall buckling is given by Equation 6-13 and is derived from the wall buckling stress due to compression $\sigma_{crit,c}$ and the cross-sectional area A:

$$P_x = \sigma_{crit,c,x} A \tag{6-13}$$

The wall buckling stress $\sigma_{crit,c}$ is approximated by the critical stress of a cylinder loaded in compression as given by NASA SP-8007 [144] whereby the additional stresses due to the deformed state of the shell are neglected. Equation 6-14 gives the local buckling stress whereby the radius is expressed through the local centerline curvature K_x that is directly derived from the FE-data (cf. subsection 5.2.2 and Appendix E2):

$$\sigma_{crit,c,x} = \frac{\gamma_x E}{\sqrt{3(1-\nu^2)}} t K_x \tag{6-14}$$

$$\gamma_x = 1 - 0.901\left(1 - e^{-\phi_x}\right)$$

$$\phi_x = \frac{1}{16}\sqrt{\frac{1}{tK_x}}$$

The compression strength due to local wall buckling P_x is normalized through the compression strength of the fully deployed mast P_0. Equation 6-15 gives the resulting compression strength in non-dimensional form:

$$\hat{P}_x = \frac{P_x}{P_0} = \frac{\sigma_{crit,c,x}}{\sigma_{crit,c,0}} \tag{6-15}$$

Figure 6-7 displays the development of the compression strength from local wall buckling throughout the Transition Zone. Discontinuities are not visible as for the calculation of the compression strength no geometry approximation is necessary through direct measurement of the centerline curvature K. In the small length region a slight fluctuation of the compression strength is visible due to initially negative centerline curvature. However the approximation interval and design range for the mast root support length starts above such small values wherefore this behavior is not of significance.

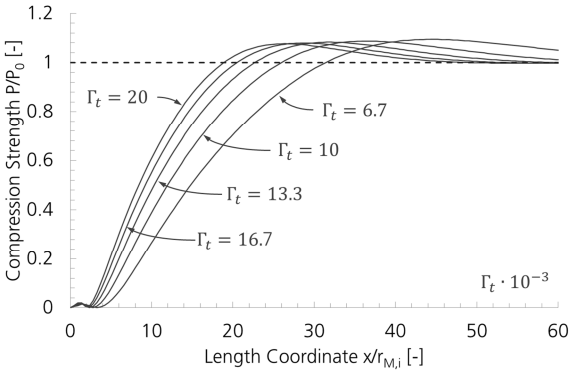

Figure 6-7: Development of the compression strength throughout the Transition Zone of the Tubular Shell Mast.

Just like the bending stiffness the compression strength is approximated in the same length and height interval through a cubic polynomial that is given by Equation 6-16 (see Appendix G2):

$$\hat{P}_{\hat{x}} = \frac{\sigma_{crit,c,\hat{x}}}{\sigma_{crit,c,0}} = e_1\hat{x}^3 + e_2\hat{x}^2 + e_3\hat{x} + e_4 \qquad 6\text{-}16$$

The coefficients e_k depend on the shell thickness ratio and are also approximated by a quadratic polynomial according to Equation 6-17 (see Appendix G2):

$$e_k = \iota_{1,k}\Gamma_t^2 + \iota_{2,k}\Gamma_t + \iota_{3,k} \qquad 6\text{-}17$$

Table 6-3 gives parameter values for calculation of the coefficients of the approximation function

Coefficient	$\iota_{1,k}$	$\iota_{2,k}$	$\iota_{3,k}$
e_1	$2.031 \cdot 10^{-1}$	$-1.595 \cdot 10^{-3}$	$-3.430 \cdot 10^{-5}$
e_2	$-8.098 \cdot 10^{-1}$	$-2.856 \cdot 10^{-1}$	$2.990 \cdot 10^{-3}$
e_3	$-1.741 \cdot 10^{2}$	10.91	$-2.693 \cdot 10^{-2}$
e_4	$7.122 \cdot 10^{2}$	-29.34	$-1.700 \cdot 10^{-2}$

Table 6-3: Parameter values for the coefficients of the compression strength approximation function.

6.3.3. Critical Bending Moment

The critical bending moment $M_{y,x}$ at a location x around the masts weak axis is given by Equation 6-18. It is a function of the wall buckling stress due to bending $\sigma_{crit,b,x}$ and the section modulus. The section modulus is derived from the second moment of area $I_{y,x}$ and the distance of the outer fiber towards the neutral layer which coincides with the centerline profile Z_x:

$$M_{y,x} = \sigma_{crit,b,x}\frac{I_{y,x}}{Z_x} \qquad 6\text{-}18$$

The critical stress $\sigma_{crit,b,x}$ is approximated by the critical bending stress of a cylinder as given by NASA SP-8007. Equation 6-19 gives the local buckling stress due to bending whereby the radius is substituted by the centerline curvature κ (cf. subsection 5.2.2 and Appendix E2):

$$\sigma_{crit,b,x} = \frac{\gamma_x E}{\sqrt{3(1-\nu^2)}} t K_x \qquad 6\text{-}19$$

$$\gamma_x = 1 - 0.731\left(1 - e^{-\phi_x}\right)$$

$$\phi_x = \frac{1}{16}\sqrt{\frac{1}{tK_x}}$$

With the second moment of area $I_{y,x}$ derived in the previous subsection, the masts critical bending moment development throughout the Transition Zone can be calculated. The critical bending moment in non-dimensional form $\widehat{M}_{y,x}$ is gained through normalization by the critical bending moment of the deployed mast $M_{y,0}$ as given by Equation 6-20:

$$\widehat{M}_{y,x} = \frac{M_{y,x}}{M_{y,0}} \qquad 6\text{-}20$$

Figure 6-8 shows the critical bending moment $\widehat{M}_{y,\hat{x}}$ plotted over the length coordinate $\hat{x}$. As described beforehand the discontinuities at the function value 1 are secondary effects of the geometry approximation.

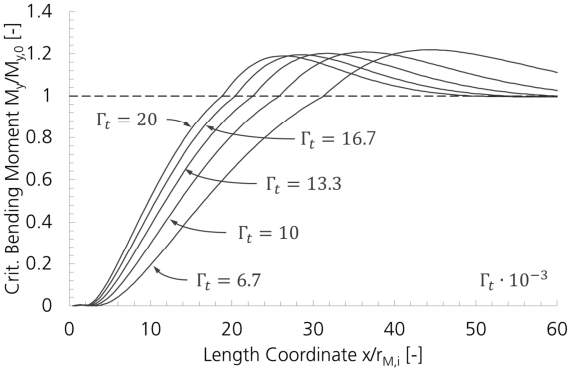

Figure 6-8: Development of the critical bending moment throughout the Transition Zone of the Tubular Shell Mast.

The approximation function for the critical bending moment in non-dimensional form is a cubic polynomial given by Equation 6-21 (see Appendix G5):

$$\widehat{M}_{y,\hat{x}} = \frac{M_{y,\hat{x}}}{M_{y,0}} = f_1\hat{x}^3 + f_2\hat{x}^2 + f_3\hat{x} + f_4 \qquad 6\text{-}21$$

The coefficients f_k depend on the shell thickness ratio Γ_t and are approximated by quadratic polynomials expressed by Equation 6-22 (see Appendix G5):

$$f_k = \tau_{1,k}\Gamma_t^2 + \tau_{2,k}\Gamma_t + \tau_{3,k} \quad \text{6-22}$$

The approximation interval is the same as for the bending stiffness. Table 6-4 gives the coefficients of the approximation function for the critical bending moment of the Tubular Shell Mast Transition Zone.

Coefficient	$\boldsymbol{\tau_{1,k}}$	$\boldsymbol{\tau_{2,k}}$	$\boldsymbol{\tau_{3,k}}$
f_1	$6.762 \cdot 10^{-2}$	$-1.076 \cdot 10^{-2}$	$1.009 \cdot 10^{-5}$
f_2	-6.161	$2.793 \cdot 10^{-1}$	$1.102 \cdot 10^{-3}$
f_3	-25.16	3.518	$-1.655 \cdot 10^{-2}$
f_4	244.6	-13.70	$1.011 \cdot 10^{-2}$

Table 6-4: Parameter values for the coefficients of the critical bending moment approximation function.

6.4. Transition Zone Scaling Functions

The scaling functions are derived through combining the expressions for the mechanical properties of the Deformable Structure with the load case specific constraint functions. Thereby the scaling functions describe the sizing response of the Deformable Structure towards the applied loading for the underlying load case.

The scaling functions for the Tubular Shell Mast with load carrying Transition Zone are developed on the basis of the scaling functions for the Tubular Shell Mast derived in section 5.2. Therefore the constraint functions for the local and global compression strength and the bending stiffness and critical bending moment are adjusted according to the above derived approximation functions for the mechanical properties. Thereby the mechanical properties are calculated for the end of the mast root support at the location $x = l_{tz}$ which is described in non-dimensional form by the parameter k_{IF} (see Equation 6-4). The scaling limits and resulting additional constraint functions are the same as for the Tubular Shell Mast and are not listed in the following.

6.4.1. Compression Strength from Local Buckling

The lowest strength regarding local wall buckling can be expected at the end of the root support. Here the mast has the smallest cross-sectional dimension and thereby the lowest curvature in the outer fiber. The compression strength in non-dimensional form is given by Equations 6-16 and 6-17. Equation 6-23 gives the resulting constraint function through multiplication with the compression strength of the fully deployed mast (see Appendix G2):

$$P_{req} \leq P_{IF} = \frac{E}{\sqrt{3(1-\nu^2)}} \frac{1}{c_c} \frac{1}{k_A^{d_c}} \left(B_1 \left(\frac{A}{k_A R^2} \right)^2 + B_2 \frac{A}{k_A R^2} + B_3 \right) A^{1+d_c} \frac{1}{R^{2d_c}} \quad \text{6-23}$$

$$B_1 = \iota_{1,1} k_{IF}^3 + \iota_{1,2} k_{IF}^2 + \iota_{1,3} k_{IF} + \iota_{1,4}$$
$$B_2 = \iota_{2,1} k_{IF}^3 + \iota_{2,2} k_{IF}^2 + \iota_{2,3} k_{IF} + \iota_{2,4}$$
$$B_3 = \iota_{3,1} k_{IF}^3 + \iota_{3,2} k_{IF}^2 + \iota_{3,3} k_{IF} + \iota_{3,4}$$

The coefficients B_1 to B_3 contain the length of the mast root support through the parameter k_{IF} that relates the supported length to the masts deployed radius of gyration. The coefficients $\iota_{1,1}$ to $\iota_{3,4}$ are given in Table 6-3.

6.4.2. Compression Strength from Global Buckling

The global compression strength is derived through Euler column buckling that depends on the masts bending stiffness. As a conservative approach it is assumed that the effective bending stiffness corresponds to that at the end of the root support. For calculation of the Euler buckling load the bending stiffness given in non-dimensional form by Equations 6-11 and 6-12 is used. The corresponding constraint function is given by Equation 6-24 that is derived through multiplication with the Euler buckling load of the fully deployed mast (see Appendix G3):

$$P_{req} \leq P_{E,IF} = \frac{\pi^2 E k_I}{\left(k_C L_{req}\right)^2}\left(C_1\left(\frac{A}{k_A R^2}\right)^2 + C_2\frac{A}{k_A R^2} + C_3\right)AR^2 \qquad 6\text{-}24$$

$$C_1 = \omega_{1,1}k_{IF}^3 + \omega_{1,2}k_{IF}^2 + \omega_{1,3}k_{IF} + \omega_{1,4}$$
$$C_2 = \omega_{2,1}k_{IF}^3 + \omega_{2,2}k_{IF}^2 + \omega_{2,3}k_{IF} + \omega_{2,4}$$
$$C_3 = \omega_{3,1}k_{IF}^3 + \omega_{3,2}k_{IF}^2 + \omega_{3,3}k_{IF} + \omega_{3,4}$$

Again the length of the root support and thereby location for the calculation of the bending stiffness is given through the coefficients C_1 to C_3 that contain the root support length parameter k_{IF}. The coefficients $\omega_{1,1}$ to $\omega_{3,4}$ are listed in Table 6-2.

6.4.3. Bending Stiffness

As a conservative approach the bending stiffness requirement EI_{req} is set equal to the bending stiffness of the mast at the end of the root support. Thereby the constraint function is derived from Equations 6-11 and 6-12 as is done for the masts Euler buckling load. Equation 6-25 expresses the resulting constraint function by multiplication with the masts fully deployed bending stiffness (see Appendix G4):

$$EI_{req} \leq EI_{y,IF} = E k_I\left(C_1\left(\frac{A}{k_A R^2}\right)^2 + C_2\frac{A}{k_A R^2} + C_3\right)AR^2 \qquad 6\text{-}25$$

6.4.4. Critical Bbending Moment

The critical bending moment depends on the masts local wall buckling strength and the cross-sectional dimensions. The lowest values are again reached at the end of the root support where the distance of the outer fiber to the neutral layer and the curvature of the shell are small. The critical bending moment at this location is calculated from Equations 6-21 and 6-22. The resulting constraint equation for the masts critical bending moment is given by Equation 6-26 and is derived through multiplication with the critical bending moment of the fully deployed mast (see Appendix G5):

$$M_{req} \leq M_{y,IF} = \frac{E}{\sqrt{3(1-\nu^2)}}\frac{1}{c_b}\frac{k_I}{k_A^{d_b}}\left(D_1\left(\frac{A}{k_A R^2}\right)^2 + D_2\frac{A}{k_A R^2} + D_3\right)A^{1+d_b}\frac{1}{R^{2d_b-1}} \qquad 6\text{-}26$$

$$D_1 = \tau_{1,1} k_{IF}^3 + \tau_{1,2} k_{IF}^2 + \tau_{1,3} k_{IF} + \tau_{1,4}$$
$$D_2 = \tau_{2,1} k_{IF}^3 + \tau_{2,2} k_{IF}^2 + \tau_{2,3} k_{IF} + \tau_{2,4}$$
$$D_3 = \tau_{3,1} k_{IF}^3 + \tau_{3,2} k_{IF}^2 + \tau_{3,3} k_{IF} + \tau_{3,4}$$

The coefficients D_1 to D_3 give the length of the root support through the parameter k_{IF}. The values for the coefficients $\tau_{1,1}$ to $\tau_{3,4}$ are provided by Table 6-4.

6.5. Scaling Behavior of a Tubular Shell Mast with Load-Carrying Transition Zone

The scaling behavior of the Tubular Shell Mast with and without consideration of the Transition Zone is compared in the following for the solar array and solar sail application.

Figure 6-9 shows the specific mass w and the specific volume v plotted over the mast length L for the solar array application where the mast is loaded in axial compression. Initially in the small scale region in both plots the scaling behavior with (dashed line) and without (solid line) consideration of a load carrying Transition Zone coincide. This behavior is caused by the scaling limits of minimum wall thickness t_{min} and maximum material strain ε_{max} which are both active for short mast length. Subsequently the curves separate whereby the principle shape is similar but with an offset in between. At a length of 10 m the specific mass w is twice as high for the mast with consideration of the Transition Zone which increases to a factor of 3.4 at a length of 100 m. The increase in specific volume v amounts to a factor of 2.5 at a length of 8 m and remains almost constant for higher length.

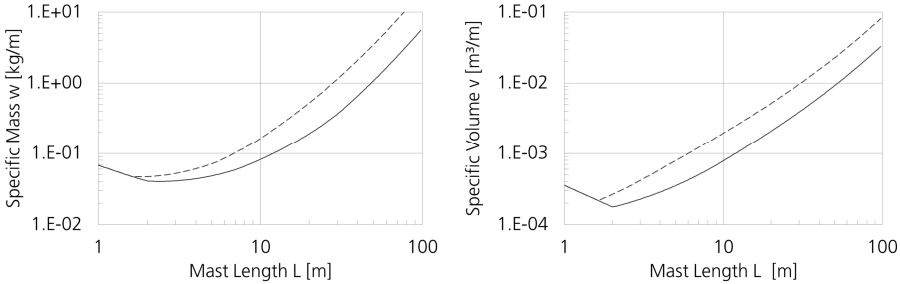

Figure 6-9: Scaling behavior of the Tubular Shell Mast with (dashed line) and without (solid line) consideration of a load carrying Transition Zone plotted over the mast length for the specific mass (left) and specific volume (right) for a solar array application.

The effective mechanical properties of a mast with consideration of the Transition Zone depends strongly on the length of the root support that is defined by the factor k_{IF}. To evaluate the impact on the scaling behavior the root support length is varied between values for k_{IF} of 5 to 15. Figure 6-10 shows the corresponding plots of the specific mass and the specific volume. For the specific mass in the small scale region with active scaling limits regarding wall thickness and flattening strain only a small

influence is visible. At the changeover in the scaling laws at a length of 2 m the increase in root support leads to an advantage in the specific mass that is maintained with increasing length. This advantage results from a reduction in shell thickness and mast radius with increasing k_{IF}. The mast mass is lowered and the dimensions of its stowed form are reduced whereby also the dimensions of the mechanism components decrease.
For the specific volume an opposite behavior is observed. The variation in root support length leads to volume savings in the small scale region below 2 m while after the changeover in scaling laws the achieved stowage volumes largely coincide for all observed values of k_{IF}. This insensitivity is caused as the gain in compactness of the stowed form though the increase of k_{IF} is compensated by the increase in length due to the longer root support.

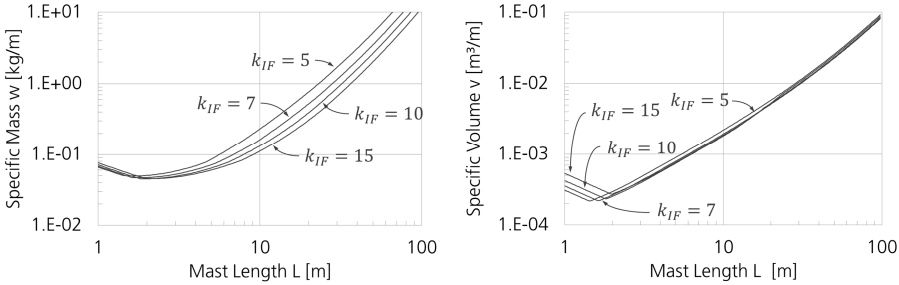

Figure 6-10: Influence of the root support length expressed through the length parameter k_{IF} on the scaling behavior regarding the specific mass (left) and the specific volume (right) for a solar array application.

The observations displayed in Figure 6-11 on the scaling behavior for the solar sail application coincide with those of the solar array. Again a region dominated by scaling limits is visible up to a length of 10 m where both curves coincide. Afterwards with the changeover in the scaling laws they separate and maintain an offset towards another while the principle shape is the same.

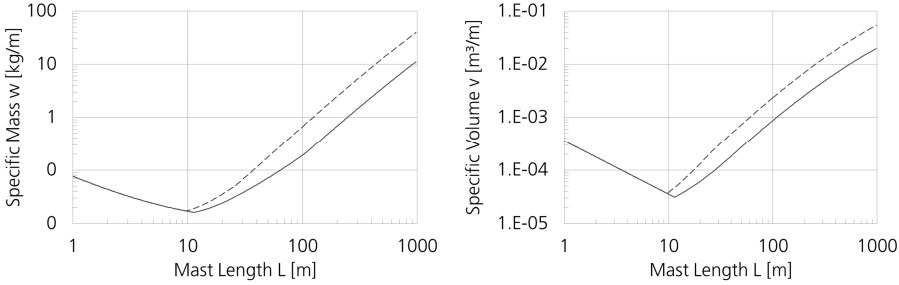

Figure 6-11: Scaling behavior of the Tubular Shell Mast with (dashed line) and without (solid line) consideration of a load carrying Transition Zone plotted over the mast length for the specific mass (left) and specific volume (right) for a solar sail application.

Figure 6-12 shows the influence of the length of the root support on the scaling behavior. Again an impact on the specific mass after the change in the scaling laws at 10 m is observed while the specific volume remains largely insensitive.s

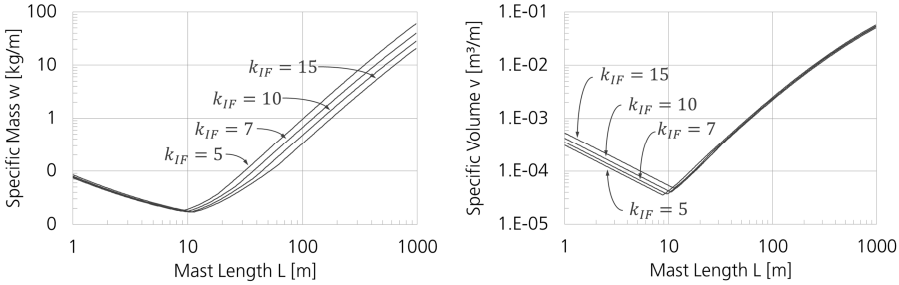

Figure 6-12: Influence of the root support length expressed through the length parameter k_{IF} on the scaling behavior regarding the specific mass (left) and the specific volume (right) for a solar sail application.

6.6. Conclusion on the Significance of Transition Zones for the Conceptual Design

The consideration of the Transition Zone of the Tubular Shell Mast shows a high impact on its scaling behavior. For both application types and load cases the performance regarding mass and stowage volume is significantly reduced in comparison to the mast that is sized in fully deployed state. Extending the external support given to the root of the mast by the Deployment Mechanism is an efficient way to enhance the overall mass efficiency but the disadvantage in stowed volume remains.

In general the results validate the hypothesis formulated in subsection 3.5.3. The consideration of the transition under load in the sizing process has potentially a high impact on the scaling behavior of Deployable Space Structures both in mass and stowed volume. Hence, the transition and the associated change in mechanical properties require consideration already in early design stages as even small deployment loads can become design driving. If the change in shape of the Deformable Structure occurs within a local Transition Zone measures for an external support should be investigated within the design process. Concerning the system design, possibilities to minimize deployment loads should be addressed as this is an effective measure to increase the overall system performance. For many deployable systems a two-stage deployment process can be realized where the Deployable Structure is deployed first and latched in deployed state. For the subsequent

deployment of the supported object such as a photovoltaic blanket the structure possesses its full load carrying capabilities. Furthermore through such a design approach the required mechanism functionalities can be reduced as guidance and support of the deploying Deformable Structure is less demanding.

7. Function Integration in the Design of Deployable Space Structures

The design task addressed within this thesis is focused aside from compliance with the functional requirements on gaining a high solution quality regarding specific design objectives. As is hypothesized in subsection 3.5.4, benefits regarding these design objectives can be gained through the design principle of function integration. Function integration addresses the concretization steps from the functional level towards the component level whereby it emphasizes to concentrate functions in a small number of components. However, current design approaches (see subsections 2.4.1 and 2.4.2) are based on subdivision of the overall function into main and sub-functions which creates a design point of view that favors function separation and complicates finding solutions with function integration.
In this chapter the benefits of function integration for Deployable Space Structures are demonstrated for the case of a deployable mast that is utilized in the beforehand introduced solar array and solar sail applications. The thereby generated results are discussed regarding their general validity for use in a design methodology.

7.1. Application of Function Integration in Deployable Space Structures

In the context of this thesis function integration in Deployable Space Structures shall enhance their solution quality regarding mass and stowage volume through reducing the number of components necessary to comply with the design objects overall function. However, the application of this design principle introduces additional design constraints whose impact may compromise potential performance benefits.

7.1.1. Principle of Function Integration and Related Design Constraints

A common example for the use of function integration in Deployable Space Structures is the use of the Deformable Structure as an energy source through storing the strain energy applied during the stowage process by elastic deformation. The CoilABLE boom [33] uses this design principle to drive its entire deployment. Therefore it does not require additional components for energy storage and generation, translation and transmission of deployment forces. Thereby the CoilABLE boom gains benefits in mass and stowage volume by reducing the required mechanism capabilities and components through integrating the function ‘Store Energy’ into the Deformable Structure.
However, the example also shows that function integration is often connected with introduction of additional design constraints with a significant impact on the scaling behavior. The CoilABLE boom stores energy through elastic deformation and is therefore limited in its longeron dimensions by the maximum elastic strain. The maximum strain requires a certain slenderness to allow stowage through elastic coiling

which limits the masts load carrying capabilities and strongly constrains its scaling behavior. On the other hand the CoilABLE booms capability to store energy and generate deployment forces is limited by the amount of strain that can be accommodated.
In consequence the use of the design principle of function integration in Deployable Space Structures can lead to benefits in the scaling behavior regarding specific applications through reducing the number of required components and/or enhancing their compliance. However, function integration is also connected with introducing additional design constraints the affected components have to comply with. Hence, it is a design trade regarding the effects of changing component scaling functions and component configurations on the overall system scaling behavior whereby necessarily the specific application requirements need to be taken into account.

7.1.2. Identification of Possibilities for Function Integration in a Deployable Mast

On the basis of the beforehand demonstrated mast designs and the analysis of their scaling behavior possibilities for function integration that may enhance the mass specific performance of a deployable mast are investigated. The investigation is done for the Tubular Shell Mast described in section 5.2 in combination with the Deployment Mechanism presented in chapter 4. Figure 7-1 displays the masses of the Deformable Structure and mechanism components of the Tubular Shell Mast summarized in functional groups relative to the overall mass for the solar array and solar sail application.

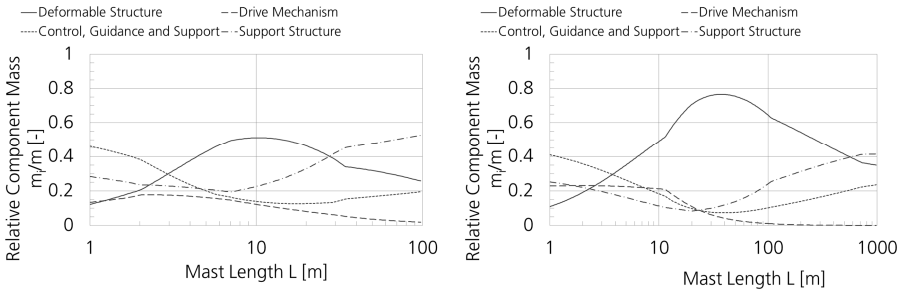

Figure 7-1: Relative component masses of the reelable Tubular Shell Mast summarized by functional groups for the application in a solar array (left) and in a solar sail (right).

Both diagrams show that the Deformable Structure is the main mass contributor in the mid-size region which can be interpreted as a good solution quality as a high percentage of the overall mass contributes to the deployable structures main task. However, for small and large dimensions the contribution of the mechanism components is dominating. Particularly the components that provide the functionalities of control, guidance and mechanical support during deployment as well as the support

structure reach combined contributions of 72% for the solar array and 65% for the solar sail application at the length interval boundaries. As these components do not contribute after deployment to the actual load carrying task, the solution quality may be enhanced through integrating the corresponding functions 'Guide the Deploying Deformable Structure' and 'Mechanically Support the Deploying Deformable Structure' as well as 'Mechanically Support the Stowed System' into fewer or even a single component. A solution which integrates these functions into the Deformable Structure is a Telescopic Tubular Mast whose design is described in the following.

7.2. Telescopic Tubular Mast as an Example for Function Integration

The Telescopic Tubular Mast consists of several cylindrical segments whose radius decreases from the bottom to the top whereby they can be stowed through nesting as is shown in Figure 7-2. Each segment is composed of a cylinder with rings at the top and bottom to provide an interface to the subsequent in the stowed and deployed configuration. Through the telescopic folding principle and the specific design of the interface rings each outer telescopic segment guides and supports the inner during deployment. Thereby the functions 'Guide the Deploying Deformable Structure' and 'Mechanically Support the Deploying Deformable Structure' are integrated into the Deformable Structures design. The same is done for the function 'Mechanically Support the Stowed System' by choosing segments that are self-supporting through definition of a certain minimum cylinder wall thickness. In combination with the interlocking interface rings a mechanically stable platform in the nested, stowed configuration is provided by the Deformable Structure that enables mounting of objects without the need of an additional support structure.

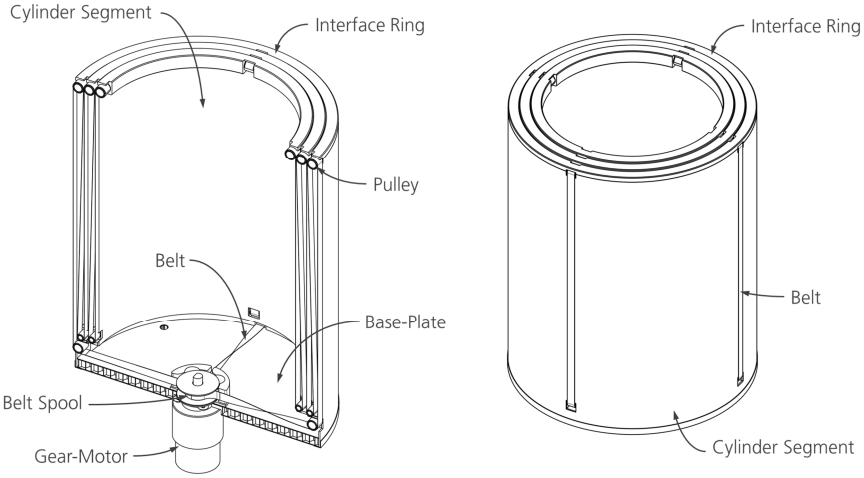

Figure 7-2: Telescopic Tubular Mast with three segments in stowed state with its main components in section view (left) and external view (right).

The deployment principle of the Telescopic Tubular Mast is similar to that of a truck-mounted crane arm. It is achieved through a belt-pulley mechanism which introduces the deployment forces generated by a gear-motor to the cylinder segments. Therefore a spool is attached to the gear-motor that coils the belts and applies a tension load. The belt is running through pulleys that are mounted in the top and bottom interface rings. By reeling the belt on the spool the bottom pulley of the respective inner cylinder is pulled towards the top pulley of the outer. Figure 7-3 shows the positions of the pulleys after deployment of the first cylinder segment. To enable mounting of the pulleys to the interface rings some clearance between the segments needs to be considered in the design. Furthermore, to achieve a stiff and stable connection the interface rings latch at discrete points once deployed.
The components of the Telescopic Tubular Mast and their accommodation are shown on the left sides of Figure 7-2 and Figure 7-3. The gear-motor is mounted in the center of a base plate that is attached to the base segment. In the displayed configuration four belts are used to enable some redundancy and uniform load introduction and the base plate is realized as a sandwich panel.

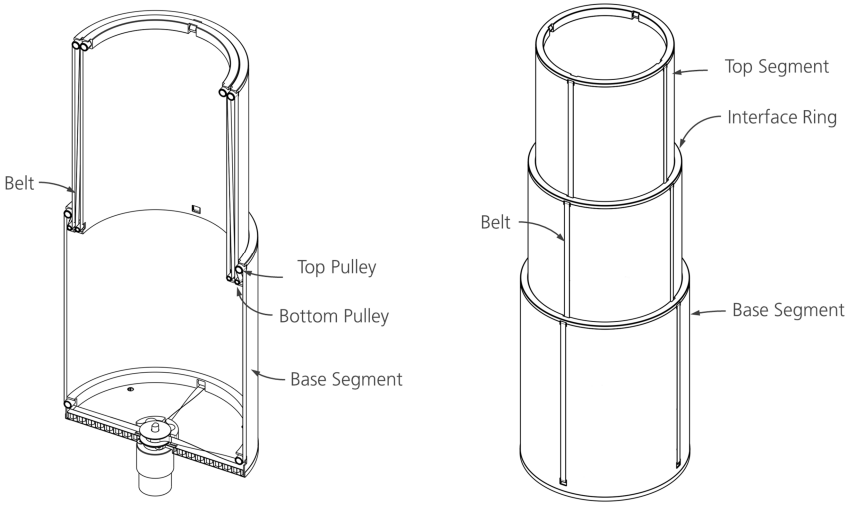

Figure 7-3: Section view of the Telescopic Tubular Mast with one segment extended (left) and full extension of the three segments (right).

The Telescopic Tubular Mast possesses fewer components than the in chapters 4 and 5 introduced reelable Tubular Shell Mast design whose relative component masses are displayed in Figure 7-1. This is achieved through function integration into the Deformable Structure. The Deformable Structure is self-supporting in the stowed configuration through the nesting segments interconnected through interface rings. Furthermore, the segments constrain themselves during deployment through the

interface rings and thereby prevent any undesired motion under load. Thus functionalities for structural support, deployment control and guidance are integrated in the design of the Deformable Structure. As the components which carry these functionalities in the design of the reelable Tubular Shell Mast have a high impact on the overall mass (see Figure 7-1) it is assumed that mass savings can be realized particularly in the high length/high load region. In the small scale region it is expected that the scaling limit of a relatively high wall thickness that is necessary to achieve a self-supporting cylinder design prevents gaining mass savings.

7.2.1.Parameterization and Scaling Functions of the Deformable Structure

As introduced beforehand the Deformable Structure of the Telescopic Tubular Mast consists of several nesting cylindrical elements that are interconnected through interface rings that latch in the deployed configuration. Thereby it is assumed that the elements are deployed sequentially triggered through latching of the respectively preceding segment wherefore the Drive Mechanism has to deploy only one segment at a time. In the following the parameterization of the Deformable Structure is described and subsequently the scaling functions are developed. The derivation of these functions is further detailed in Appendix H.

7.2.1.1. Parameterization of the Telescopic Tubular Mast

The Telescopic Tubular Mast consists of n cylinder segments whose segment radius R_i decreases from the base to the tip as displayed in Figure 7-4.

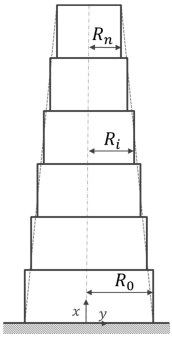

Figure 7-4: Parameterization of the Telescopic Tubular Mast with geometrical parameters of the stacked cylinder elements.

For the design of the Deformable Structure it is assumed that the wall thickness t of all segments remains constant and that the taper ratio Γ_R which relates the radius of the top segment R_n to that of the base segment R_0 is held constant. Equation 7-1 gives the expression for the taper ratio:

$$\Gamma_R = \frac{R_n}{R_0} \tag{7-1}$$

Thereby the radius R_i of a segment i and its cross-sectional area A_i can be derived according to Equations 7-2 and 7-3 (see Appendix H1):

$$R_i = R_0\left(1 - \frac{i}{n}(1-\Gamma_R)\right) \tag{7-2}$$

$$A_i = A_0\left(1 - \frac{i}{n}(1-\Gamma_R)\right) \tag{7-3}$$

Equations 7-4 and 7-5 give the cross-sectional areas of the base segment A_0 and tip segment A_n for $t \ll R_i$:

$$A_0 = k_A R_0 t \tag{7-4}$$

$$A_n = \Gamma_R A_0 \tag{7-5}$$

The resulting second moments of area for the base segment I_0 and the tip segment I_n are given by Equations 7-6 and 7-7:

$$I_0 = k_I A_0 R_0^2 \tag{7-6}$$

$$I_n = \Gamma_R^3 I_0 \tag{7-7}$$

Equation 7-8 describes the mass of the cylinder segment $m_{C,i}$ derived from Equation 7-3, the material density ρ_C and the cylinder length which depends on the mast length L and the number of segments n (see Appendix H1):

$$m_{C,i} = \rho_C A_0\left(1 - \frac{i}{n}(1-\Gamma_R)\right)\frac{L}{n} \tag{7-8}$$

The interface ring that is attached to each cylinder has a cross-sectional area $A_{IF,i}$ that depends on the segment radius R_i and the clearance between each segment ΔR. Equation 7-9 describes the segment clearance and Equation 7-10 the resulting cross-sectional area $A_{IF,i}$ (see Appendix H1):

$$\Delta R = \frac{\mathrm{R}_0 - R_n}{n} \tag{7-9}$$

$$A_{IF,i} = k_A \mathrm{R}_0^2 \frac{1}{n}(1-\Gamma_R)\left(1 - \frac{i}{n}(1-\Gamma_R)\right) \tag{7-10}$$

The height of the interface h_{IF} is defined as a multiple of the cylinder wall thickness t through the parameter k_{IF} according to Equation 7-11:

$$k_{IF} = \frac{h_{IF}}{t} \tag{7-11}$$

With the material density of the interface ring ρ_{IF} the interface mass $m_{IF,i}$ of a cylinder segment i can be expressed through Equation 7-12 (see Appendix H1):

$$m_{IF,i} = \frac{1}{n}k_{IF}(1-\Gamma_R)\left(1 - \frac{i}{n}(1-\Gamma_R)\right)\rho_{IF}A_0 R_0 \tag{7-12}$$

Equation 7-13 gives the total mass of a segment m_i of the Telescopic Tubular Mast (see Appendix H1):

$$m_i = m_{C,i} + m_{IF,i} = \rho_C A_0\big(L + k_{IF}(1-\Gamma_R)\Gamma_\rho R_0\big)\frac{1}{n}\left(1 - \frac{i}{n}(1-\Gamma_R)\right) \tag{7-13}$$

Thereby the parameter Γ_ρ describes the density of the interface ring material ρ_{IF} in relation to the cylinder material density ρ_C as expressed by Equation 7-14:

7-14

$$\Gamma_\rho = \frac{\rho_{IF}}{\rho_C}$$

The mass m of the Deformable Structure of the Telescopic Tubular Mast with constant taper ratio Γ_R and constant wall thickness t is the sum of the component masses m_i and is derived according to Equation 7-15 (see Appendix H1):

$$m = \sum_{i=0}^{n-1} m_i = \rho_C A_0 \left(L + k_{IF}(1-\Gamma_R)\Gamma_\rho R_0\right)\frac{1}{n}\left(n - \frac{1}{2}(n-1)(1-\Gamma_R)\right) \quad 7\text{-}15$$

The number of segments n depends on the desired linear compaction ratio Γ_{lL} as expressed by Equation 7-16:

$$n = \left\lfloor \frac{1}{\Gamma_{lL}} \right\rfloor \quad 7\text{-}16$$

The volume V of the Telescopic Tubular Mast coincides with that of the base segment and is given by Equation 7-17:

$$V = \pi R_0^2 \frac{L}{n} \quad 7\text{-}17$$

Based on the parametric model and basic expressions on the Deformable Structure properties the scaling functions can be derived.

7.2.1.2. Scaling Constraint Function from Global Column Buckling

The compression strength due to column buckling of the Telescopic Tubular Mast is derived through approximation as a truncated cone. Equation 7-18 gives the column buckling strength P for a mast with a fixed root and free end in the form of the Euler buckling load with a buckling factor k_{PE} that considers the form of the cone:

$$P = k_{PE}\frac{EI_0}{L^2} \quad 7\text{-}18$$

Table 7-1 lists the values for the buckling value k_{PE} depending on the ratio of the second moment of area between the top and base segment according to Timoshenko and Gere [145].

I_n/I_0	k_{PE}
0.1	1.202
0.2	1.505
0.3	1.710
0.4	1.870
0.5	2.002
0.6	2.116
0.7	2.217
0.8	2.308
0.9	2.391
1	$\frac{\pi^2}{4}$

Table 7-1: Column buckling factors for a truncated cone depending on the moment of area ratio of top to base segment [145].

The buckling factors are approximated for continuous calculation by a power function given by Equation 7-19:

$$k_{PE} \approx \frac{\pi^2}{4}\left(\frac{I_n}{I_0}\right)^{\psi} \qquad 7\text{-}19$$

$$\psi = 0.30297$$

The actual buckling values given by Timoshenko and Gere [145] and the plot of the approximation function are display in Figure 7-5.

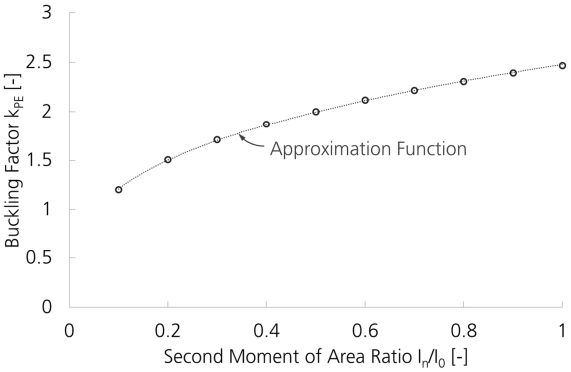

Figure 7-5: Buckling factors for a truncated cone (circles) plotted over the ratio of second moments of area between top and base segment and corresponding approximation function (dashed line).

Equation 7-20 gives the resulting scaling function due to column buckling according to an axial compression strength requirement P_{req} (see Appendix H2.1):

$$P_{req} \leq P_{crit} = \frac{\pi^2}{4}\Gamma_R^{4\psi} E k_I \frac{1}{L_{req}^2} A_0 R_0^2 \qquad 7\text{-}20$$

7.2.1.3. Scaling Constraint Function from Local Wall Buckling

The compression strength due to local wall buckling is derived through the critical buckling stress in compression loaded thin-walled cylinders given by NASA SP-8007 [144] that is approximated by Equation 7-21 (cf. subsection 5.2.2 and Appendix E2):

$$\sigma_{crit,c} = \frac{E}{\sqrt{3(1-\nu^2)}} \frac{1}{c_c \left(\frac{R}{t}\right)^{d_c}} \qquad 7\text{-}21$$

$$c_c = 0.2431$$

$$d_c = 1.4258$$

For derivation of the compression strength from local wall buckling it needs to be evaluated in which cylinder segment local wall buckling will occur first. Therefore the compression strength of the top and bottom cylinder P_n and P_0 is compared in Equation 7-22 through the ratio δ_P:

$$\delta_P = \frac{P_n}{P_0} = \frac{\sigma_{crit,c,n} A_n}{\sigma_{crit,c,0} A_0} \tag{7-22}$$

With the Equations 7-1 to 7-4 and 7-21 Equation 7-22 can be written as a function of the taper ratio Γ_R that is given by Equation 7-23 (see Appendix H2.2):

$$\delta_P = \Gamma_R^{1-d_c} \tag{7-23}$$

As $d_c > 1$ and $\Gamma_R < 1$ one obtains for the compression strength ratio of a Telescopic Tubular Mast with constant taper ratio and constant wall thickness $\delta_P > 1$. Hence, the base cylinder is the critical mast segment regarding vulnerability towards local wall buckling as $P_0 < P_n$. Equation 7-24 describes the resulting scaling function due to local wall buckling for the compression strength requirement P_{req} (see Appendix H2.2):

$$P_{req} \leq P_0 = \frac{E}{\sqrt{3(1-\nu^2)}} \frac{1}{c_c} \frac{1}{k_A^{d_c}} A_0^{1+d_c} R_0^{-2d_c} \tag{7-24}$$

7.2.1.4. Scaling Constraint Function from Bending Stiffness

The effective bending stiffness EI of the Telescopic Tubular Mast is derived through approximation as a truncated cone with fixed root and free tip that is subjected to a moment M. For derivation of the effective bending stiffness the tip displacement for the approximation is equated with that of a beam of same length and constant bending stiffness. The displacement of the truncated cone and a beam of constant cross-section at a location x is given by Equations 7-25 and 7-26 (see Appendix H3.1):

$$w(x) = \frac{1}{2} \frac{ML^2}{EI_0} \frac{1}{\Gamma_R - 1} \left(\frac{1}{\Gamma_R - 1} \left(\frac{1}{1 + (\Gamma_R - 1)\frac{x}{L}} - 1 \right) + \frac{x}{L} \right) \tag{7-25}$$

$$w(x) = \frac{1}{2} \frac{Mx^2}{EI} \tag{7-26}$$

Equating the tip displacements for $x = L$ allows derivation of the effective bending stiffness according to Equation 7-27 in relation to the bending stiffness of the base segment EI_0 (see Appendix H3.1):

$$EI = \Gamma_R EI_0 \tag{7-27}$$

Equation 7-28 gives the resulting scaling function due to bending stiffness requirement EI_{req} of the Telescopic Tubular Mast (see Appendix H3.1):

$$EI_{req} \leq EI = \Gamma_R E k_I A_0 R_0^2 \tag{7-28}$$

7.2.1.5. Scaling Constraint Function from Critical Bending Moment

The critical bending moment of the Telescopic Tubular Mast is determined through the critical wall buckling stress $\sigma_{crit,b}$ of a thin-walled cylinder loaded in bending and the section modulus. The critical buckling stress is derived through NASA SP-8007 and approximated by Equation 7-29 (cf. subsection 5.2.2 and Appendix E2):

$$\sigma_{crit,b} = \frac{E}{\sqrt{3(1-\nu^2)}} \frac{1}{c_b \left(\frac{R}{t}\right)^{d_b}} \tag{7-29}$$

$$c_b = 0.4937$$

$$d_b = 1.2455$$

The critical bending moment of the top and base cylinder M_n and M_0 is compared through the ratio δ_M given by Equation 7-30 (see Appendix H3.2):

$$\delta_M = \frac{M_n}{M_0} = \frac{\sigma_{crit,b,n} I_n R_0}{\sigma_{crit,b,0} I_0 R_n} \quad 7\text{-}30$$

With the Equations 7-1 to 7-7 and 7-29 Equation 7-30 can be written depending on the taper ratio Γ_R as given by Equation 7-31 (see Appendix H3.2):

$$\delta_M = \Gamma_R^{2-d_b} \quad 7\text{-}31$$

As $1 < d_b < 2$ and $\Gamma_R < 1$ one obtains for the critical bending moment ratio for a Telescopic Tubular Mast with constant taper ratio and constant wall thickness $\delta_M < 1$. Hence, the scaling function for the critical bending moment requirement M_{req} results from the top cylinder segment as $M_n < M_0$ and is given by Equation 7-32 (see Appendix H3.2):

$$M_{req} \leq M = \frac{E}{\sqrt{3(1-\nu^2)}} \frac{1}{c_b} \frac{k_I}{k_A^{d_b}} \Gamma_R^{2-d_b} A_0^{1+d_b} R_0^{1-2d_b} \quad 7\text{-}32$$

7.2.1.6. Scaling Limits of the Telescopic Tubular Mast

Scaling limits for the Telescopic Tubular Mast are considered for the minimum wall thickness t_{min}, the minimum clearance between cylinder segments ΔR_{min} and the minimum radius of the top segment $R_{min,n}$ expressed by Equations 7-33 to 7-35:

$$t \geq t_{min} \quad 7\text{-}33$$

$$\Delta R \geq \Delta R_{min} \quad 7\text{-}34$$

$$R_n \geq R_{min,n} \quad 7\text{-}35$$

The Telescopic Tubular Mast does not possess an external structure that supports the Deformable Structure in its stowed form. Hence, the self-supporting cylinder segments require a certain stiffness and stability according to the applied launch loads. Therefore the definition of the minimum wall thickness t_{min} is chosen higher than that of the reelable Tubular Shell Mast. The derivations of the corresponding scaling functions to these scaling limits are detailed in Appendix H2.3, H2.4 and H2.5.

7.2.2. Drive Mechanism for Telescopic Deployment

The Drive Mechanism is based on the same principle as that of the reeling mechanism detailed in subsection 4.3.5. The deployment loads are generated by an electric motor with attached gear and transmitted through belts that are reeled on a spool. The assembly of the Drive Mechanism for the Telescopic Tubular Mast is shown in Figure 7-6. It consists of four belts, eight pulleys for each cylinder segment, a Belt Spool, a gear and an electric motor. The scaling functions of these components correspond to those of the Drive Mechanism described in subsection 4.3.5 and Appendix B4 with only minor adaptation as described in Appendix H4.2. The pulley masses are included in the mass calculation of the interface rings attached to each cylinder segment through modelling these as continuous rings without considering the cut-outs for the pulleys (see Equation 7-12).

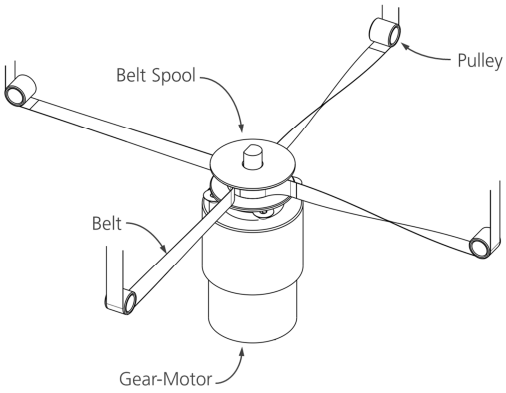

Figure 7-6: Drive Mechanism based on four tension-belts with main components.

7.2.3.Base Plate for Mechanism Mounting

The base plate is a circular plate attached to the bottom of the base segment. It carries the Drive Mechanism components and provides the interface to the host spacecraft. Figure 7-7 shows the base plate realized as a sandwich with honeycomb-core.

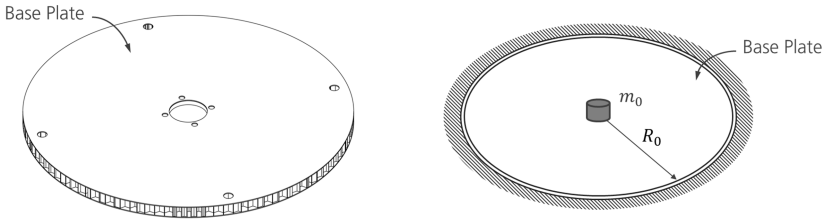

Figure 7-7: Circular base plate realized as a sandwich with honeycomb-core (left) and simplified model for derivation of the scaling function (right).

For sizing the base plate is modelled as a circular panel with a center mass m_0 that is simply supported at its edge. The radius of the plate coincides with the radius of the base segment R_0. For derivation of the scaling function it is assumed that the design is dominated by stiffness requirements from the load case of space transport expressed through the minimum eigenfrequency f_{req}. Equation 7-36 gives the resulting scaling function of the base plate (see Appendix H4.1):

$$m = \left(\frac{\pi^4}{4} \frac{k_{m,P}^3}{k_D} \frac{\rho^3 (1-\nu^2)(3+\nu)}{E(1+\nu)} R_0^8 f_{req}^2 m_0 \right)^{\frac{1}{3}} \quad 7\text{-}36$$

The parameters of the base plate scaling function are listed in Table 7-2.

Parameter	Symbol	Unit	Parameter Category	Remarks
Panel radius	R_0	m		Depending on mast design variables A and R
Supported center mass	m_0	kg		Depending on mast design variables A and R
Eigenfrequency requirement	f_{req}	Hz		
Material modulus	E	N/m²		
Material density	ρ	kg/m³		
Material Poisson's ratio	ν	-		
Plate stiffness factor	k_D	-		
Plate mass factor	k_m	-		

Table 7-2: Summary of the parameters of the base plate scaling function.

7.3. Gain in Performance due to Function Integration

The identification of benefits gained by function integration is done through comparison of the Telescopic Tubular Masts scaling behavior with that of the Tubular Shell Mast and Solid Rod Truss that are both based on the reeling mechanism introduced in chapter 4. Figure 7-8 shows the specific masses of all three mast types plotted over the mast length intervals for application in a solar array and a solar sail. Additionally the scaling function of the Tubular Shell Mast with transition under load is given.

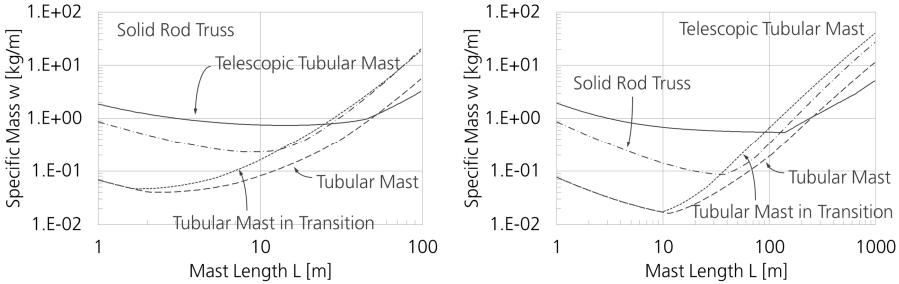

Figure 7-8: Comparison of the specific mass of the Telescopic Tubular Mast with other mast types for the application within a solar array (left) and a solar sail (right).

It is noticeable that the scaling of the Telescopic Tubular Mast is dominated for almost the entire examination intervals by the scaling limit of minimum wall thickness and in the small scale region also by the minimum segment clearance. This is visible by the

decreasing to almost constant specific mass with increasing length and causes the Telescopic Tubular Mast to be non-competitive in the small scale region. In contrast in the large size region it outperforms the Tubular Shell Mast and the Solid Rod Truss for both applications particularly when a transition under load is considered as the Telescopic Tubular Mast shows no such reduction in mechanical performance. For the solar array application the Telescopic Tubular Mast shows the best performance among the three above the length of 50 m without and 30 m with consideration of a load carrying Transition Zone in the Tubular Shell Mast. For the solar sail the corresponding length values are 250 m respectively 120 m.
The same trend is visible when comparing the scaling behavior regarding the specific volume that is displayed in Figure 7-9 for both application types. The scaling behavior is largely dominated by scaling limits which causes poor performance in the small scale region. However, for the solar array and consideration of a transition under load the Telescopic Tubular Mast achieves the best performance already for a length of 9 m. In case of the solar sail it performs best among the mast candidates at 100 m when load carrying Transition Zones are taken into account. Otherwise the Tubular Shell Mast achieves the best results.

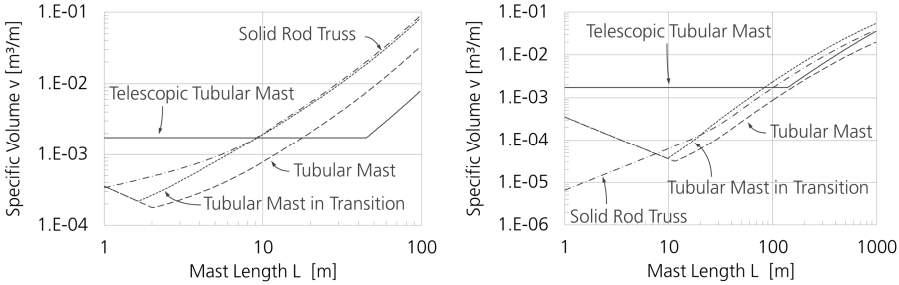

Figure 7-9: Comparison of the specific volume of the Telescopic Tubular Mast with other mast types for the application within a solar array (left) and a solar sail (right).

Comparing the mass scaling behavior in the large size region, the Telescopic Tubular Mast shows lower slopes in the scaling function than the Tubular Shell Mast and the Solid Rod Truss which increases the advantage over its competitors with increasing size.

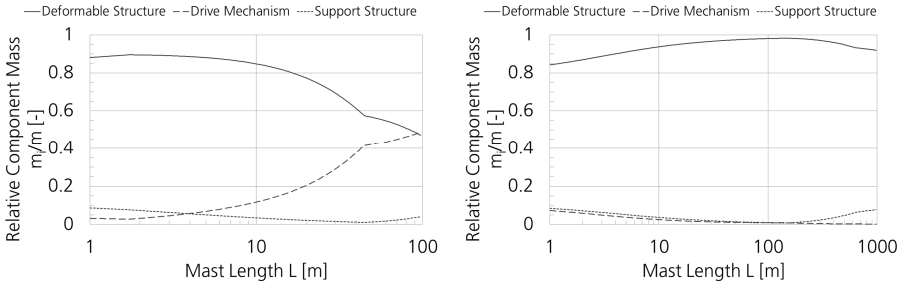

Figure 7-10: Relative component masses of the Telescopic Tubular Mast summarized by functional groups for the application in a solar array (left) and in a solar sail (right).

Figure 7-10 displays the development of the relative component masses of the Telescopic Tubular Mast analogue to the results given in Figure 7-1 for the Tubular Shell Mast. The plots of the relative masses show a high contribution of the Deformable Structure to the overall mass over the entire length interval particularly for the solar sail application. For the solar array the contribution of the Drive Mechanism increases with the array size. The difference in the scaling behavior is caused as the Drive Mechanism has to provide for the solar array a deployment force equal to the masts compression strength while for the solar sail only small deployment forces are considered in the design. Comparing the mass plots in Figure 7-1 and Figure 7-10 show significantly higher mass contributions of the Deformable Structure in the large size region where also the advantage in mass and partly volume specific performance is observed. Hence, the selective integration of mechanism functionalities regarding structural support, deployment control and guidance into the Deformable Structure has led to benefits regarding the design objectives of minimum mass and stowed volume.

7.4. Combined Application with the Design Principle of Sub-Function Minimization

Throughout the investigation of function integration in Deployable Space Structures it is found that examples utilizing this design principle also often make use of Deformable Structures which require less mechanism functionalities.
An example for minimization of mechanism functionalities through according design of the Deformable Structure is the reelable, bi-stable mast BOWL [64] which is displayed in Figure 2-4. BOWL consists of an elongated c-shaped composite tapespring and is stowed through elastic deformation. Thereby it integrates the function ‘Store Energy’ in its Deformable Structure. However, this mast features additional properties that enable a Deployment Mechanism with only minimal functional capabilities. BOWL consists of a carbon fiber composite material and uses the materials lateral contraction to gain in addition to the deployed state a second stable configuration in the stowed, reeled state due to a local strain energy minimum. To achieve this energy minimum the

fiber angle of the composite is specifically tailored throughout the masts length. This design also leads to a well-defined Transition Zone between stowed and deployed state and causes a linear self-deployment of the mast. In consequence these features reduce the number of functions the Deployment Mechanism has to provide. The reduced or dropped functions are 'Contain the Stowed Mast', 'Guide the Deploying Mast' and 'Control the Deploying Mast'. Another example for a mast that utilizes both function integration and sub-function minimization is the CoilABLE boom introduced in the beginning of this chapter.
The effect of the minimization of Deployment Mechanism functions is similar to the design principle of function integration as it results in a reduced number of components to comply with the overall function. However, the underlying general design principle is the selection of solution principles within the phase of conceptual design which cause only a low number of additional sub-functions.

7.5. Conclusions on Benefits, Side Effects and Application of Function Integration

The analysis and comparison of the scaling behavior of the Telescopic Tubular Mast with the reelable Tubular Shell Mast and the Solid Rod Truss demonstrates that the design principle of function integration can lead to enhanced solution qualities regarding mass and stowage volume. Thereby the analysis results support the hypothesis formulated in subsection 3.5.4. However, the application of function integration introduces additional constraints and scaling limits to the component design which may compromise potential benefits. For the example of the Telescopic Tubular Mast advantages are gained through integrating mechanism functions in the Deformable Structure. However, benefits are achieved only in the large size region as the required shell thickness to realize self-supporting cylinder segments becomes a design dominating scaling limit.
In the presented example the knowledge on the scaling behavior of other design solutions for the same set of requirements is used for the selective application of function integration within an alternative design. Thus, the use of function integration is particularly efficient when already some knowledge on design interdependencies and related scaling behavior of components or reference design solutions is available. This knowledge may be extracted from the literature but can also arise from the advancing design process itself.
The investigations of function integration in current Deployable Space Structure further revealed that this principle is in some cases combined with the selection of Deformable Structures that require small mechanism functionalities. The underlying design principle is to select principle solutions that add a minimum of sub-functions to achieve compliance with the overall function. Performance benefits are thereby gained through a reduced number of components which is the same principle effect as for function integration.

8. Performance Evaluation of Deployable Space Structures

At the end of the conceptual design phase a single concept among several competing is selected for further development. This decision is done on the basis of a performance comparison regarding the design objectives. Such an evaluation in an early design stage is always connected with some uncertainty regarding the actual performance. Reducing this uncertainty requires investing analysis efforts as the quality of the performance evaluation enhances with the design level of detail but also leads to increased development time and costs. Hence, for an efficient performance evaluation process a well-balanced relation between performance uncertainties and analysis efforts is of particular importance.
In this chapter means for the performance analysis of Deployable Space Structures regarding mass and stowage volume are analyzed and possibilities to reduce the analysis efforts necessary for the performance evaluation are examined. One approach reflected in the literature is to perform the evaluation in early design phases only for the Deformable Structure through performance metrics and indices. In case this approach is applicable for general design purposes the analysis efforts would be greatly reduced as a detailed Deployment Mechanism design is not required. In the following it is investigated in how far the thereby gained evaluation results are representative for the overall deployable structure and if this approach is suited for application in a conceptual design methodology. Thereby the hypothesis formulated in subsection 3.5.5 is addressed that questions such a simplified approach and states that the overall deployable structure needs to be subject of the performance evaluation. The chapter is concluded by the discussion of the analysis results regarding their applicability for a general conceptual design method for Deployable Space Structures.

8.1. Basic Considerations on Performance Evaluation

Deployable Space Structures are often complex designs with a high degree of design interaction among its components. Furthermore, the component designs are often dominated by multiple scaling limits due to the low loading conditions. Both aspects cause a high complexity in the scaling behavior of the deployable structure which is difficult to assess by intuitive and qualitative evaluation methods. Hence, for evaluation purposes a performance description through quantification is preferred.
Quantification of the performance of a deployable structure can be done through direct determination of specific properties or by use of related performance values that express performance by relating several properties towards another. For the first approach sizing results from point designs or scaling functions can be used directly. In the second case these property values are further processed by use of performance metrics or indices that aim on a performance description independent of size and design loads. Thereby a more general validity of the evaluation result is gained. This enables an application to design tasks such as the development of a model series where the performance needs to be evaluated for extensive size and load intervals instead of specific design points. Another advantage of related performance values in

the evaluation process is the comparison with solutions of the state-of-the-art. Performance data of such solutions are often published for point designs that can significantly differ in size and design loads which complicate a direct performance comparison. In these cases related performance values still allow a comparison due to their size- and load-independency.

8.2. Performance Evaluation of the Deformable Structure through Metrics and Indices

In the literature several approaches for performance evaluation of the Deformable Structure through according metrics and indices are presented. These performance metrics and indices are related performance values which are developed from constraint functions that describe the mechanical properties of a certain type of structural architecture depending on its geometrical dimensions and material properties. Hence, they can be seen as scaling functions whose function value describes the structures general performance potential with respect to specific design goals. Such performance metrics and indices are published by Mikulas et al. [119] and Murphey [28] for the case of deployable trusses. These metrics and indices as well as their underlying approach for performance quantification are analyzed in the following regarding their suitability for performance evaluation purposes within a general conceptual design method. For this analysis the scaling functions developed for the Solid Rod Truss are utilized as test functions for assessment of the evaluation results.

8.2.1.Performance Metrics by Mikulas

Mikulas et al. [119] introduce a set of performance metrics for trusses that enable evaluation of their stiffness and strength performance related to their mass and stowage volume. The metrics are developed on the basis of the constraint functions of truss architectures on bending stiffness EI and critical bending moment M and the specific mass w and specific stowage volume v. A stiffness performance metric is given in Equation 8-1 that relates the bending stiffness EI to the specific mass of the truss w:

$$\frac{EI}{w} = \frac{1}{8}\frac{E}{\rho\Sigma}D_M^2 \qquad 8\text{-}1$$

Within this equation the parameter Σ accounts for the ratio of the overall truss mass m_{all} (including longerons, diagonals, battens and nodes) towards the longeron mass m_l as given by Equation 8-2:

$$\Sigma = \frac{m_{all}}{m_l} \qquad 8\text{-}2$$

Figure 8-1 shows on the left side the stiffness performance metric $\frac{EI}{w}$ plotted over the truss diameter D_M for the Deformable Structure of the Solid Rod Truss that is introduced in chapter 5. Displayed are the sizing results for the solar array (solid line) and solar sail application (dotted line). In addition some point design performance data are given for masts of the state-of-the-art whose properties are listed in Table 8-1.

Mast	Type	Mechanical Properties, Dimensions and Materials							
		EI	M	L	D_M	w	v	E	ρ
		Nm²	Nm	M	M	kg/m	m³/m	GPa	kg/m³
ATK/ABLE S2	Coilable	$1000 \cdot 10^3$	270	19.01	0.394	0.42	$2.073 \cdot 10^{-3}$	51.7	2020
ATK/ABLE GR1	Coilable	$81.4 \cdot 10^3$	48.6	40.3	0.394	0.07	$1.073 \cdot 10^{-3}$	188	1605
ATK/ABLE GR2	Coilable	$11.1 \cdot 10^3$	10.6	25.02	0.24	0.032	-	188	1605
ILC Dover UltraBoom	Isogrid	$11.7 \cdot 10^3$	63.6	9.06	0.18	0.145	-	143.1	1462
ATK/ABLE SRTM	Articulated	$15780 \cdot 10^3$	6525	81.78	1.12	5.232	$22.66 \cdot 10^{-3}$	165.5	1633
L'Garde SSP	Inflatable rigidizable	$1536 \cdot 10^3$	1087	78.28	1.36	0.7	-	65.8	1661

Table 8-1: Mechanical properties, geometry and material data of specific deployable masts for space applications [28] [119].

As a reference to compare these performances against, the metric is used to generate curves of same stiffness performance plotted for various values of the mass ratio Σ whereby the same material properties as the Solid Rod Truss are used. The stiffness performance of the various masts can now be assessed in relation to these lines. Thereby the reference line for $\Sigma = 1$ gives the achievable maximum performance as here only the longeron mass is considered. As one can see the stiffness performance of the Solid Rod Truss follows in principle the $\Sigma = 4$ reference line but with a changeover to smaller performances at higher mast diameters. This drop in performance coincides with the changeover in the scaling laws of the Deformable Structure due to variations in active scaling limits.

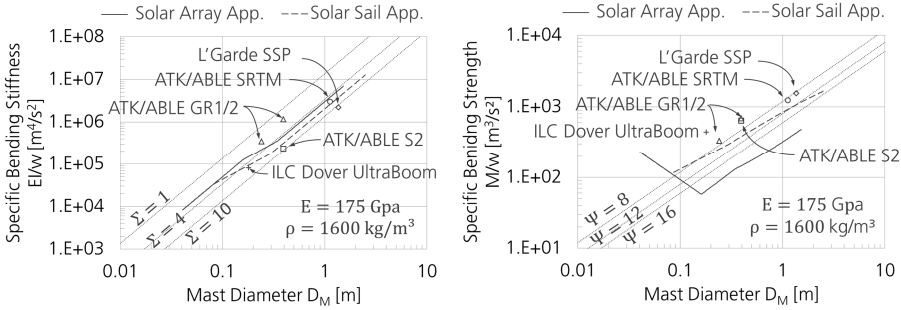

Figure 8-1: Mass specific stiffness (left) and strength (right) according to Mikulas [119] plotted over the mast diameter for the Solid Rod Truss and specific mast designs of the state-of-the-art with curves of constant performance as a reference for performance comparison.

A second metric gives the critical bending moment performance of a truss according to Equation 8-3 that relates the critical bending moment M to the specific truss mass w:

$$\frac{M}{w} = \frac{\pi^2\sqrt{2}}{4\Sigma}\frac{E}{\rho}\frac{1}{\left(\frac{l}{r_{i,l}}\right)^2}D_M \qquad 8\text{-}3$$

The strength performance depends on the longeron design represented by the ratio of the longeron length l towards the radius of gyration $r_{i,l}$. Mikulas derives different performance references through variation of the longeron design expressed by the ratio of the longeron diameter d_l towards its radius of gyration $r_{i,l}$. This ratio is given by the longeron architecture parameter Ψ according to Equations 8-4 and 8-5:

$$\left(\frac{l}{r_{i,l}}\right)^2 = \Psi\left(\frac{l}{d_l}\right)^2 \qquad 8\text{-}4$$

$$\Psi = \left(\frac{d_l}{r_{i,l}}\right)^2 \qquad 8\text{-}5$$

Thereby the metric for the critical bending moment performance is re-written in the form of Equation 8-6:

$$\frac{M}{w} = \frac{\pi^2\sqrt{2}}{4\Sigma}\frac{E}{\rho}\frac{1}{\Psi\left(\frac{l}{d_l}\right)^2}D_M \qquad 8\text{-}6$$

The critical bending moment performance $\frac{M}{w}$ is displayed on the right side of Figure 8-1 plotted over the truss diameter D_M. Again the sizing results of the Solid Rod Truss and point design data for various other trusses are given. As performance references curves that describe different longeron architecture parameters Ψ are given for comparison. The plots for the Solid Rod Truss follow at higher diameters largely the reference curves but show a significantly different behavior at small diameters. Again this is caused by the changeovers in the scaling laws due to varying active scaling limits. In the large diameter region the sizing is determined through the constraint function on critical bending moment that largely coincides with the constraint function underlying the strength performance metric. However, in the small diameter region the design is dominated by scaling limits on the minimum longeron area $A_{l,min}$ and maximum diagonal angle Θ.

A third metric is defined by Mikulas for the packaging volume performance that relates the specific stowage volume v to the bending stiffness EI as given by Equation 8-7:

$$\frac{v}{EI} = \beta\frac{8\Sigma}{ED_M^2} \qquad 8\text{-}7$$

Within the packaging volume performance metric a ratio β is introduced that relates the actual stowage volume V to the pure material volume $V_{Material}$ and is expressed by Equation 8-8:

$$\beta = \frac{V}{V_{Material}} \qquad 8\text{-}8$$

This parameter is used to generate reference curves that represent different packaging efficiencies whereby a value $\beta = 1$ gives a theoretical maximum efficiency where the actual stowage volume coincides with the material volume.

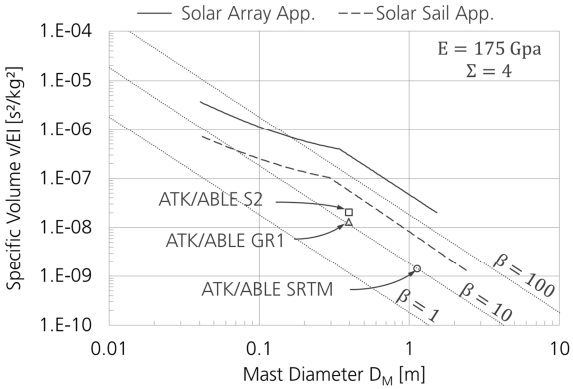

Figure 8-2: Bending stiffness specific volume according to Mikulas [119] plotted over the mast diameter for the Solid Rod Truss and specific mast designs of the state-of-the-art with curves of constant performance as a reference for performance comparison.

Figure 8-2 gives the packaging volume performance $\frac{v}{EI}$ plotted over the truss diameter D_M for the Solid Rod Truss and some examples of the state-of-the-art (see Table 8-1). Reference curves are displayed for β-values of 1, 10 and 100. Again in the high diameter region the plots of the Solid Rod Truss follow the reference curves which indicate a constant stiffness specific packaging performance. For smaller diameters where the sizing is dominated by scaling limits the packaging performance decreases with increasing diameter.

The three metrics developed by Mikulas allow an easy comparative evaluation of the mechanical performance of trusses. Although the metrics are functions of the mast diameter D_M, they enable evaluation of the structural performance independent of size. They describe lines of constant performance that are used as reference curves to compare the structures performance against. Furthermore the metrics can be used to express theoretical performance maxima as additional references for design evaluation. However, their applicability is limited by the focus of each metric on only a single design goal. Most applications for deployable masts impose requirements for both stiffness and strength which is associated with design trades that are not reflected in the metrics but influence the performance. Hence, the respective side constraint needs to be considered separately in the performance evaluation process without knowledge how stiffness translates into strength related performance and vice versa. Another aspect that needs to be considered is the presence of active scaling limits. The applicability of the metrics depends on the similarity between the evaluation subject

and the performance metric regarding the underlying scaling laws. Scaling limits cause changes in these scaling laws and can lead to misjudgments of the actual mechanical performance. This instance is particularly visible for the critical bending moment performance for small truss diameters displayed in Figure 8-1 (see right side).

8.2.2.Performance Indices by Murphey

Murphey [28] introduces performance indices for trusses that are developed for the load cases of axial compression and bending. The performance indices relate the design requirements defined by the load case to the specific truss mass w. They are derived from constraint functions that express the mechanical properties of trusses depending on their geometrical dimensions and material properties. These structure specific constraint functions are combined with those of the load case. Thereby the indices include in their basic functions both stiffness and strength requirements and incorporate the scaling laws how stiffness translates into strength related performance and vice versa. In contrast to the above presented metrics the indices express the mass specific performance through a single value that is fully independent of size and loading. Thereby the index values directly express the structures load case specific performance which can be used for comparative evaluation.

The performance index μ_c considers the load case of a truss loaded in axial compression and is derived from constraint functions of global column and local longeron buckling. It relates the length L and compression strength P to the specific truss mass w as expressed by Equation 8-9:

$$\mu_c = \frac{(LP)^{\frac{2}{3}}}{w} = \left(\frac{\pi^4}{2^3}\right)^{\frac{1}{5}} \mu_{m,c}\mu_{t,c}\mu_{l,c}\mu_{n,c} \tag{8-9}$$

Equation 8-9 also gives the performance index μ_c expressed as product of sub-indices that are given by Equations 8-10 to 8-13:

$$\mu_{m,c} = \frac{E^{\frac{2}{3}}}{\rho} \tag{8-10}$$

$$\mu_{t,c} = \frac{\beta_t}{c_t^{\frac{2}{3}}} \tag{8-11}$$

$$\mu_{l,c} = \beta_l c_l^{\frac{2}{3}} \tag{8-12}$$

$$\mu_{n,c} = \left[n \sin^2\left(\frac{\pi}{n}\right)\right]^{-\frac{1}{3}} \tag{8-13}$$

Within these equations the parameters β_t, β_l, c_t and c_l give the architecture of the truss and its longerons (for a detailed parameter description see [28]). The sub-indices describe the performance of material ($\mu_{m,c}$), truss architecture ($\mu_{t,c}$), longeron architecture ($\mu_{l,c}$) and number of longerons ($\mu_{n,c}$). They can be used to identify means for performance enhancements and evaluation of certain design decisions.

Figure 8-3 shows on the left side the performance index values μ_c for the load case of axial compression plotted over the mast length L for the Solid Rod Truss and various deployable mast point designs (see Table 8-1). In the large size region the curves for

the Solid Rod Truss are constant in case of the solar array and nearly constant for the solar sail application. Here the constraint functions for sizing of the truss are the same as those of the performance index. For smaller length where the scaling behavior of the Solid Rod Truss is dominated by scaling limits the performance becomes a function of the mast length.

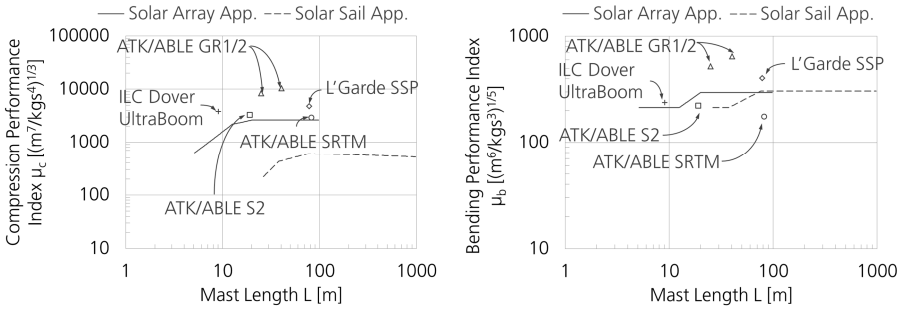

Figure 8-3: Performance indices according to Murphey [28] for the load case of axial compression (left) and bending (right) plotted over the mast length for the Solid Rod Truss and specific mast designs of the state-of-the-art.

A second performance index μ_b is developed by Murphey for the load case of bending. It relates the bending stiffness EI and critical bending moment M to the specific mass w according to Equation 8-14:

$$\mu_b = \frac{(EIM^2)^{\frac{1}{5}}}{w} = \left(\frac{\pi^4}{2}\right)^{\frac{1}{3}} \mu_{m,b}\mu_{t,b}\mu_{l,b}\mu_{n,b} \tag{8-14}$$

The bending performance index can be written as a product of sub-indices given by Equations 8-15 to 8-18 in accordance with the form of the performance index on axial compression:

$$\mu_{m,b} = \frac{E^{\frac{3}{5}}}{\rho} \tag{8-15}$$

$$\mu_{t,b} = \frac{\beta_t}{c_t^{\frac{4}{5}}} \tag{8-16}$$

$$\mu_{l,b} = \beta_l c_l^{\frac{4}{5}} \tag{8-17}$$

$$\mu_{n,b} = \left[n \sin^2\left(\frac{\pi}{n}\right)\right]^{-\frac{2}{5}} \tag{8-18}$$

Again the sub-indices allow for identification of design enhancements and quantification regarding the performance impact of certain design decisions.
Figure 8-3 shows on the right side the performance index values μ_b for the load case of bending plotted over the mast length for the Solid Rod Truss and various other mast point designs. The performance index value for the Solid Rod Truss remains in the solar

array and solar sail applications constant in the small and high length region. In between there is an increase in performance with increasing length that coincides with the changeover in the scaling laws and in particular a transition in the diagonal angle between two constant angles.

The performance indices presented by Murphey enable the performance evaluation of trusses for specific load cases fully independent of the size and design loads whereby the index value directly represents the trusses performance. Hence, interpretation relative to reference lines of constant performance as required for the metrics developed by Mikulas is not necessary. Furthermore, the indices incorporate both stiffness and strength requirements and reflect the architecture specific translation of stiffness into strength related performance and vice versa. Thus a separate evaluation regarding side constraints is not necessary. However, the applicability of the performance indices developed by Murphey is limited to the underlying load cases. Also, just like the performance metrics of Mikulas, their application requires similarity in the underlying scaling laws towards the subject of evaluation. Hence, the presence of active scaling limits needs to be considered in the evaluation process and interpretation of the results.

8.2.3.Applicability of Metrics and Indices for General Performance Evaluation Purposes

The metrics and indices developed by Mikulas and Murphey allow an easy evaluation of the mechanical performance of truss designs despite differences in sizes, materials, applications and design loads. For their use performance data of only a single point design are necessary to derive the related general performance potential of the model series. Thereby the indices presented by Murphey reflect a more thorough evaluation result as already design trades between multiple design requirements are incorporated in their formulation.

The applicability of the performance metrics and indices depends on the similarity of the underlying scaling laws to those of the subject of evaluation and its consistency throughout the analysis interval. However, the scaling behavior of the deployable structures analyzed in the previous chapters of this thesis show frequent changeovers in the scaling laws due to active scaling limits in the Deformable Structure (see Figure 7-8 and Figure 7-9). Furthermore, the system scaling behavior is the result of the individual component scaling functions and their associated scaling limits. Hence it is unlikely that a general scaling behavior of a deployable structure can be identified that provides a basis for the development of universally applicable performance metrics and indices that can be utilized within a design methodology.

Figure 8-4 shows the system scaling results for the Solid Rod Truss including the Deployment Mechanism for the stiffness performance metric $\frac{EI}{w}$ developed by Mikulas (see left side) and the axial compression performance index μ_c developed by Murphey (see right side). Both diagrams show that the performance evaluation result becomes a function of the structures size (D or L) and thereby lose their general validity. This is

particularly visible for the performance index addressing the load case of axial compression.

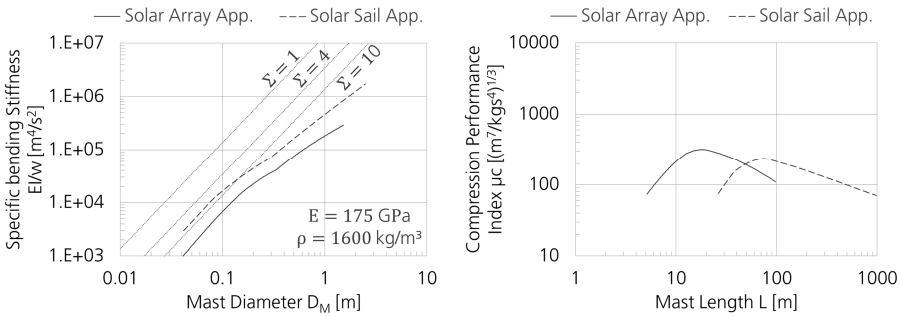

Figure 8-4: Performance evaluation of the Solid Rod Truss including the Deployment Mechanism through the stiffness performance metric developed by Mikulas (left) and the performance index for axial compression developed by Murphey (right) for the solar array (solid line) and solar sail application (dashed line).

In conclusion it is doubtful that the approach for performance evaluation reflected in the performance metrics and indices presented by Mikulas and Murphey is transferable to the performance evaluation of entire deployable structures including deployment mechanism due to the complex varying scaling behavior.

8.3. Combined Performance Evaluation of the Deformable Structure and Deployment Mechanism

In the preceding section the performance evaluation of the Deformable Structure through performance metrics and indices is investigated regarding their applicability in a conceptual design methodology. Within this section it is further investigated in how far the performance analysis of the Deformable Structure is actually representative for the overall deployable structure including the Deployment Mechanism. Therefore a comparative performance evaluation among the deployable mast concepts presented in the previous chapters of this thesis is conduct. Scaling functions for the according Deformable Structures only are derived and the corresponding evaluation results are subsequently compared to those of the overall deployable structure. Thereby only the mass specific performance is compared as the volume results are similar for both approaches as the stowage volume is largely determined through the stowed form of the Deformable Structure.

8.3.1. Deformable Structure Scaling Behavior

The scaling functions of the Deformable Structures of the Tubular Shell Mast (with and without load carrying Transition Zone), the Solid Rod Truss and the Telescopic Tubular

Mast are presented in chapters 5, 6 and 7. The scaling behavior is derived by calculation of the minimum mass results of the Deformable Structure without consideration of the mechanism components. Figure 8-5 shows the scaling behavior regarding specific mast mass w plotted over mast length L of the masts Deformable Structures for the solar array (left) and solar sail application (right).

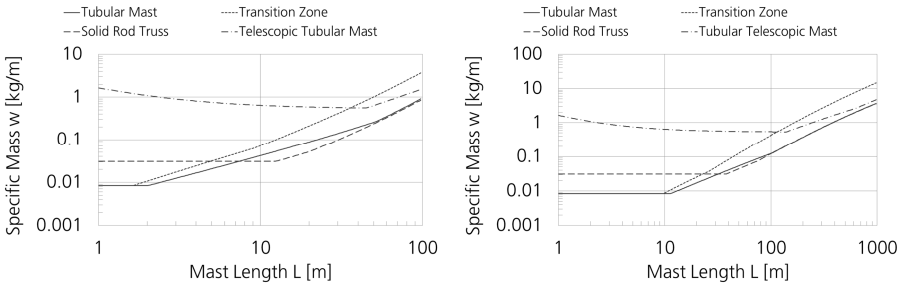

Figure 8-5: Specific mass scaling functions of the Deformable Structure plotted over the mast length for the solar array (left) and solar sail application (right).

The mass scaling plots for the Deformable Structures show a similar behavior as observed for the overall deployable masts. The sizing is largely dominated by scaling limits which is expressed by the constant or decreasing performance in the small scale region and the frequent discontinuities which mark changeovers in the scaling laws. Only in the large size region the sizing of the Deformable Structures is free of active scaling limits and determined through stiffness and strength constraints except for the Telescopic Tubular Mast.
On the basis of the mass scaling results displayed in Figure 8-5 a comparative performance evaluation is conducted in the following. The scaling function results for the stowage volume are not evaluated as here the results of the Deformable Structure are the same as for the full mast system.

8.3.2. Comparative Performance Evaluation

The performance evaluation is done comparatively between the four considered mast concepts. For each design length L the best performing concept is identified for the solar array and solar sail applications. The evaluation results gained from comparison of the scaling behavior of the Deformable Structures and the overall masts including the Deployment Mechanisms are subsequently compared.
Figure 8-6 shows the evaluation results for a solar array application and the Tubular Shell Mast without consideration of a load carrying Transition Zone. On the left side the evaluation results on the basis of the scaling behavior of the Deformable Structure is presented while on the right the results gained from the overall scaling behavior are shown. An evaluation of the basis of the Deformable Structure would lead to selection of the Tubular Shell Mast up to a length of 8 m, above the Solid Rod Truss performs

best. A significantly different concept selection result is gained through comparison of the overall scaling functions. Here the Tubular Shell Mast shows the lowest mass up to a length of 50 m while above the Telescopic Tubular Mast is selected.

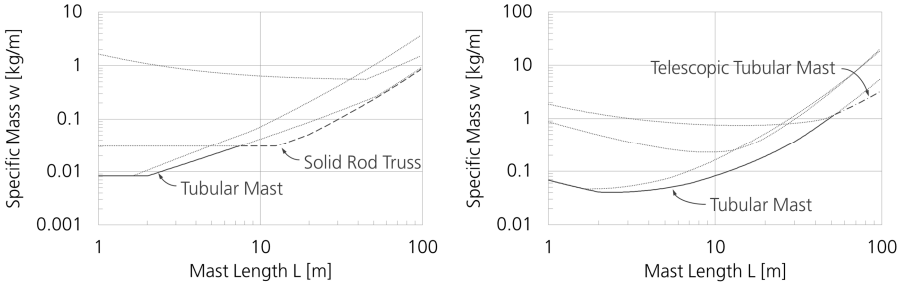

Figure 8-6: Concept selection results for a solar array application based on the specific mass scaling functions of the Deformable Structure (left) and the overall system (right) without consideration of load carrying Transition Zones.

Figure 8-7 shows the same application but with consideration of a load carrying Transition Zone for the Tubular Shell Mast. For evaluation by the Deformable Structure the Tubular Shell Mast is selected up to a length of 5 m while above the Solid Rod Truss performs best. When considering the overall scaling behavior as basis for the evaluation the Tubular Shell Mast is selected up to a length of 14 m followed by the Solid Rod Truss which shows the highest performance between 14 m and 28 m. Above again the Telescopic Tubular Mast is selected.

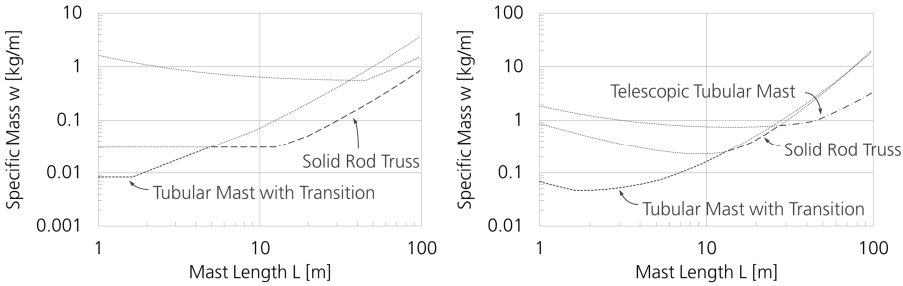

Figure 8-7: Concept selection results for a solar array application based on the specific mass scaling functions of the Deformable Structure (left) and the overall system (right) with consideration of load carrying Transition Zones.

Figure 8-8 shows the respective results for the solar sail application for the fully deployed configurations without consideration of a transition under load. Again the evaluation results gained from the Deformable Structures scaling behavior (left) significantly different to those derived from the overall scaling behavior (right). In the

first case the Tubular Shell Mast outperforms its competitors up to 30 m and again from 105 m to 450 m. In the remaining intervals the Solid Rod Truss shows the best performance but the specific masses are very similar to the Tubular Shell Mast. When considering the overall scaling behavior for the evaluation the Tubular Shell Mast performs best up to a length of 245 m, above the Telescopic Tubular Mast is selected.

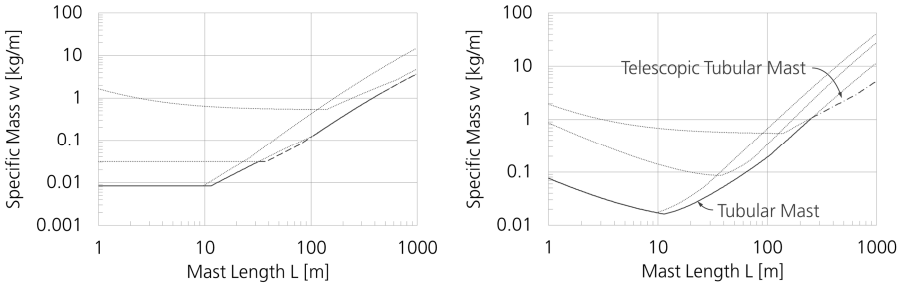

Figure 8-8: Concept selection results for a solar sail application based on the specific mass scaling functions of the Deformable Structure (left) and the overall system (right) without consideration of load carrying Transition Zones.

Figure 8-9 displays the evaluation results for the solar sail application with consideration of a transition under load for the Tubular Shell Mast. The best performing concepts when considering only the Deformable Structure (see left side) are again the Tubular Shell Mast in the small scale region and the Solid Rod Truss in the large size region. The changeover occurs at a length of 23 m. The evaluation of the overall system (see right side) shows for the Tubular Shell Mast with a load carrying Transition Zone an advantage in mass up to a length of 35 m. Above this length and up to 132 m the Solid Rod Truss shows superior values while for even larger sails the Telescopic Tubular Mast outperforms its competitors.

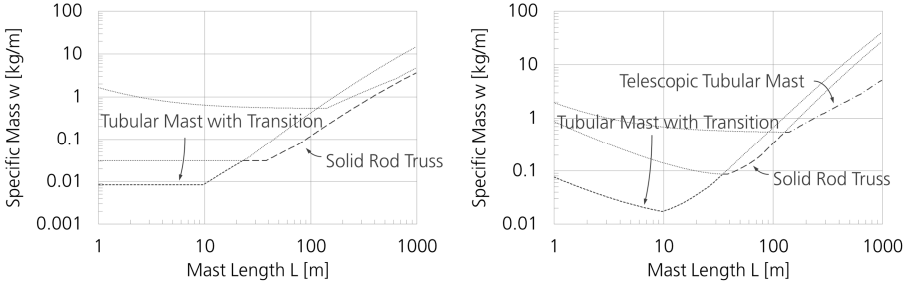

Figure 8-9: Concept selection results for a solar sail application based on the specific mass scaling functions of the Deformable Structure (left) and the overall system (right) with consideration of load carrying Transition Zones.

In conclusion, the evaluation results derived from the scaling behavior of the Deformable Structure and the overall deployable mast including the Deployment Mechanism lead to significantly different concept selection decisions. Hence, a comparative evaluation based on the scaling behavior of the Deformable Structure is not representative for the overall system. Furthermore the differences are significant wherefore this simplified approach is not suited for evaluation purposes within a general conceptual design methodology. These findings support the hypothesis formulated in subsection 3.5.5 which states that the entire deployable structure needs to be subject of the evaluation process already in the phase of conceptual design.

8.4. Conclusions on Concept Evaluation Methods for Use in the Conceptual Design

In this chapter means for the performance evaluation of Deployable Space Structures are examined. Particularly quantification of mass and volume related performance through specific metrics and indices are analyzed and it is investigated in how far a performance evaluation on the basis of the Deformable Structure only is representative for the overall system. The results contribute to the performance evaluation process that is the basis for the concept selection at the end of the phase of conceptual design.

The investigations show that performance indices and metrics are not generally applicable for evaluation purposes aside from the component level or designs that feature a low complexity in their scaling behavior due to a minimal designed Deployment Mechanism. The approach is based on the similarity of the underlying scaling functions towards that of the evaluation subject. However, the deployable structures considered for the analysis show complex scaling behaviors that are largely influenced by component scaling limits which cause multiple changeovers in the scaling laws. Hence it is doubtful that a characteristic scaling behavior of general validity can be identified that provides a basis for the development of according metrics or indices.

Furthermore it is shown that the performance evaluation for concept selection has to target the overall system and thereby supports the hypothesis formulated in subsection 3.5.5. An evaluation based on the Deformable Structure only leads to significant differences in the concept selection decisions. Hence, both the Deformable Structure and the Deployment Mechanism components have to be designed within the phase of conceptual design up to a level where performance quantification becomes possible. However, the simplified approach of considering only the Deformable Structure within the performance evaluation process may be applicable for volume related design goals as the stowed form largely depends only on the Deformable Structure. In general a direct performance comparison of the system properties reflecting the design goals is recommended.

9. Development of the Conceptual Design Methodology for Deployable Space Structures

On the basis of the system analysis described in chapters 4 to 8 a methodology for the conceptual design of Deployable Space Structures is developed and design principles are deduced. The method reflects in its processes the thereby identified design drivers and specific characteristics of this category of structures while the design principles describe means for generation of solution with potentially high solution quality.
In this chapter first the application focus of the conceptual design methodology is presented and its classification with respect to the general design methods given in VDI 2221 and VDI 2222 is described. To ensure clearness in the understanding, the terminology used in the descriptions of the methodology is defined. Subsequently the main processes of the new conceptual design method are described. The chapter is concluded by a list of general design principles applicable to Deployable Space Structures.

9.1. Application Focus of the Methodology

The conceptual design methodology is developed for the specific characteristics and design objectives of Deployable Space Structures. In the following these characteristics and objectives are defined and a classification of the methodology in relation to the general design methods described in VDI 2221 and VDI 2222 is given. Aside from Deployable Space Structures the methodology may be utilized for other deployable structures that feature similar characteristics and design goals as given in the following.

9.1.1. Characteristics of the Design Object

The specific characteristics of Deployable Space Structures result from the transport into space, the environmental conditions on-orbit and the unique mission profiles connected with space applications.
The overall function of a Deployable Space Structure is to deform or move an object from a stowed state that is beneficial for the transport into space to a deployed state that is required for its function (cf. Figure 3-1). Hence, a major characteristic of Deployable Space Structures is that the ability to change shape is not a requirement of its direct operational function but results from the limited transport capabilities of launchers regarding payload volume. Therefore Deployable Space Structures possess in general only two specific states of form which feature a large difference in size and are only little constrained regarding their deployment path between these states. The transition is done in the majority of missions and applications only once with locking in the deployed configuration. Thereby low deployment speeds are selected to avoid dynamic load events.

The Deployable Space Structure consists of two parts: a Deformable Structure and a Deployment Mechanism. The Deformable Structure provides the structural support to the object that needs to be deformed or moved and the Deployment Mechanism constrains and controls the deployment process and in most cases also generates and introduces the deployment forces. The designs of the Deformable Structure are largely influenced by the environmental conditions on-orbit. During transition and in the operational state they are subjected to only small external mechanical loads due to weightlessness. Hence, sizing according to these loads leads to lightweight designs of large deployed volume that are composed of thin-walled and slender elements.
In contrast to the conditions on-orbit, during launch high dynamic and static mechanical loads are imposed on the Deployable Space Structure in its stowed state. Therefore they possess in general a support structure that is sized according to these high mechanical loads and contains and supports the folded Deformable Structure and the mechanism components during space transport.
Table 9-1 summarizes the specific requirements and characteristics of Deployable Space Structures which describe the methods application focus. For comparison according example values for a deployable aircraft flap are given.

Characteristic	Deployable Space Structure	Deployable Aircraft Flap
States of form	2	Several
States of operational forms	1	Several
Change in size	High	Moderate
Transition speed	Small	Moderate
Transition cycles	1	Infinite
Transition direction	One-way	Dual-way
External mechanical load intensity in stowed state	High	Moderate
External mechanical load intensity during transition	Small	High
External mechanical load intensity in deployed state	Small	High

Table 9-1: General characteristics of Deployable Space Structures in comparison to a deployable aircraft flap.

9.1.2.Design Task and Objectives

The specific characteristics of Deployable Space Structures result from similarities in the design tasks and design objectives. These always contain requirements and design goals regarding the stowed volume, stowed form, deployed form and mass. Thereby the requirements for the deployed form are specific and strict as they determine the structures operational functionality, while those for the stowage volume, stowed form and mass are in general reflected in the design objectives and mark performance data that are to be optimized.
The majority of design tasks aim on a high performance regarding the design objectives with functional compliance as a necessary constraint. In most cases a high competitiveness in comparison to solutions of the state-of-the-art is desired as design

tasks addressing entirely new applications are seldom. Thereby the competitiveness of a solution is in general measured in terms of stowage volume and mass. Generating solutions with a high performance regarding these general design objectives is at the heart of this design methodology.

9.1.3. Classification of the Methodology in Relation to VDI 2221 and VDI 2222

The application focus in the design process of the conceptual design methodology for Deployable Space Structures is described in relation to the general design methods described in VDI 2221 [132] and VDI 2222 [135]. This classification is displayed in Figure 9-1.

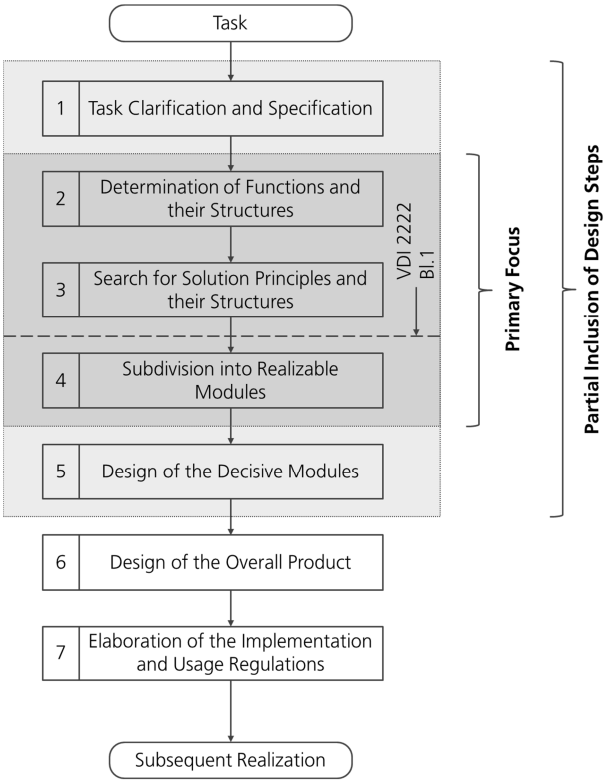

Figure 9-1: Primary focus of the conceptual design method for Deployable Space Structures and area of partially included design steps with respect to VDI 2221.

The design methodology does not fully comply with the structure of VDI 2221 but focusses primarily on the tasks 2 to 4. In addition to the primary focus some elements of the design tasks 1 and 5 are partially included in the methodologies processes. Thereby the application area is expanded over that of VDI 2222 which describes a general conceptual design methodology and focusses on the tasks 1 to 3. This broader scope results from the desired evaluation based on performance quantification. For such an evaluation a higher level of detail in the design is required. This includes basic physical models of the main components of the deployable structure to enable derivation of according properties. Thereby some elements of the preliminary design are to be included. The definition of the design task and derivation of requirements is done according to task 1 of VDI 2221. However, although a dedicated process is not defined, some comments on load cases that are specific to Deployable Space Structures and are primary sources for functional and mechanical requirements are given in subsection 9.3.1.

9.2. Terminology of the Methodology

To ensure correct understanding of the descriptions of the conceptual design methodology a well-defined terminology is of particular importance. In the following the basic terms are described in their specific meaning as utilized within these descriptions. The general terminology follows the definitions given in VDI 2221 and VDI 2222 whereby some terms are recapitulated in the following.

9.2.1. Terms Specific to Deployable Space Structures

Definitions of the Deployable Space Structure and its main elements are given on the basis of the functional analysis displayed in Figure 3-1:

→ Deployable (Space) Structure: The deployable structure supports an object that is the function carrier. This object may be an instrument or a functional surface such as a reflector mesh or a photovoltaic blanket. The deployable structure deforms or moves this object from the stowed into the deployed, operational configuration. A deployable structure consists of a Deformable Structure and a Deployment Mechanism.

→ Deformable Structure: The Deformable Structure is a structure that is foldable to enable a form transition between the stowed state of small volume or beneficial form and the deployed, operational state. It transmits the forces necessary to deform or move the supported object and provides stiffness and stability during and after deployment.

→ Deployment Mechanism: The Deployment Mechanism acts on the Deformable Structure. Its functional capabilities depend on the Deformable Structure and may include generation and introduction of the deployment forces as well as to release, guide and control the Deformable Structure during the transition and enable latching in deployed state.

9.2.2. Applicable Terms of VDI 2221 and VDI 2222

Some terms defined in VDI 2221 and VDI 2222 are essential for the description of the methodologies processes and are recapitulated here:

→ Function: A function describes the behavior or task of a product or a part of a product.

→ Overall Function: The overall function describes the overall behavior the design object has to provide.

→ Main Function: The main functions are the first layer of sub-functions of the overall function and describe the fundamental functions necessary to enable the overall function.

→ Principle Solution: The principle solution describes basic concretizations for realization of a function or functional structure through physical effects and form.

9.2.3. Terms Addressing the Design Hierarchy

Within the conceptual design methodology the degree of concretization continuously increases. The following terms describe different states of concretization of the design object and its parts:

→ Component: The component describes a construction element for the realization of one or several principle solutions. A component can be a single part or an assembly of functionally interacting parts.

→ Physical Model: The physical model is a basic realization of a component or system that allows deduction of certain physical properties such as dimensions and mass.

→ System: The system is an assembly of components that fulfils a higher ranking function (overall function) through functional interaction of its components. For example the Deployable Space Structure is a system that fulfils the overall function of deforming or moving an object between two desired states of form.

9.3. Description of the Conceptual Design Methodology

The methodology for the conceptual design of Deployable Space Structures is developed on the basis of the system analyses described throughout the chapters 4 to 8. It is subdivided into four processes which are executed sequentially. Regression and iteration loops among and within these processes are not specifically outlined but should be executed in case of invalid overall or intermediate results or in case of identified enhancements and innovations with increasing knowledge concerning the design object. Figure 9-8 displays the four processes of the conceptual design methodology and its primary outputs.

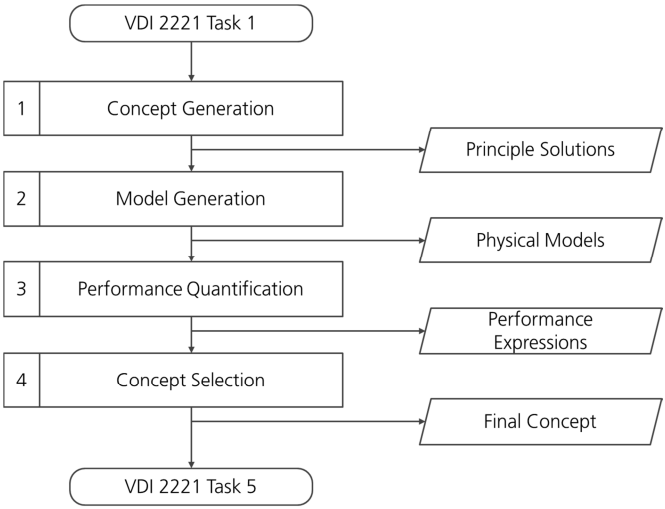

Figure 9-2: Overview on the process steps of the conceptual design method of Deployable Space Structures.

The methodology requires as input the output of VDI 2221 Task 1 'Clarification and Specification of the Design Task' and generates the necessary input for the subsequent VDI 2221 Task 5 'Design of Decisive Modules'. It starts in Process #1 with the generation of a variety of concepts in the form of principle solutions through basic design decisions on the Deformable Structure and definition of the functional capabilities of the Deployment Mechanism. In Process #2 these principle solutions are further developed to physical models that already consist of specific components with basic definitions of their physical forms. In Process #3 expressions on specific physical properties that reflect the performances regarding the design objectives are derived from the physical models. The methodology is concluded by Process #4 with the selection of a single concept for further development steps on the basis of a comparative performance evaluation.

9.3.1.Sources of Functional and Mechanical Requirements

The task and requirements definitions are done according to VDI 2221 Task 1 'Clarification and Specification of the Design Task' and are not addressed in a dedicated process within this design methodology. However, in the following some sources for requirements specific to Deployable Space Structures are presented. In the phase of conceptual design in particular functional requirements, requirements that constrain the design space and mechanical loads are to be considered. Such requirements arise primarily from four specific load cases:

→ Ground Testing: Deployable structures often reach large dimension while being mechanically only lightly loaded due to the zero-g environment on-orbit. Sizing

according to these small operational loads leads to lightweight structures composed of slender and thin-walled elements. Ground based testing of such structures in a one-g environment with additional gravity compensation systems can introduce significant mechanical loads that may be higher than during deployment and operation. However, ground testing is an integral part of the qualification process. Furthermore qualification testing often includes a high number of deployment cycles to demonstrate functional reliability although on-orbit only a single deployment event is performed in general. Hence, ground testing can introduce significant design requirements regarding mechanical loading, fatigue and general compliance with methods for ground-testing of the deployable structure.

→ Space Transport: The transport into space introduces requirements regarding mass, stowage volume and stowed form and is a source of severe mechanical loading. Additional volume, form and interface constraints are introduced by the host spacecraft whose dynamic behavior can also cause significant amplification of the mechanical loads applied by the launcher. These loads are design driving for the stowed form of the deployable structure and the mechanism components particularly in case of small and lightweight sub-systems.

→ Deployment: The unfolding of the deployable structure introduces requirements regarding the deployment path, generated deployment forces and stiffness and stability that needs to be provided to the supported object. Additionally deployment errors of the structure itself or the supported object can be sources of significant mechanical loading which requires according robustness. In many cases the main mechanical load event occurs at the end of the deployment and results from tensioning or stretching of functional surfaces such as the photovoltaic blankets of solar arrays. The definition of requirements for the load case of deployment is of high significance. Even low mechanical load requirements can have a high impact on the deployable structures design as the transition may be connected with considerably reduced mechanical properties of the Deformable Structure (cf. chapter 6).

→ Operation: During operation the deployable structure is in its fully deployed state and in general subjected to small external loads due to the zero-g environment. Significant strength requirements result from tension loads the deployable structure has to provide to the supported object. Additional mechanical loads may arise from docking events or high thrust manoeuvers. Requirements on the structures deployed stiffness are derived from constraints set by the spacecraft attitude control system and form accuracy under load.

There are several other specific sources for requirements resulting from mission profiles and design tasks which are to be considered in the phase of conceptual design. Some sources of requirements specifically applicable to Deployable Space Structures are listed in the following:

→ Stowage Time: Long stowage durations on ground before launch or on-orbit before deployment impose requirements particularly on the material selection. Creep and corrosion on ground or atomic oxygen and radiation on-orbit can

cause significant degradation. Stowage duration is design driving for applications such as drag sails that are utilized for end-of-life manoeuvers in a low earth orbit.

→ Interface Constraints: The interface between the supported object and the deployable structure imposes requirements on the structural architecture, folding principle and deployment path. An example is a mesh reflector that requires circumferential interface points for attachment of its shape giving net.

→ Shape Accuracy: Shape accuracy requirements significantly influence the design of a deployable structure as they involve the deployment precision, thermal stability, manufacturing quality and stiffness. Examples are support structures of optics, antenna reflectors or instrument booms.

→ System and Spacecraft Compatibility: Similar to the interface constraints the compatibility with the deployable system and the spacecraft causes requirements regarding volume limitations and desired stowed forms. Examples are deployable solar arrays located on the outside of the spacecraft whose stowed form is constrained by the spacecraft itself and the surrounding payload fairing. Here planar stowed forms of low height are desired.

9.3.2.Process #1: Concept Generation

Process #1 of the conceptual design methodology addresses the generation of a variety of basic concepts as the first step of the conceptual design method. The outputs are several principle solutions which incorporate first definitions of the Deformable Structures design and the definition of the required Deployment Mechanism functionalities and subsequent selection of according principle solutions. Inputs to Process #1 are the task and requirements definitions according to VDI 2221 Task 1 'Clarification and Specification of the Design Task' under consideration of the beforehand introduced load cases. Figure 9-3 displays the process for generation of concepts and its design steps with the intermediate outputs as a flow-diagram.

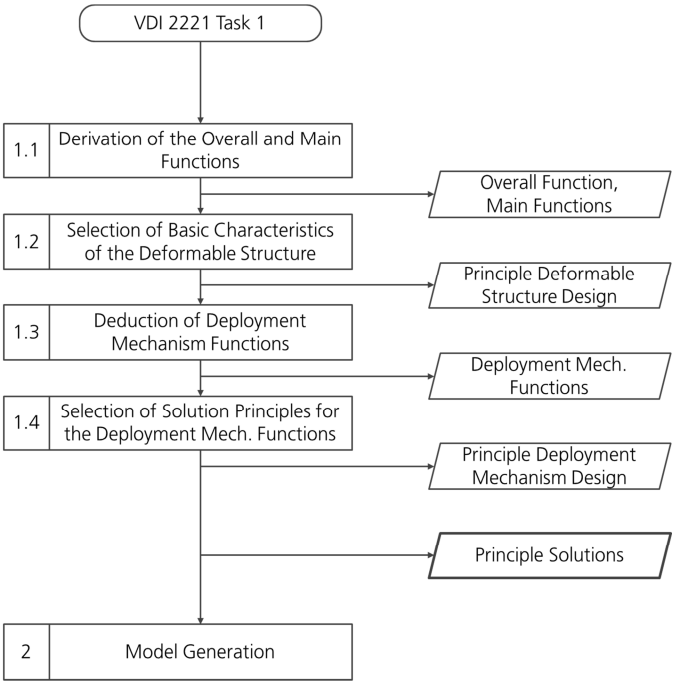

Figure 9-3: Flow diagram of Process #1 'Concept Generation' with related design steps and intermediate outputs.

The outputs of Process #1 are several principle solutions which are established sequentially through four design steps:

1.1 Derivation of the Overall and Main Functions:
In process step 1.1 the overall function and the main functions are developed. As a role model the according representation given in Figure 9-7 of section 9.4 may be utilized. The procedure is the same as given in VDI 2221 Task 2 'Determination of Functions and their Structures' (see also VDI 2222 Task 2.1 and Task 2.2).

1.2 Selection of Basic Characteristics of the Deformable Structure:
In process step 1.2 the designs of the Deformable Structures are concretized based on the beforehand derived functional description. Therefore its basic characteristics are selected which are the definition of the geometry through selection of a structural architecture, the selection of a folding principle through definition of the kinematics and the selection of a deployment principle through definition of a physical effect to achieve deployment. Outputs of this design step are the 'Principle Deformable Structure Designs' which provide the basis for the

definition of the functional capabilities of the Deployment Mechanism in the subsequent design step.

1.3 Deduction of Deployment Mechanism Functions:
Process step 1.3 addresses the definition of the required functions of the Deployment Mechanism. The required functions are deduced from the principle designs of the Deformable Structures represented by the basic characteristics. For the definition of the mechanism functions the general functional mechanism model presented hereafter in Figure 9-8 of section 9.4 may be used. Outputs of this design steps are the Deployment Mechanism functions and their structures.

1.4 Selection of Solution Principles for the Deployment Mechanism Functions:
In process step 1.4 principle solutions for the Deployment Mechanism functions are established through selection of according physical effects and basic forms. The design step comprises the Tasks 3.1 and 3.2 'Search for Solution Principles' of VDI 2222. Outputs of this design step are the 'Principle Deployment Mechanism Designs'. The summarized outputs of the design steps 1.1 to 1.4 represent the 'Principle Solutions' of the generated concepts as overall outputs of Process #1.

The structure of Process #1 is largely based on the analyses of the Deployment Mechanisms and its design interactions with the Deformable Structure conducted in chapters 4 and 5. These analyses revealed that the design of the Deployment Mechanism depends in its physical form and functional capabilities largely on the Deformable Structure. The physical form is determined through the stowed, deploying and deployed forms of the Deformable Structure which result from its architecture and folding principle. The functional capabilities are a consequence of the selected architecture and folding principle as well but are completed through selection of a deployment principle. Hence, design decisions on these three basic characteristics are to be made before a full functional description of the Deployment Mechanism becomes possible. Thereby these decisions still feature a high level of abstraction while the level of concretization remains low to not overly constrain the solution space at such an early state.

Table 9-2 summarizes Process #1 'Concept Generation'.

Process #1: Concept Generation	
Input	VDI 2221 Task 1: Task Definition VDI 2221 Task 1: Requirements Definition
Applicable Tools and Design Principles	Tool: General Overall Function (Figure 9-7) Tool: General Functional Mechanism Model (Figure 9-8) Design Principle: Sub-Function Minimization (subsection 9.5.2) Design Principle: Compact Stowage (subsection 9.5.3) Design Principle: Stowed Form Compatibility (subsection 9.5.4) Design Principle: Shifting of Scaling Limits (subsection 9.5.5) Design Principle: Avoiding Mechanical Degradation during Transition (subsection 9.5.6)

Process Steps	[1.1] Derivation of the Overall Function: From the task and requirements definitions the overall and main functions are deriveSd. [1.2] Selection of Basic Characteristics of the Deformable Structure: The principle design of the Deformable Structure is concretized. The geometry is detailed through selection of a structural architecture. A folding principle is selected that defines the kinematics and stowed form of the Deformable Structure. A deployment principle is selected through choosing physical effects and types of energy utilized for the form transition. [1.3] Deduction of Deployment Mechanism Functions: The required functional capabilities of the Deployment Mechanism are defined. From the basic characteristics of the Deformable Structure functional requirements are deduced. [1.4] Selection of Solution Principles for the Deployment Mechanism Functions: Solution principles for the Deployment Mechanism functions are established. A search for applicable solution principles is conducted and specific sets are selected.
Output	Principle Solutions
Abstract	A variety of principle solutions are established. For each solution the primary characteristics of the Deformable Structure are selected in terms of structural architecture, folding principle and deployment principle. From these primary characteristics required mechanism functionalities are deduced and applicable principle solutions are selected.

Table 9-2: Summary description of Process #1 addressing the generation of concepts.

9.3.3.Process #2: Model Generation

Process #2 addresses the translation of the principle solutions of the Deformable Structure and the Deployment Mechanism into models that allow deduction of physical properties necessary to enable performance quantification regarding the design objectives in the subsequent Process #3. The required inputs are the concepts described by the principle solutions of the Deformable Structures and Deployment Mechanisms while the outputs are the according physical models. Figure 9-4 displays the process for generation of the physical models and its design steps with the intermediate outputs as a flow-diagram.

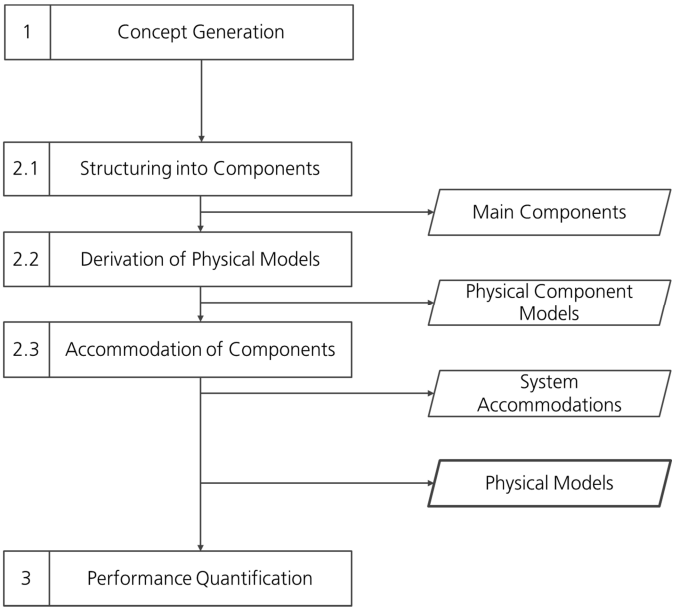

Figure 9-4: Flow diagram of Process #2 'Model Generation' with related design steps and intermediate outputs.

The outputs of Process #2 are the physical models of the according concepts generated in process #1 and are derived sequentially through three design steps:

2.1 Structuring into Components:
In process step 2.1 the concretization of the functional descriptions and selected principle solutions towards components is performed. Thereby the functions and according principle solutions are structured for realization within specific components. This design step is similar to VDI 2221 Task 4 'Structuring into Realizable Modules' but emphasizes the implementation into specific components that can be translated into separate physical models in the subsequent process step. The outputs of this process step are the main components of the concepts. Within this process step the design principle of function integration as described in chapter 7 and summarized in subsection 9.5.1 may be applied.

2.2 Derivation of Physical Models:
Within process step 2.2 the main components are translated into approximation models that enable deduction of the specific physical properties which represent the concepts performance regarding the design objectives. This translation does not necessarily have to result in a geometric representation of the component. For example the mass approximation model of an energy storage unit may be a simple mass point with a specific energy density as described in subsection 4.2.4.

Outputs of this step are the physical models of the main components of each concept.

2.3 Accommodation of Components:
In process step 2.3 the arrangements of the components in relation to each other for the stowed, deploying and deployed state are defined. From these component accommodations physical properties of the system such as the outer dimensions can be deduced. The outputs of this step are the system accommodations of each concept which may be described through design sketches for the three states of form. The summarized outputs of the three design steps represent the 'Physical Models' of the concepts which are the overall outputs of Process #2.

The structure of Process #2 is determined by the necessity to advance the designs of the generated concepts to a level where performance description through quantification in Process #3 becomes possible. These design advancements aim on component models that represent specific physical properties and are not equal to entire preliminary designs. Furthermore only those components have to be considered which contribute to the targeted system properties. For example the derivation of the stowage volume of a deployable structure requires determination of the outer envelope. Therefore the physical models generated in this Process #2 may consist only of a small number of components which drive the outer dimensions. In addition, throughout Process #2 compliance with functional requirements of the so far generated solutions should be continuously checked, whereby initial dimensioning calculations can also be used. This particularly includes the kinematic of the Deformable Structure. Furthermore detailing the design within Process #2 may introduce additional design constraints and functions for the Deformable Structure and the Deployment Mechanism.
Table 9-3 summarizes Process #2 'Model Generation'.

Process #2: Model Generation	
Input	VDI 2221 Task 1: Requirements Definition Output Process #1: Functional Concepts
Applicable Tools and Design Principles	Design Principle: Function Integration (subsection 9.5.1) Design Principle: Compact Stowed Form (subsection 9.5.3) Design Principle: Stowed Form Compatibility (subsection 9.5.4) Design Principle: Shifting of Scaling Limits (subsection 9.5.5) Design Principle: Avoiding Mechanical Degradation during Transition (subsection 9.5.6)
Process Steps	[2.1] Structuring into Components: The functions and principle solutions are concretized towards specific components. [2.2] Derivation of Physical Models: The components are translated into models that describe specific physical properties necessary for performance quantification in the subsequent process. [2.3] Accommodation of Components: The arrangements of the components in the stowed, deploying and deployed state are concretized in dedicated accommodations to enable derivation of system properties.

Output	Physical Models
Abstract	Concept models with specific physical forms are established. The principles solutions for the Deformable Structure and Deployment Mechanism are translated into basic components. Models of the components that allow deduction of physical properties are established and an accommodation of the overall model is defined.

Table 9-3: Summary description of Process #2 addressing the generation of physical models.

9.3.4.Process #3: Performance Quantification

Process #3 addresses the quantification of the concept performances with regard to the design objectives. Based on the physical models generated in the previous Process #2, expressions for those physical properties are derived which represent the design objectives. These performance expressions are the basis for the concept selection in the subsequent Process #4. Figure 9-5 displays the process for performance quantification and its design steps with the intermediate outputs as a flow-diagram.

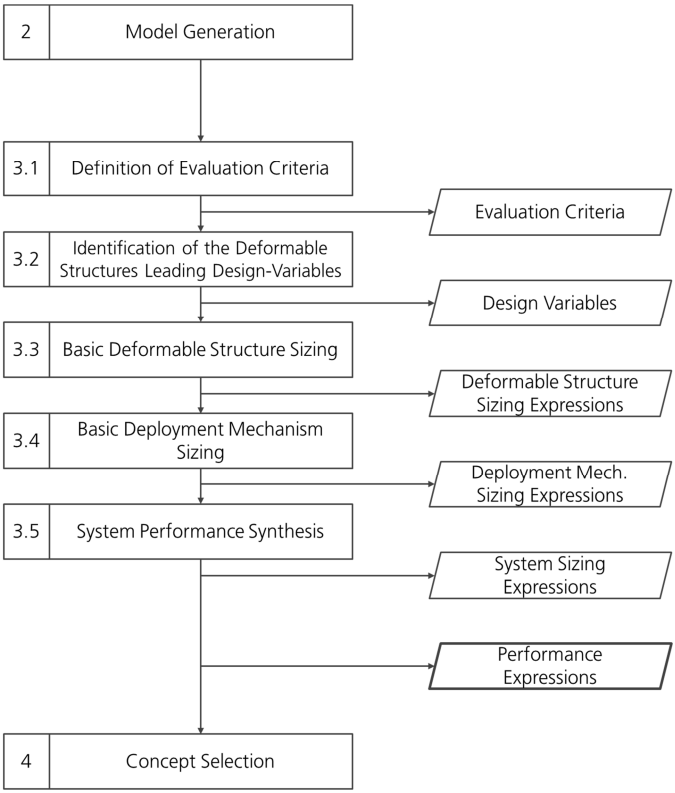

Figure 9-5: Flow diagram of Process #3 'Performance Quantification' with related design steps and intermediate outputs.

The outputs of Process #3 are performance expressions for the deployable structure which are derived through five sequential design steps:

3.1 Definition of Evaluation Criteria:
In process step 3.1 evaluation criteria in terms of specific physical properties are defined which express the design objectives. Such criteria may be the stowage volume or a certain characteristic length that expresses the compatibility with specific requirements regarding the stowed form. Output of this process step is a list of criteria that are to be included in the performance evaluation.

3.2 Identification of the Deformable Structures Leading Design Variables:
The process step 3.2 addresses the identification of the design variables of the Deformable Structure. These represent the leading design variables of the overall deployable structure as they also determine the design of the Deployment

Mechanism components (cf. chapter 4). Output of this design step is a list of design variables and possibly according design sketches.

3.3 Basic Deformable Structure Sizing:
In process step 3.3 the sizing expressions for the Deformable Structure are derived. Therefore load case specific constraint functions and according functions for the selected type of structural architecture are established and scaling limits are identified. Thereby it is essential to also establish constraint functions for each scaling limit and their combinations. The formulation of the constraint functions for the deformable should also consider sensitivities towards geometrical imperfections. Furthermore, in case of wide design intervals it may be advantageous to couple load and size requirements according to the intended type of application to minimize the number of independent design requirements. The derivation of the sizing expressions may be done according to section 5.1. Examples for sizing expressions in the form of scaling functions are given in subsections 5.2, 5.3, 6.4 and 7.2.1. Outputs of the process step are the load case specific Deformable Structures sizing expressions.

3.4 Basic Deployment Mechanism Sizing:
In process step 3.4 the sizing equations of the Deployment Mechanism are derived on the basis of the Deformable Structures sizing expressions. The expressions utilize the same design variables as the Deformable Structure and their derivation may be done through the procedure described in subsection 4.2.4. Examples for the mechanism sizing expressions in the form of scaling functions are given in section 4.3. Here again it is essential to consider the component scaling limits and their combinations in the underlying constraint functions. Outputs of this design step are the Deployment Mechanism sizing expressions.

3.5 System Performance Synthesis:
In the final process step 3.5 the system sizing expression are synthesized. For each evaluation criterion the sizing expressions of the Deformable Structures and Deployment Mechanisms are merged and refined to according system performance expressions. The fifth process step also includes generation of performance expressions for evaluation criteria which cannot be directly calculated from the underlying sizing expressions and are at least partially deduced by estimations. Such a criterion may be the system costs which in general scale with the size but where an exact expression cannot be derived. The sum of these performance expressions marks the overall output of Process #3.

Process #3 is based in its structure on the design dependencies between Deformable Structure and Deployment Mechanism identified in chapters 4 and 5 wherefore it is similar to Process #1. Thereby the Deformable Structure is the leading component which determines the Deployment Mechanism design through its stowed and deploying form. Hence, the design variables of the Deformable Structure are also valid

for the Deployment Mechanism components to describe their required geometric size and intensity of the provided physical effects. Thereby sizing of the Deformable Structure determines also the sizing result of the Deployment Mechanism components and needs to be done beforehand. Furthermore within chapter 5 it was found that in most design cases there is no need for an optimization process within early design stages. Hence, the derivation of the sizing expressions of Deformable Structure and Deployment Mechanism components is done sequentially.
Process #3 'Performance Quantification' requires significant development efforts as the concept designs have to be advanced up to a level where such quantification becomes possible. This also involves elements of the phase of preliminary design. However, as stated in section 8.1, Deployable Space Structures are complex designs with a high degree of design interactions among its components and a variety of active scaling limits which complicates its accessibility to performance evaluation by intuitive and qualitative methods. Hence, to enable a concept selection process with a small degree in performance uncertainty, evaluation by quantification is preferred and is essential for a high overall solution quality. This is particularly true for design tasks where a high competitiveness with respect to products of the state-of-the-art is desired.

Table 9-4 summarizes Process #3 'Performance Quantification'.

Process #3: Performance Quantification	
Input	VDI 2221 Task 1: Design Objectives Definition VDI 2221 Task 1: Requirements Definition Output #2: Physical Component Models Output #2: Accommodation Sketches
Applicable Tools and Design Principles	Tool: Procedure for Parameterization and Scaling Function Derivation (subsection 4.2.4)
Process Steps	[3.1] Definition of Evaluation Criteria: Specific physical properties are identified that are utilized for performance quantification. [3.2] Identification of the Deformable Structures Leading Design Variables: From the Deformable Structure the leading parameters are identified which serve as design variables for the deployable structure. [3.3] Basic Deformable Structure Sizing: Basic expressions for the sizing of the Deformable Structure according to the design requirements are established. [3.4] Basic Deployment Mechanism Sizing: Basic expressions for the sizing of the Deployment Mechanism components are established depending on the Deformable Structures sizing results and design variables. [3.5] System Performance Synthesis: The sizing expressions for the Deformable Structure and the Deployment Mechanism are synthesized in system performance expressions for each evaluation criterion.
Output	Performance Expressions
Description	Quantification of the model performances regarding the design objectives is done. Evaluation criteria are deduced from the design objectives and the leading design variables of the Deformable Structure are identified. Expressions for the sizing of the Deformable Structure are established and subsequently sizing expressions for the

	mechanism components are derived based on the Deformable Structures sizing results and design variables. From these finally sizing expressions for the system properties are synthesized and performance expressions for each evaluation criterion are derived.

Table 9-4: Summary description of Process #3 addressing the performance quantification of the models.

9.3.5.Process #4: Concept Selection

Process #4 addresses the selection of a single concept for further development through a comparative performance analysis among the generated concepts. The inputs for this selection process are the performance expressions derived in the previous Process #3. Figure 9-6 displays the process for concept selection and its design steps with the intermediate outputs as a flow-diagram.

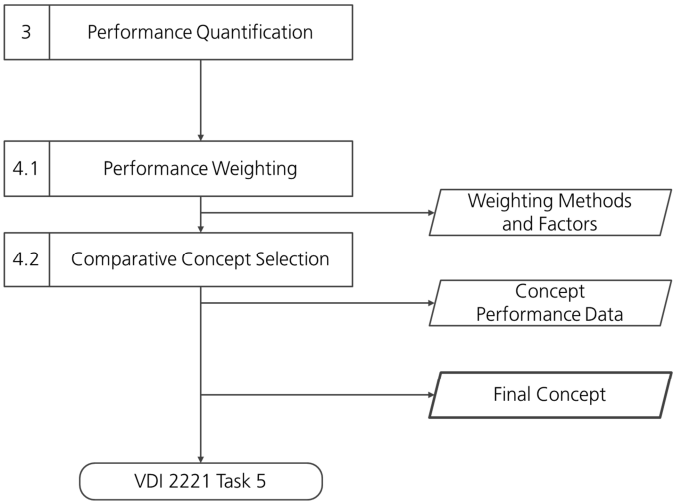

Figure 9-6: Flow diagram of Process #4 'Concept Selection' with related design steps and intermediate outputs.

The output of Process #4 is the finally selected concept that is further developed within subsequent design tasks. The process consists of two design steps:

4.1 Performance Weighting:
In process step 4.1 weighting methods and according weighting factors for the evaluation criteria are defined. In most cases the application of weighting methods is necessary as performance descriptions which combine all evaluation criteria in a single expression are seldom or their derivation is complex. Furthermore often evaluation criteria that can be clearly quantified such as mass

or stowage volume are evaluated in combination with criteria that are based on estimates such as costs. The outputs of this process step are according weighting methods and factors.

4.2 Comparative Concept Selection:
In process step 4.2 the final performance evaluation of the competing concepts is done. A performance comparison is conducted through application of the selected weighting methods and factors, performance expressions derived in the previous Process #3 and design requirements defined in the Task 1 of VDI 2221. On the basis of this comparison the best performing concept is selected as input for further design steps such as VDI 2221 Task 5 'Design of Decisive Modules'.

Table 9-5 summarizes Process #4 'Concept Selection'.

Process #4: Concept Selection	
Input	VDI 2221 Task 1: Design Task VDI 2221 Task 1: Design Objectives VDI 2221 Task 1: Requirements Definition Output #3: Evaluation Criteria Output #3: Performance Expressions
Applicable Tools and Design Principles	
Process Steps	[4.1] Performance Weighting: A method and according factors for weighting of the performances regarding the evaluation criteria are selected. [4.2] Comparative Concept Selection: The performances in each evaluation criterion are calculated, weighted and compared among all considered concepts and subsequently the best performing is selected.
Output	Final Concept
Description	A single concept is selected on the basis of a performance comparison as input for further development steps. Weighting methods and factors are selected for performance evaluation regarding the evaluation criteria. Based on this evaluation the best performing concept is selected among the competing through a performance comparison.

Table 9-5: Summary description of Process #4 addressing the selection of a single concept for further development.

Process #4 concludes the conceptual design methodology for Deployable Space Structures. In the following some tools and design principles applicable within the methods processes are described.

9.4. Functional Description of the Deployment Mechanism

For the functional description of a Deployable Space Structure performed within step 1.1 of the Process #1 'Concept Generation' the function diagram given in Figure 3-1 of chapter 3 is recapitulated in Figure 9-7. The overall function of Deployable Space

Structure will be similar to the displayed example but it may be necessary to include additional functions such as retraction into the stowed state.

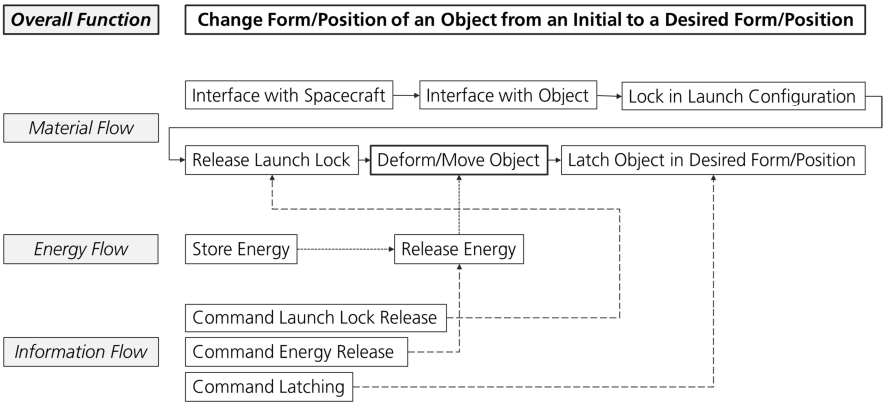

Figure 9-7: Recapitulation of the overall function of a Deployable Space Structure with separation into material, energy and information flows.

To assist the definition of the Deployment Mechanism functionalities in design step 1.3 of the Process #1 'Concept Generation' a general functional mechanism model is developed that is displayed in Figure 9-8.

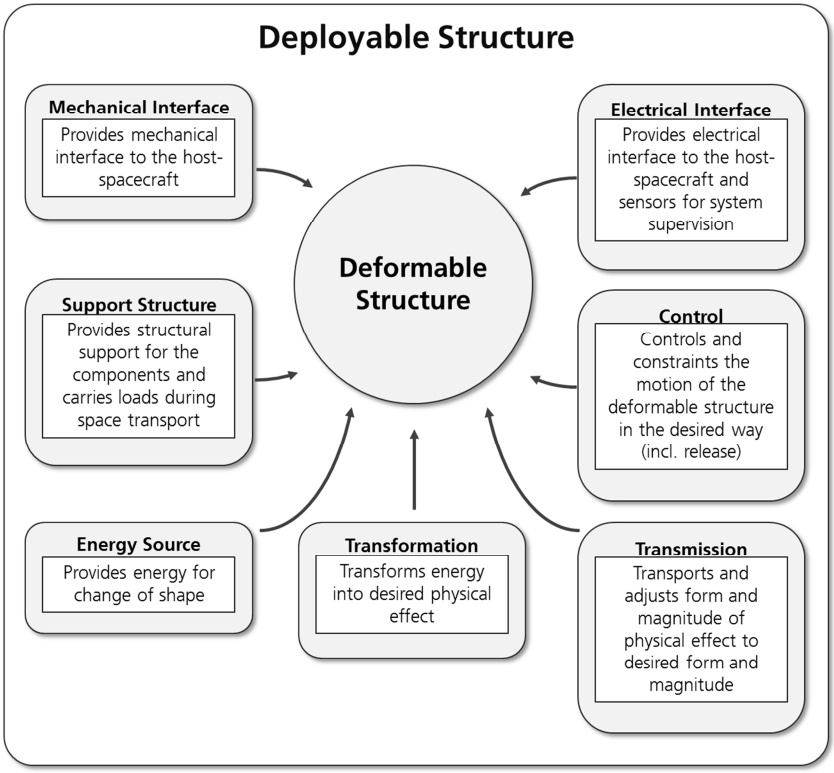

Figure 9-8: General Functional Mechanism Model with main functional categories.

The model describes the categories the functional capabilities of the Deployment Mechanisms can be assigned to. Thereby not each category has to be necessarily represented in the individual functional description of the Deployment Mechanism. The functional categories are as follows:

→ Energy Source: Provides the energy necessary for the transition from the stowed to the deployed state. Examples are pressurized gas, strain energy or electric energy.

→ Transformation: Transforms the energy into the desired physical effect. Examples are heaters, electric motors or turbines.

→ Transmission: Transmits the energy or physical effect to the Deformable Structure. Examples are gear, heat pipe or drive axles.

→ Control: Constrains and controls the deployment process of the Deformable Structure to avoid undesired motion. Examples are guide plates, rollers or motor controller.

→ Support Structure: Provides mechanical support to the Deformable Structure and mechanism components particularly during launch.

→ Mechanical Interface: Provides a mechanical interface to the host spacecraft and the object supported by the deployable structure.
→ Electrical Interface: Provides an electrical interface to the host spacecraft and the object supported by the deployable structure.

9.5. Design Principles Applicable to Deployable Space Structures

Throughout the system analysis of Deployable Space Structures some design principles are identified which are potentially beneficial to gain high solution qualities. Introduction of these principles in the form of specific processes or process steps within the design methodology potentially causes a biased design process where following these principles sets undesired constraints to the design space. Hence, these principles are described in the following in general form with references towards the applicable design steps.

9.5.1. Function Integration

Function integration enables solutions which feature a reduced number of components in comparison to designs with function separation through concentration of functional capabilities. Hence, function integration targets the concretization step from the functional to the component level. The additional functions provided by a component thereby add constraints which are to be considered in its design. The achieved reduction of component numbers may incorporate benefits regarding reducing the mass and stowage volume of a Deployable Space Structure besides lowering system complexity.
The design principle of function integration may be applied in design step 2.1 of Process #2 'Model Generation' where the translation of the functional description of the design object into an assembly of specific components is conducted. Through application of this design principle the number of concepts may be increased through establishing several variants.
The application of function integration shall be in general unbiased from considerations of the designer for performance enhancements to not compromise an open solution space. However, function integration is particularly interesting for use in re-design tasks to achieve performance enhancements of existing designs. In these cases information are already available on the manifestations of functions in certain components and their impact on the system performance wherefore a targeted use of this design principle becomes possible.

9.5.2. Sub-Function Minimization

The design principle of sub-function minimization is identified in section 7.4 and aims on reducing the number of sub-functions necessary to comply with the main and overall functions. Thereby, besides reduced system complexity, benefits regarding mass and stowage volume of a Deployable Space Structure may be achieved through minimizing the number of components. Thereby this principle is similar in its effect to

the design principle of function integration. The concretization of the design from the functional level towards specific components through selection of solution principles and their realization is connected with adding sub-functions. For example the selection of inflation as the physical effect to enable the Deformable Structures change in form causes additional sub-functions such as 'Generation of Inflation Gas' and 'Control of Gas Pressure'. Hence, the design principle of sub-function minimization aims on the selection of solution principles which involve a minimum in additional sub-functions for their realization. However, the application of this principle requires knowledge on additional sub-functions resulting from a certain design decision which is generated within the subsequent design steps. Hence, an iterative design process is required. The design principle may be applied in the design steps 1.2 to 1.4 of Process #1 'Concept Generation' and step 2.1 of Process #2 'Model Generation'.

9.5.3. Compact Stowed Form

The Deformable Structure determines through its stowed form largely the geometry of the Deployment Mechanism components and the overall assembly as is shown in chapter 4. As the mass of a component is also a function of its size, a compact stowed form is in many cases also beneficial to reduce overall mass. Particularly in case of support structures that are necessary for containment of the Deformable Structure during launch benefit from a compact stowed form. Within chapter 5 it is shown that the optimization results in case of interaction factors $g > 1$ always represent a more compact stowed form of the Deformable Structure than for $g = 1$ and subsequently gain benefits from smaller Deployment Mechanism components. This design principle may be utilized in step 1.2 to 1.4 of Process #1 'Concept Generation' and design step 2.1 of Process #2 'Model Generation'.

9.5.4. Stowed Form Compatibility

The performance of a deployable structure design depends in many design cases on the compatibility of its stowed form with a specific desired form. Such desired forms may arise from other system components such as form factors of the photovoltaic blanket in a solar array or the interface and volume constraints towards the host spacecraft or launch vehicle. According design requirements are to be defined and the design principle may be utilized in step 1.2 to 1.4 of Process #1 'Concept Generation' and design step 2.1 of Process #2 'Model Generation'.

9.5.5. Shifting of Scaling Limits

Scaling limits have a high impact on the mass and volume specific performance of lightly loaded Deployable Space Structures. Particularly in the small scale regions scaling limits often dominate the overall scaling behavior as is shown in chapters 4 and 8. Hence, avoiding or shifting boundaries set by scaling limits can result in significant performance improvements and should be considered within the early design process. This design principle applies particularly to the design steps 1.2 to 1.4 of Process #1 'Concept Generation' and step 2.1 of Process #2 'Model Generation'.

9.5.6.Avoidance of Loaded Transition Zones

In many applications of deployable structures the transition from the stowed to the deployed state is performed under load. In other cases robustness considerations require assuming worst case scenarios where significant loads during transition potentially occur. However, particularly when high compaction ratios of the Deformable Structure are desired, the transition of a deployable structure is often connected with significantly reduced mechanical properties regarding stiffness and stability. The resulting impact of a transition under load on the system performance can lead to drastic performance degradation as is demonstrated in chapter 6. Hence, even in the case of small and moderate loading during transition in comparison to the deployed state it may be beneficial to avoid structural architectures and folding principles that are associated with degradation of their mechanical properties. An efficient method to avoid load carrying Transition Zones is a deployment in two phases where the deployable structure is unfolded first until it reaches its full load carrying capabilities and the supported object second. However, this requires participation at the overall system design process. This design principle may be considered within design step 1.2 to 1.4 of Process #1 'Concept Generation' and design step 2.1 of Process #2 'Model Generation'.

10. Conceptual Design of a Solar Array

The application of the Conceptual Design Methodology developed in chapter 9 is demonstrated exemplary for a flexible blanket solar array that is similar in its design to the initial example of the ISS solar arrays (see Figure 1-1). The methodology is demonstrated only in its main process steps to limit the extent of the presentation.

10.1. Demonstration of the Methodology for a Flexible Blanket Solar Array

The demonstration starts with a brief description of the design task according to VDI 2221 Task 1 'Clarification and Specification of the Design Task'. On this basis a list of requirements is established which complements the definition of the solar array application and associated load cases presented in subsection 5.1.4. Following on the design task definition the main processes and some process steps of the newly developed conceptual design methodology are presented. The demonstration is done for a single concept but for the final step of concept selection in Process #4 according results for the Telescopic Tubular Mast and the Tubular Shell Mast (with consideration of a load carrying Transition Zone) are given in addition.

(1) Definition of the Design Task

A lightweight solar array for generation of electric power scalable between 10 kW and 50 kW (BOL) per wing shall be designed. The system architecture is a flexible blanket solar array consisting of two photovoltaic blankets which are to be supported by a central mast. The blanket is folded in a zigzag-pattern and stowed in between of two sandwich beams which also act as tip and root spreader bars and provide structural support during launch. Two array wings are attached to opposing panels of the host-satellite. They are installed in an upright position to make use of the height of the payload fairing. The stowed volume is limited by the space between the cubic satellite and the cylindrical fairing.

For initial sizing of the deployable structure the geometry of the photovoltaic blanket and the required spreader bars is defined through according size ratios. The photovoltaic array shall have a size ratio of width to length of 1:4. The ratio of blanket fold height to array length shall be 1:50. The photovoltaic cells possess an efficiency of 29.5%. The effective cell area is 70% of the blanket area. The areal mass of the combined blanket and spreader bars is assessed with 1 kg/m² while the height of a single, stowed blanket fold is approximated to 2 mm. Furthermore, the thickness of each spreader bar is assessed by 0.5% of the array length.

The corresponding list of requirements and definitions is given in Table 10-1 and complements the load case definitions given in subsection 5.1.4.

List of Requirements			
Requirement	Parameter	Value	Remark
Power Interval	P_{elec}	10 – 50 kW	
Cell Efficiency	η_{PV}	0.295	
Effective Cell Area	k_{PV}	0.7	
Array Width Ratio	Γ_{bL}	0.25	
Blanket Fold Height Ratio	Γ_{PVL}	0.02	
Spreader Bar Thickness Ratio	Γ_{SB}	0.005	
Blanket Stowed Fold Height	t_{PV}	0.0002m	
Blanket Areal Mass	γ_{Bl}	1 kg/m²	Combined Blanket and Spreader Bar Mass
…	…	…	…

Table 10-1: List of requirements and definitions for the solar array design task.

(2) Process #1: Concept Generation

Process #1 is exemplary demonstrated for the design steps 1.2 and 1.3 in which the design of the Deformable Structure and the subsequent deduction of Deployment Mechanism functions are done.

In design step 1.2 of Process #1 a variety of concepts is generated through the selection of the Deformable Structures basic characteristics. Table 10-2 displays three mast concepts whereby the first two are featuring truss architectures and the third a tubular design.

Process #1 – Step 1.2: Selection of Basic Characteristics of the Deformable Structure			
Concepts	Basic Characteristics		
	Structural Architecture	Folding Principle	Deployment Principle
#001	Truss	Concentrated Deformation through Articulation	Motorized
#002	Truss	Concentrated Deformation through Articulation	Strain Energy
#003	Tubular	Distributed Deformation through Deformable Shell and Concentrated Deformation through Fold-Lines	Strain Energy
…	…	…	…

Table 10-2: Concept generation through selection of the Deformable Structures basic characteristics.

Subsequently for each characteristic of these concepts a search for solution principles is conducted whereby certain design principles such as listed in section 9.5 may be used. Table 10-3 shows a selection of few potential solution principles whereby the design principle of 'Sub-Function Minimization' (see subsection 9.5.2) is applied. Hence the search for solution principles is focused on those which result in a minimum of mechanism functionalities. The solution principles listed for concepts #001 and #002 aim on a self-supporting truss of rigid elements with a single rotational degree of freedom for folding through shear deformation of two opposing truss faces (see left side of Figure 10-3). Folding and deployment is achieved through lengthening respectively shortening of the diagonals while the surrounding frame provides the required stiffness and stability. Thereby the deployment process does not require assistance from the deployment mechanism in the form of additional support and control functionalities.
For the tubular mast of concept #003 a flexible shell with fold lines is selected. To minimize the number of sub-functions unfolding through self-deployment driven by strain energy is selected. Particular design challenges for this concept lie in the realization of fold lines in the shell without overly compromising stiffness and stability.

Process #1 – Step 1.2: Selection of Solution Principles for the Basic Characteristics

Concepts	Design Principle	Basic Characteristics		
		Structural Architecture	Folding Principle	Deployment Principle
#001	'Sub-Function Minimization'	(A) 4 Hollow Longerons and Solid Rod Diagonals (B) 4 Hollow Longeron Truss and Cable Diagonals	(A) Rigid Truss Side-Faces and Shearing Top and Bottom Faces with SDOF Hinges	(A) Shortening of Diagonals through Pulling Cables (B) Shortening of Diagonals through Telescopic Rods
#002	'Sub-Function Minimization'	(A) 4 Hollow Longerons and Solid Rod Diagonals (B) 4 Hollow Longeron Truss and Cable Diagonals	(A) Rigid Truss Side-Faces and Shearing Top and Bottom Faces with SDOF Hinges	(A) Elastic Torsion Battens (B) Elastic Bending Diagonals (C) Elastic Elongation Diagonals
#003	'Sub-Function Minimization'	(A) Tubular Shell (B) Tubular Isogrid	(A) Flexible Composite Shell and Thinned Fold-Lines (B) Flexible Composite	(A) Self-Deployment

			Shell and High Strain Matrix with Fiber Micro-Buckling at Fold-Lines	
…	…	…	…	…

Table 10-3: Selection of solution principles for the basic characteristics of the generated concepts.

In design step 1.3 of Process #1 the Deployment Mechanism functions are deduced from the concepts principle solutions for the Deformable Structure and the overall task definition. Table 10-4 gives a list of Deployment Mechanism functions for the principle solutions #001-B-A-A and #003-A-B-A. To avoid loaded Transition Zones (see according design principle in subsection 9.5.6) a two stage array deployment is selected whereby the mast is deployed first and the photovoltaic blanket second. However, thereby additional mechanism sub-functions are introduced which are necessary for blanket unfolding and are represented by functions VII to X for concept #001 and III to VI for concept #003.

Process #1 – Step 1.3: Deduction of Deployment Mechanism Functions		
Concepts	Design Principle	Deployment Mechanism Functions
#001-B-A-A	'Avoidance of Loaded Transition Zones' through 2 Stage Deployment	(1) Hold Down Deformable Structure in Stowed State (2) Release Stowed Deformable Structure (3) Pull Diagonal Cables for Deployment (4) Provide Path-Controlled Deployment (5) Apply Tension to Deployed Deformable Structure (6) Latch Tensioned Deformable Structure (7) Release PV-Blanket (8) Unfold PV-Blanket (9) Apply Tension to Blanket (10) Latch Tensioned Blanket
#003-A-B-A	'Avoidance of Loaded Transition Zones' through 2 Stage Deployment	(1) Hold Down Deformable Structure in Stowed State (2) Release Stowed Deformable Structure (3) Release PV-Blanket (4) Unfold PV-Blanket (5) Apply Tension to Blanket (6) Latch Tensioned Blanket
…	…	…

Table 10-4: Deduction of Deployment Mechanism functions based on the Principle Solutions of the Deformable Structure.

(3) Process #2: Model Generation

Process #2 addresses the derivation of physical models to enable the performance description in the subsequent Process #3. In the following the models of concept #001 and #003 are presented without detailing the individual design steps. For the derivation of the performance expressions a geometrically representative Deformable Structure design and the accommodation of the components of the deployable structure in stowed, deploying and deployed state are required.
For further realization of the concepts #001 and #003 the design principle of 'Stowed Form Compatibility' (see subsection 9.5.4) is used. Figure 10-1 shows the stowed state of the solar array with the Telescopic Tubular Mast (left) and the Folding Truss (concept #001-B-A-A). From these design sketches the basic stowed dimensions are derived and in case of the Folding Truss geometrical dependencies regarding longeron length, truss radius and diagonal angles towards the stowed form of the solar array are deduced.

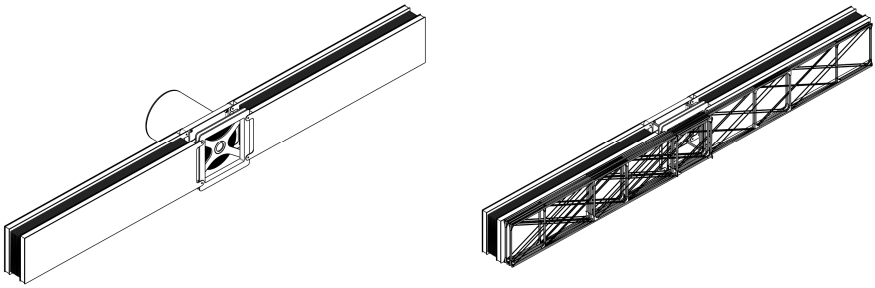

Figure 10-1: Stowed forms of the solar array consisting of the stowed photovoltaic blanket sandwiched by the spreader bars with the Telescopic Tubular Mast as deployable structure (left) and for the Folding Truss (right).

Figure 10-2 shows the stowed form of the Folding Shell Mast (concept #003-A-B-A) and a detailed view on the folding hinge and the fold-lines with concentrated strain according to Katsumata [146]. The stowed form of this concept is highly compact as there are almost no voids between the folded shells but the folding hinge design is challenging. For realization of the shell folding a solution principle is selected which considers substitution of the composite matrix by a high strain matrix applied in the vicinity of the fold lines and additional fiber micro-buckling. However the according loss in stiffness and stability and the manufacturing issues are unknowns causing potentially high development efforts.

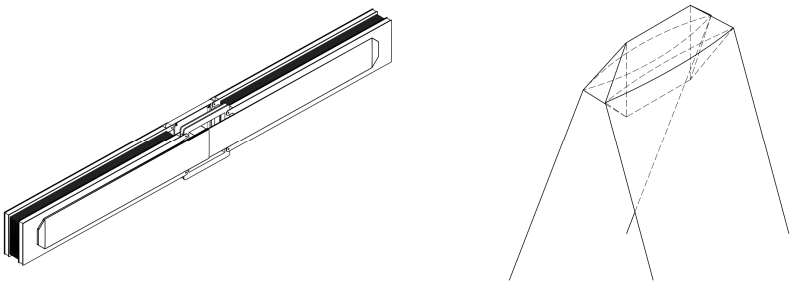

Figure 10-2: Stowed form of the Solar Array with the Folding Shell Mast (left) and detail of the fold-line hinge according to Katsumata [146].

Figure 10-3 shows the Folding Truss and the Folding Shell Mast during deployment. The Folding Truss allows for a controlled deployment through according simultaneous shortening of the diagonals possibly assisted through motion coupling of the pivoted joints. Achieving a self-deployment of the Tubular Shell Mast with a controlled release of strain energy and a specific deployment path is significantly more challenging. In both cases the generation of high deployment forces particularly in the initial deployment phase is not possible due to the zigzag folding pattern and needs to be considered in further design steps.

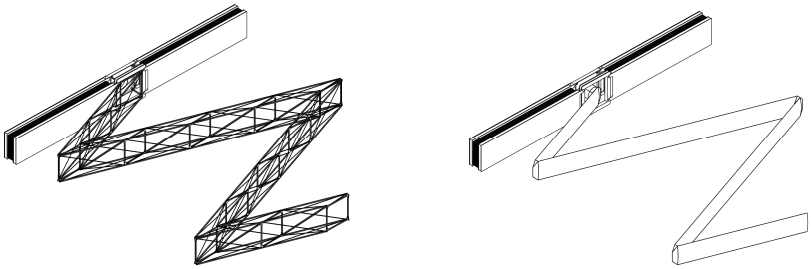

Figure 10-3: Solar array with mast support structures during first phase of deployment displayed for the Folding Truss (left) and Folding Shell Mast (right).

Figure 10-4 shows the Folding Truss in deployed state and the process of blanket unfolding. Thereby the tip spreader bars are attached to a sliding frame that uses the longerons as guide rails and the unfolding is done by a rigging system. For tensioning of the blanket the truss requires a slightly higher length than the blanket for the according rigging system. For blanket latching in tensioned state an interface of the sliding frame towards the truss possibly integrated into one of the batten frames is required. These observations on functional requirements and component interactions result in additional design constraints for the Deformable Structure and sub-functions for the Deployment Mechanism.

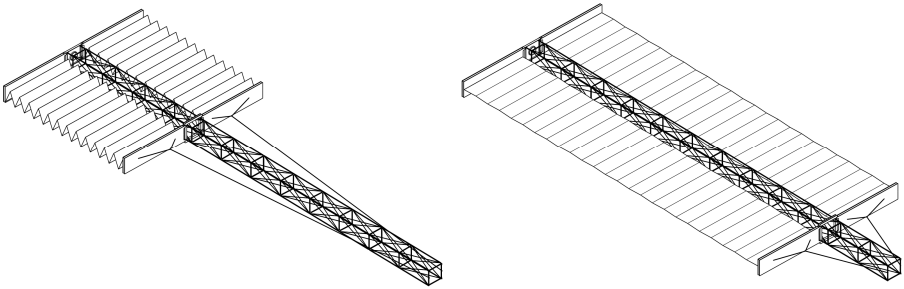

Figure 10-4: Unfolding of the solar arrays flexible photovoltaic blanket in the second deployment phase by use of a rigging system for the example of the Folding Truss.

(4) Process #3: Performance Expressions

Process #3 identifies evaluation criteria and addresses the deduction of according performance expressions from the physical models. Again the individual design steps are not described in detail and performance expressions are derived for the Folding Truss only.

The evaluation criteria for the solar array are its mass and volume specific power $P_{elec,m}$ and $P_{elec,V}$ which relate the generated array power P_{elec} to the overall array mass m_{SolAr} and volume V_{SolAr}:

$$P_{elec,m} = \frac{P_{elec}}{m_{SolAr}} \quad \text{10-1}$$

$$P_{elec,V} = \frac{P_{elec}}{V_{SolAr}} \quad \text{10-2}$$

Hence the overall array mass and volume needs to be described depending on the required array power to gain the performance expressions. The stowed volume is thereby described as the volume of the outer envelope of the solar array including the stowed mast. This definition is chosen as voids caused by a mismatch in stowed form between mast and solar array cannot be used by other components and thereby has to be considered as dead volume.

The solar array design is largely described by the initial geometrical definitions presented in the task description and summarized in Table 10-1. The according scaling functions for the photovoltaic blanket are described in Appendix I1. The design of the Folding Truss depends to a high degree on the geometry of the solar array due to the use of the design principle of 'Stowed Form Compatibility'. The according scaling functions for the Folding Truss are described in Appendix I2 and I3 and their derivation follows the procedures of chapters 4 and 5. The load case for sizing of the truss elements is the same as for the solar array application described in subsection 5.1.4.

(5) Process #4: Concept Selection

The concept selection is done through a performance comparison of the mass and volume specific power of the solar array $P_{elec,m}$ and $P_{elec,V}$. These are displayed in Figure 10-5 for flexible blanket solar arrays based on the Tubular Shell Mast, the Telescopic Tubular Mast and the Folding Truss. For the Tubular Shell Mast and the Telescopic Tubular Mast a simultaneous deployment of mast and blanket is considered whereby no additional mechanism functions are applied. Therefore the tip spreader bars are directly attached to the mast tips.

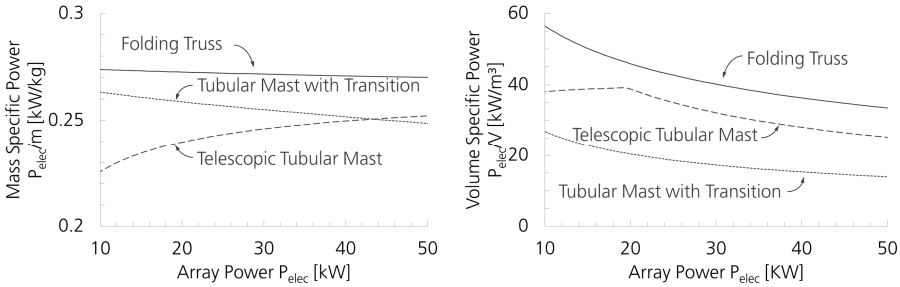

Figure 10-5: Mass (left) and volume specific power for a flexible blanket solar array based on three different deployable mast types.

The comparison of the performance values shows for the mass as well as the volume specific power that the design with a two stage deployment and application of the Folding Truss as derived within this application example leads to significantly better performances than for the other considered deployable mast concepts. Hence further weighting of the results to gain a combined evaluation is not required.

10.2. Conclusions on the Solution Quality of the Design Example

The above presented application example results in significantly enhanced performance values for the solar array application over other deployable structure designs based on established mast systems. Thereby particularly the combined use of the design principles of 'Sub-Function Minimization' (subsection 9.5.2), 'Avoidance of Loaded Transition Zones' (subsection 9.5.6) and 'Stowed Form Compatibility' (subsection 9.5.4) lead to advantages in the mass and volume specific power. In consequence the Folding Truss features a small number of mechanism components and a stowed form that is specifically tailored to match the stowed form of the solar array. Thereby a compact design is achieved although packaging of the Folding Truss is connected with several voids in between of longerons, battens and diagonals.

In addition to these results Figure 10-5 picks up the initial considerations on the mass and volume related solution quality of deployable masts described in Table 1-1 and Table 1-2. Displayed are the ratios of the mass of the Deformable Structure in relation to the total mast mass and the material volume of the Deformable Structure in relation

to the overall volume. The corresponding initially formulated critique is that the Deformable Structure contributes for a variety of deployable structures only little to the overall mass and volume although it is the carrier of the main function.

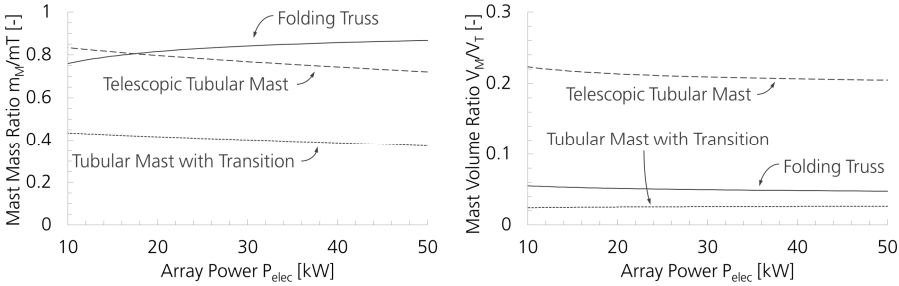

Table 10-5: Ratio of the mass of the Deformable Structure to the overall mass (left) and ratio of the material volume of the Deformable Structure to the overall volume (right).

The Folding Truss achieves considerably higher values than the systems presented in Table 1-1. Over the analysis interval the percentage of the Deformable Structures mass is mainly well above 80 % while those of the given examples are predominantly well below 50 %. Also for the stowed volume the contribution of the material volume of the stowed mast is increased and is twice as high as for the Tubular Shell Mast. However these values for the volume contribution of the Deformable Structure are still significantly lower than those of the Telescopic Tubular Mast. The reason lies in the open truss architecture which enables good deployed stiffness and stability but sets limits to the compactness of the stowed form. In this regard the Folding Shell Mast of concept #003 promises high performances as the material volume approaches nearly 100 %.

11. Application and Discussion

In conclusion to the development of the conceptual design method for Deployable Space Structures its application and associated limitations are presented. Particularly the applicability towards other design objectives and categories of deployable structures than presented within this thesis are described. Subsequently the hypotheses, the utilized approach and the gained results are discussed in some aspects.

11.1. Application of the Conceptual Design Methodology

The application of the conceptual design methodology developed within this thesis has to consider constraints that result from the focus of the underlying system analysis and characteristics of the design object. In the following first the considered application focus and intended use is described followed by a discussion regarding the expansion to other design tasks with different design goals and categories of deployable structures.

11.1.1. Application Focus and Intended Use

The application focus of the newly developed conceptual design methodology is on design tasks for Deployable Space Structures that aim on a high competitiveness regarding specific design objectives and in particular mass and stowage volume. The methodology thereby focusses particularly on the initial generation of concepts with a high diversity and identification of their respective performance potentials.
The generation of concepts is conducted in Process #1. To gain concepts of potentially high solution quality an unconstrained solution space unbiased by preferences of the designer is desired (see subsection 9.3.2). A multiplicity of initial concepts is to be generated through the selection of the basic characteristics of the Deformable Structure. Thereby the high level of abstraction emphasized in the general design methodologies VDI 2221 and VDI 2222 shall be maintained to promote finding new, innovative and unconventional concept solutions. In this regard a directed concept generation process through early considerations regarding the performance potentials should be avoided. Subsequently further variations of the initial concepts shall be generated through the application of different design principles. This also includes the stage of design concretization conducted in Process #2 whereby a high diversity of solution concepts is gained throughout the initial design steps. Thereby it is of importance to continuously check for functional compliance possibly assisted through the use of first dimensioning calculations.
The second focus of the design methodology is on accurately recognizing the performance potential of the generated concepts throughout Process #2 and #3 through quantification. The underlying assumption is that the complexity in the functional interaction of components in combination with the presence of various scaling limits does not allow for an evaluation based on intuitive or qualitative

methods. However the evaluation through quantification leads potentially to high development efforts wherefore it is of particular importance to select a performance evaluation approach that does reflect the targeted accuracy of the evaluation result. Subsequent refinement of the performance expressions to reduce the degree of uncertainty in the performance prediction may be conducted. For the evaluation process performance expressions in the form of scaling functions are particularly useful. Aside from comparison with other designs they can be used to gain insight into design interdependencies and thereby enable according deduction of design decisions to enhance the solution quality.
The conceptual design methodology is complemented through several design principles introduced in section 9.5. They are identified throughout the system analyses as potentially beneficial to gain high solution qualities and should be used to generate according concepts or create further variations of existing ones.
Furthermore several tools and procedures to assist in the design process can be found in this thesis. For the derivation of Deployment Mechanism functions the general mechanism model described in section 4.1 may be used. For the parameterization of components and subsequent derivation of scaling functions the procedure presented in subsection 4.2.4 may be used. In addition the analyses examples and procedures described throughout chapters 4 to 8 may be utilized as knowledge repositories for the design process.

11.1.2. Applicability to Other Design Goals

The presented conceptual design method is developed for design tasks whose primary design goals are a high mass and/or stowage volume related performance. Other quantifiable properties of Deployable Space Structures can be utilized as a basis for this performance driven design approach. Examples for such alternative properties may be deployment precision or thermal stability. However, the application of this methodology is not aimed on design tasks that only require functional compliance. For such tasks the development efforts arising from the performance quantification throughout Processes #2 to #4 would lead to an inefficient design process. The same is true for design tasks with minimal requirements regarding solution competitiveness. Here an evaluation approach based on qualitative or intuitive methods is preferred.

11.1.3. Applicability to Morphing Structures

There are several other deployable structures particularly in the field of morphing aircraft structures. These make use of deployable structures as "inner mechanisms" that enable and constrain the change in shape of the associated functional surface. Therefore the basic functions are similar to those of Deployable Space Structures. Also for aircrafts low mass and small stowed volume of its components are likewise design goals of general validity. However as already displayed in Table 9-1 the design tasks differ in several aspects from those of Deployable Space Structures particularly regarding design load intensity, number of target shapes and fatigue of mechanism components. Furthermore the search for a kinematic that enables compliance with the form requirements of the functional surface particularly under heavy loads is a decisive

design aspect. These differences in the design tasks cause specific design problems that are not represented in this conceptual design methodology. Hence there is only a limited applicability towards the design of morphing structures.

11.1.4. Applicability within the System Development

The development of a Deployable Space Structure is often done within the multidisciplinary development process of a specific deployable system. Such development environments impose additional design interdependencies and requirements that are also subjected to frequent changes. These aspects and the implementation into an overall system design methodology are not specifically addressed. However enhancing the methods flexibility through introduction of according regressions and iteration loops is simple and does not compromise the methods applicability. In contrast the application as a system design methodology is questionable as the processes are specifically created for the characteristics of Deployable Space Structure.

11.2. Discussion of Hypotheses and Approach

The hypotheses, verification approaches, assumptions, analysis procedures and conclusions presented within this thesis may be debated in some aspects. Few of these are discussed in the following introduced by the respective point of criticism.

11.2.1. Verification of the Leading Hypothesis

The leading hypothesis formulated at the beginning of this thesis states that current Deployable Space Structures are overly heavy and voluminous due to a methodological gap in the state-of-the-art. A direct proof for this hypothesis is not given throughout the thesis.

The leading hypothesis cannot be verified as the actual methods utilized for current Deployable Space Structure designs and the underlying design tasks are not known or published. From the literature it is found that currently there is no conceptual design method specific for Deployable Space Structures wherefore there actually is a methodological gap. The hypotheses formulated in chapter 3 on missing knowledge for the derivation of such a design methodology address further gaps whose significances are demonstrated throughout the system analyses in chapters 4 to 8. However these are only indications that based on the current state-of-the-art in Deployable Space Structure design advancements in mass and stowage volume related performance are possible through application of the new methodology.

11.2.2. Verification Approach

The approach for verification of the hypotheses formulated in chapter 3 is a detailed system analysis of a Deployable Space Structure through analytic scaling functions. The

derivation of these functions is associated with several assumptions and simplifications. Hence this approach does not fully represent the actual scaling behavior of the Deployable Space Structure and its components wherefore the validity of the results is questionable.

There are several sources for uncertainties regarding the actual scaling behavior of components and the overall system. One example is the procedure for derivation of scaling functions described in subsection 4.2.4 which is based on the selection of a single characteristic element for derivation of the component scaling functions. Other examples are the approximations made for some constraint functions to achieve compliance with the selected approach for derivation of the system scaling function presented in section 5.4 and the negligence of stiffness losses at interfaces. In consequence the absolute scaling results contain errors which influence to some extent also the global scaling behavior. However, the primary goal of the chosen verification approach is to identify general design characteristics of Deployable Space Structures throughout the chapters 4 to 8. For this analysis focus the use of analytic equations is particularly attractive as they enable identification of design interactions, design drivers and characteristics through simple inspection of the according mathematical expressions. The approach thereby enables to gain high insight into design aspects relevant for the development of an according design methodology.

11.2.3. Validity for Other Deployable Space Structures

The presented system analyses are done exclusively for deployable masts. The validity of the results and the developed design methodology towards other Deployable Space Structure is questionable.

In fact deployable masts show in comparison to other categories of Deployable Space Structures such as mesh reflectors like AstroMesh [88] pronounced Deployment Mechanisms which consequently have a high impact on the system performance and scaling behavior. However, the basic design tasks, functions and functional structures, component compositions and design interactions remain the same as these represent the general design characteristics of Deployable Space Structures. Identifying such general characteristics is the primary focus of the presented system analyses. In this regard deployable masts are particularly suited as analysis objects as they feature high solution diversity regarding architectures, folding and deployment principles and materials in comparison with other categories of Deployable Space Structures which are committed to specific types of design. Based on the thereby identified characteristics a methodology of general validity is developed and care is taken to keep the associated procedures and processes free of individual design problems. Nevertheless, according adjustments of the processes and design steps to individual design tasks are desired.

11.2.4. Inclusion of the Deployment Kinematic

The conceptual design methodology does not include a process specifically dedicated to the deployment kinematic. Thereby an essential design aspect of Deployable Space Structures is neglected.

In the design of deployable space frames, trusses and morphing aircraft structures a main focus is on the associated kinematics. However, the kinematics and corresponding design procedures depend on the selected principles for folding and deployment which may differ strongly. Exemplary a distributed deformation approach in combination with inflation as a deployment method is associated with other design problems than a motorized, articulated truss ring. Hence the selection of specific analysis and design procedures of general applicability for the kinematics of deployable structures is not possible. Instead within the presented conceptual design methodology the kinematics are addressed through according formulation of functions, design constraints and scaling limits. As a valid kinematical solution is an integral part for functional compliance it should be checked continuously throughout the development process as is addressed in the subsection 9.3.3 for Process #2.

References

[1] National Aeronautics and Space Administration (NASA), „STS-119 Shuttle Mission Imagery," 25th March 2009. [Online]. Available: https://spaceflight.nasa.gov/gallery/images/shuttle/sts-119/html/s119e010500.html. [Zugriff am 11th December 2017].

[2] Northrop Grumman, „STEM Products and Programs," [Online]. Available: http://www.northropgrumman.com/BusinessVentures/AstroAerospace/Products/Documents/pageDocs/STEM_Hardware_Programs.pdf. [Zugriff am 6th June 2016].

[3] Northrop Grumman, „Astro STEM Size and Mass," [Online]. Available: http://www.northropgrumman.com/BusinessVentures/AstroAerospace/Products/Documents/pageDocs/STEM_Parametrics.pdf. [Zugriff am 6th June 2016].

[4] N. F. Knight, K. B. Elliot, J. D. Templeton, K. Song und J. T. Rayburn, „FAST Mast Structural Response to Axial Loading: Modeling and Verification," in *53rd AIAA/ASME/ASCE/AHS/ASC Structures, Structural Dynamics and Materials Conference*, Honolulu, Hawaii, USA, 2012.

[5] J. F. Shaker, „Static Stability of a Three-Dimensional Space Truss," NASA Technical Memorandum 106944, Lewis research Center, Cleveland, Ohio, USA, 1995.

[6] T. W. Murphey, „Booms and Trosses," in *Recent Advances in Gossamer Spacecraft*, Amercian Institute of Astronautics and Aeronautics, 2006, pp. 1 - 43.

[7] National Aeronautics and Space Administration (NASA), „SRTM Mission Statistics," [Online]. Available: https://www2.jpl.nasa.gov/srtm/statistics.html. [Zugriff am 6th June 2017].

[8] Northrop Grumman, „Canister AstroMast," [Online]. Available: http://www.northropgrumman.com/BusinessVentures/AstroAerospace/Products/Documents/pageDocs/DS-303-CannisterAstroMast.pdf. [Zugriff am 6th June 2016].

[9] Orbital ATK-Goleta, „Telescoping Boom Systems," [Online]. Available: https://www.orbitalatk.com/space-systems/space-components/deployables/docs/Telescoping_Boom_Systems.pdf. [Zugriff am 24th November 2017].

[10] R. Wagner und H. Cook, Designs On Space: Blueprints For 21st Century Space Exploration, Simon & Schuster, 2001.

[11] J. W. Umland and H. Eisen, "SRTM On-Orbit Structural Dynamics," *42nd AIAA/ASME/ASCE/AHS/ASC Structures, Structural Dynamics, and Materials Conference and Exhibit,* pp. AIAA 2001-1588, 16-19 April 2001.

[12] D. L. Blanchard, „Dynamical Performance to Date of RAE-A (Explorer 38)," NASA Goddard Space Flight Center, Greenbelt, MD, United States, 1969.

[13] J. M. Fernandez, „Advanced Deployable Shell Based Composite Booms for Small Satellite Structural Applications Including Solar Sails," *4th International Symposium on Solar Sailing,* 17-20 January 2017.

[14] G. J. Klein, „Coilable Extensible Apparatus". United States Patent 3,144,215, 11 August 1964.

[15] H. J. Taylor, D. Mills und J. A. Fry, „Extensible retractable STEM Device". United States Patent 3,243,132, 29 March 1966.

[16] Northrop Grumman, "150-lb Linear Actuator STEM," [Online]. Available: http://www.northropgrumman.com/BusinessVentures/AstroAerospace/Products/Documents/pageDocs/DS-415-150lbBI-STEM.pdf. [Accessed 6th June 2016].

[17] Northrop Grumman, „40-lb Linear Actuator Bi-STEM," [Online]. Available: http://www.northropgrumman.com/BusinessVentures/AstroAerospace/Products/Documents/pageDocs/DS-414-40lbBI-STEM.pdf. [Zugriff am 6th June 2016].

[18] J. A. Banik und T. W. Murphey, „Performance Validation of the Triangular Rollable and Collapsible Mast," *24th Annual AIAA/USU Conference on Small Satellites,* 9-12 August 2010.

[19] T. W. Murphey und J. A. Banik, „Triangular Rollable and Collapsible Boom". United States Patent US 7,895,795 B1, 1 March 2011.

[20] C. P. Rubin, „Deployable Boom". United States Patent 3,434,254, 4 October 1965.

[21] B. B. Rennie, „New Closed Tubular Extendible Boom," *2nd Aerospace Mechanisms Symposium,* pp. 163-170, 15 August 1967.

[22] M. A. Brown und C. J. Butkiewiez, „Elongated Truss Boom Structures for Space Applications". United States Patent US 2002/0112417 A1, 22 August 2002.

[23] M. A. Brown, „Developments in the Superstring Deployable Truss Boom," *47th AIAA/ASME/ASCE/AHS/ASC Structures, Structural Dynamics, and Materials Conference,* 1-4 May 2006.

[24] M. F. Hillebrandt, „A New Deployable Truss for Gossamer Space Structures," *53rd AIAA/ASME/ASCE/AHS/ASC Structures, Structural Dynamics, and Materials Conference,* 23-26 April 2012.

[25] M. F. Hillebrandt, „Deployable Carbon Tape truss for Gossamer Space Structures," *12th European Conference on Spacecraft Structures, Materials and Environmental Testing,* 20-23 March 2012.

[26] Orbital ATK-Goleta, „Articulated Mast Systems," [Online]. Available: https://www.orbitalatk.com/space-systems/space-components/deployables/docs/Articulated_Mast_Systems.pdf. [Zugriff am 24th November 2017].

[27] M. V. Douglas, „Module for an Articulated Stowable and Deployable Mast". United States Patent 5,267,424, 7 December 1993.

[28] T. W. Murphey, „Booms and Trusses," in *Recent Advances in Gossamer*

Spacecraft, Amercian Institute of Astronautics and Aeronautics, 2006, pp. 1 - 43.

[29] M. D. Benton und W. M. Robbins, „Extendible Structures". United States Patent 4,599,832, 15 July 1986.

[30] M. Bowden und M. Benton, „Design of Dpeloyable-Truss Masts for Space Station," in *Aerospace Design Conference*, Irvine, California, USA, 1993.

[31] J. E. Webb, „Deployable Lattice Column". United States Patent 3,486,279, 30 December 1969.

[32] R. M. Warden, „Deployable/Retractable Mast Indepedently Rotatable When Deployed". United States Patent 5,154,027, 13 October 1992.

[33] Orbital ATK-Goleta, „CoilABLE Booms," [Online]. Available: https://www.orbitalatk.com/space-systems/space-components/deployables/docs/coilable_booms.pdf. [Zugriff am 24 November 2017].

[34] F. Rehnmark und M. Pryor, „Development of a Deployable Nonmetallic Boom for Reconfigurable Systoms of Small Spacecraft," *48th AIAA/ASME/ASCE/AHS/ASC Structures, Structural Dynamics, and Materials Conference,* 23-26 April 2007.

[35] P. A. Warren, „Open-Lattice, Foldable, Self-Deployable Structure". United States Patent US 6,345,482 B1, 12 February 2002.

[36] G. S. Agnes, R. D. Abelson, R. Miyake, J. K. H. Lin, J. Welsh und J. J. Watson, „Preliminary Analysis of the 30-m Ultraboom Flight Test Article," *46th Structural Dynamics and Materiels Conference,* 18-21 April 2005.

[37] R. E. Allred, A. E. Hoyt, P. M. McElroy, S. Scarborogh und D. P. Cadogan, „UV Rigidizable Carbon-Reinforced Isogrid Inflatable Booms," *43rd AIAA/ASME/ASCE/AHS/ASC Structures, Structural Dynamics, and Materials Conference,* 22-25 April 2002.

[38] „SRTM Mast extended at AEC-Able," [Online]. Available: https://www2.jpl.nasa.gov/srtm/images/photos/srtm_14_hi.jpg. [Zugriff am 11 January 2019].

[39] F. H. Swaim, „Intermittenly-Lapped Extendible Boom". United States Patent 3,177,987, 13 April 1965.

[40] E. C. Trexler, „Extendible-Retractable Boom". United States Patent 3,361,377, 2 January 1968.

[41] M. K. Pryor und J. O. Newlin, „Deployable Structural Assemblies, Systems for Deploying such Structural Assemblies". United States Patent US 8,042,305 B2, 25 October 2011.

[42] D. S. Chae, D. J. Rohweller und M. W. Thomson, „Deployable/Retractable Telescoping Mast Assembly and Method". United States Patent 5,315,795, 31 May 1994.

[43] Oxford Space Systems, „AstroTube Max," [Online]. Available: https://oxford.space/download/AstroTube-Max-A4-Poster-clean_2.pdf. [Zugriff am 15 December 2018].

[44] E. L. Pollard und T. W. Murphey, „Development of Deployable Elastic Composite

Shape Memory Alloy Reinforced (DECSMAR) Structures," *47th AIAA/ASME/ASCE/AHS/ASC Structures, Structural Dynamics, and Materials Conference,* 1-4 May 2006.

[45] E. L. Pollard, T. W. Murphey und G. E. Sanford, „Experimental and Numerical Analysis of a DECSMAR Structure's Deployment and Deployed Performance," *48th AIAA/ASME/ASCE/AHS/ASC Structures, Structural Dynamics, and Materials Conference,* 23-26 April 2007.

[46] O. Stohlman, Repeatability of joint-dominated deployable masts, Pasadena, California, USA: Doctoral Thesis, California Institute of Technology, 2011.

[47] C. T. Sickinger, Verifikation entfaltbarer Composite-Booms für Gossamer-Raumfahrtsysteme, Braunschweig, Germany: Doctoral Thesis, Technical University Braunschweig Carolo Wilhelmina, Department of Mechanical Engineering, 2009.

[48] M. F. Hillebrandt, S. Meyer, M. E. Zander, M. Straubel und C. Huehne, „The Boom Design of the De-Orbit Sail Satellite," *European Conference on Spacecraft Structures, Materials and Environmental Testing,* 1-4 April 2014.

[49] M. F. Hillebrandt und M. E. Zander, „Conceptual Design of the Deployable Booms for the GoSolAr-Satellite," *European Conference on Spacecraft Structures, Materials and Environmental Testing,* 28-1 April 2018.

[50] M. Straubel, P. Seefeldt, P. Spietz und C. Huehne, „The Design and Test of the GOSSAMER-1 Boom Deployment Mechanisms Engineering Model," *AIAA SciTech 2015 - Proceedings,* 5-9 January 2015.

[51] S. Meyer, M. F. Hillerbandt, M. Straubel und C. Huehne, „Design of the De-Orbit Sail Boom Deployment Unit," *European Conference on Spacecraft Structures, Materials and Environmental Testing,* 28-1 April 2014.

[52] M. Schenk, A. D. Viquerat, K. A. Seffen und S. D. Guest, „Review of Inflatable Booms for Deployable Space Structures: Packing and Rigidization," *Journal of Spacecraft and Rockets, Vol. 51, No. 3,* pp. 762-778, 2014.

[53] K. Guidanean, „An Inflatable Rigidizable Truss Structure Based on New Sub-Tg Polyurethane Composites," *43rd AIAA/ASME/ASCE/AHS/ASC Structures, Structural Dynamics, and Materials Conference,* 22-25 April 2002.

[54] A. Viquerat, M. Schenk, B. Sanders und V. Lappas, „Inflatable Rigidisable Mast for End-of-Life Deorbiting System," *European Conference on Spacraft Structures, Materials and Environmental Testing,* 28-1 April 2014.

[55] „SRTM Mast and Canister extended at AEC-Able," [Online]. Available: https://www2.jpl.nasa.gov/srtm/images/photos/srtm_17_hi.jpg. [Zugriff am 11 January 2019].

[56] R. E. Freeland, G. D. Bilyeu, G. R. Veal, M. D. Steiner und D. E. Carson, „Large Inflatable Deployable Antenna Flight Experiment Results," *48th Congress of the International,* 6-10 October 1997.

[57] I. M. Jimenez, High Strain Composites and Dual-Matrix Composite Structures, Pasadena, California, United States: California Institute of Technology, 2014.

[58] F. L. Jimenez, Mechanics of Thin Carbon Fiber Composites with a Silicone Matrix, Pasadena, California, United States: California Institute of Technology, 2011.

[59] T. W. Murphey, W. H. Francis, B. L. Davis, J. Mejia-Ariza, M. Santer, J. N. Footdale, K. Schmid, O. Soykasap, K. Guidanean und P. A. Warren, „High Strain Composites," *AIAA SciTech, 2nd AIAA Spacecraft Structures Conference,* 5-9 January 2015.

[60] W. H. Francis und M. S. Lake, „A Review of Classical Fiber Microbuckling Analytical Solutions for use with Elastic Memory Composites," *47th AIAA/ASME/ASCE/AHS/ASC Structures, Structural Dynamics, and Materials Conference,* 1-4 May 2006.

[61] H. Schuermann, Konstruieren mit Faser-Kunststoff-Verbunden, Berlin: Springer Verlag, 2005.

[62] S. Pellegrino, Deployable Structures, Wien: Springer Verlag, 2001.

[63] T. W. Murphey, S. Jeon, A. Biskner und G. Sanford, „Deployable Booms and Antennas Using Bi-stable Tape-springs," *24th Annual AIAA/USU Conference on Small Satellites,* 9-12 August 2010.

[64] J. M. Fernandez, A. Viquerat und V. Lappas, „Bistable Over the Whole Length (BOWL) CFRP Booms for Solar Sails," *Advances in Solar Sailing,* pp. 609-628, 4 February 2014.

[65] A. J. Lee und J. M. Fernandez, „Mechanics of Bistable Two-Shelled Composite Booms," *AIAA Spacecraft Structures Conference, AIAA SciTech Forum,* 8-12 January 2018.

[66] D. P. Cadogan, „Rigidizable Materials for use in Gossamer Space Inflatable Structures," *42nd AIAA/ASME/ASCE/AHS/ASC Structures, Structural Dynamics, and Materials Conference,* 16-19 April 2001.

[67] C. Cassapakis und M. Thomas, „Inflatable Structures Technology Development Overview," *Space Programs and Technologies Conference,* 26-28 September 1995.

[68] V. Barbet, S. Guionie, G. Laduree, S. Langlois, R. Potes und S. Lienard, „Mechanical Testing of Inflatable Space Structure Beams," *European Conference on Spacecraft Structures, Materials and Mechanical Testing,* 10-12 May 2005.

[69] V. Peypoudat, B. Defoort, D. Lacour, P. Brassier, O. Le Couls und S. Langlois, „Development of a 3.2m-long Inflatable and Rigidizable Solar Array Breadboard," *European Conference on Spacecraft Structures, Materials and Mechanical Testing,* 10-12 May 2005.

[70] D. Lichodziejewski, G. Veal und B. Derbes, „Spiral Wrapped Aluminum Laminate Rigidization Technology," *43rd AIAA/ASME/ASCE/AHS/ASC Structures, Structural Dynamics, and Materials Conference,* 22-25 April 2002.

[71] R. W. Schock, „Solar Array Flight Dynamic Experiment," NASA Marshall Space Flight Center, Alabama, 1986.

[72] M. J. Herriage, R. M. Kurland, C. D. Faust, E. M. Gaddy und D. J. Keys, „EOS

AM-I GaAs/Ge Flexible Blanket Solar Array," *31st IECEC Intersociety Energy Conversion Engineering Conference,* pp. 56-62, 1996.

[73] T. R. Cawsey, „A Deployment Mechanism for the Double Roll-Out Flexible Solar Array on the Space Telescope," *16th Aerospace Mechanism Symposium,* pp. 223-233, 1 May 1982.

[74] C. L. Foster, M. L. Tinker, G. S. Nurre und W. A. Till, „Solar-Array-Induced Disturbance of the Hubble Space Telescope Pointing System," *Journal of Spacecraft and Rockets, Vol. 32, No. 4,* pp. 634-644, 1995.

[75] B. R. Spence und S. F. White, „Directionally Controlled Elastically Deployable Roll-Out Solar Array". United States Patent US 8,683,755 B1, 1 April 2014.

[76] D. Manzella und K. Hack, „High-Power Solar Electric Propulsion for Future NASA Missions," *50th AIAA/ASME/SAE/ASEE Joint Propulsion Conference, AIAA Propulsion and Energy Forum,* 28-30 July 2014.

[77] J. A. Banik, „Roll-Out Solar Array (ROSA) - 12.06.17," 12 June 2017. [Online]. Available: https://www.nasa.gov/mission_pages/station/research/experiments/2139.html#results. [Zugriff am 10 January 2019].

[78] E. Groskopfs, „Storable Tubular Extensible Member Device". United States Patent 3,434,674, 25 March 1969.

[79] L. Johnson, M. Whorton, A. Heaton, R. Pinson, G. Laue und C. Adams, „NanoSail-D: A Solar Sail Demonstration Mission," *6th Symposium on Realistic Near-Term Advanced Scientific Space Missions,* 6-9 July 2009.

[80] L. Johnson, R. M. Young und E. E. Montgomery, „Recent Advances in Solar Sail Propulsion Systems at NASA," *Acta Astronautica 61 (2007) ,* pp. 376-382, 2007.

[81] L. Johnson, R. Young, E. Montgomery und D. Alhorn, „Status of Solar Sail Technology within NASA," in *2nd International Symposium on Solar Sailing*, New York, USA, July 20-22, 2010.

[82] D. W. Sleight, Y. Michii, D. Lichodziejewski, B. Derbes und T. O. Mann, „Structural Analysis of an Inflation-Deployed Solar Sail with Experimental Validation," *41st AIAA/ASME/SAE/ASEE Joint Propulsion Conference,* 10-13 July 2005.

[83] K. Miura und Y. Miyazaki, „Concept of the Tension Truss Antenna," *AIAA Journal, Vol. 28, No. 6 (1990),* pp. 1098-1104, 1990.

[84] H. Hirosawa, H. Hirabayashi, H. Kobayashi, Y. Murata, T. Kii, P. Edwards, M. Natori, T. Takano, Z.-I. Yamamoto, T. Hashimoto, K. Inoue, A. Ohnishi, T. Ohshima, T. Ichikawa, K. Fujisawa, K. Wajima, R. Okayasu, M. Inoue, N. Kawaguchi, S. Kameno, K. Shibata und Y. Asaki, „Space VLBI Satellite HALCA and its Engineering Accomplishments," *Acta Astronautica Vol. 50, No. 5,* pp. 301-309, 2002.

[85] C. Mangenot, J. Santiago-Prowald, K. van 't Klooster, N. Fonseca, L. Scolamiero, F. Coromina, P. Angeletti, M. Politano, C. Elia, D. Schmitt, M. Wittig, F. Heliere, M. Arcioni, M. Petrozzi und M. Such Taboada, „Large Reflector Antenna Working Group - Final Report," European Space Agency (ESA), Noordwijk, The

Netherlands, 2010.

[86] Proceedings of the 2nd International Conference "Advanced Lightweight Structures and Reflector Antennas", Tbilisi, Georgia, October 1-3, 2014.

[87] Northrop Grumman, „AstroMesh - Unfurlable Mesh Antenna," [Online]. Available: http://www.northropgrumman.com/BusinessVentures/AstroAerospace/Products/Documents/pageDocs/AstroMesh_DataSheet.pdf. [Zugriff am 10th January 2019].

[88] Northrop Grumman, „AstroMesh Reflector Parametrics," [Online]. Available: https://www.northropgrumman.com/BusinessVentures/AstroAerospace/Products/Documents/pageDocs/Parametrics.pdf. [Zugriff am 10th January 2019].

[89] M. W. Thomson, „The AstroMesh Deployable Reflector," *Proceedings of the IUTAM-IASS Symposium on Deployable Structures,* pp. 435-446, 6-9 September 1998.

[90] R. E. Freeland, G. D. Bilyeu, G. R. Veal und M. M. Mikulas, „Inflatable Deployable Space Structures Technology Summary," *49th International Astronautical Congress,* 28-2 September 1998.

[91] D. M. Bose, R. Winski, J. Shidner, C. Zumwalt, C. O. Johnston, D. R. Komar, F. M. Cheatwood und S. J. Hughes, „The Hypersonic Inflatable Aerodynamic Decelerator (HIAD) Mission Applications Study," *AIAA Aerodynamic Decelerator Systems (ADS) Conference,* 25-28 March 2013.

[92] R. E. Freeland, N. F. Garcia und H. Iwamoto, „Wrap-Rib Antenna Technology Development," Jet Propulsion Laboratory, California Institute of Technology, Pasadena, California, united States, 1984.

[93] D. M. Murphy, „MegaFlex - The ScalingPotentialOfUltraFlexTechnology," *53rd AIAA/ASME/ASCE/AHS/ASC Structures, Structural Dynamics and Materials Conference,* 23-26 April 2012.

[94] Northrop Grumman, „UltraFlex Solar Array Systems," [Online]. Available: http://www.northropgrumman.com/Capabilities/SolarArrays/Documents/UltraFlex_Factsheet.pdf. [Zugriff am 10 January 2019].

[95] S. D. Guest und S. Pellegrino, „A New Concept for Solid Surface Deployable Antennas," *Acta Astronautica Vol. 38, No. 2,* pp. 103-113, 1996.

[96] K. Nakamura, Y. Tsutsumi, K. Uchimaru, A. Tsujihata und A. Meguro, „Large Deployable Reflector on ETS-VIII," *17th AIAA International Communications Satellite Systems Conference,* 23-27 February 1998.

[97] A. Meguro, K. Shintate, M. Usui und A. Tsujihata, „In-Orbit Deployment Characteristics of Large Deployable Antenna Reflector Onboard Engineering Test Satellite VIII," *Acta Astronautica 65 (2009),* pp. 1306-1316, 2009.

[98] A. L. Adler, N. Hague, G. Spanjers, B. Engberg, J. Goodding, D. M. Murphy und M. M. Mikulas, „PowerSail: The Challenge of Large, Planar, Surface Structures for Space Applications," *44th AIAA/ASME/ASCE/AHS Structures, Structural Dynamics, and Materials Conference,* 7-10 April 2003.

[99] M. O'Neill, J. Howell, J. Fikes, L. Lollar, C. Carrington, N. Suzuki, M. Piszczor, D. Hoppe, M. Eskenazi, D. Aiken, M. Fulton, H. Brandhorst, M. Schuller und A. J. MacDanal, „Stretched Lens Array SquareRigger (SLASR): A New Space Array for High-Power Missions," *IEEE 4th World Conference on Photovoltaic Energy Conference,* 7-12 May 2006.

[100] M. F. Piszczor, M. J. O'Neill, M. I. Eskenazi und H. W. Brandhorst, „The Stretched Lens Array SquareRigger (SLASR) for Space Power," *4th International Energy Conversion Engineering Conference and Exhibit (IECEC),* 26-29 June 2006.

[101] Northrop Grumman, „Rigid Panel Solar Arrays," [Online]. Available: http://www.northropgrumman.com/Capabilities/SolarArrays/Documents/Rigid_Panel_Solar_Arrays.pdf. [Zugriff am 10 January 2019].

[102] Northrop Grumman, „Solar Arrays," [Online]. Available: http://www.northropgrumman.com/Capabilities/SolarArrays/Pages/default.aspx. [Zugriff am 10 January 2019].

[103] G. Tibert, Deployable Tensegrity Structures for Space Applications, Stockholm, Sweden: Doctoral Thesis, Royal Institute of Technology, Department of Mechanics, 2002.

[104] A. Kampinsky und R. K. Ritt, „Experimental and Theoretical Evaluation of a Passive Communications Satellite (Echo II)," *U.R.S.I. Symposium on Electromagnetic Wave Theory,* 1965.

[105] K. J. Kennedy, J. Raboin, G. Spexarth und G. Valle, „Inflatable Structures Technology Handbook," NASA Johnson Space Center, Houston, TX, United States, 2000.

[106] S. D. Safaei, A. Eriksson, A. Micheletti und G. Tibert, „Study of Various Tensegrity Modules as Building Blocks for Slender Booms," *International Journal of Space Structures, Vol. 28, No. 1,* 2013.

[107] J. M. Hedgepeth, „Critical Requirements for the Design of Large Space Structures," NASA Contractor Report 3484, NASA Langley Research Center, Hampton, Virginia, United States , 1981.

[108] M. M. Mikulas, „Structural Efficiency of Long Lightly Loaded Truss and Isogrid Column for Space Applications," NASA Technical Memorandum 78687, Nasa Langley Research center, Hampton, Virginia, United States, 1978.

[109] J. D. Hinkle, P. Warren und L. D. Peterson, „Geometric Imperfection Effects in an Elastically Deployable Isogrid Column," *Journal of Spacecraft and Rockets, Vol. 39, No. 5,* pp. 662-668, September - October 2002.

[110] T. W. Murphey und J. D. Hinkle, „Some Performance Trends in Hierarchical Truss Structures," *44th AIAA/ASME/ASCE/AHS/ASC Structures, Structural Dynamics, and Materials Conference,* 7-10 April 2003.

[111] T. W. Murphey, „A Material Structural Performance Index for Strain Based Deployable Trusses," *45th AIAA/ASME/ASCE/AHS/ASC Structures, Structural Dynamics & Materials Conference,* 19-22 April 2004.

[112] C. H. M. Jenkins, Recent Advances in Gossamer Spacecraft, Progress in

Astronautics and Aeronautics, American Institute of Aeronautics and Astronautics, 2006.

[113] R. F. Crawford und M. D. Benton, „Strength of Initially Wavy Lattice Columns," *AIAA Journal, Vol. 18, No. 5,* pp. 581-584, May 1980.

[114] R. F. Crawford und J. M. Hedgpeth, „Effects of Initial Waviness on the Strength and Design of Built-up Structures," *AIAA Journal, Vol. 13, No. 5,* pp. 672-675, 1975.

[115] J. N. Goodier und W. T. Thomson, „Applicability of Similarity Principles to Structural Models," National Advisory Committee for Aeronautics, Technical Note No. 933, Washington, 1944.

[116] R. F. Crawford, „Strength and Efficiency of Deployable Booms for Space Applications," *AAS/AIAA Variable Geometry and Expandable Structures Conference,* 21-23 April 1971.

[117] J. A. Garba, D. A. Kudija, B. Zeldin und E. N. Costogue, „Parametric Study of two Planar High Power Flexible Solar Array Concepts," Jet Propulsion Laboratory, JPL Publication 78-95, Pasadena, California, United States, 1978.

[118] M. M. Mikulas und C. Cassapakis, „Preliminary Design Method for Deployale Spacecraft Beams," NASA Langley Research Center, Hampton, VA, United States, 1995.

[119] M. M. Mikulas, T. J. Collins, W. Doggett, J. Dorsey und J. Watson, „Truss Performance and Packaging Metrics," *Space Technology and Applications International Forum,* 12-16 February 2006.

[120] J. A. Banik, Structural Scaling Metrics for Tensioned-Blanket Space Systems, Albuquerque, New Mexico, United States: Doctoral Thesis, University of New Mexico, Civil Engineering Department, 2014.

[121] C. Gantes, A Design Methodology for Deployable Structures, Cambridge, MA, United States: Doctoral Thesis, Massachusetts Institute of Technology, Department of Civil Engineering, 1991.

[122] C. Gantes, J. J. Connor und R. D. Logcher, „A Systematic Design Methodology for Deployable Structures," *International Journal ofSpace Structures, Vol. 9, No.2 ,* pp. 67-86, 1994.

[123] C. J. Gantes, J. J. Connor, R. D. Logcher und Y. Rosenfeld, „Structural Analysis and Design of Deployable Structures," *Computers & Structures, Vol. 32, No.3-4,* pp. 661-669, 1989.

[124] P. Farrugia, Kinematic Analysis of Foldable Structures, Guildford, Surrey, Great Britain: University of Surrey, Faculty of Engineering and Physical Sciences, 2008.

[125] Y. Chen und Z. You, „On Mobile Assemblies of Bennett Linkages," *Proceedings of the Royal Society A: Mathematical, Physical and Engineering Sciences, Vol. 464, Issue 2093,* pp. 1275-1293, 2008.

[126] S. D. Guest, Deployable Structures: Concepts and Analysis, Great Britain: Doctoral Thesis, University of Cambridge, Corpus Christi College, 1994.

[127] A. Meguro und J. Mitsugi, „Design and Analysis of Deployable Modular Structures for a Large Space Antenna," *Proceedings of the 6th European Space Mechanisms and Tribology Symposium,* pp. 319-324, 4-6 October 1995.

[128] M. Straubel, Design and Sizing Method for Deployable Space Antennas, Magdeburg: Otto-von-Guericke-University , 2012.

[129] C. H. Jenkins, Gossamer Spacecraft: Membrane And Inflatable Structures Technology For Space Applications, Cambridge, Massachussetts, United States: Progress in Astronautics and Aeronautics, American Institute of Aeronautics and Astronautics, 2001.

[130] G. Kiper und E. Soylemez, „Deployable Space Structures," *4th International Conference on Recent Advances in Space Technologies,* 11-13 June 2009.

[131] L. Puig, A. Barton und N. Rando, „A Review on Large Deployable Structures for Astrophysics Missions," *Acta Astronautica, Vol. 67 (2010),* pp. 12-26, 2010.

[132] Verein Deutscher Ingenieure, „VDI-Richtlinie 2221: Methodik zum Entwickeln und Konstruieren technischer Systeme und Produkte," in *VDI Manual Product Enginering and Design*, Berlin, Beuth Verlag GmbH, 1993.

[133] G. Pahl, W. Beitz, J. Feldhusen und K.-H. Grote, Konstruktionslehre: Grundlagen erfolgreicher Produktentwicklung - Methoden und Anwendung, 6. Auflage, Berlin: Springer Verlag, 2004.

[134] J. Jaensch und H. Birkhofer, „The Development of the Guideline VDI 2221 - The Change of Direction," *International Design Conference - DESIGN 2006,* 15-18 May 2006.

[135] Verein Deutscher Ingenieure, „VDI-Richtlinie 2222 Blatt 1: Methodisches Entwickeln von Loesungsprinzipien," in *VDI Manual Product Enginering and Design*, Berlin, Beuth Verlag GmbH, 1997.

[136] Verein Deutscher Ingenieure, „VDI-Richtlinie 2223: Methodisches Entwerfen technischer Produkte," in *VDI Manual Product Enginering and Design*, Berlin, Beuth Verlag GmbH, 2004.

[137] Verein Deutscher Ingenieure, „VDI Richtlinie 2222 Blatt 2: Erstellung und Anwendung von Konstruktionskatalogen," in *VDI Manual Product Enginering and Design*, Berlin, Beuth Verlag GmbH, 1982.

[138] V. Lajux, Methodology for the Design of Leading Edge Devices Applied to Variable Camber, Cranfield, Oxfordshire, Great Britain: Cranfield University, School of Engineering, 2007.

[139] J. Li, J. Wu und S. Yan, „Conceptual Design of Deployment Structure of Morphing Nose Cone," *Advances in Mechanical Engineering, Vol. 2013,* 29 January 2015.

[140] M. Kintscher, Entwurfsmethode fuer Formvariable Fluegelvorderkanten, Braunschweig, Germany: Doctoral Thesis, Technical University Braunschweig Carolo Wilhelmina, Department of Mechanical Engineering, 2014.

[141] Maxon Motor AG, „Maxon Motor Web-Catalogue," [Online]. Available:

https://www.maxonmotor.de/maxon/view/content/index. [Zugriff am 17 05 2018].

[142] Dr. Fritz Faulhaber GmbH & Co. KG, „Faulhaber Motor Web-Catalogue," [Online]. Available: https://www.faulhaber.com/de/startseite/. [Zugriff am 17 05 2018].

[143] Phytron GmbH, „Phytron Motor Web-Catalogue," [Online]. Available: https://www.phytron.de/. [Zugriff am 17 05 2018].

[144] National Aeronautics and Space Administration (NASA), „NASA SP-8007: Buckling of Thin-Walled Circular Cylinders," NASA Langley Research Center, Hampton, VA, United States, 1968.

[145] S. P. Timoshenko und J. M. Gere, Theory of Elastic Stability, New York: Dover Publications Inc., 1961.

[146] N. Katsumata, M. C. Natori und H. Yamakawa, „Anaylsis of Dynamic Behaviour of Inflatable Booms in Zigzag and Modified Zigzag Folding Patterns," *Acta Astronautica, Vol. 93,* pp. 45-54, 2014.

[147] J. P. Den Hartog, Mechanische Schwingungen, Berlin: Springer Verlag, 1952.

[148] U. Fischer, F. Naeher, W. Roehrer, M. Heinzler, S. Oesterle, A. Stephan, R. Kilgus, H. Paetzold und R. Winkow, Tabellenbuch Metall, 42. Auflage, Haan-Gruiten: Verlag Europa-Lehrmittel, Noruney, Vollmer GmbH & Co., 2002.

[149] M. Mikulas, R. Pappa, J. Warren und G. Rose, „Telescoping Solar Array Concept for Achieving High Packaging Efficiency," in *AIAA SciTech 2nd AIAA Spacecraft Structures Conferenc*e, Kissimmee, Florida, 5-9 January 2015.

Appendix A

A Basic Construction Element Scaling Functions

Within Appendix A scaling functions of general construction elements are derived as a basis for the derivation of component scaling functions. Addressed are beams (see A1 and A2), plates (see A3 and A4), connector elements (see A5) and ball bearings (see A6).

Note: Due to the high number of parameters there may be overlapping in the nomenclature of sub-parameters. However, these are only applied in the according section of the Appendix and not part of the solutions referenced in the main document.

A1 Beam Parameterization

Beams are basic construction elements for realization of larger structures. In the following a general parameterization is given and examples for specific beam designs which are utilized in the following descriptions of the component scaling functions are presented.

A1.1 General Beam Parameterization

A beam is parameterized by its cross-sectional area A which results from its cross-sectional size r (radius, side length …) and an area factor k_A that depends on the specific cross-sectional form:

$$A = k_A r^2$$

The corresponding second moment of area I is determined through a factor k_I which also depends on the specific cross-sectional form:

$$I = k_I A r^2 = k_I k_A r^4$$

The beam mass m results from the cross-sectional area A, the material density ρ and beam length l:

$$m = k_\rho \rho A l = k_A \rho l r^2$$

In case of an inhomogeneous material density such as in a sandwich beam a reference density ρ^* and according density factor k_ρ is defined:

$$\rho = k_\rho \rho^*$$

$$m = k_\rho \rho^* A l = k_\rho k_A \rho^* l r^2$$

For calculation of the critical stress of a beam of asymmetric cross-section loaded in bending the maximum distance of the outer fiber to the neutral layer y_{max} is given by an according factor k_y in relation to the cross-sectional size r:

$$y_{max} = k_y r$$

Here r is the characteristic size of the beam cross-section and ρ^* is the reference density of the beam. In case of a beam with homogenous material the reference density ρ^* coincides with the material density ρ. The values of the coefficients k depend on the corresponding beam cross-section and are non-dimensional.

The general beam properties are summarized in Tab. A - 1. In the following according properties for four different types of beams are presented: A1.2 solid beam, A1.3 hollow beam, A1.4 sandwich beam, A1.5 stiffened beam.

General Beam Properties		
Property	**Parameter**	**Unit**
Beam cross-sectional size/radius	r	m
Beam cross-section factor	k_A	-
Beam moment of area factor	k_I	-
Beam neutral layer factor	k_y	-
Beam density factor	k_ρ	-
Material modulus	E	N/m²
Reference density	ρ^*	kg/m³
Cross-sectional area	$A = k_A r^2$	m²
Second Moment of area	$I = k_I k_A r^4$	m⁴
Outer fiber offset to neutral layer	$y_{max} = k_y r$	m
Density	$\rho = k_\rho \rho^*$	kg/m³
Mass	$m = k_\rho k_A \rho^* l r^2$	kg

Tab. A - 1: General beam properties.

A1.2 Solid Beam

The solid beam possesses a fully filled cross-section that is symmetric in both axes and has equal dimensions in both spatial dimensions. The cross-sectional size r is equal to the radius of a circular beam and equal to the half edge size of a rectangular beam (see Fig. A - 1).

Fig. A - 1: Cross-sectional shapes of the solid beams.

The cross-sectional areas A of a circle (index $_{circ}$) and a rectangle (index $_{quad}$) are as follows:

$$A_{circ} = \pi r^2$$
$$A_{quad} = 4r^2$$
$$A = c_A r^2 = k_A r^2$$

The according second moments of areas I are as follows:

$$I_{circ} = \frac{1}{4} A r^2$$

$$I_{quad} = \frac{A(2r)^2}{12} = \frac{1}{3}Ar^2$$
$$I = c_I Ar^2 = k_I Ar^2 = k_I k_A r^4$$

The mass m of the solid beam is as follows:

$$m = \rho Al = k_\rho k_A \rho^* r^2 l$$

The maximum distance of the outer fiber to the neutral layer y_{max} is as follows:

$$y_{max} = r = k_y r$$

Constraint values for selected cross-sectional shapes and definitions of characteristic size r are summarized in Tab. A - 2.

Properties of a Solid Beam					
Cross-sectional shape	r	k_A	k_I	k_ρ	k_y
Circular	Radius	π	$\frac{1}{4}$	1	1
Quadratic	Half edge size	4	$\frac{1}{3}$	1	1

Tab. A - 2: Properties of hollow beams.

A1.3 Hollow Beam

The hollow beam is similar in cross-sectional dimensions to the solid beam but consists of thin shells (see Fig. A - 2).

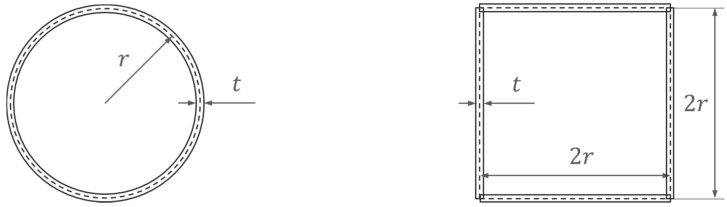

Fig. A - 2: Cross-sections of hollow beams.

Again the cross-sectional size r represents the radius or half edge size of the cross-section. The shell thickness t is given in relation r through the wall thickness ratio Γ_t:

$$\Gamma_t = \frac{t}{r}$$

The cross-sectional areas A of a circular and quadratic tube for $t << r$ are as follows:

$$A_{ctub} \approx 2\pi rt = 2\pi\Gamma_t r^2$$
$$A_{qtub} \approx 8rt = 8\Gamma_t r^2$$
$$A \approx c_A rt = c_A \Gamma_t r^2 = k_A r^2$$

The second moments of area I are as follows:

$$I_{ctub} = \frac{A}{4}\left(\left(r + \frac{t}{2}\right)^2 + \left(r - \frac{t}{2}\right)^2\right) = \frac{A}{4}\left(2r^2 + \frac{t^2}{2}\right) \approx \frac{1}{2}Ar^2$$

$$I_{qtub} = 2\left(\frac{A}{4}\frac{(2r)^2}{12} + \frac{A}{4}\frac{t^2}{12} + \frac{A}{4}r^2\right) \approx \frac{2}{3}Ar^2$$
$$I \approx k_I A r^2 = k_I k_A r^4$$

The mass m is as follows:

$$m = \rho A l = k_\rho k_A \rho^* r^2 l$$

The maximum distance of the outer fiber to the neutral layer y_{max} is as follows:

$$y_{max} = r = k_y r$$

Constraint values for selected cross-sectional shapes and definitions of characteristic size r are summarized in Tab. A - 3.

Properties of a Hollow Beam					
Cross-sectional shape	r	k_A	k_I	k_ρ	k_y
Tubular	Radius	$2\pi\Gamma_t$	$\frac{1}{2}$	1	1
Quadratic	Half edge size	$8\Gamma_t$	$\frac{2}{3}$	1	1
Geometry parameters	Wall thickness ratio: $\Gamma_t = \frac{t}{r}$				

Tab. A - 3: Properties of hollow beams.

A1.4 Sandwich Beam

The sandwich beam possesses a rectangular cross-section that is symmetric in both axes. It is composed of a lightweight core with face sheets at top and bottom (see Fig. A - 3).

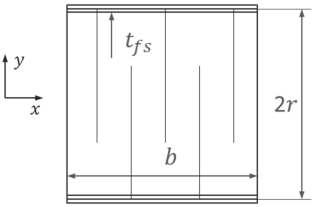

Fig. A - 3: ross-section of the sandwich beam.

The cross-sectional size r corresponds to the beams half edge size and its width is given by b. For the thickness of the facesheets t_{fs} it is assumed that $t_{fs} \ll r, b$. The beam width and the facesheet thicknesses are given as ratios of the cross-sectional size parameter r through the width ratio Γ_b and face sheet or wall thickness ratio Γ_t:

$$b = \Gamma_b r$$
$$t_{fs} = \Gamma_t r$$

To account for the difference in between the core material density ρ_{core} and facesheet material density ρ_{fs} a density ratio Γ_ρ is defined:

$$\rho_{core} = \Gamma_\rho \rho_{fs}$$

The cross-sectional area A is as follows:

$$A \approx 2rb = 2\Gamma_b r^2 = k_A r^2$$

The second moment of area I is considers only the face-sheets as contributors:

$$I_x = 2bt_{fs}r^2 = 2\Gamma_t\Gamma_b r^4 \approx \Gamma_t A r^2 = k_I k_A r^4$$

The mass m is thereby as follows:

$$m = \rho Al = \left(\rho_{core}\frac{V_c}{V} + \rho_{fs}\frac{V_{fs}}{V}\right)Al = \left(\rho_{core}\frac{(2r - t_{fs})b}{A} + \rho_{fs}\frac{2bt_{fs}}{A}\right)Al$$

$$m = \left(\rho_{core}\frac{(2-\Gamma_t)rb}{A} + \rho_{fs}\frac{\Gamma_t 2rb}{A}\right)Al = \left(\rho_{core}\left(1-\frac{\Gamma_t}{2}\right) + \rho_{fs}\Gamma_t\right)Al$$

$$m = \left(\Gamma_\rho\left(1-\frac{\Gamma_t}{2}\right) + \Gamma_t\right)\rho_{fs}Al \approx k_\rho\rho_{fs}Al = k_\rho k_A\rho_{fs}r^2 l$$

The maximum distance of the outer fiber to the neutral layer is as follows:

$$y_{max} = r = k_y r$$

Constraint values for selected cross-sectional shapes and definitions of characteristic size r are summarized in Tab. A - 4.

Properties of a Sandwich Beam					
Cross-sectional shape	r	k_A	k_I	k_ρ	k_y
Rectangle	Half-height	$2\Gamma_b$	Γ_t	$\Gamma_\rho\left(1-\frac{\Gamma_t}{2}\right) + \Gamma_t$	1
Geometry parameters	Facesheet/wall thickness ratio: $\Gamma_t = \frac{t_{fs}}{r}$ Beam width ratio: $\Gamma_b = \frac{b}{r}$ Beam density ratio: $\Gamma_\rho = \frac{\rho_{core}}{\rho_{fs}}$				
Remarks	The reference material values are those of the facesheet.				

Tab. A - 4: Properties of the sandwich beam.

A1.5 Stiffened Beam

The stiffened beam possesses a T-shaped cross-section that is symmetric in one axis. It consists of a horizontal baseplate and a vertical stringer (see Fig. A - 4).

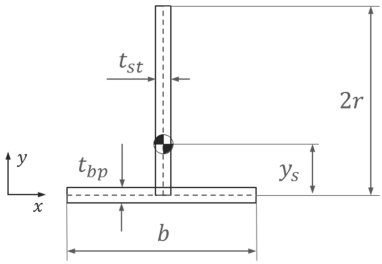

Fig. A - 4: Cross-section of the stiffened beam.

The cross-sectional size r corresponds to half of the profile height and the width is given through b. For the stringer thickness t_{st} it is assumed that $t_{st} \ll r, b$ and the same is done for the baseplate thickness t_{bp} where it is assumed that $t_{bp} \ll r, b$. The beam width b and the baseplate thickness t_{bp} are again expressed through according ratios Γ_b and Γ_t in relation to r:

$$b = \Gamma_b r$$
$$t_{bp} = \Gamma_t r$$

The ratio of stringer to baseplate size is defined by an area ratio Γ_A as follows:

$$\Gamma_A = \frac{A_{st}}{A_{bp}}$$

Thereby the cross-sectional area A of the stiffened beam can be calculated from the baseplate cross-sectional area A_{bp} and the stringer cross-sectional area A_{st}:

$$A_{bp} = t_{bp} b = \Gamma_t \Gamma_b r^2$$
$$A_{st} = 2 t_{st} r = \Gamma_A A_{bp} = \Gamma_A \Gamma_t \Gamma_b r^2$$
$$A = A_{bp} + A_{st} = A_{bp}(1 + \Gamma_A) = (1 + \Gamma_A)\Gamma_t \Gamma_b r^2 = k_A r^2$$

The neutral axis of the stiffened beam y_s is thereby as follows:

$$y_s = \frac{A_{st}}{A} r = \frac{\Gamma_A}{1 + \Gamma_A} r$$

The second moment of area I is derived as follows whereby it is assumed that cross-sectional properties are selected which cause $I_x \leq I_y$:

$$I_x = \frac{(2r)^2}{12} A_{st} + (r - y_s)^2 A_{st} + \frac{t_{bp}^2}{12} A_{bp} + y_s^2 A_{bp} \approx \frac{r^2}{3} A_{st} + (r - y_s)^2 A_{st} + y_s^2 A_{bp}$$
$$I_x \approx \frac{r^2}{3} A_{st} + \left(r - \frac{A_{st}}{A} r\right)^2 A_{st} + \left(\frac{A_{st}}{A} r\right)^2 A_{bp} = \left(\frac{1}{3} A_{st} + \left(1 - \frac{A_{st}}{A}\right)^2 A_{st} + \left(\frac{A_{st}}{A}\right)^2 A_{bp}\right) r^2$$
$$I_x \approx \left(\frac{1}{3} A_{st} + \left(1 - 2\frac{A_{st}}{A} + \left(\frac{A_{st}}{A}\right)^2\right) A_{st} + \left(\frac{A_{st}}{A}\right)^2 A_{bp}\right) r^2$$
$$I_x \approx \left(\frac{4}{3} A_{st} - 2\frac{A_{st}^2}{A} + \frac{A_{st}^3}{A^2} + \frac{A_{st}^2}{A^2} A_{bp}\right) r^2 = \left(\frac{4}{3} - 2\frac{A_{st}}{A} + \frac{A_{st}^2}{A^2} + \frac{A_{st} A_{bp}}{A^2}\right) A_{st} r^2$$
$$I_x \approx \left(\frac{4}{3} - 2\frac{\Gamma_A A_{bp}}{A} + \frac{\Gamma_A^2 A_{bp}^2}{A^2} + \frac{\Gamma_A A_{bp}^2}{A^2}\right) \Gamma_A A_{bp} r^2 = \left(\frac{4}{3} - 2\Gamma_A \frac{A_{bp}}{A} + \Gamma_A^2 \left(\frac{A_{bp}}{A}\right)^2 + \Gamma_A \left(\frac{A_{bp}}{A}\right)^2\right) \Gamma_A A_{bp} r^2$$
$$I_x \approx \left(\frac{4}{3} - 2\Gamma_A \frac{A_{bp}}{A} + \Gamma_A (1 + \Gamma_A) \left(\frac{A_{bp}}{A}\right)^2\right) \Gamma_A A_{bp} r^2 = \left(\frac{4}{3} - \frac{\Gamma_A}{1 + \Gamma_A}\right) \frac{\Gamma_A}{1 + \Gamma_A} A r^2$$
$$I_x \approx \left(\frac{4}{3} - \frac{\Gamma_A}{1 + \Gamma_A}\right) \frac{\Gamma_A}{1 + \Gamma_A} k_A r^4 = k_I k_A r^4$$

The mass m of the beam is as follows:

$$m = \rho A l = k_\rho k_A \rho^* r^2 l$$

The maximum distance of the outer fiber to the neutral layer y_{max} is as follows:

$$y_{max} = \left(2 - \frac{\Gamma_A}{1 + \Gamma_A}\right) r = k_y r$$

Constraint values for selected cross-sectional shapes and definitions of characteristic size r are summarized in Tab. A - 5.

Properties of a Stiffened Beam					
Cross-sectional shape	r	k_A	k_I	k_ρ	k_y
T-Shape	Half-height	$(1 + \Gamma_A)\Gamma_t \Gamma_b$	$\left(\frac{4}{3} - \frac{\Gamma_A}{1 + \Gamma_A}\right) \frac{\Gamma_A}{1 + \Gamma_A}$	1	$\left(2 - \frac{\Gamma_A}{1 + \Gamma_A}\right)$

Geometry parameters	Base plate wall thickness ratio: $\Gamma_t = \frac{t_{bp}}{r}$ Beam width ratio: $\Gamma_b = \frac{b}{r}$ Stringer to base plate area ratio: $\Gamma_A = \frac{A_{st}}{A_{bp}}$

Tab. A - 5: Properties of the stiffened beam.

A2 Beam Scaling Functions

Beams are applied in the simplified component models in several configurations. In the following beam scaling functions for these configurations are derived as a basis for derivation of according component scaling functions. The scaling functions are derived for two constraint functions which represent the main design requirements applied to structural components during launch where the highest mechanical loads occur. The first function is a constraint on the minimum eigenfrequency f which has to be above a certain requirement f_{req}:

$$f \geq f_{req}$$

The second function is a constraint on the maximum beam stress σ_{max} as a result from a lateral acceleration load. Thereby the maximum stress in the outer fiber has to be below a certain critical stress σ_{crit}:

$$\sigma_{max} \leq \sigma_{crit}$$

For these constraint functions beam scaling functions are derived in the following. The equations are derived on the basis of the beam parameterization presented in A1 and are not further referenced in detail (the cross-sectional size parameter r is depicted as beam radius in the following).

A2.1 Beam with Simply Supported Ends

A beam with two simply supported ends under own weight is considered.

Scaling Functions from First Eigenfrequency

The eigenfrequency f of a beam with stiffness K, uniformly distributed mass m and simply supported ends is according to Den Hartog [147] as follows:

$$f = \frac{\omega}{2\pi} = \frac{k_C^2}{2\pi}\sqrt{\frac{K}{m}} = \frac{k_C^2}{2\pi}\sqrt{\frac{EI}{ml^3}}$$

For the first eigenfrequency the related boundary coefficient value is $k_C = \pi$. Further substituting the expressions for the beam second moment of area I and beam mass m leads to:

$$f = \frac{\pi}{2}\sqrt{\frac{EI}{ml^3}} = \frac{\pi}{2}\sqrt{k_I \frac{E}{k_\rho \rho^*}\frac{r}{l^2}}$$

Equating with the eigenfrequency requirement f_{req} gives:

$$f_{req} = \frac{\pi}{2}\sqrt{k_I \frac{E}{k_\rho \rho^*}\frac{r}{l^2}}$$

Solving for the required radius r gives the beam radius scaling function:

$$r = \frac{2}{\pi}\sqrt{\frac{1}{k_I}\frac{k_\rho \rho^*}{E}}\, l^2 f_{req}$$

Substituting the radius expression in the beam mass function gives the beam mass scaling function:

$$m = k_\rho k_A \rho^* r^2 l$$

$$m = k_\rho k_A \rho^* \left(\frac{2}{\pi}\sqrt{\frac{1}{k_I}\frac{k_\rho \rho^*}{E}}\, l^2 f_{req}\right)^2 l$$

$$m = \frac{4}{\pi^2}\frac{k_A}{k_I}\frac{k_\rho^2 \rho^{*2}}{E}\, l^5 f_{req}^2$$

Scaling Functions from Critical Stress

The beam is subjected to a lateral acceleration load a_{acc} and wherefore the according stress depends on the mass distribution throughout the beam. For a beam under constant distributed load q the maximum stress σ_{max} is as follows:

$$q = \frac{m a_{acc}}{l}$$

$$\sigma_{max} = \frac{M_{max}}{W} = \frac{M_{max}}{I} y_{max}$$

The maximum bending moment M_{max} in the beam from the lateral acceleration is as follows:

$$M_{max} = \frac{q l^2}{8} = \frac{m a_{acc} l}{8}$$

$$\sigma_{max} = \frac{1}{8} m a_{acc} l \frac{y_{max}}{I}$$

Substituting the mass term by the beam linear mass represented by ρA leads to:

$$\sigma_{max} = \frac{1}{8} \rho A a_{acc} l^2 \frac{y_{max}}{I}$$

Substituting the expressions for the cross-sectional area A, material density ρ, second moment of area I and distance of the outer fiber y_{max} leads to:

$$\sigma_{max} = \frac{1}{8} k_\rho \rho^* k_A r^2 a_{acc} l^2 \frac{k_y r}{k_I k_A r^4}$$

$$\sigma_{max} = \frac{1}{8}\frac{k_y}{k_I} k_\rho \rho^* a_{acc} \frac{l^2}{r}$$

Subsequently the beam radius scaling function is derived from the critical stress as follows:

$$\sigma_{max} \leq \sigma_{crit}$$

$$\sigma_{crit} = \frac{1}{8}\frac{k_y}{k_I} k_\rho \rho^* a_{acc} \frac{l^2}{r}$$

$$r = \frac{1}{8}\frac{k_y}{k_I}\frac{k_\rho \rho^*}{\sigma_{crit}} l^2 a_{acc}$$

Substituting the radius expression in the beam mass function leads to the corresponing beam mass scaling function:

$$m = k_\rho k_A \rho^* r^2 l$$

$$m = k_\rho k_A \rho^* \left(\frac{1}{8}\frac{k_y}{k_I}\frac{k_\rho \rho^*}{\sigma_{crit}} l^2 a_{acc}\right)^2 l$$

$$m = \frac{1}{64}\frac{k_A k_y^2}{k_I^2}\frac{k_\rho^3 \rho^{*3}}{\sigma_{crit}^2} l^5 a_{acc}^2$$

Scaling Function Summary

The resulting scaling functions for the beam with simply supported ends are summarized in Tab. A - 6.

Scaling Functions of a Beam with Simply Supported Ends	
Scaling Approach: Eigenfrequency Solution	Scaling Approach: Critical Stress Solution
$m = \frac{4}{\pi^2}\frac{k_A}{k_l}\frac{k_\rho^2 \rho^{*2}}{E} l^5 f_{req}^2$	$m = \frac{1}{64}\frac{k_A k_y^2}{k_l^2}\frac{k_\rho^3 \rho^{*3}}{\sigma_{crit}^2} l^5 a_{acc}^2$
$r = \frac{2}{\pi}\sqrt{\frac{1}{k_l}\frac{k_\rho \rho^*}{E}} l^2 f_{req}$	$r = \frac{1}{8}\frac{k_y}{k_l}\frac{k_\rho \rho^*}{\sigma_{crit}} l^2 a_{acc}$

Tab. A - 6: Mass and radius scaling functions for a beam with simply supported ends.

A2.2 Beam with Simply Supported Ends and Additional Distributed Mass

A beam with two simply supported ends and an additional mass uniformly distributed throughout its length is considered. The approach is the same as for the beam with two simply supported ends in A2.1 but requires manipulation of the mass term by adding the additional distributed mass q to the length specific beam mass w. The resulting term for the length specific mass including the distributed mass w^* is as follows:

$$w^* = q + w$$

As the length specific mass is constant the corresponding beam mass m^* is as follows:

$$m^* = ql + m = m_q + m$$

Scaling Functions from First Eigenfrequency

The mass term including the distributed mass is substituted in the eigenfrequency expression given in A2.1:

$$f = \frac{\pi}{2}\sqrt{\frac{EI}{m^* l^3}}$$

$$f = \frac{\pi}{2}\sqrt{\frac{EI}{(m_q + m) l^3}}$$

Substitution of the mass and moment of inertia expressions gives:

$$f = \frac{\pi}{2}\sqrt{\frac{E k_l k_A r^4}{(m_q + k_\rho k_A \rho^* r^2 l) l^3}}$$

Equating with the eigenfrequency requirement f_{req} gives:

$$f_{req} = \frac{\pi}{2}\sqrt{\frac{E k_l k_A r^4}{(m_q + k_\rho k_A \rho^* r^2 l) l^3}}$$

Solving for the beam radius results in a fourth-degree polynomial:

$$f_{req}^2 = \frac{\pi^2}{4}\frac{E k_l k_A r^4}{(m_q + k_\rho k_A \rho^* r^2 l) l^3}$$

$$m_q + k_\rho k_A \rho^* r^2 l = \frac{\pi^2}{4}\frac{E k_l k_A r^4}{f_{req}^2 l^3}$$

$$0 = \frac{\pi^2}{4}\frac{Ek_Ik_Ar^4}{f_{req}^2 l^3} - k_\rho k_A \rho^* r^2 l - m_q$$

$$0 = r^4 - \frac{4}{\pi^2}\frac{f_{req}^2 l^3}{Ek_Ik_A} k_\rho k_A \rho^* r^2 l - \frac{4}{\pi^2}\frac{f_{req}^2 l^3}{Ek_Ik_A} m_q$$

$$0 = r^4 - \frac{4}{\pi^2}\frac{1}{k_I}\frac{k_\rho \rho^*}{E} f_{req}^2 l^4 r^2 - \frac{4}{\pi^2}\frac{1}{k_Ik_A}\frac{1}{E} m_q f_{req}^2 l^3$$

Substitution of the beam radius by $\lambda = r^2$ leads to:

$$0 = \lambda^2 - \frac{4}{\pi^2}\frac{1}{k_I}\frac{k_\rho \rho^*}{E} f_{req}^2 l^4 \lambda - \frac{4}{\pi^2}\frac{1}{k_Ik_A}\frac{1}{E} m_q f_{req}^2 l^3$$

The solutions for λ are thereby as follows:

$$\lambda_{1,2} = \frac{2}{\pi^2}\frac{1}{k_I}\frac{k_\rho \rho^*}{E} f_{req}^2 l^4 \pm \sqrt{\left(\frac{2}{\pi^2}\frac{1}{k_I}\frac{k_\rho \rho^*}{E} f_{req}^2 l^4\right)^2 + \frac{4}{\pi^2}\frac{1}{k_Ik_A}\frac{1}{E} m_q f_{req}^2 l^3}$$

Thus the solutions for the beam radius are as follows:

$$r_{1,2} = \pm\sqrt{\lambda_1}$$

$$r_{3,4} = \pm\sqrt{\lambda_2}$$

The solution needs to be positive wherefore solution r_2 and r_4 are invalid. By equating coefficients it is further found that the solution r_3 is invalid as well due to negative λ_2. Therefore the solution for the beam radius scaling function is as follows:

$$r = r_1 = \sqrt{\frac{2}{\pi^2}\frac{1}{k_I}\frac{k_\rho \rho^*}{E} f_{req}^2 l^4 + \sqrt{\left(\frac{2}{\pi^2}\frac{1}{k_I}\frac{k_\rho \rho^*}{E} f_{req}^2 l^4\right)^2 + \frac{4}{\pi^2}\frac{1}{k_Ik_A}\frac{1}{E} m_q f_{req}^2 l^3}}$$

Substituting of the radius expression in the beam mass function leads to the beam mass scaling function:

$$m = k_\rho k_A \rho^* r^2 l$$

$$m = k_\rho k_A \rho^* l\left(\frac{2}{\pi^2}\frac{1}{k_I}\frac{k_\rho \rho^*}{E} f_{req}^2 l^4 + \sqrt{\left(\frac{2}{\pi^2}\frac{1}{k_I}\frac{k_\rho \rho^*}{E} f_{req}^2 l^4\right)^2 + \frac{4}{\pi^2}\frac{1}{k_Ik_A}\frac{1}{E} m_q f_{req}^2 l^3}\right)$$

$$m = \frac{2}{\pi^2}\frac{k_A}{k_I}\frac{k_\rho^2 \rho^{*2}}{E} f_{req}^2 l^5 + k_\rho k_A \rho^* l\sqrt{\left(\frac{2}{\pi^2}\frac{1}{k_I}\frac{k_\rho \rho^*}{E} f_{req}^2 l^4\right)^2 + \frac{4}{\pi^2}\frac{1}{k_Ik_A}\frac{1}{E} m_q f_{req}^2 l^3}$$

$$m = \frac{2}{\pi^2}\frac{k_A}{k_I}\frac{k_\rho^2 \rho^{*2}}{E} f_{req}^2 l^5 + \sqrt{\left(\frac{2}{\pi^2}\frac{k_A}{k_I}\frac{k_\rho^2 \rho^{*2}}{E} f_{req}^2 l^5\right)^2 + \frac{4}{\pi^2}\frac{k_A}{k_I}\frac{k_\rho^2 \rho^{*2}}{E} m_q f_{req}^2 l^5}$$

Substitution of the recurring terms simplifies the beam mass scaling function as follows:

$$\Phi = \frac{2}{\pi^2}\frac{k_A}{k_I}\frac{k_\rho^2 \rho^{*2}}{E} f_{req}^2 l^5$$

$$m = \Phi + \sqrt{\Phi^2 + 2\Phi m_q}$$

Formulation of the beam radius scaling function by use of the above term Φ leads to:

$$r = \sqrt{\frac{2}{\pi^2}\frac{1}{k_I}\frac{k_\rho \rho^*}{E} f_{req}^2 l^4 + \sqrt{\left(\frac{2}{\pi^2}\frac{1}{k_I}\frac{k_\rho \rho^*}{E} f_{req}^2 l^4\right)^2 + \frac{4}{\pi^2}\frac{1}{k_Ik_A}\frac{1}{E} m_q f_{req}^2 l^3}}$$

$$r = \sqrt{\left(\frac{1}{k_A}\frac{1}{k_\rho \rho^*}\frac{1}{l}\right)\Phi + \sqrt{\left(\frac{1}{k_A}\frac{1}{k_\rho \rho^*}\frac{1}{l}\right)^2 \Phi^2 + 2\left(\frac{1}{k_A}\frac{1}{k_\rho \rho^*}\frac{1}{l}\right)^2 \Phi m_q}}$$

$$r = \sqrt{\frac{1}{k_A}\frac{1}{k_\rho \rho^*}\frac{1}{l}}\sqrt{\Phi + \sqrt{\Phi^2 + 2\Phi m_q}}$$

Scaling Functions from Critical Stress

The mass term including the distributed mass is substituted in the critical stress expression given in A2.1:

$$\sigma_{max} = \frac{M_{max}}{W} = \frac{M_{max}}{I} y_{max}$$
$$\sigma_{max} = \frac{1}{8} m^* a_{acc} l \frac{y_{max}}{I}$$
$$\sigma_{max} = \frac{1}{8}(m_q + m) a_{acc} l \frac{y_{max}}{I}$$

Substitution of the mass m, second moment of area I and outer fiber distance y_{max} gives:

$$\sigma_{max} = \frac{1}{8}(m_q + k_\rho k_A \rho^* r^2 l) a_{acc} l \frac{k_y r}{k_I k_A r^4}$$
$$\sigma_{max} = \frac{1}{8}(m_q + k_\rho k_A \rho^* r^2 l) a_{acc} l \frac{k_y}{k_I k_A r^3}$$

Equating with the critical stress σ_{crit} gives:

$$\sigma_{crit} = \frac{1}{8}(m_q + k_\rho k_A \rho^* r^2 l) a_{acc} l \frac{k_y}{k_I k_A r^3}$$

Solving for the beam radius r leads to a cubic polynomial:

$$8\frac{\sigma_{crit}}{a_{acc} l}\frac{k_I k_A r^3}{k_y} = m_q + k_\rho k_A \rho^* r^2 l$$
$$0 = r^3 - \frac{1}{8}\frac{a_{acc} l}{\sigma_{crit}}\frac{k_y}{k_I k_A} k_\rho k_A \rho^* l r^2 - \frac{1}{8}\frac{a_{acc} l}{\sigma_{crit}}\frac{k_y}{k_I k_A} m_q$$
$$0 = r^3 - \frac{1}{8}\frac{k_y}{k_I}\frac{k_\rho \rho^*}{\sigma_{crit}} a_{acc} l^2 r^2 - \frac{1}{8}\frac{1}{\sigma_{crit}}\frac{k_y}{k_I k_A} m_q a_{acc} l$$

The general form of the cubic equation is as follows:

$$0 = r^3 + ar^2 + br + c$$

The according coefficients are thereby as follows:

$$a = -\frac{1}{8}\frac{k_y}{k_I}\frac{k_\rho \rho^*}{\sigma_{crit}} a_{acc} l^2$$
$$b = 0$$
$$c = -\frac{1}{8}\frac{1}{\sigma_{crit}}\frac{k_y}{k_I k_A} m_q a_{acc} l$$

Substitution of the radius expression by $r = z - \frac{a}{3}$ leads to the reduced form of the cubic equation:

$$0 = z^3 + pz + q$$

The coefficients p and q are as follows:

$$p = b - \frac{a^2}{3} = -\frac{a^2}{3}$$
$$q = \frac{2a^3}{27} - \frac{ab}{3} + c = \frac{2a^3}{27} + c$$

The solution is found by Cardano's Method as follows:

$$\Delta = \left(\frac{q}{2}\right)^2 + \left(\frac{p}{3}\right)^3 = \frac{1}{4}\left(\frac{2a^3}{27} + c\right)^2 + \frac{1}{27}\left(-\frac{a^2}{3}\right)^3$$
$$\Delta = \frac{1}{4}\left(\frac{4}{729}a^6 + \frac{4}{27}a^3 c + c^2\right) - \frac{1}{729}a^6$$

$$\Delta = \frac{1}{27}a^3c + \frac{1}{4}c^2$$

Substituting the coefficients leads to:

$$\Delta = \frac{1}{27}\left(-\frac{1}{8}\frac{k_y}{k_l}\frac{k_\rho\rho^*}{\sigma_{crit}}a_{acc}l^2\right)^3\left(-\frac{1}{8}\frac{1}{\sigma_{crit}}\frac{k_y}{k_lk_A}m_qa_{acc}l\right)+\frac{1}{4}\left(-\frac{1}{8}\frac{1}{\sigma_{crit}}\frac{k_y}{k_lk_A}m_qa_{acc}l\right)^2$$

$$\Delta = \frac{1}{3^32^{12}}\frac{k_y^4}{k_l^4k_A}\frac{k_\rho^3\rho^{*3}}{\sigma_{crit}^4}a_{acc}^4l^7m_q+\frac{1}{2^8}\frac{k_y^2}{k_l^2k_A^2}\frac{1}{\sigma_{crit}^2}a_{acc}^2l^2m_q^2$$

The value of Δ is always positive wherefore there is only one real solution for the reduced form:

$$z_1 = u + v$$

With:

$$u = \sqrt[3]{-\frac{q}{2}+\sqrt{\Delta}} = \sqrt[3]{-\left(\frac{a}{3}\right)^3-\frac{c}{2}+\sqrt{\frac{1}{27}a^3c+\frac{1}{4}c^2}}$$

$$v = \sqrt[3]{-\frac{q}{2}-\sqrt{\Delta}} = \sqrt[3]{-\left(\frac{a}{3}\right)^3-\frac{c}{2}-\sqrt{\frac{1}{27}a^3c+\frac{1}{4}c^2}}$$

The solution for the beam radius scaling function is as follows:

$$r = r_1 = z_1 - \frac{a}{3} = u + v - \frac{a}{3}$$

Substitution of the radius in the mass equation gives the according beam mass scaling function as follows:

$$m = k_\rho k_A\rho^* r^2 l$$

$$m = k_\rho k_A\rho^*\left(u+v-\frac{a}{3}\right)^2 l$$

Scaling Function Summary

The resulting scaling functions for the beam with simply supported ends and additional distributed mass are summarized in Tab. A - 7.

Scaling Functions of a Beam with Simply Supported Ends and Additional Distributed Mass	
Scaling Approach: Eigenfrequency Solution	Scaling Approach: Critical Stress Solution
$m = \Phi + \sqrt{\Phi^2 + 2\Phi m_q}$	$m = k_\rho k_A\rho^*\left(u+v-\frac{a}{3}\right)^2 l$
$r = \sqrt{\frac{1}{k_A}\frac{1}{k_\rho\rho^*}\frac{1}{l}}\sqrt{\Phi+\sqrt{\Phi^2+2\Phi m_q}}$	$r = u + v - \frac{a}{3}$
$\Phi = \frac{2}{\pi^2}\frac{k_A}{k_l}\frac{k_\rho^2\rho^{*2}}{E}f_{req}^2l^5$	$u = \sqrt[3]{-\left(\frac{a}{3}\right)^3-\frac{c}{2}+\sqrt{\frac{1}{27}a^3c+\frac{1}{4}c^2}}$ $v = \sqrt[3]{-\left(\frac{a}{3}\right)^3-\frac{c}{2}-\sqrt{\frac{1}{27}a^3c+\frac{1}{4}c^2}}$

	$a = -\frac{1}{8}\frac{k_y}{k_I}\frac{k_\rho \rho^*}{\sigma_{crit}} a_{acc} l^2$ $c = -\frac{1}{8}\frac{1}{\sigma_{crit}}\frac{k_y}{k_I k_A} m_q a_{acc} l$

Tab. A - 7: Mass and radius scaling functions for a beam with simply supported ends and additional distributed mass.

A2.3 Beam with Fixed Root and Tip Mass

A beam with a fixed root and an additional point mass at its tip is considered.

Scaling Functions from First Eigenfrequency

The eigenfrequency of a beam with spring stiffness K, fixed root, uniformly distributed beam mass m and additional tip mass m_T is given by Den Hartog [147] as follows:

$$K = \frac{3EI}{l^3}$$

$$m^* = m_T + 0.23m$$

$$f = \frac{\omega}{2\pi} = \frac{1}{2\pi}\sqrt{\frac{K}{m^*}} = \frac{1}{2\pi}\sqrt{\frac{3EI}{(m_T + 0.23m)l^3}}$$

Substituting the expressions for the second moment of area I and the beam mass m leads to:

$$f = \frac{1}{2\pi}\sqrt{\frac{3Ek_I k_A r^4}{\left(m_T + 0.23k_\rho k_A \rho^* r^2 l\right)l^3}}$$

Equating with the eigenfrequency requirement f_{req} gives:

$$f_{req} = \frac{1}{2\pi}\sqrt{\frac{3Ek_I k_A r^4}{\left(m_T + 0.23k_\rho k_A \rho^* r^2 l\right)l^3}}$$

Solving for the beam radius r leads to a fourth degree polynomial:

$$4\pi^2 f_{req}^2 = \frac{3Ek_I k_A r^4}{\left(m_T + 0.23k_\rho k_A \rho^* r^2 l\right)l^3}$$

$$m_T + 0.23k_\rho k_A \rho^* l r^2 = \frac{3}{4\pi^2} E k_I k_A \frac{1}{f_{req}^2}\frac{1}{l^3} r^4$$

$$0 = \frac{3}{4\pi^2} E k_I k_A \frac{1}{f_{req}^2}\frac{1}{l^3} r^4 - 0.23k_\rho k_A \rho^* l r^2 - m_T$$

$$0 = r^4 - \frac{4\pi^2 0.23 k_\rho k_A \rho^* l^4 f_{req}^2}{3Ek_I k_A} r^2 - \frac{4\pi^2 m_T f_{req}^2 l^3}{3Ek_I k_A}$$

$$0 = r^4 - \frac{0.92\pi^2}{3}\frac{k_\rho \rho^*}{E}\frac{1}{k_I} f_{req}^2 l^4 r^2 - \frac{4\pi^2}{3}\frac{1}{E}\frac{1}{k_I k_A} m_T f_{req}^2 l^3$$

Substitution of beam radius by $\lambda = r^2$ leads to:

$$0 = \lambda^2 - \frac{0.92\pi^2}{3}\frac{k_\rho \rho^*}{E}\frac{1}{k_I} f_{req}^2 l^4 \lambda - \frac{4\pi^2}{3}\frac{1}{E}\frac{1}{k_I k_A} m_T f_{req}^2 l^3$$

The solutions for λ are as follows:

$$\lambda_{1,2} = \frac{0.92\pi^2}{6}\frac{k_\rho \rho^*}{E}\frac{1}{k_I} f_{req}^2 l^4 \pm \sqrt{\left(\frac{0.92\pi^2}{6}\frac{k_\rho \rho^*}{E}\frac{1}{k_I} f_{req}^2 l^4\right)^2 + \frac{4\pi^2}{3}\frac{1}{E}\frac{1}{k_I k_A} m_T f_{req}^2 l^3}$$

Thus the solutions for the radius are as follows:

$$r_{1,2} = \pm\sqrt{\lambda_1}$$
$$r_{3,4} = \pm\sqrt{\lambda_2}$$

The solution needs to be positive wherefore solution r_2 and r_4 are invalid. By equating coefficients it is further found that the solution r_3 is invalid as well due to negative λ_2. Therefore the solution for the beam radius scaling function is as follows:

$$r = r_1 = \sqrt{\frac{0.92\pi^2}{6}\frac{k_\rho \rho^*}{E}\frac{1}{k_I}f_{req}^2 l^4 + \sqrt{\left(\frac{0.92\pi^2}{6}\frac{k_\rho \rho^*}{E}\frac{1}{k_I}f_{req}^2 l^4\right)^2 + \frac{4\pi^2}{3}\frac{1}{E}\frac{1}{k_I k_A}m_T f_{req}^2 l^3}}$$

Substituting the radius expression in the beam mass function leads to beam mass scaling function:

$$m = k_\rho k_A \rho^* r^2 l$$
$$m = k_\rho k_A \rho^* l\left(\frac{0.92\pi^2}{6}\frac{k_\rho \rho^*}{E}\frac{1}{k_I}f_{req}^2 l^4 + \sqrt{\left(\frac{0.92\pi^2}{6}\frac{k_\rho \rho^*}{E}\frac{1}{k_I}f_{req}^2 l^4\right)^2 + \frac{4\pi^2}{3}\frac{1}{E}\frac{1}{k_I k_A}m_T f_{req}^2 l^3}\right)$$
$$m = \frac{0.92\pi^2}{6}\frac{k_\rho^2 \rho^{*2}}{E}\frac{k_A}{k_I}f_{req}^2 l^5 + k_\rho k_A \rho^* l\sqrt{\left(\frac{0.92\pi^2}{6}\frac{k_\rho \rho^*}{E}\frac{1}{k_I}f_{req}^2 l^4\right)^2 + \frac{4\pi^2}{3}\frac{1}{E}\frac{1}{k_I k_A}m_T f_{req}^2 l^3}$$
$$m = \frac{0.92\pi^2}{6}\frac{k_\rho^2 \rho^{*2}}{E}\frac{k_A}{k_I}f_{req}^2 l^5 + \sqrt{\left(\frac{0.92\pi^2}{6}\frac{k_\rho^2 \rho^{*2}}{E}\frac{k_A}{k_I}f_{req}^2 l^5\right)^2 + \frac{4\pi^2}{3}\frac{k_\rho^2 \rho^{*2}}{E}\frac{k_A}{k_I}m_T f_{req}^2 l^5}$$
$$m = \frac{0.23}{2}\frac{4\pi^2}{3}\frac{k_\rho^2 \rho^{*2}}{E}\frac{k_A}{k_I}f_{req}^2 l^5 + \sqrt{\left(\frac{0.23}{2}\frac{4\pi^2}{3}\frac{k_\rho^2 \rho^{*2}}{E}\frac{k_A}{k_I}f_{req}^2 l^5\right)^2 + \frac{4\pi^2}{3}\frac{k_\rho^2 \rho^{*2}}{E}\frac{k_A}{k_I}f_{req}^2 l^5 m_T}$$

Substitution of the recurring terms simplifies the beam mass scaling function as follows:

$$\Phi = \frac{0.23}{2}\frac{4\pi^2}{3}\frac{k_\rho^2 \rho^{*2}}{E}\frac{k_A}{k_I}f_{req}^2 l^5$$
$$m = \Phi + \sqrt{\Phi^2 + \frac{2}{0.23}\Phi m_T}$$

Formulation of the beam radius scaling function by use of the above introduced term Φ leads to:

$$r = \sqrt{\frac{0.92\pi^2}{6}\frac{k_\rho \rho^*}{E}\frac{1}{k_I}f_{req}^2 l^4 + \sqrt{\left(\frac{0.92\pi^2}{6}\frac{k_\rho \rho^*}{E}\frac{1}{k_I}f_{req}^2 l^4\right)^2 + \frac{4\pi^2}{3}\frac{1}{E}\frac{1}{k_I k_A}m_T f_{req}^2 l^3}}$$
$$r = \sqrt{\left(\frac{1}{k_\rho \rho^*}\frac{1}{k_A}\frac{1}{l}\right)\Phi + \sqrt{\left(\frac{1}{k_\rho \rho^*}\frac{1}{k_A}\frac{1}{l}\right)^2\Phi^2 + \frac{2}{0.23}\left(\frac{1}{k_\rho \rho^*}\frac{1}{k_A}\frac{1}{l}\right)^2\Phi m_T}}$$
$$r = \sqrt{\frac{1}{k_\rho \rho^*}\frac{1}{k_A}\frac{1}{l}}\sqrt{\Phi + \sqrt{\Phi^2 + \frac{2}{0.23}\Phi m_T}}$$

Scaling Functions from Critical Stress

The maximum stress σ_{max} in a beam loaded in bending is as follows:

$$\sigma_{max} = \frac{M_{max}}{W} = \frac{M_{max}}{I}y_{max}$$

The maximum bending moment M_{max} on a beam with fixed root, uniform linear mass ρA and tip mass m_T resulting from a lateral acceleration load a_{acc} occurs at its root and depends on the mass distribution:

$$M_{max} = m_T a_{acc} l + \frac{1}{2}\rho A a_{acc} l^2$$

Substitution gives the maximum stress in the outer fiber:

$$\sigma_{max} = \left(m_T a_{acc} l + \frac{1}{2}\rho A a_{acc} l^2\right)\frac{y_{max}}{I}$$

Substituting the expressions for the cross-sectional area A, material density ρ, second moment of area I and distance of the outer fiber y_{max} leads to:

$$\sigma_{max} = \left(m_T a_{acc} l + \frac{1}{2}k_\rho \rho^* k_A r^2 a_{acc} l^2\right)\frac{k_y r}{k_I k_A r^4}$$

$$\sigma_{max} = \left(m_T a_{acc} l + \frac{1}{2}k_\rho k_A \rho^* a_{acc} l^2 r^2\right)\frac{k_y}{k_I k_A r^3}$$

Equating with the critical stress σ_{crit} gives:

$$\sigma_{crit} = \left(m_T a_{acc} l + \frac{1}{2}k_\rho k_A \rho^* a_{acc} l^2 r^2\right)\frac{k_y}{k_I k_A r^3}$$

Solving for the beam radius leads to a cubic polynomial:

$$\sigma_{crit} r^3 = m_T a_{acc} l \frac{k_y}{k_I k_A} + \frac{1}{2}k_\rho k_A \rho^* a_{acc} l^2 \frac{k_y}{k_I k_A} r^2$$

$$\sigma_{crit} r^3 = \frac{k_y}{k_I k_A} m_T a_{acc} l + \frac{1}{2}\frac{k_y}{k_I} k_\rho \rho^* a_{acc} l^2 r^2$$

$$0 = \sigma_{crit} r^3 - \frac{1}{2}\frac{k_y}{k_I} k_\rho \rho^* a_{acc} l^2 r^2 - \frac{k_y}{k_I k_A} m_T a_{acc} l$$

$$0 = r^3 - \frac{1}{2}\frac{k_y}{k_I}\frac{k_\rho \rho^*}{\sigma_{crit}} a_{acc} l^2 r^2 - \frac{k_y}{k_I k_A}\frac{1}{\sigma_{crit}} m_T a_{acc} l$$

The general form of the cubic equation is as follows:

$$0 = r^3 + ar^2 + br + c$$

The coefficients are as follows:

$$a = -\frac{1}{2}\frac{k_y}{k_I}\frac{k_\rho \rho^*}{\sigma_{crit}} a_{acc} l^2$$

$$b = 0$$

$$c = -\frac{k_y}{k_I k_A}\frac{1}{\sigma_{crit}} m_T a_{acc} l$$

Substitution of the radius expression by $r = z - \frac{a}{3}$ leads to the reduced form of the cubic equation:

$$0 = z^3 + pz + q$$

The coefficients p and q are as follows:

$$p = b - \frac{a^2}{3} = -\frac{a^2}{3}$$

$$q = \frac{2a^3}{27} - \frac{ab}{3} + c = \frac{2a^3}{27} + c = 2\left(\frac{a}{3}\right)^3 + c$$

The solution is found by Cardano's Method as follows:

$$\Delta = \left(\frac{q}{2}\right)^2 + \left(\frac{p}{3}\right)^3 = \frac{1}{4}\left(\frac{2a^3}{27} + c\right)^2 + \frac{1}{27}\left(-\frac{a^2}{3}\right)^3$$

$$\Delta = \frac{1}{4}\left(\frac{4}{729}a^6 + \frac{4}{27}a^3 c + c^2\right) - \frac{1}{729}a^6$$

$$\Delta = \frac{1}{27}a^3 c + \frac{1}{4}c^2 = \left(\frac{a}{3}\right)^3 c + \left(\frac{c}{2}\right)^2$$

Substituting the coefficients leads to:

$$\Delta = \frac{1}{27}\left(-\frac{1}{2}\frac{k_y}{k_l}\frac{k_\rho \rho^*}{\sigma_{crit}}a_{acc}l^2\right)^3 \left(-\frac{k_y}{k_l k_A}\frac{1}{\sigma_{crit}}m_T a_{acc} l\right) + \frac{1}{4}\left(-\frac{k_y}{k_l k_A}\frac{1}{\sigma_{crit}}m_T a_{acc} l\right)^2$$

$$\Delta = \frac{1}{216}\frac{k_y^4}{k_l^4 k_A}\frac{k_\rho^3 \rho^{*3}}{\sigma_{crit}^4}a_{acc}^4 l^7 m_T + \frac{1}{4}\frac{k_y^2}{k_l^2 k_A^2}\frac{1}{\sigma_{crit}^2}m_T^2 a_{acc}^2 l^2$$

The value of Δ is always positive wherefore there is only one real solution for the reduced form:

$$z_1 = u + v$$

With:

$$u = \sqrt[3]{-\frac{q}{2} + \sqrt{\Delta}} = \sqrt[3]{-\left(\frac{a}{3}\right)^3 - \frac{c}{2} + \sqrt{\left(\frac{a}{3}\right)^3 c + \left(\frac{c}{2}\right)^2}}$$

$$v = \sqrt[3]{-\frac{q}{2} - \sqrt{\Delta}} = \sqrt[3]{-\left(\frac{a}{3}\right)^3 - \frac{c}{2} - \sqrt{\left(\frac{a}{3}\right)^3 c + \left(\frac{c}{2}\right)^2}}$$

The solution for the beam radius scaling function is as follows:

$$r_1 = z_1 - \frac{a}{3} = u + v - \frac{a}{3}$$

Substitution of the radius expression in the mass equation gives the beam mass scaling function as follows:

$$m = k_\rho k_A \rho^* r^2 l$$

$$m = k_\rho k_A \rho^* \left(u + v - \frac{a}{3}\right)^2 l$$

Scaling Function Summary

The resulting scaling functions for the beam with fixed root and tip mass are summarized in Tab. A - 8.

Scaling Functions of a Beam with Fixed Root and Tip Mass	
Scaling Approach: Eigenfrequency Solution	Scaling Approach: Critical Stress Solution
$m = \Phi + \sqrt{\Phi^2 + \frac{2}{0.23}\Phi m_T}$	$m = k_\rho k_A \rho^* \left(u + v - \frac{a}{3}\right)^2 l$
$r = \sqrt{\frac{1}{k_\rho \rho^*}\frac{1}{k_A}\frac{1}{l}}\sqrt{\Phi + \sqrt{\Phi^2 + \frac{2}{0.23}\Phi m_T}}$	$r = u + v - \frac{a}{3}$
$\Phi = \frac{0.23}{2}\frac{4\pi^2}{3}\frac{k_\rho^2 \rho^{*2}}{E}\frac{k_A}{k_l}f_{req}^2 l^5$	$z_1 = u + v$ $u = \sqrt[3]{-\left(\frac{a}{3}\right)^3 - \frac{c}{2} + \sqrt{\left(\frac{a}{3}\right)^3 c + \left(\frac{c}{2}\right)^2}}$ $v = \sqrt[3]{-\left(\frac{a}{3}\right)^3 - \frac{c}{2} - \sqrt{\left(\frac{a}{3}\right)^3 c + \left(\frac{c}{2}\right)^2}}$

	$a = -\frac{1}{2}\frac{k_y}{k_I}\frac{k_\rho \rho^*}{\sigma_{crit}} a_{acc} l^2$ $c = -\frac{k_y}{k_I k_A}\frac{1}{\sigma_{crit}} m_T a_{acc} l$

Tab. A - 8: Mass and radius scaling functions for a beam with fixed root and tip mass.

A3 Plate Parameterization

Just like beams, plates are basic construction elements for realization of larger structures. In the following a general parameterization is given and examples for specific plate designs which are utilized in the following descriptions of the component scaling functions are presented.

A3.1 General Plate Parameterization

The mass m result from its length a, width b, thickness t and material density ρ:

$$m = abt\rho$$

To account for different types of plate architectures with different cross-sectional designs a mass architecture parameter k_m may be introduced as follows:

$$m = k_m abt\rho$$

In case of an inhomogeneous material density such as in a sandwich plate a reference density ρ^* and according density factor k_ρ is defined:

$$\rho = k_\rho \rho^*$$

Thereby the plate mass is written as follows:

$$m = k_m k_\rho abt\rho^*$$

The resulting area mass γ of the plate is as follows:

$$\gamma = k_m k_\rho t\rho^*$$

The plate's deformation under load is determined through its flexural rigidity D which results for an isotropic material from the material modulus E, Poisson ratio ν and :

$$D = \frac{E}{1-\nu^2}\int z^2 dz$$

For a general plate the resulting flexural rigidity may be written as follows whereby k_D is the flexural rigidity architecture parameter which contains the plate's specific cross-sectional design:

$$D = k_D \frac{Et^3}{1-\nu^2}$$

The general properties of a plate are summarized in Tab. A - 9. In the following according properties of solid plates (see A3.2), sandwich plates (see A3.3) and stiffened plates (see A3.4) are derived.

General Plate Properties		
Property	**Parameter**	**Unit**
Plate length	a	m
Plate width	b	m
Plate thickness	t	m
Material modulus	E	N/m²

Poisson ratio	ν	-
Reference density	ρ^*	kg/m³
Plate mass architecture factor	k_m	-
Plate flexural rigidity architecture factor	k_D	-
Plate density factor	k_ρ	-
Mass	$m = k_m k_\rho abt\rho^*$	kg
Density	$\rho = k_\rho \rho^*$	kg/m³
Areal mass	$\gamma = k_m k_\rho t\rho^*$	kg/m²
Flexural rigidity	$D = k_D \frac{Et^3}{1-\nu^2}$	Nm

Tab. A - 9: General plate properties.

A3.2 Solid Plate

The mass m and the areal mass γ of a solid panel coincides with the general plate mass:

$$m = abt\rho$$
$$\gamma = t\rho$$

The flexural rigidity D is as follows:

$$D = \frac{1}{12}\frac{Et^3}{1-\nu^2}$$

The properties of the solid plate are summarized in Tab. A - 10.

Properties of a Solid Plate			
Plate Architecture	k_m	k_D	k_ρ
Solid	1	$\frac{1}{12}$	1

Tab. A - 10: Properties of the solid plate.

A3.3 Sandwich Plate

The mass of the sandwich panel m depends on its basic dimensions a, b and t. The cross-section and its parameterization is the same as for the sandwich beam (see A1.4 and Fig. A - 3). However, the sandwich is an assembly of a sandwich core of density ρ_c and the facesheets of density ρ_{fs} and thickness t_{fs}. For calculation of the mass it is assumed that $t_{fs} \ll t$:

$$m \approx ab\left(\rho_c\left(t - t_{fs}\right) + 2\rho_{fs}t_{fs}\right)$$

Substituting the core material density by the material density ratio Γ_ρ leads to:

$$\Gamma_\rho = \frac{\rho_c}{\rho_{fs}}$$
$$m = ab\rho_{fs}\left(\Gamma_\rho\left(t - t_{fs}\right) + 2t_{fs}\right)$$

Substituting the face-sheet thickness with the thickness ratio Γ_t gives:

$$\Gamma_t = \frac{t_{fs}}{t}$$
$$m = ab\rho_{fs}\left(\Gamma_\rho\left(t - \Gamma_t t\right) + 2\Gamma_t t\right)$$
$$m = abt\rho_{fs}\left(\Gamma_\rho\left(1 - \Gamma_t\right) + 2\Gamma_t\right)$$

The areal mass γ of the panel is thereby:

$$\gamma = \frac{m_P}{ab}$$
$$\gamma = t\rho_{fs}\left(\Gamma_\rho\left(1 - \Gamma_t\right) + 2\Gamma_t\right)$$

For calculation of the flexural rigidity of the sandwich plate it is assumed that only the cover sheets contribute to the overall stiffness. Therefore the flexural rigidity D is as follows:

$$D = \frac{E_{fs}}{1 - \nu_{fs}^2} 2 \int_{\frac{t}{2} - \frac{t_{fs}}{2}}^{\frac{t}{2} + \frac{t_{fs}}{2}} z^2 dz$$
$$D = \frac{E_{fs}}{1 - \nu_{fs}^2} \frac{2}{3} \left(\left(\frac{t}{2} + \frac{t_{fs}}{2} \right)^3 - \left(\frac{t}{2} - \frac{t_{fs}}{2} \right)^3 \right)$$
$$D = \frac{E_{fs}}{1 - \nu_{fs}^2} \frac{2}{3} \left(\frac{t^3}{8} + 3\frac{t^2}{4}\frac{t_{fs}}{2} + 3\frac{t}{2}\frac{t_{fs}^2}{4} + \frac{t_{fs}^3}{8} - \frac{t^3}{8} + 3\frac{t^2}{4}\frac{t_{fs}}{2} - 3\frac{t}{2}\frac{t_{fs}^2}{4} + \frac{t_{fs}^3}{8} \right)$$
$$D = \frac{E_{fs}}{1 - \nu_{fs}^2} \left(\frac{1}{2} t^2 t_{fs} + \frac{t_{fs}^3}{6} \right)$$

For $t_{fs} \ll t$ the higher order term of t_{fs} can be neglected and the flexural rigidity becomes:

$$D = \frac{E_{fs}}{1 - \nu_{fs}^2} \frac{t_{fs} t^2}{2}$$

Substituting the face-sheet thickness by the thickness ratio Γ_t, the flexural rigidity can be written as follows:

$$D = \frac{\Gamma_t}{2} \frac{E_{fs} t^3}{1 - \nu_{fs}^2}$$

The properties of the sandwich plate are summarized in Tab. A - 11.

Properties of a Sandwich Plate			
Plate Architecture	k_m	k_D	k_ρ
Sandwich	$\Gamma_\rho(1 - \Gamma_t) + 2\Gamma_t$	$\frac{\Gamma_t}{2}$	$\frac{\rho_c}{\rho_{fs}}$
Geometry Parameters	Facesheet/wall thickness ratio: $\Gamma_t = \frac{t_{fs}}{t}$ Plate density ratio: $\Gamma_\rho = \frac{\rho_c}{\rho_{fs}}$		
Remarks	The reference material properties are those of the face sheets.		

Tab. A - 11: Properties of the sandwich plate.

A3.4 Stiffened Plate

The stiffened plate is in its cross-sectional design similar to the stiffened beam (see A1.5 and Fig. A - 4) in both plate main directions. It consists of a base plate of thickness d and vertical stiffeners of height t and same thickness d (with $d \ll t$). Stiffeners are aligned in both panel directions and are crossing each other. The cross-section is parameterized by the wall thickness to panel height ratio Γ_{dt} and the stiffener to base-plate area ratio Γ_A which relates the cross-sectional area of the stiffeners A_{st} to the cross-sectional area of the base plate A_{bp}:

$$\Gamma_{dt} = \frac{d}{t}$$

$$\Gamma_A = \frac{A_{st}}{A_{bp}}$$

Hence, the baseplate cross-sectional area $A_{BP,x}$ normal to the x-direction is as follows:

$$A_{bp,x} = ad = \Gamma_{dt} at$$

The cross-sectional area of the stringer $A_{st,x}$ normal to the x-direction is as follows:

$$A_{st,x} = \Gamma_A A_{bp}$$

$$A_{st,x} = \Gamma_A \Gamma_{dt} at$$

For the y-direction the cross-sectional values are gained through replacing plate length a by plate width b. Thereby the mass m of the stiffened panel is calculated from the baseplate mass m_{bp} and the masses of stiffeners in x- and y-direction $m_{st,x}$ and $m_{st,y}$ as follows:

$$m = m_{bp} + m_{st,x} + m_{st,y}$$

$$m = \left(A_{bp,x} b + A_{st,x} b + A_{st,y} a\right)\rho$$

$$m = \left(abd + \Gamma_A A_{bp,x} b + \Gamma_A A_{bp,y} a\right)\rho$$

$$m = (abd + \Gamma_A abd + \Gamma_A abd)\rho$$

$$m = \rho abd(1 + 2\Gamma_A)$$

Substituting the base-plate thickness d gives:

$$m = \Gamma_{dt}(1 + 2\Gamma_A) abt\rho$$

The specific plate mass is thereby as follows:

$$\gamma = \Gamma_{dt}(1 + 2\Gamma_A) t\rho$$

The stiffened plate does not have a continuous flexural rigidity and $d \ll t$. Therefore the expression needs to be modified to account for the discontinuous panel design. Assuming rectangular longitudinal and lateral stiffeners and according loading in these directions only, there is (almost) no coupling between longitudinal and transverse stresses. The lateral contraction can therefore be neglected and the panel flexural rigidity becomes the beam bending stiffness per unit length (for $d \ll t$):

$$D = \frac{EI}{a} = \frac{E}{a} \int z^2 dA$$

The boundaries of the integral are depending on the neutral layer of the stiffened panel. In relation to the neutral layer of the base-plate, the distance to the neutral layer of the stiffened panel y_S is as follows:

$$y_S = \frac{A_{st} \frac{t}{2}}{A_{bp} + A_{st}}$$

$$y_S = \frac{\Gamma_A A_{bp}}{A_{bp} + \Gamma_A A_{bp}} \frac{t}{2}$$

$$y_S = \frac{\Gamma_A}{2(1 + \Gamma_A)} t$$

The contribution of the stiffeners to the flexural rigidity depends on their combined width $\frac{A_{st}}{t}$ compared to the panel width a:

$$\frac{A_{St}}{at} = \frac{\Gamma_A \Gamma_{dt} at}{at} = \Gamma_A \Gamma_{dt}$$

The flexural rigidity of the stiffeners with respect to the panel neutral layer is as follows:

$$D_{st} = \frac{E}{a}\int_{-y_S}^{t-y_S} z^2 dA$$

$$D_{st} = E\Gamma_A \Gamma_{dt}\int_{-y_S}^{t-y_S} z^2 dz$$

$$D_{st} = \frac{1}{3}E\Gamma_A \Gamma_{dt}((t-y_S)^3 - (-y_S)^3)$$

$$D_{st} = \frac{1}{3}E\Gamma_A \Gamma_{dt}(t^3 - 3t^2 y_S + 3t y_S^2 - y_S^3 + y_S^3)$$

$$D_{st} = \frac{1}{3}E\Gamma_A \Gamma_{dt}(t^3 - 3t^2 y_S + 3t y_S^2)$$

$$D_{st} = \frac{1}{3}E\Gamma_A \Gamma_{dt}\left(t^3 - 3t^3\frac{\Gamma_A}{2(1+\Gamma_A)} + 3t^3\left(\frac{\Gamma_A}{2(1+\Gamma_A)}\right)^2\right)$$

$$D_{st} = Et^3\Gamma_A \Gamma_{dt}\left(\frac{1}{3} - \frac{\Gamma_A}{2(1+\Gamma_A)} + \left(\frac{\Gamma_A}{2(1+\Gamma_A)}\right)^2\right)$$

The contribution of the base-plate is derived as follows:

$$D_{bp} = \frac{E}{a}\int_{-\left(y_S+\frac{d}{2}\right)}^{-\left(y_S-\frac{d}{2}\right)} z^2 dA$$

$$D_{bp} = E\int_{-\left(y_S+\frac{d}{2}\right)}^{-\left(y_S-\frac{d}{2}\right)} z^2 dz$$

$$D_{bp} = \frac{1}{3}E\left(\left(-\left(y_S - \frac{d}{2}\right)\right)^3 - \left(-\left(y_S + \frac{d}{2}\right)\right)^3\right)$$

$$D_{bp} = \frac{1}{3}E\left(-\left(y_S - \frac{d}{2}\right)^3 + \left(y_S + \frac{d}{2}\right)^3\right)$$

$$D_{bp} = \frac{1}{3}E\left(-\left(y_S^3 - 3y_S^2\frac{d}{2} + 3y_S\left(\frac{d}{2}\right)^2 - \left(\frac{d}{2}\right)^3\right) + \left(y_S^3 + 3y_S^2\frac{d}{2} + 3y_S\left(\frac{d}{2}\right)^2 + \left(\frac{d}{2}\right)^3\right)\right)$$

$$D_{bp} = \frac{1}{3}E\left(6y_S^2\frac{d}{2} + 2\left(\frac{d}{2}\right)^3\right)$$

$$D_{bp} = E\left(y_S^2 d + \frac{1}{12}d^3\right)$$

For $d \ll t$ the cubic term can be neglected. Substituting the base-plate thickness d leads to:

$$D_{bp} = Et^3\left(\frac{\Gamma_A}{2(1+\Gamma_A)}\right)^2 \Gamma_{dt}$$

The stiffened panel flexural rigidity is as follows:

$$D = D_{st} + D_{bp}$$

$$D = Et^3\Gamma_A \Gamma_{dt}\left(\frac{1}{3} - \frac{\Gamma_A}{2(1+\Gamma_A)} + \left(\frac{\Gamma_A}{2(1+\Gamma_A)}\right)^2\right) + Et^3\left(\frac{\Gamma_A}{2(1+\Gamma_A)}\right)^2 \Gamma_{dt}$$

$$D = Et^3\Gamma_A \Gamma_{dt}\left(\frac{1}{3} - \frac{\Gamma_A}{2(1+\Gamma_A)} + \frac{\Gamma_A}{(2(1+\Gamma_A))^2} + \left(\frac{\Gamma_A}{2(1+\Gamma_A)}\right)^2\right)$$

$$D = Et^3\Gamma_A \Gamma_{dt}\left(\frac{1}{3} + \frac{\Gamma_A^2 + \Gamma_A - 2\Gamma_A(1+\Gamma_A)}{(2(1+\Gamma_A))^2}\right)$$

$$D = Et^3\Gamma_A\Gamma_{dt}\left(\frac{1}{3} - \frac{\Gamma_A + \Gamma_A^2}{\left(2(1+\Gamma_A)\right)^2}\right)$$

$$D = Et^3\Gamma_A\Gamma_{dt}\left(\frac{1}{3} - \frac{\Gamma_A(1+\Gamma_A)}{4(1+\Gamma_A)^2}\right)$$

Thereby the flexural rigidity of the plate with longitudinal and lateral stiffeners is as follows:

$$D = \Gamma_A\Gamma_{dt}\left(\frac{1}{3} - \frac{\Gamma_A}{4(1+\Gamma_A)}\right)Et^3$$

The properties of the stiffened plate are summarized in Tab. A - 12.

Properties of a Stiffened Plate			
Plate Architecture	$\boldsymbol{k_m}$	$\boldsymbol{k_D}$	$\boldsymbol{k_\rho}$
Stiffened	$\Gamma_{dt}(1+2\Gamma_A)$	$\Gamma_A\Gamma_{dt}\left(\frac{1}{3} - \frac{\Gamma_A}{4(1+\Gamma_A)}\right)$	1
Geometry Parameters	Wall thickness ratio for stiffeners and baseplate: $\Gamma_{dt} = \frac{d}{t}$ Cross-sectional area ratio between stiffeners and baseplate: $\Gamma_A = \frac{A_{st}}{A_{bp}}$		
Remarks	With $\nu = 0$ for rectangular, longitudinal and lateral stiffeners and $d \ll t$		

Tab. A - 12: Properties of the stiffened plate.

A4 Plate Scaling Functions

Plates are applied in the simplified component models in several configurations. In the following plate scaling functions for these configurations are derived as a basis for derivation of according component scaling functions. The scaling functions are derived for the constraint function on the minimum eigenfrequency f which has to be above a certain requirement f_{req} during launch:

$$f \geq f_{req}$$

Plate scaling functions are utilized for derivation of panel scaling functions which span large areas. Hence it is assumed that the stiffness requirements resulting from the minimum eigenfrequency constraints are dominating. Therefore the derivation of according plate scaling functions from critical stresses is neglected.

A4.1 Rectangular Plate with Two Fixed Edges

The plate with two fixed, opposing edges is approximated as an elongated beam with fixed ends. For derivation of the scaling function the according expression for the first eigenfrequency given by Den Hartog [147] is utilized:

$$f = \frac{k_C^2}{2\pi}\sqrt{\frac{EI}{ml^3}}$$

Equating with the eigenfrequency constraint function gives:

$$f_{req} = \frac{k_C^2}{2\pi}\sqrt{\frac{EI}{ml^3}}$$

For these boundary conditions the according coefficient value is $k_C^2 = 22.4$. The beam length l corresponds to the plate width b and the mass m of the general plate is described in Tab. A - 9. The beam bending stiffness EI is approximated by the plate flexural rigidity D for $\nu = 0$:

$$D = k_D \frac{Et^3}{1-\nu^2} \approx \frac{EI}{a}$$

Substitution in the eigenfrequency expression gives:

$$f_{req} = \frac{k_C^2}{2\pi}\sqrt{k_D E \frac{at^3}{mb^3}}$$

Substitution of the plate thickness through the mass expression according to Tab. A - 9 gives:

$$m = k_m k_\rho abt\rho^*$$

$$t = \frac{m}{k_m k_\rho ab\rho^*}$$

$$f_{req} = \frac{k_C^2}{2\pi}\sqrt{k_D E \frac{a}{mb^3}\left(\frac{m}{k_m k_\rho ab\rho^*}\right)^3}$$

$$f_{req} = \frac{k_C^2}{2\pi}\sqrt{k_D \frac{E}{k_\rho^3 \rho^{*3}} \frac{1}{a^2 b^6} \frac{1}{k_m^3} m^2}$$

Solving for the plate mass m gives:

$$m = \sqrt{\frac{4\pi^2}{k_C^4} \frac{k_m^3}{k_D} \frac{k_\rho^3 \rho^{*3}}{E} a^2 b^6 f_{req}^2}$$

The resulting scaling function for the beam with fixed ends is summarized in Tab. A - 13.

Scaling Functions of a Plate with Two Fixed Edges
Scaling Approach: Eigenfrequency Solution
$m = \sqrt{\frac{4\pi^2}{k_C^4} \frac{k_m^3}{k_D} \frac{k_\rho^3 \rho^{*3}}{E} a^2 b^6 f_{req}^2}$

Tab. A - 13: Mass scaling function of a plate with two fixed, opposing edges due to a minimum eigenfrequency criterion approximated as an elongated beam.

A4.2 Rectangular Plate with Four Simply Supported Edges and Additional Center Mass

The first eigenfrequency of the rectangular plate with center mass and simply supported edges is derived by approximation as a spring pendulum. Thereby the center mass m_0 corresponds to the end mass and it is assumed that the mass of the plate m is significantly lower than the supported center mass ($m_0 \gg m$). The spring stiffness K is derived from the middle displacement of the plate w_0 where a load F is applied:

$$F = K\Delta L$$

$$K = \frac{F}{\Delta L} = \frac{Q}{w_0}$$

The panel displacement w_0 due to an acceleration load a_{acc} acting on the center mass m_0 results from the corresponding lateral load Q:

$$Q = a_{acc} m_0$$

Timoshenko and Gere [145] provide for calculation of the displacement w of a simply supported plate subjected to a single lateral load the following expression:

$$w(x,y) = \sum_{i=1}^{\infty}\sum_{j=1}^{\infty} a_{ij} \sin\left(\frac{i\pi x}{a}\right) \sin\left(\frac{j\pi y}{b}\right)$$

The shape of the displacement field is described through sine functions in longitudinal and length direction with i respectively j antinodes. The related amplitude coefficients a_{ij} are given by Timoshenko as follows whereby the coefficients ξ and η describe the lateral loads location of attack in relation to the plates edge length a and b:

$$a_{ij} = \frac{4Q \sin\left(\frac{i\pi\xi}{a}\right) \sin\left(\frac{j\pi\eta}{b}\right)}{abD\pi^4 \left(\frac{i^2}{a^2} + \frac{j^2}{b^2}\right)^2}$$

In the following a simple sinusoidal displacement in both spatial axes is assumed. The load application point is in the center of the panel due to the location of the supported mass. For $i = j = 1$, $\xi = \frac{a}{2}$ and $\eta = \frac{b}{2}$ one obtains for the amplitude coefficient:

$$a_{11} = \frac{4Q}{abD\pi^4 \left(\frac{1}{a^2} + \frac{1}{b^2}\right)^2}$$

The displacement is thereby:

$$w(x,y) = \frac{4Q}{abD\pi^4 \left(\frac{1}{a^2} + \frac{1}{b^2}\right)^2} \sin\left(\pi\frac{x}{a}\right) \sin\left(\pi\frac{y}{b}\right)$$

Due to $x = \frac{a}{2}$ and $y = \frac{b}{2}$ the middle displacement of the plate w_0 coincides with the amplitude coefficient a_{11}:

$$w_0 = \frac{4}{\pi^4} \frac{Q}{Dab \left(\frac{1}{a^2} + \frac{1}{b^2}\right)^2}$$

Substitution of w_0 in the spring stiffness expression leads to:

$$K = \frac{\pi^4}{4} Dab \left(\frac{1}{a^2} + \frac{1}{b^2}\right)^2$$

Thereby the eigenfrequency f of the spring pendulum is as follows:

$$f = \frac{1}{2\pi}\omega_0 = \frac{1}{2\pi}\sqrt{\frac{K}{m_0}}$$

$$f = \frac{1}{2\pi}\sqrt{\frac{\frac{\pi^4}{4} Dab \left(\frac{1}{a^2} + \frac{1}{b^2}\right)^2}{m_0}}$$

$$f = \sqrt{\frac{\pi^2}{16}\frac{D}{m_0} ab \left(\frac{1}{a^2} + \frac{1}{b^2}\right)^2}$$

Substituting the flexural rigidity expression of the general plate leads to:

$$f = \sqrt{\frac{\pi^2}{16}\frac{k_D E t^3}{m_0(1-\nu^2)} ab \left(\frac{1}{a^2} + \frac{1}{b^2}\right)^2}$$

Substituting the panel thickness t by the panel mass expression leads to:

$$t = \frac{m}{k_m k_\rho ab\rho^*}$$

$$f = \sqrt{\frac{\pi^2}{16}\frac{k_D E}{m_0(1-\nu^2)}\left(\frac{m}{k_m k_\rho ab\rho^*}\right)^3 ab\left(\frac{1}{a^2}+\frac{1}{b^2}\right)^2}$$

Thereby the eigenfrequency of the panel is as follows:

$$f = \left(\frac{\pi^2}{16}\frac{k_D E}{k_\rho^3 \rho^{*3}(1-\nu^2)}\frac{m^3}{k_m^3 m_0}\frac{1}{a^2 b^2}\left(\frac{1}{a^2}+\frac{1}{b^2}\right)^2\right)^{\frac{1}{2}}$$

Equating with the required eigenfrequency f_{req} gives:

$$f_{req} = \left(\frac{\pi^2}{16}\frac{k_D E}{k_\rho^3 \rho^{*3}(1-\nu^2)}\frac{m^3}{k_m^3 m_0}\frac{1}{a^2 b^2}\left(\frac{1}{a^2}+\frac{1}{b^2}\right)^2\right)^{\frac{1}{2}}$$

The according plate mass scaling function is derived through solving the eigenfrequency expression for the plate mass m:

$$f_{req}^2 = \frac{\pi^2}{16}\frac{k_D E}{k_\rho^3 \rho^{*3}(1-\nu^2)}\frac{m^3}{k_m^3 m_0}\frac{1}{a^2 b^2}\left(\frac{1}{a^2}+\frac{1}{b^2}\right)^2$$

$$m = \left(\frac{16}{\pi^2}k_m^3\frac{a^2 b^2}{\left(\frac{1}{a^2}+\frac{1}{b^2}\right)^2}\frac{(1-\nu^2)k_\rho^3\rho^{*3}}{k_D E}f_{req}^2 m_0\right)^{\frac{1}{3}}$$

The corresponding plate areal mass scaling function is as follows:

$$\gamma = \frac{m}{ab}$$

$$\gamma = \left(\frac{16}{\pi^2}k_m^3\frac{1}{ab\left(\frac{1}{a^2}+\frac{1}{b^2}\right)^2}\frac{(1-\nu^2)k_\rho^3\rho^{*3}}{k_D E}f_{req}^2 m_0\right)^{\frac{1}{3}}$$

The resulting scaling functions for the beam with fixed root and tip mass are summarized in Tab. A - 14.

Scaling Functions of a Plate with Four Simply Supported Edges and Additional Center Mass
Scaling Approach: Eigenfrequency Solution
$$m = \left(\frac{16}{\pi^2}k_m^3\frac{a^2 b^2}{\left(\frac{1}{a^2}+\frac{1}{b^2}\right)^2}\frac{(1-\nu^2)k_\rho^3\rho^{*3}}{k_D E}f_{req}^2 m_0\right)^{\frac{1}{3}}$$ $$\gamma = \left(\frac{16}{\pi^2}k_m^3\frac{1}{ab\left(\frac{1}{a^2}+\frac{1}{b^2}\right)^2}\frac{(1-\nu^2)k_\rho^3\rho^{*3}}{k_D E}f_{req}^2 m_0\right)^{\frac{1}{3}}$$

Tab. A - 14: Mass and areal mass scaling function of a rectangular plate with four simply supported edges and a heavy center mass.

A4.3 Circular Plate with Simply Supported Edge and Additional Center Mass

For scaling of the circular plate with heavy center mass due to a first eigenfrequency requirement it is approximated as a spring pendulum. Thereby it is assumed that the center mass m_0 is significantly larger than the panel mass m ($m_0 \gg m$). The stiffness K of a circular plate that is simply supported at its edges and subjected to a central load F is given by Den Hartog [147] as follows:

$$K = 16\pi \frac{D}{R^2} \frac{1+\nu}{3+\nu}$$

The flexural rigidity D of the plate is as follows:

$$D = k_D \frac{Et^3}{1-\nu^2}$$

Thereby the plate stiffness can be re-written as follows:

$$K = 16\pi k_D \frac{E(1+\nu)}{(1-\nu^2)(3+\nu)} t^3 \frac{1}{R^2}$$

In the general formulation the panel mass m and the specific panel mass γ are as follows:

$$m = \pi k_{m,P} R^2 t \rho$$

$$\gamma = k_{m,P} t \rho$$

The eigenfrequency of a spring pendulum is as follows:

$$f = \frac{1}{2\pi}\omega_0 = \frac{1}{2\pi}\sqrt{\frac{K}{m_0}}$$

Substitution of the spring stiffness gives:

$$f = \frac{1}{2\pi}\sqrt{16\pi k_D \frac{E(1+\nu)}{(1-\nu^2)(3+\nu)} t^3 \frac{1}{R^2}\frac{1}{m_0}}$$

$$f^2 = \frac{4}{\pi} k_D \frac{E(1+\nu)}{(1-\nu^2)(3+\nu)} t^3 \frac{1}{R^2}\frac{1}{m_0}$$

The panel thickness t is substituted by the panel mass m:

$$m = \pi k_{m,P} R^2 t \rho$$

$$t = \frac{m_P}{\pi k_{m,P} R^2 \rho}$$

$$f^2 = \frac{4}{\pi} k_D \frac{E(1+\nu)}{(1-\nu^2)(3+\nu)} \left(\frac{m_P}{\pi k_{m,P} R^2 \rho}\right)^3 \frac{1}{R^2}\frac{1}{m_0}$$

$$f^2 = \frac{4}{\pi^4}\frac{k_D}{k_{m,P}^3} \frac{E(1+\nu)}{\rho^3(1-\nu^2)(3+\nu)} m_P^3 \frac{1}{R^8}\frac{1}{m_0}$$

Solving for the panel mass m gives:

$$m = \left(\frac{\pi^4}{4}\frac{k_{m,P}^3}{k_D}\frac{\rho^3(1-\nu^2)(3+\nu)}{E(1+\nu)} R^8 f_{req}^2 m_0\right)^{\frac{1}{3}}$$

The corresponding plate areal mass scaling function is as follows:

$$\gamma = \frac{m}{\pi R^2}$$

$$\gamma = \left(\frac{\pi}{4}\frac{k_{m,P}^3}{k_D}\frac{\rho^3(1-\nu^2)(3+\nu)}{E(1+\nu)} R^2 f_{req}^2 m_0\right)^{\frac{1}{3}}$$

The resulting scaling functions for the beam with fixed root and tip mass are summarized in Tab. A - 15.

Scaling Functions of a Circular Plate with a Simply Supported Edge and Additional Center Mass
Scaling Approach: Eigenfrequency Solution
$$m = \left(\frac{\pi^4}{4}\frac{k_{m,P}^3}{k_D}\frac{\rho^3(1-\nu^2)(3+\nu)}{E(1+\nu)}R^8 f_{req}^2 m_0\right)^{\frac{1}{3}}$$ $$\gamma = \left(\frac{\pi}{4}\frac{k_{m,P}^3}{k_D}\frac{\rho^3(1-\nu^2)(3+\nu)}{E(1+\nu)}R^2 f_{req}^2 m_0\right)^{\frac{1}{3}}$$

Tab. A - 15: Mass and areal mass scaling function of a circular plate with a simply supported edge and a heavy center mass.

A5 Connector Element Scaling Functions

Connector elements such as screws, bolts, inserts and nuts are additional structural elements with a considerable contribution to the overall mass.

A5.1 General Connector Element

The baseline connector element selected for parameterization is a screw of the type ISO 4762 with a threaded cylindrical counterpart and a free shaft of certain length in between (see Fig. A - 5).

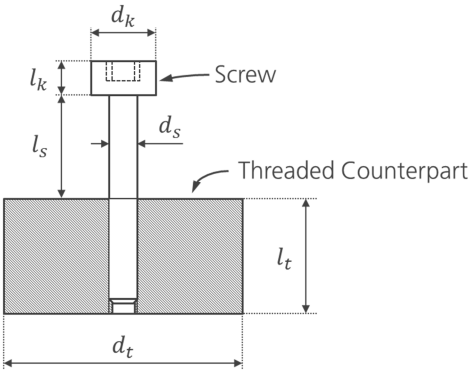

Fig. A - 5: Model of a screw connector element consisting of a screw type ISO 4762 and a cylindrical threaded counterpart.

The screw and the according counterpart are parameterized according to Tab. A - 16. Furthermore a series of size ratios are defined which relate the screw and counterpart dimensions to the screw diameter d_s.

ISO 4762 Screw Connector Element and Threaded, Cylindrical Counterpart Properties		
Property	**Parameter**	**Unit**
Screw shaft diameter	d_s	m
Free screw shaft length	l_s	m
Screw head diameter	d_k	m
Screw head length	l_k	m
Threaded counterpart diameter	d_t	m
Threaded counterpart length	l_t	m
Screw material density	ρ_s	kg/m³
Threaded counterpart material density	ρ_t	kg/m³
Maximum allowable tensile stress	σ_{max}	N/m²
Maximum allowable shear stress	τ_{max}	N/m²
Screw head diameter ratio	$\Gamma_{dk} = \frac{d_k}{d_s}$	-
Screw head length ratio	$\Gamma_{lk} = \frac{l_k}{d_s}$	-
Screw free shaft length ratio	$\Gamma_{ls} = \frac{l_s}{d_s}$	-
Counterpart length ratio	$\Gamma_{lt} = \frac{l_t}{d_s}$	-
Counterpart outer diameter ratio	$\Gamma_{dt} = \frac{d_t}{d_s}$	-
Thread – screw material density ratio	$\Gamma_{\rho} = \frac{\rho_t}{\rho_s}$	-

Tab. A - 16: Connector element properties of a screw of type ISO 4762 and according cylindrical threaded counterpart.

The general connector element mass m_{CE} is derived from the masses of the screw head m_{head}, screw shaft m_{shaft} and the threaded counterpart $m_{counterpart}$:

$$m_{CE} = m_{head} + m_{shaft} + m_{counterpart}$$

$$m_{CE} = \frac{\pi}{4}\rho_s d_k^2 l_k + \frac{\pi}{4}\rho_s d_s^2 (l_s + l_t) + \frac{\pi}{4}\rho_t (d_t^2 - d_s^2) l_t$$

The mass expression is further generalized by formulation in terms of the cube of the screw diameter d_s while all other dimensions are expressed as ratios in relation to d_s:

$$m_{CE} = \frac{\pi}{4}\rho_s d_s^3 \left(\frac{d_k}{d_s}\right)^2 \frac{l_k}{d_s} + \frac{\pi}{4}\rho_s d_s^3 \left(\frac{l_s}{d_s} + \frac{l_t}{d_s}\right) + \frac{\pi}{4}\rho_t d_s^3 \left(\left(\frac{d_t}{d_s}\right)^2 - 1\right) \frac{l_t}{d_s}$$

$$m_{CE} = \frac{\pi}{4} d_s^3 \left(\rho_s \left(\left(\frac{d_k}{d_s} \right)^2 \frac{l_k}{d_s} + \frac{l_s}{d_s} + \frac{l_t}{d_s} \right) + \rho_s \frac{\rho_t}{\rho_s} \left(\left(\frac{d_t}{d_s} \right)^2 - 1 \right) \frac{l_t}{d_s} \right)$$

Substituting the screw size ratios and material density ratio, the connector element mass function can be rewritten as follows:

$$m_{CE} = \frac{\pi}{4} d_s^3 \rho_s \left(\Gamma_{dk}^2 \Gamma_{lk} + \Gamma_{ls} + \Gamma_{lt} + \Gamma_\rho \Gamma_{lt} (\Gamma_{dt}^2 - 1) \right)$$

The diameter of the screw is defined by the loading and a maximum allowable stress σ_{crit}. The maximum stress includes a factor of safety and considers subtraction of the screw pre-load. For simplification it is assumed that the connectors are sized by axial loads P_{ax} only while shear loads are decoupled from the connectors e.g. by use of undercuts and bending loads are negligible. The stress in the connector is thereby as follows:

$$\sigma = \frac{P_{ax}}{A_s} \leq \sigma_{crit}$$

Substituting the screw shaft area A_s leads to:

$$\sigma_{crit} = \frac{4}{\pi} \frac{P_{ax}}{d_s^2}$$

Solving for the screw shaft diameter d_s gives the require diameter:

$$d_s = \sqrt{\frac{4}{\pi} \frac{P_{ax}}{\sigma_{crit}}}$$

Thereby the connector element mass can be written as follows:

$$m_{CE} = \frac{\pi}{4} \left(\frac{4}{\pi} \frac{P_{ax}}{\sigma_{crit}} \right)^{\frac{3}{2}} \rho_s \left(\Gamma_{dk}^2 \Gamma_{lk} + \Gamma_{ls} + \Gamma_{lt} + \Gamma_\rho \Gamma_{lt} (\Gamma_{dt}^2 - 1) \right)$$

$$m_{CE} = \left(\frac{4}{\pi} \frac{P_{ax}^3}{\sigma_{crit}^3} \right)^{\frac{1}{2}} \rho_s \left(\Gamma_{dk}^2 \Gamma_{lk} + \Gamma_{ls} + \Gamma_{lt} + \Gamma_\rho \Gamma_{lt} (\Gamma_{dt}^2 - 1) \right)$$

For an acceleration load a_{acc} acting on an attached mass m_0 the axial load P_{ax} can be substituted and results in the following connector element mass scaling function:

$$m_{CE} = \left(\frac{4}{\pi} \frac{a_{acc}^3 m_0^3}{\sigma_{crit}^3} \right)^{\frac{1}{2}} \rho_s \left(\Gamma_{dk}^2 \Gamma_{lk} + \Gamma_{ls} + \Gamma_{lt} + \Gamma_\rho \Gamma_{lt} (\Gamma_{dt}^2 - 1) \right)$$

The load driven approach chosen here leads to small screw dimensions and therefore low connector mass. For a real satellite subsystem only a small number of screw connections are sized by a load approach. Instead the number of component attachment points dictates the number of screws and in addition problems in handling of small screws during integration determine their minimum size. Therefore, in general a high number of oversized connectors cause a significant increase in the overall structural mass that is not covered by the load approach. This tendency is even more pronounced the smaller the subsystem becomes. Hence, it is convenient to define small critical stresses σ_{crit} and a minimum screw diameter $d_{s,min}$ as a lower scaling limit:

$$m_{CE,min} = \frac{\pi}{4} d_{s,min}^3 \rho_s \left(\Gamma_{dk}^2 \Gamma_{lk} + \Gamma_{ls} + \Gamma_{lt} + \Gamma_\rho \Gamma_{lt} (\Gamma_{dt}^2 - 1) \right)$$

The scaling functions are summarized in Tab. A - 17.

Scaling Functions of a General Screw Connector Element with Cylindrical Threaded Counterpart
Scaling Approach: Pull Out Force Solution
$m_{CE} = \left(\frac{4}{\pi} \frac{a_{acc}^3 m_0^3}{\sigma_{crit}^3} \right)^{\frac{1}{2}} \rho_s \left(\Gamma_{dk}^2 \Gamma_{lk} + \Gamma_{ls} + \Gamma_{lt} + \Gamma_\rho \Gamma_{lt} (\Gamma_{dt}^2 - 1) \right)$

$$m_{CE,min} = \frac{\pi}{4} d_{s,min}^3 \rho_s \left(\Gamma_{dk}^2 \Gamma_{lk} + \Gamma_{ls} + \Gamma_{lt} + \Gamma_\rho \Gamma_{lt} (\Gamma_{dt}^2 - 1) \right)$$

Tab. A - 17: General screw connector mass scaling functions considering a cylindrical threaded counterpart.

Some of the size and material ratios can be deduced from actual screw dimensions and design rules of thumb. For the given type of screw ISO 4762 the screw head ratios Γ_{dk} and Γ_{lk} are given in Tab. A - 18.

Screw Head Ratios for Screw ISO 4762		
Screw diameter	$\boldsymbol{\Gamma_{dk}}$	$\boldsymbol{\Gamma_{lk}}$
M1.6	$15/8$	1
M2	$19/10$	
M3	$11/6$	
M4	$7/4$	
M5	$17/10$	
M6	$5/3$	
M8	$13/8$	
M10	$8/5$	
≥M12	$3/2$	

Tab. A - 18: Screw head diameter and length ratios for ISO 4762

Furthermore the minimum thread depth and thereby counterpart length ratio Γ_{lt} can be determined by design rules of thumb. Depending on the material of the panel, the length ratio Γ_{lt} is given in Tab. A - 19 for screws of different hardness grade [148].

Required Thread Length Ratios for Screw Connectors				
Counterpart material	**Minimum thread length ratio $\boldsymbol{\Gamma_{lt,min}}$**			
Screw hardness grade	8.8	8.8	10.9	10.9
Thread fineness $\frac{d}{P}$	< 9	≥ 9	< 9	≥ 9
Aluminum alloy, high strength	$11/10$	$7/5$		–
Cast steel and steel, low strength	1	$5/4$		$7/5$
Steel, medium strength	$9/10$	1		$6/5$
Steel, high strength	$4/5$	$9/10$		1

Tab. A - 19: Counterpart length ratio of a screw connector depending on the counterpart material [148].

The density ratio Γ_ρ depends on the material mix of screw and counterpart. Established material mixtures and thereby density ratios Γ_ρ are given in Tab. A - 20.

Density Ratios between Screw and Counterpart	
Counterpart – screw material mix	**Material density ratio Γ_ρ**
Aluminum alloy – Steel	$9/26$
Steel – Steel	1

Tab. A - 20: Material density ratios of common screw and counterpart pairings.

The remaining size ratios Γ_{dt} and Γ_{ls} defining the counterpart outer diameter and free shaft length of the screw are defined according to the type of connector element and the corresponding panel type. In the following these are derived for a connector applied with a counterpart of high strength such as solid or stiffened metal panel and counterpart of low strength such as a sandwich panel with a lightweight core material.

A5.2 Connector Element for Solid and Stiffened Panels

For the solid and stiffened panel the threaded counterpart is integrated into the panel. The diameter ratio can again be derived by design rules of thumb. Depending on the material of the counterpart, the minimum outer diameter ratio Γ_{dt} is given in Tab. A - 21.

Threaded Counterpart Diameter Ratio for high Strength Materials	
Counterpart material	**Minimum diameter ratio $\Gamma_{dt,min}$**
Aluminum alloy	3
Steel	$5/2$

Tab. A - 21 : Minimum values for the threaded counterpart diameter ratios for a high strength material.

The baseline screw connector element chosen here is a steel screw ISO 4762 of hardness 8.8 combined with an aluminum alloy counterpart. For simplification the head diameter ratio is set constant and taken from a screw of size M4 (see Tab. A - 18). The connector element is thereby characterized by the following size and material ratios whereby the minimum ratios are increased by a factor of 1.4:

$$\Gamma_{dk} = 7/4$$
$$\Gamma_{lk} = 1$$
$$\Gamma_{lt} = 2$$
$$\Gamma_{dt} = 21/5$$
$$\Gamma_{\rho} = 9/26$$

For the free screw shaft length it is assumed that the component to be fixed has connector flange size which corresponds to three times the screw diameter:

$$\Gamma_{ls} = 3$$

Thereby the connector element mass scaling function for a counterpart featuring a high strength material is as follows:

$$m_{CE} = \left(\frac{4}{\pi}\frac{a_{acc}^3 m_0^3}{\sigma_{crit}^3}\right)^{\frac{1}{2}} \rho_s \left(\frac{49}{16} + 3 + 2 + \frac{9}{26} 2 \left(\frac{441}{25} - 1\right)\right)$$

$$m_{CE} \approx 19.6 \left(\frac{4}{\pi}\frac{a_{acc}^3 m_0^3}{\sigma_{crit}^3}\right)^{\frac{1}{2}} \rho_s$$

The mass scaling function considering a lower minimum screw diameter $d_{s,min}$ is thereby as follows:

$$m_{CE,min} \approx 4.9 \pi d_{s,min}^3 \rho_s$$

The scaling functions are summarized in Tab. A - 22.

Scaling Functions of a Screw Connector Element for Solid and Stiffened Panels
Scaling Approach: Pull Out Force Solution assuming High Strength Counterpart Material
$m_{CE} \approx 19.6 \left(\frac{4}{\pi}\frac{a_{acc}^3 m_0^3}{\sigma_{crit}^3}\right)^{\frac{1}{2}} \rho_s$ $m_{CE,min} \approx 4.9 \pi d_{s,min}^3 \rho_s$

Tab. A - 22: Scaling functions for connector elements applied with solid or stiffened panels made of a high strength material.

For attachment of a component of mass m_0 a number of z_{CE} screw connectors may be considered. In this regard in addition to a scaling limit on the minimum diameter $d_{s,min}$ also a scaling limit on the maximum number of screws $z_{CE,max}$ may be defined. Therefore in the following the mass scaling behavior of a component connection through screw connectors in a solid and stiffened panel consisting of a high strength material is examined.
Equating the minimum connector element mass $m_{CE,min}$ multiplied by the number of connectors z_{CE} with the connector mass derived by the load approach leads to:

$$z_{CE} m_{CE,min} = m_{CE}$$

$$\frac{\pi}{4} z_{CE} d_{s,min}^3 \rho_s \left(\Gamma_{dk}^2 \Gamma_{lk} + \Gamma_{ls} + \Gamma_{lt} + \Gamma_\rho \Gamma_{lt} (\Gamma_{dt}^2 - 1)\right)$$

$$= \left(\frac{4}{\pi}\frac{m_0^3 a_{acc}^3}{z_{CE} \sigma_{max}^3}\right)^{\frac{1}{2}} \rho_s \left(\Gamma_{dk}^2 \Gamma_{lk} + \Gamma_{ls} + \Gamma_{lt} + \Gamma_\rho \Gamma_{lt} (\Gamma_{dt}^2 - 1)\right)$$

$$d_{s,min}^3 = \left(\frac{64}{\pi^3}\frac{m_0^3 a_{acc}^3}{z_{CE}^3 \sigma_{max}^3}\right)^{\frac{1}{2}}$$

Solving for the number of connectors leads to:

$$d_{s,min}^6 = \frac{64}{\pi^3}\frac{m_0^3 a_{acc}^3}{z_{CE}^3 \sigma_{max}^3}$$

$$z_{CE}^3 = \frac{64}{\pi^3}\frac{m_0^3 a_{acc}^3}{d_{s,min}^6 \sigma_{max}^3}$$

$$z_{CE} = \left\lceil \frac{4}{\pi}\frac{m_0 a_{acc}}{d_{s,min}^2 \sigma_{max}} \right\rceil$$

Multiplying the minimum connector element mass by the number of connectors gives the overall minimum connector element mass:

$$m_{CE,min} = \left\lceil \frac{4}{\pi}\frac{m_0 a_{acc}}{d_{s,min}^2 \sigma_{max}} \right\rceil \frac{\pi}{4} d_{s,min}^3 \rho_s \left(\Gamma_{dk}^2 \Gamma_{lk} + \Gamma_{ls} + \Gamma_{lt} + \Gamma_\rho \Gamma_{lt} (\Gamma_{dt}^2 - 1)\right)$$

Dividing by the supported mass m_0 gives the minimum connector mass ratio that is independent of the supported mass:

$$\frac{m_{CE,min}}{m_0} = \frac{1}{m_0}\left[\frac{4}{\pi}\frac{m_0 a_{acc}}{d_{s,min}^2 \sigma_{max}}\right]\frac{\pi}{4} d_{s,min}^3 \rho_s \left(\Gamma_{dk}^2 \Gamma_{lk} + \Gamma_{ls} + \Gamma_{lt} + \Gamma_\rho \Gamma_{lt}(\Gamma_{dt}^2 - 1)\right)$$

In the small size region where z_{CE} becomes unity, the connector mass ratio decreases with increasing attached mass as follows:

$$\frac{m_{CE,min}}{m_0} = \frac{1}{m_0}\frac{\pi}{4} d_{s,min}^3 \rho_s \left(\Gamma_{dk}^2 \Gamma_{lk} + \Gamma_{ls} + \Gamma_{lt} + \Gamma_\rho \Gamma_{lt}(\Gamma_{dt}^2 - 1)\right)$$

For an upper scaling limit the maximum number of connector elements may be limited to $z_{CE,max}$. The connector mass ratio thereby becomes:

$$\frac{m_{CE}}{m_0} = \left(\frac{4}{\pi}\frac{m_0 a_{acc}^3}{z_{CE,max} \sigma_{max}^3}\right)^{\frac{1}{2}} \rho_s \left(\Gamma_{dk}^2 \Gamma_{lk} + \Gamma_{ls} + \Gamma_{lt} + \Gamma_\rho \Gamma_{lt}(\Gamma_{dt}^2 - 1)\right)$$

An example for the resulting scaling behavior of a component connection of mass m_0 through 1 to 16 screw connectors in a solid or stiffened plate consisting of a high strength material is displayed in Fig. A - 6. One can see that in the small mass region the relative connector mass decreases due to the minimum screw diameter $d_{s,min}$ as active scaling limit. By continuously increasing the number of connectors the relative mass remains almost constant in the middle section and finally increases when the maximum number of connectors $z_{CE,max}$ is reached. This behavior results from the cubic increase in screw connector mass with the screw shaft diameter d_s while the load carrying cross-section only increases with the square.

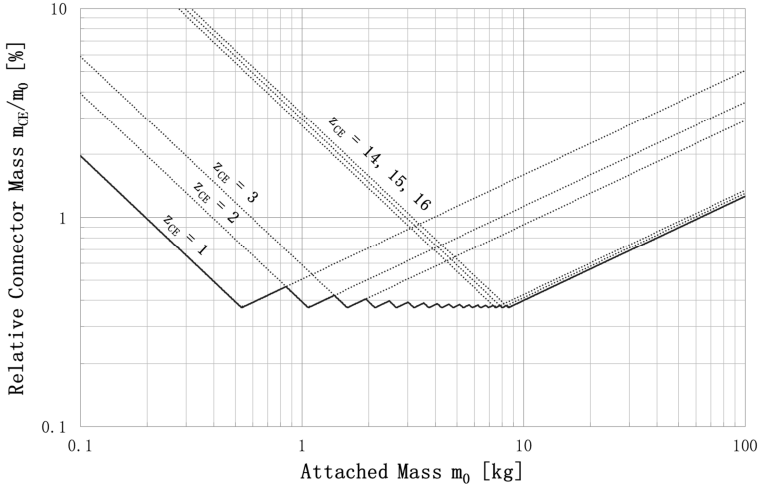

Fig. A - 6: Minimum relative connector mass $\frac{m_{CE}}{m_0}$ plotted over the attached mass m_0 with varying number of connectors z_{CE} and a maximum number of sixteen connectors for a solid or stiffened panel consisting of a high strength material.

A5.3 Connector Element for Sandwich Panels

In a sandwich panel the counterparts of the connector elements are inserts as the core material is in general of low strength. An (in-plane) insert is approximated as a solid circular block whose

mass is determined by the axial pull-out force P_{ax} and the shear strength τ_{crit} of the sandwich core to which the loads are transmitted. The shear strength determines the required outer surface of the insert which corresponds to the outer surface of the threaded counterpart A_t as follows:

$$\tau = \frac{P_{ax}}{A_t} \leq \tau_{crit}$$

Substituting the inserts outer surface by the counterpart diameter d_t and length l_t gives:

$$\tau_{crit} = \frac{P_{ax}}{\pi d_t l_t}$$

As the sandwich thickness is unknown, the insert thickness is substituted by the thread length ratio Γ_{lt}:

$$\tau_{crit} = \frac{P_{ax}}{\pi d_t d_s \Gamma_{lt}}$$

Solving for the outer diameter d_t gives:

$$d_t = \frac{P_{ax}}{\pi \Gamma_{lt} \tau_{crit}} \frac{1}{d_s}$$

Thereby the outer diameter ratio Γ_{dt} is as follows:

$$\Gamma_{dt} = \frac{d_t}{d_s}$$

Substituting the outer diameter d_t leads to:

$$\Gamma_{dt} = \frac{1}{\pi} \frac{1}{\Gamma_{lt}} \frac{P_{ax}}{\tau_{crit}} \frac{1}{d_s^2}$$

Expressing the axial load P_{ax} by the critical stress σ_{crit} eliminates the screw shaft diameter d_s:

$$P_{ax} = \frac{\pi}{4} \sigma_{crit} d_s^2$$

$$\Gamma_{dt} = \frac{1}{4\Gamma_{lt}} \frac{\sigma_{crit}}{\tau_{crit}}$$

Thereby the connector element mass scaling function for sandwich panels with low strength core materials is as follows:

$$m_{CE} = \left(\frac{4}{\pi} \frac{a_{acc}^3 m_0^3}{\sigma_{crit}^3} \right)^{\frac{1}{2}} \rho_s \left(\Gamma_{dk}^2 \Gamma_{lk} + \Gamma_{ls} + \Gamma_{lt} + \Gamma_\rho \Gamma_{lt} \left(\left(\frac{1}{4\Gamma_{lt}} \frac{\sigma_{crit}}{\tau_{crit}} \right)^2 - 1 \right) \right)$$

For a lower scaling limit with a minimum screw diameter $d_{s,min}$ the according scaling function is as follows:

$$m_{CE} = \frac{\pi}{4} d_{s,min}^3 \rho_s \left(\Gamma_{dk}^2 \Gamma_{lk} + \Gamma_{ls} + \Gamma_{lt} + \Gamma_\rho \Gamma_{lt} \left(\left(\frac{1}{4\Gamma_{lt}} \frac{\sigma_{crit}}{\tau_{crit}} \right)^2 - 1 \right) \right)$$

Again the baseline screw connector element is a steel screw ISO 4762 of hardness 8.8 combined with an aluminum alloy counterpart. The connector element is characterized by the following size and material ratios whereby the minimum ratios are increased by a factor of 1.4:

$$\Gamma_{dk} = 7/4$$
$$\Gamma_{lk} = 1$$
$$\Gamma_{lt} = 2$$
$$\Gamma_\rho = 9/26$$

Again for the free screw shaft length it is assumed that the component to be fixed has connector flange size which corresponds to three times the screw diameter:

$$\Gamma_{ls} = 3$$

Thereby the connector element mass scaling function is as follows:

$$m_{CE} = \left(\frac{4}{\pi}\frac{a_{acc}^3 m_0^3}{\sigma_{crit}^3}\right)^{\frac{1}{2}} \rho_s \left(\frac{49}{16} + 3 + 2 + \frac{9}{26} 2 \left(\left(\frac{1}{8}\frac{\sigma_{crit}}{\tau_{crit}}\right)^2 - 1\right)\right)$$

$$m_{CE} = \left(\frac{4}{\pi}\frac{a_{acc}^3 m_0^3}{\sigma_{crit}^3}\right)^{\frac{1}{2}} \rho_s \left(\frac{129}{16} + \frac{9}{13}\left(\left(\frac{1}{8}\frac{\sigma_{crit}}{\tau_{crit}}\right)^2 - 1\right)\right)$$

The corresponding scaling function for the minimum screw diameter $d_{s,min}$ is as follows:

$$m_{CE} = \frac{\pi}{4} d_{s,min}^3 \rho_s \left(\frac{129}{16} + \frac{9}{13}\left(\left(\frac{1}{8}\frac{\sigma_{crit}}{\tau_{crit}}\right)^2 - 1\right)\right)$$

In this approach the insert thickness does not coincide to the actual thickness of the sandwich core. As the in-plane connectors are distributed throughout the panel, they contribute by their mass to the panel loading and thereby influence the required panel thickness. Therefore, for simplification instead of the panel thickness, the fixed thread length ratio Γ_{lt} is utilized for sizing of the in-plane inserts. By using ratios close to the minimum allowable ratio this approach is conservative as rather large insert radii are gained. This is due to the fact that the insert mass increases by the square of the diameter but the outer surface transmitting the shear loads of the pull-out force increases only linearly.

The scaling functions are summarized in Tab. A - 23.

Scaling Functions of a Screw Connector Element for Sandwich Panels
Scaling Approach: Pull Out Force Solution assuming Low Strength Counterpart Material
$m_{CE} = \left(\frac{4}{\pi}\frac{a_{acc}^3 m_0^3}{\sigma_{crit}^3}\right)^{\frac{1}{2}} \rho_s \left(\frac{129}{16} + \frac{9}{13}\left(\left(\frac{1}{8}\frac{\sigma_{crit}}{\tau_{crit}}\right)^2 - 1\right)\right)$ $m_{CE} = \frac{\pi}{4} d_{s,min}^3 \rho_s \left(\frac{129}{16} + \frac{9}{13}\left(\left(\frac{1}{8}\frac{\sigma_{crit}}{\tau_{crit}}\right)^2 - 1\right)\right)$

Tab. A - 23: Scaling functions for connector elements applied with sandwich panels considering a low strength core material.

In the following the scaling behavior of a component connection through screw connectors in a sandwich panel similar to the same approach described for a solid and stiffened panel in A5.2 is examined. Thereby the basic equations remain the same except for the term describing the connector geometry through the according size ratios. Hence the mass scaling function in the small size region where z_{CE} becomes unity is as follows:

$$\frac{m_{CE,min}}{m_0} = \frac{1}{m_0}\frac{\pi}{4} d_{s,min}^3 \rho_s \left(\Gamma_{dk}^2 \Gamma_{lk} + \Gamma_{ls} + \Gamma_{lt} + \Gamma_\rho \Gamma_{lt}\left(\left(\frac{1}{4\Gamma_{lt}}\frac{\sigma_{crit}}{\tau_{crit}}\right)^2 - 1\right)\right)$$

The according mass scaling function for the maximum number of connector elements $z_{CE,max}$ is as follows:

$$\frac{m_{CE}}{m_0} = \left(\frac{4}{\pi}\frac{m_0 a^3}{z_{CE,max}\sigma_{max}^3}\right)^{\frac{1}{2}} \rho_s \left(\Gamma_{dk}^2 \Gamma_{lk} + \Gamma_{ls} + \Gamma_{lt} + \Gamma_\rho \Gamma_{lt}\left(\left(\frac{1}{4\Gamma_{lt}}\frac{\sigma_{crit}}{\tau_{crit}}\right)^2 - 1\right)\right)$$

Fig. A - 7 shows the relative mass scaling plot for a component attachment to a sandwich panel with low strength core material. The principle behavior is the same as observed for the solid and stiffened panel displayed in Fig. A - 6. However, the relative connector mass is almost five times higher than for the solid and stiffened panel due to the mass impact of the insert.

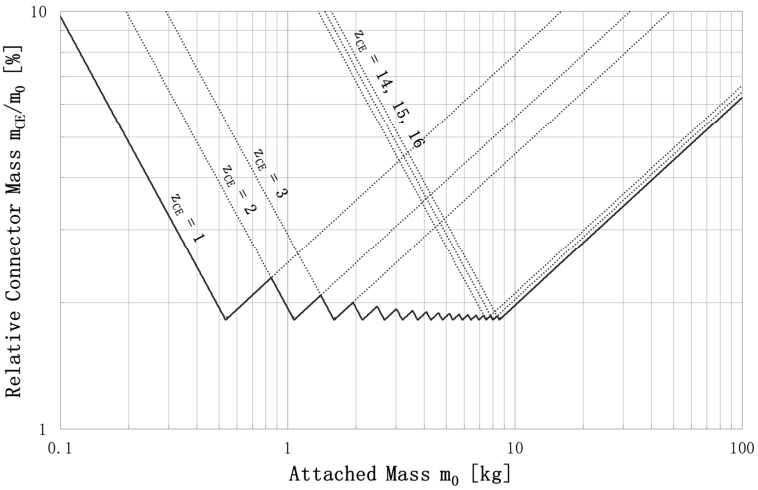

Fig. A - 7: Minimum relative connector mass $\frac{m_{CE}}{m_0}$ plotted over the attached mass m_0 with varying number of connectors z_{CE} and a maximum number of sixteen connectors for a sandwich panel with a low strength core material.

A6 Bearing Scaling Function

Rolling-element bearings are required for many mechanism components with moving parts. As they often consist of steel or other high density materials and some mechanisms use a high number of such elements, a mass model of a ball bearing is introduced.

A6.1 Ball Bearing Parameterization

The significant elements concerning mass are the bearing races and the balls in between. The geometry parameters are the inner radius r_i, the outer radius r_a, the ball radius r_b, the thicknesses of the inner and outer rings ring t_{ir} and t_{ar} and the width of the bearing w. Furthermore, the distribution angle α_b of the balls is defined. The corresponding model is displayed in Fig. A - 8.

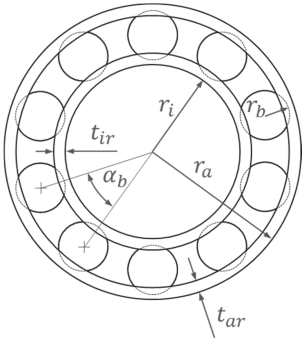

Fig. A - 8: Ball bearing model with roller ball, outer and inner ring and main geometry parameters.

The parameters are expressed in relation to the inner radius r_i which may result from a required axle diameter. Defined are a ball size ratio Γ_b, ring thickness ratio Γ_t and bearing width ratio Γ_w:

$$\Gamma_b = \frac{r_b}{r_i}$$

$$\Gamma_t = \frac{t_{ir}}{r_i}$$

$$\Gamma_w = \frac{w}{r_b} > 2$$

The parameters and according ratios are summarized in Tab. A - 24.

Ball Bearing Properties		
Property	**Parameter**	**Unit**
Inner radius	r_i	m
Outer radius	r_a	m
Ball radius	r_b	m
Inner ring thickness	t_{ir}	m

Outer ring thickness	t_{ar}	m
Bearing width	w	m
Ball distribution angle	α_b	rad
Material density	ρ	kg/m³
Ball size ratio	$\Gamma_b = \frac{r_b}{r_i}$	-
Ring thickness ratio	$\Gamma_t = \frac{t_{ir}}{r_i}$	-
Bearing width ratio	$\Gamma_w = \frac{w}{r_b} > 2$	-

Tab. A - 24: Ball bearing geometry parameters and ratios.

A6.2 Ball Bearing Scaling Function

For derivation of the mass scaling function similarity principles are used. Therefore the following geometrical similarities are defined:

$$t_{ar} = t_{ir}$$
$$r_a = r_i + \frac{t_{ir}}{2} + 2r_b + \frac{t_{ar}}{2}$$

The geometrical dimensions of the ball bearing are formulated depending on the inner radius r_i as follows:

$$t_{ir} = t_{ar} = \Gamma_t r_i$$
$$r_b = \Gamma_b r_i$$
$$w = \Gamma_w r_b = \Gamma_w \Gamma_b r_i$$
$$r_a = r_i + \frac{t_{ir}}{2} + 2r_b + \frac{t_{ar}}{2} = r_i + \Gamma_t r_i + 2\Gamma_b r_i = (1 + \Gamma_t + 2\Gamma_b) r_i$$

The mass of a single ball m_b is as follows:

$$m_b = \frac{4\pi}{3} r_b^3 \rho = \frac{4\pi}{3} \rho \Gamma_b^3 r_i^3$$

The number of balls n_b is given by the angle α_b. To avoid overlapping the angle needs to fulfil the following requirement:

$$\alpha_b > 2 \arcsin\left(\frac{r_b}{r_i + \frac{t_{ir}}{2} + r_b}\right) = 2 \arcsin\left(\frac{\Gamma_b}{1 + \frac{1}{2}\Gamma_t + \Gamma_b}\right)$$

Furthermore the number of balls n_b needs to be an integer rounded to the lower value:

$$n_b = \left\lfloor \frac{2\pi}{\alpha_b} \right\rfloor = \left\lfloor \frac{\pi}{\arcsin\left(\frac{\Gamma_b}{1 + \frac{1}{2}\Gamma_t + \Gamma_b}\right)} \right\rfloor$$

The mass of the inner ring m_i is as follows:

$$m_i = \pi((r_i + t_{ir})^2 - r_i^2) w \rho = \Gamma_w \pi (2 r_i t_{ir} + t_{ir}^2) r_b \rho$$
$$m_i = \Gamma_w \pi (2\Gamma_t r_i^2 + \Gamma_t^2 r_i^2) \Gamma_b r_i \rho$$
$$m_i = \pi (2\Gamma_t + \Gamma_t^2) \Gamma_w \Gamma_b \rho r_i^3$$

The mass of the outer ring m_a is as follows:

$$m_a = \pi(r_a^2 - (r_a - t_{ar})^2)w\rho = \Gamma_w\pi(2r_a t_{ar} - t_{ar}^2)r_b\rho$$
$$m_a = \Gamma_w\pi(2(1 + \Gamma_t + 2\Gamma_b)\Gamma_t r_i^2 - \Gamma_t^2 r_i^2)\Gamma_b r_i\rho$$
$$m_a = \pi(2(1 + \Gamma_t + 2\Gamma_b)\Gamma_t - \Gamma_t^2)\Gamma_w\Gamma_b\rho r_i^3$$

The overall mass m of the bearing is the sum of the above described bearing components:

$$m = m_i + n_b m_b + m_a$$

$$m = \left(\pi(2\Gamma_t + \Gamma_t^2)\Gamma_w + \left[\frac{\pi}{\arcsin\left(\frac{\Gamma_b}{1 + \frac{1}{2}\Gamma_t + \Gamma_b} \right)} \right] \frac{4\pi}{3}\Gamma_b^2 + \pi(2(1 + \Gamma_t + 2\Gamma_b)\Gamma_t - \Gamma_t^2)\Gamma_w \right) \Gamma_b\rho r_i^3$$

$$m = \left(2\pi\Gamma_t\Gamma_w + \pi\Gamma_t^2\Gamma_w + \left[\frac{\pi}{\arcsin\left(\frac{\Gamma_b}{1 + \frac{1}{2}\Gamma_t + \Gamma_b} \right)} \right] \frac{4\pi}{3}\Gamma_b^2 + 2\pi(1 + \Gamma_t + 2\Gamma_b)\Gamma_t\Gamma_w - \pi\Gamma_t^2\Gamma_w \right) \Gamma_b\rho r_i^3$$

$$m = 2\pi\left(\left[\pi\left(\arcsin\left(\frac{\Gamma_b}{1 + \frac{1}{2}\Gamma_t + \Gamma_b} \right) \right)^{-1} \right] \frac{2}{3}\Gamma_b^2 + (2 + \Gamma_t + 2\Gamma_b)\Gamma_t\Gamma_w \right) \Gamma_b\rho r_i^3$$

The resulting ball bearing mass scaling function depends on the inner radius r_i and is summarized in Tab. A - 25.

Scaling Functions of a Ball Bearing
Scaling Approach: Geometric Similarity based on a Design Reference Model with the Axle Radius as Leading Dimension
$m = 2\pi\left(\left[\pi\left(\arcsin\left(\frac{\Gamma_b}{1 + \frac{1}{2}\Gamma_t + \Gamma_b} \right) \right)^{-1} \right] \frac{2}{3}\Gamma_b^2 + (2 + \Gamma_t + 2\Gamma_b)\Gamma_t\Gamma_w \right) \Gamma_b\rho r_i^3$

Tab. A - 25: Ball bearing scaling function depending on the radius of the corresponding axle.

Appendix B

B Deployment Mechanism Component Scaling Functions

Within Appendix B the derivations of the Deployment Mechanism scaling functions are described.

B1 Mast Spool

The 'Mast Spool' supports the reeled mast during launch and is divided into three parts whose designs are addressed in the following sub-sections:

→ One 'Spool Cylinder' to carry the stowed boom,
→ Two 'Spool End Caps' to avoid slippage of the boom off the cylinder,
→ One 'Spool Axle' for mounting of the spool to the support structure.

B1.1 Spool Cylinder

The Mast Spool Cylinder (index MSC) is a circular cylinder that is realized as a grid structure to ensure also good scalability also in the large size region. The grid consists of a number of n_{st} interconnected by helical diagonals (see Fig. B - 1). The decisive structural elements for sizing of the cylinder are the stringers.

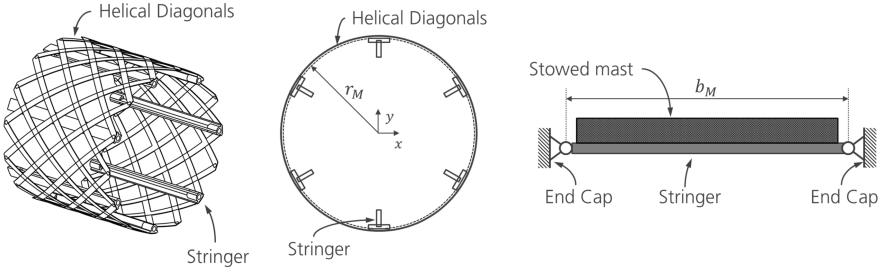

Fig. B - 1: Mast Spool Cylinder design as a helical structure (left and middle) and simplified stringer model (right).

The stringers are idealized as beams with simply supported ends that support a uniformly distributed mass resulting from the stowed mast. Thereby it is assumed that the diagonals do not contribute to the load carrying task of the stringers. For sizing of the stringers the beam scaling functions derived in A2.2 and summarized in Tab. A - 7 are applied. Therefore the scaling function parameters need to be adjusted accordingly. The width of the cylinder b_{MSC} and thereby the stringer length l is determined by the flattened width of the mast b_M:

$$b_{MSC} = l = b_M$$

The distributed mass m_q applied to one stringer by the mass m_M of the stowed mast depends on the number of stringers n_{st} and a factor k_{Mm} that accounts for the mass fraction the highest loading stringer has to carry:

$$m_q = k_{Mm} \frac{m_M}{n_{st}}$$

Furthermore the eigenfrequency and acceleration load requirements are increased by factors k_f and k_a to account for local amplification.
The total mass of the Spool Cylinder m_{MSC} is gained from the stringer mass $m_{MSC,st}$ and a mass amplification factor $k_{MSC,m} > 1$ that accounts for the contribution of the diagonal mass:

$$m_{MSC} = k_{MSC,m} n_{st} m_{MSC,st}$$

The solution for the spool core mass scaling function due to the eigenfrequency requirement f_{req} is thereby as follows:

$$m_{MSC,f} = k_{MSC,m} n_{st} \left(\Phi + \sqrt{\Phi^2 + 2\Phi k_{Mm} \frac{m_M}{n_{st}}} \right)$$

$$\Phi = \frac{2}{\pi^2} \frac{k_A}{k_I} \frac{k_\rho^2 \rho^{*2}}{E} k_f^2 f_{req}^2 b_M^5$$

The corresponding solution for the Spool Cylinder scaling function due to the critical stress requirement σ_{crit} is as follows:

$$m_{MSC,\sigma} = k_{MSC,m} n_{st} k_\rho k_A \rho^* \left(u + v - \frac{a}{3} \right)^2 b_M$$

$$u = \sqrt[3]{-\left(\frac{a}{3}\right)^3 - \frac{c}{2} + \sqrt{\frac{1}{27} a^3 c + \frac{1}{4} c^2}}$$

$$v = \sqrt[3]{-\left(\frac{a}{3}\right)^3 - \frac{c}{2} - \sqrt{\frac{1}{27} a^3 c + \frac{1}{4} c^2}}$$

$$a = -\frac{1}{8} \frac{k_y}{k_I} \frac{k_\rho \rho^*}{\sigma_{crit}} k_a a_{acc} b_M^2$$

$$c = -\frac{1}{8} \frac{1}{\sigma_{crit}} \frac{k_y}{k_A k_I} k_a a_{acc} k_{Mm} \frac{m_M}{n_{st}} b_M$$

A scaling limit is introduced in terms of a minimum stringer radius $r_{MSC,st,min}$. The resulting Spool Cylinder mass scaling function $m_{MSC,min}$ is according to Tab. A - 1 and substitution of the related parameters as follows:

$$m_{MSC,min} = k_{MSC,m} n_{st} k_\rho k_A \rho^* b_M r_{MSC,st,min}^2$$

The parameters describing the scaling functions of the Mast Spool Cylinder and the values for calculation of the according properties are summarized in Tab. B - 1.

Parameters of the Mast Spool Cylinder			
Parameter	**Symbol**	**Unit**	**Value**
Flattened mast width	b_M	m	Input value
Number of stringers	n_{st}	-	6
Material density	ρ^*	kg/m³	2700
Material modulus	E	N/m²	70 GPa
Material critical stress	σ_{crit}	N/m²	200 MPa
Beam density factor	k_ρ	-	1
Beam cross-section factor	k_A	-	0.4

Beam moment of area factor	k_I	-	0.417
Beam neutral layer factor	k_y	-	1.5
Mass factor to account for diagonals	$k_{MSC,m}$	-	2
Distributed mass factor	k_{Mm}	-	1/3
Eigenfrequency requirement adjustment factor	k_f	-	1.5
Acceleration load adjustment factor	k_a	-	1.5
Mast mass	m_M	kg	Input value
Lateral acceleration	a_{acc}	m/s²	30 g
First eigenfrequency	f_{req}	Hz	100
Minimum stringer radius	$r_{MSC,st,min}$	m	0.002 (Stiffened Beam)

Tab. B - 1: Parameters and according values of the Mast Spool Cylinder scaling functions.

The spool core scaling functions are summarized in Tab. B - 2.

Scaling Functions of the Spool Cylinder	
Scaling Approach: Eigenfrequency Solution	Scaling Approach: Critical Stress Solution
$m_{MSC,f} = k_{MSC,m} n_{st} \left(\Phi + \sqrt{\Phi^2 + 2\Phi k_{Mm} \frac{m_M}{n_{st}}} \right)$	$m_{MSC,\sigma} = k_{MSC,m} n_{st} k_\rho k_A \rho^* \left(u + v - \frac{a}{3} \right)^2 b_M$
$\Phi = \frac{2}{\pi^2} \frac{k_A}{k_I} \frac{k_\rho^2 \rho^{*2}}{E} k_f^2 f_{req}^2 b_M^5$	$u = \sqrt[3]{-\left(\frac{a}{3}\right)^3 - \frac{c}{2} + \sqrt{\frac{1}{27}a^3 c + \frac{1}{4}c^2}}$ $v = \sqrt[3]{-\left(\frac{a}{3}\right)^3 - \frac{c}{2} - \sqrt{\frac{1}{27}a^3 c + \frac{1}{4}c^2}}$ $a = -\frac{1}{8} \frac{k_y}{k_I} \frac{k_\rho \rho^*}{\sigma_{crit}} k_a a_{acc} b_M^2$ $c = -\frac{1}{8} \frac{1}{\sigma_{crit}} \frac{k_y}{k_A k_I} k_a a_{acc} k_{Mm} \frac{m_M}{n_{st}} b_M$

$$m_{MSC,min} = k_{MSC,m} n_{st} k_\rho k_A \rho^* b_M \mathrm{r}_{MSC,st,min}^2$$

Tab. B - 2: Spool Cylinder mass scaling functions for the eigenfrequency and critical stress criteria as well as the scaling limit of minimum stringer diameter.

B1.2 Spool End Cap

The Spool End Caps (index MSE) are of circular shape and each is realized as a set of n_{rib} radial ribs interconnected by a ring joint and outer circular flange which connect the Spool Cylinder with the spool mount (see Fig. B - 2). The decisive structural elements for the sizing of the end cap are the ribs.

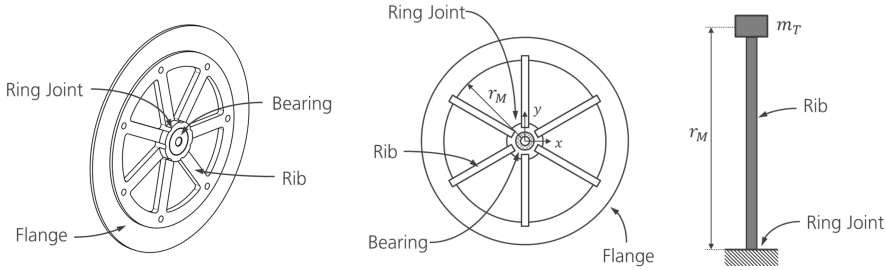

Fig. B - 2: Design of the Mast Spool End Caps as radial ribs interconnected by an outer and inner ring (left and middle) and rib approximation model (right).

The ribs are idealized as beams with one fixed end at the spool mount and a tip mass m_T. For sizing of the ribs the beam scaling functions derived in A2.3 and summarized in Tab. A - 8 are applied. Therefore the scaling function parameters need to be adjusted accordingly. The length of the ribs coincides with the spool core radius r_{MSC} which corresponds to the mast reeling radius r_M:

$$l_{MSE} = r_{MSC} = r_M$$

The tip mass m_T results from the attached cylinder mass m_{MSC} and mast mass m_M and the number of radial ribs n_{rib} per end-cap:

$$m_T = \frac{m_{MSC} + m_M}{2 n_{rib}}$$

Furthermore the eigenfrequency and acceleration load requirements are increased by factors k_f and k_a to account for local amplification.

The total mass of the end-cap is derived from the number of ribs n_{rib}, the mass of a rib $m_{MSE,rib}$ and a mass amplification factor $k_{MSE,m} > 1$ that accounts for the mass of inner ring joint and outer flange:

$$m_{MSE} = k_{MSE,m} n_{rib} m_{MSE,rib}$$

The solution for the spool core mass scaling function due to the eigenfrequency requirement f_{req} is thereby as follows:

$$m_{MSE} = k_{MSE,m} n_{rib} \left(\Phi + \sqrt{\Phi^2 + \frac{1}{0.23} \Phi \frac{m_{MSC} + m_M}{n_{rib}}} \right)$$

$$\Phi = \frac{0.23}{2}\frac{4\pi^2}{3}\frac{k_\rho^2 \rho^{*2}}{E}\frac{k_A}{k_I}k_f^2 f_{req}^2 r_M^5$$

The corresponding solution for the Spool Cylinder scaling function due to the critical stress requirement σ_{crit} is as follows:

$$m_{MSE} = k_{MSE,m} n_{rib} k_\rho k_A \rho^* \left(u + v - \frac{a}{3}\right)^2 r_M$$

$$u = \sqrt[3]{-\left(\frac{a}{3}\right)^3 - \frac{c}{2} + \sqrt{\frac{1}{27}a^3 c + \frac{1}{4}c^2}}$$

$$v = \sqrt[3]{-\left(\frac{a}{3}\right)^3 - \frac{c}{2} - \sqrt{\frac{1}{27}a^3 c + \frac{1}{4}c^2}}$$

$$a = -\frac{1}{2}\frac{k_y}{k_I}\frac{k_\rho \rho^*}{\sigma_{crit}} k_a a_{acc} r_M^2$$

$$c = -\frac{k_y}{k_I k_A}\frac{1}{\sigma_{crit}}\frac{m_{MSC} + m_M}{2n_{rib}} k_a a_{acc} r_M$$

A scaling limit is introduced in terms of a minimum rib radius $r_{MSE,rib,min}$. The resulting Spool Cylinder end cap mass scaling function $m_{MSE,min}$ is according to Tab. A - 1 and substitution of the related parameters as follows:

$$m_{MSE,min} = k_{MSE,m} n_{rib} k_\rho k_A \rho^* r_M r_{MSE,rib,min}^2$$

The parameters describing the scaling functions of the Mast Spool Cylinder and the values for calculation of the according properties are summarized in Tab. B - 3.

Parameters of the Mast Spool Cylinder End Caps			
Parameter	**Symbol**	**Unit**	**Value**
Mast reeling radius	r_M	m	Input value
Number of ribs	n_{rib}	-	6
Material density	ρ^*	kg/m³	2700
Material modulus	E	N/m²	70 GPa
Material critical stress	σ_{crit}	N/m²	200 MPa
Beam density factor	k_ρ	-	1
Beam cross-section factor	k_A	-	0.8
Beam moment of area factor	k_I	-	0.417
Beam neutral layer factor	k_y	-	1.5
Flange and joint mass factor	$k_{MSE,m}$	-	1.3

Eigenfrequency requirement adjustment factor	k_f	-	1.5
Acceleration load adjustment factor	k_a	-	1.5
Mast mass	m_M	kg	Input value
Central cylinder mass	m_{MSC}	kg	Input value
Lateral acceleration	a_{acc}	m/s²	30 g
First eigenfrequency	f_{req}	Hz	100
Minimum rib radius	$r_{MSE,rib,min}$	m	0.002 (Stiffened Beam)

Tab. B - 3: Parameters and according values of the Mast Spool Cylinder end cap scaling functions.

The spool core scaling functions are summarized in Tab. B - 4.

Scaling Functions of the Spool Cylinder	
Scaling Approach: Eigenfrequency Solution	Scaling Approach: Critical Stress Solution
$m_{MSE} = k_{MSE,m} n_{rib} \left(\Phi + \sqrt{\Phi^2 + \frac{1}{0.23} \Phi \frac{m_{MSC} + m_M}{n_{rib}}} \right)$	$m_{MSE} = k_{MSE,m} n_{rib} k_\rho k_A \rho^* \left(u + v - \frac{a}{3} \right)^2 r_M$
$\Phi = \frac{0.23}{2} \frac{4\pi^2}{3} \frac{k_\rho^2 \rho^{*2}}{E} \frac{k_A}{k_I} k_f^2 f_{req}^2 r_M^5$	$u = \sqrt[3]{-\left(\frac{a}{3}\right)^3 - \frac{c}{2} + \sqrt{\frac{1}{27} a^3 c + \frac{1}{4} c^2}}$ $v = \sqrt[3]{-\left(\frac{a}{3}\right)^3 - \frac{c}{2} - \sqrt{\frac{1}{27} a^3 c + \frac{1}{4} c^2}}$ $a = -\frac{1}{2} \frac{k_y}{k_I} \frac{k_\rho \rho^*}{\sigma_{crit}} k_a a_{acc} r_M^2$ $c = -\frac{k_y}{k_I k_A} \frac{1}{\sigma_{crit}} \frac{m_{MSC} + m_M}{2 n_{rib}} k_a a_{acc} r_M$
$m_{MSE,min} = k_{MSE,m} n_{rib} k_\rho k_A \rho^* r_M r_{MSE,rib,min}^2$	

Tab. B - 4: Spool Cylinder end cap mass scaling functions for the eigenfrequency and critical stress criteria as well as the scaling limit of minimum stringer diameter.

B1.3 Spool Axle

The Spool Axle (index MSA) carries the boom spool and is realized as a continuous rod or tube. For sizing the shear strength of the axle is utilized. Lateral forces acting on the axle result from the mass supported by the axle m_0 and a lateral acceleration a_{acc} increased by a factor k_a to account for local load amplifications. The supported mass is the sum of the mast mass m_M, Spool End Cap mass m_{MSE} and Spool Cylinder mass m_{MSC}:

$$m_0 = m_M + 2m_{MSE} + m_{MSC}$$

It is assumed that there is only a small gap between the mounting points of the axle in the support structure and the mounting point of the spool. Therefore induced bending loads are negligible. The required cross-sectional area A_{MSA} of the Spool Axle is as follows:

$$A_{MSA} = \frac{m_0 k_a a_{acc}}{\tau_{max}}$$

The resulting mass of the axle m_{MAS} is as follows:

$$m_{SA} = \rho A_{MSA} b_{MSA}$$

The width of the axle b_{MSA} is determined by the Spool Cylinder width b_{MSC} which corresponds to the flattened mast width b_M:

$$b_{MSA} = b_M$$

To account for the width of the mount in the support structure a mass amplification factor $k_{MSA,m} > 1$ is applied. Thereby the mass scaling function of the Spool Axle can be written as follows:

$$m_{MSA} = \frac{\rho}{\tau_{max}}(m_M + 2m_{MSE} + m_{MSC}) k_a a_{acc} k_{MSA,m} b_M$$

A scaling limit is introduced in terms of a minimum axle diameter $d_{MSA,min}$. The resulting Spool Axle mass scaling function $m_{MSA,min}$ is as follows:

$$m_{MSA,min} = \frac{\pi}{4} d_{MSA,min}^2 b_M \rho$$

The parameters describing the scaling functions of the Mast Spool Axle and the values for calculation of the according properties are summarized in Tab. B - 5.

Parameters of the Mast Spool Axle			
Parameter	**Symbol**	**Unit**	**Value**
Flattened mast width	b_M	m	Input value
Material density	ρ	kg/m³	7800
Maximum shear stress	τ_{max}	N/m²	150 MPa
Mass amplification factor	$k_{MSA,m}$	-	1.2
Mast mass	m_M	kg	Input value
Central cylinder mass	m_{MSC}	kg	Input value
End cap mass	m_{MSE}	kg	Input value
Acceleration load adjustment factor	k_a	-	1.5
Lateral acceleration	a_{acc}	m/s²	30 g

Minimum axle diameter	$d_{MSA,min}$	m	0.001 (Solid Circular Rod)

Tab. B - 5: Parameters and according values of the Mast Spool Axle scaling functions.

The Spool Axle scaling functions are summarized in Tab. B - 6.

Scaling Functions of the Spool Axle
Scaling Approach: Maximum Shear Stress Solution
$m_{MSA} = \frac{\rho}{\tau_{max}}(m_M + 2m_{MSE} + m_{MSC})k_a a_{acc} k_{MSA,m} b_M$
$m_{MSA,min} = \frac{\pi}{4} d_{MSA,min}^2 b_M \rho$

Tab. B - 6: Spool Axle mass scaling functions for the maximum shear stress criterion and the scaling limit of a minimum axle diameter.

B2 Spool Brake Mechanism

The spool brake generates a counter torque through spring loaded arms gearing into a Tooth Ring. The brake consists of four components with significant mass contribution (see Fig. B - 3):

→ One 'Spool Brake Tooth Ring',
→ One 'Spool Brake Arm Mount',
→ A number of n_{la} 'Spool Brake Arms',
→ A number of n_{la} 'Spool Brake Springs'.

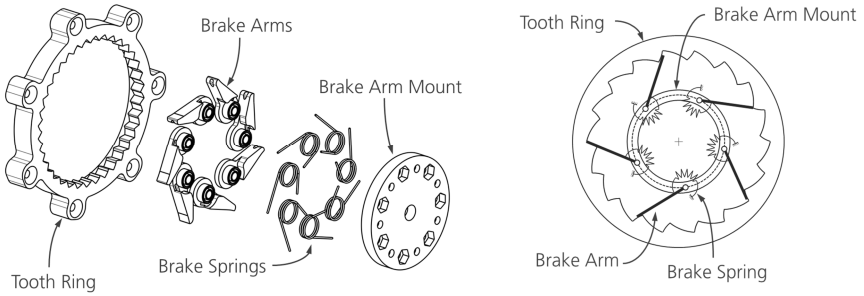

Fig. B - 3: Components of the Spool Brake Mechanism in exploded view (left) and approximation model (right).

B2.1 Brake Mechanism Parameterization

The brake is parameterized by geometrical similarity principles through according size ratios. All ratios thereby relate to the outer brake diameter as leading geometry parameter. As the brake is

integrated into the Mast Spool, the outer radius r_a is the same as the Mast Spool Cylinder radius r_{MSC} which equals the reeling radius of the mast r_M.

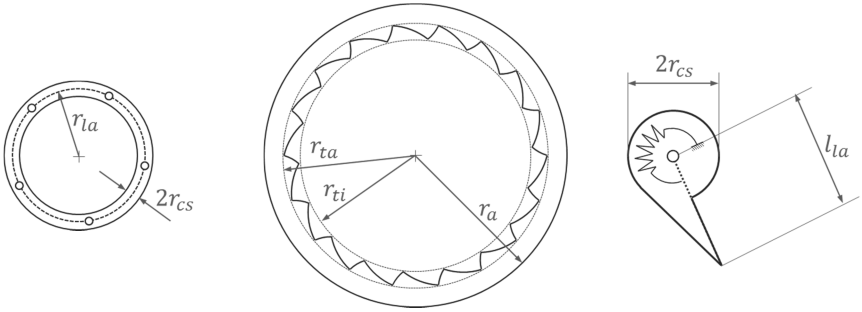

Fig. B - 4: Overview on the dimensions of the Brake Arm Mount (left), brake Tooth Ring (middle) and Brake Spring arms (right).

The geometry parameters and according size ratios of the Spool Brake Mechanism are summarized in Tab. B - 7.

Parameters of the Spool Brake Mechanism			
Parameter	**Symbol**	**Unit**	**Value**
Outer ring radius	r_a	m	-
Inner tooth radius	r_{ti}	m	-
Outer tooth radius	r_{ta}	m	-
Brake height	h_a	m	-
Brake Arm Mount radius	r_{la}	m	-
Brake Arm length	l_{la}	m	-
Brake Arm Mounting angle	γ_{la}	rad	-
Brake Arm deflection angle	$\gamma_{la,0}$	rad	$\pi/4$
Brake Arm number	n_{la}	-	7
Spring wire diameter	d_{cs}	m	-
Spring coiling radius	r_{cs}	m	-
Coil Spring stiffness	K_{cs}	Nm/rad	-
Spring coil number	n_{cs}	-	7
Critical coil spring	$\sigma_{cs,crit}$	N/m²	600 MPa

stress			
Material density	ρ	kg/m³	2700
Coil spring material modulus	E	N/m²	210 GPa
Coil spring material density	ρ_{cs}	kg/m³	7800
Maximum arm contact line pressure	$p_{t,max}$	N/m	1000
Inner tooth radius ratio	$\Gamma_{rti} = \frac{r_{ti}}{r_a}$	-	0.82
Outer tooth radius ratio	$\Gamma_{rta} = \frac{r_{ta}}{r_a}$	-	0.88
Brake Arm length ratio	$\Gamma_{lla} = \frac{l_{la}}{r_a}$	-	0.52
Brake Arm Mount radius ratio	$\Gamma_{rla} = \frac{r_{la}}{r_a}$	-	0.5
Spring coiling radius ratio	$\Gamma_{rcs} = \frac{r_{cs}}{r_a}$	-	0.12

Tab. B - 7: Parameters and according values of the Spool Brake Mechanism.

B2.2 Required Braking Torque

The braking torque $M_{B,req}$ that needs to be generated by the Brake Mechanism depends on the torque generated by the reeled mast M_{Mr} increased by a factor $k_B > 1$ to maintain a minimum tension on the mast during deployment:

$$M_{B,req} = k_B M_{Mr}$$

As a first approximation the stowed mast can be seen as a spiral spring whose moment depends on the cross-sectional dimensions of the flattened mast, the material properties and the reeling radius. The moment generated by the flattened mast M_{Mr} results from the bending stiffness of the flattened mast $(EI)_{M,flat}$ and the mast reeling radius r_M:

$$M_{Mr} = \frac{(EI)_{M,flat}}{r_M}$$

The bending stiffness of the flattened mast depends on the according mast architecture and material. Hence the required braking torque is as follows:

$$M_{B,req} = k_B \frac{(EI)_{M,flat}}{r_M}$$

B2.3 Brake Spring Torque

The torque generated by a single Brake Spring depends on its integration into the overall brake assembly which is displayed in Fig. B - 5.

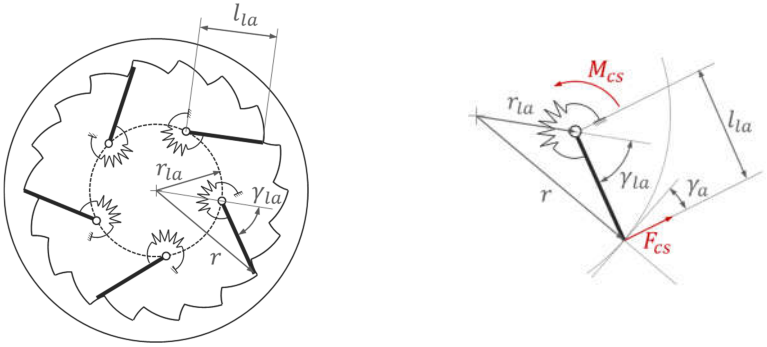

Fig. B - 5: Parameters describing the integration of the Brake Springs into the overall brake assembly.

The spring moment M_{cs} depends on the deflection angle γ_{la}, the initial spring mounting angle $\gamma_{la,0}$ and the coil spring stiffness K_{cs}:

$$M_{cs} = K_{cs}(\gamma_{la} + \gamma_{la,0})$$

The coil spring stiffness depends on the wire diameter d_{cs} and moment of inertia I_{cs}, the material modulus E, the coil radius r_{cs} and the coil number n_{cs}:

$$K_{cs} = \frac{M}{\gamma} = \frac{EI_{cs}}{n_{cs}\pi d_{cs}} = \frac{EI_{cs}}{n_{cs}\pi(2r_{cs})}$$

Substitution of the moment of inertia by assuming a circular wire cross-section leads to:

$$K_{cs} = \frac{E\frac{d_{cs}^4\pi}{64}}{n_{cs}\pi 2r_{cs}} = \frac{Ed_{cs}^4}{128n_{cs}\Gamma_{rcs}r_a}$$

Hence, the moment of a single spring M_{cs} can be written as follows:

$$M_{cs} = \frac{Ed_{cs}^4}{128n_{cs}\Gamma_{rcs}r_a}(\gamma_{la} + \gamma_{la,0})$$

Braking Torque Generated by a Single Spring Loaded Brake Arm

The corresponding braking torque M_a generated by a single spring loaded Brake Arm depends on the force F_{cs} applied by the spring to the toothed edge and its angle of attack γ_a.

$$M_a = F_{cs}\cos(\gamma_a)\,r = \frac{K_{cs}(\gamma_{la} + \gamma_{la,0})}{l_{la}}\cos(\gamma_a)\,r$$

$$M_a = \frac{K_{cs}(\gamma_{la} + \gamma_{la,0})}{\Gamma_{lla}}\cos(\gamma_a)\frac{r}{r_a}$$

The applied force F_{cs} for a certain deflection angle γ_{la} depends on the spring length l_{la} as follows:

$$F_{cs} = \frac{M_{cs}}{l_{la}} = \frac{K_{cs}(\gamma_{la} + \gamma_{la,0})}{l_{la}}$$

The angle γ_{la} depends on the mounting radius of the lever arm r_{la}, the arm length l_{la} and the position r of the arm tip as follows:

$$\cos(\pi - \gamma_{la}) = \frac{r_{la}^2 + l_{la}^2 - r^2}{2r_{la}l_{la}}$$

$$\gamma_{la} = \pi - \arccos\left(\frac{\Gamma_{rla}^2 + \Gamma_{lla}^2 - \left(\frac{r}{r_a}\right)^2}{2\Gamma_{rla}\Gamma_{lla}}\right)$$

The angle γ_a is derived as follows:

$$\cos(\gamma_a) = \frac{l_{la}^2 + r^2 - r_{la}^2}{2 l_{la} r}$$

$$\cos(\gamma_a) = \frac{\Gamma_{lla}^2 + \left(\frac{r}{r_a}\right)^2 - \Gamma_{rla}^2}{2\Gamma_{lla}\frac{r}{r_a}}$$

$$\gamma_a = \arccos\left(\frac{\Gamma_{lla}^2 + \left(\frac{r}{r_a}\right)^2 - \Gamma_{rla}^2}{2\Gamma_{lla}\frac{r}{r_a}}\right)$$

For calculation of the total moment it is assumed that the moment of each spring loaded arm M_a corresponds to the mean moment between the maximum and minimum position of the arm tip r:

$$r = \frac{r_{ti} + r_{ta}}{2} = \frac{\Gamma_{rti} + \Gamma_{rta}}{2} r_a$$

Substitution of the radius r in the expressions for the spring deflection angle γ_{la} and the spring angle of attack γ_a leads to:

$$\gamma_{la} = \pi - \arccos\left(\frac{\Gamma_{rla}^2 + \Gamma_{lla}^2 - \frac{1}{4}(\Gamma_{rti} + \Gamma_{rta})^2}{2\Gamma_{rla}\Gamma_{lla}}\right)$$

$$\gamma_a = \arccos\left(\frac{\Gamma_{lla}^2 + \frac{1}{4}(\Gamma_{rti} + \Gamma_{rta})^2 - \Gamma_{rla}^2}{\Gamma_{lla}(\Gamma_{rti} + \Gamma_{rta})}\right)$$

Thereby the moment contribution M_a of a single spring to the overall moment is as follows:

$$M_a = \frac{K_{cs}(\gamma_{la} + \gamma_{la,0})}{\Gamma_{lla}} \cos(\gamma_a) \frac{\Gamma_{rti} + \Gamma_{rta}}{2}$$

$$M_a = K_{cs}\left(\pi - \arccos\left(\frac{\Gamma_{rla}^2 + \Gamma_{lla}^2 - \frac{1}{4}(\Gamma_{rti} + \Gamma_{rta})^2}{2\Gamma_{rla}\Gamma_{lla}}\right) + \gamma_{la,0}\right) \frac{\Gamma_{lla}^2 + \frac{1}{4}(\Gamma_{rti} + \Gamma_{rta})^2 - \Gamma_{rla}^2}{\Gamma_{lla}^2(\Gamma_{rti} + \Gamma_{rta})} \frac{\Gamma_{rti} + \Gamma_{rta}}{2}$$

$$M_a = K_{cs}\left(\pi - \arccos\left(\frac{\Gamma_{rla}^2 + \Gamma_{lla}^2 - \frac{1}{4}(\Gamma_{rti} + \Gamma_{rta})^2}{2\Gamma_{rla}\Gamma_{lla}}\right) + \gamma_{la,0}\right) \frac{\Gamma_{lla}^2 + \frac{1}{4}(\Gamma_{rti} + \Gamma_{rta})^2 - \Gamma_{rla}^2}{2\Gamma_{lla}^2}$$

Substitution of the spring stiffness K_{cs} leads to the braking torque expression generated by a single spring arm:

$$M_a = \frac{1}{128} E \frac{1}{n_{cs}}\left(\pi - \arccos\left(\frac{\Gamma_{rla}^2 + \Gamma_{lla}^2 - \frac{1}{4}(\Gamma_{rti} + \Gamma_{rta})^2}{2\Gamma_{rla}\Gamma_{lla}}\right) + \gamma_{la,0}\right) \frac{\Gamma_{lla}^2 + \frac{1}{4}(\Gamma_{rti} + \Gamma_{rta})^2 - \Gamma_{rla}^2}{2\Gamma_{lla}^2 \Gamma_{rcs}} \frac{d_{cs}^4}{r_a}$$

Substitution in the expression for the spring moment leads to:

$$M_{cs} = \frac{1}{128} E \frac{1}{n_{cs}}\left(\pi - \arccos\left(\frac{\Gamma_{rla}^2 + \Gamma_{lla}^2 - \frac{1}{4}(\Gamma_{rti} + \Gamma_{rta})^2}{2\Gamma_{rla}\Gamma_{lla}}\right) + \gamma_{la,0}\right) \frac{d_{cs}^4}{r_a}$$

Calculation of Spring Wire Diameter and Number of Coils

The remaining variables that are not determined by linear scaling ratios are the diameter of the spring wire d_{cs} and the number of coils n_{cs}. The two parameters are derived from two constraint functions on the required brake moment $M_{B,req}$ and the critical stress in the spring $\sigma_{cs,crit}$. The constraint functions are as follows:

$$\sigma_{cs,max} \leq \sigma_{cs,crit}$$
$$M_{Brake} \geq M_{B,req}$$

The maximum stress in the spring wire depends on the spring moment M_{cs} and the section modulus W_{cs} which is a function of the wire moment of inertia I_{cs} and the maximum distance of the outer fiber to the neutral layer $y_{cs,max}$:

$$\sigma_{cs,max} = \frac{M_{cs}}{W_{cs}} = \frac{M_{cs}}{I_{cs}} y_{cs,max}$$
$$\sigma_{cs,max} = \frac{M_{cs}}{\frac{d_{cs}^4 \pi}{64}} \frac{d_{cs}}{2} = \frac{32}{\pi d_{cs}^3} M_{cs}$$

Substitution of the spring moment M_{cs} leads to:

$$\sigma_{cs,max} = \frac{32}{\pi d_{cs}^3} K_{cs} \gamma_{cs,max}$$

The angle $\gamma_{cs,max}$ is the maximum deflection angle the spring has to provide and is derived as follows:

$$\gamma_{cs,max} = \gamma_{la,max} + \gamma_{la,0}$$
$$\gamma_{cs,max} = \pi - \arccos\left(\frac{\Gamma_{rla}^2 + \Gamma_{lla}^2 - \left(\frac{r(\gamma_{la,max})}{r_a}\right)^2}{2\Gamma_{rla}\Gamma_{lla}}\right) + \gamma_{la,0}$$

The maximum angle of the spring $\gamma_{la,max}$ is reached for a spring tip radius that coincides with the inner radius of the Tooth Ring r_{ti}:

$$\gamma_{cs,max} = \pi - \arccos\left(\frac{\Gamma_{rla}^2 + \Gamma_{lla}^2 - \left(\frac{r_{ti}}{r_a}\right)^2}{2\Gamma_{rla}\Gamma_{lla}}\right) + \gamma_{la,0}$$
$$\gamma_{cs,max} = \pi - \arccos\left(\frac{\Gamma_{rla}^2 + \Gamma_{lla}^2 - \Gamma_{rti}^2}{2\Gamma_{rla}\Gamma_{lla}}\right) + \gamma_{la,0}$$

Substitution in the expression for the maximum stress leads to:

$$\sigma_{cs,max} = \frac{32}{\pi d_{cs}^3} K_{cs} \left(\pi - \arccos\left(\frac{\Gamma_{rla}^2 + \Gamma_{lla}^2 - \Gamma_{rti}^2}{2\Gamma_{rla}\Gamma_{lla}}\right) + \gamma_{la,0}\right)$$

Substitution of the spring stiffness K_{cs} gives:

$$\sigma_{cs,max} = \frac{1}{4\pi} E \frac{1}{n_{cs}} \frac{1}{\Gamma_{rcs}} \left(\pi - \arccos\left(\frac{\Gamma_{rla}^2 + \Gamma_{lla}^2 - \Gamma_{rti}^2}{2\Gamma_{rla}\Gamma_{lla}}\right) + \gamma_{la,0}\right) \frac{d_{cs}}{r_a}$$

Substitution of the maximum stress expression in the critical stress constraint function leads to:

$$\sigma_{cs,max} \leq \sigma_{cs,crit}$$
$$\sigma_{cs,crit} = \frac{1}{4\pi} E \frac{1}{n_{cs}} \frac{1}{\Gamma_{rcs}} \left(\pi - \arccos\left(\frac{\Gamma_{rla}^2 + \Gamma_{lla}^2 - \Gamma_{rti}^2}{2\Gamma_{rla}\Gamma_{lla}}\right) + \gamma_{la,0}\right) \frac{d_{cs}}{r_a}$$

For simplification the terms containing geometry parameters of the brake are substituted by the parameter $\Phi_{B,1}$ which leads to the stress constraint function for the coil springs:

$$\sigma_{cs,crit} = \frac{1}{4\pi} E \frac{1}{n_{cs}} \Phi_{B,1} \frac{d_{cs}}{r_a}$$
$$\Phi_{B,1} = \frac{1}{\Gamma_{rcs}} \left(\pi - \arccos\left(\frac{\Gamma_{rla}^2 + \Gamma_{lla}^2 - \Gamma_{rti}^2}{2\Gamma_{rla}\Gamma_{lla}} \right) + \gamma_{la,0} \right)$$

For calculation of the brake moment M_{Brake} it is assumed that the spring arms all possess different phase angles and that $n_{la} - 1$ of the arms gear into the Tooth Ring while the remaining one is in the short phase of flapping back into the starting position:

$$M_{Brake} = (n_{la} - 1) M_a$$

Equating with the moment constraint function leads to:

$$M_{Brake} \geq M_{B,req}$$
$$M_{B,req} = (n_{la} - 1) M_a$$

Substitution of the spring moment contribution M_a gives:

$$M_{B,req} = \frac{1}{128} (n_{la} - 1) E \frac{1}{n_{cs}} \left(\pi - \arccos\left(\frac{\Gamma_{rla}^2 + \Gamma_{lla}^2 - \frac{1}{4}(\Gamma_{rti} + \Gamma_{rta})^2}{2\Gamma_{rla}\Gamma_{lla}} \right) + \gamma_{la,0} \right) \frac{\Gamma_{lla}^2 + \frac{1}{4}(\Gamma_{rti} + \Gamma_{rta})^2 - \Gamma_{rla}^2}{2\Gamma_{lla}^2 \Gamma_{rcs}} \frac{d_{cs}^4}{r_a}$$

For simplification the terms containing geometry parameters of the brake are substituted by the parameter Φ_M which leads to the braking torque constraint function:

$$M_{B,req} = \frac{1}{128} (n_{la} - 1) E \frac{1}{n_{cs}} \Phi_{B,2} \Phi_{B,3} \frac{d_{cs}^4}{r_a}$$
$$\Phi_{B,2} = \left(\pi - \arccos\left(\frac{\Gamma_{rla}^2 + \Gamma_{lla}^2 - \frac{1}{4}(\Gamma_{rti} + \Gamma_{rta})^2}{2\Gamma_{rla}\Gamma_{lla}} \right) + \gamma_{la,0} \right)$$
$$\Phi_{B,3} = \frac{\Gamma_{lla}^2 + \frac{1}{4}(\Gamma_{rti} + \Gamma_{rta})^2 - \Gamma_{rla}^2}{2\Gamma_{lla}^2 \Gamma_{rcs}}$$

From the stress and braking torque constraint function the wire diameter and required number of spring coils is derived. Solving the stress constraint function for the spring wire diameter d_{cs} leads to:

$$\sigma_{cs,crit} = \frac{1}{4\pi} E \frac{1}{n_{cs}} \Phi_{B,1} \frac{d_{cs}}{r_a}$$
$$d_{cs} = 4\pi \frac{1}{\Phi_{B,1}} \frac{1}{E} n_{cs} \sigma_{cs,crit} r_a$$

Substitution of the wire diameter in the moment expression leads to:

$$M_{B,req} = \frac{1}{128} (n_{la} - 1) E \frac{1}{n_{cs}} \Phi_{B,2} \Phi_{B,3} \frac{d_{cs}^4}{r_a}$$
$$M_{B,req} = \frac{1}{128} (n_{la} - 1) E \frac{1}{n_{cs}} \Phi_{B,2} \Phi_{B,3} \frac{1}{r_a} \left(4\pi \frac{1}{\Phi_{B,1}} \frac{1}{E} n_{cs} \sigma_{cs,crit} r_a \right)^4$$
$$M_{req} = 2\pi^4 (n_{la} - 1) \frac{\sigma_{cs,crit}^4}{E^3} n_{cs}^3 \frac{\Phi_{B,2} \Phi_{B,3}}{\Phi_{B,1}^4} r_a^3$$

Solving for the number of spring coils n_{cs} leads to:

$$n_{cs} = \left(\frac{1}{2\pi^4} \frac{\Phi_{B,1}^4}{\Phi_{B,2} \Phi_{B,3}} \frac{1}{(n_{la} - 1)} \frac{E^3}{\sigma_{cs,crit}^4} M_{B,req} \frac{1}{r_a^3} \right)^{\frac{1}{3}}$$

The spring wire diameter d_{cs} is thereby as follows:

$$d_{cs} = \left(\frac{32}{\pi} \frac{\Phi_{B,1}}{\Phi_{B,2}\Phi_{B,3}} \frac{1}{(n_{la}-1)} \frac{1}{\sigma_{cs,crit}} M_{B,req} \right)^{\frac{1}{3}}$$

With the solutions on the spring wire diameter and number of spring coils the spring moment can be calculated:

$$M_{cs} = \frac{1}{128} \Phi_{B,2} E \frac{1}{n_{cs}} \frac{d_{cs}^4}{r_a}$$

The equations for calculation of the required spring moment, wire diameter and number of coils are summarized in Tab. B - 8.

Scaling Function of the Required Spring Moment of the Spool Brake Mechanism
Scaling Approach: Geometric Similarity based on a Design Reference Model with the Outer Brake Radius as Leading Dimension
$$M_{cs} = \frac{1}{128} \Phi_{B,2} E \frac{1}{n_{cs}} \frac{d_{cs}^4}{r_a}$$ $$d_{cs} = \left(\frac{32}{\pi} \frac{\Phi_{B,1}}{\Phi_{B,2}\Phi_{B,3}} \frac{1}{(n_{la}-1)} \frac{1}{\sigma_{cs,crit}} M_{B,req} \right)^{\frac{1}{3}}$$ $$n_{cs} = \left(\frac{1}{2\pi^4} \frac{\Phi_{B,1}^4}{\Phi_{B,2}\Phi_{B,3}} \frac{1}{(n_{la}-1)} \frac{E^3}{\sigma_{cs,crit}^4} M_{B,req} \frac{1}{r_a^3} \right)^{\frac{1}{3}}$$
$$\Phi_{B,1} = \frac{1}{\Gamma_{rcs}} \left(\pi - \arccos\left(\frac{\Gamma_{rla}^2 + \Gamma_{lla}^2 - \Gamma_{rti}^2}{2\Gamma_{rla}\Gamma_{lla}} \right) + \gamma_{la,0} \right)$$ $$\Phi_{B,2} = \left(\pi - \arccos\left(\frac{\Gamma_{rla}^2 + \Gamma_{lla}^2 - \frac{1}{4}(\Gamma_{rti} + \Gamma_{rta})^2}{2\Gamma_{rla}\Gamma_{lla}} \right) + \gamma_{la,0} \right)$$ $$\Phi_{B,3} = \frac{\Gamma_{lla}^2 + \frac{1}{4}(\Gamma_{rti} + \Gamma_{rta})^2 - \Gamma_{rla}^2}{2\Gamma_{lla}^2\Gamma_{rcs}}$$

Tab. B - 8: Required spring moment, wire diameter and number of coils for the Spool Brake Mechanism.

B2.4 Spool Brake Tooth Ring Scaling Function

The mass of the spool brake Tooth Ring (index SBT) m_{SBT} results from its dimensions displayed in Fig. B - 4 and the material density ρ as follows:

$$m_{SBT} = \pi \left(r_a^2 - \left(\frac{r_{ta} + r_{ti}}{2} \right)^2 \right) h_a \rho$$

$$m_{SBT} = \pi \left(1 - \left(\frac{\Gamma_{rta} + \Gamma_{rti}}{2} \right)^2 \right) r_a^2 h_a \rho$$

The outer radius of the ring r_a corresponds to the reeling radius of the mast r_M. The height of the ring h_a is derived from the contact pressure caused by the spring loaded arms. The contact area between the arm and the tooth flank of the ring is a line. To avoid wear on the teeth or the arm during operation of the brake an allowable line load $p_{t,max}$ is defined. By this line load and the

contact force between tooth and spring loaded arm, the height of the Tooth Ring h_a of the brake is determined as follows:

$$h_a = \frac{F_{cs}}{p_{t,max}} = \frac{M_{cs}}{l_{la} p_{t,max}} = \frac{M_{cs}}{\Gamma_{lla} p_{t,max} r_a}$$

Hence, the mass scaling function for the outer ring is as follows whereby the spring moment M_{cs} is calculated according to Tab. B - 8:

$$m_{SBT} = \pi \frac{1}{\Gamma_{lla}} \left(1 - \left(\frac{\Gamma_{rta} + \Gamma_{rti}}{2}\right)^2\right) \frac{M_{cs}}{p_{t,max}} \rho r_M$$

The parameters of the spool brake Tooth Ring scaling function are summarized in Tab. B - 9.

Parameters of the Spool Brake Tooth Ring			
Parameter	**Symbol**	**Unit**	**Value**
Mast reeling radius	r_M	m	Input value
Material density	ρ	kg/m³	2700
Coil spring moment	M_{cs}	Nm	Input value
Allowable tooth line pressure	$p_{t,max}$	N/m	1000
Brake Arm length ratio	Γ_{lla}	-	0.52
Outer tooth radius ratio	Γ_{rta}	-	0.88
Inner tooth radius ratio	Γ_{rti}	-	0.82

Tab. B - 9: Design parameters of the spool brake Tooth Ring.

The scaling function is summarized in Tab. B - 10.

Scaling Function of the Spool Brake Tooth Ring
Scaling Approach: Geometric Similarity based on a Design Reference Model with the Outer Brake Radius as Leading Dimension
$m_{SBT} = \pi \frac{1}{\Gamma_{lla}} \left(1 - \left(\frac{\Gamma_{rta} + \Gamma_{rti}}{2}\right)^2\right) \frac{M_{cs}}{p_{t,max}} \rho r_M$

Tab. B - 10: Scaling function of the spool brake Tooth Ring.

B2.5 Spool Brake Arm Mount Scaling Function

The mass of the spool Brake Arm Mount (index SBM) m_{SBM} results from its dimensions displayed in Fig. B - 4 and the material density ρ. The middle radius of the inner ring coincides with the arm

mounting radius r_{la} and the width coincides with the spring diameter $2r_{cs}$ while the height is the same as for the outer ring h_a. Thereby the mass of the Brake Arm Mount m_{BAM} is as follows:

$$m_{SBM} = \pi((r_{la} + r_{cs})^2 - (r_{la} - r_{cs})^2)h_a\rho$$
$$m_{SBM} = \pi((\Gamma_{rla} + \Gamma_{rcs})^2 - (\Gamma_{rla} - \Gamma_{rcs})^2)r_a^2 h_a\rho$$
$$m_{SBM} = \pi\left(\Gamma_{rla}^2 + 2\Gamma_{rla}\Gamma_{rcs} + \Gamma_{rcs}^2 - (\Gamma_{rla}^2 - 2\Gamma_{rla}\Gamma_{rcs} + \Gamma_{rcs}^2)\right)r_a^2 h_a\rho$$
$$m_{SBM} = 4\pi\Gamma_{rla}\Gamma_{rcs}r_a^2 h_a\rho$$

Substitution of the outer radius r_a by the reeling radius of the mast r_M and of the height parameter h_a gives the mass scaling function for the spool Brake Arm Mount whereby the spring moment M_{cs} is calculated according to Tab. B - 8:

$$m_{SBM} = 4\pi\frac{\Gamma_{rla}\Gamma_{rcs}}{\Gamma_{lla}}\frac{M_{cs}}{p_{t,max}}\rho r_M$$

The parameters of the spool Brake Arm Mount scaling function are summarized in Tab. B - 11.

Parameters of the Spool Brake Arm Mount			
Parameter	**Symbol**	**Unit**	**Value**
Mast reeling radius	r_M	m	Input value
Material density	ρ	kg/m³	2700
Coil spring moment	M_{cs}	Nm	Input value
Allowable tooth line pressure	$p_{t,max}$	N/m	1000
Brake Arm length ratio	Γ_{lla}	-	0.52
Spring coiling radius ratio	Γ_{rcs}	-	0.12
Brake Arm Mount radius ratio	Γ_{rla}	-	0.5

Tab. B - 11: Design parameters of the spool Brake Arm Mount.

The scaling function is summarized in Tab. B - 12.

Scaling Function of the Spool Brake Arm Mount
Scaling Approach: Geometric Similarity based on a Design Reference Model with the Outer Brake Radius as Leading Dimension
$m_{SBM} = 4\pi\frac{\Gamma_{rla}\Gamma_{rcs}}{\Gamma_{lla}}\frac{M_{cs}}{p_{t,max}}\rho r_M$

Tab. B - 12: Scaling function of the spool Brake Arm Mount.

B2.6 Spool Brake Arm Scaling Function

The combined mass of the spring loaded Brake Arms (index SBA) m_{SBA} results from its dimensions displayed in Fig. B - 4 and the material density ρ as follows:

$$m_{SBA} = n_{la}\left(\frac{1}{2} l_{la} r_{cs} + \pi r_{cs}^2\right) h_a \rho$$

$$m_{SBA} = n_{la}\left(\frac{1}{2} \Gamma_{lla} \Gamma_{rcs} + \pi \Gamma_{rcs}^2\right) r_a^2 h_a \rho$$

Substitution of the outer radius r_a by the reeling radius of the mast r_M and of the height parameter gives the mass scaling function for spool Brake Arms whereby the spring moment M_{cs} is calculated according to Tab. B - 8:

$$m_{SBA} = n_{la} \frac{1}{\Gamma_{lla}}\left(\frac{1}{2} \Gamma_{lla} \Gamma_{rcs} + \pi \Gamma_{rcs}^2\right) \frac{M_{cs}}{p_{t,max}} \rho r_M$$

The parameters of the spool Brake Arm scaling function are summarized in Tab. B - 13.

Parameters of the Spool Brake Arms			
Parameter	**Symbol**	**Unit**	**Value**
Mast reeling radius	r_M	m	Input value
Material density	ρ	kg/m³	2700
Coil spring moment	M_{cs}	Nm	Input value
Allowable tooth line pressure	$p_{t,max}$	N/m	1000
Brake Arm length ratio	Γ_{lla}	-	0.52
Spring coiling radius ratio	Γ_{rcs}	-	0.12

Tab. B - 13: Design parameters of the spool Brake Arms.

The scaling function is summarized in Tab. B - 14.

Combined Scaling Function of the Spool Brake Arms
Scaling Approach: Geometric Similarity based on a Design Reference Model with the Outer Brake Radius as Leading Dimension
$m_{SBA} = n_{la} \frac{1}{\Gamma_{lla}}\left(\frac{1}{2} \Gamma_{lla} \Gamma_{rcs} + \pi \Gamma_{rcs}^2\right) \frac{M_{cs}}{p_{t,max}} \rho r_M$

Tab. B - 14: Combined scaling function of the spool Brake Arms.

B2.7 Spool Brake Spring Scaling Function

The combined mass of the Brake Springs (index SBS) m_{SBS} results from its dimensions displayed in Fig. B - 4 and Fig. B - 5 and the wire material density ρ as follows:

$$m_{SBS} = \frac{\pi}{4} d_{cs}^2 (2l_{la} + 2\pi n_{cs} r_{cs}) \rho$$

$$m_{SBS} = \frac{\pi}{4} d_{cs}^2 (2\Gamma_{lla} + 2\pi n_{cs} \Gamma_{rcs}) \rho r_a$$

Substitution of the outer brake radius r_a by the mast reeling radius r_M gives the spool brake sping mass scaling function:

$$m_{SBS} = \frac{\pi}{4} d_{cs}^2 (2\Gamma_{lla} + 2\pi n_{cs} \Gamma_{rcs}) \rho r_M$$

The wire diameter d_{cs} and number of spring coils n_{cs} is derived according to Tab. B - 8.

The parameters of the spool Brake Arm scaling function are summarized in Tab. B - 15.

Parameters of the Spool Brake Springs			
Parameter	**Symbol**	**Unit**	**Value**
Mast reeling radius	r_M	m	Input value
Material density	ρ	kg/m³	7800
Coil spring moment	M_{cs}	Nm	Input value
Spring diameter	d_{cs}	N/m	Input value
Number of spring coils	n_{cs}	-	Input value
Brake Arm length ratio	Γ_{lla}	-	0.52
Spring coiling radius ratio	Γ_{rcs}	-	0.12

Tab. B - 15: Design parameters of the spool Brake Springs.

The scaling function is summarized in Tab. B - 16.

Combined Scaling Function of the Spool Brake Springs
Scaling Approach: Geometric Similarity based on a Design Reference Model with the Outer Brake Radius as Leading Dimension
$m_{SBS} = \frac{\pi}{4} d_{cs}^2 (2\Gamma_{lla} + 2\pi n_{cs} \Gamma_{rcs}) \rho r_M$

Tab. B - 16: Combined scaling function of the spool Brake Springs.

B3 Mast Root Support and Guidance

The mast root support and guidance components provide structural support to the deploying mast and guide their deployment direction. This module consists of two components:

→ Two 'Support Plates',
→ Two 'Guide Rolls'.

B3.1 Mast Guide and Support Plate

The mast guide and support shells (index MGS) are rectangular in their basic geometry and are fixed to the mechanism support structure along their longitudinal, opposing edges (see Fig. B - 6).

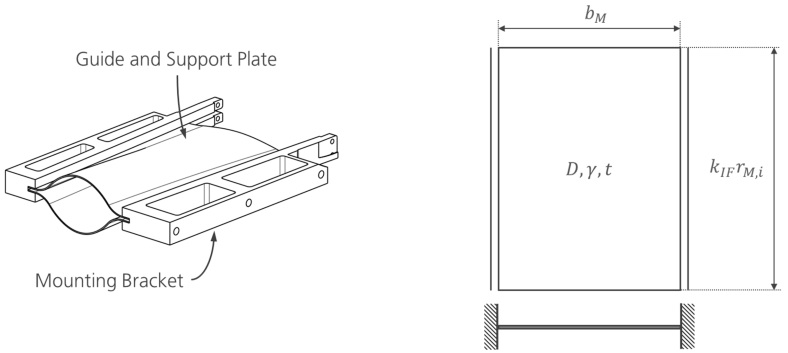

Fig. B - 6 : Support Plates for root support of the deploying mast (left) and approxmation model (right).

The shells are approximated as plates with fixed longitudinal edges. The shells do have to support only their own mass as the mast mass is negligible in comparison. Also the loads introduced into the shells from the loaded mast can be assumed to be negligible as well. Therefore the shells are sized by a minimum eigenfrequency criterion. For sizing the plate scaling functions described in A4.1 and Tab. A - 13 are applied. Therefore the scaling function parameters need to be adjusted accordingly. The width of the plate b_{MGS} corresponds to the width of the flattened mast b_M:

$$b_{MGS} = b = b_M$$

The length a of the plate is described by the mast-mechanism interface factor k_{IF} which relates the length of the Guide and Support Plates to the masts radius of gyration $r_{M,i}$:

$$a_{MGS} = a = k_{IF} r_{M,i}$$

To separate the local modes from the overall minimum eigenfrequency f_{req}, it is increased by a factor k_f. The resulting Support Plate mass scaling function is as follows:

$$m_{MGS} = \left(4\pi^2 \frac{1}{k_C^4} \frac{k_m^3}{k_D} \frac{k_\rho^3 \rho^{*3}}{E} \left(k_{IF} r_{M,i} \right)^2 b_M^6 k_f^2 f_{req}^2 \right)^{\frac{1}{2}}$$

A scaling limit is introduced in terms of a minimum shell thickness $t_{MGS,min}$. The resulting Support Plate mass scaling function $m_{MGS,min}$ is as follows:

$$m_{MGS,min} = k_{IF} r_{M,i} b_M t_{MGS,min} k_\rho \rho^*$$

The parameters of the Support Plate scaling functions are summarized in Tab. B - 17.

Parameters of the Support Plates			
Parameter	**Symbol**	**Unit**	**Value**
Mast radius of gyration	$r_{M,i}$	m	Input value

Flattened mast width	b_M	m	Input value
Material modulus	E	N/m²	60 GPa
Reference density	ρ^*	kg/m³	1600
Minimum eigenfrequency	f_{req}	Hz	100
Density factor	k_ρ	-	50/1600
Plate mass architecture factor	k_m	-	0.111
Plate flexural rigidity architecture factor	k_D	-	0.0125
Plate mounting factor	k_C	-	4.73
Mast-Mechanism Interface Factor	k_{IF}	-	5
Eigenfrequency amplification factor	k_f	-	1.5
Minimum shell thickness	$t_{MGS,min}$	m	0.003 (Sandwich Architecture)

Tab. B - 17: Design parameters of the mast Guide and Support Plates.

The scaling functions are summarized in Tab. B - 18.

Scaling Functions of the Support Plates
Scaling Approach: Eigenfrequency Solution
$m_{MGS} = \left(4\pi^2 \frac{1}{k_C^4} \frac{k_m^3}{k_D} \frac{k_\rho^3 \rho^{*3}}{E} \left(k_{IF} r_{M,i}\right)^2 b_M^6 k_f^2 f_{req}^2\right)^{\frac{1}{2}}$
$m_{MGS,min} = k_{IF} r_{M,i} b_M t_{MGS,min} k_\rho \rho^*$

Tab. B - 18: Mass scaling functions of the mast guide and Support Plates.

Exemplary a comparison of the mass scaling behavior of mast guide and support shells realized as solid, sandwich and stiffened plates is displayed in Fig. B - 7. In the small scale region the advantage of the solid plate regarding the minimum scaling limit is visible.

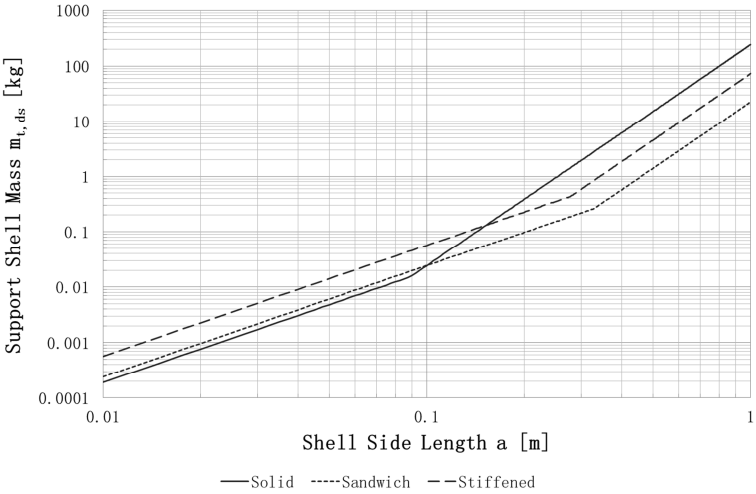

Fig. B - 7: Exemplary comparison of the support shell mass scaling behavior for solid, sandwich and stiffened plate architectures plotted of the shell side length.

B3.2 Guide Roll

The mast Guide Rolls (index MGR) are slender circular cylinders equipped with a ball bearing at both ends for rotatable mounting (see Fig. B - 8). Mounting is done through bolts at both ends or an axle is considered.

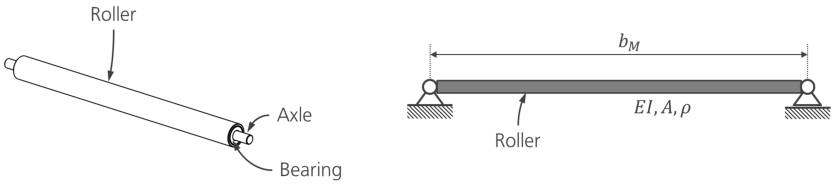

Fig. B - 8: Guide Roll with ball bearings and axle (left) and approximation model for sizing (right).

The Guide Roll is approximated as a beam with simply supported ends. They have to support only their own weight wherefore they are sized by a minimum required eigenfrequency criterion. For sizing the beam scaling functions derived in A2.1and Tab. A - 6 are applied. Therefore the scaling function parameters need to be adjusted accordingly. The length l_{MGR} of the Guide Roll corresponds to the width of the flattened mast b:

$$l_{MGR} = l = b_M$$

Furthermore the eigenfrequency requirement is amplified by a factor k_f and the additional mass of an axle is considered by a mass amplification factor $k_{MGR,m}$. The resulting Guide Roll mass scaling function is as follows:

$$m_{MGR} = \frac{4}{\pi^2} k_{MGR,m} \frac{k_A}{k_I} \frac{k_\rho^2 \rho^{*2}}{E} b_M^5 k_f^2 f_{req}^2$$

A scaling limit is introduced in terms of a minimum Guide Roll radius $r_{MGR,min}$. The resulting Guide Roll mass scaling function $m_{MGR,min}$ is as follows:

$$m_{MGR,min} = k_{MGR,m} k_A k_\rho \rho^* b r_{MGR,min}^2$$

The ball bearings are sized according to A6.2 and Tab. A - 25. The required input value depends on the radius of the Guide Roll r_{MGR} (see Tab. A - 6) and the ball bearing size ratio of outer to inner radius $\frac{r_a}{r_i}$:

$$r_{MGR} = \frac{2}{\pi} \sqrt{\frac{1}{k_I} \frac{k_\rho \rho^*}{E}} b_M^2 k_f f_{req}$$

$$\frac{r_a}{r_i} = 1 + \Gamma_t + 2\Gamma_b$$

Assuming that the outer bearing radius corresponds to $\frac{4}{5}$ of the Guide Roll radius, the resulting input value for ball bearing sizing is as follows:

$$r_a = \frac{4}{5} r_{MGR}$$

$$r_i = \frac{r_a}{1 + \Gamma_t + 2\Gamma_b}$$

$$r_i = \frac{8}{5\pi} \frac{1}{1 + \Gamma_t + 2\Gamma_b} \sqrt{\frac{1}{k_I} \frac{k_\rho \rho^*}{E}} b_M^2 k_f f_{req}$$

The mass of the ball bearings can now be derived according to Tab. A - 25.

The parameters of the support shell scaling functions are summarized in Tab. B - 19

Parameters of the Guide Rolls			
Parameter	**Symbol**	**Unit**	**Value**
Mast flattened width	b_M	m	Input value
Material modulus	E	N/m²	70 GPa
Reference density	ρ^*	kg/m³	2700
Minimum eigenfrequency	f_{req}	Hz	100
Density factor	k_ρ	-	1
Cross-section area factor	k_A	-	0.2π
Cross-section second moment of area factor	k_I	-	0.5
Mass amplification factor	$k_{MGR,m}$	-	1.2
Eigenfrequency amplification factor	k_f	-	1.5

Minimum roll diameter	$r_{MGR,min}$	m	0.002 (Circular Tube)

Tab. B - 19: Mast Guide Roll design parameters.

The scaling functions are summarized in Tab. B - 20.

Scaling Functions of the Guide Rolls
Scaling Approach: Eigenfrequency Solution
$m_{MGR} = \frac{4}{\pi^2} k_{MGR,m} \frac{k_A}{k_l} \frac{k_\rho^2 \rho^{*2}}{E} b_M^5 k_f^2 f_{req}^2$
$m_{MGR,min} = k_{MGR,m} k_A k_\rho \rho^* b r_{MGR,min}^2$

Tab. B - 20: Mast Guide Roll scaling functions.

B4 Drive Mechanism

The Drive Mechanism generates, transforms and transmits the forces necessary for deployment of the mast. It consists of four components:

→ One 'Belt' for transmission of the loads,
→ One 'Belt Spool' for introducing the loads into the belt,
→ One 'Gear' to transform the forces generated by the motor,
→ One 'Electric Motor' to generate the deployment forces in the first place.

B4.1 Belt

The belt (index DMB) is a flexible, thin walled tape of rectangular cross-section (see Fig. B - 9). It is sized by the load P it has to transmit and the elastic deformation the belt is subjected to when being coiled on the spool or deflected by a pulley.

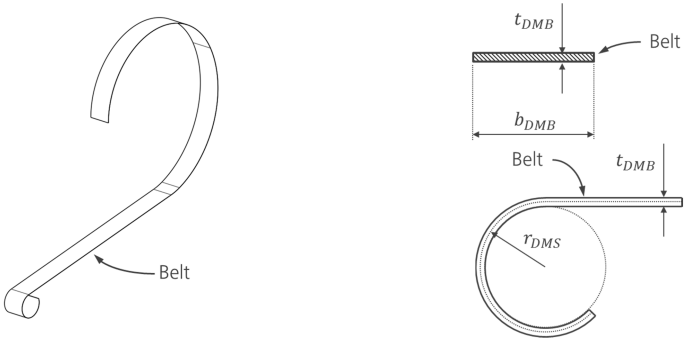

Fig. B - 9: Flexible belt in its form integrated into the Deployment Mechanism (left), cross-sectional dimensions (top right) and reeling process on the Belt Spool (bottom right).

The overall strain ε results from the strains $\varepsilon_{P,B}$ and $\varepsilon_{r,B}$ in the belt induced by loading P and coiling onto the Belt Spool with radius $r_{DMS,i}$ as follows:

$$\varepsilon = \varepsilon_{P,B} + \varepsilon_{r,B}$$

$$\varepsilon = \frac{P}{EA_{DMB}} + \frac{t_{DMB}}{2r_{DMS,i}}$$

Here A_{DMB} is the belt cross-sectional area, $r_{BS,i}$ is the minimum radius of the Belt Spool or pulley, P is the applied load on the belt and t_{DMB} is the thickness of the belt. The total strain shall not exceed the maximum elastic strain ε_{max} including a strain safety factor $F_{S,\varepsilon,B}$:

$$\varepsilon \leq \frac{1}{F_{S,\varepsilon,B}}\varepsilon_{max}$$

Furthermore a ratio $\Gamma_{\varepsilon,P,B}$ of the strain $\varepsilon_{P,B}$ applied by the pulling force P in relation to the total strain ε is introduced:

$$\frac{\varepsilon_{P,B}}{\varepsilon} = \Gamma_{\varepsilon,P,B}$$

Thereby the total strain equation can be written as follows:

$$\frac{\varepsilon_{max}}{F_{S,\varepsilon,B}} = \Gamma_{\varepsilon,P,B}\varepsilon + \frac{t_{DMB}}{2r_{DMS,i}}$$

$$\frac{\varepsilon_{max}}{F_{S,\varepsilon,B}} = \frac{\Gamma_{\varepsilon,P,B}}{F_{S,\varepsilon,B}}\varepsilon_{max} + \frac{t_{DMB}}{2r_{DMS,i}}$$

$$\left(1 - \Gamma_{\varepsilon,P,B}\right)\frac{\varepsilon_{max}}{F_{S,\varepsilon,B}} = \frac{t_{DMB}}{2r_{DMS,i}}$$

Solving the belt strain equation for $r_{DMS,i}$ leads to:

$$r_{DMS,i} = \frac{1}{2\left(1 - \Gamma_{\varepsilon,P,B}\right)}\frac{F_{S,\varepsilon,B}}{\varepsilon_{max}}t_{DMB}$$

The belt cross-sectional area A_{DMB} is as follows:

$$A_{DMB} = t_{DMB}b_{DMB}$$

The required belt cross-sectional area A_{DMB} is derived from the pulling force strain limit:

$$\varepsilon_{P,B} = \Gamma_{\varepsilon,P,B}\frac{\varepsilon_{max}}{F_{S,\varepsilon,B}} = \frac{P}{EA_{DMB}}$$

Solving for A_{DMB} leads to:

$$A_{DMB} = \frac{F_{S,\varepsilon,B}}{\varepsilon_{max}}\frac{1}{\Gamma_{\varepsilon,P,B}}\frac{1}{E}P$$

By introducing a belt thickness to width ratio Γ_b the belt width is eliminated as a variable:

$$\Gamma_b = \frac{t_{DMB}}{b_{DMB}}$$

Thereby the area becomes:

$$A_{DMB} = \frac{t_{DMB}^2}{\Gamma_b}$$

Solving for t_{DMB} leads to:

$$t_{DMB} = \sqrt{\Gamma_b A_{DMB}}$$

Substituting the area expression leads to the required belt thickness t_B expression:

$$t_{DMB} = \sqrt{\Gamma_b \frac{F_{S,\varepsilon,B}}{\Gamma_{\varepsilon,P,B}}\frac{P}{E\varepsilon_{max}}}$$

The belt width b_{DMB} is thereby:

$$b_{DMB} = \sqrt{\frac{F_{S,\varepsilon,B}}{\Gamma_b\Gamma_{\varepsilon,P,B}}\frac{P}{E\varepsilon_{max}}}$$

The mass m_{DMB} of the belt can now be derived. Here it is assumed that the belt length corresponds to the required length of the mast L_{req}:

$$m_{DMB} = A_{DMB} L_{req} \rho$$

$$m_{DMB} = \frac{t_{DMB}^2}{\Gamma_b} L_{req} \rho$$

Thereby the belt mass scaling function is as follows:

$$m_{DMB} = \frac{F_{S,\varepsilon,B}}{\Gamma_{\varepsilon,P,B}} \frac{\rho}{E \varepsilon_{max}} L_{req} P$$

The definition of the load that needs to be transmitted by the belt depends on the required deployment force which is defined by the designer.

The parameters of the support shell scaling functions are summarized in Tab. B - 21.

Parameters of the Belt			
Parameter	**Symbol**	**Unit**	**Value**
Belt length	L_{req}	m	Input value
Deployment force	P	N	Input value
Material modulus	E	N/m²	210 GPa
Material density	ρ	kg/m³	7800
Maximum elastic strain	ε_{max}	-	0.008
Belt strain ratio	$\Gamma_{\varepsilon,P,B}$	-	0.25
Factor of safety	$F_{S,\varepsilon,B}$	-	2

Tab. B - 21: Belt design parameters.

The scaling functions are summarized in Tab. B - 22.

Scaling Functions of the Belt
Scaling Approach: Maximum Elastic Strain
$m_{DMB} = \frac{F_{S,\varepsilon,B}}{\Gamma_{\varepsilon,P,B}} \frac{\rho}{E \varepsilon_{max}} L_{req} P$

Tab. B - 22: Belt scaling function according to a maximum elastic strain criterion.

B4.2 Belt Spool

The Belt Spool coils the belt and thereby transmits the deployment forces generated by the gear-motor to the belt. It consists of a cylinder with end caps to prevent slippage of the boom off the spool. The Belt Spool mass scaling function is derived from similarity to a reference design as displayed in Fig. B - 10.

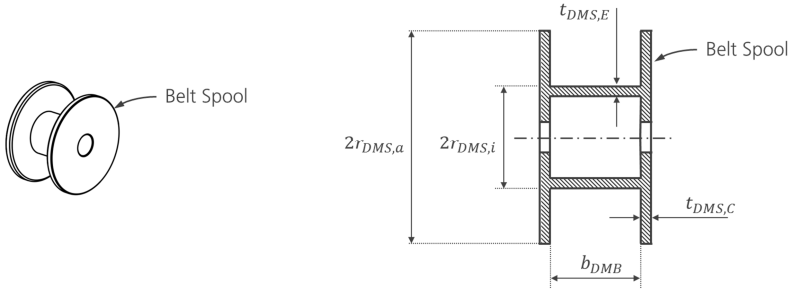

Fig. B - 10: Belt Spool for coiling of the belt (left) and geometrical properties of the reference design (right).

The radius of the cylindrical part of the Belt Spool $r_{DMS,i}$ is derived already in B4.1:

$$r_{DMS,i} = \frac{1}{2\left(1-\Gamma_{\varepsilon,P,B}\right)}\frac{F_{S,\varepsilon,B}}{\varepsilon_{max}}t_{DMB}$$

Substitution of the belt thickness t_{DMB} in the expression for the inner Belt Spool radius $r_{DMS,i}$ leads to:

$$r_{DMS,i} = \frac{\sqrt{\Gamma_b \frac{F_{S,\varepsilon,B}}{\Gamma_{\varepsilon,P,B}}\frac{P}{E\varepsilon_{max}}}}{2\varepsilon_{max}}\frac{F_{S,\varepsilon,B}}{\left(1-\Gamma_{\varepsilon,P,B}\right)}$$

$$r_{DMS,i} = \sqrt{\frac{\Gamma_b F_{S,\varepsilon,B}^3}{4\Gamma_{\varepsilon,P,B}\left(1-\Gamma_{\varepsilon,P,B}\right)^2}\frac{P}{E\varepsilon_{max}^3}}$$

The width of the spool is given by the belt width b_{DMB}. The outer radius of the spool $r_{DMS,a}$ is derived from the inner spool radius $r_{DMS,i}$ and the length L and thickness of the belt t_{DMB}:

$$\pi r_{DMS,a}^2 = \pi r_{DMS,i}^2 + L t_{DMB}$$

$$r_{DMS,a} = \sqrt{\frac{\pi r_{DMS,i}^2 + L t_{DMB}}{\pi}}$$

To account for gaps between windings and to avoid slipping of the belt off the edge of the Spool End Caps, the outer radius is increased by a factor $k_{DMS,ra}$:

$$r_{DMS,a} = k_{DMS,ra}\sqrt{r_{DMS,i}^2 + \frac{1}{\pi}L t_{DMB}}$$

Substituting the expressions for the inner radius and the belt thickness results in:

$$r_{DMS,a} = k_{DMS,ra}\sqrt{\frac{1}{4}\frac{\Gamma_b F_{S,\varepsilon,B}^3}{\Gamma_{\varepsilon,P,B}\left(1-\Gamma_{\varepsilon,P,B}\right)^2}\frac{P}{E\varepsilon_{max}^3} + \frac{1}{\pi}L\sqrt{\Gamma_b\frac{F_{S,\varepsilon,B}}{\Gamma_{\varepsilon,P,B}}\frac{P}{E\varepsilon_{max}}}}$$

As the dimensions of the inner and outer radius $r_{DMS,i}$ and $r_{DMS,a}$ as well as the spool width b_{DMB} are known, the mass scaling function can be derived. As introduced above the mass of the Belt Spool m_{DMS} is calculated by assuming a spool that consists of a cylindrical spool core of radius $r_{DMS,i}$ enclosed by two end caps of radius $r_{DMS,a}$. The thickness of the end caps $t_{DMS,E}$ is given as a ratio $\Gamma_{t,E}$ of the spool width which coincides with the belt width b_{DMB}:

$$\frac{t_{DMS,E}}{b_{DMB}} = \Gamma_{t,E}$$

The thickness of the Belt Spool core $t_{DMS,C}$ is also given as a ratio $\Gamma_{t,C}$ of the belt width b_{DMB}:

$$\frac{t_{DMS,C}}{b_{DMB}} = \Gamma_{t,C}$$

The expression for the belt width b_{DMB} can be replaced in both ratios by the belt thickness t_{DMB}:

$$\frac{t_{DMS,E}}{t_{DMB}} = \frac{\Gamma_{t,E}}{\Gamma_b}$$

$$\frac{t_{DMS,C}}{t_{DMB}} = \frac{\Gamma_{t,C}}{\Gamma_b}$$

Thereby the mass of the Belt Spool m_{DMS} can be calculated as follows:

$$m_{DMS} \approx \left(2\pi r_{DMS,a}^2 t_{DMS,E} + 2\pi r_{DMS,i} t_{DMS,C} b_{DMB}\right)\rho$$

Substitution of the end cap and spool core thickness leads to:

$$m_{DMS} \approx 2\pi\left(r_{DMS,a}^2 \frac{\Gamma_{t,E}}{\Gamma_b} t_{DMB} + r_{DMS,i} \frac{\Gamma_{t,C}}{\Gamma_b} t_{DMB} b_{DMB}\right)\rho$$

$$m_{DMS} \approx 2\pi\left(r_{DMS,a}^2 \frac{\Gamma_{t,E}}{\Gamma_b} t_{DMB} + r_{DMS,i} \frac{\Gamma_{t,C}}{\Gamma_b^2} t_{DMB}^2\right)\rho$$

Substituting the inner and outer radii results in:

$$m_{DMS} \approx 2\pi\left(\left(k_{DMS,ra}\sqrt{\frac{1}{4}\frac{\Gamma_b F_{S,\varepsilon,B}^3}{\Gamma_{\varepsilon,P,B}\left(1-\Gamma_{\varepsilon,P,B}\right)^2}\frac{P}{E\varepsilon_{max}^3} + \frac{1}{\pi}L\sqrt{\Gamma_b\frac{F_{S,\varepsilon,B}}{\Gamma_{\varepsilon,P,B}}\frac{P}{E\varepsilon_{max}}}}\right)^2 \frac{\Gamma_{t,E}}{\Gamma_b} t_{DMB} + \sqrt{\frac{\Gamma_b F_{S,\varepsilon,B}^3}{4\Gamma_{\varepsilon,P,B}\left(1-\Gamma_{\varepsilon,P,B}\right)^2}\frac{P}{E\varepsilon_{max}^3}}\frac{\Gamma_{t,C}}{\Gamma_b^2} t_{DMB}^2\right)\rho$$

$$m_{DMS} \approx 2\pi\left(k_{DMS,ra}^2\left(\frac{1}{4}\frac{\Gamma_b F_{S,\varepsilon,B}^3}{\Gamma_{\varepsilon,P,B}\left(1-\Gamma_{\varepsilon,P,B}\right)^2}\frac{P}{E\varepsilon_{max}^3} + \frac{1}{\pi}L\sqrt{\Gamma_b\frac{F_{S,\varepsilon,B}}{\Gamma_{\varepsilon,P,B}}\frac{P}{E\varepsilon_{max}}}\right)^2 \frac{\Gamma_{t,E}}{\Gamma_b} t_{DMB} + \sqrt{\frac{\Gamma_b F_{S,\varepsilon,B}^3}{4\Gamma_{\varepsilon,P,B}\left(1-\Gamma_{\varepsilon,P,B}\right)^2}\frac{P}{E\varepsilon_{max}^3}}\frac{\Gamma_{t,C}}{\Gamma_b^2} t_{DMB}^2\right)\rho$$

Substitution of the belt thickness expression and equating the belt length with the mast length L_{req} leads to:

$$m_{DMS} \approx 2\pi\left(k_{DMS,ra}^2\left(\frac{1}{4}\frac{\Gamma_b F_{S,\varepsilon,B}^3}{\Gamma_{\varepsilon,P,B}\left(1-\Gamma_{\varepsilon,P,B}\right)^2}\frac{P}{E\varepsilon_{max}^3} + \frac{1}{\pi}L_{req}\sqrt{\Gamma_b\frac{F_{S,\varepsilon,B}}{\Gamma_{\varepsilon,P,B}}\frac{P}{E\varepsilon_{max}}}\right)^2 \frac{\Gamma_{t,E}}{\Gamma_b}\sqrt{\Gamma_b\frac{F_{S,\varepsilon,B}}{\Gamma_{\varepsilon,P,B}}\frac{P}{E\varepsilon_{max}}} + \sqrt{\frac{\Gamma_b F_{S,\varepsilon,B}^3}{4\Gamma_{\varepsilon,P,B}\left(1-\Gamma_{\varepsilon,P,B}\right)^2}\frac{P}{E\varepsilon_{max}^3}}\frac{\Gamma_{t,C}}{\Gamma_b^2}\Gamma_b\frac{F_{S,\varepsilon,B}}{\Gamma_{\varepsilon,P,B}}\frac{P}{E\varepsilon_{max}}\right)\rho$$

$$m_{DMS} \approx 2\pi\left(k_{DMS,ra}^2\left(\frac{1}{4}\frac{\Gamma_b F_{S,\varepsilon,B}^3}{\Gamma_{\varepsilon,P,B}\left(1-\Gamma_{\varepsilon,P,B}\right)^2}\frac{P}{E\varepsilon_{max}^3} + \frac{1}{\pi}L_{req}\sqrt{\Gamma_b\frac{F_{S,\varepsilon,B}}{\Gamma_{\varepsilon,P,B}}\frac{P}{E\varepsilon_{max}}}\right)^2 \frac{\Gamma_{t,E}}{\Gamma_b}\sqrt{\Gamma_b\frac{F_{S,\varepsilon,B}}{\Gamma_{\varepsilon,P,B}}\frac{P}{E\varepsilon_{max}}} + \sqrt{\frac{\Gamma_b F_{S,\varepsilon,B}^3}{4\Gamma_{\varepsilon,P,B}\left(1-\Gamma_{\varepsilon,P,B}\right)^2}\frac{P}{E\varepsilon_{max}^3}}\frac{\Gamma_{t,C}}{\Gamma_b\Gamma_{\varepsilon,P,B}}\frac{F_{S,\varepsilon,B}}{E\varepsilon_{max}}P\right)\rho$$

Through substitution of the recurring term by Υ the mass scaling function of the Belt Spool can be written as follows:

$$m_{DMS} \approx 2\pi \left(k_{DMS,ra}^2 \left(\frac{1}{4} \frac{F_{S,\varepsilon,B}^2}{\left(1-\Gamma_{\varepsilon,P,B}\right)^2} \Upsilon + \frac{1}{\pi} L_{req} \sqrt{\Upsilon} \right)^2 \frac{\Gamma_{t,E}}{\Gamma_b} \sqrt{\Upsilon} + \frac{\Gamma_{t,C}}{\Gamma_b^2} \sqrt{\frac{F_{S,\varepsilon,B}^2}{4\left(1-\Gamma_{\varepsilon,P,B}\right)^2} \Upsilon^3} \right) \rho$$

$$\Upsilon = \Gamma_b \frac{F_{S,\varepsilon,B}}{\Gamma_{\varepsilon,P,B}} \frac{P}{E\varepsilon_{max}}$$

The parameters of the support shell scaling functions are summarized in Tab. B - 23.

Parameters of the Belt Spool			
Parameter	**Symbol**	**Unit**	**Value**
Belt length	L_{req}	m	Input value
Deployment force	P	N	Input value
Material modulus	E	N/m²	210 GPa
Material density	ρ	kg/m³	2700
Maximum elastic strain	ε_{max}	-	0.008
Belt width ratio	Γ_b	-	0.0025
Belt strain ratio	$\Gamma_{\varepsilon,P,B}$	-	0.25
Belt Spool End Cap wall thickness ratio	$\Gamma_{t,E}$	-	0.05
Belt Spool central cylinder wall thickness ratio	$\Gamma_{t,C}$	-	0.05
Belt volume factor	$k_{DMS,ra}$	-	1.5
Factor of safety	$F_{S,\varepsilon,B}$	-	2

Tab. B - 23: Belt Spool design parameters.

The scaling functions are summarized in Tab. B - 24.

Scaling Functions of the Belt Spool
Scaling Approach: Geometric Similarity based on a Design Reference Model in combination with a Design Load
$m_{DMS} \approx 2\pi \left(k_{DMS,ra}^2 \left(\frac{1}{4} \frac{F_{S,\varepsilon,B}^2}{\left(1-\Gamma_{\varepsilon,P,B}\right)^2} \Upsilon + \frac{1}{\pi} L_{req} \sqrt{\Upsilon} \right)^2 \frac{\Gamma_{t,E}}{\Gamma_b} \sqrt{\Upsilon} + \frac{\Gamma_{t,C}}{\Gamma_b^2} \sqrt{\frac{F_{S,\varepsilon,B}^2}{4\left(1-\Gamma_{\varepsilon,P,B}\right)^2} \Upsilon^3} \right) \rho$
$\Upsilon = \Gamma_b \frac{F_{S,\varepsilon,B}}{\Gamma_{\varepsilon,P,B}} \frac{P}{E\varepsilon_{max}}$

Tab. B - 24: Belt Spool scaling function.

B4.3 Gear

For sizing of the gear (index DMG) the required output torque has to be known.

Gear Output Torque

The required gear output torque T_G is given by the outer radius of the spool with fully coiled belt and the pulling force the system has to provide. The outer radius r_o of the spool with coiled belt corresponds to the Belt Spool End Cap radius $r_{BS,a}$ without consideration of the belt volume factor as follows:

$$r_o = \frac{r_{DMS,a}}{k_{DMS,ra}} = \sqrt{\frac{1}{4}\frac{\Gamma_b F_{S,\varepsilon,B}^3}{\Gamma_{\varepsilon,P,B}\left(1-\Gamma_{\varepsilon,P,B}\right)^2}\frac{P}{E\varepsilon_{max}^3} + \frac{1}{\pi}L\sqrt{\Gamma_b\frac{F_{S,\varepsilon,B}}{\Gamma_{\varepsilon,P,B}}\frac{P}{E\varepsilon_{max}}}}$$

The required torque provided by the gear is as follows:

$$T_G = r_o P$$

The force P that needs to be transmitted by the Belt Mechanism depends on the required deployment force of the mast, internal friction in the mechanism and other constraining components such as the brake of the boom spool to prevent self-deployment. Here a safety factor $F_{S,P,BM}$ for design of the Belt Mechanism is introduced to account for these effects:

$$P = F_{S,P,BM}P_{pull}$$

For derivation of the nominal pulling force P_{pull} several approaches may be used:

→ Design load: P_{req}
→ Maximum load: P_{max}
→ Euler load: P_E
→ …

The resulting torque that needs to be provided by the gear T_G is as follows:

$$T_G = r_o P$$

$$T_G = \sqrt{\frac{\Gamma_b F_{S,\varepsilon,B}^3}{4\Gamma_{\varepsilon,P,B}\left(1-\Gamma_{\varepsilon,P,B}\right)^2}\frac{P}{E\varepsilon_{max}^3} + \sqrt{\frac{1}{\pi^2}\Gamma_b\frac{F_{S,\varepsilon,B}}{\Gamma_{\varepsilon,P,B}}\frac{P}{E\varepsilon_{max}}L_{req}^2 P}}$$

$$T_G = \left(\frac{1}{4}\Gamma_b\frac{F_{S,\varepsilon,B}^3}{\Gamma_{\varepsilon,P,B}\left(1-\Gamma_{\varepsilon,P,B}\right)^2}\frac{1}{E\varepsilon_{max}^3}P^3 + \left(\frac{1}{\pi^2}\Gamma_b\frac{F_{S,\varepsilon,B}}{\Gamma_{\varepsilon,P,B}}\frac{1}{E\varepsilon_{max}}P^5 L_{req}^2\right)^{\frac{1}{2}}\right)^{\frac{1}{2}}$$

The parameters for the gear output torque scaling function are the same as for the Belt Spool summarized in Tab. B - 24.

Gear Mass Scaling Function

The gear mass is described based on the torque T_G it has to provide. As a gear is a complex assembly of many components and its design influenced by several parameters, catalogue data of commercially available gears from Maxon Motor AG [141] and Dr. Fritz Faulhaber GmbH & Co. KG [142] suited for high vacuum and space applications are used to derive the relation between torque and gear mass. Fig. B - 11 plots the gear mass m_G (in g) and an approximation curve over the output torque T_G.

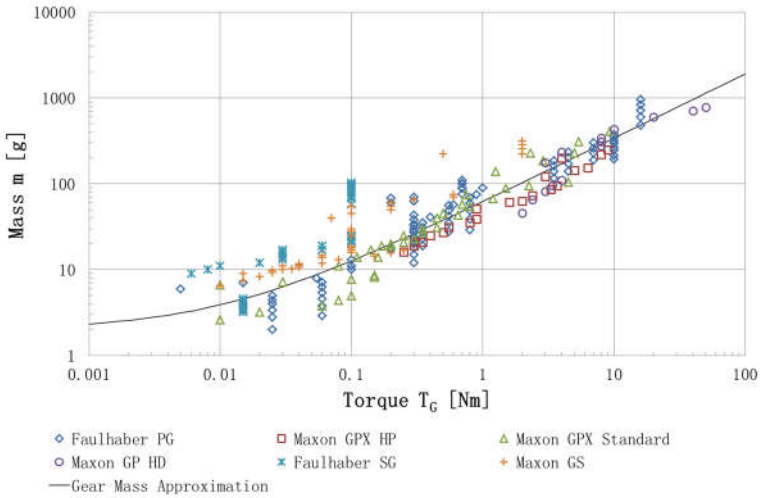

Fig. B - 11: Gear mass of commercially available products of the companies Maxon Motor AG [141] and Dr. Fritz Faulhaber GmbH & Co. KG [142] and an approximation curve plotted over output torque.

From these catalogue data the gear mass is described by the following power law:

$$m_{DMG} = \xi_{G,1} T_G^{\xi_{G,2}} + \xi_{G,3}$$

The constant $\xi_{G,3}$ describes the lower scaling limit of a gear. The coefficients of the approximation function are selected as follows:

$$\xi_{G,1} = 60 \left[\frac{\mathrm{g}}{(\mathrm{Nm})^{b_G}}\right]$$

$$\xi_{G,2} = 0.75 \text{ [-]}$$

$$\xi_{G,3} = 2 \text{ [g]}$$

In addition to these parameters, the gear mass scaling function depends on the same parameters as for the Belt Spool summarized in Tab. B - 24.

The torque and gear mass scaling function are summarized in Tab. B - 25.

Scaling Functions of the Gear Output Torque and Mass
Scaling Approach: Processing of Catalogue Data
$T_G = \left(\frac{1}{4}\Gamma_b \frac{F_{S,\varepsilon,B}^3 F_{S,P,BM}^2}{\Gamma_{\varepsilon,P,B}\left(1-\Gamma_{\varepsilon,P,B}\right)^2} \frac{1}{E\varepsilon_{max}^3} P_{req}^3 + \left(\frac{1}{\pi^2}\Gamma_b \frac{F_{S,\varepsilon,B} F_{S,P,BM}^5}{\Gamma_{\varepsilon,P,B}} \frac{1}{E\varepsilon_{max}} P_{req}^5 L_{req}^2\right)^{\frac{1}{2}}\right)^{\frac{1}{2}}$
$m_{DMG} = \xi_{G,1} T_G^{\xi_{G,2}} + \xi_{G,3}$

Tab. B - 25: Gear torque and mass scaling functions.

B4.4 Electric Motor

The electric motor (index DMM) generates the deployment forces in the first place from electric energy provided by the host spacecraft. For sizing of the motor first the required motor torque has to be determined.

Motor Output Torque

The required output torque of the electric motor T_{EM} is given by the output torque of the gear T_G, the gear transmission ratio k_G and the efficiency of the gear η_G:

$$T_{EM} = \frac{1}{\eta_G}\frac{T_G}{k_G}$$

The gear transmission ratio is chosen qualitatively with respect to the desired deployment speed. Common gear ratios of planetary gears are between $1{:}50$ and $1{:}500$. Common gear efficiencies of planetary gears are between 80% for a small number of gear stages and 50% for a high number.

Electric Motor Mass Scaling Function

The mass is derived based on the generated torque of the motor. As an electric motor is a complex assembly of many components and its design influenced by several parameters, here the motor mass equation is derived by catalogue data of commercially available motors of the companies Maxon Motor AG [141], Dr. Fritz Faulhaber GmbH & Co. KG [142] and Phytron GmbH [143] that are suited for high vacuum and space applications. Fig. B - 12 plots the motor mass (in g) and an approximation curve over the generated torque (in mNm).

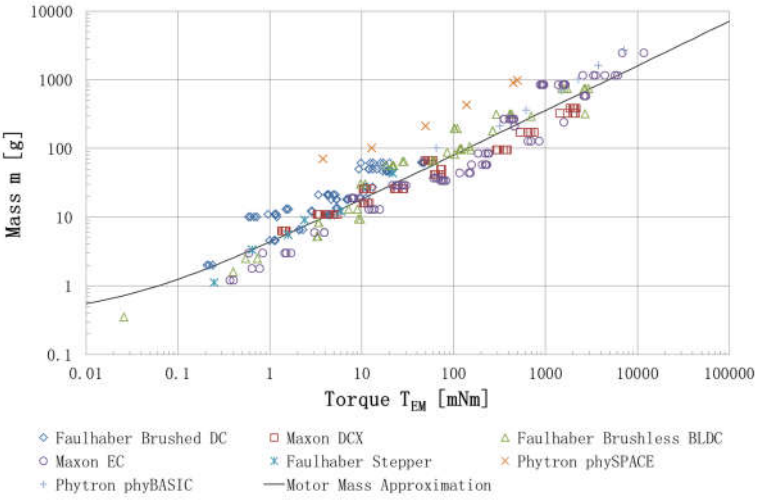

Fig. B - 12: Electric motor mass of commercially available products of the companies Maxon Motor AG [141], Dr. Fritz Faulhaber GmbH & Co. KG [142] and Phytron GmbH [143] and an approximation curve plotted over output torque.

The motor mass m_{DMM} is described by the following power law:

$$m_{DMM} = \chi_{EM,1} T_{EM}^{\chi_{EM,2}} + \chi_{EM,3}$$

The constant $\chi_{EM,3}$ describes the lower scaling limit of electric motors. The coefficients of the approximation function are as follows:

$$\chi_{EM,1} = 4 \left[\frac{\mathrm{g}}{(\mathrm{mNm})^{b_M}}\right]$$
$$\chi_{EM,2} = 0.65 \text{ [-]}$$
$$\chi_{EM,3} = 0.35 \text{ [g]}$$

Substitution of the required motor torque leads to the motor mass scaling function:

$$m_{DMM} = \chi_{EM,1} \left(\frac{1}{\eta_G} \frac{T_G}{k_G}\right)^{\chi_{EM,2}} + \chi_{EM,3}$$

The electric motor mass scaling function is summarized in Tab. B - 26.

Scaling Functions of the Electric Motor Output Mass
Scaling Approach: Processing of Catalogue Data
$m_{DMM} = \chi_{EM,1} \left(\frac{1}{\eta_G} \frac{T_G}{k_G}\right)^{\chi_{EM,2}} + \chi_{EM,3}$

Tab. B - 26: Electric motor mass scaling funtion.

B5 Mechanical Support Structure

The Mechanical Support Structure (index SS) consists of a rectangular box composed of six panels which all possess same architecture and thickness. The panels which are decisive for the mechanical sizing are the side panels which support the internal mechanism components and the stowed mast. Thereby it is assumed that the masses of the supported components are concentrated in a central point mass m_0 and significantly larger than the panel mass. The scaling function of the side panels is derived through approximation as a spring pendulum on the basis of the scaling function of a plate with four simply supported edges and a heavy center mass as detailed in A4.2. Therefore the parameters are adjusted accordingly. The plate dimensions of the length a and width b are substituted by parameters that are to be defined in relation to the masts stowed form such as displayed in Fig. B - 13:

$$a = S_a$$
$$b = S_b$$

The attached mass m_0 includes the masses of the mast and all mechanism components and is not further detailed. The areal mass scaling function of the side panel γ_{SS}:

$$\gamma_{SS} = \left(\frac{16}{\pi^2} k_m^3 \frac{1}{S_a S_b \left(\frac{1}{S_a^2} + \frac{1}{S_b^2}\right)^2} \frac{(1-\nu^2) k_\rho^3 \rho^{*3}}{k_D E} f_{req}^2 m_0 \right)^{\frac{1}{3}}$$

The mass scaling function of the Support Structure is as gained through multiplication with the outer surface as follows:

$$m_{SS} = 2(S_a S_b + S_a S_c + S_b S_c)\left(\frac{16}{\pi^2} k_m^3 \frac{1}{S_a S_b \left(\frac{1}{S_a^2} + \frac{1}{S_b^2}\right)^2} \frac{(1-\nu^2) k_\rho^3 \rho^{*3}}{k_D E} f_{req}^2 m_0\right)^{\frac{1}{3}}$$

$$m_{SS} = \left(\frac{128}{\pi^2} k_m^3 \frac{(S_a S_b + S_a S_c + S_b S_c)^3}{S_a S_b \left(\frac{1}{S_a^2} + \frac{1}{S_b^2}\right)^2} \frac{(1-\nu^2) k_\rho^3 \rho^{*3}}{k_D E} f_{req}^2 m_0\right)^{\frac{1}{3}}$$

A scaling limit is introduced in terms of a minimum wall thickness $t_{SS,min}$. The resulting support structure mass scaling function $m_{SS,min}$ is as follows:

$$m_{SS,min} = 2(S_a S_b + S_a S_c + S_b S_c) k_\rho \rho^* t_{SS,min}$$

Furthermore the outer dimensions of the support structure define the volume of the Deployment Mechanism and thereby the volume V of the entire mast as all other mechanism components are enclosed by the support structure:

$$V_{SS} = S_a S_b S_c$$

The volume is derived from a design sketch such as displayed in Fig. B - 13 which relates the support structure dimensions S_a, S_B and S_c to the dimensions of the stowed mast.

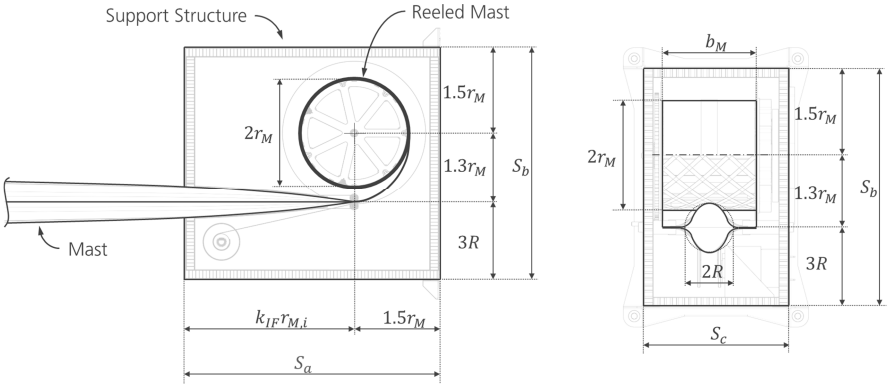

Fig. B - 13: Design sketch of the outer support structure dimensions in relation to the geometry properties of the stowed mast.

The parameters of the Support Structure scaling functions are summarized in Tab. B - 27.

Parameters of the Support Structure			
Parameter	**Symbol**	**Unit**	**Value**
Structure length	S_a	m	Input value
Structure height	S_b	m	Input value

Structure width	S_c	m	Input value
Material modulus	E	N/m²	60 GPa
Reference density	ρ^*	kg/m³	1600
Poisson ratio	ν	-	0.3
Minimum eigenfrequency	f_{req}	Hz	100
Attached mass	m_0	kg	Input value
Density factor	k_ρ	-	100/1600 (Sandwich Architecture)
Plate mass architecture factor	k_m	-	0.111 (Sandwich Architecture)
Plate flexural rigidity architecture factor	k_D	-	0.0125 (Sandwich Architecture)
Minimum wall thickness	$t_{SS,min}$	m	0.003 (Sandwich Architecture)

Tab. B - 27: Support Structure design parameters.

The scaling functions are summarized in Tab. B - 28.

Scaling Functions of a Plate with Four Simply Supported Edges and Additional Center Mass
Scaling Approach: Eigenfrequency Solution (Mass) and Relation to Stowed Mast Form (Volume)
$$m_{SS} = \left(\frac{128}{\pi^2} k_m^3 \frac{(S_a S_b + S_a S_c + S_b S_c)^3}{S_a S_b \left(\frac{1}{S_a^2} + \frac{1}{S_b^2}\right)^2} \frac{(1-\nu^2) k_\rho^3 \rho^{*3}}{k_D E} f_{req}^2 m_0 \right)^{\frac{1}{3}}$$
$$m_{SS,min} = 2(S_a S_b + S_a S_c + S_b S_c) k_\rho \rho^* t_{SS,min}$$
$$V_{SS} = S_a S_b S_c$$

Tab. B - 28: Mass and volume scaling function of the box-shaped Deployment Mechanism Support Structure.

Appendix C

C Overall System Scaling Function

Within Appendix C the derivation of the system scaling function for deployable masts is described.

C1 General Mast Sizing Solution

The scaling functions of the mechanism components largely depend on the sizing results of the Deformable Structure. The sizing of the Deformable Structure is done through constraint functions derived from the specific load case and the structural architecture of the mast. As there are two design variables (mast cross-sectional area A and mast radius R) two constraint functions are required. The specific constraint functions utilized within this system analysis can be written as power functions which enables formulation of a general mast sizing solution. The constraint functions can be written in the following form with a constant left side represented by the parameter c and a term consisting of the design variables A and R:

$$c_1 \leq A^{i_1} R^{j_1}$$
$$c_2 \leq A^{i_2} R^{j_2}$$

The minimum mass solution exactly fulfills both constraint equations:

$$c_1 = A^{i_1} R^{j_1}$$
$$c_2 = A^{i_2} R^{j_2}$$

Solving equation 1 for R:

$$R = \left(\frac{c_1}{A^{i_1}}\right)^{\frac{1}{j_1}}$$

Substituting in equation 2:

$$c_2 = A^{i_2}\left(\left(\frac{c_1}{A^{i_1}}\right)^{\frac{1}{j_1}}\right)^{j_2}$$

Solving for A:

$$c_2 = \frac{A^{i_2}}{A^{i_1\frac{j_2}{j_1}}} c_1^{\frac{j_2}{j_1}}$$

$$c_2 = \frac{c_1^{\frac{j_2}{j_1}}}{A^{i_1\frac{j_2}{j_1} - i_2}}$$

$$c_2 = \frac{c_1^{\frac{j_2}{j_1}}}{A^{\frac{i_1 j_2 - i_2 j_1}{j_1}}}$$

$$A = \left(\frac{c_1^{\frac{j_2}{j_1}}}{c_2}\right)^{\frac{j_1}{i_1 j_2 - i_2 j_1}}$$

The general solution for the required cross-sectional area A to comply with the constraint equations is as follows:

$$A = \left(\frac{c_1^{j_2}}{c_2^{j_1}}\right)^{\frac{1}{i_1 j_2 - i_2 j_1}}$$

Substituting A in the radius expression R:

$$R = \left(\frac{c_1}{\left(\left(\frac{c_1^{j_2}}{c_2^{j_1}} \right)^{\frac{1}{i_1 j_2 - i_2 j_1}} \right)^{i_1}} \right)^{\frac{1}{j_1}}$$

$$R = \frac{c_1^{\frac{1}{j_1}}}{\left(\frac{c_1^{j_2}}{c_2^{j_1}} \right)^{\frac{i_1}{j_1 (i_1 j_2 - i_2 j_1)}}}$$

$$R = \frac{c_1^{\frac{1}{j_1}}}{c_1^{\frac{i_1 j_2}{j_1 (i_1 j_2 - i_2 j_1)}}} c_2^{\frac{i_1}{i_1 j_2 - i_2 j_1}}$$

$$R = \frac{c_2^{\frac{i_1}{i_1 j_2 - i_2 j_1}}}{c_1^{\frac{i_1 j_2}{j_1 (i_1 j_2 - i_2 j_1)} - \frac{1}{j_1}}}$$

$$R = \frac{c_2^{\frac{i_1}{i_1 j_2 - i_2 j_1}}}{c_1^{\frac{i_1 j_2}{j_1 (i_1 j_2 - i_2 j_1)} - \frac{i_1 j_2 - i_2 j_1}{j_1 (i_1 j_2 - i_2 j_1)}}}$$

The general solution for the required cross-sectional radius R to comply with the constraint equations is as follows:

$$R = \left(\frac{c_2^{i_1}}{c_1^{i_2}} \right)^{\frac{1}{i_1 j_2 - i_2 j_1}}$$

The general mast sizing solutions for mast cross-sectional area A and mast radius R are summarized in Tab. C - 1.

General Mast Sizing Solution	
First constraint function	$c_1 \leq A^{i_1} R^{j_1}$
Second constraint function	$c_2 \leq A^{i_2} R^{j_2}$
Mast cross-section area solution	$A = \left(\frac{c_1^{j_2}}{c_2^{j_1}} \right)^{\frac{1}{i_1 j_2 - i_2 j_1}}$
Mast radius solution	$R = \left(\frac{c_2^{i_1}}{c_1^{i_2}} \right)^{\frac{1}{i_1 j_2 - i_2 j_1}}$

Tab. C - 1: Constraint equations and general mast sizing solution.

C2 Design Interaction Factor

The general approach to derive the mast parameters presented above is to calculate those parameter values that just satisfy the load case constraints and thereby give the minimum mass of the mast structure. Thereby the design is already fully determined and the system mass only a result of the structural mast design. However, the working hypothesis is that the minimum of the overall system mass differs from the system mass derived by the approach of the minimum mast mass. It is hypothesized that it is beneficial to "invest" additional mass into the mast structure as other components can be made more lightweight in response which lowers the overall system mass. Hence, the approach for the overall system mass minimum is to increase the mast cross-sectional area A above the required minimum solution A^*. Thereby the cross-sectional geometry can be altered in a certain interval and still complies with the load case constraints. To gain the overall minimum system mass the required additional mast mass needs to be determined.
Fig. C - 1 shows an example of a tubular column under compression load. The compression strength ratio P_E/P_{req} for global Euler buckling and P_σ/P_{req} for local wall buckling is plotted over the radius ratio R/R^*. The increasing parts of the curves are the global Euler and the decreasing parts the local wall buckling strength. The required global and local compression strength is satisfied for the minimum mass column in exactly one point at $[1,1]$. Therefore no variation of radius R is possible. By increasing the cross-sectional area A (and thereby mass) of the column by 10%, the requirements are satisfied for a radius ratio interval between 0.95 and 1.08.

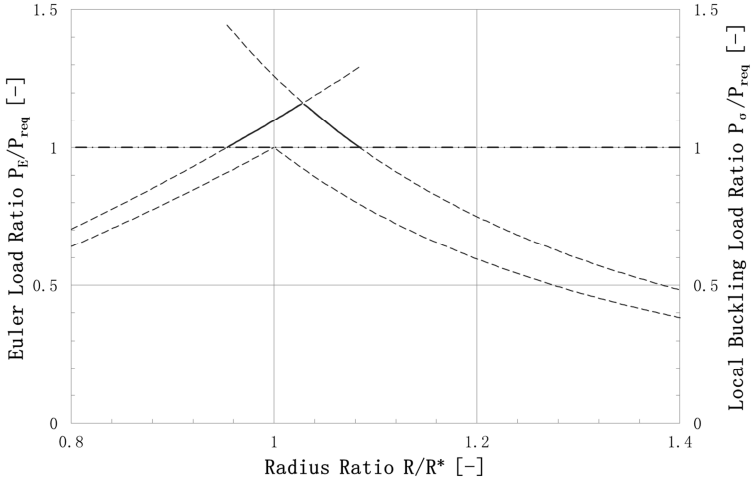

Fig. C - 1: Constraint function results for normalized global (primary y-axis) and local buckling load (secondary y-axis) plotted over the normalized radius for the minimum mass solution (lower dotted curve) and increased mass solution (upper dotted curve) with highlighted valid results (solid curve).

Fig. C - 2 shows an example of a tubular column under bending load. The bending stiffness ratio EI/EI_{req} and the critical bending moment ratio M/M_{req} is plotted over the radius ratio R/R^*. The increasing parts of the curves represent the bending stiffness ratios and the decreasing parts the

critical bending moment ratios. The required bending stiffness and critical bending moment are satisfied for the minimum mass column in exactly one point at $[1,1]$. Therefore no variation of radius R is possible. By increasing the cross-sectional area A (and thereby mass) of the column by 10%, the requirements are satisfied for a radius ratio interval between 0.95 and 1.15.

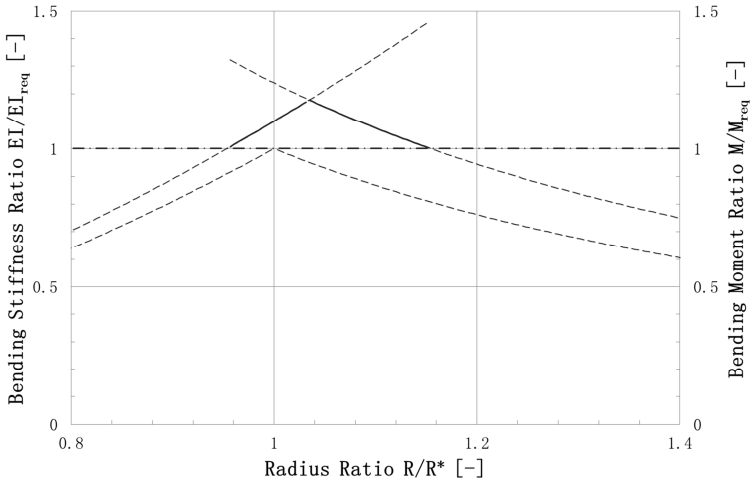

Fig. C - 2: Constraint function results for normalized bending stiffness (primary y-axis) and critical bending moment (secondary y-axis) plotted over the normalized radius for the minimum mass solution (lower dotted curve) and increased mass solution (upper dotted curve) with highlighted valid results (solid curve).

The increase in cross-sectional area and thereby mass of the mast relative to the exact solution A^* is given by the parameter g:

$$\frac{A}{A^*} = g$$

For $g > 1$ the structural and geometrical requirements are satisfied not only in one single set of cross-sectional parameters but in an interval allowing variation of these parameters. The minimum system mass is gained at the boundaries of the interval. Otherwise an overly large value for g is chosen and thereby an overly heavy mast is used. Therefore, equating the structural and geometrical requirements to gain the mast mass equation is no longer valid. Instead a single constraint is exactly met while the other is exceeded. The radius R corresponding to the cross-sectional area A increased by the parameter g in relation to the reference solution A^* is calculated from the remaining constraint equation:

$$c = A^i R^j$$

The cross-sectional area A is known by the parameter g and the reference solution A^*. The reference solution for the radius R^* is as follows:

$$c = A^{*i} R^{*j}$$

$$R^* = \left(\frac{c}{A^{*i}}\right)^{\frac{1}{j}}$$

Solving the remaining constraint equation for the radius R leads to:

$$c = (gA^*)^i R^j$$

$$R = \left(\frac{c}{(gA^*)^i}\right)^{\frac{1}{j}}$$

Substitution with the radius reference solution R^* allows formulation of the corresponding radius R dependent on the parameter g:

$$R = \left(\frac{1}{g^i}\frac{c}{A^{*i}}\right)^{\frac{1}{j}}$$

$$R = \frac{1}{g^{\frac{i}{j}}}R^*$$

$$\frac{R}{R^*} = g^{-\frac{i}{j}}$$

It needs to be checked if the solution of one constraint equation causes exceeding or violating the other:

$$c_1 = A^{i_1}R^{j_1}$$

$$c_2 \leq A^{i_2}R^{j_2}$$

The solution of the first constraint is as follows:

$$A = A^*g$$

$$R = R^*g^{-\frac{i_1}{j_1}}$$

Substituting the expressions in the second constraint equation leads to:

$$c_2 \leq (A^*g)^{i_2}\left(R^*g^{-\frac{i_1}{j_1}}\right)^{j_2}$$

The left side is given by the reference solution:

$$c_2 = A^{*i_2}R^{*j_2}$$

Substitution leads to:

$$A^{*i_2}R^{*j_2} \leq A^{*i_2}g^{i_2}R^{*j_2}g^{-\frac{i_1 j_2}{j_1}}$$

$$1 \leq g^{i_2-\frac{i_1 j_2}{j_1}}$$

For a valid solution that does not violate the unconsidered constrain equation, the following inequation needs to be satisfied (inequality signs may be reversed):

$$1 \leq g^{\frac{i_2 j_1 - i_1 j_2}{j_1}}$$

As it is always $g \geq 1$, the exponent $\frac{i_2 j_1 - i_1 j_2}{j_1}$ needs to be above or below zero depending on the type of inequality sign to gain a valid solution:

$$\frac{i_2 j_1 - i_1 j_2}{j_1} \geq 0 \text{ for } c_2 \leq A^{i_2}R^{j_2}$$

$$\frac{i_2 j_1 - i_1 j_2}{j_1} \leq 0 \text{ for } c_2 \geq A^{i_2}R^{j_2}$$

The solutions for the mast with increased cross-sectional area A over the reference solution A^* and the corresponding radius as well as the criteria for valid solutions are summarized in Tab. C - 2.

Mast Sizing Solution with Increased Cross-Sectional Area by g	
Mast cross-sectional area solution	$A = A^*g$
Mast radius solution	$R = R^*g^{-\frac{i}{j}}$

Validity criteria	$\frac{i_2 j_1 - i_1 j_2}{j_1} \geq 0$ for $c_2 \leq A^{i_2} R^{j_2}$ $\frac{i_2 j_1 - i_1 j_2}{j_1} \leq 0$ for $c_2 \geq A^{i_2} R^{j_2}$

Tab. C - 2: Sizing solutions for the mast with increased cross-sectional area over the refenrence and criteria for solution validity.

C3 System Scaling Function

For derivation of the system scaling function the Deployment Mechanism components are sized according to the sizing results of the mast. To reduce the number of variables the load and size requirements are coupled which can be done for many deployable systems as load in general scales with size for same remaining mission and system requirements. For many structures the size can be expressed by one characteristic length L to which all other dimensions are related. Hence, the design relevant loads can be expressed as a function of the characteristic length:

$$P_{req} = f_P(L)$$
$$M_{req} = f_M(L)$$
$$EI_{req} = f_{EI}(L)$$

Based on the coupling of load and size the system properties are derived. Fig. C - 3 describes the analysis flow to derive the system mass of a mast concept for a certain size interval $L_0 \leq L \leq L_{max}$ and size increment ΔL. For each length the mass functions for a size factor interval $1 \leq g \leq g_{max}$ are calculated and the values g_{opt} leading to the lowest masses are derived.

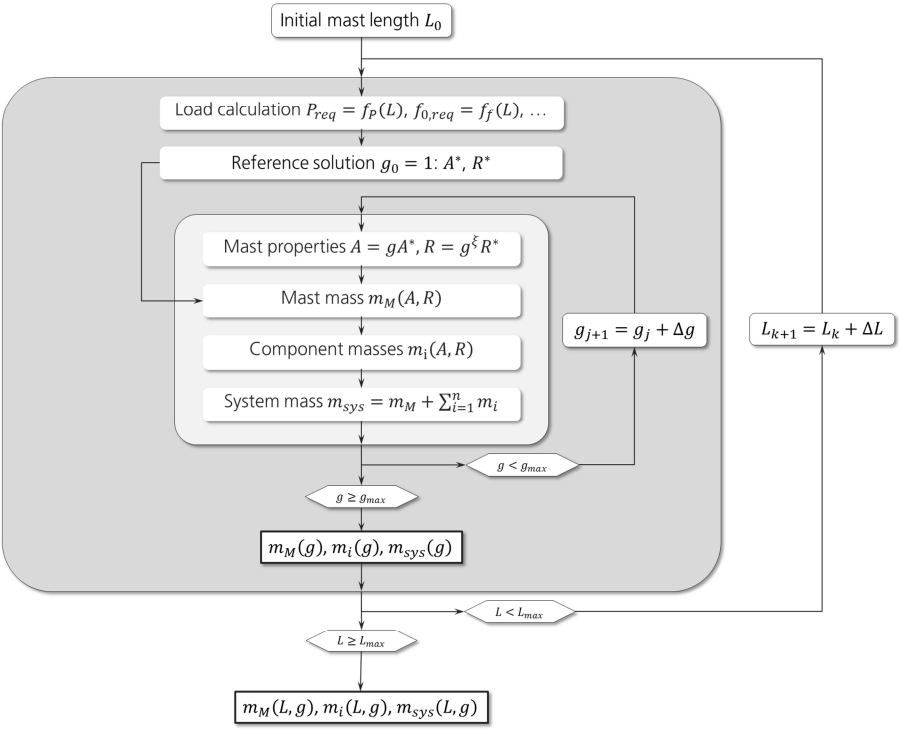

Fig. C - 3: Flow diagram for the derivation of the system mass of the deployable structure (the same procedure is applied for the derivation of the system stowage volume).

Fig. C - 4 shows principle diagrams of the system analysis process through use of the interaction factor g. For each component and the overall system an optimum value $g \geq 1$ can be derived that represents the influence of the mechanism on the Deformable Structure (mast) design as a result from the system optimization process.

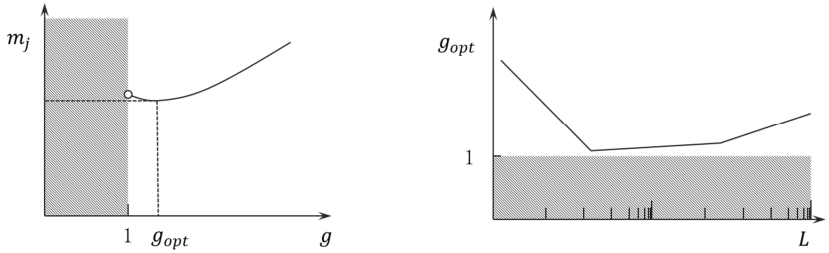

Fig. C - 4: Principle diagrams of the mast-mechanism interaction factor: derivation of the optimum value for a single component (left) and according plot over the design interval (right).

Appendix D

D Design Load Cases

Within Appendix D the design load cases are derived from a solar sail and solar array application and according constraint functions are formulated.

D1 Solar Sail Application

For the solar sail a design similar to that of Sunjammer [82] is considered. Sunjammer uses a sail that is supported by a net of cables that are attached to the masts in several points along their length. Thereby the sail does not require any tension through allowing it to billow in between the cables. Thereby only bending loads arising from the solar pressure are applied to the sail in operational state.

D1.1 Basic Equations

For the calculation of the mast loading the pressure on the sail p and the distribution of the mass has to be known. The sail pressure p is dependent on the solar pressure p_{sol} at 1 AE and the distance d_{AE} of the sail towards the sun given as a fraction in relation to 1 AE:

$$p = \frac{2p_{sol}}{d_{AE}^2}$$

The resulting acceleration a of the sail depends on the overall areal mass γ as follows:

$$a = \frac{p}{\gamma}$$

For calculation of the mass distribution it is assumed that the sail consists of a center mass m_C and four cross-wise aligned masts that support the square membrane. The mass of the sails and masts is combined in the mass m_{SM} that is is assumed to be uniformly distributed throughout the sail. The overall mass m is thereby as follows:

$$m = m_C + m_{SM}$$

The areal mass of the sail and masts is given by γ_{SM} and for the overall sail by γ:

$$\gamma_{SM} = \frac{m_{SM}}{A}$$

$$\gamma = \frac{m_{SM} + m_C}{A}$$

The sail area A is dependent on the mast length as follows:

$$A = 2L^2$$

The mass distribution is described by the mass distribution factor k_γ:

$$k_\gamma = \frac{m_{SM}}{m} = \frac{\gamma_{SM}}{\gamma}$$

The mass distribution varies with the size of the sail. For a small sail a higher center mass relative to the sail can be expected as components such as power, communication and control do not scale with the sail. For a sail of infinite size the mass distribution factor k_γ will approach 1.

The areal mass of the sail and masts γ_{SM} and of the overall areal mass γ are approximated through power functions:

$$\gamma_{SM} = a_{SM} L^{n_{SM}} + \gamma_{SM,0}$$

$$\gamma = aL^n + \gamma_{SM,0}$$

Thereby the mass distribution factor becomes as follows:

$$k_\gamma = \frac{a_{SM} L^{n_{SM}} + \gamma_{SM,0}}{a L^n + \gamma_{SM,0}}$$

The constant term $\gamma_{SM,0}$ corresponds to the areal sail mass that is reached for an infinite large sail for both areal mass terms as the contribution of the payload becomes infinite small. Therefore two points are defined for derivation of the coefficients:

$$\gamma_{SM,1}(L_1)$$
$$\gamma_{SM,2}(L_2)$$
$$\gamma_1(L_1)$$
$$\gamma_2(L_2)$$

Solving the first constraint equation for the coefficient a_{SM}:

$$\gamma_{SM,1} = a_{SM} L_1^{n_{SM}} + \gamma_{SM,0}$$
$$a_{SM} = \left(\gamma_{SM,1} - \gamma_{SM,0}\right) \frac{1}{L_1^{n_{SM}}}$$

Substitution in the second constraint equation gives:

$$\gamma_{SM,2} = \left(\gamma_{SM,1} - \gamma_{SM,0}\right) \left(\frac{L_2}{L_1}\right)^{n_{SM}} + \gamma_{SM,0}$$
$$\frac{\gamma_{SM,2} - \gamma_{SM,0}}{\gamma_{SM,1} - \gamma_{SM,0}} = \left(\frac{L_2}{L_1}\right)^{n_{SM}}$$
$$n_{SM} = \log_{\frac{L_2}{L_1}} \left(\frac{\gamma_{SM,2} - \gamma_{SM,0}}{\gamma_{SM,1} - \gamma_{SM,0}}\right)$$

The solution for the overall areal is mass is according to the sail mass:

$$a = \left(\gamma_1 - \gamma_{SM,0}\right) \frac{1}{L_1^n}$$
$$n = \log_{\frac{L_2}{L_1}} \left(\frac{\gamma_2 - \gamma_{SM,0}}{\gamma_1 - \gamma_{SM,0}}\right)$$

Fig. D - 1 shows the areal masses and the mass distribution factor plotted over a mast length for the following constraints:

$$L_1 = 1 \text{ m}$$
$$L_2 = 100 \text{ m}$$
$$\gamma_{SM,1}(L_1) = 0.05 \frac{\text{kg}}{\text{m}}$$
$$\gamma_1(L_1) = 0.5 \frac{\text{kg}}{\text{m}}$$
$$\gamma_{SM,2}(L_2) = 0.0075 \frac{\text{kg}}{\text{m}}$$
$$\gamma_2(L_2) = 0.0125 \frac{\text{kg}}{\text{m}}$$
$$\gamma_{SM,0} = 0.005 \frac{\text{kg}}{\text{m}}$$

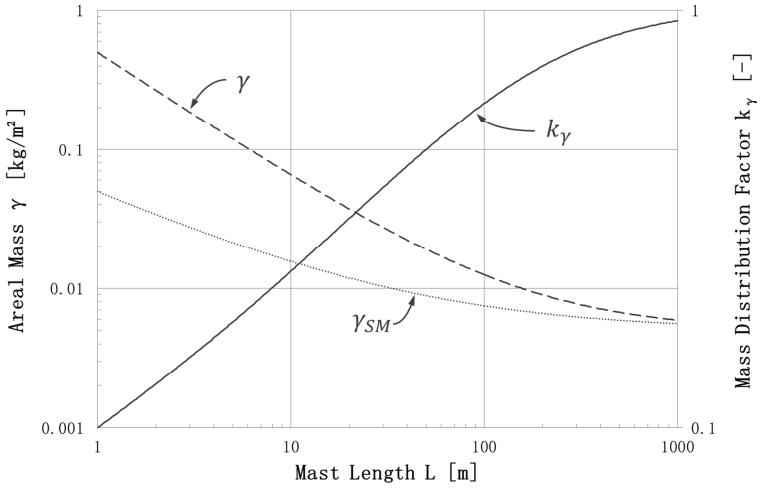

Fig. D - 1: Areal mass and mass distribution factor plotted over the mast length.

D1.2 Critical Bending Moment Requirement

The loading on a single mast is derived from a quadrant of the sail symmetric to the corresponding mast. For a continuous load introduction into the mast the distributed load q at a location s along the mast from the sails center is as follows for the inner half of the mast $0 \leq s \leq \frac{L}{2}$:

$$q(s) = 2ps - 2s\gamma_{SM}a \text{ for } 0 \leq s \leq \frac{L}{2}$$

$$q(s) = 2ps - 2ps\frac{\gamma_{SM}}{\gamma}$$

The distributed load q for the outer half $\frac{L}{2} \leq s \leq L$ is as follows:

$$q(s) = 2p(L-s) - 2(L-s)\gamma_{SM}a \text{ for } \frac{L}{2} \leq s \leq L$$

$$q(s) = 2p(L-s) - 2p(L-s)\frac{\gamma_{SM}}{\gamma}$$

Substitution of the distributed mass factor k_γ gives:

$$q(s) = 2ps\left(1 - k_\gamma\right) \text{ for } 0 \leq s \leq \frac{L}{2}$$

$$q(s) = 2p(L-s)\left(1 - k_\gamma\right) \text{ for } \frac{L}{2} \leq s \leq L$$

The bending moment M at a location s of the mast resulting from the distributed load is as follows:

$$M(s) = \int_s^L q(s)(L-s)ds$$

For the outer half of the mast the bending moment is as follows:

$$M(s) = \int_s^L 2p(L-s)^2\left(1 - k_\gamma\right)ds$$

$$M(s) = 2p(1-k_\gamma)\int_s^L (L^2 - 2Ls + s^2)ds$$

$$M(s) = 2p(1-k_\gamma)\left(L^2 s - Ls^2 + \frac{1}{3}s^3\right)\Big|_s^L$$

$$M(s) = 2p(1-k_\gamma)\left(\frac{1}{3}L^3 - L^2 s + Ls^2 - \frac{1}{3}s^3\right) \text{ for } \frac{L}{2} \le s \le L$$

For the inner half of the mast the bending moment is as follows:

$$M(s) = \frac{1}{12}pL^3(1-k_\gamma) + \int_s^{\frac{L}{2}} 2p(1-k_\gamma)s(L-s)ds$$

$$M(s) = \frac{1}{12}pL^3(1-k_\gamma) + 2p(1-k_\gamma)\int_s^{\frac{L}{2}} (Ls - s^2)ds$$

$$M(s) = \frac{1}{12}pL^3(1-k_\gamma) + 2p(1-k_\gamma)\left(\frac{1}{2}Ls^2 - \frac{1}{3}s^3\right)\Big|_s^{\frac{L}{2}}$$

$$M(s) = \frac{1}{12}pL^3(1-k_\gamma) + 2p(1-k_\gamma)\left(\frac{1}{12}L^3 - \frac{1}{2}Ls^2 + \frac{1}{3}s^3\right)$$

$$M(s) = 2p(1-k_\gamma)\left(\frac{1}{8}L^3 - \frac{1}{2}Ls^2 + \frac{1}{3}s^3\right) \text{ for } 0 \le s \le \frac{L}{2}$$

The bending moment at the root of the masts for $s = 0$ is as follows:

$$M = \frac{1}{4}(1-k_\gamma)pL^3$$

Substitution of the pressure on the sail p gives the required critical bending moment of the mast M_{req}:

$$M_{req} = \frac{1}{2}(1-k_\gamma)\frac{p_{sol}}{d_{AE}^2}L_{req}^3$$

D1.3 Bending Stiffness Requirement

An additional requirement is the bending stiffness EI_{req} of the masts to ensure a certain flatness of the sail under load. For a constant bending stiffness EI the displacement of the tip under the solar pressure is derived from the course of bending moment $M(s)$ and the resulting curvature z'' which is the second derivative of the lateral displacement z:

$$z'' = -\frac{M(s)}{EI}$$

The integrals for the inner half of the mast $0 \le s \le \frac{L}{2}$ are as follows:

$$z'' = -\frac{1}{EI}2p(1-k_\gamma)\left(\frac{1}{8}L^3 - \frac{1}{2}Ls^2 + \frac{1}{3}s^3\right)$$

$$z' = -\frac{1}{EI}2p(1-k_\gamma)\left(\frac{1}{8}L^3 s - \frac{1}{6}Ls^3 + \frac{1}{12}s^4\right) + C_1$$

$$z = -\frac{1}{EI}2p(1-k_\gamma)\left(\frac{1}{16}L^3 s^2 - \frac{1}{24}Ls^4 + \frac{1}{60}s^5\right) + C_1 s + C_2$$

The constraint equations to solve for the constants are as follows:

$$z(0) = 0$$

$$z'(0) = 0$$

Thereby the constants are as follows:

$$C_1 = C_2 = 0$$

The constraints for lateral displacement solution of the second half of the mast $\frac{L}{2} \le s \le L$ are as follows:

$$z''\left(\frac{L}{2}\right) = -\frac{1}{12}\frac{1}{EI}p(1-k_\gamma)L^3$$
$$z'\left(\frac{L}{2}\right) = -\frac{3}{32}\frac{1}{EI}p(1-k_\gamma)L^4$$
$$z\left(\frac{L}{2}\right) = -\frac{13}{480}\frac{1}{EI}p(1-k_\gamma)L^5$$

The solution for the second half of the mast is as follows whereby a constant C_3 is added to account for the curvature at the middle of the mast:

$$z'' = -\frac{1}{EI}2p(1-k_\gamma)\left(\frac{1}{3}L^3 - L^2 s + Ls^2 - \frac{1}{3}s^3\right) + C_3$$
$$z' = -\frac{1}{EI}2p(1-k_\gamma)\left(\frac{1}{3}L^3 s - \frac{1}{2}L^2 s^2 + \frac{1}{3}Ls^3 - \frac{1}{12}s^4\right) + C_3 s + C_4$$
$$z = -\frac{1}{EI}2p(1-k_\gamma)\left(\frac{1}{6}L^3 s^2 - \frac{1}{6}L^2 s^3 + \frac{1}{12}Ls^4 - \frac{1}{60}s^5\right) + C_3 s^2 + C_4 s + C_5$$

The constants are derived through equivalence at the middle of the mast at $s = \frac{L}{2}$:

$$z''\left(\frac{L}{2}\right) = -\frac{1}{12}\frac{1}{EI}p(1-k_\gamma)L^3 + C_3$$
$$z'\left(\frac{L}{2}\right) = -\frac{5}{32}\frac{1}{EI}p(1-k_\gamma)L^4 + \frac{1}{2}C_3 L + C_4$$
$$z\left(\frac{L}{2}\right) = -\frac{49}{960}\frac{1}{EI}p(1-k_\gamma)L^5 + \frac{1}{4}C_3 L^2 + \frac{1}{2}C_4 L + C_5$$

The constants are thereby as follows:

$$-\frac{1}{12}\frac{1}{EI}p(1-k_\gamma)L^3 + C_3 = -\frac{1}{12}\frac{1}{EI}p(1-k_\gamma)L^3$$
$$C_3 = 0$$
$$-\frac{5}{32}\frac{1}{EI}p(1-k_\gamma)L^4 + C_4 = -\frac{3}{32}\frac{1}{EI}p(1-k_\gamma)L^4$$
$$C_4 = \frac{1}{16}\frac{1}{EI}p(1-k_\gamma)L^4$$
$$-\frac{49}{960}\frac{1}{EI}p(1-k_\gamma)L^5 + \frac{1}{32}\frac{1}{EI}p(1-k_\gamma)L^5 + C_5 = -\frac{13}{480}\frac{1}{EI}p(1-k_\gamma)L^5$$
$$-\frac{19}{960}\frac{1}{EI}p(1-k_\gamma)L^5 + C_5 = -\frac{13}{480}\frac{1}{EI}p(1-k_\gamma)L^5$$
$$C_5 = -\frac{7}{960}\frac{1}{EI}p(1-k_\gamma)L^5$$

For a constant bending stiffness the tip displacement $z(L)$ is thereby as follows:

$$z(L) = -\frac{2}{15}\frac{1}{EI}p(1-k_\gamma) + \frac{1}{16}\frac{1}{EI}p(1-k_\gamma)L^5 - \frac{7}{960}\frac{1}{EI}p(1-k_\gamma)L^5$$
$$z(L) = \left(-\frac{128}{960} + \frac{60}{960} - \frac{7}{960}\right)\frac{1}{EI}p(1-k_\gamma)L^5$$
$$z(L) = -\frac{15}{192}\frac{1}{EI}p(1-k_\gamma)L^5$$

To limit the tip displacement to a fraction of the mast length k_z the required bending stiffness is as follows:

$$k_z = \frac{|z(L)|}{L}$$
$$\frac{15}{192}\frac{1}{(EI)_{req}}p(1-k_\gamma)L^5 = k_z L$$
$$(EI)_{req} = \frac{15}{192}\frac{1}{k_z}p(1-k_\gamma)L^4$$

Substitution of the sail pressure gives the required bending stiffness as follows:

$$(EI)_{req} = \frac{15}{96}\frac{1}{k_z}\left(1 - k_\gamma\right)\frac{p_{sol}}{d_{AE}^2}L_{req}^4$$

Fig. D - 2 shows the course of the critical bending moment and bending stiffness requirements over the mast length for the following constraints:

$$k_z = 0.02$$
$$d_{AE} = 0.25$$
$$p_{sol} = 4.6 \cdot 10^{-6}\ \text{Pa}$$

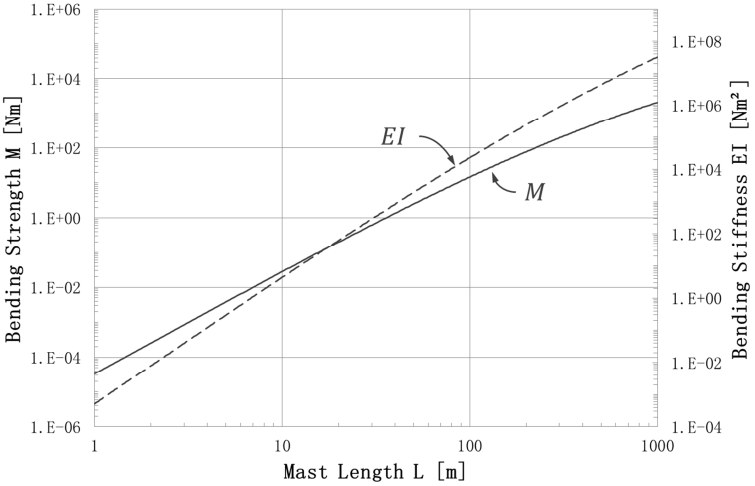

Fig. D - 2: Development of the moment and bending stiffness requirement over the mast length.

D1.4 Load Case Constraint Functions: Solar Sail

The resulting constraint functions for the solar sail application are summarized in Tab. D - 1.

Constraint Functions for the Solar Sail Application	
Required Critical bending moment	$M_{req} = \frac{1}{2}\left(1 - k_\gamma\right)\frac{p_{sol}}{d_{AE}^2}L_{req}^3$
Required Bending Stiffness	$(EI)_{req} = \frac{15}{96}\frac{1}{k_z}\left(1 - k_\gamma\right)\frac{p_{sol}}{d_{AE}^2}L_{req}^4$
Sail mass distribution factor	$k_\gamma = \frac{a_{SM}L^{n_{SM}} + \gamma_{SM,0}}{aL^n + \gamma_{SM,0}}$

Tab. D - 1: Solar sail application constraint functions.

The related constraint function parameters are summarized in Tab. D - 2.

Constraint Function Parameters for the Solar Sail Application			
Parameter	**Symbol**	**Unit**	**Value**
Mast length	L_{req}	m	Input value
Overall areal mass equation constant term	a	$\frac{\text{kg/m}^2}{\text{m}^n}$	0.495
Sail areal mass equation constant term	a_{SM}	$\frac{\text{kg/m}^2}{\text{m}^{n_{SM}}}$	0.045
Overall areal mass equation power term	n	-	-0.910
Sail areal mass equation power term	n_{SM}	-	-0.628
Minimum overall and sail areal mass	$\gamma_{SM,0}$	kg/m²	0.005
Lateral tip displacement factor	k_z	-	0.02
Distance from the sun	d_{AE}	AE	0.25
Solar pressure at 1 AE	p_{sol}	Pa	$4.6 \cdot 10^{-6}$

Tab. D - 2: Solar sail application constraint function parameters.

D2 Solar Array Application

The solar array design is a flexible blanket array similar to that of the ISS with a central mast and two adjacent PV-blankets. Mast and blanket are deployed in the same plane wherefore the mast is loaded in axial compression.

D2.1 Basic Equations

The mass distribution of the solar array is expressed by the areal mass γ that gives the ratio of the array mass m to its surface area A:

$$\gamma = \frac{m}{A}$$

The surface area A of the array is derived through the array length L and the aspect ratio Γ_{bL} that relates the array width b to its length L:

$$\Gamma_{bL} = \frac{b}{L}$$
$$A = bL = \Gamma_{bL} L^2$$

Thereby the linear mass w of the array along its longitudinal axis is as follows:

$$w = \frac{m}{L} = \frac{\gamma A}{L} = \gamma \Gamma_{bL} L$$

D2.2 Eigenfrequency

The array is designed for a certain deployed stiffness expressed through a minimum eigenfrequency requirement f. The eigenfrequency requirement is defined dependent on the size

of the array as for large arrays it becomes the dominating design driver [149]. It is defined through a power function as follows:

$$f = a_f L^{n_f} + f_0$$

The constant term f_0 refers to the eigenfrequency requirement for an infinite large array. Thereby two reference values are defined as follows:

$$f_1(L_1)$$
$$f_2(L_2)$$

The corresponding equations are as follows:

$$f_1 = a_f L_1^{n_f} + f_0$$
$$f_2 = a_f L_2^{n_f} + f_0$$

Solving the first equation for a_f gives:

$$a_f = (f_1 - f_0)\frac{1}{L_1^{n_f}}$$

Substitution in the second constraint equation gives:

$$f_2 = (f_1 - f_0)\left(\frac{L_2}{L_1}\right)^{n_f} + f_0$$
$$\frac{f_2 - f_0}{f_1 - f_0} = \left(\frac{L_2}{L_1}\right)^{n_f}$$
$$n_f = \log_{\frac{L_2}{L_1}}\left(\frac{f_2 - f_0}{f_1 - f_0}\right)$$

Banik gives an expression for the eigenfrequency of a flexible blanket solar array [120] depending on the masts bending stiffness EI and linear array mass w:

$$f = \delta \frac{3.516}{2\pi}\left(\frac{EI}{wL^4}\right)^{\frac{1}{2}}$$

The coefficient δ is an empirical knockdown factor with a value of 0.76. The loading of the mast corresponds to 21% of the Euler buckling load P_E:

$$P_E = \frac{\pi^2 EI}{L^2}$$

Although the mast has a fixed root and free end, the boundary factor k_C has a value of 1 due to the load introduction through the blanket that is fixed at the masts root. Thereby the direction of load introduction changes due to the mast deformation.

D2.3 Compression Strength Requirement

Solving the eigenfrequency expression for the mast bending stiffness EI gives:

$$f^2 = \delta^2\left(\frac{3.516}{2\pi}\right)^2 \frac{EI}{wL^4}$$
$$EI = \left(\frac{2\pi}{3.516}\right)^2 \frac{1}{\delta^2} f^2 w L^4$$

The resulting global compression strength is given by the Euler buckling load of the mast:

$$P_E = \frac{\pi^2 EI}{L^2} = \left(\frac{2\pi^2}{3.516}\right)^2 \frac{1}{\delta^2} f^2 w L^2$$

As the tension load on the membrane corresponds to 21% of the Euler buckling load the local compression strength of the mast can be lower than the global compression strength. However, in the design of a solar array some robustness against off-nominal loading due to blanket deployment errors is required. Hence, in the following the local buckling load requirement is set equal to the global buckling load. The required compression strength P_{req} of the mast is thereby as follows:

$$P_{req} = \left(\frac{2\pi^2}{3.516}\right)^2 \frac{1}{\delta^2} f^2 w L^2$$

Substitution of the linear mass gives:

$$P_{req} = \left(\frac{2\pi^2}{3.516}\right)^2 \left(\frac{f}{\delta}\right)^2 \gamma \Gamma_{bL} L_{req}^3$$

Fig. D - 3 gives the compression strength requirement plotted over the mast length for the following constraints:

$$L_1 = 1 \text{ m}$$
$$L_2 = 10 \text{ m}$$
$$f(L_1) = 0.25 \text{ Hz}$$
$$f(L_2) = 0.05 \text{ Hz}$$
$$f_0 = 0.01 \text{ Hz}$$
$$\delta = 0.76$$
$$\gamma = 1.2 \frac{\text{kg}}{\text{m}}$$
$$\Gamma_{bL} = 0.25$$

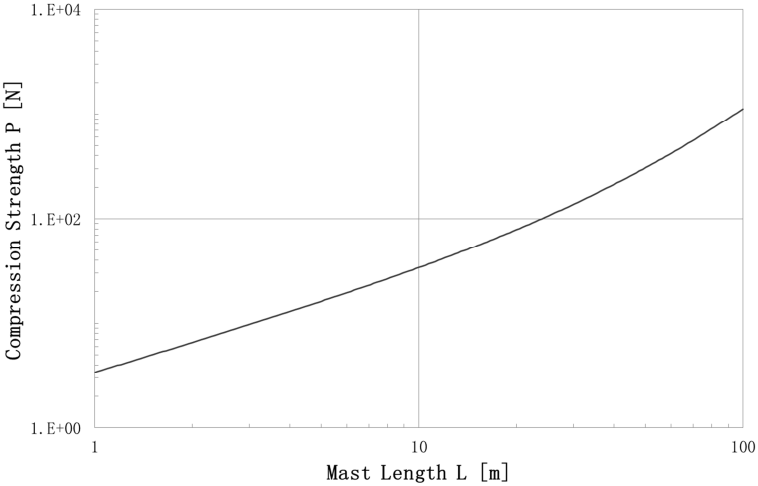

Fig. D - 3: Required compression strength plotted over the mats length.

D2.4 Load Case Constraint Functions: Solar Array

The resulting constraint functions for the solar array application are summarized in Tab. D - 3.

Constraint Functions for the Solar Array Application	
Required axial compression strength	$P_{req} = \left(\frac{2\pi^2}{3.516}\right)^2 \left(\frac{f}{\delta}\right)^2 \gamma \Gamma_{bL} L_{req}^3$
Required eigenfrequency	$f = a_f L^{n_f} + f_0$

Tab. D - 3: Solar array application constraint functions.

The related constraint function parameters are summarized in Tab. D - 4.

Constraint Function Parameters for the Solar Sail Application			
Parameter	**Symbol**	**Unit**	**Value**
Required mast length	L_{req}	m	Input value
Required eigenfrequency	f	Hz	Input value
Eigenfrequency equation constant term	f_0	Hz	0.01
Eigenfrequency equation linear term	a_f	$\frac{\text{Hz}}{\text{m}^{n_f}}$	0.495
Eigenfrequency equation power term	n_f	-	-1.041
Eigenfrequency knock-down factor	δ	-	0.76
Solar array areal mass	γ	kg/m²	1.2
Blanket size ratio	Γ_{bL}	-	0.25

Tab. D - 4: Solar array constraint function parameters.

Appendix E

E Tubular Shell Mast Scaling Function

Within Appendix E the scaling functions for the Tubular Shell Mast are derived for the load cases of axial compression and bending.

E1 Tubular Shell Mast Parameterization

The Tubular Shell Mast is parameterized similar to a hollow circular beam described in A1.1 and A1.3. Hence the cross-sectional area A is described by a factor k_A that accounts for a specific cross-sectional shape and relates the cross-sectional area to the masts radius R and shell thickness t:

$$A = k_A R t$$

In the same way the second moment of area I is expressed by a factor k_I that describes depending on the specific cross-sectional shape the relation to the cross-sectional area A and radius R:

$$I = k_I A R^2$$

Thereby the mass m and specific mass w of the Tubular Shell Mast is given by the cross-sectional area A, mast length L and material density ρ as follows:

$$m = \rho A L$$

$$w = \rho A$$

In addition scaling limits are applied for the minimum shell thickness t_{min} and the maximum elastic strain ε_{max} during flattening of the cross-section.

The parameters of the Tubular Shell Mast are summarized in Tab. E - 1.

Tubular Shell Mast Parameters			
Property	**Parameter**	**Unit**	**Values**
Radius	R	m	Sizing result
Wall thickness	t	m	Sizing result
Length	L	m	-
Cross-section factor	k_A	-	2π
Second moment of area factor	k_I	-	0.5
Column mounting parameter	k_C	-	2
Material modulus	E	N/m²	60 GPa
Material density	ρ	kg/m³	1600
Cross-sectional area	$A = k_A R t$	m²	-
Second Moment of area	$I = k_I A R^2$	m^4	-
Mass	$m = \rho A L$	kg	-

Minimum shell thickness	t_{min}	m	0.0001
Maximum elastic flattening strain	ε_{max}	-	0.006

Tab. E - 1: Parameterization of the Tubular Shell Mast.

E2 Consideration of Geometric Shell Imperfections

The Tubular Shell Mast consists of a thin, flexible shell that is sensitive regarding its local buckling strength to geometrical imperfections. Thereby the degree of sensitivity increases with the ratio of shell thickness t to radius R. For thin walled cylinders loaded in axial compression and bending according equations to approximate the critical stresses σ_{crit} are given in NASA SP-8007 [144]. For axial compression the expression is as follows:

$$\sigma_{crit} = \frac{E}{\sqrt{3(1-\nu^2)}}\frac{t}{R}\gamma_c$$
$$\gamma_c = 1 - 0.901(1 - e^{-\phi})$$
$$\phi = \frac{1}{16}\sqrt{\frac{R}{t}}$$

For bending the expression is as follows:

$$\sigma_{crit} = \frac{E}{\sqrt{3(1-\nu^2)}}\frac{t}{R}\gamma_b$$
$$\gamma_b = 1 - 0.731(1 - e^{-\phi})$$
$$\phi = \frac{1}{16}\sqrt{\frac{R}{t}}$$

To comply with the method for derivation of the mast-mechanism interactions described in Appendix C the according constraint functions have to be formulated as power functions. However, the equations for the critical compression and bending stresses given by the NASA SP-8007 [144] lead to complex expressions when solved for the variables R and t. Therefore approximation functions within a certain interval $[\Gamma_{Rt,1}, \Gamma_{Rt,2}]$ of the wall thickness ratios $\Gamma_{Rt} = \frac{R}{t}$ are used. The following substitution is done:

$$\frac{\Gamma_{Rt}}{\gamma(\Gamma_{Rt})} \approx c\Gamma_{Rt}^{d}$$

Thereby the maximum stress is as follows:

$$\sigma_{crit} = \frac{E}{\sqrt{3(1-\nu^2)}}\frac{1}{c\Gamma_{Rt}^{d}}$$

The approximation interval is chosen according to the working strain for elastically deformed shell booms. The material strain ε is in general within the interval $[0.01, 0.00025]$ which results in the interval $[50, 2000]$ for the wall thickness ratio Γ_{Rt} according to:

$$\varepsilon_f = \frac{t}{2R} = \frac{1}{2\Gamma_{Rt}}$$

Wherefore the intervals are:

$$\{\varepsilon_f \in \mathbb{R} | 0.00025 \leq \varepsilon_f \leq 0.01\}$$
$$\{\Gamma_{Rt} \in \mathbb{R} | 2000 \geq \Gamma_{Rt} \geq 50\}$$

The constant c and the exponent d are chosen accordingly. For compression loads the values are as follows:

$$c_c = 0.2431$$
$$d_c = 1.4258$$

For bending loads the values are as follows:

$$c_b = 0.4937$$
$$d_b = 1.2455$$

From this approximation an error in the calculation of the critical stresses arises. The resulting error Ψ_{Rt} is given by:

$$\Psi_{Rt} = 100\% \cdot \left(\frac{c\Gamma_{Rt}^{d}}{\Gamma_{Rt}\frac{1}{\gamma(\Gamma_{Rt})}} - 1 \right) = 100\% \cdot (c\Gamma_{Rt}^{d-1}\gamma(\Gamma_{Rt}) - 1)$$

For a conservative approximation the error should be predominantly positive. Fig. E - 1 shows the critical stress derived by NASA SP-8007 [144] and its approximation and the resulting approximation error for compression loading. The largest deviations occur for small wall thickness ratios. The maxima are between -12.6% for a wall thickness ratio Γ_{Rt} of 50 and $+11.6\%$ for a wall thickness ratio Γ_{Rt} of 330.

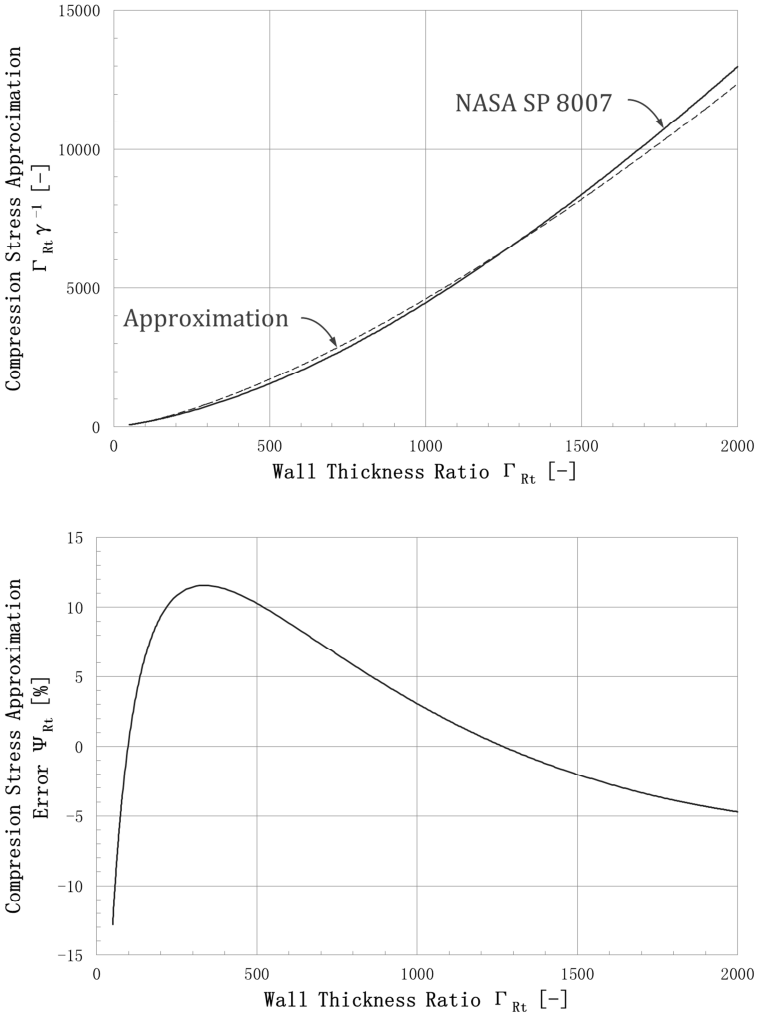

Fig. E - 1: Comparison of the compression stress expression $\frac{\Gamma_{Rt}}{\gamma_c}$ derived by NASA SP-8007 [144] and its approximation plotted over the considered wall thickness ratio interval (top) and plot of the resulting error (bottom).

Fig. E - 2 shows the critical stress derived by NASA SP-8007 [144] and its approximation and the resulting approximation error for bending. The error shows again the largest values for small wall thickness ratios. The maxima are between -4.7% for a wall thickness ratio Γ_{Rt} of 50 and $+3.6\%$ for a wall thickness ratio Γ_{Rt} of 240.

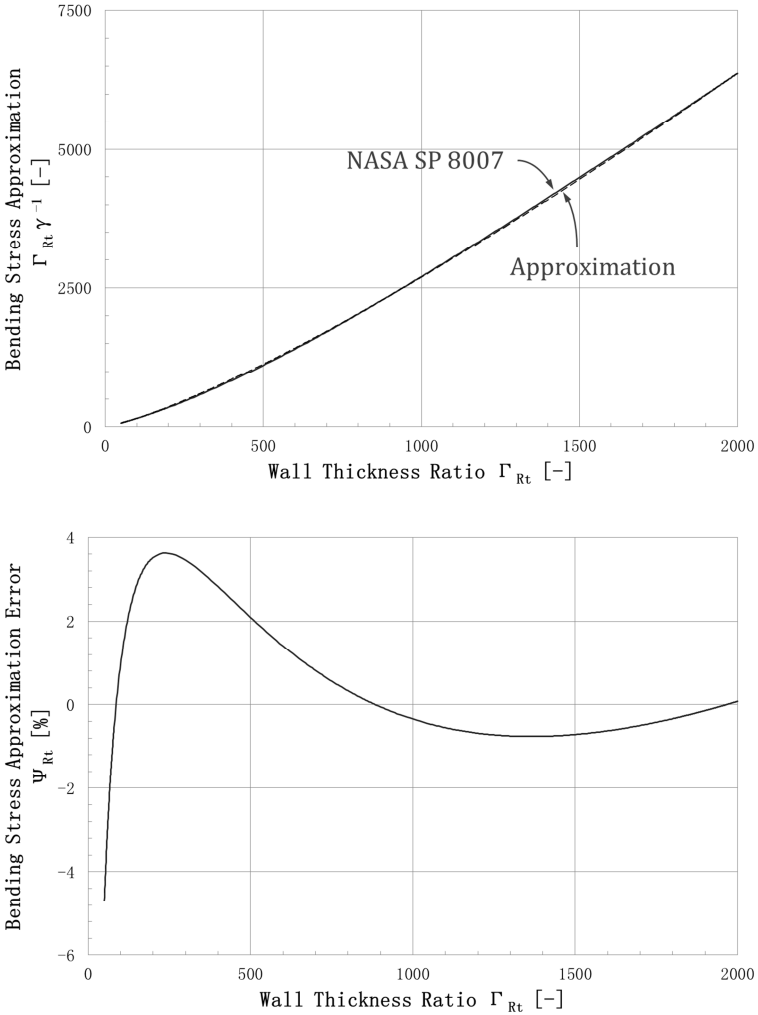

Fig. E - 2: Comparison of the bending stress expression $\frac{\Gamma_{Rt}}{\gamma_b}$ derived by NASA SP-8007 [144] and its approximation plotted over the considered wall thickness ratio interval (left) and plot of the resulting error (right).

The local buckling stresses for a Tubular Shell Mast loaded in compression and bending are summarized in Tab. E - 2.

Tubular Shell Mast Local Buckling Stresses Approximation for Compression and bending Loading		
Performance Parameter	**Symbol/Expression**	**Value**
Local buckling stress approximation function	$\sigma_{max} = \frac{E}{\sqrt{3(1-\nu^2)}} \frac{1}{c\Gamma_{Rt}^d}$	-
Linear approximation coefficient for compression loading	c_c	0.2431
Power approximation coefficient for compression loading	d_c	1.4258
Linear approximation coefficient for bending loading	c_b	0.4937
Power approximation coefficient for bending loading	d_b	1.2455

Tab. E - 2: Buckling stresses approximation function for the Tubular Shell Mast loaded in bending and compression.

E3 Scaling Constraint Functions for the Load Case of Axial Compression

The constraint functions of the Tubular Shell Mast for the load case of axial compression are global buckling P_{global} and local buckling P_{local} as well as the scaling limit functions for the minimum wall thickness t_{min} and maximum elastic material strain ε_{max}.

E3.1 Global Column Buckling

The constraint function of global column buckling is derived for a slender mast from Euler buckling:

$$P_{req} \leq P_{global} = P_E = \frac{\pi^2 EI}{\left(k_C L_{req}\right)^2}$$

With the cross-sectional parameters given in Tab. E - 1 the constraint equation for global Euler buckling is re-written:

$$P_{req} \leq \frac{\pi^2 EI}{\left(k_C L_{req}\right)^2}$$

$$P_{req} \leq \frac{\pi^2 E k_I R^2 A}{\left(k_C L_{req}\right)^2}$$

The general form of the constraint equation from global column buckling is as follows:

$$\frac{1}{\pi^2}\frac{1}{E}\frac{1}{k_I} k_C^2 L_{req}^2 P_{req} \leq AR^2$$

Hence, the constraint function parameters according to Appendix C are as follows:

$$c = \frac{1}{\pi^2}\frac{1}{E}\frac{1}{k_I} k_C^2 L_{req}^2 P_{req}$$

$$i = 1$$

$$j = 2$$

E3.2 Local Wall Buckling

The constraint function for local wall buckling is derived from the critical wall buckling stress σ_{crit}:

$$P_{req} \leq P_{local} = \sigma_{crit} A$$

Through use of the stress formulation according to E2 and the cross-sectional parameters given in Tab. E - 1 the constraint can be written as follows:

$$P_{req} \leq \frac{E}{\sqrt{3(1-\nu^2)}} \frac{1}{c_c \Gamma_{Rt}^{d_c}} A$$

$$P_{req} \leq \frac{E}{\sqrt{3(1-\nu^2)}} \frac{1}{c_c \left(\frac{R}{t}\right)^{d_c}} A$$

Substituting the wall thickness:

$$A = k_A R t$$

$$t = \frac{A}{k_A R}$$

$$P_{req} \leq \frac{E}{\sqrt{3(1-\nu^2)}} \frac{1}{c_c \left(\frac{k_A R^2}{A}\right)^{d_c}} A$$

$$P_{req} \leq \frac{E}{\sqrt{3(1-\nu^2)}} \frac{1}{c_c k_A^{d_c} R^{2d_c}} A^{1+d_c}$$

The general form of the second constraint equation from local wall buckling is:

$$c_c k_A^{d_c} \frac{\sqrt{3(1-\nu^2)}}{E} P_{req} \leq A^{1+d_c} R^{-2d_c}$$

Hence, the constraint function parameters according to Appendix C are as follows:

$$c = c_c k_A^{d_c} \frac{\sqrt{3(1-\nu^2)}}{E} P_{req}$$

$$i = 1 + d_c$$

$$j = -2d_c$$

E3.3 Minimum Wall Thickness

A scaling limit is applied in the form of a minimum wall thickness t_{min} of the Tubular Shell Mast as this is restricted by manufacturing limitations and procurement of thin materials. The resulting constraint function is as follows:

$$A \geq A_{min} = k_A R t_{min}$$

Re-arranging in the general form gives:

$$k_A t_{min} \leq A R^{-1}$$

Hence, the constraint function parameters according to Appendix C are as follows:

$$c = k_A t_{min}$$

$$i = 1$$

$$j = -1$$

E3.4 Maximum Strain

A scaling limit is applied in the form of a maximum elastic material strain ε_{max} to ensure foldability of the Tubular Shell Mast that is stowed through elastic deformation. The resulting constraint function is as follows:

$$\varepsilon = \frac{t}{2R} \leq \varepsilon_{max}$$

Substitution of the wall thickness according to Tab. E - 1 and re-arranging in the general form gives:

$$\frac{t}{2R} \leq \varepsilon_{max}$$
$$A = k_A R t$$
$$t = \frac{A}{k_A R}$$
$$\frac{A}{2k_A R^2} \leq \varepsilon_{max}$$
$$2k_A \varepsilon_{max} \geq A R^{-2}$$

Hence, the constraint function parameters according to Appendix C are as follows:

$$c = 2k_A \varepsilon_{max}$$
$$i = 1$$
$$j = -2$$

E3.5 Summary of Tubular Shell Mast Scaling Constraint Functions for Axial Compression

The scaling functions of the Tubular Shell Mast for the load case of axial compression are summarized in Tab. E - 3.

Scaling Functions of the Tubular Shell Mast for the Load Case of Axial Compression				
Constraint Criterion	**Constraint Function**	c	i	j
Global column buckling	$\frac{1}{\pi^2}\frac{1}{E}\frac{1}{k_I} k_C^2 L_{req}^2 P_{req} \leq A R^2$	$\frac{1}{\pi^2}\frac{1}{E}\frac{1}{k_I} k_C^2 L_{req}^2 P_{req}$	1	2
Local wall buckling	$c_c k_A^{d_c} \frac{\sqrt{3(1-\nu^2)}}{E} P_{req} \leq A^{1+d_c} R^{-2d_c}$	$c_c k_A^{d_c} \frac{\sqrt{3(1-\nu^2)}}{E} P_{req}$	$1 + d_c$	$-2d_c$
Minimum wall thickness	$k_A t_{min} \leq A R^{-1}$	$k_A t_{min}$	1	-1
Maximum material strain	$2k_A \varepsilon_{max} \geq A R^{-2}$	$2k_A \varepsilon_{max}$	1	-2

Tab. E - 3: Summary of the Tubular Shell Mast scaling functions for the load case of axial compression.

E4 Scaling Constraint Functions for the Load Case of Bending

The constraint functions of the Tubular Shell Mast for the load case of bending are bending stiffness EI and critical bending moment M as well as the scaling limit function of the minimum wall thickness t_{min} and maximum elastic material strain ε_{max}. The latter are the same as for the load case of axial compression and are not further addressed.

E4.1 Bending Stiffness

The constraint function for the bending stiffness requirements is as follows:

$$(EI)_{req} \leq EI = Ek_I AR^2$$

Re-written in the form according to Appendix C gives:

$$\frac{1}{E}\frac{1}{k_I}(EI)_{req} \leq AR^2$$

Hence, the constraint function parameters according to Appendix C are as follows:

$$c = \frac{1}{E}\frac{1}{k_I}(EI)_{req}$$
$$i = 1$$
$$j = 2$$

E4.2 Critical Bending Moment

The constraint function for the critical bending moment requirements is as follows:

$$M_{req} \leq M = \sigma_{crit}\frac{I}{R}$$

Through use of the stress formulation according to E2 and the cross-sectional parameters given in Tab. E - 1 the constraint can be written as follows:

$$M_{req} \leq \sigma_{crit} k_I AR$$
$$M_{req} \leq \frac{E}{\sqrt{3(1-\nu^2)}}\frac{1}{c_b\left(\frac{R}{t}\right)^{d_b}}k_I AR$$
$$M_{req} \leq \frac{E}{\sqrt{3(1-\nu^2)}}\frac{1}{c_b\left(\frac{k_A R^2}{A}\right)^{d_b}}k_I AR$$
$$M_{req} \leq \frac{E}{\sqrt{3(1-\nu^2)}}\frac{1}{c_b}\frac{k_I}{k_A^{d_b}}A^{1+d_b}R^{1-2d_b}$$

Re-written in the form according to Appendix C gives:

$$\frac{\sqrt{3(1-\nu^2)}}{E}c_b\frac{k_A^{d_b}}{k_I}M_{req} \leq A^{1+d_b}R^{1-2d_b}$$

Hence, the constraint function parameters according to Appendix C are as follows:

$$c = \frac{\sqrt{3(1-\nu^2)}}{E}c_b\frac{k_A^{d_b}}{k_I}M_{req}$$
$$i = 1 + d_b$$
$$j = 1 - 2d_b$$

E4.3 Summary of Tubular Shell Mast Scaling Constraint Functions for Bending

The scaling constraint functions of the Tubular Shell Mast for the load case of axial compression are summarized in Tab. E - 4.

Scaling Constraint Functions of the Tubular Shell Mast for the Load Case of Bending				
Constraint Criterion	**Constraint Function**	c	i	j
Bending Stiffness	$\frac{1}{E}\frac{1}{k_I}(EI)_{req} \leq AR^2$	$\frac{1}{E}\frac{1}{k_I}(EI)_{req}$	1	2
Critical bending moment	$\frac{\sqrt{3(1-\nu^2)}}{E}c_b\frac{k_A^{d_b}}{k_I}M_{req} \leq A^{1+d_b}R^{1-2d_b}$	$c_c k_A^d\frac{\sqrt{3(1-\nu^2)}}{E}P_{req}$	$1+d_b$	$1-2d_b$

Minimum wall thickness	$k_A t_{min} \leq AR^{-1}$	$k_A t_{min}$	1	-1
Maximum material strain	$2k_A \varepsilon_{max} \geq AR^{-2}$	$2k_A \varepsilon_{max}$	1	-2

Tab. E - 4: Summary of the Tubular Shell Mast scaling constraint functions for the load case of bending.

Appendix F

F Solid Rod Truss Scaling Function

Within Appendix F the scaling functions for the solid rod truss are derived for the load cases of axial compression and bending.

F1 Truss Parameterization

The parameterization of a truss requires several more parameters than the beforehand presented Tubular Shell Mast as a truss is an assembly of longerons, battens and diagonals components. In the following the approach presented by Murphey [28] for truss parameterization is followed in general.

The truss mass m is the sum of the masses of longerons m_l, battens m_b and diagonals m_d:

$$m = m_l + m_b + m_d$$

Substitution by the linear mass terms $A_i\rho_i$ and the number of longerons n leads to:

$$m = \frac{nA_l\rho_l l + nA_b\rho_b l_b + nA_d\rho_d l_d}{l} L$$

$$m = n\left(A_l\rho_l + A_b\rho_b\frac{l_b}{l} + A_d\rho_d\frac{l_d}{l}\right)L$$

For a conservative assumption of same linear mass of longerons, battens and diagonals, the mass expression can be rewritten as follows:

$$m = nA_l\rho_l\left(1 + \frac{l_b}{l} + \frac{l_d}{l}\right)L$$

The ratios for the length of battens and diagonals can be expressed by the diagonal angle Θ between batten and diagonal:

$$m = nA_l\rho_l\left(1 + \frac{1}{\tan(\Theta)} + \frac{1}{\sin(\Theta)}\right)L$$

The term considering the diagonal angle Θ is referred to as the equivalent truss mass factor β:

$$\beta = 1 + \frac{1}{\tan(\Theta)} + \frac{1}{\sin(\Theta)}$$

The equivalent truss cross-sectional area A is thereby as follows:

$$A = n\beta A_l$$

Scaling limits are applied for the solid rod truss regarding the minimum and maximum diagonal angles Θ_{min} and $\Theta_{max}$and the minimum longeron cross-sectional radius $r_{l,min}$. Thereby the minimum longeron cross-sectional area is calculated as follows:

$$A_{l,min} = k_{A,l}r_{l,min}^2$$

The parameters and properties of the solid rod truss are summarized in Tab. F - 1.

Solid Rod Truss Parameters			
Property	**Parameter**	**Unit**	**Values**
Truss radius	R	m	Sizing result
Longeron radius	r_l	m	-

Truss length	L	m	-
Longeron length	$l = 2\tan(\Theta)\, R \sin\left(\frac{\pi}{n}\right)$	m	-
Equivalent truss cross-sectional area	$A = n\beta A_l$	m²	Sizing result
Longeron cross-sectional area	$A_l = k_{A,l} r^2$	m²	-
Truss second moment of area	$I = \frac{n}{2} A_l R^2$	m⁴	-
Longeron second moment of area	$I_l = k_{I,l} r^2 A_l = \frac{k_{I,l}}{k_{A,l}} A_l^2$	m⁴	-
Material modulus	E	N/m²	175 GPa
Material density	ρ	kg/m³	1600
Number of longerons	n	-	4
Truss axial mass fraction	$\beta = 1 + \frac{1}{\tan(\Theta)} + \frac{1}{\sin(\Theta)}$	-	-
Diagonal angle	Θ	rad	$\Theta_{opt,c} = 31.4°$ $\Theta_{opt,b} = 19.9°$
Longeron cross-section factor	$k_{A,l}$	-	π
Longeron second moment of area factor	$k_{I,l}$	-	$\frac{1}{4}$
Truss mounting factor	k_C	-	2
Longeron mounting factor	$k_{C,l}$	-	1
Truss mass	$m = n\beta A_l \rho L$	kg	-
Minimum diagonal angle	Θ_{min}	rad	$\frac{\pi}{12}$
Maximum diagonal angle	Θ_{max}	rad	$\frac{\pi}{3}$
Minimum longeron cross-sectional radius	$r_{l,min}$	m²	0.00075

Tab. F - 1: Summary of the solid rod truss parameters.

F2 Truss Axial Mass Fraction

As demonstrated above the truss axial mass fraction β depends on the diagonal angle Θ. For many design cases the diagonal angle is fixed while for other the diagonal angle does vary. These cases are examined in the following.

F2.1 Constant Diagonal Angle

The truss diagonal angle is constant for scaling without consideration of scaling limits and in the case of active scaling limits on the maximum and minimum diagonal angle. For truss scaling without scaling limits Murphey [28] has shown that there is a global, load case specific optimum for the diagonal angle Θ. For the load cases of axial compression (index c) and bending (index b) the values are as follows:

$$\Theta_{opt,c} = 31.4°$$
$$\Theta_{opt,b} = 19.9°$$

Therefore the equivalent truss mass factor is a constant β_{opt}:

$$\beta_{opt,c} = 1 + \frac{1}{\tan(\Theta_{opt,c})} + \frac{1}{\sin(\Theta_{opt,c})} = 4.56$$
$$\beta_{opt,c} = 1 + \frac{1}{\tan(\Theta_{opt,b})} + \frac{1}{\sin(\Theta_{opt,b})} = 6.70$$

Thereby the equivalent truss cross-sectional area is as follows:

$$A = n\beta_{opt}A_l$$

The truss mass m is as follows:

$$m = A\rho L = n\beta_{opt}A_l\rho L$$

For the scaling limits of maximum and minimum diagonal angle the derivation of axial mass fraction and truss mass is the same.

The properties of a truss of constant diagonal angle are summarized in Tab. F - 2.

Truss Properties for Constant Diagonal Angles	
Truss axial mass fraction	$\beta_{const} = 1 + \frac{1}{\tan(\Theta_{const})} + \frac{1}{\sin(\Theta_{const})}$
Truss equivalent cross-sectional area	$A = n\beta_{const}A_l$
Truss mass	$m = n\beta_{const}A_l\rho L$

Tab. F - 2: Truss properties for constant diagonal angle.

F2.2 Varying Diagonal Angle

When certain scaling limits are reached an additional constraint equation is introduced and the truss diagonal angle Θ becomes an additional variation parameter. Therefore the ratio for batten length and diagonal length in the truss mass factor expressions β varies. The length of battens l_b and diagonals l_d depends on the number of longerons n, truss radius R and longeron length l as follows:

$$l_b = 2R\sin\left(\frac{\pi}{n}\right)$$
$$l_d = \left(l^2 + 4R^2\sin^2\left(\frac{\pi}{n}\right)\right)^{\frac{1}{2}}$$

The ratios towards the longeron length l are as follows:

$$\frac{l_b}{l} = 2\frac{R}{l}\sin\left(\frac{\pi}{n}\right)$$

$$\frac{l_d}{l} = \left(1 + 4\left(\frac{R}{l}\right)^2 \sin^2\left(\frac{\pi}{n}\right)\right)^{\frac{1}{2}}$$

Thereby the equivalent axial mass factor β can be rewritten as follows:

$$\beta = 1 + 2\frac{R}{l}\sin\left(\frac{\pi}{n}\right) + \left(1 + 4\left(\frac{R}{l}\right)^2 \sin^2\left(\frac{\pi}{n}\right)\right)^{\frac{1}{2}}$$

For the examination of the interaction between structure and mechanism by the interaction factor g, a formulation of the mast constraint functions in the following form is chosen (see Appendix C):

$$c \leq A^i R^j$$

To enable this type of formulation the equivalent truss mass factor β is approximated by a power function as follows:

$$\beta \approx \frac{1}{c_t\left(\frac{R}{l}\right)^{d_t}}$$

If a scaling limit is active and the diagonal angle becomes a variable the angle either continuously increases from the optimum value Θ_{opt} to the maximum value Θ_{max} or continuously decreases to the minimum value Θ_{min} or vice versa. To achieve a continuous transition at these interval boundaries, the coefficients of the approximation are derived by equating with the actual truss mass factors at these boundaries. For the diagonal angle interval $\Theta_{opt,c}$ to Θ_{max} the truss mass factors are as follows:

$$\beta_{opt,c} = 1 + \frac{1}{\tan(\Theta_{opt,c})} + \frac{1}{\sin(\Theta_{opt,c})}$$

$$\beta_{max} = 1 + \frac{1}{\tan(\Theta_{max})} + \frac{1}{\sin(\Theta_{max})}$$

The corresponding ratios of the truss radius to the longeron length are derived by the expression for the longeron length l as follows:

$$l = 2\tan(\Theta)\, R \sin\left(\frac{\pi}{n}\right)$$

$$\frac{R}{l} = \frac{1}{2\tan(\Theta)\sin\left(\frac{\pi}{n}\right)}$$

The coefficients c_t and d_t of the approximation function are derived by the constraint equation at the interval boundaries. The first constraint equation for $\Theta_{opt,c}$ is as follows:

$$\beta_{opt,c} = \frac{1}{c_t\left(\left(\frac{R}{l}\right)_{opt,c}\right)^{d_t}}$$

$$\beta_{opt,c} = \frac{1}{c_t\left(\frac{1}{2\tan(\Theta_{opt,c})\sin\left(\frac{\pi}{n}\right)}\right)^{d_t}}$$

$$\beta_{opt,c} = \frac{1}{c_t}\left(2\tan(\Theta_{opt,c})\sin\left(\frac{\pi}{n}\right)\right)^{d_t}$$

Solving for the linear coefficient c_t gives:

$$c_t = \frac{\left(2\tan(\Theta_{opt,c})\sin\left(\frac{\pi}{n}\right)\right)^{d_t}}{\beta_{opt,c}}$$

The second constraint equation for Θ_{max} is as follows:

$$\beta_{max} = \frac{1}{c_t \left(\left(\frac{R}{l}\right)_{max}\right)^{d_t}}$$

$$\beta_{max} = \frac{1}{c_t \left(\frac{1}{2\tan(\Theta_{max})\sin\left(\frac{\pi}{n}\right)}\right)^{d_t}}$$

$$\beta_{max} = \frac{1}{c_t}\left(2\tan(\Theta_{max})\sin\left(\frac{\pi}{n}\right)\right)^{d_t}$$

Substitution of the coefficient c_t gives:

$$\beta_{max} = \beta_{opt,c}\frac{\left(2\tan(\Theta_{max})\sin\left(\frac{\pi}{n}\right)\right)^{d_t}}{\left(2\tan(\Theta_{opt,c})\sin\left(\frac{\pi}{n}\right)\right)^{d_t}}$$

$$\frac{\beta_{max}}{\beta_{opt,c}} = \left(\frac{\tan(\Theta_{max})}{\tan(\Theta_{opt,c})}\right)^{d_t}$$

Solving for the exponent d_t leads to:

$$d_t = \log_{\left(\frac{\tan(\Theta_{max})}{\tan(\Theta_{opt,c})}\right)}\left(\frac{\beta_{max}}{\beta_{opt,c}}\right)$$

Thereby the linear coefficient c is as follows:

$$c_t = \frac{1}{\beta_{opt,c}}\left(2\tan(\Theta_{opt,c})\sin\left(\frac{\pi}{n}\right)\right)^{\log_{\left(\frac{\tan(\Theta_{max})}{\tan(\Theta_{opt,c})}\right)}\left(\frac{\beta_{max}}{\beta_{opt,c}}\right)}$$

The same procedure is followed for the diagonal angle intervals $[\Theta_{opt,c}, \Theta_{min}]$, $[\Theta_{opt,b}, \Theta_{max}]$ and $[\Theta_{opt,b}, \Theta_{min}]$. With the thereby derived approximation functions on the truss axial mass fraction β the truss equivalent cross-sectional area A for a truss with varying diagonal angle is derived as follows:

$$A = \frac{n}{c_t \left(\frac{R}{l}\right)^{d_t}} A_l$$

The mass m of a truss is thereby as follows:

$$m = nA\rho L = \frac{n}{c_t \left(\frac{R}{l}\right)^{d_t}} A_l \rho L$$

The properties of a truss of constant diagonal angle are summarized in Tab. F - 3.

Truss Properties for Varying Diagonal Angles	
Truss axial mass fraction	$\beta_{vary} \approx \frac{1}{c_t \left(\frac{R}{l}\right)^{d_t}}$
Truss equivalent cross-sectional area	$A = \frac{n}{c_t \left(\frac{R}{l}\right)^{d_t}} A_l$

Truss mass	$m = \frac{n}{c_t \left(\frac{R}{l}\right)^{d_t}} A_l \rho L$

Tab. F - 3: Truss properties for a varying diagonal angle.

F3 Consideration of Geometrical Longeron Imperfections

The longerons in a solid rod truss are slender elements that are sensitive to geometric imperfections. Imperfections in the longerons cause lateral deflections well before reaching the buckling load. The impact of initial imperfection on effective extensional stiffness and strength of the longeron is of interest here as they are decisive for the overall truss performance. In the following the imperfections are considered based on the approaches of Timoshenko and Gere [145] and Crawford [113].

F3.1 Lateral Deflection

A sinusoidal initial imperfection of amplitude a_0 is considered in the longeron:

$$y_0 = a_0 \sin\left(\frac{\pi}{l}x\right)$$

The overall deformation y consists of the initial deformation y_0 and the load induced deformation from the axial compression of the longeron y_P:

$$y = y_0 + y_P$$

The moment in the longeron resulting from the deformation is:

$$M_l = P_l(y_0 + y_P)$$

Substituting the moment expression in the equation of the beam curvature leads to the differential equation for loading related longeron deformation:

$$\frac{d^2 y_P}{dx^2} = -\frac{M_l}{(EI)_l} = -\frac{P_l(y_0 + y_P)}{(EI)_l} = -k^2(y_0 + y_P)$$

$$\frac{d^2 y_P}{dx^2} + k^2 y_P = -a_0 k^2 \sin\left(\frac{\pi}{l}x\right)$$

The approach for the solution of this differential equation is:

$$y_P = A\sin(kx) + B\cos(kx) + \frac{1}{\left(\frac{\pi^2}{k^2 l^2}\right) - 1} a_0 \sin\left(\frac{\pi x}{l}\right)$$

With the longeron boundary constraints $y(x = 0) = 0$ and $y(x = l) = 0$ the coefficients A and B are both zero:

$$y = y_0 + y_P = a_0 \sin\left(\frac{\pi}{l}x\right) + \frac{1}{\left(\frac{\pi^2}{k^2 l^2}\right) - 1} a_0 \sin\left(\frac{\pi x}{l}\right)$$

$$y = a_0 \left(1 + \frac{1}{\left(\frac{\pi^2}{k^2 l^2}\right) - 1}\right) \sin\left(\frac{\pi}{l}x\right)$$

$$y = a_0 \left(1 + \frac{1}{\frac{\pi^2 (EI)_l}{P_l l^2} - 1}\right) \sin\left(\frac{\pi}{l}x\right)$$

Substitution by the Euler equation of a beam simply supported at both ends leads to:

$$P_{E,l} = \frac{\pi^2 (EI)_l}{l^2}$$

$$y = a_0 \frac{1}{1 - \frac{P_l}{P_{E,l}}} \sin\left(\frac{\pi}{l} x\right)$$

The displacement a in the middle of the longeron at $l/2$ is as follows:

$$a = a_0 \frac{1}{1 - \frac{P_l}{P_{E,l}}}$$

F3.2 Axial Shortening

The initial shape of an imperfect longeron is given by $y_0(x)$. The shape of the longeron under load is given by $y(x)$ which does not consider deformations in the x-direction to simplify the approach. The arc-length ds of an increment dx in the initial state is (see Fig. F - 1):

$$d_s^2 = d_x^2 + d_{y_0}^2$$

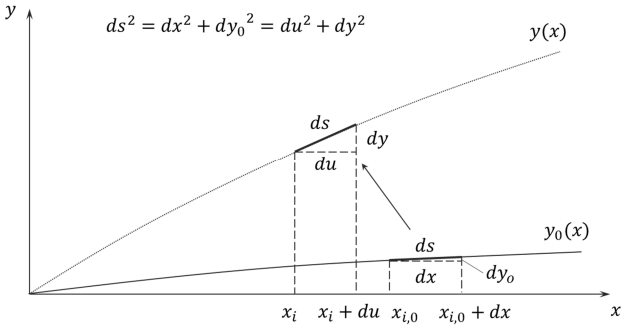

Fig. F - 1: Axial shortening of an imperfect longeron from initial to deformed state under load.

It is assumed that the longeron is incompressible wherefore its total arc-length l_0 does not change under load. The longeron is deformed due to the load and the arc-length increment is shifted. The initial coordinates of the end points of the increment are $x_{i,0}$ and $y_0(x_{i,0})$ and $x_{i,0} + dx$ and $y_0(x_{i,0} + dx)$. The coordinates of the end points for the loaded beam are x_i and $y(x_{i,0})$ and $x_i + du$ and $y(x_{i,0} + dx)$. Of interest is the axial shortening λ of the longeron due to the deflection which is defined as follows:

$$d\lambda = du - dx$$

$$ds^2 = dx^2 + dy_0^2 = du^2 + dy^2$$

$$du = \sqrt{1 - \left(\frac{dy - dy_0}{dx}\right)^2}\, dx$$

$$d\lambda = \left(\sqrt{1 - \left(\frac{dy - dy_0}{dx}\right)^2} - 1\right) dx$$

The axial shortening from an initially straight longeron of length l is as follows:

$$\lambda = \int_0^l \left(\sqrt{1 - \left(\frac{dy}{dx}\right)^2} - 1 \right) dx$$

The deformed shape of a longeron that is simply supported at both ends and loaded by an axial compression force P_l is given as follows (without considering axial shortening):

$$y = a \sin(bx)$$

Whereby a is the amplitude of the sine wave and b is the length factor $b = \frac{\pi}{l}$. The derivative is as follows:

$$y = ab \cos(bx)$$

Substituting the expression in the integral leads to:

$$\lambda = \int_0^l \left(\sqrt{1 - a^2 b^2 \cos^2(bx)} - 1 \right) dx$$

$$\lambda = \int_0^l \sqrt{1 - a^2 b^2 \cos^2(bx)}\, dx - \int_0^l dx$$

$$\lambda = \int_0^l f(x)\, dx - \int_0^l dx$$

The expression in the first integral $f(x)$ is replaced by an expression $g(x)$ that allows a simpler solution. The approach for $g(x)$ is chosen by examination of the graph of the shape fuction $f(x)$ displayed in Fig. F - 2:

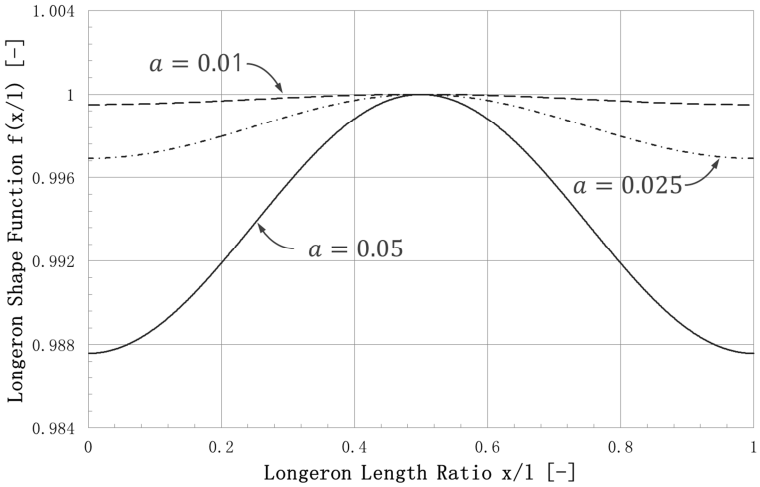

Fig. F - 2: Shape function (note: not actual shape of the deformed longeron) of the deformed longeron plotted over the longeron length ratio.

The behavior at the boundaries is as follows:

$$f'(x = 0) = f'\left(x = \frac{l}{2}\right) = f'(x = l) = 0$$

$$f\left(x = \frac{l}{2}\right) = 1$$

$$f(x = 0) = f(x = l)$$

$$f(x) = f(x = l - x) \text{ for } 0 \le x \le \frac{l}{2}$$

It is visible that an offset-value h is superposed by a negative cos-function in the interval $[0; 2\pi]$ of certain amplitude d. While the mid-point has always the value 1 independent of a and b, the amplitude does vary with a and b. To satisfy these constraints the offset-value h as well as the amplitude d are both functions of a and b. Thereby the approach for $g(x)$ is as follows:

$$g(x) = h(a,b) - d(a,b)\cos(2bx)$$

To satisfy $f\left(x = \frac{l}{2}\right) = 1$ the offset value h is written as follows:

$$h(a,b) = 1 - d(a,b)$$

This leads to:

$$g(x) = 1 - d(a,b)(1 + \cos(2bx))$$

The expression for d is found by equating $f(x)$ and $g(x)$ for $x = 0$:

$$\sqrt{1 - a^2b^2\cos^2(bx)} = 1 - d(a,b)(1 + \cos(2bx))$$

$$\sqrt{1 - a^2b^2} = 1 - 2d(a,b)$$

Thereby the expression for the amplitude d is:

$$d(a,b) = \frac{1}{2}\left(1 - \sqrt{1 - a^2b^2}\right)$$

Now $g(x)$ can be written as follows:

$$g(x) = 1 - \frac{1}{2}\left(1 - \sqrt{1 - a^2b^2}\right)(1 + \cos(2bx))$$

$$g(x) = 1 - \frac{1}{2}\left(1 - \sqrt{1 - a^2\left(\frac{\pi}{l}\right)^2}\right)\left(1 + \cos\left(2\frac{\pi}{l}x\right)\right)$$

Comparing the graphs of both functions $g(x)$ and $f(x)$ one can see that they thoroughly coincide wherefore:

$$f(x) \equiv g(x)$$

$$\int_0^l g(x)\,dx = \int_0^l f(x)\,dx$$

The solution of the axial shortening is thereby as follows:

$$\lambda = \int_0^x g(x)\,dx - \int_0^x dx$$

$$\lambda = \int_0^x \left(1 - d(1 + \cos(2bx))\right)dx - \int_0^x dx$$

$$\lambda = (1 - d)\int_0^x dx - d\int_0^x \cos(2bx)\,dx - \int_0^x dx$$

$$\lambda = (1 - d)x - d\frac{\sin(2bx)}{2b} - x$$

$$\lambda = -dx - d\frac{\sin(2bx)}{2b}$$

$$\lambda = -d\left(x + \frac{\sin(2bx)}{2b}\right)$$

The full expression is as follows:

$$\lambda = -\frac{1}{2}\left(1 - \sqrt{1 - a^2b^2}\right)\left(x + \frac{\sin(2bx)}{2b}\right)$$

$$\lambda = -\frac{1}{2}\left(1 - \sqrt{1 - a^2\left(\frac{\pi}{l}\right)^2}\right)\left(x + l\frac{\sin\left(2\frac{\pi}{l}x\right)}{2\pi}\right)$$

The total axial shortening from a sinusoidal deformation of amplitude a for $x = l$ is thereby:

$$\lambda = \frac{l}{2}\left(\sqrt{1 - a^2\left(\frac{\pi}{l}\right)^2} - 1\right)$$

Fig. F - 3 shows a comparison of the derived solution with the approximation solution δ given by Timoshenko and Gere [145]:

$$\delta = -\frac{\pi^2 a^2}{4l}$$

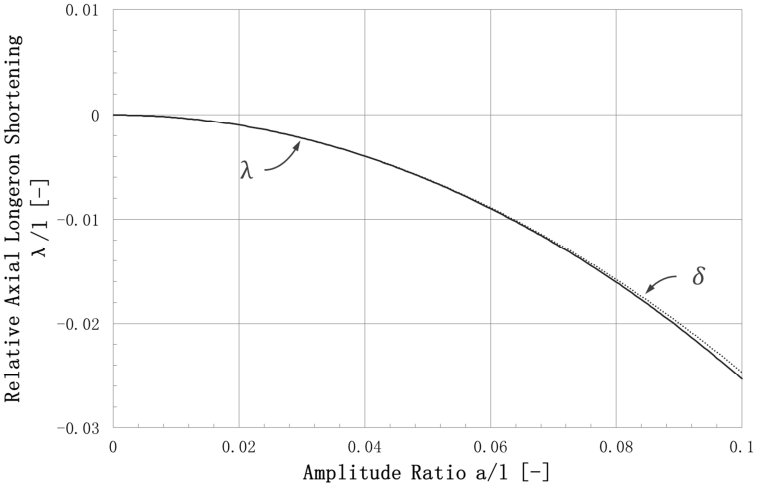

Fig. F - 3: Relative axial longeron shortening plotted over the amplitude ratio and comparison with the simplified solution given by Timoshenko and Gere [145].

The comparison shows that a substantial difference occurs only at high amplitudes. Hence in the following the approximation solution δ is utilized.

The axial shortening from bending of a simply supported longeron with a sinusoidal imperfection of amplitude a_0 due to an axial compression force P_l is derived by substituting the amplitude a by the mid-deflection of the compressed longeron [145]:

$$y\left(x = \frac{l}{2}\right) = a = a_0 \frac{1}{1 - \frac{P_l}{P_{E,l}}}$$

The overall axial shortening of the approximation δ is thereby as follows:

$$\delta = -\frac{\pi^2 a_0^2}{4l} \frac{1}{\left(1 - \frac{P_l}{P_{E,l}}\right)^2} + \frac{\pi^2 a_0^2}{4l} - \frac{P_l l}{EA}$$

$$\delta = \frac{\pi^2 a_0^2}{4l}\left(1 - \frac{1}{\left(1 - \frac{P_l}{P_{E,l}}\right)^2}\right) - \frac{P_l l}{EA}$$

F3.3 Axial Stiffness

The axial stiffness EA is now derived by calculation of the inverse axial stiffness:

$$\frac{d\sigma}{d\varepsilon} = E = \frac{l}{A_l}\frac{dP_l}{d\delta}$$

$$\frac{1}{(EA)_l} = \frac{1}{l}\frac{d\delta}{dP_l}$$

For the approximation of the axial shortening δ the derivative is as follows:

$$\frac{d\delta}{dP_l} = -\frac{\pi^2 a_0^2}{2lP_{E,l}}\frac{1}{\left(1-\frac{P_l}{P_{E,l}}\right)^3} - \frac{l}{(EA)_l} = -l\left(\frac{a_0^2}{2}\frac{1}{\left(1-\frac{P_l}{P_{E,l}}\right)^3}\frac{1}{(EI)_l} + \frac{1}{(EA)_l}\right)$$

Therefore the inverse axial stiffness is as follows:

$$\left|\frac{1}{E_{tan,l}A_l}\right| = \frac{a_0^2}{2}\frac{1}{\left(1-\frac{P_l}{P_{E,l}}\right)^3}\frac{1}{(EI)_l} + \frac{1}{(EA)_l}$$

$$\left|\frac{E}{E_{tan,l}}\right| = \frac{a_0^2}{2}\frac{1}{\left(1-\frac{P_l}{P_{E,l}}\right)^3}\frac{A_l}{I_l} + 1$$

Substitution of the second moment of area I_l by the longeron radius of gyration $r_{i,l}$:

$$\left|\frac{E}{E_{tan,l}}\right| = \frac{1}{2}\left(\frac{a_0}{r_{i,l}}\right)^2\frac{1}{\left(1-\frac{P_l}{P_{E,l}}\right)^3} + 1$$

The modulus ratio $\frac{E}{E_{tan}}$ shows a strong sensitivity to the initial imperfection of the longeron. In Fig. F - 4 the plots for three different initial imperfection ratios $\frac{a_0}{r_{i,l}}$ are given.

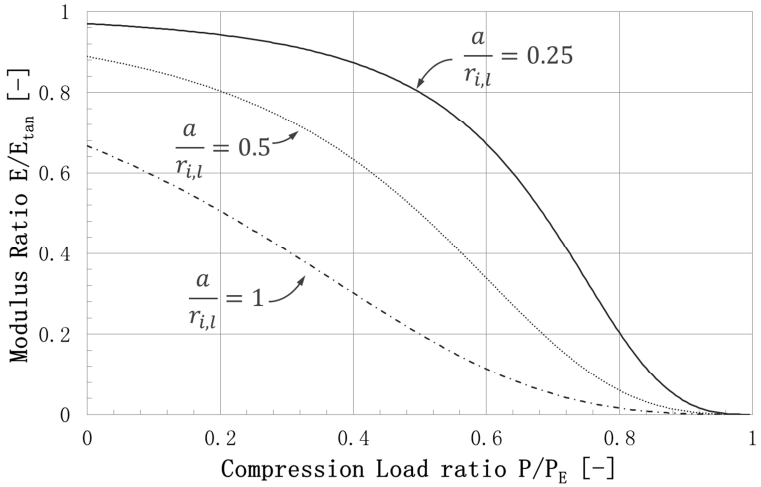

Fig. F - 4: Longeron modulus ratio plotted over compression load ratio for varios initial imperfection sizes.

For design purposes the mechanical properties of the unloaded structure are considered wherefore the modulus is derived for $P_l = 0$:

$$\left|\frac{E}{E_{tan,0,l}}\right| = \frac{1}{2}\left(\frac{a_0}{r_{i,l}}\right)^2 + 1$$

Substituting the longeron imperfection ratio:

$$\zeta = \frac{a_0}{r_{i,l}}$$

One gets the initial tangent modulus $E_{tan,0,l}$ of the imperfect longeron:

$$E_{tan,0,l} = \frac{E}{\frac{1}{2}\zeta^2 + 1}$$

As the initial modulus is a function of the imperfection ratio only, the expression is substituted by the initialmodulus knockdown factor $k_{E,0}$ as follows:

$$E_{tan,0} = k_{E,0}E$$

Fig. F - 5 shows the initial modulus ratio plotted over the imperfection ratio.

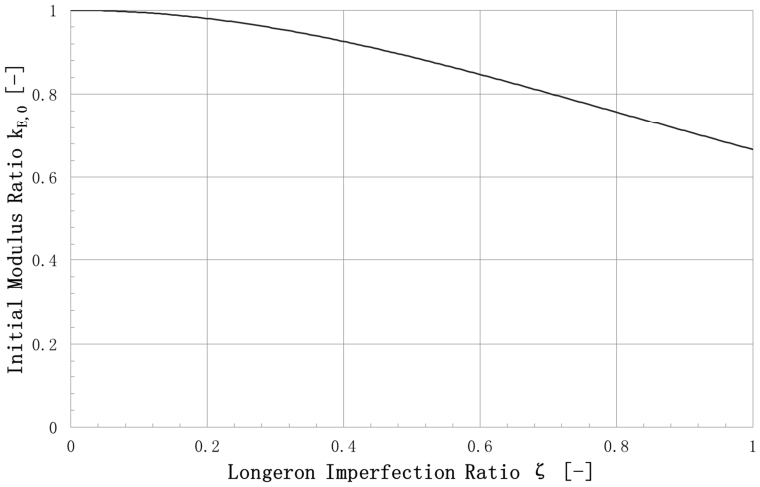

Fig. F - 5: Initial modulus ratio plotted over the longeron imperfection ratio.

F3.4 Column Compression Strength

In the following the compression strength P_{crit} of the truss is derived. The axial stiffness of the longerons is load dependent. Thereby a truss composed of imperfect longerons can be seen as a column with non-linear material modulus $E(P)$:

$$P_{crit} = \frac{\pi^2 E(P) I}{(k_C L)^2}$$

$$P_{crit} = P_E \frac{E_{tan,l}}{E}$$

$$P_{crit} = P_E \frac{1}{\frac{1}{2}\zeta^2 \frac{1}{\left(1 - \frac{P_l}{P_{E,l}}\right)^3} + 1}$$

The longeron loading and the overall loading are connected as follows for a straight column without global imperfection under compression:

$$P_l = \frac{P}{n_l}$$

Substituting the expression leads to:

$$P_{crit} = P_E \frac{1}{\frac{1}{2}\zeta^2 \frac{1}{\left(1 - \frac{P_{crit}}{n_l P_{E,l}}\right)^3} + 1}$$

A ratio of the critical overall Euler load and the longeron Euler load is introduced as follows according to Crawford [113]:

$$K = \frac{P_E}{nP_{E,l}}$$

Substitution leads to:

$$P_{crit} = P_E \frac{1}{\frac{1}{2}\zeta^2 \frac{1}{\left(1 - K\frac{P_{crit}}{P_E}\right)^3} + 1}$$

For the design case of $K = 1$ local and global buckling occurs simultaneously and the equation can be written as follows:

$$\frac{P_{crit}}{P_E} = \frac{1}{\frac{1}{2}\zeta^2 \frac{1}{\left(1 - \frac{P_{crit}}{P_E}\right)^3} + 1}$$

With:

$$\frac{P_{crit}}{P_E} = \alpha_{max}$$
$$\frac{1}{2}\zeta^2 = c$$

The equation becomes:

$$\alpha_{max} = \frac{1}{\frac{c}{(1 - \alpha_{max})^3} + 1}$$

Solving for zero on the right side:

$$\alpha_{max}\left(\frac{c}{(1 - \alpha_{max})^3} + 1\right) = 1$$
$$\frac{c\alpha_{max}}{(1 - \alpha_{max})^3} = 1 - \alpha_{max}$$
$$(1 - \alpha_{max})^4 - c\alpha_{max} = 0$$

Substitution by $x = 1 - \alpha_{max}$ leads to:

$$x^4 + cx - c = 0$$

The reduced form of a polynomial of fourth-power is:

$$x^4 + Px^2 + Qx + R = 0$$

The cubic resolvent of the reduced form is:

$$z^3 - 2Pz^2 + (P^2 - 4R)z + Q^2 = 0$$

Substituting the coefficients:

$$P = 0$$
$$Q = c$$

$$R = -c$$

Leads to:

$$z^3 + 4cz + c^2 = 0$$

The roots of the cubic resolvent are obtained by Cardano's method. The cubic equation is already in the reduced form:

$$z^3 + pz + q = 0$$

With:

$$p = 4c$$
$$q = c^2$$

The solution is obtained by substitution of $z = u + v$:

$$u = \sqrt[3]{-\frac{q}{2} + \sqrt{\Delta}}$$
$$v = \sqrt[3]{-\frac{q}{2} - \sqrt{\Delta}}$$

Whereby:

$$\Delta = \left(\frac{q}{2}\right)^2 + \left(\frac{p}{3}\right)^2$$

Substituting the expressions leads to:

$$u = \sqrt[3]{-\frac{c^2}{2} + \sqrt{\left(\frac{c^2}{2}\right)^2 + \left(\frac{4c}{3}\right)^3}} = \sqrt[3]{-\frac{c^2}{2} + \frac{c}{2}\sqrt{c\left(c + \frac{256}{27}\right)}} = \sqrt[3]{\frac{c}{2}\left(\sqrt{c\left(c + \frac{256}{27}\right)} - c\right)}$$

$$v = \sqrt[3]{-\frac{c^2}{2} - \sqrt{\left(\frac{c^2}{2}\right)^2 + \left(\frac{4c}{3}\right)^3}} = \sqrt[3]{-\frac{c}{2}\left(\sqrt{c\left(c + \frac{256}{27}\right)} + c\right)}$$

Examination of the expressions for u and v shows that for $c > 0$ the term for u is always positive while for v it is always negative. As the absolute value of v is higher than of u, the sum $u + v$ is always negative. The subtraction $u - v$ is always positive.

With:

$$\varepsilon_1 = -\frac{1}{2} + i\frac{1}{2}\sqrt{3}$$
$$\varepsilon_2 = \varepsilon_1^2 = -\frac{1}{2} - i\frac{1}{2}\sqrt{3}$$

The roots of the cubic equation are:

$$z_1 = u + v$$
$$z_2 = u\varepsilon_1 + v\varepsilon_2 = -\frac{u+v}{2} + i\sqrt{3}\frac{u-v}{2}$$
$$z_3 = u\varepsilon_2 + v\varepsilon_1 = -\frac{u+v}{2} - i\sqrt{3}\frac{u-v}{2}$$

To simplify the notation of the equations, substitution of the real part and the imaginary part is done as follows:

$$-\frac{u+v}{2} = T_{RE}$$
$$\sqrt{3}\frac{u-v}{2} = T_{IM}$$

Therefore the roots can be rewritten as follows:

$$z_1 = -2T_{RE}$$
$$z_2 = T_{RE} + iT_{IM}$$
$$z_3 = T_{RE} - iT_{IM}$$

The roots of the original equation are now as follows:

$$x_1 = \frac{1}{2}\left(\sqrt{-z_1} + \sqrt{-z_2} + \sqrt{-z_3}\right)$$

$$x_2 = \frac{1}{2}\left(\sqrt{-z_1} - \sqrt{-z_2} - \sqrt{-z_3}\right)$$
$$x_3 = \frac{1}{2}\left(-\sqrt{-z_1} + \sqrt{-z_2} - \sqrt{-z_3}\right)$$
$$x_4 = \frac{1}{2}\left(-\sqrt{-z_1} - \sqrt{-z_2} + \sqrt{-z_3}\right)$$

Whereby the algebraic signs must be chosen to satisfy:

$$\sqrt{-z_1}\sqrt{-z_2}\sqrt{-z_3} = -Q$$

The square-root of a complex number J is defined as follows:

$$\sqrt{J} = \sqrt{J_{RE} + iJ_{IM}} = \pm\left(\sqrt{\frac{|J| + J_{RE}}{2}} + i\,\mathrm{sgn}(J_{IM})\sqrt{\frac{|J| - J_{RE}}{2}}\right)$$

The square-roots of the negatives of the numbers z_1, z_2 and z_3 are as follows:

$$\sqrt{-z_1} = \sqrt{2T_{RE}}$$
$$\sqrt{-z_2} = \sqrt{-T_{RE} - iT_{IM}} = \pm\left(\sqrt{\frac{\sqrt{T_{RE}^2 + T_{IM}^2} - T_{RE}}{2}} - i\sqrt{\frac{\sqrt{T_{RE}^2 + T_{IM}^2} + T_{RE}}{2}}\right)$$
$$\sqrt{-z_3} = \sqrt{-T_{RE} + iT_{IM}} = \pm\left(\sqrt{\frac{\sqrt{T_{RE}^2 + T_{IM}^2} - T_{RE}}{2}} + i\sqrt{\frac{\sqrt{T_{RE}^2 + T_{IM}^2} + T_{RE}}{2}}\right)$$

The result x_2 gives the required solution:

$$x_2 = -\frac{1}{2}\left(\sqrt{2T_{RE}} - 2\sqrt{\frac{\sqrt{T_{RE}^2 + T_{IM}^2} - T_{RE}}{2}}\right)$$
$$x_2 = -\frac{1}{2}\left(\sqrt{-(u+v)} - 2\sqrt{\frac{\sqrt{\left(-\frac{u+v}{2}\right)^2 + \left(\sqrt{3}\frac{u-v}{2}\right)^2} - \left(-\frac{u+v}{2}\right)}{2}}\right)$$
$$x_2 = -\frac{1}{2}\left(\sqrt{-(u+v)} - 2\sqrt{\frac{\sqrt{(u+v)^2 + 3(u-v)^2} + u + v}{4}}\right)$$
$$x_2 = -\frac{1}{2}\left(\sqrt{-(u+v)} - 2\sqrt{\frac{2\sqrt{u^2 - uv + v^2} + u + v}{4}}\right)$$

Re-substitution of x_2 into α_{max} leads to:

$$\alpha_{max} = 1 + \frac{1}{2}\left(\sqrt{-(u+v)} - 2\sqrt{\frac{2\sqrt{u^2 - uv + v^2} + u + v}{4}}\right)$$

Substituting the longeron imperfection ratio in the expressions for u and v leads to:

$$u = \sqrt[3]{\frac{\zeta^2}{4}\left(\sqrt{\frac{\zeta^2}{2}\left(\frac{\zeta^2}{2} + \frac{256}{27}\right)} - \frac{\zeta^2}{2}\right)} = \sqrt[3]{\frac{\zeta^2}{4}\left(\sqrt{\frac{\zeta^2}{4}\left(\zeta^2 + \frac{512}{27}\right)} - \frac{\zeta^2}{2}\right)} = \sqrt[3]{\frac{\zeta^3}{8}\left(\sqrt{\zeta^2 + \frac{512}{27}} - \zeta\right)}$$

$$v = \sqrt[3]{-\frac{\zeta^2}{4}\left(\sqrt{\frac{\zeta^2}{2}\left(\frac{\zeta^2}{2}+\frac{256}{27}\right)}+\frac{\zeta^2}{2}\right)} = \sqrt[3]{-\frac{\zeta^2}{4}\left(\sqrt{\frac{\zeta^2}{4}\left(\zeta^2+\frac{512}{27}\right)}+\frac{\zeta^2}{2}\right)}$$

$$= \sqrt[3]{-\frac{\zeta^3}{8}\left(\sqrt{\left(\zeta^2+\frac{512}{27}\right)}+\zeta\right)}$$

Thereby u and v can be written as follows:

$$u = \frac{\zeta}{2}\sqrt[3]{\sqrt{\zeta^2+\frac{512}{27}}-\zeta}$$

$$v = -\frac{\zeta}{2}\sqrt[3]{\sqrt{\zeta^2+\frac{512}{27}}+\zeta}$$

And the compression load strength P_{crit} of the truss with imperfect longerons is:

$$P_{crit} = P_E\left(1+\frac{1}{2}\left(\sqrt{-(u+v)}-2\sqrt{\frac{2\sqrt{u^2-uv+v^2}+u+v}{4}}\right)\right)$$

As the reduction of the column Euler load is a function of the longeron imperfection ratio ζ only, the expression is substituted by the compression strength knockdown factor k_ζ:

$$P_{crit} = P_E k_\zeta$$

Fig. F - 6 shows the maximum compression load ratio k_ζ plotted over the longeron imperfection ratio ζ.

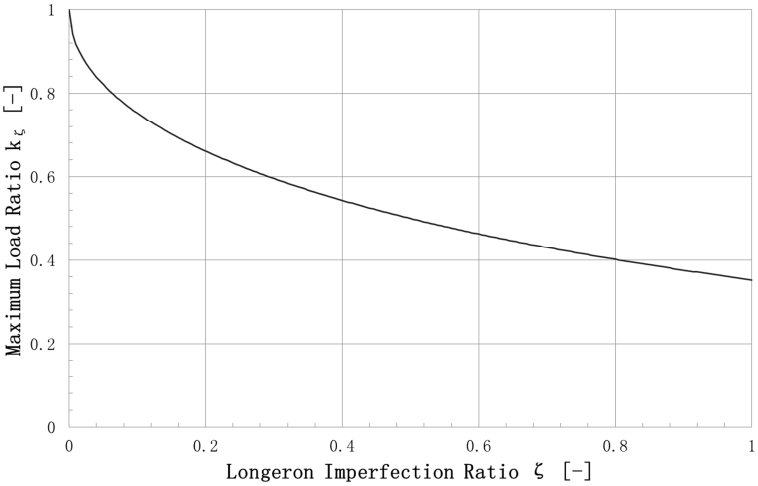

Fig. F - 6: Column maximum load ratio plotted over longeron imperfection ratio.

F3.5 Summary of Truss Performance Equations with Geometrical Longeron Imperfections

The equations for the truss performance considering initial longeron imperfections are summarized in Tab. F - 1.

Truss Performance Equations Considering initial Geometrical Longeron Imperfections		
Performance Parameter	**Symbol/Expression**	**Value**
Longeron imperfection ratio	$\zeta = \frac{a_0}{r_g}$	0.15
Initial modulus knockdown factor	$k_{E,0} = \frac{1}{\frac{1}{2}\zeta^2 + 1}$	-
Initial modulus	$E_{tan,0} = k_{E,0} E$	-
Column compression strength knockdown factor	$k_\zeta = \left(1 + \frac{1}{2}\left(\sqrt{-(u+v)} - 2\sqrt{\frac{2\sqrt{u^2 - uv + v^2} + u + v}{4}}\right)\right)$ $u = \frac{\zeta}{2}^3 \sqrt{\sqrt{\zeta^2 + \frac{512}{27}} - \zeta}$ $v = -\frac{\zeta}{2}^3 \sqrt{\sqrt{\zeta^2 + \frac{512}{27}} + \zeta}$	-
Column compression strength	$P_{crit} = P_E k_\zeta$	-

Tab. F - 4: Truss performance equations considering initial geomtrical longeron imperfections.

F4 Scaling Constraint Functions for the Load Case of Axial Compression

The derivation of the truss scaling constraint functions depends on the definition of the diagonal angle Θ. For scaling with constant diagonal angle the truss axial mass fraction is a constant as well (see F2.1). Hence the design variables are the equivalent truss cross-sectional area A and the truss radius R and the scaling functions can be derived accordingly by the scaling functions on global column and local longeron buckling. When the diagonal angle becomes a variable due to an active scaling limit a third variable is introduced. Hence, the diagonal angle Θ or according truss axial mass fraction β is determined through the additional constraint function provided by the scaling limits.

F4.1 Axial Compression Constraint Functions

The general constraint equations for the truss are local and global column buckling derived by Euler's buckling equation:

$$P_{req} \leq P_{global} = P_E k_\zeta = \frac{\pi^2 EI}{(k_C L)^2} k_\zeta$$

$$P_{req} \leq P_{local} = nP_{E,l} = n\frac{\pi^2 (EI)_l}{\left(k_{C,l} l\right)^2}$$

The bending stiffness expressions EI and $(EI)_l$ are functions of the longeron cross-sectional area A_l:

$$EI = E\frac{n}{2} A_l R^2$$

$$(EI)_l = E\frac{k_{I,l}}{k_{A,l}} A_l^2$$

The equivalent cross-sectional area A is as follows:

$$A = n\beta A_l$$

Substitution of the longeron cross-sectional area A_l by the equivalent cross-sectional area A leads to:

$$EI = E\frac{1}{2}\frac{A}{\beta} R^2$$

$$(EI)_l = E\frac{k_{I,l}}{k_{A,l}}\left(\frac{A}{n\beta}\right)^2$$

Thereby the constraint equations for the global column buckling can be re-written as follows:

$$P_{req} \leq \frac{\pi^2 EI}{\left(k_C L_{req}\right)^2} k_\zeta$$

$$P_{req} \leq \frac{\pi^2}{\left(k_C L_{req}\right)^2} k_\zeta E\frac{n}{2}\frac{A}{n\beta} R^2$$

$$P_{req} \leq \frac{\pi^2}{2} k_\zeta \frac{1}{k_C^2}\frac{1}{L_{req}^2}\frac{1}{\beta} EAR^2$$

The constraint equation for the local longeron buckling can be re-written as follows:

$$P_{req} \leq n\frac{\pi^2 (EI)_l}{\left(k_{C,l} l\right)^2}$$

$$P_{req} \leq n\frac{\pi^2}{\left(k_{C,l} l\right)^2} E\frac{k_{I,l}}{k_{A,l}}\left(\frac{A}{n\beta}\right)^2$$

$$P_{req} \leq \pi^2 \frac{1}{n}\frac{1}{l^2}\frac{1}{k_{C,l}^2}\frac{k_{I,l}}{k_{A,l}}\frac{1}{\beta^2} EA^2$$

Additional constraint functions result from scaling limits. For the minimum and maximum diagonal angle Θ_{min} and Θ_{max} these are:

$$\Theta_{min} \leq \Theta$$

$$\Theta_{max} \geq \Theta$$

These can also be formulated on the basis of the truss axial mass fraction β:

$$\beta_{min} \leq \beta = \frac{1}{c_t\left(\frac{R}{l}\right)^{d_t}}$$

$$\beta_{max} \geq \beta = \frac{1}{c_t\left(\frac{R}{l}\right)^{d_t}}$$

A third scaling limit and corresponding constraint function is defined through a minimum longeron cross-sectional area $A_{l,min}$:

$$A_{l,min} \leq A_l$$

The constraint functions for a truss loaded in axial compression are summarized in Tab. F - 5.

Constraint Functions for a Truss Column loaded in Compression	
Constraint Parameter	**Constraint Function**
Global column buckling	$P_{req} \leq \frac{\pi^2}{2} k_\zeta \frac{1}{k_C^2} \frac{1}{L_{req}^2} \frac{1}{\beta} EAR^2$
Local longeron buckling	$P_{req} \leq \pi^2 \frac{1}{n} \frac{1}{l^2} \frac{1}{k_{C,l}^2} \frac{k_{I,l}}{k_{A,l}} \frac{1}{\beta^2} EA^2$
Minimum diagonal angle	$\Theta_{min} \leq \Theta$ or $\beta_{min} \leq \beta = \frac{1}{c_t \left(\frac{R}{l}\right)^{d_t}}$
Maximum diagonal angle	$\Theta_{max} \geq \Theta$ or $\beta_{max} \geq \beta = \frac{1}{c_t \left(\frac{R}{l}\right)^{d_t}}$
Minimum longeron cross-sectional area	$A_{l,min} \leq A_l$

Tab. F - 5: Constraint functions for a truss loaded in axial compression.

F4.2 Axial Compression with Fixed Diagonal Angle

For constant diagonal angles Θ_{const} the scaling functions the constraint functions are developed in the following. The resulting truss axial mass fraction is a constant as well:

$$\beta_{const} = 1 + \frac{1}{\tan(\Theta_{const})} + \frac{1}{\sin(\Theta_{const})}$$

For a constant diagonal angle the longeron length l can be expressed as a function of the truss radius R and number of longerons n [28]:

$$l = 2 \tan(\Theta_{const}) R \sin\left(\frac{\pi}{n}\right)$$

Thereby the scaling function for constant diagonal angles local longeron buckling is as follows:

$$P_{req} \leq \frac{\pi^2}{4} \frac{1}{n} \frac{1}{\left(\tan(\Theta_{const}) \sin\left(\frac{\pi}{n}\right)\right)^2} \frac{1}{k_{C,l}^2} \frac{k_{I,l}}{k_{A,l}} \frac{1}{\beta_{const}^2} EA^2 R^{-2}$$

The resulting constraint function on local longeron buckling re-written in the form according to Appendix C is as follows:

$$\frac{4}{\pi^2} \beta_{const}^2 n \left(\tan(\Theta_{const}) \sin\left(\frac{\pi}{n}\right)\right)^2 k_{C,l}^2 \frac{k_{A,l}}{k_{I,l}} \frac{1}{E} P_{req} \leq A^2 R^{-2}$$

The resulting constraint function on global column buckling re-written in the form according to Appendix C is as follows:

$$\frac{2}{\pi^2} \frac{1}{k_\zeta} k_C^2 \beta_{const} \frac{1}{E} P_{req} L_{req}^2 \leq AR^2$$

The constraint function on the minimum cross-sectional longeron area $A_{l,min}$ for a truss with constant diagonal angle is as follows:

$$A_{l,min} \leq A_l$$

Substitution of the equivalent truss cross-sectional area A gives:

$$A = n\beta_{const}A_l$$

$$A_{l,min} \leq \frac{1}{n\beta_{const}}A$$

The resulting constraint function on the minimum cross-sectional longeron area re-written in the form according to Appendix C is as follows:

$$n\beta_{const}A_{l,min} \leq AR^0$$

Tab. F - 6 summarizes the constraint functions for scaling of a truss with constant diagonal angle applicable for the cases of scaling without active scaling limits represented by $\Theta_{opt,c}$ and the cases where the maximum and minimum diagonal angles Θ_{min} and Θ_{max} are reached.

Scaling Constraint Functions of the Truss with Fixed Diagonal Angle for the Load Case of Axial Compression				
Constraint Criterion	**Constraint Function**	c	i	j
Global column buckling	$\frac{2}{\pi^2}\frac{1}{k_\zeta}k_c^2\beta_{const}\frac{1}{E}P_{req}L_{req}^2 \leq AR^2$	$\frac{2}{\pi^2}\frac{1}{k_\zeta}k_c^2\beta_{const}\frac{1}{E}P_{req}L_{req}^2$	1	2
Local longeron buckling	$\frac{4}{\pi^2}\beta_{const}^2 n\left(\tan(\Theta_{const})\sin\left(\frac{\pi}{n}\right)\right)^2 k_c^2 \leq A^2R^{-2}$	$\frac{4}{\pi^2}\beta_{const}^2 n\left(\tan(\Theta_{const})\sin\left(\frac{\pi}{n}\right)\right)^2 k$	2	-2
Minimum cross-sectional longeron area	$n\beta_{const}A_{l,min} \leq AR^0$	$n\beta_{const}A_{l,min}$	1	0
Applicable for diagonal angles $\Theta_{opt,c}$, Θ_{min}, Θ_{max}				

Tab. F - 6: Scaling constraint functions for the truss with fixed diagonal angle loaded in compression.

F4.3 Axial Compression with Varying Diagonal Angle

For a truss with varying diagonal angle three constraint functions need to be solved. These are re-formulated in two scaling functions to achieve compatibility of the constraint functions with the form according to Appendix C.

The truss diagonal angle Θ varies when the minimum longeron cross-sectional dimensions are reached. The resulting constraint equation for the equivalent cross-sectional truss area A is thereby as follows:

$$A \geq n\beta A_{min,l}$$

Substitution of the truss mass factor approximation leads to:

$$A \geq \frac{n}{c_t\left(\frac{R}{l}\right)^{d_t}}A_{min,l}$$

$$A \geq \frac{n}{c_t R^{d_t}}l^{d_t}A_{min,l}$$

The longeron length l is derived from local longeron buckling:

$$P_{req} \leq \pi^2 \frac{1}{n} \frac{1}{l^2} \frac{1}{k_{C,l}^2} \frac{k_{I,l}}{k_{A,l}} \frac{1}{\beta^2} EA^2$$

Substitution of the truss mass factor approximation leads to:

$$P_{req} \leq \pi^2 \frac{1}{n} \frac{1}{l^2} \frac{1}{k_{C,l}^2} \frac{k_{I,l}}{k_{A,l}} \left(c_t \left(\frac{R}{l} \right)^{d_t} \right)^2 EA^2$$

$$P_{req} = \pi^2 c_t^2 \frac{1}{n} \frac{1}{k_{C,l}^2} \frac{k_{I,l}}{k_{A,l}} \frac{1}{l^{2+2d_t}} EA^2 R^{2d_t}$$

Solving for the longeron length l gives:

$$l^{2+2d_t} = \pi^2 c_t^2 \frac{1}{n} \frac{1}{k_{C,l}^2} \frac{k_{I,l}}{k_{A,l}} \frac{1}{P_{req}} EA^2 R^{2d_t}$$

$$l = \left(\pi^2 c_t^2 \frac{1}{n} \frac{1}{k_{C,l}^2} \frac{k_{I,l}}{k_{A,l}} \frac{1}{P_{req}} EA^2 R^{2d_t} \right)^{\frac{1}{2+2d_t}}$$

Substitution of the longeron length in the expression for the equivalent cross-sectional truss area gives the first constraint equation:

$$A \geq \frac{n}{c_t R^{d_t}} l^{d_t} A_{min,l}$$

$$A \geq \frac{n}{c_t R^{d}} \left(\pi^2 c_t^2 \frac{1}{n} \frac{1}{k_{C,l}^2} \frac{k_{I,l}}{k_{A,l}} \frac{1}{P_{req}} EA^2 R^{2d_t} \right)^{\frac{d_t}{2+2d_t}} A_{min,l}$$

$$A^{\frac{2+2d_t}{d_t}} \geq \frac{n^{\frac{2+2d_t}{d_t}}}{c_t^{\frac{2+2d_t}{d_t}} R^{2+2d_t}} \pi^2 c_t^2 \frac{1}{n} \frac{1}{k_{C,l}^2} \frac{k_{I,l}}{k_{A,l}} \frac{1}{P_{req}} EA^2 R^{2d_t} A_{min,l}^{\frac{2+2d_t}{d_t}}$$

$$\frac{A^{\frac{2+2d_t}{d_t}}}{A^2} \geq \pi^2 \frac{n^{\frac{2+2d_t}{d_t}}}{n} \frac{c_t^2}{c_t^{\frac{2+2d_t}{d_t}}} \frac{1}{k_{C,l}^2} \frac{k_{I,l}}{k_{A,l}} \frac{1}{P_{req}} E \frac{R^{2d_t}}{R^{2+2d_t}} A_{min,l}^{\frac{2+2d_t}{d_t}}$$

$$A^{\frac{2}{d_t}} \geq \pi^2 n^{\frac{2+d_t}{d_t}} \frac{1}{c_t^{\frac{2}{d_t}}} \frac{1}{k_{C,l}^2} \frac{k_{I,l}}{k_{A,l}} \frac{1}{P_{req}} E \frac{1}{R^2} A_{min,l}^{\frac{2+2d_t}{d_t}}$$

Re-written in the form according to Appendix C results in:

$$\pi^2 \frac{1}{c_t^{\frac{2}{d_t}}} n^{\frac{2+d_t}{d_t}} \frac{1}{k_{C,l}^2} \frac{k_{I,l}}{k_{A,l}} EA_{min,l}^{\frac{2+2d_t}{d_t}} \frac{1}{P_{req}} \leq A^{\frac{2}{d_t}} R^2$$

$$\pi^{2d_t} \frac{1}{c_t^2} n^{2+d_t} \frac{1}{k_{C,l}^{2d_t}} \left(\frac{k_{I,l}}{k_{A,l}} \right)^{d_t} E^{d_t} A_{min,l}^{2+2d_t} \frac{1}{P_{req}^{d_t}} \leq A^2 R^{2d_t}$$

Substitution of the expressions for the truss mass factor approximation and the longeron length in the constraint equation for global column buckling gives the second constraint equation:

$$P_{req} \leq \frac{\pi^2}{2} k_\zeta \frac{1}{k_C^2} \frac{1}{L_{req}^2} \frac{1}{\beta} EAR^2$$

$$P_{req} \leq \frac{\pi^2}{2} k_\zeta \frac{1}{k_C^2} \frac{1}{L_{req}^2} c_t \left(\frac{R}{l} \right)^{d_t} EAR^2$$

$$P_{req} \leq \frac{\pi^2}{2} c_t k_\zeta \frac{1}{k_C^2} \frac{1}{l^{d_t}} \frac{1}{L_{req}^2} EAR^{2+d_t}$$

$$P_{req} \leq \frac{\pi^2}{2} c_t \frac{1}{k_C^2} k_\zeta E \frac{1}{\left(\pi^2 c_t^2 \frac{1}{n} \frac{1}{k_{C,l}^2} \frac{k_{I,l}}{k_{A,l}} \frac{1}{P_{req}} EA^2 R^{2d_t} \right)^{\frac{d_t}{2+2d_t}}} \frac{1}{L_{req}^2} AR^{2+d_t}$$

$$P_{req}^{\frac{2+2d_t}{d_t}}$$

$$\leq \frac{\pi^{2\frac{2+2d_t}{d_t}}}{2^{\frac{2+2d_t}{d_t}}} c_t^{\frac{2+2d_t}{d_t}} \frac{1}{k_C^{2\frac{2+2d_t}{d_t}}} k_\zeta^{\frac{2+2d_t}{d_t}} E^{\frac{2+2d_t}{d_t}} \frac{1}{\pi^2 c_t^2 \frac{1}{n} \frac{1}{k_{C,l}^2} \frac{k_{I,l}}{k_{A,l}} \frac{1}{P_{req}} E A^2 R^{2d_t}} \frac{1}{L_{req}^{2\frac{2+2d_t}{d_t}}} A^{\frac{2+2d_t}{d_t}} R^{\frac{(2+d_t)(2+2d_t)}{d_t}}$$

$$\frac{P_{req}^{\frac{2+2d_t}{d_t}}}{P_{req}} \leq \frac{\pi^{2\frac{2+2d_t}{d_t}}}{\pi^2} \frac{1}{2^{\frac{2+2d_t}{d_t}}} \frac{c_t^{\frac{2+2d_t}{d_t}}}{c_t^2} \frac{1}{k_C^{2\frac{2+2d_t}{d_t}}} k_\zeta^{\frac{2+2d_t}{d_t}} \frac{E^{\frac{2+2d_t}{d_t}}}{E} n k_{C,l}^2 \frac{k_{A,l}}{k_{I,l}} \frac{1}{L_{req}^{2\frac{2+2d_t}{d_t}}} \frac{A^{\frac{2+2d_t}{d_t}}}{A^2} \frac{R^{\frac{(2+d_t)(2+2d_t)}{d_t}}}{R^{2d_t}}$$

$$P_{req}^{\frac{2+d_t}{d_t}} \leq \frac{\pi^{\frac{4+2d_t}{d_t}}}{2^{\frac{2+2d_t}{d_t}}} c_t^{\frac{2}{d_t}} \frac{1}{k_C^{\frac{4+4d_t}{d_t}}} k_\zeta^{\frac{2+2d_t}{d_t}} E^{\frac{2+d_t}{d_t}} n k_{C,l}^2 \frac{k_{A,l}}{k_{I,l}} \frac{1}{L_{req}^{\frac{4+4d_t}{d_t}}} A^{\frac{2}{d_t}} R^{\frac{4+6d_t}{d_t}}$$

Re-written in the form according to Appendix C results in:

$$\frac{2^{\frac{2+2d_t}{d_t}}}{\pi^{\frac{4+2d_t}{d_t}}} \frac{1}{c_t^{\frac{2}{d_t}}} k_C^{\frac{4+4d_t}{d_t}} \frac{k_{I,l}}{k_{A,l}} \frac{1}{k_\zeta^{\frac{2+2d_t}{d_t}}} \frac{1}{E^{\frac{2+d_t}{d_t}}} \frac{1}{n} \frac{1}{k_{C,l}^2} L_{req}^{\frac{4+4d_t}{d_t}} P_{req}^{\frac{2+d_t}{d_t}} \leq A^{\frac{2}{d_t}} R^{\frac{4+6d_t}{d_t}}$$

$$\frac{2^{2+2d_t}}{\pi^{4+2d_t}} \frac{1}{c_t^2} k_C^{4+4d_t} \left(\frac{k_{I,l}}{k_{A,l}}\right)^{d_t} \frac{1}{k_\zeta^{2+2d_t}} \frac{1}{E^{2+d_t}} \frac{1}{n^{d_t}} \frac{1}{k_{C,l}^{2d_t}} L_{req}^{4+4d_t} P_{req}^{2+d_t} \leq A^2 R^{4+6d_t}$$

Tab. F - 7 summarizes the constraint functions for scaling of a truss with varying diagonal angle for the case that the minimum longeron dimensions are reached.

Scaling Constraint Functions of the Truss with Varying Diagonal Angle for the Load Case of Axial Compression				
Constraint Criterion	**Constraint Function**	c	i	j
Global column buckling with minimum longeron cross-sectional dimensions	$\frac{2^{2+2d_t}}{\pi^{4+2d_t}} \frac{1}{c_t^2} k_C^{4+4d_t} \left(\frac{k_{I,l}}{k_{A,l}}\right)^{d_t} \frac{1}{k_\zeta^{2+2d_t}} \frac{1}{E^{2+d_t}} \frac{1}{n^{d_t}} \frac{1}{k_{C,l}^{2d_t}} \leq A^2 R^{4+6d_t}$	$\frac{2^{2+2d_t}}{\pi^{4+2d_t}} \frac{1}{c_t^2} k_C^{4+4d_t} \left(\frac{k_{I,l}}{k_{A,l}}\right)^{d_t} \frac{1}{k_\zeta^{2+2d_t}} \frac{1}{E^{2+d_t}} n$	2	$4 + 6d_t$
Local longeron buckling with minimum longeron cross-sectional dimensions	$\pi^{2d_t} \frac{1}{c_t^2} n^{2+d_t} \frac{1}{k_{C,l}^{2d_t}} \left(\frac{k_{I,l}}{k_{A,l}}\right)^{d_t} E^{d_t} A_{min,l}^{2+2d_t} \leq A^2 R^{2d_t}$	$\pi^{2d_t} \frac{1}{c_t^2} n^{2+d_t} \frac{1}{k_{C,l}^{2d_t}} \left(\frac{k_{I,l}}{k_{A,l}}\right)^{d_t} E^{d_t} A_m^2$	2	$2d_t$

Tab. F - 7: Scaling constraint functions for a truss with varying diagonal angle and minimum cross-sectional longeron dimensions for the load case of axial compression.

F5 Scaling Constraint Functions for the Load Case of Bending

The scaling constraint functions for the truss loaded in bending are derived in the same way as for the load case of axial compression.

F5.1 Bending Constraint Functions

The general constraint equations for the truss are a certain bending stiffness that needs to be provided and local longeron buckling due to an applied bending moment. The bending stiffness constraint equation is as follows:

$$EI_{req} \leq EI = k_{E,0} E \frac{n}{2} A_l R^2$$

Substitution of the longeron area gives:

$$A = n\beta A_l$$

$$A_l = \frac{A}{n\beta}$$

$$EI_{req} \leq EI = \frac{1}{2} k_{E,0} E \frac{1}{\beta} A R^2$$

The critical bending moment constraint equation is as follows:

$$M_{req} \leq M = \frac{n}{2} P_l R$$

The longeron compression strength P_l is as follows:

$$P_l = \frac{\pi^2 (EI)_l}{\left(k_{C,l} l\right)^2}$$

$$M_{req} \leq M = \frac{n}{2} \frac{\pi^2 (EI)_l}{\left(k_{C,l} l\right)^2} R$$

For simply supported longerons $k_{C,l}$ becomes 1 and by substituting the longeron moment of inertia I_l the moment expression can be written as follows:

$$M_{req} \leq M = \frac{\pi^2}{2} nE \frac{k_{I,l}}{k_{A,l}} \frac{A_l^2}{l^2} R$$

Substitution of the longeron area A_l by the equivalent truss cross-sectional area A gives:

$$A = n\beta A_l$$

$$A_l = \frac{A}{n\beta}$$

$$M_{req} \leq M = \frac{\pi^2}{2} nE \frac{k_{I,l}}{k_{A,l}} \frac{1}{l^2} \left(\frac{A}{n\beta}\right)^2 R$$

Thereby the constraint equation for the critical bending moment is as follows:

$$M_{req} \leq M = \frac{\pi^2}{2} \frac{1}{n} \frac{1}{\beta^2} \frac{k_{I,l}}{k_{A,l}} \frac{1}{l^2} E A^2 R$$

Additional constraint functions resulting from scaling limits are the same as for the load case of axial compression.

The constraint functions for a truss loaded in bending are summarized in Tab. F - 8.

Constraint Functions for a Truss Column loaded in Bending	
Constraint Parameter	**Constraint Function**
Bending Stiffness	$EI_{req} \leq EI = \frac{1}{2} k_{E,0} E \frac{1}{\beta} AR^2$
Critical bending moment	$M_{req} \leq M = \frac{\pi^2}{2} \frac{1}{n} \frac{1}{\beta^2} \frac{k_{I,l}}{k_{A,l}} \frac{1}{l^2} EA^2R$
Minimum diagonal angle	$\Theta_{min} \leq \Theta$ or $\beta_{min} \leq \beta = \frac{1}{c_t \left(\frac{R}{l}\right)^{d_t}}$
Maximum diagonal angle	$\Theta_{max} \geq \Theta$ or $\beta_{max} \geq \beta = \frac{1}{c_t \left(\frac{R}{l}\right)^{d_t}}$
Minimum longeron cross-sectional area	$A_{l,min} \leq A_l$

Tab. F - 8: Constraint functions for a truss loaded in bending.

F5.2 Bending with Fixed Diagonal Angle

As introduced for the load case of axial compression the truss axial mass ratio becomes a constant for constant diagonal angles in the cases of $\Theta_{opt,b}$, Θ_{min} and Θ_{max} and the longeron length can be expressed as a function of the truss radius R and number of longerons n:

$$\beta_{const} = 1 + \frac{1}{\tan(\Theta_{const})} + \frac{1}{\sin(\Theta_{const})}$$

$$l = 2 \tan(\Theta_{const}) R \sin\left(\frac{\pi}{n}\right)$$

Substitution in the scaling constraint function on the bending stiffness gives:

$$EI_{req} \leq \frac{1}{2} k_{E,0} E \frac{1}{\beta_{const}} AR^2$$

Re-written in the form according to Appendix C the scaling constraint function is as follows:

$$2 \frac{1}{k_{E,0} E} \beta_{const} EI_{req} \leq AR^2$$

Substitution in the expression of the scaling constraint function on the critical bending moment gives:

$$M_{req} \leq \frac{\pi^2}{8} \frac{1}{n} \frac{1}{\beta_{const}^2} \frac{k_{I,l}}{k_{A,l}} \frac{1}{\left(\tan(\Theta_{const}) \sin\left(\frac{\pi}{n}\right)\right)^2} EA^2R^{-1}$$

Re-written in the form according to Appendix C the scaling constraint function is as follows:

$$\frac{8}{\pi^2} n \beta_{const}^2 \frac{k_{A,l}}{k_{I,l}} \left(\tan(\Theta_{const}) \sin\left(\frac{\pi}{n}\right)\right)^2 \frac{1}{E} M_{req} \leq A^2R^{-1}$$

The scaling constraint function on the minimum cross-sectional longeron area is the same as for the load case of axial compression.

Tab. F - 9 summarizes the constraint functions for scaling of a truss with constant diagonal angle applicable for the cases of scaling without active scaling limits represented by $\Theta_{opt,b}$ and the cases where the maximum and minimum diagonal angles Θ_{min} and Θ_{max} are reached.

Scaling Constraint Functions of the Truss with Fixed Diagonal Angle for the Load Case of Bending				
Constraint Criterion	**Constraint Function**	c	i	j
Bending Stiffness	$2\frac{1}{k_{E,0}E}\beta_{const}EI_{req} \leq AR^2$	$2\frac{1}{k_{E,0}E}\beta_{const}EI_{req}$	1	2
Critical bending moment	$\frac{8}{\pi^2}n\beta_{const}^2\frac{k_{A,l}}{k_{I,l}}\left(\tan(\Theta_{const})\sin\left(\frac{\pi}{n}\right)\right) \leq A^2R^{-1}$	$\frac{8}{\pi^2}n\beta_{const}^2\frac{k_{A,l}}{k_{I,l}}\left(\tan(\Theta_{const})\sin\left(\frac{\pi}{n}\right)\right)$	2	-1
Minimum cross-sectional longeron area	$n\beta_{const}A_{l,min} \leq AR^0$	$n\beta_{const}A_{l,min}$	1	0
Applicable for diagonal angles $\Theta_{opt,b}$, Θ_{min}, Θ_{max}				

Tab. F - 9: Scaling constraint functions for the truss with fixed diagonal angle loaded in bending.

F5.3 Bending with Varying Diagonal Angle

As introduced for the load case of axial compression the diagonal angle becomes a variable when the minimum longeron cross-sectional area is reached. The scaling limit for minimum longeron area is solved for the truss mass factor β:

$$n\beta A_{l,min} = A$$
$$\beta = \frac{A}{nA_{l,min}}$$

The approximation function for the truss mass factor is solved for the longeron length l:

$$\beta \approx \frac{1}{c_t\left(\frac{R}{l}\right)^{d_t}}$$
$$l = c_t^{\frac{1}{d_t}}\beta^{\frac{1}{d_t}}R$$
$$l = c_t^{\frac{1}{d_t}}\left(\frac{A}{nA_{l,min}}\right)^{\frac{1}{d}}R$$
$$l = c_t^{\frac{1}{d_t}}\frac{1}{n^{\frac{1}{d_t}}}\frac{1}{A_{l,min}^{\frac{1}{d_t}}}A^{\frac{1}{d_t}}R$$

Substitution of longeron length and truss mass factor in the constraint equation for bending stiffness and re-written in the form according to Appendix C gives:

$$2\frac{1}{k_{E,0}E}\beta(EI)_{req} \leq AR^2$$
$$2\frac{1}{k_{E,0}E}\frac{A}{nA_{l,min}}(EI)_{req} \leq AR^2$$
$$2\frac{1}{k_{E,0}E}\frac{1}{n}\frac{1}{A_{l,min}}(EI)_{req} \leq A^0R^2$$

Substitution of longeron length and truss mass factor in the constraint equation for critical bending moment and re-written in the form according to Appendix C gives:

$$\frac{2}{\pi^2} n \beta^2 \frac{k_{A,l}}{k_{I,l}} l^2 \frac{1}{E} M_{req} \leq A^2 R$$

$$\frac{2}{\pi^2} n \left(\frac{A}{n A_{l,min}} \right)^2 \frac{k_{A,l}}{k_{I,l}} \left(c_t^{\frac{1}{d_t}} \frac{1}{n^{\frac{1}{d_t}}} \frac{1}{A_{l,min}^{\frac{1}{d_t}}} A^{\frac{1}{d_t}} R \right)^2 \frac{1}{E} M_{req} \leq A^2 R$$

$$\frac{2}{\pi^2} \frac{1}{n^{1+\frac{2}{d_t}}} \frac{1}{A_{l,min}^{2+\frac{2}{d_t}}} \frac{k_{A,l}}{k_{I,l}} c_t^{\frac{2}{d_t}} \frac{1}{E} M_{req} \leq A^{-\frac{2}{d_t}} R^{-1}$$

Tab. F - 10 summarizes the constraint functions for scaling of a truss with varying diagonal angle for the case that the minimum longeron dimensions are reached.

Scaling Constraint Functions of the Truss with Varying Diagonal Angle for the Load Case of Bending				
Constraint Criterion	**Constraint Function**	c	i	j
Bending stiffness with minimum longeron cross-sectional dimensions	$2 \frac{1}{k_{E,0} E} \frac{1}{n} \frac{1}{A_{l,min}} (EI)_{req} \leq A^0 R^2$	$2 \frac{1}{k_{E,0} E} \frac{1}{n} \frac{1}{A_{l,min}} (EI)_{req}$	0	2
Critical bending moment with minimum longeron cross-sectional dimensions	$\frac{2}{\pi^2} \frac{1}{n^{1+\frac{2}{d_t}}} \frac{1}{A_{l,min}^{2+\frac{2}{d_t}}} \frac{k_{A,l}}{k_{I,l}} c_t^{\frac{2}{d_t}} \frac{1}{E} M_{req} \leq A^{-\frac{2}{d_t}} R^{-1}$	$\frac{2}{\pi^2} \frac{1}{n^{1+\frac{2}{d_t}}} \frac{1}{A_{l,min}^{2+\frac{2}{d_t}}} \frac{k_{A,l}}{k_{I,l}} c_t^{\frac{2}{d_t}} \frac{1}{E} M_r$	$-\frac{2}{d_t}$	-1

Tab. F - 10: Scaling constraint functions for a truss with varying diagonal angle and minimum cross-sectional longeron dimensions for the load case of bending.

Appendix G

G Transition Zone Scaling Constraint Functions

Within Appendix G the scaling constraint functions for the Tubular Shell Mast with consideration of a load carrying Transition Zone are derived for the load cases of axial compression and bending.

G1 Transition Zone Parameterization

Fig. G - 1 displays the parameterization of the Transition Zone through three functions describing the centerline profile $Z(x)$, the centerline curvature $\mathrm{K}(x)$ and the flange profile $Y(x)$. Furthermore the Transition Zone of the deploying mast is supported by the mechanism over the length l_{tz}.

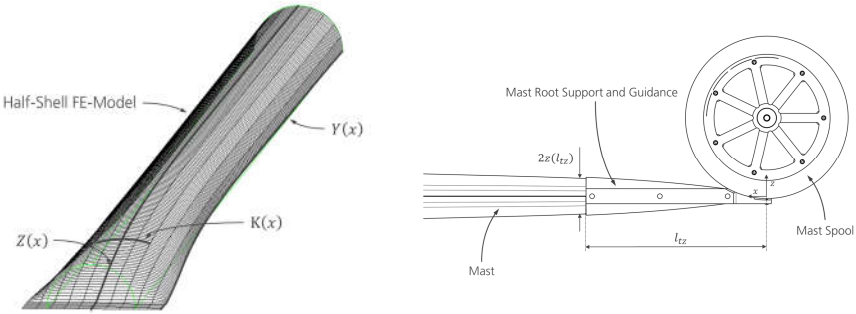

Fig. G - 1: Shape of the transition (left) and support given by the Deployment Mechanism (right).

To enable a description of the Transition Zones geometry independent of size the length coordinate x is normalized by the mast radius of gyration $r_{M,i}$ and geometry functions $Y(x)$ and $Z(x)$ are normalized by the deployed cross-sectional radius R and the curvature $\mathrm{K}(x)$ by the deployed curvature κ:

$$\hat{x} = \frac{x}{r_{M,i}}$$

$$\hat{Y}(\hat{x}) = \frac{Y(x)}{R}$$

$$\hat{Z}(\hat{x}) = \frac{Z(\hat{x})}{R}$$

$$\hat{\mathrm{K}}(\hat{x}) = \frac{\mathrm{K}(\hat{x})}{\kappa}$$

Furthermore the length of the supported part of the Transition Zone l_{tz} is described in relation to the masts radius of gyration by the mast-mechanism interface factor k_{IF}:

$$k_{IF} = \frac{l_{tz}}{r_{M,i}}$$

The cross-sectional shape of the mast is described in non-dimensional form through the wall thickness ratio Γ_t which relates the shell thickness t to the mast radius R:

$$\Gamma_t = \frac{t}{R}$$

Furthermore the cross-sectional shape is described by the angle α that describes the peripheral half-angle of the deployed half-shell. The cross-sectional shape of the mast with the according parameters is displayed in Fig. G - 2.

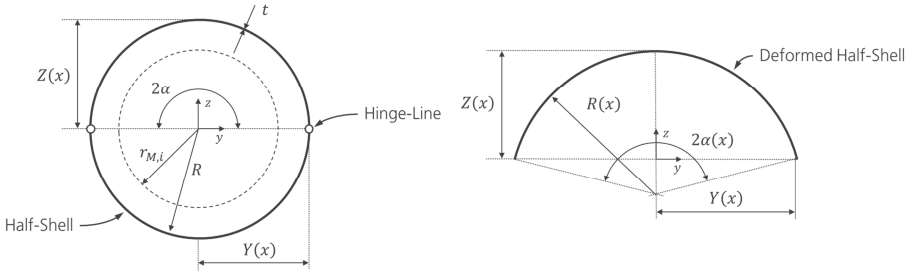

Fig. G - 2: Cross-sectional shape of the Tubular Shell Mast in deployed state (left) and shape approximation of the deformed state (right).

For the description of the deformed state of the Tubular Shell Mast within the Transition Zone the cross-sectional shape is approximated as a segment of a circle according to Fig. G - 2. With this form approximation the properties of the mast throughout the Transition Zone can be calculated from the three geometry functions $Y(x)$, $Z(x)$ and $\mathrm{K}(x)$. The second moment of area around the masts weak axis I_y is derived from the second moment of area of a segment of a circle as shown in Fig. G - 3.

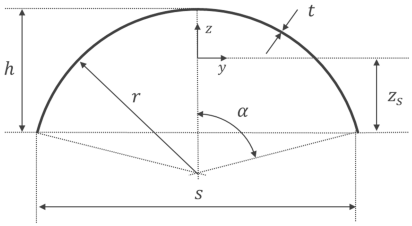

Fig. G - 3: Geometrical properties of a segment of a circle.

The distance of the center of the circle segment towards the center of area z_s is as follows:

$$z_s = \frac{r\sin(\alpha)}{\alpha}$$

The radius of the segments r and the half-angle α of a circle segment are calculated as follows:

$$r = \frac{4h^2 + s^2}{8h}$$

$$\alpha = \arcsin\left(\frac{s}{2r}\right)$$

The second moment of area of a segment of a circle that is symmetrical towards the z-axis is as follows:

$$I_{y,s} = r^3 t\left(\alpha + \frac{\sin(2\alpha)}{2} - \frac{2\sin^2(\alpha)}{\alpha}\right)$$

The overall moment of inertia I_y of the Tubular Shell Mast with deformed cross-section is the sum of the second moments of area of the circle segments and the offset towards the axis of symmetry Δz:

$$I_y = 2\left(I_{y,s} + \Delta z^2 \frac{A}{2}\right)$$

The segment base length s, the segment height h and the offset of the segments Δz are calculated from the centerline and flange profiles $Z(x)$ and $Y(x)$ as follows:

$$s(x) = 2Y(x)$$
$$h(x) = Z(x)$$
$$\Delta z(x) = Z(x) - \left(r(x) - z_s(x)\right) = Z(x) + \left(\frac{\sin(\alpha(x))}{\alpha(x)} - 1\right) r(x)$$

The properties of the mast Transition Zone are summarized in Tab. G - 1.

Tubular Shell Mast Transition Zone Parameters			
Property	**Parameter**	**Unit**	**Values**
Deployed radius	R	m	Sizing result
Cross-sectional area	A	m²	Sizing result
Shell thickness	t	m	-
Mast radius of gyration	r_{Mi}	m	-
Deployed mast curvature	κ	1/m	-
Cross-sectional half-angle	α	rad	$\frac{\pi}{2}$
Circle segment width	s	m	-
Circle segment height	h	m	-
Center of area offset	z_s	m	-
Circle segment offset to mast neutral axis	Δz	m	-
Circle segment second moment of area	$I_{y,s}$	m⁴	-
Mast second moment of area around weak axis	I_y	m⁴	-
Length coordinate	x	m	-
Normalized length coordinate	$\hat{x}$	-	-
Centerline profile	Z	m	FE-data
Normalized centerline profile	$\hat{Z}$	-	-

Flange profile	Y	m	FE-data
Normalized flange profile	$\hat{Y}$	-	-
Centerline curvature	K	1/m	FE-data
Normalized centerline curvature	$\hat{\mathrm{K}}$	-	-
Wall thickness ratio	Γ_t	-	-
Transition Zone length	l_{tz}	m	-
Mast-mechanism interface factor	k_{IF}	-	7

Tab. G - 1: Parameters of the Transition Zone of the Tubular Shell Mast.

G2 Compressions Strength from Local Wall Buckling

The constraint equation for the critical stress is formulated for the mast at the interface to the mechanism as follows:

$$P_{req} \leq \sigma_{crit,IF} A$$

The approximation function for the compression strength $\hat{P}$ of the Tubular Shell Mast regarding local wall buckling is as follows (see subsection 6.3.2):

$$\hat{P}_{\hat{x}} = \frac{P_{\hat{x}}}{P_0} = \frac{\sigma_{crit,c,\hat{x}}}{\sigma_{crit,c,0}} = e_1 \hat{x}^3 + e_2 \hat{x}^2 + e_3 \hat{x} + e_4$$

The coefficients e_k are as follows:

$$\Gamma_t = \frac{t}{R}$$

$$e_k = \iota_{1,k} \Gamma_t^2 + \iota_{2,k} \Gamma_t + \iota_{3,k}$$

The length coordinate at the interface is as follows:

$$\hat{x}_{IF} = \frac{x_{IF}}{r_{M,i}} = \frac{l_{tz}}{r_{M,i}} = k_{IF}$$

Substitution in the compression strength expressions gives:

$$P_{\hat{x}_{IF}} = P_{IF} = (e_1 k_{IF}^3 + e_2 k_{IF}^2 + e_3 k_{IF} + e_4) P_0$$

Substitution of the coefficients e_k gives:

$$P_{IF} = \left(\left(\iota_{1,1} \left(\frac{t}{R}\right)^2 + \iota_{2,1} \frac{t}{R} + \iota_{3,1} \right) k_{IF}^3 + \left(\iota_{1,2} \left(\frac{t}{R}\right)^2 + \iota_{2,2} \frac{t}{R} + \iota_{3,2} \right) k_{IF}^2 + \left(\iota_{1,3} \left(\frac{t}{R}\right)^2 + \iota_{2,3} \frac{t}{R} + \iota_{3,3} \right) k_{IF} + \left(\iota_{1,4} \left(\frac{t}{R}\right)^2 + \iota_{2,4} \frac{t}{R} + \iota_{3,4} \right) \right) P_0$$

$$P_{IF} = \left(\iota_{1,1} k_{IF}^3 \left(\frac{t}{R}\right)^2 + \iota_{2,1} k_{IF}^3 \frac{t}{R} + \iota_{3,1} k_{IF}^3 + \iota_{1,2} k_{IF}^2 \left(\frac{t}{R}\right)^2 + \iota_{2,2} k_{IF}^2 \frac{t}{R} + \iota_{3,2} k_{IF}^2 + \iota_{1,3} k_{IF} \left(\frac{t}{R}\right)^2 + \iota_{2,3} k_{IF} \frac{t}{R} + \iota_{3,3} k_{IF} + \iota_{1,4} \left(\frac{t}{R}\right)^2 + \iota_{2,4} \frac{t}{R} + \iota_{3,4} \right) P_0$$

$$P_{IF} = \left(\left(\iota_{1,1} k_{IF}^3 + \iota_{1,2} k_{IF}^2 + \iota_{1,3} k_{IF} + \iota_{1,4}\right) \left(\frac{t}{R}\right)^2 + \left(\iota_{2,1} k_{IF}^3 + \iota_{2,2} k_{IF}^2 + \iota_{2,3} k_{IF} + \iota_{2,4}\right) \frac{t}{R} + \iota_{3,1} k_{IF}^3 + \iota_{3,2} k_{IF}^2 + \iota_{3,3} k_{IF} + \iota_{3,4} \right) P_0$$

Substitution of the wall thickness t gives:

$$A = k_A R t$$
$$t = \frac{A}{k_A R}$$

$$P_{IF} = \left(\left(\iota_{1,1} k_{IF}^3 + \iota_{1,2} k_{IF}^2 + \iota_{1,3} k_{IF} + \iota_{1,4}\right) \left(\frac{A}{k_A R^2}\right)^2 + \left(\iota_{2,1} k_{IF}^3 + \iota_{2,2} k_{IF}^2 + \iota_{2,3} k_{IF} + \iota_{2,4}\right) \frac{A}{k_A R^2} + \iota_{3,1} k_{IF}^3 + \iota_{3,2} k_{IF}^2 + \iota_{3,3} k_{IF} + \iota_{3,4} \right) P_0$$

The deployed compression strength P_0 is as follows:

$$P_0 = \sigma_{crit,c} A$$
$$P_0 = \frac{E}{\sqrt{3(1-\nu^2)}} \frac{t}{R} \gamma_c A$$

Substitution of the term $\frac{t}{R}\gamma_c$ by the approximation gives (see Tubular Column):

$$P_0 = \frac{E}{\sqrt{3(1-\nu^2)}} \frac{1}{c_c \left(\frac{R}{t}\right)^{d_c}} A$$
$$P_0 = \frac{E}{\sqrt{3(1-\nu^2)}} \frac{1}{c_c \left(\frac{k_A R^2}{A}\right)^{d_c}} A$$
$$P_0 = \frac{E}{\sqrt{3(1-\nu^2)}} \frac{1}{c_c} \frac{1}{k_A^{d_c}} A^{1+d_c} \frac{1}{R^{2d_c}}$$

Thereby the constraint equation for the compression strength from local wall buckling is as follows:

$$P_{req} \leq P_{IF} = \frac{E}{\sqrt{3(1-\nu^2)}} \frac{1}{c_c} \frac{1}{k_A^{d_c}} \left(\left(\iota_{1,1} k_{IF}^3 + \iota_{1,2} k_{IF}^2 + \iota_{1,3} k_{IF} + \iota_{1,4}\right) \left(\frac{A}{k_A R^2}\right)^2 + \left(\iota_{2,1} k_{IF}^3 + \iota_{2,2} k_{IF}^2 + \iota_{2,3} k_{IF} + \iota_{2,4}\right) \frac{A}{k_A R^2} + \iota_{3,1} k_{IF}^3 + \iota_{3,2} k_{IF}^2 + \iota_{3,3} k_{IF} + \iota_{3,4} \right) A^{1+d_c} \frac{1}{R^{2d_c}}$$

To simplify the expression the following substitutions are made:

$$P_{req} \leq P_{IF} = \frac{E}{\sqrt{3(1-\nu^2)}} \frac{1}{c_c} \frac{1}{k_A^{d_c}} \left(B_1 \left(\frac{A}{k_A R^2}\right)^2 + B_2 \frac{A}{k_A R^2} + B_3 \right) A^{1+d_c} \frac{1}{R^{2d_c}}$$

With:

$$B_1 = \iota_{1,1} k_{IF}^3 + \iota_{1,2} k_{IF}^2 + \iota_{1,3} k_{IF} + \iota_{1,4}$$
$$B_2 = \iota_{2,1} k_{IF}^3 + \iota_{2,2} k_{IF}^2 + \iota_{2,3} k_{IF} + \iota_{2,4}$$
$$B_3 = \iota_{3,1} k_{IF}^3 + \iota_{3,2} k_{IF}^2 + \iota_{3,3} k_{IF} + \iota_{3,4}$$

The scaling constraint function of the Tubular Shell Mast with Transition Zone from local wall buckling due to axial compression is summarized in Tab. G - 2.

Scaling Constraint Function for Local Wall Buckling due to Axial Compression
$$P_{req} \le P_{IF} = \frac{E}{\sqrt{3(1-\nu^2)}} \frac{1}{c_c} \frac{1}{k_A^{d_c}} \left(B_1 \left(\frac{A}{k_A R^2} \right)^2 + B_2 \frac{A}{k_A R^2} + B_3 \right) A^{1+d_c} \frac{1}{R^{2d_c}}$$
$$B_1 = \iota_{1,1} k_{IF}^3 + \iota_{1,2} k_{IF}^2 + \iota_{1,3} k_{IF} + \iota_{1,4}$$ $$B_2 = \iota_{2,1} k_{IF}^3 + \iota_{2,2} k_{IF}^2 + \iota_{2,3} k_{IF} + \iota_{2,4}$$ $$B_3 = \iota_{3,1} k_{IF}^3 + \iota_{3,2} k_{IF}^2 + \iota_{3,3} k_{IF} + \iota_{3,4}$$

Tab. G - 2: Scaling constraint function on local wall buckling due to axial compression within the Transition Zone of a Tubular Shell Mast.

G3 Compression Strength from Global Column Buckling

The global column buckling load is strongly influenced by the Transition Zone as for a beam with fixed root the cross-section is reduced at the location where the highest bending loads occur. As a conservative assumption the bending stiffness $(EI)_{IF}$ at the interface to the mechanism is used to calculate the Euler buckling load of the column P_E:

$$P_{req} \le P_E = \frac{\pi^2 (EI)_{IF}}{\left(k_C L_{req}\right)^2}$$

The bending stiffness approximation function is as follows (see subsection 6.3.1):

$$\widehat{EI}_{y,\hat{x}} = \frac{EI_{y,\hat{x}}}{EI_{y,0}} = d_1 \hat{x}^3 + d_2 \hat{x}^2 + d_3 \hat{x} + d_4$$

With the coefficients d_k:

$$\Gamma_t = \frac{t}{R}$$

$$d_k = \omega_{1,k} \Gamma_t^2 + \omega_{2,k} \Gamma_t + \omega_{3,k}$$

The length coordinate at the interface is as follows:

$$\hat{x}_{IF} = \frac{x_{IF}}{r_{M,i}} = \frac{l_{tz}}{r_{M,i}} = k_{IF}$$

Substitution in the bending stiffness expressions gives:

$$EI_{y,\hat{x}_{IF}} = EI_{y,IF} = (d_1 k_{IF}^3 + d_2 k_{IF}^2 + d_3 k_{IF} + d_4) EI_{y,0}$$

Substitution of the coefficients d_k gives:

$$EI_{y,IF} = \left(\left(\omega_{1,1} \left(\frac{t}{R}\right)^2 + \omega_{2,1} \frac{t}{R} + \omega_{3,1} \right) k_{IF}^3 + \left(\omega_{1,2} \left(\frac{t}{R}\right)^2 + \omega_{2,2} \frac{t}{R} + \omega_{3,2} \right) k_{IF}^2 + \left(\omega_{1,3} \left(\frac{t}{R}\right)^2 + \omega_{2,3} \frac{t}{R} + \omega_{3,3} \right) k_{IF} + \left(\omega_{1,4} \left(\frac{t}{R}\right)^2 + \omega_{2,4} \frac{t}{R} + \omega_{3,4} \right) \right) EI_{y,0}$$

$$EI_{y,IF} = \left(\omega_{1,1} k_{IF}^3 \left(\frac{t}{R}\right)^2 + \omega_{2,1} k_{IF}^3 \frac{t}{R} + \omega_{3,1} k_{IF}^3 + \omega_{1,2} k_{IF}^2 \left(\frac{t}{R}\right)^2 + \omega_{2,2} k_{IF}^2 \frac{t}{R} + \omega_{3,2} k_{IF}^2 + \omega_{1,3} k_{IF} \left(\frac{t}{R}\right)^2 + \omega_{2,3} k_{IF} \frac{t}{R} + \omega_{3,3} k_{IF} + \omega_{1,4} \left(\frac{t}{R}\right)^2 + \omega_{2,4} \frac{t}{R} + \omega_{3,4} \right) EI_{y,0}$$

$$EI_{y,IF} = \left(\left(\omega_{1,1} k_{IF}^3 + \omega_{1,2} k_{IF}^2 + \omega_{1,3} k_{IF} + \omega_{1,4} \right) \left(\frac{t}{R}\right)^2 + \left(\omega_{2,1} k_{IF}^3 + \omega_{2,2} k_{IF}^2 + \omega_{2,3} k_{IF} + \omega_{2,4} \right) \frac{t}{R} + \omega_{3,1} k_{IF}^3 + \omega_{3,2} k_{IF}^2 + \omega_{3,3} k_{IF} + \omega_{3,4} \right) EI_{y,0}$$

Substitution of the wall thickness t gives:

$$A = k_A R t$$
$$t = \frac{A}{k_A R}$$

$$EI_{y,IF} = \left(\left(\omega_{1,1} k_{IF}^3 + \omega_{1,2} k_{IF}^2 + \omega_{1,3} k_{IF} + \omega_{1,4}\right) \left(\frac{A}{k_A R^2}\right)^2 + \left(\omega_{2,1} k_{IF}^3 + \omega_{2,2} k_{IF}^2 + \omega_{2,3} k_{IF} + \omega_{2,4}\right) \frac{A}{k_A R^2} + \omega_{3,1} k_{IF}^3 + \omega_{3,2} k_{IF}^2 + \omega_{3,3} k_{IF} + \omega_{3,4} \right) EI_{y,0}$$

The deployed bending stiffness is as follows:

$$EI_{y,0} = E k_I A R^2$$

Thereby the bending stiffness at the interface is as follows:

$$EI_{y,IF} = E k_I \left(\left(\omega_{1,1} k_{IF}^3 + \omega_{1,2} k_{IF}^2 + \omega_{1,3} k_{IF} + \omega_{1,4}\right) \left(\frac{A}{k_A R^2}\right)^2 + \left(\omega_{2,1} k_{IF}^3 + \omega_{2,2} k_{IF}^2 + \omega_{2,3} k_{IF} + \omega_{2,4}\right) \frac{A}{k_A R^2} + \omega_{3,1} k_{IF}^3 + \omega_{3,2} k_{IF}^2 + \omega_{3,3} k_{IF} + \omega_{3,4} \right) AR^2$$

Substitution of the bending stiffness in the Euler buckling equation gives:

$$P_{req} \leq P_E = \frac{\pi^2 E k_I}{\left(k_C L_{req}\right)^2} \left(\left(\omega_{1,1} k_{IF}^3 + \omega_{1,2} k_{IF}^2 + \omega_{1,3} k_{IF} + \omega_{1,4}\right) \left(\frac{A}{k_A R^2}\right)^2 + \left(\omega_{2,1} k_{IF}^3 + \omega_{2,2} k_{IF}^2 + \omega_{2,3} k_{IF} + \omega_{2,4}\right) \frac{A}{k_A R^2} + \omega_{3,1} k_{IF}^3 + \omega_{3,2} k_{IF}^2 + \omega_{3,3} k_{IF} + \omega_{3,4} \right) AR^2$$

To simplify the expression the following substitutions are made:

$$P_{req} \leq P_E = \frac{\pi^2 E k_I}{\left(k_C L_{req}\right)^2} \left(C_1 \left(\frac{A}{k_A R^2}\right)^2 + C_2 \frac{A}{k_A R^2} + C_3 \right) AR^2$$

With:

$$C_1 = \omega_{1,1} k_{IF}^3 + \omega_{1,2} k_{IF}^2 + \omega_{1,3} k_{IF} + \omega_{1,4}$$
$$C_2 = \omega_{2,1} k_{IF}^3 + \omega_{2,2} k_{IF}^2 + \omega_{2,3} k_{IF} + \omega_{2,4}$$
$$C_3 = \omega_{3,1} k_{IF}^3 + \omega_{3,2} k_{IF}^2 + \omega_{3,3} k_{IF} + \omega_{3,4}$$

The scaling constraint function of the Tubular Shell Mast with Transition Zone from local wall buckling due to axial compression is summarized in Tab. G - 3.

Scaling Constraint Function for Global Column Buckling due to Axial Compression
$$P_{req} \leq P_E = \frac{\pi^2 E k_I}{\left(k_C L_{req}\right)^2} \left(C_1 \left(\frac{A}{k_A R^2}\right)^2 + C_2 \frac{A}{k_A R^2} + C_3 \right) AR^2$$

$$C_1 = \omega_{1,1}k_{IF}^3 + \omega_{1,2}k_{IF}^2 + \omega_{1,3}k_{IF} + \omega_{1,4}$$
$$C_2 = \omega_{2,1}k_{IF}^3 + \omega_{2,2}k_{IF}^2 + \omega_{2,3}k_{IF} + \omega_{2,4}$$
$$C_3 = \omega_{3,1}k_{IF}^3 + \omega_{3,2}k_{IF}^2 + \omega_{3,3}k_{IF} + \omega_{3,4}$$

Tab. G - 3: Scaling constraint function on global column buckling due to axial compression within the Transition Zone of a Tubular Shell Mast.

G4 Bending Stiffness at the Mast-Mechanism Interface

The bending stiffness approximation function is as follows (see subsection 6.3.1):

$$\widehat{EI}_{y,\hat{x}} = \frac{EI_{y,\hat{x}}}{EI_{y,0}} = d_1\hat{x}^3 + d_2\hat{x}^2 + d_3\hat{x} + d_4$$

With the coefficients d_k:

$$\Gamma_t = \frac{t}{R}$$
$$d_k = \omega_{1,k}\Gamma_t^2 + \omega_{2,k}\Gamma_t + \omega_{3,k}$$

The length coordinate at the interface is as follows:

$$\hat{x}_{IF} = \frac{x_{IF}}{r_{M,i}} = \frac{l_{tz}}{r_{M,i}} = k_{IF}$$

Substitution in the bending stiffness expressions gives:

$$EI_{y,\hat{x}_{IF}} = EI_{y,IF} = (d_1k_{IF}^3 + d_2k_{IF}^2 + d_3k_{IF} + d_4)EI_{y,0}$$

Substitution of the coefficients d_k gives:

$$EI_{y,IF} = \left(\left(\omega_{1,1}\left(\frac{t}{R}\right)^2 + \omega_{2,1}\frac{t}{R} + \omega_{3,1}\right)k_{IF}^3 + \left(\omega_{1,2}\left(\frac{t}{R}\right)^2 + \omega_{2,2}\frac{t}{R} + \omega_{3,2}\right)k_{IF}^2 + \left(\omega_{1,3}\left(\frac{t}{R}\right)^2 + \omega_{2,3}\frac{t}{R} + \omega_{3,3}\right)k_{IF} + \left(\omega_{1,4}\left(\frac{t}{R}\right)^2 + \omega_{2,4}\frac{t}{R} + \omega_{3,4}\right)\right)EI_{y,0}$$

$$EI_{y,IF} = \left(\omega_{1,1}k_{IF}^3\left(\frac{t}{R}\right)^2 + \omega_{2,1}k_{IF}^3\frac{t}{R} + \omega_{3,1}k_{IF}^3 + \omega_{1,2}k_{IF}^2\left(\frac{t}{R}\right)^2 + \omega_{2,2}k_{IF}^2\frac{t}{R} + \omega_{3,2}k_{IF}^2 + \omega_{1,3}k_{IF}\left(\frac{t}{R}\right)^2 + \omega_{2,3}k_{IF}\frac{t}{R} + \omega_{3,3}k_{IF} + \omega_{1,4}\left(\frac{t}{R}\right)^2 + \omega_{2,4}\frac{t}{R} + \omega_{3,4}\right)EI_{y,0}$$

$$EI_{y,IF} = \left(\left(\omega_{1,1}k_{IF}^3 + \omega_{1,2}k_{IF}^2 + \omega_{1,3}k_{IF} + \omega_{1,4}\right)\left(\frac{t}{R}\right)^2 + \left(\omega_{2,1}k_{IF}^3 + \omega_{2,2}k_{IF}^2 + \omega_{2,3}k_{IF} + \omega_{2,4}\right)\frac{t}{R} + \omega_{3,1}k_{IF}^3 + \omega_{3,2}k_{IF}^2 + \omega_{3,3}k_{IF} + \omega_{3,4}\right)EI_{y,0}$$

Substitution of the wall thickness t gives:

$$A = k_A R t$$
$$t = \frac{A}{k_A R}$$

$$EI_{y,IF} = \Bigg(\left(\omega_{1,1}k_{IF}^3 + \omega_{1,2}k_{IF}^2 + \omega_{1,3}k_{IF} + \omega_{1,4}\right)\left(\frac{A}{k_A R^2}\right)^2 + \left(\omega_{2,1}k_{IF}^3 + \omega_{2,2}k_{IF}^2 + \omega_{2,3}k_{IF} + \omega_{2,4}\right)\frac{A}{k_A R^2} + \omega_{3,1}k_{IF}^3 + \omega_{3,2}k_{IF}^2 + \omega_{3,3}k_{IF} + \omega_{3,4} \Bigg) EI_{y,0}$$

The deployed bending stiffness is as follows:

$$EI_{y,0} = Ek_I AR^2$$

Thereby the constraint equation for the bending stiffness at the interface is as follows:

$$(EI)_{req,IF} \leq EI_{y,IF} = Ek_I \Bigg(\left(\omega_{1,1}k_{IF}^3 + \omega_{1,2}k_{IF}^2 + \omega_{1,3}k_{IF} + \omega_{1,4}\right)\left(\frac{A}{k_A R^2}\right)^2 + \left(\omega_{2,1}k_{IF}^3 + \omega_{2,2}k_{IF}^2 + \omega_{2,3}k_{IF} + \omega_{2,4}\right)\frac{A}{k_A R^2} + \omega_{3,1}k_{IF}^3 + \omega_{3,2}k_{IF}^2 + \omega_{3,3}k_{IF} + \omega_{3,4} \Bigg) AR^2$$

To simplify the expression the following substitutions are made:

$$(EI)_{req,IF} \leq EI_{y,IF} = Ek_I \left(C_1 \left(\frac{A}{k_A R^2}\right)^2 + C_2 \frac{A}{k_A R^2} + C_3 \right) AR^2$$

With:

$$C_1 = \omega_{1,1}k_{IF}^3 + \omega_{1,2}k_{IF}^2 + \omega_{1,3}k_{IF} + \omega_{1,4}$$
$$C_2 = \omega_{2,1}k_{IF}^3 + \omega_{2,2}k_{IF}^2 + \omega_{2,3}k_{IF} + \omega_{2,4}$$
$$C_3 = \omega_{3,1}k_{IF}^3 + \omega_{3,2}k_{IF}^2 + \omega_{3,3}k_{IF} + \omega_{3,4}$$

The scaling constraint function of the Tubular Shell Mast with Transition Zone from local wall buckling due to axial compression is summarized in Tab. G - 4.

Scaling Constraint Function for Bending Stiffness
$(EI)_{req,IF} \leq EI_{y,IF} = Ek_I \left(C_1 \left(\frac{A}{k_A R^2}\right)^2 + C_2 \frac{A}{k_A R^2} + C_3 \right) AR^2$
$C_1 = \omega_{1,1}k_{IF}^3 + \omega_{1,2}k_{IF}^2 + \omega_{1,3}k_{IF} + \omega_{1,4}$ $C_2 = \omega_{2,1}k_{IF}^3 + \omega_{2,2}k_{IF}^2 + \omega_{2,3}k_{IF} + \omega_{2,4}$ $C_3 = \omega_{3,1}k_{IF}^3 + \omega_{3,2}k_{IF}^2 + \omega_{3,3}k_{IF} + \omega_{3,4}$

Tab. G - 4: Scaling constraint function on the bending stiffness within the Transition Zone of a Tubular Shell Mast.

G5 Critical Bending Moment at the Mast-Mechanism Interface

The critical bending moment approximation function is as follows (see subsection 6.3.3):

$$\widehat{M}_{y,\hat{x}} = \frac{M_{y,\hat{x}}}{M_{y,0}} = f_1 \hat{x}^3 + f_2 \hat{x}^2 + f_3 \hat{x} + f_4$$

With the coefficients f_k:

$$\Gamma_t = \frac{t}{R}$$
$$f_k = \tau_{1,k}\Gamma_t^2 + \tau_{2,k}\Gamma_t + \tau_{3,k}$$

The length coordinate at the interface is as follows:

$$\hat{x}_{IF} = \frac{x_{IF}}{r_{M,i}} = \frac{l_{tz}}{r_{M,i}} = k_{IF}$$

Substitution in the critical bending moment expressions gives:

$$M_{y,\hat{x}_{IF}} = M_{y,IF} = (f_1 k_{IF}^3 + f_2 k_{IF}^2 + f_3 k_{IF} + f_4) M_{y,0}$$

Substitution of the coefficients f_k gives:

$$M_{y,IF} = \left(\left(\tau_{1,1}\left(\frac{t}{R}\right)^2 + \tau_{2,1}\frac{t}{R} + \tau_{3,1}\right)k_{IF}^3 + \left(\tau_{1,2}\left(\frac{t}{R}\right)^2 + \tau_{2,2}\frac{t}{R} + \tau_{3,2}\right)k_{IF}^2 + \left(\tau_{1,3}\left(\frac{t}{R}\right)^2 + \tau_{2,3}\frac{t}{R} + \tau_{3,3}\right)k_{IF} + \left(\tau_{1,4}\left(\frac{t}{R}\right)^2 + \tau_{2,4}\frac{t}{R} + \tau_{3,4}\right)\right)M_{y,0}$$

$$M_{y,IF} = \left(\tau_{1,1}k_{IF}^3\left(\frac{t}{R}\right)^2 + \tau_{2,1}k_{IF}^3\frac{t}{R} + \tau_{3,1}k_{IF}^3 + \tau_{1,2}k_{IF}^2\left(\frac{t}{R}\right)^2 + \tau_{2,2}k_{IF}^2\frac{t}{R} + \tau_{3,2}k_{IF}^2 + \tau_{1,3}k_{IF}\left(\frac{t}{R}\right)^2 + \tau_{2,3}k_{IF}\frac{t}{R} + \tau_{3,3}k_{IF} + \tau_{1,4}\left(\frac{t}{R}\right)^2 + \tau_{2,4}\frac{t}{R} + \tau_{3,4}\right)M_{y,0}$$

$$M_{y,IF} = \left(\left(\tau_{1,1}k_{IF}^3 + \tau_{1,2}k_{IF}^2 + \tau_{1,3}k_{IF} + \tau_{1,4}\right)\left(\frac{t}{R}\right)^2 + \left(\tau_{2,1}k_{IF}^3 + \tau_{2,2}k_{IF}^2 + \tau_{2,3}k_{IF} + \tau_{2,4}\right)\frac{t}{R} + \tau_{3,1}k_{IF}^3 + \tau_{3,2}k_{IF}^2 + \tau_{3,3}k_{IF} + \tau_{3,4}\right)M_{y,0}$$

Substitution of the wall thickness t gives:

$$A = k_A R t$$
$$t = \frac{A}{k_A R}$$

$$M_{y,IF} = \left(\left(\tau_{1,1}k_{IF}^3 + \tau_{1,2}k_{IF}^2 + \tau_{1,3}k_{IF} + \tau_{1,4}\right)\left(\frac{A}{k_A R^2}\right)^2 + \left(\tau_{2,1}k_{IF}^3 + \tau_{2,2}k_{IF}^2 + \tau_{2,3}k_{IF} + \tau_{2,4}\right)\frac{A}{k_A R^2} + \tau_{3,1}k_{IF}^3 + \tau_{3,2}k_{IF}^2 + \tau_{3,3}k_{IF} + \tau_{3,4}\right)M_{y,0}$$

The deployed critical bending moment is as follows:

$$M_{y,0} = \sigma_{crit,b} W_{y,0} = \sigma_{crit,b}\frac{I_{y,0}}{z_0}$$
$$M_{y,0} = \frac{E}{\sqrt{3(1-\nu^2)}}\frac{t}{R}\gamma_b k_I A R$$

Substitution of the term $\frac{t}{R}\gamma_b$ by the approximation gives:

$$M_{y,0} = \frac{E}{\sqrt{3(1-\nu^2)}}\frac{1}{c_b\left(\frac{R}{t}\right)^{d_b}}k_I A R$$

Substitution of the wall thickness gives:

$$M_{y,0} = \frac{E}{\sqrt{3(1-\nu^2)}}\frac{1}{c_b\left(\frac{k_A R^2}{A}\right)^{d_b}}k_I A R$$
$$M_{y,0} = \frac{E}{\sqrt{3(1-\nu^2)}}\frac{1}{c_b}\frac{k_I}{k_A^{d_b}}A^{1+d_b}\frac{1}{R^{2d_b-1}}$$

Thereby the constraint equation on the critical bending moment is as follows:

$$M_{req,IF} \leq M_{y,IF} = \frac{E}{\sqrt{3(1-\nu^2)}} \frac{1}{c_b} \frac{k_I}{k_A^{d_b}} \Bigg(\left(\tau_{1,1} k_{IF}^3 + \tau_{1,2} k_{IF}^2 + \tau_{1,3} k_{IF} + \tau_{1,4}\right) \left(\frac{A}{k_A R^2}\right)^2 + \left(\tau_{2,1} k_{IF}^3 + \tau_{2,2} k_{IF}^2 + \tau_{2,3} k_{IF} + \tau_{2,4}\right) \frac{A}{k_A R^2} + \tau_{3,1} k_{IF}^3 + \tau_{3,2} k_{IF}^2 + \tau_{3,3} k_{IF} + \tau_{3,4} \Bigg) A^{1+d_b} \frac{1}{R^{2d_b-1}}$$

To simplify the expression the following substitutions are made:

$$M_{req,IF} \leq M_{y,IF} = \frac{E}{\sqrt{3(1-\nu^2)}} \frac{1}{c_b} \frac{k_I}{k_A^{d_b}} \left(D_1 \left(\frac{A}{k_A R^2}\right)^2 + D_2 \frac{A}{k_A R^2} + D_3 \right) A^{1+d_b} \frac{1}{R^{2d_b-1}}$$

With:

$$D_1 = \tau_{1,1} k_{IF}^3 + \tau_{1,2} k_{IF}^2 + \tau_{1,3} k_{IF} + \tau_{1,4}$$
$$D_2 = \tau_{2,1} k_{IF}^3 + \tau_{2,2} k_{IF}^2 + \tau_{2,3} k_{IF} + \tau_{2,4}$$
$$D_3 = \tau_{3,1} k_{IF}^3 + \tau_{3,2} k_{IF}^2 + \tau_{3,3} k_{IF} + \tau_{3,4}$$

The scaling constraint function of the Tubular Shell Mast with Transition Zone from local wall buckling due to axial compression is summarized in Tab. G - 5.

Scaling Constraint Function for Critical Bending Moment
$M_{req,IF} \leq M_{y,IF} = \frac{E}{\sqrt{3(1-\nu^2)}} \frac{1}{c_b} \frac{k_I}{k_A^{d_b}} \left(D_1 \left(\frac{A}{k_A R^2}\right)^2 + D_2 \frac{A}{k_A R^2} + D_3 \right) A^{1+d_b} \frac{1}{R^{2d_b-1}}$
$D_1 = \tau_{1,1} k_{IF}^3 + \tau_{1,2} k_{IF}^2 + \tau_{1,3} k_{IF} + \tau_{1,4}$ $D_2 = \tau_{2,1} k_{IF}^3 + \tau_{2,2} k_{IF}^2 + \tau_{2,3} k_{IF} + \tau_{2,4}$ $D_3 = \tau_{3,1} k_{IF}^3 + \tau_{3,2} k_{IF}^2 + \tau_{3,3} k_{IF} + \tau_{3,4}$

Tab. G - 5: Scaling constraint function on the critical bending moment within the Transition Zone of a Tubular Shell Mast.

Appendix H

H Telescopic Tubular Mast Scaling Function

Within Appendix H the scaling functions for the Telescopic Tubular Mast are derived for the load cases of axial compression and bending.

H1 Mast Parameterization and Mass Functions

For the Telescopic Tubular Mast with constant taper ratio Γ_R and constant wall thickness t the segment radius R_i is as follows:

$$\Gamma_R = \frac{R_n}{R_0} = \text{const.}$$

$$R_i = R_0 - \frac{i}{n}(R_0 - R_n)$$

$$R_i = R_0 - R_0\frac{i}{n}\left(1 - \frac{R_n}{R_0}\right)$$

$$R_i = R_0\left(1 - \frac{i}{n}(1 - \Gamma_R)\right)$$

The cross-sectional area A_i of the cylinder segment is thereby:

$$A_i = k_A R_i t$$

$$A_i = k_A R_0 t\left(1 - \frac{i}{n}(1 - \Gamma_R)\right)$$

$$A_i = A_0\left(1 - \frac{i}{n}(1 - \Gamma_R)\right)$$

Thus, the mass of a cylinder segment $m_{C,i}$ is as follows:

$$m_{C,i} = \rho_C A_i l$$

$$m_{C,i} = \rho_C A_0\left(1 - \frac{i}{n}(1 - \Gamma_R)\right)\frac{L}{n}$$

The interface cross-sectional area $A_{IF,i}$ is again given by the radius of the segment R_i and the clearance between each cylinder segment ΔR:

$$A_{IF,i} = k_A R_i \Delta R$$

$$A_{IF,i} = k_A R_i \frac{\mathrm{R}_0 - R_n}{n}$$

$$A_{IF,i} = k_A R_i \mathrm{R}_0 \frac{1}{n}(1 - \Gamma_R)$$

$$A_{IF,i} = k_A \mathrm{R}_0^2 \frac{1}{n}(1 - \Gamma_R)\left(1 - \frac{i}{n}(1 - \Gamma_R)\right)$$

The height of the interface is again derived by the wall thickness multiplied by a factor h_{IF}. Due to the constant wall thickness also the interface height is a constant:

$$h_{IF} = k_{IF} t$$

Thereby the mass of an interface m_{IF} is as follows:

$$m_{IF,i} = \rho_{IF} A_{IF,i} h_{IF}$$

$$m_{IF,i} = \rho_{IF} k_A \mathrm{R}_0^2 \frac{1}{n}(1 - \Gamma_R)\left(1 - \frac{i}{n}(1 - \Gamma_R)\right) k_{IF} t$$

$$m_{IF,i} = \frac{1}{n} k_{IF}(1-\Gamma_R)\left(1-\frac{i}{n}(1-\Gamma_R)\right)\rho_{IF} A_0 R_0$$

The material density of interface is expressed by a density ratio Γ_ρ:

$$\Gamma_\rho = \frac{\rho_{IF}}{\rho_C}$$

The interface mass is re-written as follows:

$$m_{IF,i} = \frac{1}{n} k_{IF}(1-\Gamma_R)\left(1-\frac{i}{n}(1-\Gamma_R)\right)\Gamma_\rho \rho_C A_0 R_0$$

The number of telescopic segments is derived from the desired compaction ratio Γ_{lL}:

$$n = \left\lceil \frac{L}{l} \right\rceil = \left\lceil \frac{1}{\Gamma_{lL}} \right\rceil$$

Thereby the mass of a single segment is m_i is as follows:

$$m_i = m_{C,i} + m_{IF,i}$$

$$m_i = \rho_C A_0 \left(1-\frac{i}{n}(1-\Gamma_R)\right)\frac{L}{n} + \frac{1}{n} k_{IF}(1-\Gamma_R)\left(1-\frac{i}{n}(1-\Gamma_R)\right)\Gamma_\rho \rho_C A_0 R_0$$

$$m_i = \rho_C A_0 \big(L + k_{IF}(1-\Gamma_R)\Gamma_\rho R_0\big)\frac{1}{n}\left(1-\frac{i}{n}(1-\Gamma_R)\right)$$

The mass of the Telescopic Tubular Mast m with constant taper ratio and constant wall thickness is as follows:

$$m = \sum_{i=0}^{n-1} m_i$$

$$m = \rho_C A_0 \big(L + k_{IF}(1-\Gamma_R)\Gamma_\rho R_0\big)\frac{1}{n}\sum_{i=0}^{n-1}\left(1-\frac{i}{n}(1-\Gamma_R)\right)$$

The sum can be re-written as follows:

$$\sum_{i=0}^{n-1}\left(1-\frac{i}{n}(1-\Gamma_R)\right)$$

$$n=1: \sum_{i=0}^{1-1}\big(1-i(1-\Gamma_R)\big) = 1$$

$$n=2: \sum_{i=0}^{2-1}\left(1-\frac{i}{2}(1-\Gamma_R)\right) = 2-\frac{1}{2}(1-\Gamma_R)$$

$$n=3: \sum_{i=0}^{3-1}\left(1-\frac{i}{3}(1-\Gamma_R)\right) = 3-(1-\Gamma_R)$$

$$n=4: \sum_{i=0}^{4-1}\left(1-\frac{i}{4}(1-\Gamma_R)\right) = 4-\frac{3}{2}(1-\Gamma_R)$$

$$n=5: \sum_{i=0}^{5-1}\left(1-\frac{i}{5}(1-\Gamma_R)\right) = 5-2(1-\Gamma_R)$$

$$\sum_{i=0}^{n-1}\left(1-\frac{i}{n}(1-\Gamma_R)\right) = n-\frac{1}{2}(n-1)(1-\Gamma_R)$$

The total mass m is thereby as follows:

$$m = \rho_C A_0 \left(L + k_{IF}(1-\Gamma_R)\Gamma_\rho R_0\right)\frac{1}{n}\left(n - \frac{1}{2}(n-1)(1-\Gamma_R)\right)$$

The parameters and properties of the Telescopic Tubular Mast are summarized in Tab. H - 1.

Telescopic Tubular Mast Parameters			
Property	**Parameter**	**Unit**	**Values**
Base segment radius	R_0	m	Sizing result
Top segment radius	R_n	m	-
Base segment area	A_0	m²	Sizing result
Top segment area	A_n	m²	-
Base segment second moment of area	I_0	m⁴	-
Tip segment second moment of area	I_n	m⁴	-
Cylinder segment modulus	E	N/m²	60 GPa
Cylinder segment density	ρ_C	kg/m³	1600
Interface ring density	ρ_{IF}	kg/m³	2700
Wall thickness	t	m	-
Segment clearance	ΔR	m	-
Number of segments	n	-	$\left\lceil \frac{1}{\Gamma_{lL}} \right\rceil$
Taper ratio	Γ_R	-	0.25
Density ratio	Γ_ρ	-	27/16
Segment length ratio	Γ_{lL}	-	0.02
Cross-section factor	k_A	-	2π
Second moment of area factor	k_I	-	½
Column mounting parameter	k_C	-	2
Interface size factor	k_{IF}	-	10
Minimum wall thickness	t_{min}	m	0.0005
Minimum tip radius	$R_{n,min}$	m	0.02
Minimum segment clearance factor	$k_{\Delta,min} = \frac{\Delta R_{min}}{t}$	-	5

Tab. H - 1: Telescopic Tubular Mast parameters.

The geometry and mass functions of the Telescopic Tubular Mast are summarized in Tab. H - 2.

Telescopic Tubular Mast Geometry and Mass Functions	
Parameter	**Expression**
Segment radius	$R_i = R_0\left(1 - \frac{i}{n}(1-\Gamma_R)\right)$
Segment area	$A_i = A_0\left(1 - \frac{i}{n}(1-\Gamma_R)\right)$
Deformable Structure overall mass	$m = \rho_C A_0\left(L + k_{IF}(1-\Gamma_R)\Gamma_\rho R_0\right)\frac{1}{n}\left(n - \frac{1}{2}(n-1)(1-\Gamma_R)\right)$

Tab. H - 2: Geometry and mass functions of the Telescopic Tubular Mast.

H2 Scaling Constraint Functions for Axial Compression

The scaling constraint functions for the load case of axial compression are derived in the following.

H2.1 Global Column Buckling

For a column loaded in compression that does not possess constant cross-sectional properties throughout its length, the general Euler buckling equation cannot be applied. For simplification of the buckling load calculation, the Telescopic Tubular Mast is approximated in the following by a cylindrical cone with linear decreasing radius R from the bottom (index 0) to the top (index n).

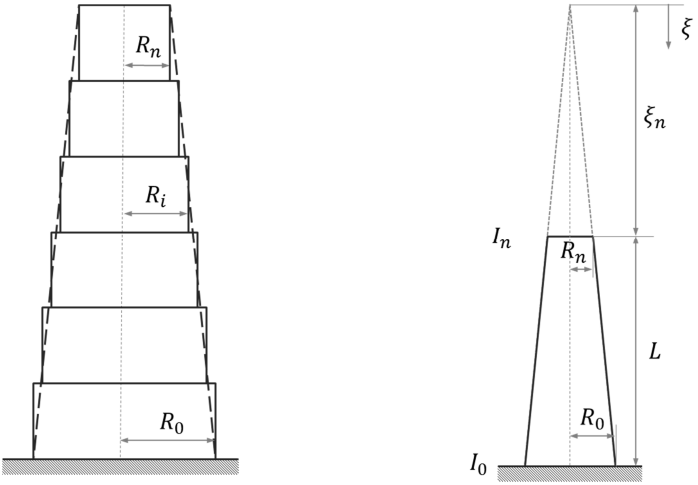

Fig. H - 1: Approximation of the Telescopic Tubular Mast as a truncated cone with radii definitions (left) and cone geometry parameter definition (right).

For a truncated conical cylinder the radius is as follows:

$$R(\xi) = R_n \frac{\xi}{\xi_n}$$

The parameter ξ is the axial coordinate with respect to the tip of the cone. The parameter ξ_n is the distance from the tip of the cone to the tip of the mast with the end radius R_n. The local cross-sectional moment of inertia is as follows:

$$I = k_I k_A R^3 t$$

By assuming a fixed ratio Γ_{tR} of the wall thickness t to the radius R the moment of inertia becomes:

$$\Gamma_{tR} = \frac{t}{R}$$

$$I = k_I k_A \Gamma_{tR} R^4$$

Thereby the development of the moment of inertia throughout the cone is described as follows:

$$I = k_I k_A \Gamma_{tR} \left(R_n \frac{\xi}{\xi_n} \right)^4$$

$$I = k_I k_A \Gamma_{tR} R_n^4 \left(\frac{\xi}{\xi_n} \right)^4$$

$$I = I_n \left(\frac{\xi}{\xi_n} \right)^4$$

The general form of the Euler buckling equation for a conical bar with fixed root and free end with compression load P is given by Timoshenko and Gere [145] as follows:

$$P_{crit} = k_{PE} \frac{E I_0}{L^2}$$

Timoshenko and Gere give solutions for the buckling value k_{PE} which are listed in Tab. H - 3 (in [145] Table 2-12 in section 2.16).

Column Buckling Factors for a Truncated Cone	
I_n/I_0	k_{PE}
0.1	1.202
0.2	1.505
0.3	1.710
0.4	1.870
0.5	2.002
0.6	2.116
0.7	2.217
0.8	2.308
0.9	2.391
1	$\frac{\pi^2}{4}$

Tab. H - 3: Column buckling factors for a truncated cone load in axial compression according to Timoshenko and Gere [145].

The buckling values can be approximated by a power function as follows:

$$k_{PE} = \frac{\pi^2}{4}\left(\frac{I_n}{I_0}\right)^f$$

The factor f is derived from the mean of the buckling values:

$$f = \log_{\frac{I_n}{I_0}}\left(k_{PE}\frac{4}{\pi^2}\right) \approx 0.30297$$

Fig. H - 2 shows a comparison of the values given by Timoshenko and Gere with the approximation function.

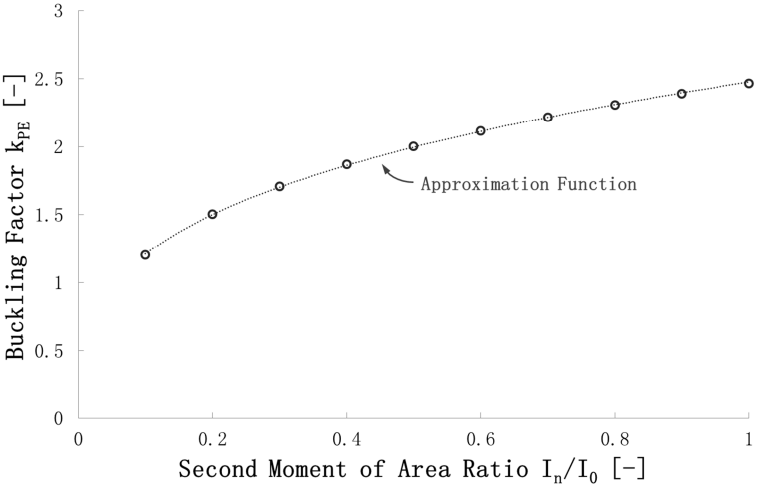

Fig. H - 2: Column buckling factors for a truncated cone loaded in axial compression according to Timoshenko and Gere [145] and overlayed approximation function.

Thereby the critical compression load of the Telescopic Tubular Mast depends on the taper ratio $\frac{I_n}{I_0}$ of the moment of inertia as follows:

$$P_{crit} = \frac{\pi^2}{4}\left(\frac{I_n}{I_0}\right)^f \frac{EI_0}{L^2}$$

Substitution of the moment of inertia at the root I_0 and at the tip I_n gives:

$$P_{crit} = \frac{\pi^2}{4}\left(\frac{k_l k_A \Gamma_{tR} R_n^4}{k_l k_A \Gamma_{tR} R_0^4}\right)^f \frac{EI_0}{L^2}$$

$$P_{crit} = \frac{\pi^2}{4}\left(\frac{R_n}{R_0}\right)^{4f} \frac{EI_0}{L^2}$$

Therefore the constraint equation for global buckling is as follows:

$$P_{req} \leq P_{crit} = \frac{\pi^2}{4}\left(\frac{R_n}{R_0}\right)^{4f} \frac{EI_0}{L^2}$$

$$P_{req} \leq \frac{\pi^2 EI_0}{4L^2}\Gamma_R^{4f}$$

Substitution of the moment of inertia gives:

$$P_{req} \leq \frac{\pi^2}{4} \Gamma_R^{4f} E k_l \frac{1}{L_{req}^2} A_0 R_0^2$$

Re-written in the form according to Appendix C gives:

$$\frac{4}{\pi^2} \frac{1}{\Gamma_R^{4f}} \frac{1}{E} \frac{1}{k_l} L_{req}^2 P_{req} \leq A_0 R_0^2$$

H2.2 Local Wall Buckling due to Compression

The critical stress in the cylinder walls is derived by NASA SP-8007 as introduced in Appendix E2. Here the same functions are used to calculate the critical stress σ_{crit}:

$$\sigma_{crit} = \frac{E}{\sqrt{3(1-\nu^2)}} \frac{t}{R} \gamma_c$$

$$\gamma_c = 1 - 0.901(1 - e^{-\phi})$$

$$\phi = \frac{1}{16} \sqrt{\frac{R}{t}}$$

The approximation is as follows:

$$\sigma_{crit} = \frac{E}{\sqrt{3(1-\nu^2)}} \frac{1}{c_c \left(\frac{R}{t}\right)^{d_c}}$$

With:

$$c_c = 0.2431$$

$$d_c = 1.4258$$

Therefore, the constraint equation for a segment i is as follows:

$$P_{req} \leq P_{crit} = \sigma_{crit} A_i$$

$$P_{req} \leq P_{crit} = \frac{E}{\sqrt{3(1-\nu^2)}} \frac{1}{c_c \left(\frac{R_i}{t_i}\right)^{d_c}} A_i$$

$$P_{req} \leq P_{crit} = \frac{E}{\sqrt{3(1-\nu^2)}} \frac{1}{c_c} \left(\frac{t_i}{R_i}\right)^{d_c} A_i$$

In the following the local wall buckling loads of the top and bottom cylinders are compared. The constraint equations are as follows:

$$P_{req} \leq P_0 = \frac{E}{\sqrt{3(1-\nu^2)}} \frac{1}{c_c} \left(\frac{t_0}{R_0}\right)^{d_c} A_0$$

$$P_{req} \leq P_n = \frac{E}{\sqrt{3(1-\nu^2)}} \frac{1}{c_c} \left(\frac{t_n}{R_n}\right)^{d_c} A_n$$

The ratio of the buckling loads is given by the value q:

$$q = \frac{P_n}{P_0}$$

$$q = \frac{\frac{E}{\sqrt{3(1-\nu^2)}} \frac{1}{c_c} \left(\frac{t_n}{R_n}\right)^{d_c} A_n}{\frac{E}{\sqrt{3(1-\nu^2)}} \frac{1}{c_c} \left(\frac{t_0}{R_0}\right)^{d_c} A_0}$$

$$q = \frac{\left(\frac{t_n}{R_n}\right)^{d_c} A_n}{\left(\frac{t_0}{R_0}\right)^{d_c} A_0}$$

$$q = \left(\frac{t_n}{t_0}\frac{R_0}{R_n}\right)^{d_c}\frac{A_n}{A_0}$$

For the case of constant wall thickness t the expression for q becomes:

$$t_0 = t_n = t$$
$$A_i = k_A R_i t$$
$$q = \left(\frac{t}{t}\frac{R_0}{R_n}\right)^{d_c}\frac{k_A R_n t}{k_A R_0 t}$$
$$q = \left(\frac{R_0}{R_n}\right)^{d_c}\frac{R_n}{R_0}$$
$$q = \left(\frac{R_0}{R_n}\right)^{d_c-1}$$
$$q = \left(\frac{1}{\Gamma_R}\right)^{d_c-1} = \Gamma_R^{1-d_c}$$

As $\Gamma_R < 1$ and $d_c > 1$ follows that $q > 1$. Hence, for $R_0 > R_n$ the buckling load of the base cylinder is smaller than that of the top cylinder. Therefore, the base cylinder is critical for dimensioning and the scaling constraint function on local wall buckling is as follows:

$$P_{req} \leq \frac{E}{\sqrt{3(1-\nu^2)}}\frac{1}{c_c}\left(\frac{t_0}{R_0}\right)^{d_c} A_0$$
$$P_{req} \leq \frac{E}{\sqrt{3(1-\nu^2)}}\frac{1}{c_c}\left(\frac{A_0}{k_A R_0^2}\right)^{d_c} A_0$$
$$P_{req} \leq \frac{E}{\sqrt{3(1-\nu^2)}}\frac{1}{c_c}\frac{1}{k_A^{d_c}} A_0^{1+d_c}\frac{1}{R_0^{2d_c}}$$

Re-written in the form according to Appendix C gives:

$$\frac{\sqrt{3(1-\nu^2)}}{E} c_c k_A^{d_c} P_{req} \leq A_0^{1+d_c} R_0^{-2d_c}$$

H2.3 Minimum Wall Thickness

The Telescopic Tubular Mast does not have a supporting structure that carries the loads applied during launch. Thus introduction of a certain minimum wall thickness t_{min} is justified additionally to the limitations set by manufacturing capabilities and procurement of thin materials. The corresponding constraint equation is as follows:

$$A_i \geq k_A R_i t_{min}$$
$$k_A t_{min} \leq A_i R_i^{-1}$$

As the base segment dimensions provide the reference for the other segments, the scaling constraint equation according to Appendix C is as follows:

$$k_A t_{min} \leq A_0 R_0^{-1}$$

H2.4 Minimum Tip Radius

The radius of the tip segment shall not be below certain minimum tip radius $R_{n,min}$:

$$R_{n,min} \leq R_n = \Gamma_R R_0$$

Thus the constraint equation according to Appendix C is as follows:

$$\frac{1}{\Gamma_R} R_{n,min} \leq A_0^0 R_0$$

H2.5 Minimum Segment Clearance

The clearance between the cylinders shall not be below a certain minimum $(\Delta R)_{min}$:

$$(\Delta R)_{min} \leq \Delta R = R_{i-1} - R_i$$

$$(\Delta R)_{min} \leq R_0 \left(1 - \frac{i-1}{n}(1-\Gamma_R)\right) - R_0 \left(1 - \frac{i}{n}(1-\Gamma_R)\right)$$

$$(\Delta R)_{min} \leq R_0 \left(1 - \frac{i}{n}(1-\Gamma_R) + \frac{1}{n}(1-\Gamma_R)\right) - R_0 \left(1 - \frac{i}{n}(1-\Gamma_R)\right)$$

$$(\Delta R)_{min} \leq R_0 \frac{1}{n}(1-\Gamma_R)$$

The segment clearance may be expressed by a multiple of the wall thickness t:

$$(\Delta R)_{min} = k_{\Delta,min} t$$

$$k_{\Delta,min} t \leq R_0 \frac{1}{n}(1-\Gamma_R)$$

Substitution of the wall thickness gives:

$$k_{\Delta,min} \frac{A_0}{k_A R_0} \leq R_0 \frac{1}{n}(1-\Gamma_R)$$

Thus the constraint equation according to Appendix C is as follows:

$$n \frac{1}{1-\Gamma_R} \frac{k_{\Delta,min}}{k_A} \leq A_0^{-1} R_0^2$$

H2.6 Summary of the Scaling Constraint Functions for Axial Compression

The scaling constraint functions for the Telescopic Tubular Mast loaded in axial compression are summarized in Tab. H - 4.

Scaling Constraint Functions of the Telescopic Tubular Mast for Axial Compression				
Constraint Criterion	**Constraint Function**	c	i	j
Global column buckling	$\frac{4}{\pi^2}\frac{1}{\Gamma_R^{4f}}\frac{1}{E}\frac{1}{k_I} L_{req}^2 P_{req} \leq A_0 R_0^2$	$\frac{4}{\pi^2}\frac{1}{\Gamma_R^{4f}}\frac{1}{E}\frac{1}{k_I} L_{req}^2 P_{req}$	1	2
Local wall buckling	$\frac{\sqrt{3(1-\nu^2)}}{E} c_c k_A^{d_c} P_{req} \leq A_0^{1+d_c} R_0^{-2d_c}$	$\frac{\sqrt{3(1-\nu^2)}}{E} c_c k_A^{d_c} P_{req}$	$1 + d_c$	$-2d_c$
Minimum wall thickness	$k_A t_{min} \leq A_0 R_0^{-1}$	$k_A t_{min}$	1	-1
Minimum tip radius	$\frac{1}{\Gamma_R} R_{n,min} \leq A_0^0 R_0$	$\frac{1}{\Gamma_R} R_{n,min}$	0	1
Minimum segment clearance	$n \frac{1}{1-\Gamma_R} \frac{k_{\Delta,min}}{k_A} \leq A_0^{-1} R_0^2$	$n \frac{1}{1-\Gamma_R} \frac{k_{\Delta,min}}{k_A}$	-1	2

Tab. H - 4: Summary of the scaling constraint functions of the Telescopic Tubular Mast for the load case of axial compression.

H3 Scaling Constraint Functions for Bending

The scaling constraint functions for the load case of bending are derived in the following.

H3.1 Bending Stiffness

For derivation of the effective bending stiffness of the Telescopic Tubular Mast a continuous variation of the mast radius from the base to the tip is assumed. The local radius $R(x)$ is thereby as follows:

$$R(x) = R_0 - (R_0 - R_n)\frac{x}{L}$$

Substitution of the tip radius by the taper ratio Γ_R gives:

$$\Gamma_R = \frac{R_n}{R_0}$$

$$R(x) = R_0\left(1 - (1 - \Gamma_R)\frac{x}{L}\right)$$

For constant wall thickness t the local cross-sectional area $A(x)$ is as follows:

$$A(x) = k_A R(x) t$$

$$A(x) = k_A R_0\left(1 - (1 - \Gamma_R)\frac{x}{L}\right) t$$

The local moment of inertia is as follows:

$$I(x) = k_I A(x)\big(R(x)\big)^2$$

$$I(x) = k_I k_A\left(1 - (1 - \Gamma_R)\frac{x}{L}\right)^3 R_0^3 t$$

For a constant moment M the differential equation for a beam is as follows:

$$w''(x) = \frac{M(x)}{EI(x)}$$

$$w''(x) = \frac{M}{Ek_I k_A\left(1 - (1 - \Gamma_R)\frac{x}{L}\right)^3 R_0^3 t}$$

$$w''(x) = \frac{M}{EI_0}\frac{1}{\left(1 - (1 - \Gamma_R)\frac{x}{L}\right)^3}$$

The integrals are as follows:

$$w'(x) = \frac{M}{EI_0}\frac{-L^3}{2L^2\Gamma_R - 2L^2 + x^2(2\Gamma_R^3 - 6\Gamma_R^2 + 6\Gamma_R - 2) + x(4L\Gamma_R^2 - 8L\Gamma_R + 4L)} + C_1$$

$$w(x) = \frac{M}{EI_0}\frac{L^3}{2L\Gamma_R^2 - 4L\Gamma_R + 2L + x(2\Gamma_R^3 - 6\Gamma_R^2 + 6\Gamma_R - 2)} + C_1 x + C_2$$

For a beam with fixed root and free tip under constant moment the constants are derived from the following constraints:

$$w'(0) = 0$$

$$0 = \frac{M}{EI_0}\frac{-L^3}{2L^2\Gamma_R - 2L^2} + C_1$$

$$C_1 = \frac{M}{EI_0}\frac{L}{2\Gamma_R - 2}$$

$$w(0) = 0$$

$$0 = \frac{M}{EI_0}\frac{L^3}{2L\Gamma_R^2 - 4L\Gamma_R + 2L} + C_2$$

$$C_2 = -\frac{M}{EI_0}\frac{L^2}{2\Gamma_R^2 - 4\Gamma_R + 2}$$

Thus, the displacement from a constant moment M is as follows:

$$w(x) = \frac{M}{EI_0}\frac{L^3}{2L\Gamma_R^2 - 4L\Gamma_R + 2L + x(2\Gamma_R^3 - 6\Gamma_R^2 + 6\Gamma_R - 2)} + \frac{M}{EI_0}\frac{L}{2\Gamma_R - 2}x - \frac{M}{EI_0}\frac{L^2}{2\Gamma_R^2 - 4\Gamma_R + 2}$$

$$w(x) = \frac{M}{EI_0}\left(\frac{L^3}{2L\Gamma_R^2 - 4L\Gamma_R + 2L + x(2\Gamma_R^3 - 6\Gamma_R^2 + 6\Gamma_R - 2)} + \frac{L}{2\Gamma_R - 2}x - \frac{L^2}{2\Gamma_R^2 - 4\Gamma_R + 2}\right)$$

$$w(x) = \frac{ML^2}{EI_0}\left(\frac{1}{(2\Gamma_R - 2)(\Gamma_R - 1) + (2\Gamma_R - 2)(\Gamma_R - 1)^2\frac{x}{L}} + \frac{1}{2\Gamma_R - 2}\frac{x}{L} - \frac{1}{(2\Gamma_R - 2)(\Gamma_R - 1)}\right)$$

$$w(x) = \frac{ML^2}{EI_0}\frac{1}{2\Gamma_R - 2}\left(\frac{1}{(\Gamma_R - 1) + (\Gamma_R - 1)^2\frac{x}{L}} + \frac{x}{L} - \frac{1}{\Gamma_R - 1}\right)$$

$$w(x) = \frac{ML^2}{EI_0}\frac{1}{2}\frac{1}{\Gamma_R - 1}\left(\frac{1}{\Gamma_R - 1}\left(\frac{1}{1 + (\Gamma_R - 1)\frac{x}{L}} - 1\right) + \frac{x}{L}\right)$$

In the following an equivalent bending stiffness is derived by equating the tip displacement $w(L)$ for a certain moment M of the telescopic mast with a mast of constant bending stiffness EI and same length L. The displacement function for such a beam is as follows:

$$w''(x) = \frac{M}{EI}$$

$$w'(x) = \frac{M}{EI}x + C_1$$

$$w(x) = \frac{M}{EI}\frac{1}{2}x^2 + C_1 x + C_2$$

The constants are as follows:

$$w'(0) = 0$$

$$0 = C_1$$

$$w(0) = 0$$

$$0 = C_2$$

The displacement is thereby as follows:

$$w(x) = \frac{M}{EI}\frac{1}{2}x^2$$

Equating the displacement function with the telescopic beam gives:

$$\frac{M}{EI}\frac{1}{2}x^2 = \frac{ML^2}{EI_0}\frac{1}{2}\frac{1}{\Gamma_R - 1}\left(\frac{1}{\Gamma_R - 1}\left(\frac{1}{1 + (\Gamma_R - 1)\frac{x}{L}} - 1\right) + \frac{x}{L}\right)$$

$$\frac{1}{EI}x^2 = \frac{L^2}{EI_0}\frac{1}{\Gamma_R - 1}\left(\frac{1}{\Gamma_R - 1}\left(\frac{1}{1 + (\Gamma_R - 1)\frac{x}{L}} - 1\right) + \frac{x}{L}\right)$$

For same deformation at the beam tip the equivalent bending stiffness EI is as follows:

$$\frac{1}{EI}L^2 = \frac{L^2}{EI_0}\frac{1}{\Gamma_R - 1}\left(\frac{1}{\Gamma_R - 1}\left(\frac{1}{\Gamma_R} - 1\right) + 1\right)$$

$$\frac{1}{EI} = \frac{1}{EI_0}\frac{1}{\Gamma_R - 1}\left(\frac{1}{\Gamma_R - 1}\left(\frac{1}{\Gamma_R} - 1\right) + 1\right)$$

$$EI = \frac{\Gamma_R - 1}{\frac{1}{\Gamma_R - 1}\left(\frac{1}{\Gamma_R} - 1\right) + 1}EI_0$$

$$EI = \frac{(\Gamma_R - 1)^2}{\frac{1}{\Gamma_R} + \Gamma_R - 2}EI_0$$

$$EI = \frac{\Gamma_R - 1}{1 - \frac{1}{\Gamma_R}}EI_0$$

$$EI = \Gamma_R EI_0$$

Thereby the constraint equation for the bending stiffness is as follows:

$$EI_{req} \leq EI = \Gamma_R EI_0$$
$$EI_{req} \leq \Gamma_R E k_I A_0 R_0^2$$

Thus the constraint equation according to Appendix C is as follows:

$$\frac{1}{\Gamma_R}\frac{1}{E}\frac{1}{k_I} EI_{req} \leq A_0 R_0^2$$

H3.2 Critical Bending Moment

Again a constant bending moment is used to characterize the performance for this load case. Therefore the critical bending moment is checked for the tip segment as it possesses the smallest cross-sectional dimensions. The maximum buckling stress of the cylinder wall for a cylinder in bending is as follows:

$$\sigma_{max} = \frac{E}{\sqrt{3(1-\nu^2)}}\frac{t}{R}\gamma_b$$
$$\gamma_b = 1 - 0.731(1 - e^{-\phi})$$
$$\phi = \frac{1}{16}\sqrt{\frac{R}{t}}$$

Formulation with the approximation is as follows:

$$\sigma_{max} = \frac{E}{\sqrt{3(1-\nu^2)}}\frac{1}{c_b\left(\frac{R}{t}\right)^{d_b}}$$

Thus the constraint equation for the critical bending moment is as follows:

$$M_{req} \leq M = \frac{E}{\sqrt{3(1-\nu^2)}}\frac{1}{c_b\left(\frac{R}{t}\right)^{d_b}}\frac{I}{R}$$
$$M_{req} \leq M = \frac{E}{\sqrt{3(1-\nu^2)}}\frac{1}{c_b\left(\frac{k_A R^2}{A}\right)^{d_b}} k_I A R$$
$$M_{req} \leq M = \frac{E}{\sqrt{3(1-\nu^2)}}\frac{1}{c_b}\frac{k_I}{k_A^{d_b}} A^{1+d_b} R^{1-2d_b}$$

The critical bending moment of the base segment is as follows:

$$M_0 = \frac{E}{\sqrt{3(1-\nu^2)}}\frac{1}{c_b}\frac{k_I}{k_A^{d_b}} A_0^{1+d_b} R_0^{1-2d_b}$$

The critical bending moment of the tip segment is as follows:

$$M_n = \frac{E}{\sqrt{3(1-\nu^2)}}\frac{1}{c_b}\frac{k_I}{k_A^{d_b}} A_n^{1+d_b} R_n^{1-2d_b}$$

Substitution of the expressions for the tip segment radius and cross-sectional area depending on the base segment properties gives:

$$R_n = \Gamma_R R_0$$
$$A_n = k_A R_n t = k_A \Gamma_R R_0 t$$
$$A_n = \Gamma_R A_0$$

$$M_n = \frac{E}{\sqrt{3(1-\nu^2)}}\frac{1}{c_b}\frac{k_I}{k_A^{d_b}} A_n^{1+d_b} R_n^{1-2d_b}$$
$$M_n = \frac{E}{\sqrt{3(1-\nu^2)}}\frac{1}{c_b}\frac{k_I}{k_A^{d_b}} \Gamma_R^{1+d_b} A_0^{1+d_b} \Gamma_R^{1-2d_b} R_0^{1-2d_b}$$
$$M_n = \frac{E}{\sqrt{3(1-\nu^2)}}\frac{1}{c_b}\frac{k_I}{k_A^{d_b}} \Gamma_R^{2-d_b} A_0^{1+d_b} R_0^{1-2d_b}$$

Comparing the critical bending moment of the base and the tip segment through the ratio υ gives:

$$\upsilon = \frac{M_n}{M_0}$$
$$\upsilon = \Gamma_R^{2-d_b}$$

As $0 < \Gamma_R < 1$ and $1 < d_b < 2$ one gains for the critical bending moment ratio $\upsilon < 1$. Hence the critical bending moment of the top segment is critical and the constraint equation for critical bending moment is as follows:

$$M_{req} \leq M = \frac{E}{\sqrt{3(1-\nu^2)}} \frac{1}{c_b} \frac{k_I}{k_A^{d_b}} \Gamma_R^{2-d_b} A_0^{1+d_b} R_0^{1-2d_b}$$

Thus the constraint equation according to Appendix C is as follows:

$$\frac{\sqrt{3(1-\nu^2)}}{E} c_b \frac{k_A^{d_b}}{k_I} \frac{1}{\Gamma_R^{2-d_b}} M_{req} \leq A_0^{1+d_b} R_0^{1-2d_b}$$

H3.3 Summary of the Scaling Constraint Functions for Bending

The scaling constraint functions for the Telescopic Tubular Mast loaded in bending are summarized in Tab. H - 5 whereby the constraint functions on the scaling limits are the same as for the load case of axial compression.

Scaling Constraint Functions of the Telescopic Tubular Mast for Bending				
Constraint Criterion	**Constraint Function**	c	i	j
Bending stiffness	$\frac{1}{\Gamma_R}\frac{1}{E}\frac{1}{k_I} EI_{req} \leq A_0 R_0^2$	$\frac{1}{\Gamma_R}\frac{1}{E}\frac{1}{k_I} EI_{req}$	1	2
Critical bending moment	$\frac{\sqrt{3(1-\nu^2)}}{E} c_b \frac{k_A^{d_b}}{k_I} \frac{1}{\Gamma_R^{2-d_b}} M_{req} \leq A_0^{1+d_b} R_0^{1-2d_b}$	$\frac{\sqrt{3(1-\nu^2)}}{E} c_b \frac{k_A^{d_b}}{k_I} \frac{1}{\Gamma_R^{2-d_b}}$	$1 + d_b$	$1 - 2d_b$
Minimum wall thickness	$k_A t_{min} \leq A_0 R_0^{-1}$	$k_A t_{min}$	1	-1
Minimum tip radius	$\frac{1}{\Gamma_R} R_{n,min} \leq A_0^0 R_0$	$\frac{1}{\Gamma_R} R_{n,min}$	0	1
Minimum segment clearance	$n \frac{1}{1-\Gamma_R} \frac{k_{\Delta,min}}{k_A} \leq A_0^{-1} R_0^2$	$n \frac{1}{1-\Gamma_R} \frac{k_{\Delta,min}}{k_A}$	-1	2

Tab. H - 5: Summary of the scaling constraint functions of the Telescopic Tubular Mast for the load case of bending.

H4 Deployment Mechanism Scaling Constraint Functions

In the following the derivations of the scaling functions for the Deployment Mechanism of the Telescopic Tubular Mast are described.

H4.1 Base Plate

The base plate is mounted to the bottom of the base cylinder, carries the mechanism components of mass m_0 and provides the interface to the host spacecraft. The base plate model is that of a circular plate with a central mass. The plate radius corresponds to the base segment radius R_0. Dimensioning is done by an eigenfrequency requirement f_{req} whereby the mass of the plate is as follows according to A4.3:

$$m = \left(\frac{\pi^4}{4} \frac{k_m^3}{k_D} \frac{k_\rho^3 \rho^{*3} (1-\nu^2)(3+\nu)}{E(1+\nu)} R_0^8 f_{req}^2 m_0 \right)^{\frac{1}{3}}$$

A scaling limit is applied to the minimum plate thickness t_{min}. Thereby the plate mass is as follows:

$$m_{min} = k_m k_\rho \rho^* t_{min} R_0^2$$

The parameters of the base plate scaling functions are summarized in Tab. H - 6.

Parameters of the Base Plate			
Parameter	**Symbol**	**Unit**	**Value**
Base plate radius	R_0	m	Input value
Center mass	m_0	kg	Input value
Material modulus	E	N/m²	60 GPa
Reference density	ρ^*	kg/m³	1600
Poisson ratio	ν	-	0.3
Eigenfrequency requirement	f_{req}	Hz	100
Plate mass architecture factor	k_m	-	0.111 (Sandwich Architecture)
Plate flexural rigidity architecture factor	k_D	-	0.0125 (Sandwich Architecture)
Density factor	k_ρ	-	27/16
Minimum plate thickness	t_{min}	m	0.003 (Sandwich Architecture)

Tab. H - 6: Parameters of the base plate scaling function of the Telescopic Tubular Mast.

The scaling function is summarized in Tab. H - 7.

Scaling Function of the Base Plate
Scaling Approach: First Eigenfrequency
$$m = \left(\frac{\pi^4}{4}\frac{k_{m,P}^3}{k_D}\frac{k_\rho^3 \rho^{*3}(1-\nu^2)(3+\nu)}{E(1+\nu)} R_0^8 f_{req}^2 m_0\right)^{\frac{1}{3}}$$ $$m_{min} = k_m k_\rho \rho^* t_{min} R_0^2$$

Tab. H - 7: Mass scaling functions of the base plate of the Telescopic Tubular Mast.

H4.2 Belt Drive Mechanism

The belt Drive Mechanism corresponds to that of the reeling mechanism described in Appendix B4. In difference to the described solution four belts are utilized instead of one whereby each carries a quarter of the actual pulling force:

$$P^* = \frac{P}{4}$$

The resulting belt mass is the same as for a single belt given in B4.1 but the dimensions of the Belt Spool and the corresponding torque the gear motor has to provide differ. Hence, the belt length has to be adjusted to four times the mast length in the Belt Spool geometry function in difference to those given in B4.2:

$$L^* = 4L$$

The subsequent sizing of the gear and motor is done as described in B4.3 and B4.4.

Appendix I

I Telescopic Tubular Mast Scaling Function

Within Appendix I the scaling functions for the flexible blanket solar array and the Folding Truss are derived.

I1 Solar Array Scaling Functions

The solar array is a flexible blanket design with two zigzag folded blankets deployed by a deployable mast in the center between the blankest. The blankets are stowed in between of two sandwich beams that also act as root and tip spreader bars.

I1.1 Array Geometry Scaling Functions

For initial sizing of blanket and spreader bar their geometry is expressed in terms of geometry ratios depending on the mast length L. The width of the combined blankets b_{BL} is defined by the ratio Γ_{bL} as follows:

$$\Gamma_{BL} = \frac{b_{BL}}{L} = 0.25$$

The fold height h_{PV} is defined by the ratio Γ_{PVL} as follows:

$$\Gamma_{PVL} = \frac{h_{PV}}{L} = 0.02$$

Thereby also the number of folds n_{PV} is a constant:

$$n_{PV} = \frac{1}{\Gamma_{PVL}}$$

The stowed thickness of each fold t_{PV} is set to 0.002 m. Thereby the stack size s_{PV} is constant:

$$s_{PV} = n_{PV} t_{PV} = \frac{t_{PV}}{\Gamma_{PVL}} = 0.1 \text{ m}$$

Furthermore the areal mass of the blanket including spreader bar mass γ_{BL} is set to 1 kg/m².

The area A_{BL} and length L of the blanket depends on the required electric power output $P_{elec,req}$, the solar constant $G_{SC} = 1367 \text{ W/m}^2$, the efficiency of the photovoltaic cells $\eta_{PV} = 0.295$ and the effective cell area factor $k_{PV} = 0.7$:

$$P_{elec,req} = A_{BL} G_{SC} \eta_{PV} k_{PV}$$
$$A_{BL} = b_{BL} L = \Gamma_{bL} L^2$$

Substitution of the area expression and solving for the length L gives:

$$P_{elec,req} = \Gamma_{bL} L^2 G_{SC} \eta_{PV} k_{PV}$$
$$L = \left(\frac{P_{elec,req}}{\Gamma_{bL} G_{SC} \eta_{PV} k_{PV}} \right)^{\frac{1}{2}}$$

I1.2 Array Mass Scaling Functions

The mass scaling function of the blanket including the spreader bars m_{BL} is as follows:

$$m_{BL} = A_{BL} \gamma_{BL}$$
$$A_{BL} = \frac{P_{elec,req}}{G_{SC} \eta_{PV} k_{PV}}$$

$$m_{BL} = \frac{P_{elec,req}}{G_{SC}\eta_{PV}k_{PV}}\gamma_{BL}$$

The total mass of the solar array m_{SolAr} is the sum of the array blanket mass m_{BL} and the mast mass m_M

$$m_{SolAr} = m_{BL} + m_M$$

The resulting mass specific power $P_{elec,m}$ is thereby as follows:

$$P_{elec,m} = \frac{P_{elec}}{m_{SolAr}}$$

I1.3 Array Volume Scaling Functions

The stowed volume of the blanket including the spreader bars V_{BL} is assessed by the depth of the photovoltaic stack s_{PV} and a ratio Γ_{SB} that describes the thickness of the spreader bars t_{SB} whereby it is assumed that these scale with the length of the array as follows:

$$\Gamma_{SB} = \frac{t_{SB}}{L} = 0.005$$

Thereby the volume of the blanket including spreader bars is as follows:

$$V_{BL} = h_{PV}b_{BL}(2t_{SB} + s_{PV})$$

Substitution of the size expressions through the according ratios gives:

$$V_{BL} = \Gamma_{PVL}\Gamma_{bL}\left(2\Gamma_{SB}L + \frac{t_{PV}}{\Gamma_{PVL}}\right)L^2$$

Substitution of the array length gives the volume scaling function of the blanket including the spreader bars:

$$V_{BL} = \Gamma_{PVL}\left(2\Gamma_{SB}L + \frac{t_{PV}}{\Gamma_{PVL}}\right)\frac{P_{elec,req}}{G_{SC}\eta_{PV}k_{PV}}$$

The effective volume of the solar array is defined as that of the outer rectangular envelope V_{SolAr}. The width and height of the envelope is determined by the width b_{BL} and height h_{PV} of the stowed blanket. The depth of the envelope is the sum of the depth of the stowed photovoltaic s_{PV}, the thickness of the spreader bars t_{SB} and the depth of the stowed mast s_M:

$$V_{SolAr} = h_{PV}b_{BL}(2t_{SB} + s_{PV} + s_M)$$

$$V_{SolAr} = V_{BL} + \Gamma_{PVL}\Gamma_{bL}s_M L^2$$

The outer envelope is chosen for calculation of the array volume, as a void volume caused by the stowed mast cannot be occupied by other array components. Hence a stowed form of the mast compatible to the stowed blanket is advantageous. The volume specific power of the array $P_{elec,V}$ is thereby as follows:

$$P_{elec,V} = \frac{P_{elec}}{V_{SolAr}}$$

I1.4 Summary of Array Geometry, Mass and Volume Scaling Functions

The parameters of the blanket and solar array are summarized in Tab. I - 1.

Parameters of the Photovoltaic Blanket and the Solar Array			
Parameter	**Symbol**	**Unit**	**Value**
Required electric power	P_{elec}	W	Input value

Array Length	L	m	-
Blanket width	b_{BL}	m	-
Photovoltaic (PV) fold thickness	t_{PV}	m	0.002
PV fold height	h_{PV}	m	-
Spreader bar thickness	t_{SB}	m	-
Stowed PV stack size	s_{PV}	m	-
Stowed mast depth	s_M	m	-
Number of PV folds	n_{PV}	-	-
Efficiency of the PV	η_{PV}	-	0.295
Solar constant	G_{SC}	W/m²	1367
Effective PV area factor	k_{PV}	-	0.7
Blanket with ratio	Γ_{bL}	-	0.25
PV fold height ratio	Γ_{PVL}	-	0.02
Spreader bar thickness ratio	Γ_{SB}	-	0.005
Blanket and spreader bar areal mass	γ_{BL}	kg/m²	1
Blanket and spreader bar mass	m_{BL}	kg	-
Mast mass	m_M	kg	-
Solar array total mass	m_{SolAr}	kg	-
Blanket and spreader bar volume	V_{BL}	m³	-
Solar array envelope volume	V_{SolAr}	m³	-
Solar array mass specific power	$P_{elec,m}$	W/kg	-
Solar array volume specific power	$P_{elec,V}$	W/m³	-

Tab. I - 1: Parameters of the solar array and photovoltaic blanket.

The blanket and array mass and volume scaling functions are summarized in Tab. I - 2.

Scaling Function of the Photovoltaic Blanket and the Solar Array	
Scaling Approach: Geometric Similarity expressed through according Size Ratios	
Blanket and spreader bar mass	$m_{BL} = \frac{P_{elec,req}}{G_{SC}\eta_{PV}k_{PV}}\gamma_{BL}$
Solar array total mass	$m_{SolAr} = m_{BL} + m_M$
Blanket and spreader bar volume	$V_{BL} = \Gamma_{PVL}\left(2\Gamma_{SB}L + \frac{t_{PV}}{\Gamma_{PVL}}\right)\frac{P_{elec,req}}{G_{SC}\eta_{PV}k_{PV}}$
Solar array total volume	$V_{SolAr} = V_{BL} + \Gamma_{PVL}\Gamma_{bL}s_M L^2$

Tab. I - 2: Mass and volume scaling functions of the solar array and photovoltaic blanket.

I2 Folding Truss Scaling Functions

The scaling functions for the folding truss are derived according to the truss parameterization described in Appendix F1.

I2.1 Folding Truss Geometry Scaling Functions

The radius R is coupled to the height of the stowed blanket which corresponds to the fold height of the photovoltaic h_{PV}:

$$h_{PV} = 2\sin\left(\frac{\pi}{n}\right)R$$

Substitution of the fold height gives:

$$R = \frac{\Gamma_{PVL}L}{2\sin\left(\frac{\pi}{n}\right)}$$

Substitution of the length by the required power expression gives the truss radius scaling function:

$$R = \frac{\Gamma_{PVL}}{2\sin\left(\frac{\pi}{n}\right)}\left(\frac{P_{elec,req}}{\Gamma_{bL}G_{SC}\eta_{PV}k_{PV}}\right)^{\frac{1}{2}}$$

$$R = \left(\frac{1}{4}\frac{\Gamma_{PVL}^2}{\Gamma_{bL}}\frac{1}{\sin^2\left(\frac{\pi}{n}\right)}\frac{P_{elec,req}}{G_{SC}\eta_{PV}k_{PV}}\right)^{\frac{1}{2}}$$

Furthermore the length of a longeron l is coupled to the blanket width b_{BL} as it has to be a fraction of an even integer given by the number of longeron n_{lB}:

$$l = \frac{b_{BL}}{n_{lB}}$$

Substitution of the blanket width gives:

$$l = \frac{\Gamma_{bL}L}{n_{lB}}$$

Substitution of the length by the required power expression gives the longeron length scaling function:

$$l = \frac{\Gamma_{bL}}{n_{lB}}\left(\frac{P_{elec,req}}{\Gamma_{bL}G_{SC}\eta_{PV}k_{PV}}\right)^{\frac{1}{2}}$$

$$l = \left(\frac{\Gamma_{bL}}{n_{lB}^2}\frac{P_{elec,req}}{G_{SC}\eta_{PV}k_{PV}}\right)^{\frac{1}{2}}$$

The diagonal angle Θ and thereby the truss axial mass ratio β is as follows:

$$l = 2\tan(\Theta)\,R\sin\left(\frac{\pi}{n}\right)$$

$$\tan(\Theta) = \frac{l}{2R\sin\left(\frac{\pi}{n}\right)}$$

$$\tan(\Theta) = \frac{1}{2\frac{\Gamma_{PVL}}{2\sin\left(\frac{\pi}{n}\right)}\left(\frac{P_{elec,req}}{\Gamma_{bL}G_{SC}\eta_{PV}k_{PV}}\right)^{\frac{1}{2}}\sin\left(\frac{\pi}{n}\right)}\frac{\Gamma_{bL}}{n_{lB}}\left(\frac{P_{elec,req}}{\Gamma_{bL}G_{SC}\eta_{PV}k_{PV}}\right)^{\frac{1}{2}}$$

$$\tan(\Theta) = \frac{\Gamma_{bL}}{\Gamma_{PVL}n_{lB}}$$

Thereby the diagonal angle scaling function is as follows:

$$\Theta = \arctan\left(\frac{\Gamma_{bL}}{\Gamma_{PVL}n_{lB}}\right)$$

I2.2 Folding Truss Mass Scaling Functions from Global Column Buckling

As the radius R, the longeron length l and the diagonal angle Θ depend on the requirements and geometrical definitions of the blanket, the remaining design variable is the cross-sectional area A:

$$A = n\beta A_l$$

The solution for the longeron area A_l is derived for the solar array application and the load case of axial compression defined in Appendix D2. The constraint functions are global column buckling and local longeron buckling as follows:

$$P_{req} \le P_{global} = k_\zeta\frac{\pi^2 EI}{(k_C L)^2}$$

$$P_{req} \le P_{local} = \frac{\pi^2 (EI)_l}{n\left(k_{C,l}l\right)^2}$$

As there is only a single design variable the two constraint functions lead to two scaling functions. The scaling function from global column buckling is as follows:

$$P_{req} = k_\zeta\frac{\pi^2}{(k_C L)^2}\frac{n}{2}EA_l R^2$$

Substitution of the truss radius and the length gives:

$$P_{req} = k_\zeta\frac{\pi^2}{k_C^2\frac{P_{elec,req}}{\Gamma_{bL}G_{SC}\eta_{PV}k_{PV}}}\frac{n}{2}EA_l\frac{1}{4}\frac{\Gamma_{PVL}^2}{\Gamma_{bL}}\frac{1}{\sin^2\left(\frac{\pi}{n}\right)}\frac{P_{elec,req}}{G_{SC}\eta_{PV}k_{PV}}$$

$$P_{req} = \frac{\pi^2}{k_C^2}k_\zeta\frac{n}{2}EA_l\frac{1}{4}\Gamma_{PVL}^2\frac{1}{\sin^2\left(\frac{\pi}{n}\right)}$$

Solving for the longeron cross-sectional area gives:

$$A_l = \frac{8}{\pi^2}\frac{1}{k_\zeta}k_C^2\frac{1}{\Gamma_{PVL}^2}\frac{\sin^2\left(\frac{\pi}{n}\right)}{n}\frac{1}{E}P_{req}$$

Hence the scaling function for the truss cross-sectional area from global column buckling is as follows:

$$A_{global} = n\beta A_l$$

$$A_{global} = \frac{8}{\pi^2}\frac{1}{k_\zeta}k_C^2\frac{1}{\Gamma_{PVL}^2}\sin^2\left(\frac{\pi}{n}\right)\beta\frac{1}{E}P_{req}$$

The mass scaling function for the global column buckling is thereby as follows:

$$m_{M,global} = A_{global}\rho L$$

$$m_{M,global} = \frac{8}{\pi^2}\frac{1}{k_\zeta}k_C^2\frac{1}{\Gamma_{PVL}^2}\sin^2\left(\frac{\pi}{n}\right)\beta\frac{\rho}{E}P_{req}L$$

Substitution of the array length gives:

$$m_{M,global} = \frac{8}{\pi^2}\frac{1}{k_\zeta}k_C^2\frac{1}{\Gamma_{PVL}^2}\sin^2\left(\frac{\pi}{n}\right)\beta\frac{\rho}{E}P_{req}\left(\frac{P_{elec,req}}{\Gamma_{bL}G_{SC}\eta_{PV}k_{PV}}\right)^{\frac{1}{2}}$$

$$m_{M,global} = \left(\frac{64}{\pi^4}\frac{1}{k_\zeta^2}k_C^4\frac{1}{\Gamma_{PVL}^4}\sin^4\left(\frac{\pi}{n}\right)\beta^2\frac{\rho^2}{E^2}\frac{P_{elec,req}}{\Gamma_{bL}G_{SC}\eta_{PV}k_{PV}}P_{req}^2\right)^{\frac{1}{2}}$$

The scaling function for the corresponding specific mass $w_{M,global}$ is as follows:

$$w_{M,global} = \frac{8}{\pi^2}\frac{1}{k_\zeta}k_C^2\frac{1}{\Gamma_{PVL}^2}\sin^2\left(\frac{\pi}{n}\right)\beta\frac{\rho}{E}P_{req}$$

I2.3 Folding Truss Mass Scaling Function from Local Longeron Buckling

The scaling function from longeron buckling is as follows:

$$P_{req} \le P_{local} = \frac{\pi^2(EI)_l}{n\left(k_{C,l}l\right)^2}$$

$$P_{req} = \frac{1}{n}\frac{\pi^2}{k_{C,l}^2 l^2}E\frac{k_{I,l}}{k_{A,l}}A_l^2$$

Substitution of the longeron length gives:

$$P_{req} = \frac{1}{n}\frac{\pi^2}{k_{C,l}^2\frac{\Gamma_{bL}}{n_{lB}^2}\frac{P_{elec,req}}{G_{SC}\eta_{PV}k_{PV}}}E\frac{k_{I,l}}{k_{A,l}}A_l^2$$

$$A_l = \left(\frac{1}{\pi^2}n\frac{1}{E}\frac{k_{A,l}}{k_{I,l}}k_{C,l}^2\frac{\Gamma_{bL}}{n_{lB}^2}\frac{P_{elec,req}}{G_{SC}\eta_{PV}k_{PV}}P_{req}\right)^{\frac{1}{2}}$$

Hence the scaling function for the truss cross-sectional area from longeron buckling is as follows:

$$A_{local} = n\beta A_l$$

$$A_{local} = \left(\frac{1}{\pi^2}n^3\beta^2\frac{1}{E}\frac{k_{A,l}}{k_{I,l}}k_{C,l}^2\frac{\Gamma_{bL}}{n_{lB}^2}\frac{P_{elec,req}}{G_{SC}\eta_{PV}k_{PV}}P_{req}\right)^{\frac{1}{2}}$$

The mass scaling function for the local longeron buckling is as follows:

$$m_{M,local} = A_{local}\rho L$$

$$m_{M,local} = \left(\frac{1}{\pi^2}n^3\beta^2\frac{1}{E}\frac{k_{A,l}}{k_{I,l}}k_{C,l}^2\frac{\Gamma_{bL}}{n_{lB}^2}\frac{P_{elec,req}}{G_{SC}\eta_{PV}k_{PV}}P_{req}\right)^{\frac{1}{2}}\rho L$$

Substitution of the array length gives:

$$m_{M,local} = \left(\frac{1}{\pi^2}n^3\beta^2\frac{1}{E}\frac{k_{A,l}}{k_{I,l}}k_{C,l}^2\frac{\Gamma_{bL}}{n_{lB}^2}\frac{P_{elec,req}}{G_{SC}\eta_{PV}k_{PV}}P_{req}\right)^{\frac{1}{2}}\rho\left(\frac{P_{elec,req}}{\Gamma_{bL}G_{SC}\eta_{PV}k_{PV}}\right)^{\frac{1}{2}}$$

$$m_{M,local} = \left(\frac{1}{\pi^2}n^3\beta^2\frac{\rho^2}{E}\frac{k_{A,l}}{k_{I,l}}k_{C,l}^2\frac{1}{n_{lB}^2}\frac{P_{elec,req}^2}{G_{SC}^2\eta_{PV}^2k_{PV}^2}P_{req}\right)^{\frac{1}{2}}$$

The scaling function for the corresponding specific mass $w_{M,local}$ is as follows:

$$w_{M,local} = \left(\frac{1}{\pi^2} n^3 \beta^2 \frac{\rho^2}{E} \frac{k_{A,l}}{k_{I,l}} k_{C,l}^2 \frac{\Gamma_{bL}}{n_{IB}^2} \frac{P_{elec,req}}{G_{SC} \eta_{PV} k_{PV}} P_{req}\right)^{\frac{1}{2}}$$

I2.4 Required Compression Strength from Array Scaling Function

The required compression strength P_{req} is derived according to Appendix D2.3 as follows:

$$P_{req} = \left(\frac{2\pi^2}{3.516}\right)^2 \left(\frac{f}{\delta}\right)^2 \gamma_{BL} \Gamma_{bL} L^3$$

Substitution of the array length gives:

$$P_{req} = \left(\frac{2\pi^2}{3.516}\right)^2 \left(\frac{f}{\delta}\right)^2 \gamma_{BL} \Gamma_{bL} \left(\frac{P_{elec,req}}{\Gamma_{bL} G_{SC} \eta_{PV} k_{PV}}\right)^{\frac{3}{2}}$$

$$P_{req} = \left(\left(\frac{2\pi^2}{3.516}\right)^4 \left(\frac{f}{\delta}\right)^4 \gamma_{BL}^2 \frac{P_{elec,req}^3}{\Gamma_{bL} G_{SC}^3 \eta_{PV}^3 k_{PV}^3}\right)^{\frac{1}{2}}$$

I2.5 Folding Truss Volume Scaling Function

The volume of the array is derived according to Appendix I1.3. Therefore the stowed size s_M of the mast needs to be derived. For the Folding Truss the corresponding value is depending on the longeron radius r_l and the array width ratio Γ_{bL} as this defines the number of folds of the truss. For each fold two longerons lie next to each other. To account for some clearance a factor k_{FTV} is considered. Thereby the stowed mast for the Folding Truss size is as follows:

$$s_M = 2k_{FTV}\left(\frac{1}{\Gamma_{bL}} + 1\right) r_l$$

The radius of the longeron is derived through the scaling result longeron cross-sectional area A_l derived in Appendix I2.2 and I2.3:

$$A_l = k_{A,l} r_l^2$$

$$r_l = \left(\frac{A_l}{k_{A,l}}\right)^{\frac{1}{2}}$$

Hence the stowed mast size is as follows:

$$s_M = 2k_{FTV}\left(\frac{1}{\Gamma_{bL}} + 1\right)\left(\frac{A_l}{k_{A,l}}\right)^{\frac{1}{2}}$$

I2.6 Summary of Folding Truss Geometry, Mass and Volume Scaling Functions

The parameters of the Folding Truss are summarized in Tab. I - 3.

Parameters of the Folding Truss			
Parameter	**Symbol**	**Unit**	**Value**
Required electric power	P_{elec}	W	Input value
Required compression strength	P_{req}	N	-
Array Length	L	m	-
Truss radius	R	m	-

Longeron length	l	m	-
Truss cross-sectional area	A	m²	Design variable
Longeron cross-sectional area	A_l	m²	-
Longeron radius	r_l	m	-
Diagonal angle	Θ	rad	-
Stowed mast depth	s_M	m	-
Material modulus	E	N/m²	175 GPa
Material density	ρ	kg/m³	1600
Truss axial mass ratio	β	-	-
Number of longerons	n	-	4
Longeron area factor	$k_{A,l}$	-	4
Longeron second moment of area factor	$k_{I,l}$	-	1/3
Longeron mounting factor	$k_{C,l}$	-	1
Truss mounting factor	k_C	-	2
Stowage volume factor	k_{FTV}	-	1.2
Number of PV folds	n_{PV}	-	-
Efficiency of the PV	η_{PV}	-	0.295
Eigenfrequency	f	Hz	-
Eigenfrequency knockdown factor	δ	-	0.76
Solar constant	G_{SC}	W/m²	1367
Effective PV area factor	k_{PV}	-	0.7
Blanket with ratio	Γ_{bL}	-	0.25
PV fold height ratio	Γ_{PVL}	-	0.02
Spreader bar thickness ratio	Γ_{SB}	-	0.005
Blanket and spreader bar areal mass	γ_{BL}	kg/m²	1
Mast mass	m_M	kg	-

Tab. I - 3: Parameters of the Foldin Truss.

The Folding Truss geometry, mass and volume scaling functions are summarized in Tab. I - 4.

Scaling Functions of the Folding Truss for a Solar Array Application	
Scaling Approach: Axial Compression	
Truss radius	$R = \left(\frac{1}{4} \frac{\Gamma_{PVL}^2}{\Gamma_{bL}} \frac{1}{\sin^2\left(\frac{\pi}{n}\right)} \frac{P_{elec,req}}{G_{SC}\eta_{PV}k_{PV}} \right)^{\frac{1}{2}}$
Longeron length	$l = \left(\frac{\Gamma_{bL}}{n_{lB}^2} \frac{P_{elec,req}}{G_{SC}\eta_{PV}k_{PV}} \right)^{\frac{1}{2}}$
Diagonal angle	$\Theta = \arctan\left(\frac{\Gamma_{bL}}{\Gamma_{PVL} n_{lB}} \right)$
Mass from global column buckling	$m_{M,global} = \left(\frac{64}{\pi^4} \frac{1}{k_\zeta^2} k_C^4 \frac{1}{\Gamma_{PVL}^4} \sin^4\left(\frac{\pi}{n}\right) \beta^2 \frac{\rho^2}{E^2} \frac{P_{elec,req}}{\Gamma_{bL} G_{SC}\eta_{PV}k_{PV}} P_{req}^2 \right)^{\frac{1}{2}}$
Mass from local wall buckling	$m_{M,local} = \left(\frac{1}{\pi^2} n^3 \beta^2 \frac{\rho^2}{E} \frac{k_{A,l}}{k_{I,l}} k_{C,l}^2 \frac{1}{n_{lB}^2} \frac{P_{elec,req}^2}{G_{SC}^2 \eta_{PV}^2 k_{PV}^2} P_{req} \right)^{\frac{1}{2}}$
Required compression strength	$P_{req} = \left(\left(\frac{2\pi^2}{3.516} \right)^4 \left(\frac{f}{\delta} \right)^4 \gamma_{BL}^2 \frac{P_{elec,req}^3}{\Gamma_{bL} G_{SC}^3 \eta_{PV}^3 k_{PV}^3} \right)^{\frac{1}{2}}$
Stowed size	$s_M = 2k_{FTV} \left(\frac{1}{\Gamma_{bL}} + 1 \right) \left(\frac{A_l}{k_{A,l}} \right)^{\frac{1}{2}}$

Tab. I - 4: Mass and volume scaling functions for the Folding Truss in a solar array application.

I3 Folding Truss Drive Mechanism

The Drive Mechanism consists of mechanism to pull the in the stowed state elongated diagonals of the folding truss to achieve deployment of the mast and a second Drive Mechanism to deploy the photovoltaic blanket. For both Drive Mechanisms a design as described in section 4.3.5 and Appendix B4 are utilized. As a first approximation the design values given in the related sections (see Tab. B - 21 and Tab. B - 23) remain the same. The mass of the shortened diagonals which are part of the Deployment Mechanism is already contained within the truss axial mass ratio β.